AD-A164 693 DAMAGE TOLERANCE CONCEPTS FOR CRITICAL ENGINE COMPONENTS(U) ADVISORY GROUP FOR AEROSPACE RESEARCH AND DEVELOPMENT NEUILLY-SUR-SEINE (FRANCE) OCT 85 1/4

UNCLASSIFIED AGARD-CP-393 F/G 21/5 NL

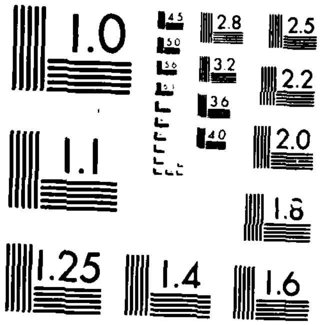
1.0
4.5
5.0
5.6
2.8
2.5
3.2
2.2
3.6
4.0
2.0
1.1
1.8
1.25
1.4
1.6

MICROCOPY RESOLUTION TEST CHART
NATIONAL BUREAU OF STANDARDS 1963 A

(2)

AGARD-CP-393

AGARD

ADVISORY GROUP FOR AEROSPACE RESEARCH & DEVELOPMENT

7 RUE ANCELLE 92200 NEUILLY SUR SEINE FRANCE

AD-A164 693

AGARD CONFERENCE PROCEEDINGS No.393

Damage Tolerance Concepts for Critical Engine Components

DISTRIBUTION STATEMENT A
Approved for public release;
Distribution Unlimited

DTIC
ELECTE
FEB 24 1986
S D

NORTH ATLANTIC TREATY ORGANIZATION

DTIC FILE COPY

DISTRIBUTION AND AVAILABILITY
ON BACK COVER

86 2 24 037

AGARD-CP-393

NORTH ATLANTIC TREATY ORGANIZATION

ADVISORY GROUP FOR AEROSPACE RESEARCH AND DEVELOPMENT

(ORGANISATION DU TRAITE DE L'ATLANTIQUE NORD)

AGARD Conference Proceedings No.393

DAMAGE TOLERANCE CONCEPTS FOR CRITICAL ENGINE COMPONENTS

Papers presented at the 60th Meeting of the Structures and Materials Panel
in San Antonio, Texas, USA on 22–26 April 1985.

THE MISSION OF AGARD

The mission of AGARD is to bring together the leading personalities of the NATO nations in the fields of science and technology relating to aerospace for the following purposes:

— Exchanging of scientific and technical information;

— Continuously stimulating advances in the aerospace sciences relevant to strengthening the common defence posture;

— Improving the co-operation among member nations in aerospace research and development;

— Providing scientific and technical advice and assistance to the North Atlantic Military Committee in the field of aerospace research and development;

— Rendering scientific and technical assistance, as requested, to other NATO bodies and to member nations in connection with research and development problems in the aerospace field;

— Providing assistance to member nations for the purpose of increasing their scientific and technical potential;

— Recommending effective ways for the member nations to use their research and development capabilities for the common benefit of the NATO community.

The highest authority within AGARD is the National Delegates Board consisting of officially appointed senior representatives from each member nation. The mission of AGARD is carried out through the Panels which are composed of experts appointed by the National Delegates, the Consultant and Exchange Programme and the Aerospace Applications Studies Programme. The results of AGARD work are reported to the member nations and the NATO Authorities through the AGARD series of publications of which this is one.

Participation in AGARD activities is by invitation only and is normally limited to citizens of the NATO nations.

The content of this publication has been reproduced
directly from material supplied by AGARD or the authors.

Published October 1985

Copyright © AGARD 1985
All Rights Reserved

ISBN 92-835-0380-5

Printed by Specialised Printing Services Limited
40 Chigwell Lane, Loughton, Essex IG10 3TZ

PREFACE

The Structures and Materials Panel has discussed the problems of materials in the gas turbine environment on a number of occasions in past years. In 1982 a sub-committee was formed to promote a Specialists' Meeting on the overall philosophy and the implications of introducing damage tolerance concepts (DTC) into the design and use of critical engine components. The damage tolerant philosophy offers potential cost savings of considerable magnitude when compared with a 'safe-life' approach, if only such a concept can be implemented with an asurance that current safety standards will not be prejudiced. As an example of possible cost savings, it has been estimated that over 80% of engine discs have 10 or more low cycle fatigue lives remaining when discarded under 'safer-life' rules, and its is this useful remaining life that the DTC aims to exploit in service. Apart from economic advantages, the DTC approach offers a practical method of using modern high-strength disc materials that could be rejected by the application of safe-life conditions of usage.

The structure of the meeting was such that it concentrated upon the parameters important in the application of DTC and the specialist techniques supporting this approach. The treatment of the engine as a complete system was addressed in the opening and penultimate sessions, which permitted liaison between the AGARD Panels, dealing with Structures and Materials on the one hand and Propulsion and Energetics on the other, and a joint discussion on the problems of engine lifing. The audience, in the final discussion, clearly expressed a continuing interest in DTC and encouraged the SMP to arrange further specialist sessions on this topic.

D.A.FANNER
Chairman — Sub-Committee on
"Damage tolerance concepts for
critical engine components"

Accesion For
NTIS CRA&I ☑
DTIC TAB ☐
Unannounced ☐
Justification ....
By ....
Distribution /
Availability Codes
Dist | Avail and/or Special
A-1

CONTENTS

Page

PREFACE iii

INTRODUCTORY REMARKS
by M.J.Weaver vi

Reference

SESSION I – OVERALL PHILOSOPHY

DAMAGE TOLERANCE CONCEPTS FOR CRITICAL ENGINE COMPONENTS
by R.H.Jeal 1

ENGINE CYCLIC DURABILITY BY ANALYSIS AND TESTING – HIGHLIGHTS OF THE SPRING 1984 PEP MEETING
by A.A.Martino 2

DAMAGE TOLERANCE DESIGN CONCEPTS FOR MILITARY ENGINES
by T.T.King, W.D.Cowie and W.H.Reimann 3

SESSION II – PARAMETERS IMPORTANT TO DTC

PARAMETERS THAT INPUT TO APPLICATION OF DAMAGE TOLERANCE CONCEPTS TO CRITICAL ENGINE COMPONENTS
by D.W.Hoeppner 4

LIMITATIONS OF MANUAL NDT SYSTEMS AND THE 'NO EYES' CONCEPT
by R.G.Taylor 5

THE ROLE OF THERMAL AND STRESS ANALYSES IN THE APPLICATION OF DAMAGE TOLERANT DESIGN
by G.F.Harrison and T.H.Edmunds 6

DAMAGE TOLERANCE ACCEPTANCE METHODS IN STRUCTURAL COMPONENTS OF A MEDIUM CARBON STEEL AND A MEDIUM-STRENGTH AL-Mg ALLOY
by C.M.Branco 7

MANUFACTURING TECHNOLOGY FOR NONDESTRUCTIVE EVALUATION (NDE) SYSTEM TO IMPLEMENT RETIREMENT FOR CAUSE (RFC) PROCEDURES FOR GAS TURBINE ENGINE COMPONENTS
by D.L.Birx and F.M.Taylor 8

AGARD COOPERATIVE TEST PROGRAMME ON TITANIUM ALLOY ENGINE DISC MATERIAL
by A.J.A.Mom and M.D.Raizenne 9

SESSION III – SPECIALIST TECHNIQUES TO SUPPORT DTC

ASPECTS OF SMALL CRACK GROWTH
by M.N.James and J.F.Knott 10

CRACK GROWTH IN NEAR-ALPHA TITANIUM ALLOYS
by C.R.Gostelow 11

MESURE DE LONGUEUR DE FISSURE, DEFORMATION ET ENDOMMAGEMENT PAR UNE TECHNIQUE DE POTENTIEL ELECTRIQUE
par H.Policella, G.Baudin et G.Cailletaud 12

SMALL DEFECT CHARACTERIZATION IN POWDER METALLURGY MATERIALS
by S.Re Fiorentin and H.Walther 13

Reference

ADVANCED EXPERIMENTAL METHODS FOR MONITORING THE BEHAVIOR OF SMALL CRACKS
by J.M.Larsen 14

MULTIAXIAL AND THERMOMECHANICAL FATIGUE CONSIDERATIONS IN DAMAGE TOLERANT DESIGN
by G.E.Leese and R.C.Bill 15

ADVANCED QUANTITATIVE METHODS FOR NONDESTRUCTIVE EVALUATION
by D.E.Chimenti and T.J.Moran 16

STATISTICAL ANALYSIS OF SPIN PIT FAILURE DATA TO PREDICT INSERVICE B.1 LIVES OF GAS TURBINE DISKS
by R.Mahorter, S.Fowler and J.Salvino 17

FRACTURE MECHANICS AND LCF-PROPERTIES OF ENGINE DISCS OF Ti 6 Al-4V, INCONEL 718 AND UDIMET 700 P/M-HIP
by W.Schütz and R.Heidenreich 18

EVALUATION OF CYCLIC SPIN PIT TESTS FOR THE DAMAGE TOLERANCE OF DISKS
by H.Huff and G.W.König 19

TURBISTAN, A STANDARD LOAD SEQUENCE FOR AIRCRAFT ENGINE DISCS
by A.J.A.Mom, W.J.Evans and A.A.ten Have 20

SESSION IV – CASE HISTORIES AND IMPLEMENTING

AN ANALYSIS OF RIG TEST DISC FAILURES
by G.Asquith 21

CONTRIBUTION OF TURBINE BLADE SERVICE FAILURES TO A DAMAGE TOLERANCE APPROACH
by R.J.H.Wanhill and A.J.A.Mom 22

PRACTICAL EXPERIENCE WITH DAMAGE TOLERANCE BASED LIFE EXTENSION OF TURBINE ENGINE COMPONENTS
by A.K.Koul, R.Thamburaj, M.D.Raizenne, W.Wallace and M.C.DeMalherbe 23

SESSION V

RECORDER'S REPORT OF FINAL DISCUSSION
by G.F.Harrison D

DAMAGE TOLERANCE CONCEPTS FOR CRITICAL ENGINE COMPONENTS

INTRODUCTORY REMARKS

by

M J WEAVER

Materials and Engineering Research Division
Propulsion Department
Royal Aircraft Establishment
Pyestock, Farnborough, Hants, UK.

Up until about ten years ago both engine and airframe components were, in general, designed and lifed according to a "Safe-life" philosophy. Following a number of unexpected, defect related airframe failures in the late 60's and early 70's, a damage tolerance airframe design code was adopted[1] which made the assumption that specific flaws could always be present and that the structure had to be shown to be tolerant of these defects with regard to safety for a given period of time. Engine design and lifing philosophy, on the other hand, has remained Safe-life oriented and only relatively recently has it been widely suggested that damage tolerance design and lifing procedures should be applied to critical aero engine components.

Before introducing the subject of damage tolerance and, in particular, defining the objectives and format of this Conference it is worthwhile to review briefly the concept of Safe-life design and lifing procedures as applied to engine components, especially discs. Disc Safe-life limits are defined by undertaking a statistical analysis of representative fatigue data in order to establish the cyclic, in-service life at which about 1 in 750 (in USA this figure is approximately 1 in 1000) components will have initiated a fatigue induced crack of approximately 800 microns (1/32 inch) in length[2]. In the UK these representative data are determined by spin-rig testing actual engine components whereas in the USA more reliance is placed on declaring safe-lives based on data obtained from complex test piece evaluations. It has been estimated that 80% of discs have over ten low cycle fatigue lifetimes remaining when discarded under the Safe-life rules[3]. It is this apparent inefficient usage of potential component life that prompted the United States Air Force (USAF) to institute its Retirement-for-Cause (RFC) lifing policy, a policy aimed initially at running discs on beyond their declared Safe-life until quantifiable damage had been identified. Reducing cost-of-ownership is one argument, therefore, that can be put forward for moving away from the established Safe-life policy.

A further disadvantage of the Safe-life concept is that it assumes components entering service to be free from any major, untoward defects. To some extent the statistics of Safe-life testing take account of the possibility of there being a defect present but, bearing in mind the small sample of test specimens used to establish the representative fatigue data, it is unreal to assume that every possible size, shape and location of defect could be taken into consideration. What is more, the likelihood of a premature, defect-related failure occurring is closely related to the maximum stress to which a disc is subjected in service. The advent of advanced, high strength disc alloys is tempting designers to increase disc operating stresses in order to allow both higher rotational speeds and reduced weight. Unfortunately, a situation can arise where, if a very high stress is in combination with even a small rogue defect, then crack growth from the defect may be induced and a disc burst precipitated well before the declared Safe-life has been achieved. Utilisation of the full strength potential of modern disc alloys may only be possible if an alternative to the Safe-life philosophy is adopted, otherwise the current safety margins could be eroded.

Although the Safe-life concepts currently in use have coped very successfully with the demands imposed upon them during the past 20 to 30 years, the above examples highlight limitations that are beginning to surface now that significant upward movements in component utilisation and stressing levels are being sought. Both of these limitations can, in theory, be overcome by augmenting or replacing Safe-life with a damage tolerance lifing concept, a fundamental principle of which is the acceptance by both manufacturer and customer/licensing authority that critical engine components are not necessarily free from cracks or harmful defects. Confronted with this situation, a manufacturer has to demonstrate, probably by utilising advanced stress analysis and fracture mechanics methodology, a cyclic lifetime for each component whilst maintaining an adequate level of safety. After the initial declared life has been achieved the component may be cleared for further periods of service depending on detailed circumstances and the issuing of a clean bill of health following a meticulous NDT inspection.

This, very briefly, is damage tolerance; any move away from Safe-life to this alternative means of lifing critical engine components will have widespread implications on many of the established design and lifing practices, e.g. materials selection, failure criteria, safety and inspection requirements. A major objective of this Conference is to define and debate the important issues governing the implementation of damage tolerance concepts. The opening Session is intended to set the overall scene with papers describing the current philosophies as seen from American and European viewpoints.

To predict how a component containing defects will behave in an engine requires the detailed knowledge of a wide range of parameters. These include:-

- the nature, size and likely distribution of defects,
- the predicted component usage in order that the stresses, strains, temperatures and loading patterns being imposed on the defects can be calculated,
- a detailed understanding of the factors influencing the rate of cyclic crack growth for the particular material in question,
- the metallurgical structure throughout the component.

These and other factors important to damage tolerance concepts will be debated in the 2nd and 3rd Sessions of this Conference. In Session 4, a series of case histories will be presented which, it is hoped, will help to identify the strengths and weaknesses of the current state of the art of predicting the behaviour of defects in real gas turbine components.

Finally, there are three questions that should be tabled right at the start of the Conference in the hope that some measure of agreement can be reached between attendees by the time the Conference ends. The first of these is: "What is really meant by damage tolerance?" At present almost everyone has his or her own detailed interpretation of what is implied by the phrase "Damage tolerance", particularly when applied to gas turbine engines. If these concepts are to become part of the accepted engine design and lifing procedures then there are obvious advantages if the engine fraternity as a whole is, right from the outset, thinking in terms of a unified concept.

The second question is: "Are damage tolerance concepts really required?" It would appear that one of the major driving forces behind the introduction of a damage tolerance design philosophy for engine components is the USAF, first with its intention to implement RFC and, latterly, with the ENSIP approach. It will be interesting to assess whether the arguments in favour of the US military moving towards damage tolerance concepts are equally applicable both to other military users and to the civil engine field. The preface to the programme announcing this meeting states that the introduction of damage tolerance concepts into the design and use of critical engine components offers considerable economic benefits through the safe and extended life thus permitted. If these benefits can only be realised by having at one's disposal a complex and expensive non-destructive testing (NDT) facility, then their implementation by a relatively small fleet operator may not be cost effective unless, of course, the operator is prepared to buy a service elsewhere from a specialist NDT facility. This may be practical for a civil operator but military air force chiefs are unlikely to be very happy about such an arrangement. There is likely to be much debate both at, and subsequent to, this Conference over the role of NDT in damage tolerance lifing schemes.

The final question is: "How safe is a damage tolerance lifing philosophy?". The maintenance of adequate levels of safety is paramount in any engine design and lifing scheme; in damage tolerance, as with Safe-life, the statistical aspects are crucial. Although none of the papers is specifically addressing this point, it is hoped that contributors will, where possible, discuss and stimulate discussion on this important topic. If, for lifing purposes, it has to be assumed that the biggest defect is situated in the most highly stressed area, which also happens to be an area of poor microstructure, then how likely is it that a disc designed to a damage tolerance code will ever be allowed to leave the ground?

R V Jones, in his book "Most Secret War",[4] recounts a saying that he attributes to a University colleague and which is appropriate to iterate at the start of this Conference:

"Do not think what you want to think until you know what you ought to know."

The fact that this International Conference has been called is a positive indication that the engine community is already thinking in terms of damage tolerance design; it will be interesting to ascertain during the course of the meeting whether sufficient knowledge is to hand in order to allow its immediate safe and beneficial implementation.

REFERENCES:

1. J I Rudd, "Airforce Damage Tolerance Design Philosophy"; ASTM STP842, 1984, p134-141.
2. W J Evans et al, "Disc Fatigue Life Predictions for Gas Turbines"; AGARD-CP-368, 1984, Paper 11.
3. J A Harris et al, "Engine Component Retirement for Cause"; AGARD-CP-317, 1982, Paper 5.
4. R V Jones, "Most Secret War". Published by Hamish Hamilton Ltd, 1978.

DAMAGE TOLERANCE CONCEPTS FOR CRITICAL ENGINE COMPONENTS

R H Jeal
Chief Materials Engineer
Rolls-Royce Limited
Derby
UK

1. INTRODUCTION

The cost of failures in gas turbines has always been so high, both in human and financial terms, that it has been recognised since the earliest days that the behaviour of components had to be fully characterised before the engines were used in service.

The integrity of the gas turbine has therefore always been based upon two separate phases of development.

The first has been the basic design itself where, as well as ensuring that the individual components meet their basic mechanical purpose, the designer attempts to match his understanding of the operating conditions to his perception of the capability of material chosen. The second has been the 'development' phase where the actual behaviour of the component has been assessed either as part of an operating engine - 'bench engine testing' - or as an individual component - 'rig testing' - under conditions which are related to those the engine is expected to see in service.

The results of this work are then used, together with prior experience, to identify the critical components of the engine, those that prejudice the safety of the aircraft if they fail. Safe lives are set, after which components must be removed if engine integrity is to be maintained.

Because of the time and costs involved in testing engines to failure under service conditions, coupled with the uncertain knowledge of those conditions, various assumptions and models have been used to accelerate such engine tests and also devise individual component tests. For the same reasons various criteria have been devised to set limits to the conditions worked to in the design phase so that a component did not go round the design-development loop too many times.

The net result of all this work has been to set a 'damage tolerance concept' for critical engine components which was valid for the design requirements at that time. If the design requirements had not changed there would probably be no need to alter the earlier perceived concepts. However, the constant search for cheaper, more efficient engines with higher thrust/weight ratios has led to components operating under higher loads and temperatures for longer times and the use of more complex metallic materials with different behaviour modes than those which formed the basis of the original behaviour models. Such changes have therefore led to the need for different damage tolerance concepts and in particular a change in emphasis from the earlier empirically based approaches to ones based upon a more fundamental understanding of the physical phenomena involved in material and component behaviour. The behaviour of the materials needed to meet the component demands of the new engines now being designed are so far removed from those used in the early engines that concepts based upon a real understanding of total behaviour are essential if reasonable engine integrity is to be established in any safe, cost effective manner rather than be driven in empirical steps by the after effects of in-service failures as has been the tendency in the past.

This paper traces the development of damage tolerance concepts from the earliest days, examines the current situation in the light of design needs and available technology and looks at possible directions for the future.

2. ORIGINAL CONCEPTS

The earliest design concepts used for gas turbines were based, in the main, on experience derived from reciprocating engines and superchargers made from ferritic and austenitic steels, and aluminium alloys. Mechanical integrity of rotating parts was based, therefore, on the simple overspeed criteria still enshrined in the majority of regulations governing gas turbine design using models of materials behaviour based upon the solid mechanics assumptions that all materials are elastic isotropic homogeneous continua. Provided that stress levels were limited to below the yield stress such an approach was reasonably valid. Deviations from the material model due to defects and discontinuities were dealt with by controlling and assessing the component during manufacture, rejecting those that did not meet the model. The real problems of the day, concerning combustion cans, turbine blades and vibration problems, where there was little, if any, relevant prior experience, were dealt with during extensive development engine testing. The short life of hot end parts led to frequent in-service engine strips and the critical components were rejected whenever cracking was seen on inspection. However, the low loading factors imposed by other limitations meant cracking rarely occurred. When creep was recognised as a failure mechanism limitations were imposed to avoid operating in that regime.

Cyclic bench engine tests were kept running under representative service cycles ahead of the engines out in the field, the problems so revealed acted upon before, hopefully, they occurred in service.

In summary, therefore, the approach was very simple.

a) A simple materials behaviour model was assumed - Fig 1.

b) Components were designed using criteria set to stay within the model (avoiding creep and plasticity considerations).

c) The material was chosen, manufactured and inspected to meet the model behaviour.

d) Life was evaluated using bench engine testing.

e) All parts were examined on frequent strip overhauls and cracked parts rejected - a sort of on condition approach.

As the demands on designers grew, materials with higher yield stress, higher creep limits, and lower densities were needed leading to the introduction of nickel base superalloys and titanium alloys. Up until this time, in the mid to late 1950's, fatigue had been considered a phenomenon associated with vibration and resonance, something to be designed round. Now with the higher operating stress levels allowed by the tensile properties of the new materials, the longer time between overhauls created by better hot end materials and the differing behaviour of new alloy systems it was found that the old design/development concepts were not sufficient. A number of bench engine and in service failures occurred at unacceptably low lives.

5. THE LOW CYCLE FATIGUE APPROACH

Analysis of the failures soon showed that, at the stresses permitted by the overspeed design criterion, fatigue failures could occur in a small number of cycles related to numbers of aircraft flights or missions. This phenomenon was soon reproduced in simple laboratory tests and, by the late 1960's empirical data banks were established of stress/life (S/N) plots covering various temperatures and component features i.e. "notches". This approach was grafted onto the early component behaviour concept as setting an additional stress limitation during the design phase. The maximum permitted stress was set by the required life - or vice versa - and read off fatigue design curves which were derived from the laboratory measured data, modified by component test results, and treated with suitable factors to allow for scatter in properties

The existing arbitary life end point of first visible (or engineering') crack was taken for components and separation was used for specimen end point. Stress analysis of the components and specimens whilst using increasing sophisticated mathematical techniques, was still based upon the same simple behaviour model assuming an elastic continuum. Increasing control was placed upon manufacturers to produce uniform homogeneous components which were subjected to rigorous NDI of the surfaces to avoid or reject any "defects".

Some divergence of approach emerged in North America and Europe. The regulating authorities in the USA (in the main FAA) allowed component life declaration on the basis of design curves, whereas in Europe (both for civil and military engines) the life of individual components had to be established by cyclic rig testing to failure under appropriate stress and temperature conditions.

Three major difficulties limited the use of the simple approach as described above.

a) The deviation from simple specimen stress-strain behaviour in components due to local geometry and cyclic hardening or softening of the material.

b) Flight cycles were rarely a simple up and down stress system but consisted of a complex series of changes and holds in stress - especially in military engines - that were difficult to relate to the design curve based upon simple cycles.

c) Time dependant effects became apparent at temperatures below the commonly assumed creep limits which made accelerated testing somewhat dubious in some cases.

Empirical approaches were used to handle all these difficulties but the model continued to be that of using the universal design assumptions with correction factors to allow for the deviations in behaviour.

This approach, which is still current in many areas, depended upon:-

a) The original simple materials behaviour mode, modified to allow for fatigue assumptions.

b) The end point of component life being defined as first visible crack.

c) Material behaviour being fully characterised by simple stress/life curves.

d) Manufacture and inspection of components to "defect free" standards.

e) The evaluation of individual component lives by representative rig testing (as far as Europe was concerned).

The definition of end point was further refined to 'first engineering crack' of a defined size (usually .010" deep by .030" surface length) to prevent declared component lives being reduced by improving inspection methods. Those defects - defined as 'discontinuities that produced failure outside the previously defined scatter band' - that could not be found by inspection were eliminated by improved, and more expensive, manufacturing methods such as vacuum melting, forging for refined microstructures and controlled machining operations.

Engine design concepts continued to demand higher operating loads and temperatures leading to further unpredicted failures on rigs and in engines due to the following factors:-

a At higher stress levels the life margin between first engineering crack and component failure became too small to be useful (in some cases negative) - Fig 2.

b Discontinuities that could neither be found by available NDT methods or eliminated by process control nucleated early cracks.

c Environmental effects (e.g. frettage, corrosion) could cause early cracking.

d The strengthening methods used to increase the tensile, creep and low cycle fatigue properties of alloys produced fracture modes that are not covered by the conventional behaviour mode.

Once these problems are accepted an alternative approach has to be found if we are to continue using materials under the currently envisaged operating conditions.

4. INSPECTION RELATED APPROACHES

If the assumption is made that components contain discontinuities that act as propagating cracks a new approach can be used.

This type of approach, variously called life on condition, retirement for cause or just "fracture mechanics", assumes the presence of a crack just smaller than the detection limit of the inspection method used to examine the component. This crack is then assumed to grow in a manner predicted by linear elastic fracture mechanics or some similar type of model which can be characterised by simple laboratory data. Cyclic rig testing of pre cracked components has shown that such predictions are remarkedly accurate (Fig 3) provided appropriate laboratory data is used. In particular for gas turbine discs it is important to use corner crack data rather than "through crack" data because crack closure and other such effects modify the effective crack tip stress intensity (Fig 4).

On this basis a life to failure can be calculated (Fig 5) and a safe proportion used to declare a service life. Once this is completed and the part passes re-inspection a further life can be used and so on until a crack is found.

So one can adopt a simple system:-

a Select the appropriate fracture mechanics model for the applied condition to be analysed.

b Characterise the crack growth parameters of material using laboratory tests.

c Establish the detection limits of the inspection methods to be used.

d Calculate the safe life increment for the component.

e Re inspect and, if crack free, run for another increment.

The method assumes that the component cracking mode is that characterised by the laboratory test and that the material still acts as an isotropic continuum. It has been used very successfully to control in service situations both where the presence of defects cannot be eliminated by process control or where early cracking greater than 'first engineering crack' occurs in relatively low stress areas of discs such as bolt holes or blade attachment features.

As both a design approach and a model of real component behaviour the method has a number of major disadvantages:-

a The crack propagation properties of materials depend upon alloy type rather than strength so that the high operating stresses permitted by tensile and fatigue properties of the newer alloys translates *into shorter crack* propagation lives - Fig 6.

b The defect sizes that need to be reliably found to give reasonable safe life increments are at or beyond the physical limits of todays NDI Technology. Fig 7. These sizes are now really setting the operating stress limits when this approach is used.

c The behaviour of small cracks cannot be predicted from that of large cracks, particularly when they are a similar size to the material microstructure - Fig 8. In the latter the basic assumption of the approach is violated.

These disadvantages mean that the inspection related methods only give short life increments which get shorter as stress levels rise. They also lead to long expensive inspection methods whose reliability *can only be considered in a* statistical manner (Fig 9).

The method also depends upon similitude between the crack propagation in the component and that in the characterising laboratory specimens - if microstructurally dominated crack growth occurs the method no longer gives accurate predictions and yet the latter mode is dominant in current high strength alloys.

5. TOTAL LIFE CONCEPTS

If we are to continue using materials at higher stress levels it is necessary to fully characterise their total behaviour and design against the appropriate usable strength criterion.

The cyclic behaviour of any component goes through a number of life phases:

a Nucleation of first crack.

b Microstructurally dominated crack growth.

c Mechanics dominated crack growth.

d Final unstable growth.

These are shown in Fig 10 related to component total life.

When the mode of behaviour of materials at discontinuities is examined two types of occurrance can be seen:

a The discontinuity acts as a propagating crack.

b The discontinuity acts as a local stress raiser and a crack nucleates in the surrounding matrix.

The latter case is by far the most common under envisaged component stress *strain* conditions and careful control of the manufacturing process enables the first type to be eliminated for those conditions. Crack nucleation always takes place at a discontinuity, either on extraneous particles or some microstructural anomaly such as a triple point or unfavourably orientated grain. In high strength materials the nature of that crack nucleation is invariably microstructurally related with the metallurgical crack size characterised by the appropriate microstructural parameter. This parameter is governed by the degree of process control exercised but it is now becoming possible to control component microstructure to an extent that makes it a usable approach.

Subsequent crack growth is also microstructurally dominated as the crack moves in a series of steps. Strain energy builds up in the unit ahead of the crack tip and then crack proceeds rapidly across that unit. Fig 11. Once the crack has covered a sufficiently large number of units it can be regarded as moving *in a* continuum and the approach considered in section 4 above become valid. The initial crack size can however be characterised from microstructural considerations rather than inspection limits leading to a more realistic method.

The inter-relationship of crack nucleation from discontinuities and subsequent growth with the material microstructure can be investigated in the laboratory using small crack growth tests. Such work reveals that the mechanisms traditionally used to produce high tensile properties in materials - solutioning hardening to limit slip and reduction in grain size - are the mechanisms that also decrease the ability of the material to cope with local discontinuities. Correct choice of microstructure based upon this type of understanding enables a safe predictable "short crack" life to be established so that the total short and long crack life can be properly defined by manufacturing process control.

This approach therefore introduces a number of factors to combat the disadvantages of the traditional fracture mechanics approach:-

a) The presence of crack-like discontinuities can be either eliminated or controlled by manufacturing process and selection of defect tolerant microstructures.

b) A true nucleation and short crack life can be characterised and evaluated to provide a model (or models for each type of cracking mechanism) for component life prediction.

c) The traditional 'long crack' fracture mechanics approach can be used based on a starting size related to microstructural consideration where similitude has been established.

This type of concept demands new models of material behaviour based upon the realisation that materials cannot be treated as elastic isotropic continuous media but can be considered as a series of anisotropic continuum units that sequentially absorb strain and finally crack.

The concept demands levels of manufacturing process control that prevent the formation of large discontinuities and controls the nature of small ones (such as microstructure) in a way that produces reproducable behaviour. This level of process control is now virtually available for Titanium alloys but there is some way to go with Nickel Superalloys.

The concept demands new types of alloys and microstructures to control local deformation and crack behaviour within the material, rather than producing the highest macro strength properties in the section. This has already been demonstrated with Titanium alloys and similar concepts are beginning to show promise with the superalloys.

Above all the concept demands that the predictive models used to assess the integrity of components are based upon the real behaviour of materials rather than trying to make the alloy fit the traditional model.

6. THE FUTURE

The future approach to the integrity of engine components, and the speed of incorporation of advanced damage tolerance concepts, must recognise two factors.

a) Current approaches are the result of accumulated experience, empirically relating laboratory, rig and bench engine testing with in-service behaviour. This experience is only as good as our understanding of the last "failure" - extrapolation of the system to more arduous operating conditions and 'stronger materials' must recognise the danger of introducing new, unforseen modes of behaviour which can, and will, cause early failure.

b) Current design goals for engines, in terms of efficiency, thrust/weight ratios and costs, cannot be met by using current materials within todays experience - we have to go to higher temperatures and stresses for longer times. To achieve this safely we have to modify our approach to properly define the behaviour of materials under the required conditions before committing designs to achievable behavioural targets.

The current low cycle fatigue approach to a poorly defined life end point cannot be dismissed over night, as it enshrines much of our current experience. It must, however be modified in the light of our new understanding of real materials behaviour - in particular setting the boundaries of applicability of the basic assumptions, and a recognition of the relationship between 'crack initiation' and subsequent crack propagation.

If these limitations are combined with a full characterisation of the material related to its method of manufacture, the approach will remain a useful, if empirical tool in aiding component life prediction.

Extensions of the approach to new conditions must, however, be fully covered by rig testing of components under representative conditions.

Wherever the bounds of the approach are exceeded, either during the design phase, or where unforseen circumstances such as corrosion or frettage cause early cracking, a fracture mechanics approach based upon inspection related initial crack sizes offers a safe approach.

The inherent assumption that relatively large undetected propagating cracks, are present from the beginning of life, is however, a very inefficient way of using materials. We must find a way of accounting for the presence of these discontinuities, which act as local stress raisers promoting what has been called in the past 'excessive fatique scatter'. Fig 12 plots this out as a series of cyclic life curves where the end point is total failure of the part. The left hand lowest life curve represents the inspection related approach. The extreme right curve is that attributal to the engineers "perfect" material. Those in between cover discontinuities of decreasing effect. The life increment over and above the 'fracture mechanics' line is the sum of phases 1 (nucleation) and 2 (short crack propagation) from Fig 10.

The behaviour of any discontinuity can be established from understanding its 'severity' and the imposed stress/strain field.

The severity will be dependant upon shape and size of the discontinuity relative to the microstructure it is in - all factors which can properly and exactly be controlled.

The severity will also be changed if the mode of material behaviour changes - hence such characterisation must taken into account the full range of possible operating conditions. With the *change from cross slip ductile modes* to limited slip microstructure modes commonly seen in todays high strength materials the short crack phase becomes dominant in *local* behaviour.

Component behaviour then can be assessed by knowledge of discontinuity distribution and stress/strain field.

Discontinuity severity and distribution have traditionally been taken into account by the concept of scatter - materials have been controlled during manufacture to give minimum scatter.

Such an approach is still valid - provided it is *now recognised we must identify* and control the factors in the manufacturing process causing scatter separately and assess their real behaviour rather than try *to relate back the "ideal"* continuum.

Such approaches offer the only real ways of dealing with the next generation of materials - whether ceramics or composites. The non continuum nature of these materials coupled with their lack of ability to accept localised high strains without cracking gives similar problems to high strength metallic materials.

7. CONCLUSIONS

The integrity of components can be maintained under todays *high stressing* conditions, without necessarily resorting to a 'initial inspection crack' approach provided the real behaviour of the materials is recognised rather than represented by the continuous approach of traditional models.

Such an approach has to include full investigation of the following facts:

a) Material microstructure.

b) *Deformation and failure modes.*

c) Discontinuity severity and distribution.

d) Relationship of manufacture process to the real material produced.

e) Relationship of the material behaviour modes to a total life concept of component behaviour.

Recognition of the critical factors determining component life and proper control of them offers a secure way of ensuring the integrity of components under the *arduous condition now being experienced in new engines* without resorting to the conservative life approach based upon non destructive testing. It is the only way that new materials will *be safely incorporated into engines.*

8. ACKNOWLEDGEMENTS

The concepts discussed in this paper have evolved from discussions with,and the work of,many people, both metallurgists and engineers. In particular the author would like to thank Geoff Asquith of Rolls-Royce and Dave Hoeppner of University of Toronto for their single minded approach to seek out the truth.

9. REFERENCES

1. R H Jeal - Defects and their effects on the behaviour of Gas Turbine Discs. AGARD-CP-317 September 1981.

2. R H Jeal - Relationship between fatigue modelling and component integrity. Fatigue 84 University of Birmingham September 1984.

3. Reliability of Non Destructive Inspection (NDI) of Aircraft Engine Components. SA-ALC-MM 0 8151 January 1984 (Fig 9).

Engineering premise

All materials are homogeneous, elastic, isotropic media, free from defects and amenable to conventional fatigue cumulative damage analysis within normal scatter limits

SML 18157

FIG 1 - THE "ENGINEERS PREMISE"

Rolls-Royce Limited 198

MATERIAL VS LIFE TO BURST FROM A 0.03" CRACK

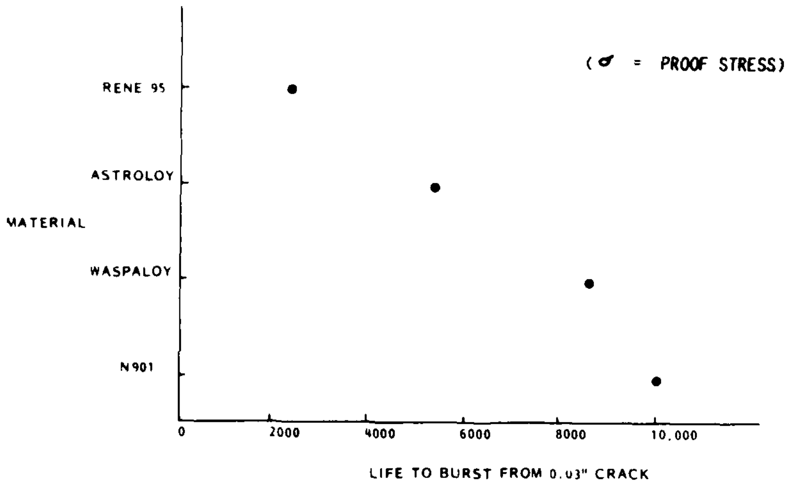

1 APR 1985

FIG. 2 VML 23786

FIG 2 - MATERIAL VERSUS LIFE TO BURST

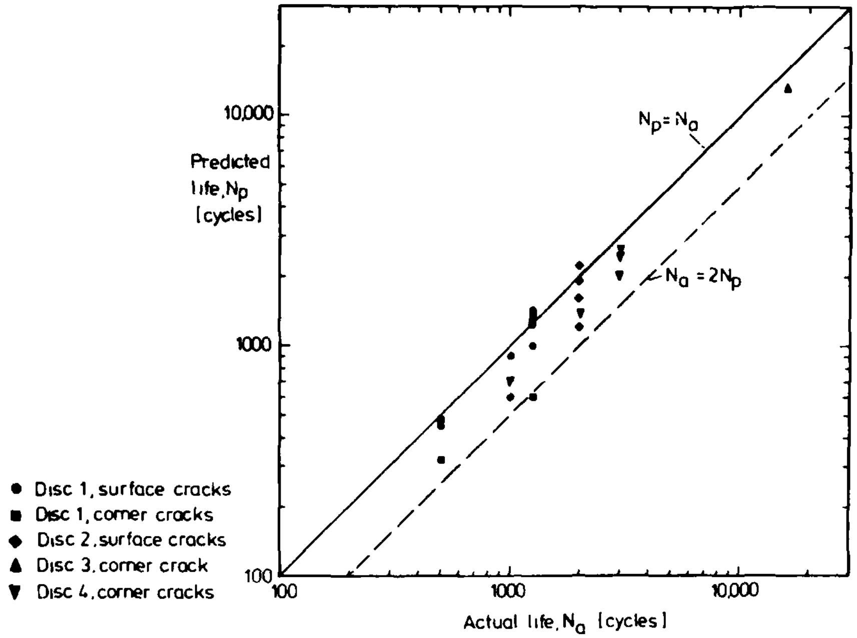

FIG 3 - CORRELATION BETWEEN PREDICTED AND ACTUAL DISC LIVES USING CORNER CRACK DATA

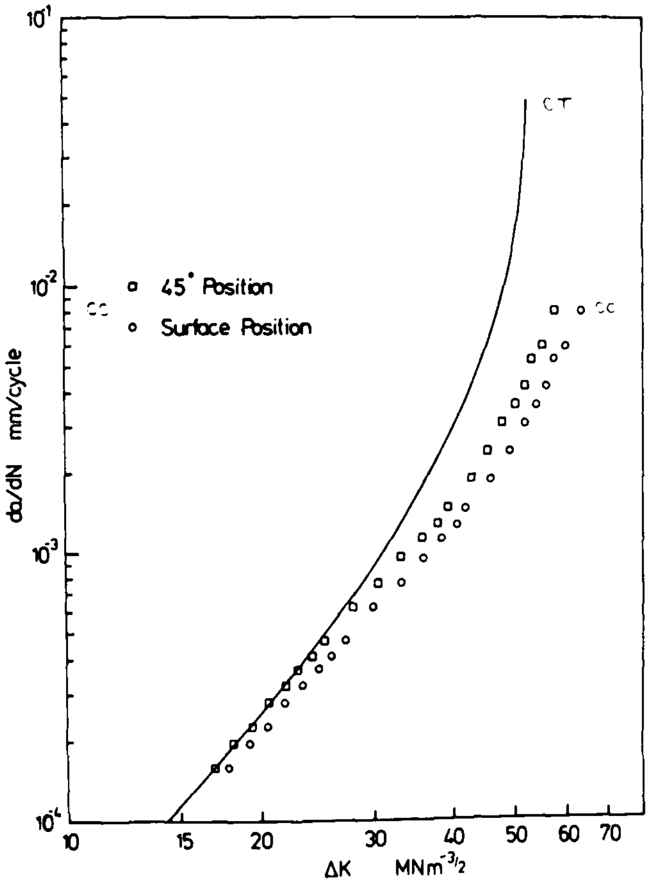

FIG 4 - COMPARISON OF CORNER CRACK AND COMPACT TENSION CRACK PROPAGATION DATA FOR Ti6-4

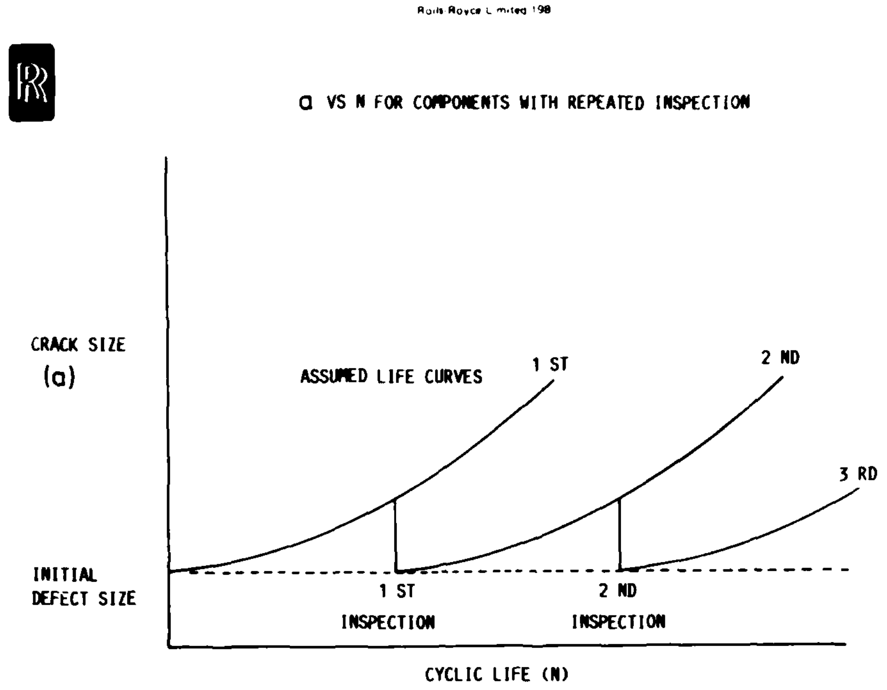
Rolls Royce Limited 198
a VS N FOR COMPONENTS WITH REPEATED INSPECTION
CRACK SIZE
(a)
ASSUMED LIFE CURVES
1 ST
2 ND
3 RD
INITIAL DEFECT SIZE
1 ST INSPECTION
2 ND INSPECTION
CYCLIC LIFE (N)

FIG 5 - CRACK LENGTH VS CYCLES FOR COMPONENTS WITH REPEATED INSPECTION

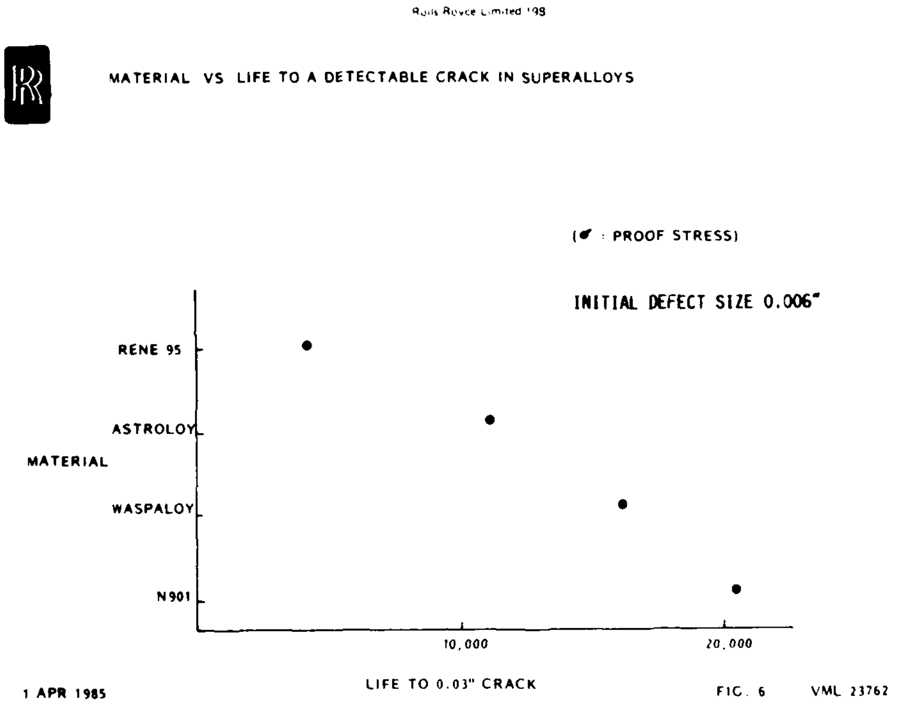

FIG 6 - MATERIAL VS LIFE TO A DETECTABLE CRACK IN SUPERALLOYS

RB211-22B HP Turbine. Detection capability required for life on condition approach

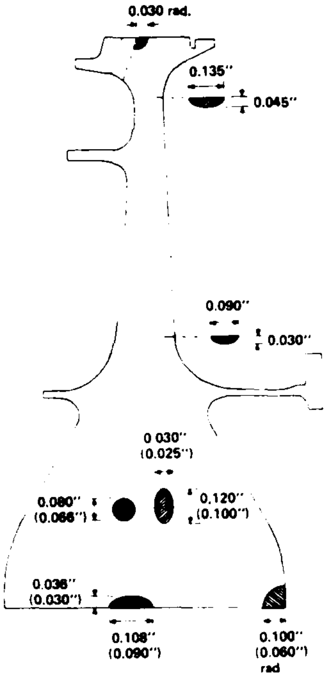

FIG 7 - DETECTION CAPABILITY REQUIRED FOR LIFE ON CONDITION APPROACH

DEFINITION OF CRACK TYPES IN PLANAR SLIP MATERIALS

MATERIAL MICROSTRUCTURE \ STRUCTURAL SECTION	LONG CRACK COMPARED TO SECTION SIZE DESIGNATION OL	SHORT CRACK COMPARED TO SECTION SIZE DESIGNATION OS
LONG CRACK COMPARED TO MICROSTRUCTURAL UNIT SIZE DESIGNATION LO	- CONVENTIONAL CONTINUUM MECHANICS APPROACH - LEFM - THROUGH - CRACK DATA IS APPROPRIATE E.G. COMPACT TENSION - LARGELY INDEPENDENT OF MICRO-STRUCTURE DESIGNATION LL	- CONVENTIONAL CONTINUUM MECHANICS APPROACH APPROPRIATE - SIMILITUDE WITH LL PROVIDED CLOSURE EFFECTS ARE TAKEN INTO ACCOUNT - TENDS TO GIVE SLOWER CRACK PROPN RATES IF EXPRESSED AGAINST NOMINAL Δ K. (IN LABORATORY AIR ENVIRONMENT) DESIGNATION LS
SHORT CRACK COMPARED TO MICROSTRUCTURAL UNIT SIZE DESIGNATION SO	- MODIFIED LEFM APPROACH REQUIRED WHICH INCORPORATES CRYSTAL ANISOTROPY - CRACK DIRECTION AND STEP LENGTH DEPENDENT ON SECTION GEOMETRY AND CRYSTALLOGRAPHY NO SIMILITUDE WITH OTHER MODES DESIGNATION SL (SPECIAL CASE - SINGLE CRYSTAL)	- INDIVIDUAL STRUCTURAL UNITS CAN BE TREATED AS "ANISOTROPIC CONTINUUM" - LEFM INVALIDATED BECAUSE THE CRACK SIZE IS COMPARABLE TO THE EXTENT OF CRACK TIP PLASTICITY - CRACK DIRECTION, STEP LENGTH DOMINATED BY CRYSTALLOGRAPHIC CONSIDERATIONS DESIGNATION SS

FIG 8 - DEFINITION OF CRACK TYPES IN PLANAR SLIP MATERIALS

ENSIP NDT

PRELIMINARY CONCLUSIONS - AERO ENGINE PARTS

	AVERAGE	BEST
MAGNETIC INSPECTION POD	60% -.300" CRACK	65% -.250"
PENETRANT INSPECTON	90% -.220"	90% -.175"
EDDY CURRENT	90% -.090"	90% -.030"
ULTRASONIC	80% -.375"	90% -.180"

- AVERAGE RESULTS OBTAINED FROM MAJORITY OF TECHNICIANS
- BEST RESULTS OBTAINED FROM TOP 10% TECHNICIANS
- USAF TECHNICIANS ARE NORMALLY BETTER TRAINED THAN MOST AIRLINE TECHNICIANS.

FIG 9 - INSPECTION RELIABILITY

Rolls Royce Limited 198

Stages of fatigue life

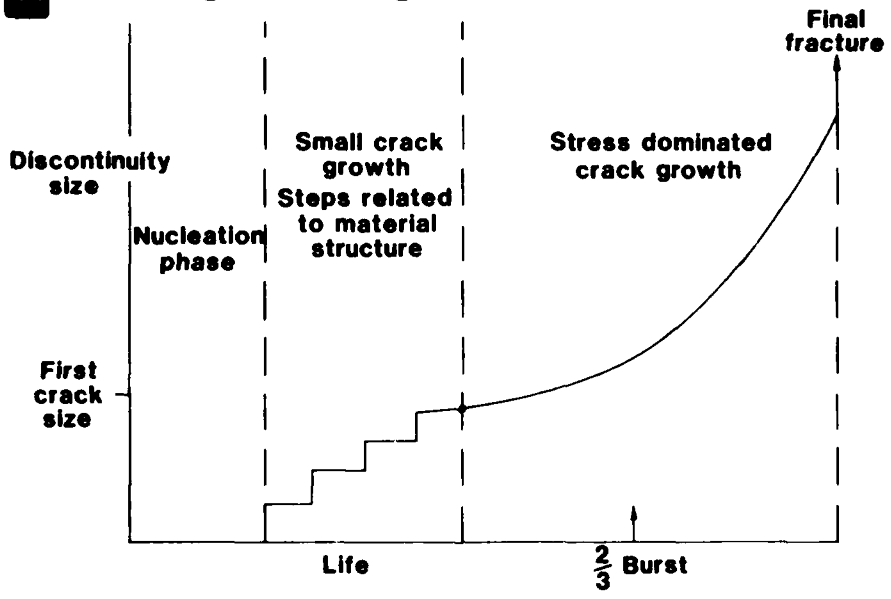

FIG 10 - VS N MODEL

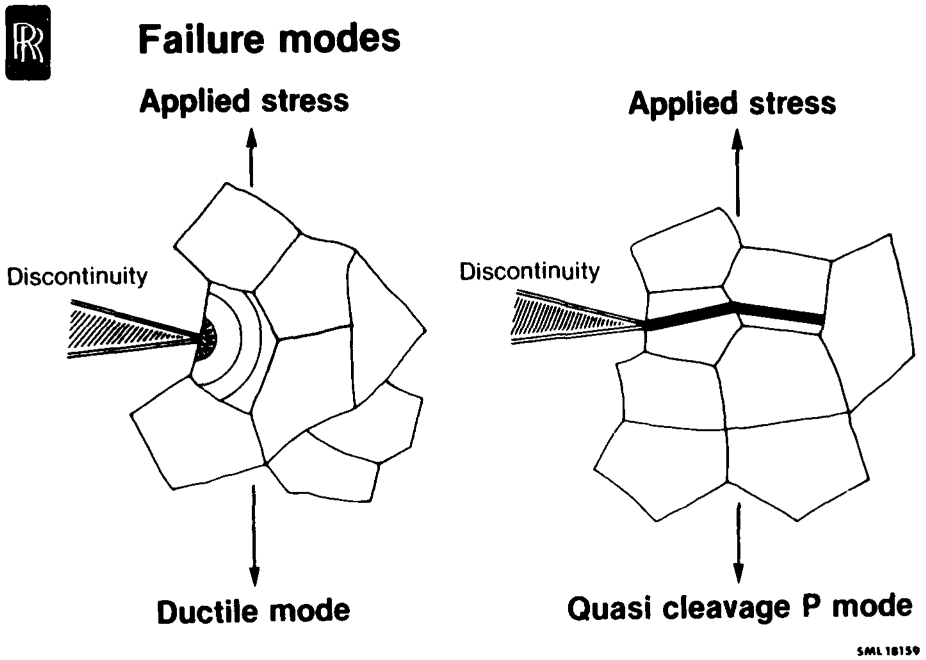
Failure modes
Applied stress
Applied stress
Discontinuity
Discontinuity
Ductile mode
Quasi cleavage P mode
SML 18159

FIG 11 - CRACK TIP FAILURE MODES

Rolls-Royce Limited 1985

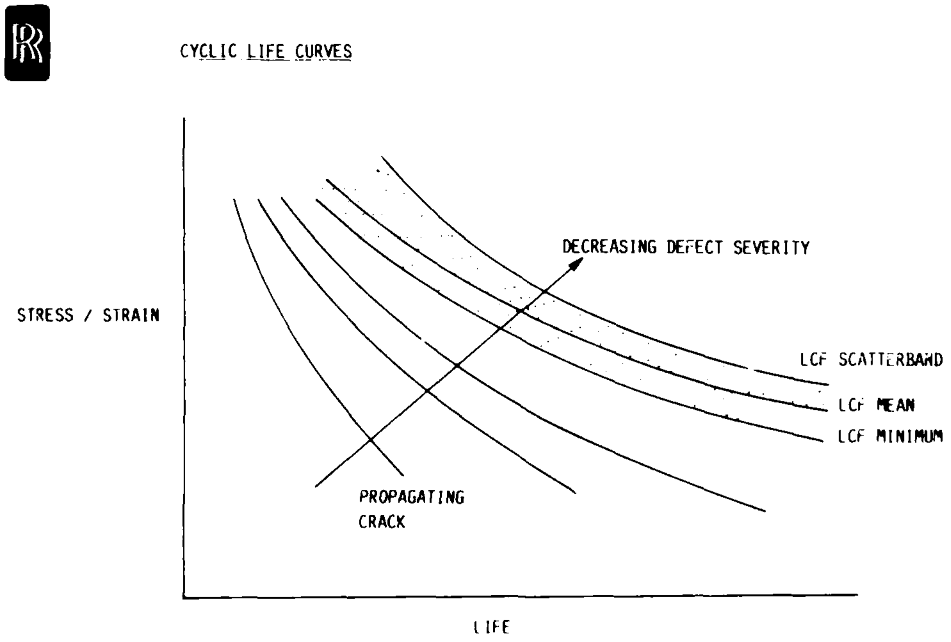

FIG 12 - CYCLIC LIFE CURVES

ENGINE CYCLIC DURABILITY BY ANALYSIS AND TESTING - HIGHLIGHTS OF THE SPRING 1984 PEP MEETING

Albert A. Martino
Manager, Systems Development and Evaluation Group
Naval Air Propulsion Center
P.O. Box 7176
Trenton, NJ 08628-0176

INTRODUCTION

Research on gas turbine engine development during the past decade in NATO nations has concentrated heavily on gaining better understanding of the relationship between material characteristics, failure mechanisms, structural analysis and validation testing for increased service life.

Recognizing this intense interest and activity level the Propulsion and Energetics Panel (PEP) sponsored a specialists' meeting that surveyed the state-of-art technical areas related to improving engine life and considered the technical and economical problems and possibilities of advanced cyclic testing in the development of engines. Discussions focused on relationships between engine use and failure modes, accelerated mission testing (AMT) development, critical material characteristics, component life assessment methods, recent results of component and engine cyclic testing, and future requirements were discussed.

Members of the Structures and Material Panel (SMP) made outstanding contributions.

This 63rd Specialists' Meeting was held in Lisse, Netherlands, 30 May to 1 June 1984. The complete proceedings, including questions and answers of the discussions that followed each paper are included in the report AGARD-CP-368, dated September 1984 and entitled "Engine Cyclic Durability by Analysis and Testing." The highlights of those papers follow.

BACKGROUND

Historically it is recognized that powerplant development has set the pace in aircraft system capability. Improvements in overall propulsion system capability have been impressive and continuous. While performance in terms of thrust, thrust-to-weight and specific fuel consumption has improved dramatically, so too have engine durability and life. Both performance and durability have increased well beyond the best ever experienced for reciprocating engines in fighter/bomber applications noted Col. J.R. Nelson, USAF, who served as the Technical Evaluator for this PEP meeting. However, he adds, that "due to sharply increasing engine acquisition cost and very large overall costs of ownership, it is essential that engine life be further increased. Almost as important as this increase in life is a requirement that life values be accurately predicted at initial fleet introduction for the engine and its components. In addition, usage must be tracked carefully in order to maintain a close relationship not only between predicted and actual life, but also between predicted and actual support requirements. This latter point is central not only to fleet readiness to insure stability of operations, but also to controlling support costs which, aside from the expense of fuel itself, are still several times the initial acquisition cost and are very sensitive to unexpected durability/reliability shortfalls."

A major reason for the high cost of ownership he explains, has been due not only to shorter engine life than desired, but more significantly shorter engine/component/part lives. The resultant instabilities in the engine support system, especially initially, have caused significant, unplanned cost variances as well as shortfalls in system reliability and availability, whether military or civilian. This situation has led to intense government and industry interest and research and engineering efforts to improve not only engine life itself but the ability to assess and predict engine and engine component life/durability characteristics. Progress in the past decade in both testing and analysis techniques has been significant, particularly in the improved understanding of the major impact of low cycle fatigue (LCF) on engine/engine part life, especially with respect to engine hot section part life. Considering this historical background, Colonel Nelson says this specialists' meeting was very timely.

ENGINE UTILIZATION

Understanding temperature and load induced stress on critical engine components is essential in predicting life for thermally sensitive parts, Nelson reported. A major problem is that there is no simple correlation between primary recordable engine parameters and the resultant response at the component locations. This leads to questions as to how much of data is required and how accurate meaningful life prediction capability must be. To measure these parameters, some manufacturers and users have an interest in recording and real-time processing of in-flight data. The purpose here is to have a real-time understanding of engine life usage.

In reference 1, the authors Breitkopf and Speer identify three basic methods for determining engine usage:

> "The use of overall cyclic exchange rates for converting the flying hours into the number of completed reference cycles or sequences;
>
> The use of different cyclic exchange rates depending on the nature of the mission flown, and
>
> Calculation subsequent to each flight on the basis of the time history of the relevant flight and engine parameters."

They say experience shows that the life consumption based on flying hours varies for the same type of aircraft and engine in military use and differences of a factor of 10 from flight to flight are not uncommon.

Therefore, for both economy and safety reasons, the use of overall cyclic exchange rates can be acceptable only when the mission mix of all the aircraft is known, when all engines undergo the same mission mix, and when the life consumption for this mission mix is known. However they say all three prerequisites are not usually met, meaning that high exchange rates must be used.

Breitkopf and Speer add "Evaluation of the flown missions using different cyclic exchange rates is probably the most commonly used method. In contrast to the method of using the overall cyclic exchange rates, this procedure offers the chance of appreciably greater accuracy."

"If flown missions are classified according to specific characteristics and the relevant cyclic exchange rates are determined on a broad data basis for each class, this method can have sufficient accuracy for cold section parts, and it can be the optimal solution for such components in respect of the contradictory aspects of safety and life cycle costs. But this is not very probable when it comes to the hot section components, since appropriate classification of flights in this case is very elaborate." Figure 1 represents the flight course based on the time behavior of the rotor speed.

They concluded that "apparently the beginning and end of the flight, including the elements ground time and departure, and landing and taxi, respectively, are of a deterministic character, with regard to both the succession of the elements and the pattern of the elements."

"The figure shows the main characteristics which exert the greatest influence on the stress behaviour of the hot section parts, and consequently on the life consumption during the flight. In principle, the influence of any single parameter cannot be regarded separately from that of the others."

As an example, the authors cite a duty cycle with three different warm-up periods of 3, 10 and 20 minutes is represented in figure 2. They found the shorter the warm-up phase, the lesser is the stress minimum and the greater is the main cycle's span. With a warm-up period of 3 minutes in comparison to 20 minutes, the life consumption during this flight increases by 52%.

Brietkopf and Speer (reference 1) report that "the on-line computation of the life consumed during the flight, and individually for each engine, out of the measured relevant flight and engine parameters offers itself as the best solution." They claim this procedure is more accurate, less cumbersome and without the large logistical expenditure the on-ground evaluation of recorded flight data requires. The general procedure is summarized in Figure 3.

Breitkopf and Speer add that "because the thermal stresses have very great influence on the life consumption, they must be calculated with great accuracy. In particular, the determination of the time behaviour of the temperature distribution in the critical components, necessary to achieve this high accuracy, presents a problem. Precise numerical methods (finite-element or difference methods), which would otherwise be used, do not come into question because of the time and the amount of computer hardware they require. Consequently, a rapid and accurate approximation procedure must be used." Such a procedure is described in reference 1, and the authors conclude that this calculations procedure permits rapid approximation of transient temperatures and thermal stresses in the rotor structure of a gas turbine engine, and that, a microprocessor system can help implement the method, also permitting the LCF life consumpton of components subject to thermal stresses, such as HP turbine and compressor stages, to be calculated accurately in flight.

Edmunds and Lawrence (reference 2), also noted that "the high performance and rapid response of modern military engines means that transient thermal stresses make a significant contribution to the fatigue life utilization of critical rotating components. This, coupled with the variability of actual usage, raises a requirement for calculating transient thermal stresses from flight recorded data." They believe that the methodology described in reference 2 is a "computationally efficient procedure for meeting this requirement. The analysis is based on a simplified model of the heat transfer and mechanics of the engine that is tuned with results of more sophisticated finite difference and finite element computations. Applications to an engine disc are described using data collected by on-board recordings. The results are validated by comparisons with more detailed theoretical analyses - practical constraints preventing a direct measuring of in-flight stresses. The integration of the results into the overall lifing procedure is also briefly described."

The authors (reference 2) recognize that "the numerical analysis models all require substantial computational power and storage and can only be effectively used on a mainframe installation. However, a major restraint on the service monitoring operation is the requirement to operate on a mini-computer at a maintenance base and, ultimately, on an on-board micro-processor. The use of the above tools is impractical in these environments and hence, in order to meet the previously established requirement, it is necessary to construct a simplified heat transfer/stress analysis model that represents an acceptable compromise between computational power requirements and accuracy." The remainder of their paper concerned itself with such a model and the demonstration of the simplified model to reproduce the results of a more detailed analysis of the high pressure turbine assembly of a military engine.

A great deal of discussion took place regarding the approaches presented in these two papers. Some arguments concerned the amount of data needed to ensure "life accuracy"; which fatigue model(s) should be used; and whether to perform real-time calculations of transient thermomechanical stresses for all parts. No resolution was reached.

Col. Nelson, a man of extensive experience with the development, procurement and operation of U.S. Air Force aircraft noted that "the U.S. Air Force is committed to onboard engine health monitoring and has required this capability on all new engines both for tracking events/usage and for understanding overall engine trending and fleet support management. However, the level, format, and volume of data to be presented to maintenance personnel for effective maintenance action is the subject of intense interest and activity with no accepted solution as yet."

ACCELERATE MISSION TESTING

The overwhelming acceptance of Accelerated Mission Testing (AMT) throughout government and industry was reflected by comments made by meeting attendees. This approach is generally agreed to be a significant improvement over past gas turbine propulsion system qualification testing techniques.

W.R. Taylor (reference 3) reviews the evolution of engine development test requirements in the United States Engine qualification tests in other countries (references 1 & 2) follow a similar pattern. Mr. Taylor stresses that the cost of owning of gas turbine aircraft engines today makes it imperative that the development process produce a production engine that will minimize life cycle cost.

The U.S. Air Force "recognized this problem and one of the most significant changes that has been made in the last 10 years is the incorporation of AMT into U.S. development programs," Taylor says.

He defines AMT as:

> "An engine test conducted in a ground test facility in which the test profile bears a direct relationship to mission usage. The profile accounts for all significant throttle excursions and time at high power that would typically be seen in a composite operational mission."

Taylor emphasizes these points: "1) That AMT directly relates to field usage and 2) That AMT accounts for major throttle excursions and time at high engine power settings. AMT is primarily a structural durability test and it is important that the detrimental portions of the mission be included in the test. The major throttle excursions drive low cycle fatigue and thermal fatigue failure modes. The dwell time at high power conditions contributes to creep, stress rupture and erosion failure phenomenon."

In reference 3, there is an identification of the background of mission related testing, test cycle derivation, data sources and key parameters. Because AMT is expensive, Nelson notes that it is highly desirable that more extensive analysis in the areas mentioned be accelerated to reduce the amount of required testing and, therefore, test costs. The Technical Evaluator, Colonel Nelson, highlights during his summarizing remarks the important area of facilities for the conduct of AMT. He notes: "this extensive cyclic testing, especially of augmented turbofans, has required redesign of facility hardware, both for creation of the proper environmental test conditions and for durability of facility hardware itself. Particular attention must be paid now to fuels, oils, and horsepower extraction equipment in order to assure temperatures and flows appropriate to engine AMT conditions are maintained. Strengthened test stand frames, inlet screens and louvres, and exhaust diffusers are required. Overall facility maintenance costs are increased. Attention is required to devise means of reducing these costs."

Since cost is very important, he says this session shows that efficiency of test and modeling techniques must be improved. "While good correlation of AMT and field usage-related distress is being achieved, AMT adds significantly to test hours of a typical engine development with resultant increased cost of hardware, fuel and test support," Nelson says.

References 1, 2, and 3 discussed a variety of ways used to acquire actual mission profiles of power setting or speed versus time. Taylor explains: "these profiles are then combined into a single composite mission or set of missions representing an average aircraft mission usage. The composites are then reduced by the elimination of part power dwell times and minor throttle transients that are not considered to contribute to the overall life consumption of the engine." There is no universal methodology to complete the task just described. But Taylor notes that the elimination process is a key step in obtaining an optimized AMT cycle because it reduces expensive and superfluous test cell time" (reference 3). The engine problem being addressed and the experience of the organization seem to impact this process heavily.

Taylor summarizes the benefits and limitations of AMT by noting that in the past 10 years, AMT has shown that it correlated well with field usage in life demonstration. He adds that it is a useful tool for substantiating designs and revealing problems that require redesign. AMT is also useful for establishing field and overhaul limits and the verification of rework procedures. But he continues, "AMT cannot completely address performance degradation because of the flight conditions are not simulated in this static test. The total answer to engine structural durability is not provided due to the stochastic nature of engine component life and synergistic effects between the simulated and nonsimulated failure mechanisms."

Taylor stresses that AMT does not provide the complete answer to engine structural durability, and good design criteria, bench and component tests, continued update of mission usage, and "lead the fleet" programs, are needed. "AMT is a major life management tool that is a useful tool in promoting safety, reducing cost and increasing system readiness," he says. The discussions throughout the meeting strongly supported these statements.

LIFE ASSESSMENT METHODOLOGIES

Several papers discussed the capabilities and limitations of current analytical modeling techniques, and agreed that significant strides have been made in the last two decades in engine structural analysis modeling techniques and design tools. However, as Nelson reports, the application of these tools, highlights the need for further development. This SMP Specialists' Meeting on "Damage Tolerance Concepts for Critical Engine Components" should be a major step in that direction. Brief reviews of some of the models developed earlier showed that they did not accurately assess the complex loading relationships of gas turbine engine components. These shortcomings were addressed to some degree in references 8 and 16 where the Pratt & Whitney and General Electric Company have each developed empirical models to address this problem. These models are relatively simple and do not yet address multiple crack initiation that actually occurs. Nelson believes the occurrence of these and other real life events requires that development of analytical techniques continue. Furthermore, resolution of additional questions is needed regarding: boundary constraints and their accurate measurement needed to perform local stress fracture analyses; the required materials property data for these analyses (especially with PM materials); and how to combine these considerations into a life determination.

Many presenters discussed the aspects that must be accommodated if a durability assessment is to be predicted from a modelled engine component. The following lists some of these aspects and related pertinent discussion:

a. Boundary Constraints are the temperature, pressure and body forces. It is necessary to determine these items accurately in order to have a "valid model result". In many papers, the point took on different forms such as: duty cycle effects on components, on-board recording of data, degradation effects, etc. However, for valid results, one must either measure the environment or accurately predict it in order to achieve a meaningful durability assessment.

b. Stress Analysis determines the stresses that the component local area experiences as a function of the fluctuations of the boundary constraints during the actual flights. As Nelson says the need for this is pointed out in reference 4, "a 10 percent lower stress can produce a 60 percent higher life." The major problem is "What level of accuracy is required?" Many presenters expressed the need for accurate stress analysis but apparently this led to a compressed answer dependent upon the amount of time and funding available. During any specific engine design and development, Nelson reports "the intent is to require the minimum effort to accomplish the minimum level of acceptable accuracy. Also, an important facet of durability analysis is the assessment of the design for fracture potential. In order to do this, a fracture mechanics analysis must be conducted using the calculated stress values as primary input."

c. Fracture Analysis is perhaps the fastest growing technology in the turbine engine industry. This was discussed in detail in reference 5, and pointed out as a need generated by the onset of powder metallurgy in references 6, 7 and 8. There is a need to consider the environmental and synergistic effects of stress sequence and temperature in conducting a detailed fracture assessment of an engine component. "However, one must keep in mind that basic to the fracture assessment is "material property" generation at the appropriate environmental conditions and with material specimens of proper metallurgical condition," Nelson reports.

d. Life/Durability Determination was highlighted in many references. All discussed different aspects of life determination and methods used for accounting for damage accumulation. Nelson noted, "What can be said about each is that all were different and none were totally wrong! In fact, this independent activity and discussion of areas of disagreement as to parameter validity, sequencing, correction factors, creep characteristics, use of classical models, etc., is healthy and needs further encouragement. There was but one short discussion of multiple cracking and then only with respect to a given single location. While this case is of interest and should be modeled and analyzed for cause and effect, the case of multiple cracking must be addressed wherein second, third, etc., cracks appear in remote locations of a single structure, e.g., first in a bolt hole of a turbine disc then in a second bolt hole for the web nonadjacent to the first crack. There was general agreement at the PEP meeting that his analysis would be very difficult and very dependent upon the successful development of models that consider single cracks, it does represent real experience with some evidence that secondary remote cracking may delay or otherwise affect initial crack growth in some structures. Such sophisticated analysis is an area which should be reviewed for progress and focused effort."

In reference 9, Larsen and Nicholas note that during the past two decades the design criteria and material property requirements for critical structural components in United States Air Force gas turbine engines have changed drastically. "In the 1960's, most critical components such as turbine disks and spacers were life limited by the creep and stress rupture properties of their materials," they say "less than one percent of all rotating components were life limited by Low Cycle Fatigue (LCF). However, demands for improved performance of advanced engines have led to design increases in component operating temperatures and stresses, and the result has been a transition from creep to low cycle fatigue as the dominant life limiting mechanism in the majority of rotating components. In fact, low cycle fatigue has become the life limiting factor for turbine disks in over 75 percent of designs." They also review the U.S. Air Force change from a "safe life" to "retirement for cause" (RFC) life management philosophy Larsen and Nicholas continue: "Low cycle fatigue, defined by the time required to initiate a crack, is a stochastic process having considerable variabiity. In order to provide a safe component operating life, the conventional approach has been to use a lower bound on the mean LCF life that is equivalent to a probability of 1/1000 of initiating a detectable crack during the design lifetime of the component. In practice, all components are removed from service after reaching this design lifetime, and this translates into 999 out of 1000 disks being retired from service which are still structurally sound." Figure 4, from a USAF analysis of the F100 1st stage turbine disc at retirement, indicates that 80 percent of the discs should have at least ten lifetimes remaining (reference 10).

In order to use the remaining life of these 999 disks without sacrificing structural safety, the U.S. Air Force started a revised life management philosophy termed Retirement-For-Cause (RFC) on some components in advanced engines. Under RFC, components must undergo periodic inspections and be returned to service if no cracks larger than a certain size are detected. The authors say this procedure requires two technologies: the ability to detect cracks larger than a given "detectable size" with a high degree of reliability, and the ability to predict crack growth rates and to show that a crack of the "detectable size" or smaller will not grow to a catastrophic size during one inspection interval.

Koul, Wallace, and Thamburaj, reference 11 report that "damage tolerance concepts are being considered for use both at the design stage, for stress analysis and for lifing procedures, and to establish intervals for inspection and repair during service. It is assumed that flaws exist in parts as manufactured, at a size just below the NDI detection limit, and these may be located in the most highly stressed regions or hot-spots of the component. It is further assumed that these flaws will grow in-service, at a rate determined by the local stress (mechanical and thermal) distribution around the flaw, the operating temperature and the environment. These parameters will vary with time as a function of engine power setting (demand) and the detailed time histories will therefore be a function of the operational mission profile or use. The general objective of the damage tolerance approach is to establish expected crack growth rates for realistic operating conditions and to implement NDI procedures with an appropriate level of sensitivity, reliability, and frequency to ensure that cracks can be detected and if feasible monitored in service to a point where risk of rapid or unstable crack propagation becomes severe. Flawed parts are therefore retired on an individual basis when their condition dictates. The "critical" crack length, or length at retirement is therefore a function of many variables including material type, component design, operating environment, engine usage, engine use monitoring system employed and NDI procedures employed." Figure 5 illustrates the USAF damage tolerance approach to life management of LCF limited engine components.

In reference 11, the authors also provided an interesting look at the life extension possibilities of major components - namely turbine blades and turbine and compressor discs.

As Koul, Wallace, and Thamburaj report: "Improvements in component operational capability have essentially been achieved through proper adjustment of the alloy chemistry to increase the volume fraction and to decrease surface degradation. Progress has also occurred in new processing techniques. Perhaps the most remarkable development in this respect have been the introduction of directionally solidified and single crystal blades, and the manufacture of powder metallurgy compressor and turbine discs."

"Data showing the beneficial effects of hot isostatic processing on the stress-rupture properties of new and service exposed Ni-based superalloy turbine blades were presented. Creep design methods that are generally used to highlight the service induced degeneration effects were critically analyzed. A new life prediction method that systematically analyzes the creep degeneration effects with increasing service life was proposed."

"The influence of machining operations on the LCF properties of IN901 have been evaluated (reference 12) and the results indicate a 3-5 fold increase in LCF life of Electro-discharge machining (EDM) plus abrasive flow machining (AFM) samples when compared with samples machined by conventional methods."

CRITICAL MATERIAL CHARACTERIZATION

Ir. A.J.A. Mom presented an outstanding paper (reference 5), a comprehensive overview of the AGARD SMP activities on turbine engine technology over the last 10 years. These activities covered most of the material related aspects in gas turbine technology from the initial design to the retirement of components. Topics were grouped as: 1) the development and application of advanced materials, 2) material properties and behaviour, 3) material processing and fabrication techniques, 4) maintenance and repair and 5) life prediction methods.

One of the strongest messages developed at the PEP meeting was that the key to meaningful life prediction analyses and cyclic test evaluation is the generation of, and sound understanding of, materials properties under proper environmental and metallurgical conditions. In reference 5, Ir. Mom reviewed life prediction methods. When one considers the complexity of the relationships, the loading definitions required, the knowledge of material performance necessary to predict component life, and the desire to incorporate all this into an effective system, you realize the enormity of the technical challenge. Everyone also recognizes the need for such a tool for aircraft propulsion development to continue and meet the safety, performance, and economical goals of the future. The amount of activity in all related areas identified at the PEP meeting was encouraging.

Ir. Mom's paper included an extensive discussion on powder metallurgy. He noted that "the production of engine components (and also aircraft structural components) out of superalloy or titanium powders has received considerable attention in recent years. Powder Metallurgy (PM) offers considerable potential advantages: in large components a much better uniformity in properties can be obtained then by conventional forging of ingot material. Furthermore the technique also offers a considerable cost reduction potential because of (near) net shape forging by hot isostatic pressing (HIP) capabilities."

In reference 6, Dr. Konig, evaluated "the mechanical properties of powder-metallurgical nickel-base superalloys in order to predict the behaviour of advanced aero-engine discs in comparison with conventional wrought nickel-base (e.g. Waspaloy; IN 718) discs. The assessment included tensile strength, crack initiation and propagation fatigue life as well as the influence of mean stress. Special emphasis was put on the question about the scatter in fatigue lives resulting from defects in the material (e.g. oxide inclusions) and on the surface (e.g. grooves). The tolerance with respect to these defects was estimated on the basis of fracture mechanics methods."

It was interesting to note that Dr. Konig - recognizing that the most common feature to produce high strain ranges in discs are notches, such as bolt holes, cooling holes or blade slots - used specimens with internal holes in cyclic spin tests to obtain material data for the behaviour of these type of notches. Some meeting attendees were interested in the effectiveness of this evaluation method. Further discussions seem warranted.

Many authors, especially Poret, Guedon, and Pineau, showed that grain size alone has significantly different effects on crack growth rates in the same material composition. In addition, the location of the crack in the surface or subsurface and the surrounding stress gradient play an important role in the resultant fracture life value.

Dr. Schneider and Grunling (reference 13) discussed the mechanical aspects of high temperature coatings. The role of protective coatings in modern gas turbine engines was re-emphasized. Coatings are essential in preventing erosion, corrosion, oxidation and overall wear. The selection of the best coating process is, however, a compromise typical of most unique design processes. Coating durability, adherence, environmental protection, and the impact of the coating on base metal mechanical properties must be considered. In the second part of reference 13, the two men noted the influence of the coating on the mechanical properties of the coated component. Under either static and/or cyclic loadings, they said "a coating has some influence either through changes in the material properties due to a different heat treatment or through changes in the surface of a component due to the presence of the coating. Therefore, a coating alters the condition for crack initiation. The changes in materials may be positive, negative, or negligible."

COMPONENT AND ENGINE CYCLIC TESTING

Turbine blades and rotors are expensive and critical engine components. A reliable and accurate lifetime prediction of these components is essential for optimal use of gas turbines. A major difficulty in predicting the crack initiation life is accounting for the high temperature effects of creep-fatigue interaction and environmental attack. Various life prediction approaches seem to work well for some alloy systems but not for others and this is attributed mainly to differences in materials response or capacity to absorb different types of damage. In reference 14, Nazmy, Wettstein and Wicki reported the results of their examination of the high temperature low cycle fatigue (HTLCF) behavior of the blading alloy IN738 in air at 850°C. They said this enabled them to have a basic understanding of the behavior of this alloy as well as to test the different methodologies used in life time prediction. Another part of the investigation focused on the influence of environmental effects on the HTLCF behavior. These conditions were chosen to simulate the conditions imposed on the gas turbine blades, and therefore mainly sulfur containing environments were used.

These authors concluded that:

a. "Using one set of HTLCF data three different lifetime prediction methods were evaluated. The strain range partitioning and Ostergren methods both showed comparable predictive capabilities that were better as compared to the frequency-separation method.

b. HTLCF life is affected in a pronounced manner by prior exposure at 850°C in the hot corroding environments studied here. Prior exposure at 750°C in the studied hot corroding environments caused some reduction in the HTLCF life of IN 738 specimens. The prior exposure at 700°C for 600 hr. in the studied hot corroding conditions did not affect the HTLCF life of IN 738 specimens."

With reference 15, Ponsford and Waddington took the meeting attendees into the very real world surrounding the design and development of a cast directionally solidifed high pressure turbine blade for the Rolls Royce RB211-22B engine.

Rolls Royce recognized that it needed a method of proving the design beyond the normal endurance testing to simulate the service life of the turbine blade. This led to the creation of the intensive cyclic endurance program. The program aimed to prove that the new HP turbine blade could achieve the design objective of a 10,000 hour service life. Their paper covered the program's objectives, the definition of the endurance cycles and the automation used in running the cyclic tests. Discussion included comments on the modifications incorporated to ensure that testing represented the service environment. They also presented the results of the program which demonstrated that the design objective would be achieved in airline service.

The experiences related in reference 15 and the program modifications made to keep the program moving properly toward its goal were most enlightening and should provide useful input into the testers' handbook of lessons learned. As reported by Ponsford and Waddington "Following the successful demonstration of the cast directionally solidified HP turbine blade in the intensive cyclic endurance program, cyclic testing is now used to test all major developments of the RB211."

The U.S. Air Force and the U.S. gas turbine industry have realized that there is a need, during the early phases of engine development when an engine has components of advanced design and materials and their intended use is unclear, for a testing philosophy and program that will cost effectively assess the "design ability" of advanced components. Hill, in reference 4, reported on this relatively new philosophy termed Life Assessment Technology (LAT). His paper gave what he called "a status report on the results of current rig and component testing being conducted under the Life Assessment Testing approach to turbine engine durability validation. The focus of the paper is the combination of using material of reduced life capability and creating conditions of higher stress to produce short-time failure for cost effective validation of the tools and rules of life prediction. The three components discussed were combustors, compressor disks and turbine blades."

Using Figure 6, Hill described the three basic approaches to testing components for durability--"whole" life, "potential" life and "reduced" life. In "whole" life, one tests the component under actual spectrum loads until it fails, he said. This produces a one-to-one mapping of the test data on actual life expectancy. The "whole" life approach is the best data, but it also may require most expense and time.

The "potential" life approach involves testing the component to real-time spectrum loads but for only a percentage of life--not until failure. Hill reported that with this method, it is very difficult to determine what percentage of life should be exhausted and how much life was demonstrated without a calibrated residual life test.

The "reduced" life test approach involves either manipulating the component geometry to produce a "short life" specimen or creating an overstress on the component by changing the environment or both, Hill said, this method gives a cost effective assessment of the tools and rules of design by allowing the test article to be tested to a failed state in a short test time. However, he noted, the only difficulty is the assurance of maintaining the proper failure mode in the manipulation of the component or the boundary conditions. "Methods of higher stress inducement may be faster load rates, use of artifical stress risers, more severe thermal gradients, higher temperatures, use of lower strength (characterized) materials and coatings, high mechanical loading, or combinations of any of these methods," Hill said.

"The LAT philosophy uses both the "potential" life and the "reduced" life approach to supply a baseline durability characterization of a component's design. The actual testing under LAT can be the testing of a component on either a bench, rig, core or full engine or a combination of these methods. The key to LAT testing is the creation and control of the test by using loads and temperature (stress/strain) rather than mission usage (throttle motion). This requires the LAT tests to be fully instrumented to quantify the component's boundary conditions such that "valid" data is obtained for use in correlation of the tools/modes of design."

Hill concluded that "through the component testing described in his paper and other test efforts, it has been determined that the Life Assessment Testing philosophy offers a significant cost effective means of using component testing to validate or create life prediction models and methods."

In reference 3, Taylor notes that the engine development requirements today are generally based on the requirements of MIL-E-5007D, but have been augmented by the AMT concept and the soon to be released Engine Structural Integrity Program (ENSIP). These requirements will be incorporated into one new Mil-Prime Specification.

In his presentation (no paper published) C.D. Clayton, General Electric Company, illustrated how engine cyclic testing and the ENSIP philosophy integrate in the validation of engine life prediction. Figure 7 (reference 16) illustrates the progression through the ENSIP. The engine test program can be considered as three phases: 1) the Operability Engine Testing phase that will evaluate the sea level and altitude performance and engine control; 2) the Endurance Test AMT Cycle engine phase where engines are run to the specification requirement AMT cycles; 3) the Parameter Measurement Engine testing where temperature/pressure/speed/vibration, aeromechanical, and other imposed loads are measured.

The ENSIP method provides a structured program for total engine development and it includes a durability and damage tolerance assessment, a durability and damage tolerance control plan, and a structural maintenance plan. It is also of significance to note both AMT and ENSIP are now part of all U.S. Air Force initial engine development programs and are required to be carried forward through the life of the engine program in order to accommodate field usage changes, multiple system applications, engine upgrades, etc. The total process will hopefully produce more durable, reliable engines with much better defined support requirements.

The initial phases of the ENSIP are being applied to the production verification procedures of the GE F101-GE-102 and F110-GE-100 turbofan engines for the USAF.

REFERENCES

1. Breitkopf, G.E.; Speer, T.M., (Motoren-und Turbinen - Union Munchen GmbH, West Germany): In-Flight Evaluation of LCF Life Consumption of Critical Rotor Components Subjected to High Transient Thermal Stress.
2. Edmunds, T.M.; Lawrence, R.A., (Rolls Royce Limited, Bristol, England): Monitoring Engine Thermal Stresses.
3. Taylor, W.R., (Aeronautical Systems Div., WPAFB, Ohio): Accelerated Mission Endurance Testing (AMT).
4. Hill R.J., (Aero Propulsion Laboratory, AFWAL, WPAFB, Ohio): Verification of Life Prediction Through Component Testing.
5. Mom, A.J.A., (National Aerospace Laboratory NLR, Amsterdam, The Netherlands): Overview of the AGARD SMP Activities on Turbine Engine Materials Technology in the 1972-1982 Period.
6. Konig, G.W., (Materials Laboratory, MTU, West Germany): Comparison Between the Properties of Conventional Wrought and Powder Metallurgical Alloys for Turbine Disc Applications.
7. Poret, L., Guedon, J.Y., Pineau, A., (SNECMA and Ecole des Mines de Paris, France): Resistane A La Propagation De Fissures De L'Alliage Inconel 718.
8. Farmer, E.T., (Pratt & Whitney Aircraft Group, United Technologies Corp., West Palm Beach, Florida): View of Future Requirements for Engine Cyclic Durability by Analysis and Testing.
9. Larsen, J.M., Nicholas, T., (Air Force Wright Aeronautical Laboratories, WPAFB, Ohio): Cumulative Damage Modeling of Fatigue Crack Growth.
10. Harris, J.A. Jr., Annis, C.A. Jr., Van Wanderham, M.C., Sims, D.L.: Engine Component Retirement for Cause.
11. Koul, A.K., Wallace, W., (National Research Council, Canada), Thamburaj, R.,(Carleton University, Ottawa, Canada): Problems and Possibilities for Life Extension in Gas Turbine Components.
12. Dixon, I., Gladysz, V.: Unpublished Work, 1983.
13. Schneider, K., Grunling, H.W., (Borwn, Boveri & Cie AG, Mannheim Germany): Mechanical Aspects of High Temperature Coatings.
14. Nazmy, M.Y., Wettstein, H., Wicki, A., (Brown Boveri Research Center, Baden, Switzerland): Experiences With the Material Behaviour and High Temperature Low Cycle Fatigue Life Prediction of the IN 738 Blading Alloy.
15. Ponsford, J.S., Waddington, G.K., (Rolls Royce Limited, Derby, England): Cyclic Endurance Testing of the RB211-22B Cast HP Turbine Blade.
16. Clayton, C.D., (General Electric Co., Evendale, Ohio): The Role of Engine Cyclic Testing in the Validation of Life Predictions.

ACCELERATED MISSION TESTING (AMT)

AN ENGINE TEST CONDUCTED IN A GROUND TEST FACILITY IN WHICH THE TEST PROFILE BEARS A DIRECT RELATIONSHIP TO MISSION USAGE. THE PROFILE ACCOUNTS FOR ALL SIGNIFICANT THROTTLE EXCURSIONS AND TIME AT HIGH POWER THAT WOULD TYPICALLY BE SEEN IN A COMPOSITE OPERATIONAL MISSION.

GENERAL MISSION PATTERN WITH LCF-RELEVANT MAIN PARAMETERS

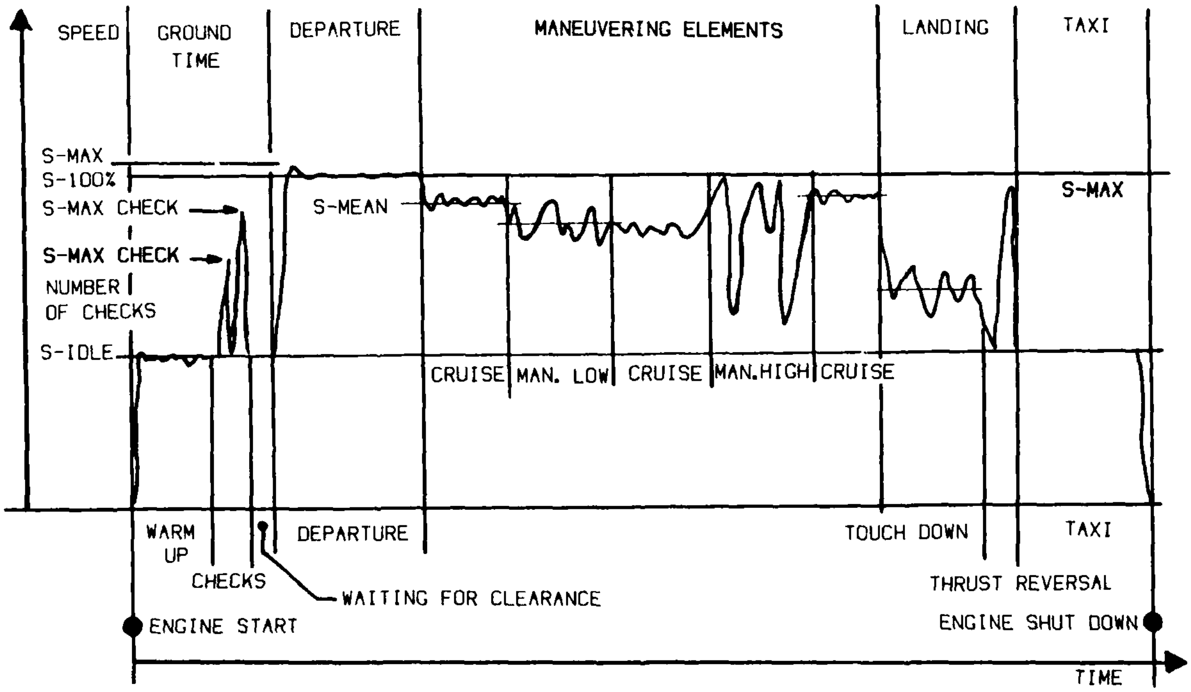

SPEED
GROUND TIME
DEPARTURE
MANEUVERING ELEMENTS
LANDING
TAXI
S-MAX
S-100%
S-MAX CHECK
S-MAX CHECK
NUMBER OF CHECKS
S-IDLE
S-MEAN
S-MAX
CRUISE
MAN. LOW
CRUISE
MAN.HIGH
CRUISE
WARM UP
CHECKS
DEPARTURE
WAITING FOR CLEARANCE
ENGINE START
TOUCH DOWN
TAXI
THRUST REVERSAL
ENGINE SHUT DOWN
TIME

FIGURE 1

DIFFERENCE IN HPC DISK RIM STRESS HISTORY DUE TO DIFFERENT GROUND TIMES

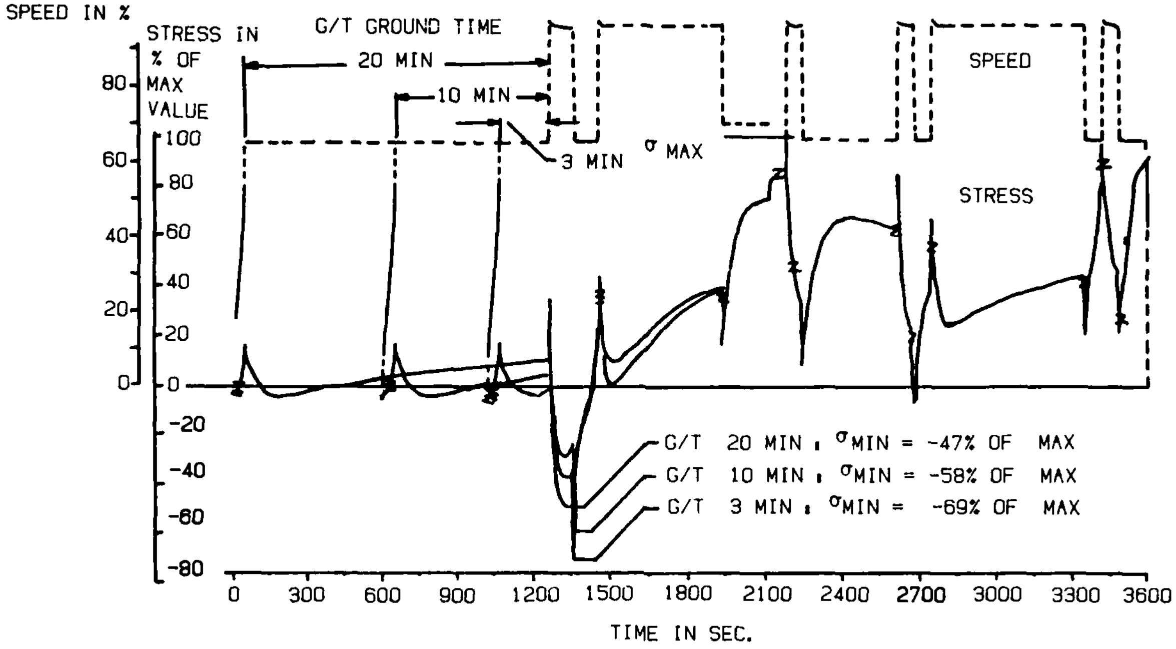

FIGURE 2

FLOW CHART MISSION ANALYSIS

CALCULATION OF LCF-LIFE CONSUMPTION

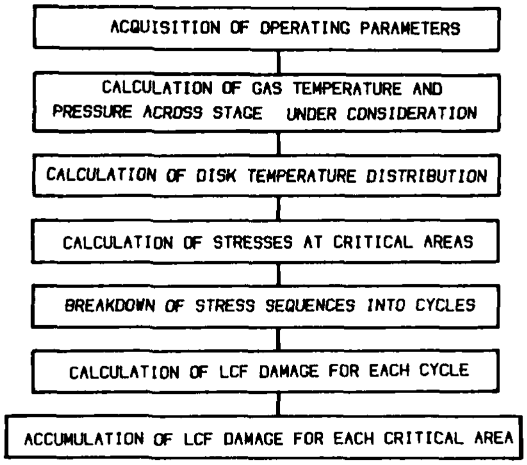
ACQUISITION OF OPERATING PARAMETERS
CALCULATION OF GAS TEMPERATURE AND PRESSURE ACROSS STAGE UNDER CONSIDERATION
CALCULATION OF DISK TEMPERATURE DISTRIBUTION
CALCULATION OF STRESSES AT CRITICAL AREAS
BREAKDOWN OF STRESS SEQUENCES INTO CYCLES
CALCULATION OF LCF DAMAGE FOR EACH CYCLE
ACCUMULATION OF LCF DAMAGE FOR EACH CRITICAL AREA

FIGURE 3

THE MAJORITY OF DISCS HAVE USEFUL LIFE AFTER RETIREMENT. THE RETIREMENT CRITERION IS BASED ON SAFE LIFE APPROACH

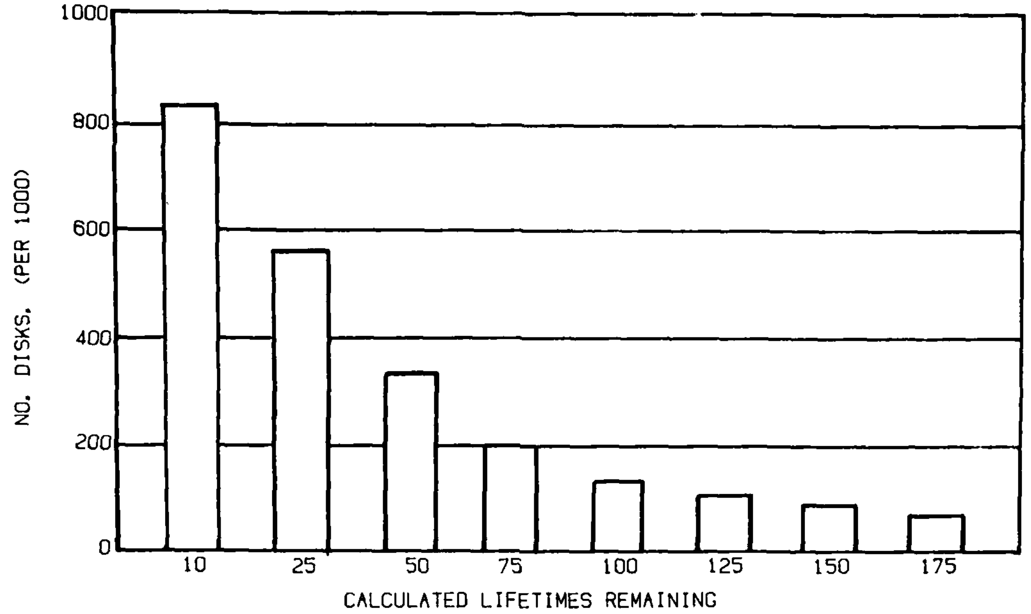

FIGURE 4

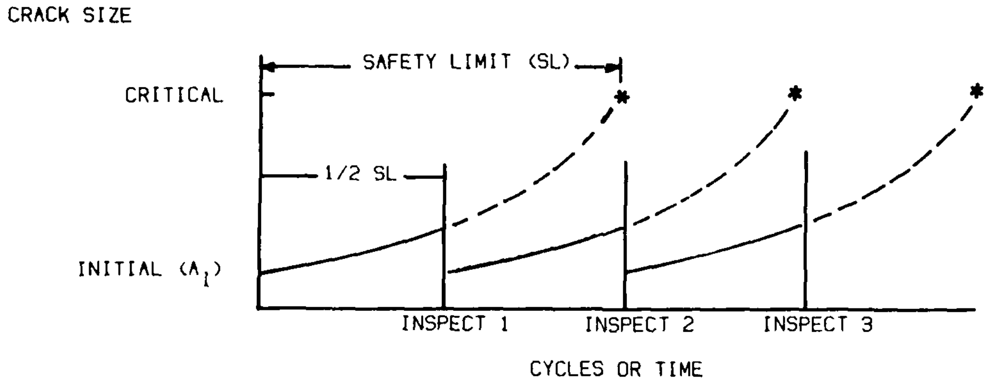
CRACK SIZE
SAFETY LIMIT (SL)
CRITICAL
1/2 SL
INITIAL (A_I)
INSPECT 1
INSPECT 2
INSPECT 3
CYCLES OR TIME

CRITERIA

- SAFETY LIMIT IS TIME FOR INITIAL FLAW (Ai) TO GROW AND CAUSE PART FAILURE
- INSPECT AT 1/2 SL INSPECTION INTERVAL 1 LIFETIME (DES. GOAL) OR 1 DEPOT INTERVAL (MIN DESIGN REQMT)
- APPLIES TO FRACTURE CRITICAL PARTS
- PRODUCTION Ai BASED ON NDE METHOD OR MATERIAL DEFECT DISTRIBUTION
- DEPOT Ai BASED ON NDE METHOD

FIGURE 5

DURABILITY TEST APPROACHES

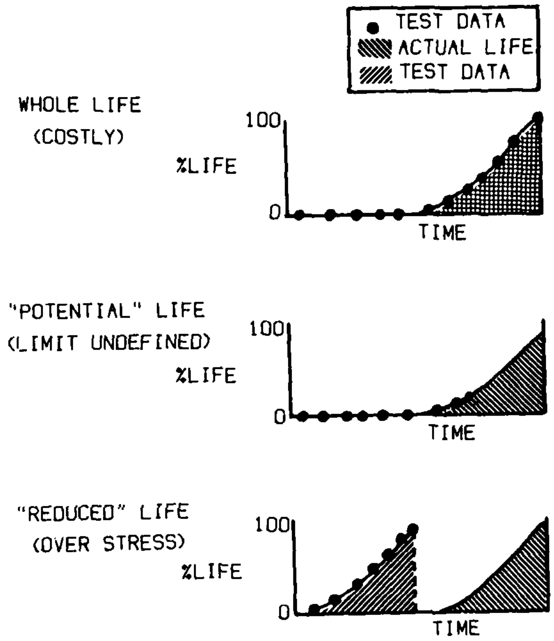

FIGURE 6

PROGRESSION THROUGH THE ENSIP PROGRAM

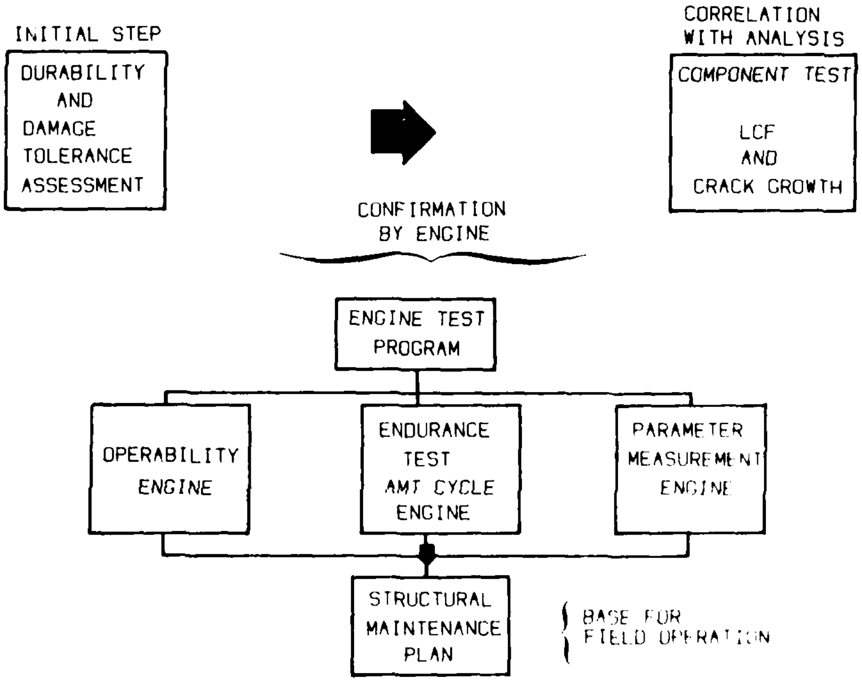
INITIAL STEP
DURABILITY AND DAMAGE TOLERANCE ASSESSMENT
CORRELATION WITH ANALYSIS
COMPONENT TEST
LCF AND CRACK GROWTH
CONFIRMATION BY ENGINE
ENGINE TEST PROGRAM
OPERABILITY ENGINE
ENDURANCE TEST AMT CYCLE ENGINE
PARAMETER MEASUREMENT ENGINE
STRUCTURAL MAINTENANCE PLAN
BASE FOR FIELD OPERATION

FIGURE 7

DAMAGE TOLERANCE DESIGN CONCEPTS
FOR MILITARY ENGINES

T. T. King, ASD/EN, W. D. Cowie, ASD/YZEE and W. H. Reimann, AFWL/MLLN
Wright-Patterson Air Force Base, Ohio 45433 USA

SUMMARY

This paper summarizes the damage tolerance requirements that are applied to Air Force engine development programs. These requirements are an integral part of the Engine Structural Integrity Program (ENSIP) contained in MIL-STD-1783 (USAF) dated 30 November 1984. Application of damage tolerance requirements to existing inventory engines (F100 and TF34) and to the development programs (F100-PW-220, F101-GE-102, F110-GE-100 and F109-GA-100) have resulted in implementation of enhanced nondestructive evaluation methods (i.e., eddy current) at manufacturing and at field/depot. Experience has shown that these inspections have been successful in detecting early cracking and accelerating corrective actions. It has been highlighted that several development efforts in the last five years have identified FPI process improvements that must be implemented within industry and Air Force depots to improve flaw detection reliability. The need to quantify detection reliability for imbedded defects is also identified.

The engine development process has been evolutionary in terms of application of upgraded requirements. The new process is contained in ENSIP. Recent experience clearly demonstrates that the damage tolerance requirement is cost effective when assessed on a life cycle basis.

INTRODUCTION

Surely, one of man's greatest achievements in machine design is the aircraft turbine engine. Further, designing one of these machines to produce the highest performance the state-of-the-art will allow, while simultaneously exhibiting the characteristics of durability, reliability, and light weight is indeed a formidable challenge.

In order to meet this challenge, lessons learned from previous turbine engine development programs have been incorporated and utilized. Steps have been taken to understand and identify the numerous and complex failure modes early in the development process. A disciplined approach to turbine engine structural development reflecting these lessons learned is now being utilized to assist in achieving the durability goals desired in military turbine engines. This program is referred to as the Engine Structural Integrity Program (ENSIP) and is contained in MIL-STD-1783 (USAF) dated 30 November 1984. This paper will discuss the use of damage tolerance design concepts which is an important and intrinsic part of ENSIP.

OVERVIEW OF ENSIP

In the past fifteen years, a large number of structural problems have occurred in Air Force turbine engines. Many of these were safety problems causing loss of aircraft and an even greater number affect durability, causing a high level of maintenance and modification costs. All of these problems have adversely affected fleet readiness. The Engine Structrual Integrity Program (ENSIP) was developed based on the specific lessons learned (Figure 1) and was intended to substantially reduce these problems. ENSIP was recommended by the Scientific Advisory Board and established by the Air Force to provide an organized and disciplined approach to the structural design, analysis, development, production and life management of gas turbine engines with the goal of assuring engine structural safety, increased service readiness and reduced life cycle costs.

As shown in Figure 2, there are five major tasks associated with ENSIP; namely, design information task, design analysis, component and material characterization task, component and core engine testing task, ground and flight engine testing task, and production quality control and life management task. Each major task is subdivided into a number of subtasks which guide the development process.

ENGINE STRUCTURAL MAINTENANCE PLAN

The engine structrual maintenance plan represents the output of the engine ENSIP process. This plan will identify and define the individual part life limits, the necessary inspection periods for each part as well as the inspection procedure. Repair options and limits are also presented.

ENSIP - [illegible]

Structural safety is obtained in ENSIP by requiring damage tolerance structure that is capable of [illegible] flaws induced either in manufacturing or in service.

Durability requirements require the economic life of the engine to exceed the specified [illegible] aircraft when flown to the design usage spectra.

Maintainability [illegible] that old parts fit and function with new parts, repair [illegible] inspectability and structrual diagnostics be designed into the [illegible] Materials and Process Characterization Plan shall control materials [illegible] engine development points. Environmental Definition requirements [illegible] dynamic, steady state stress, status spectra, and [illegible] Ground Test Policy is utilized to assure com- [illegible] maintainability requirements. A Usage and Tracking [illegible] engine life management program.

FATIGUE/DAMAGE TOLERANCE TRENDS

The conventional fatigue design approach is shown in Figure 3. Components are designed so that the Low Cycle Fatigue (LCF) limit exceeds the required usage interval in terms of engine flight hours or cycles. The LCF limit is based on the lower bound (-3σ or 1/1000) of the distribution of crack initiation times. The lower bound limit has been chosen to prevent occurrence of cracking and resultant failure and the need for repair (economics). The main concern with the conventional approach is that no recognition or provision exists regarding the impact initial defects can have on total component life (i.e., component failure can and has occurred prior to reaching the LCF limit). Implementation of the safe life philosophy requires that all like components be removed from service upon expiration of the safe life. Since there is wide scatter in materials data for fatigue, the analysis is usually based on -3 sigma material properties which implies that all components are treated like the worst case component in the population.

It can further be noted that the fatigue design philosophy is strongly based on the premise that the material is free of initial defects. This philosophy makes no allowance for material, manufacturing, producibility, and handling anomalies or defects. In MIL-STD-1783, the damage tolerance requirement has been incorporated to prevent safety or flight structural failures caused by material defects, manufacturing defects or fatigue induced cracks. There have been numerous engine failures in the past where initial defects grew in size due to the use of high strength, low fracture toughness material and improper detail design resulting in high stress levels and structural discontinuities, and lack of adequate quality control.

The primary need for damage tolerance requirements has occurred due to the ever present drive to minimize engine weight through development of materials with increased strength and resistance to crack initiation. An undesirable but attendant feature of these new materials has been a decrease resistance to crack propagation (Figure 4 and 5). As a result of these trends, the F100 and TF34 engine durability and damage tolerance assessments were performed.

Results of these analysis are shown in Figure 6.

ENSIP DAMAGE TOLERANCE REQUIREMENTS

General. Damage tolerance is defined as the ability of the engine to resist failure due to the presence of flaws, cracks or other damage for a specified period of usage. The damage tolerance approach to life management of cycle limited engine components is shown in Figure 7. Components are designed so that the safety limit exceed 2X the required inspection interval. The safety limit or residual life is the time for assumed initial flaws to grow and cause failure. Since the requirement is to inspect at one-half the safety limit, the design goal for the safety limit is 2X the required design life (i.e., no inspections). The minimum design requirement for the safety limit is 2X the planned depot visit interval. The basis and assumptions for initial flaws are covered elsewhere in this paper. An important aspect of the damage tolerance requirement is that it applies only to fracture critical parts which is also discussed elsewhere in this paper.

It is required that the "cost" as a function of the "requirement" be defined via trade studies since the magnitude of the safety limit impacts overall engine configuration variables such as weight, costs, material selection, inspection methods and detail design. Trade study results are used to set the damage tolerance requirement and associated variables.

Fracture Critical Components. Fracture critical components are defined as those components whose failure will result in probable loss of the aircraft as a result of noncontainment or, for single engine aircraft, power loss preventing sustained flight due to direct part failure or by causing other progressive part failures. Damage tolerance requirements are applied only to fracture critical components and not, in general, to durability critical components. As can be expected, component classification is affected by aircraft engine configuration, i.e., single engine or multi-engine. Component classification can, in some instances, be rather subjective and historical records and experience gained during development tests should be used to aid in classification. Component classification is established early and is identified in the contract.

Initial Flaw Size. Initial flaws are assumed to exist in fracture critical components. Experience has shown that premature cracking (i.e., crack initiation prior to the LCF limit) occurs at high stressed areas and initial conditions have included both material and manufacturing related quality variations (i.e., voids, inclusions, machining marks, scratches, sharp cracks, etc.). The damage tolerance requirement uses a sharp crack initial flaw assumption to characterize these abnormal initial conditions. Assumed initial imbedded flaw sizes are based on the intrinsic material defect distribution or the Nondestructive Evaluation (NDE) methods to be used during manufacture. An inspection reliability of 90 percent Probability of Detection (POD) at the lower bound 95 percent Confidence Level (CL) is required for the assumed initial flaw sizes.

The assumed initial flaw size to account for intrinsic material defect distribution should encompass 99.9 percent of the defect population if a scatter factor of two is used to establish the inspection interval or 99.99 percent if a scatter factor of one is used.

An initial flaw size not less than 0.030 inch length (surface) or 0.015 inch by 0.015 inch length (corners) for nonconcentrated stress areas (bores, webs, etc.) is required. Initial flaw sizes for other surface locations (holes, fillets, scallops, etc.) will be consistent with the demonstrated capability (90% POD/95% CL) of the inspection systems proposed for use. It is recommend that initial design and sizing of components be based on 0.030 inch length surface flaws or 0.015 inch by 0.015 inch corner cracks. The basis for this recommendation is two-fold: (1) To establish an intial flaw size that can be screened by use of Fluorescent Penetrant Inspection (FPI) as the standard NDE method and (2) To provide capability for application of upgraded NDE methods at a few locations when required.

These flaw sizes ar intended to represent the maximum size damage that can be present in a critical location after manufacture and/or inspection. The basis for these flaw sizes is the data on detection capability of the various NDE methods. These data are included and discussed elsewhere in this paper.

The assumed initial flaw sizes for use in design are summarized in Figure 8.

Residual Strength. Residual strength is defined as the load carrying capability of a component at any time during service exposure period considering the presence of damage and accounting for the growth of damage as a function of exposure time. The requirement is to provide limit load residual strength capability throughout the service life of the component. Expressed in another way, the minimum residual strength for each component (and location) must be equal to the maximum stress that occurs within the applicable stress spectra based on the design duty cycle. Normal or expected overspeed due to control system tolerance and engine deterioration is included in the residual strength requirement but fail safe conditions such as burst margin are excluded. A pictorial presentation of the residual strength requirement is shown in Figure 9.

Inspection Intervals. It is highly desirable to have no damage tolerance inspections required during the design lifetime of the engine. This inservice non-inspectable classification requires that components be designed such that the residual life or safety limit be twice the design life. Designing components as inservice non-inspectable is a requirement for those components or locations which cannot be inspected during the depot maintenance cycle (i.e., imbedded defect considerations and other non-inspectable areas).

It is recognized though that the weight penalty incurred to achieve a safety limit/ residual life/damage growth interval twice the design life may be prohibitive on some components/locations. Therefore, inservice inspections will be allowed on some components subject to justification. The basis for the justification is characterization of the costs as a function of the requirements as established by trade studies. Cost is usually in terms of weight or Life Cycle Cost (LCC) and the requirement in terms of safety limit/ residual life/damage growth interval.

The depot or base level inspection interval for damage tolerance considerations should be compatible with the overall engine maintenance plan. Once again, it is highly desirable that the inspection interval be equal to the hot part design service life as this is the expected minimum depot or maintenance interval for the engine or module. It is required that the damage tolerance inspection interval be contained in the contract specification.

Flaw Growth. Flaw growth interval, safety limit and residual life are used interchangeably in this paper. It is required that the assumed initial flaw sizes will not grow to critical size and cause failure of a component due to the application of the required residual strength load in 2 times (2X) the inspection inerval. The flaw growth interval is set equal to 2X the inspection interval to provide margin for the variability that exists in the total process (i.e., inspection reliability, material properties, usage, stress predictions, etc.), Factors other than 2 should be used when individual assessments of the variables that affect crack growth can be made (e.g., to account for observed scatter in crack growth during testing).

It is very important that the effects of vibratory stress on unstable crack growth be accounted for in establishing the safety limit. Experience shows that the threshold crack size can be significantly less than the critical crack size associated with the material fracture toughness depending on the material, major stress cycle and the vibratory stress. Indeed, as shown by Figure 10, the conventional Goodman Diagram may not disclose the true sensitivity of initial defects to vibratory stresses. The threshold crack size must be established at each individual sustained power condition (idle, cruise, intermediate) using the appropriate values of steady stress and vibratory stress. The smallest threshold crack size will be used as a limiting value in calculation the safety limit if it is less than the critical crack size associated with the material fracture toughness.

The damage tolerance requirement allows rational assessment/accounting of the variables which can affect the safety limit and calculation thereof subject to verification by test. Examples include effects of surface enhancements such as cold expanded holes, shot peening and proof test. Also, continuing damage is assumed at critical locations where the initial damage assumptions does not result in failure of the component (e.g., the case of a free surface at a bolthole).

VERIFICATION.

Verification that damage tolerance criteria is met is assured via development and implementation of a damage tolerance control plan, by analysis and test, and by implementation of reliable inspection methods during manufacture and field/depot maintenance.

A damage tolerance control plan is prepared that identifies and schedules each of the tasks and interfaces in the functional areas of design, materials selection, test, manufacturing control and inspection. Specific tasks that are addressed in control plan are shown in Figure 11.

Most of the tasks to be contained in the damage tolerance control plan have been accomplished by engine manufacturers in past development and production programs. However, the damage tolerance requirement now established by the Air Force imposes the need for new tasks as well as tighter controls and more involvement between the functional areas. Experience indicates that the development and implementation of a damage tolerance control plan is very difficult but experience also shows very strongly that development of a plan results in an improved understanding of what must be done. The importance of having a plan rests on the involvement of multiple functional areas and the criticality of having assigned responsibilities for each task.

A particularly important part of the damage tolerance control plan is the requirement for early trade studies for design concepts/material/weight/performance/cost. These trade studies are critical to defining cost versus requirement (e.g., weight impact versus inspection interval).

Analysis and Test Requirement. Schematics for damage tolerance are shown in Figures 12 and 13. Particular emphasis is placed on establishing correlation between analytical predictions and test measurements for growth of cracks in critical areas. Refined analysis models that predict the stress state at and away from the surface as well as multiple cyclic tests of coupons, subcomponents and full scale components in the presence of initial damage are required. As with the overall ENSIP development philosophy, damage tolerance analysis and tests are conducted early with minimum impact. Test requirements included speciment tests to define basic materials fracture data (i.e., K_{IC}, Kc, K_{ISCC}, da/dn), subcomponent tests to evaluate crack growth at typical critical features (i.e., boltholes, fillet radii, snaps, etc.), spin pit test of full scale components (e.g., disks, spacers, etc.) and engine test of pre-flawed components. Typical test configurations and imperical data are shown in Figures 14 - 17. Verification requirements also include engine test with components that are pre-flawed or cracked in critical locations to determine the effects of the "real" environment (temperature and gradient, vibration, etc.). Such tests must be closely controlled and monitored using the inspection requirements planned for service engines to assure safety of the test engine.

Non-Destructive Evaluation (NDE) requirements are implemented on fracture critical parts during manufacture and during field/depot inspection to protect safety. Specific inspection requirements are derived via design analysis tradeoffs between initial flaw size assumption, stress level, and material properties for a given usage (stress environment spectrum). As discussed in the section on initial flaw size, a flaw size assumption less than 0.030 inch surface length requires implementation of enhanced NDE (i.e., eddy current). The ability of eddy current to reliably detect surface flaws down to 0.005 inch depth has been demonstrated in several applications. Primary emphasis on use of eddy current is for stress concentration areas where a small flaw size assumption is required to achieve the required residual life without excessive weight penalty. Typical probability of detection data for eddy current is shown in Figure 18. A summary of eddy current inspection requirements for Air Force engines is shown in Figure 19.

In general, Fluorescent Penetrant inspection (FPI) is specified for areas requiring 0.030 inch surface length or larger to achieve the required residual life. The ability of current FPI processes in common use today to reliably detect .030 inch flaws is not clear. Therefore, in some instances, eddy current may be specified for large areas if susceptibility data indicates the need. Data generated on numerous demonstration programs clearly indicates that the FPI process can be significantly improved over that in gneneral use today via implementation of upgraded training, equipment and procedures (proper cleaning including etch, hydrophilic emulsifier and wet developer). These demonstration programs have been conducted on several Air Force/Industry engine development programs (F100, F101, F110) and laboratory technology programs (Air Force Wright Aeronautical Laboratories). Some typical detection improvements that have been demonstrated for upgraded FPI processes is shown in Figure 20. The critical need is to implement the best FPI process within industry and within the Air Force logistics centers since FPI will remain to be the most widely used method to inspect large areas for crack like damage.

Another critical NDE need is to quantify the POD of ultrasonics to detect imbedded defects in bulk volumes and to develop inspection methods for finished shapes. Very limited data indicates that reliable detection limits may be as large as 2000 square mils (i.e., approximately equal to a planar disc of 3/64 inch diameter). The goal is to develop and implement ultrasonic inspection methods such that a residual life equal to 2X the required life or inspection interval can be achieved assuming the largest undetectable flaw size without excessive impact on weight.

Retirement-for-Cause. Traditionally, components whose dominant failure mode is Low Cycle Fatigue (LCF) have been designed to a "crack initiation" criterion. Using this approach, only one component in a population of 1000 would have actually initiated a crack and the remaining 999 components would be discarded with substantial undefined useful life to crack initiation remaining. Figure 21 shows that the difference between the number of cycles to reach the "design allowable" curve and the population "average" curve for an "average" component would have consumed only 10% or less of its potential useful life-to-crack initiation. Under the initiation criterion, there is no way to utilize this potential life without accepting a higher probability or failure of the remaining components.

Under the Retirement-for-Cause (RFC), this additional useful life can be utilized by adopting a rejection criterion that uses each component in a population until it specifically initiates a crack rather than rejecting the entire population on the behavior of the statistical minimum. The development of fracture mechanics concepts over the last several years has permitted the degree of predictability for crack propagation rates necessary to implement such an approach on a safe basis.

The RFC concept would use the damage tolerance approach (shown in Figure 7) to life management. In using RFC as an operating system, all components would be inspected first at the end of a safety limit period divided by an appropriate safety margin and only those components containing detectable cracks equal to or greater than A_i would be retired or repaired. All others would be returned for additional service (with the assumption that if a flaw existed it would be smaller than A_s) or another inspection interval. In this way, the crack propagation residual life is continually reset to a safe value. By following this approach, components are only rejected for cause (cracks) and each component is allowed to operate for its own specific crack initiation life. It should be noted that if a crack is missed at the first inspection interval, another chance should exist to find a larger crack.

It is clear that not all fatigue-limited components may be handled in this way, and that each component must be evaluated individually to determine the economic feasibility of RFC. The inspection interval must be such that it does not place undue constraints on the operation of the component or that the cost of the necessary "tear-down" and inspection does not negate the advantage the life extension gained. It seems unlikely that RFC can be applied to components limited by high cycle fatigue considerations, but for many high cost components limited by LCF, such as engine disks, this approach does offer significant economic advantages.

It is also clear that in applying RFC, Non-Destructive Evaluation (NDE) becomes acritical factor. The crack length determines the residual life of the component and its detection is limited by the resolution and reliability of the inspection system employed. In many cases, the decision as to whether or not RFC can be applied to a component will be predicated upon the ability of available NDE approaches to detect initial flaw A_i with sufficient sensitivity and reliability. Because RFC procedure is based on damage tolerance concepts, the NDE techniques can be selected, refined, and focused on a particular local area than attempting to critically inspect large areas.

In 1986, the United States Air Force will implement RFC on the F100 engine which powers both the F-15 and F-16 fleets. Figure 22 shows the anticipated cost savings for the remaining life of these weapon systems.

CONCLUSIONS

Damage tolerance requirements are major tools in the Engine Structural Integrity Program to increase safety, readiness, and reduce life cycle costs. Non-destructive Inspection methods are making rapid advances, particularly eddy current techniques for focused inspections. Development efforts have identified process improvements that can be implemented to improve FPI flaw detection reliability for large area inspections. Damage tolerance design permits the use of Retirement-for-Cause (RFC) maintenance philosophy on costly engine components which will reduce overhaul costs.

REFERENCES

Tiffany, C. F., Cowie, W. D., The American Society of Mechanical Engineers (ASME), "Progress on the ENSIP Approach to Improved Structural Integrity in Gas Turbine Engine/An Overview", August 30, 1978, 78-WA/GT-13; was presented at the Winter Annual Meeting, San Francisco, California, December 10-15, 1978.

Cowie, W. D., Stein, T. A., The American Institute of Aeronautics and Astronautics for publication (AIAA), "Damage Tolerant Design and Test Considerations in the Engine Structural Integrity Program"; was presented at the propulsion session of the 21st Structures, Structural Dynamics, and Materials Conference in Seattle, Washington on 12-14 May 1980.

- IT IS UNREALISTIC (AND CAN BE DANGEROUS) TO ASSUME DEFECT-FREE STRUCTURE IN SAFETY OF FLIGHT COMPONENTS
- CRITICAL PARTS (& PART DETAILS) AND POTENTIAL FAILURE MODES MUST BE IDENTIFIED EARLY AND APPROPRIATE CONTROL MEASURES IMPLEMENTED
- INTERNAL THERMAL & VIBRATORY ENVIRONMENTS MUST BE IDENTIFIED EARLY IN THE ENGINE DEV
- PREDICTED ANALYTICAL STRESSES MUST BE VERIFIED BY TEST FOR COMPLEX COMPONENTS
- MATERIALS & PROCESSES MUST BE ADEQUATELY CHARACTERIZED (PARTICULARLY, THE FRACTURE PROPERTIES)

Figure 1 - Specific Lessons Learned

- DESIGN STRESS SPECTRA, COMPONENT TEST SPECTRA, AND FULL SCALE ENGINE TEST SPECTRA MUST BE BASED ON THE ANTICIPATED SERVICE USAGE OF THE ENGINE. (I.E., ACCELERATED MISSION RELATED TESTING)
- POTENTIAL ENGINE/AIRFRAME STRUCTURAL INTERACTIONS MUST BE DEFINED AND ACCOUNTED FOR
- CLOSED LOOP FORCE MANAGEMENT PROCEDURES MUST BE DEFINED AND ENFORCED
  - REALISTIC INSPECTION AND MAINTENANCE REQUIREMENTS
  - INDIVIDUAL ENGINE TRACKING PROCEDURES
  - DEFICIENCY REPORTING
  - UPDATES IN PROCEDURES BASED ON ACTUAL USAGE

Figure 1 (Continued) - Specific Lessons Learned

TASK I	TASK II	TASK III	TASK IV	TASK V
DESIGN INFORMATION	DESIGN ANAL MAT'L CHARACT & DEV TESTS	COMPONENT & CORE ENGINE TESTS	GROUND & FLIGHT ENGINE TESTS	ENGINE LIFE MANAGEMENT
DEVELOPMENT PLANS • ENSIP MASTER • **DURABILITY & DAM TOL CONTROL** • **MAT'L & PROCESS CHARACTERIZATION** • CORROSION PREV & CONTROL • INSPECTION & DIAGNOSTICS OPERATIONAL RQMTS • DESIGN SERVICE LIFE & DESIGN USAGE RQMTS • DESIGN CRITERIA	• DESIGN DUTY CYCLE • **MATERIAL CHARACTERIZATION** • **DESIGN DEV TESTS** • **STRUCTURAL/ THERMAL ANALYSIS** • INSTALLED ENGINE INSPECTABILITY • **MFG AND QUALITY CONTROL**	COMPONENT TESTS • STRENGTH • VIBRATION • **DAMAGE TOLERANCE** • DURABILITY CORE ENGINE TESTS • THERMAL SURVEY • VIBRATION STRAIN & FLUTTER BOUNDARY SURVEY	GROUND ENGINE TESTS • STRENGTH • **DAMAGE TOLERANCE** • ACCELERATED MISSION TEST (AMT) • THERMAL SURVEY • VIBRATION STRAIN & FLUTTER BOUNDARY SURVEY FLT ENGINE TESTS • FAN STRAIN SURVEY • THERMAL SURVEY • INSTALLED VIBRATION • DETERIORATION	• UPDATED ANALYSES • **STRUCTURAL MAINTENANCE PLAN** • OPERATIONAL USAGE SURVEY • INDIVIDUAL ENGINE TRACKING • **DURABILITY & DAMAGE TOLERANCE CONTROL ACTIONS (PRODUCTION)**

Figure 2 - ENSIP Tasks with Damage Tolerance Tasks Shaded

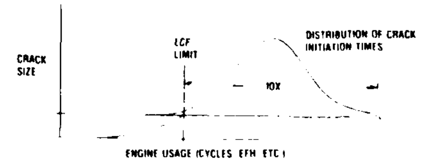

CRITERIA	LOW CYCLE FATIGUE (LCF) LIMIT BASED ON LOWER BOUND (-3σ OR 1/1000) DISTRIBUTION OF CRACK INITIATION TIME
ACTION	100% PART REPLACEMENT AT LCF LIMIT
CONCERNS	NO RECOGNITION OF IMPACT INITIAL DEFECTS CAN HAVE ON TOTAL PART LIFE (PART FAILURE CAN OCCUR PRIOR TO LCF LIMIT)
	MAJORITY OF PARTS MAY BE DISCARDED PRIOR TO REACHING THEIR INDIVIDUAL CRACK INITIATION TIME (I.E., IF LCF LIMIT IS LESS THAN FULL LIFE)

Figure 3 - Conventional Approach to Life Management of Cyclic Limited Engine Components

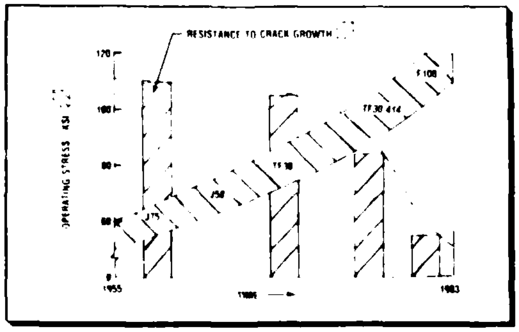

Figure 4 - Some Material Trends

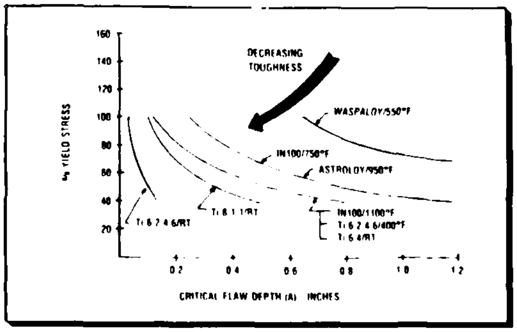

Figure 5 - Some Material Trends

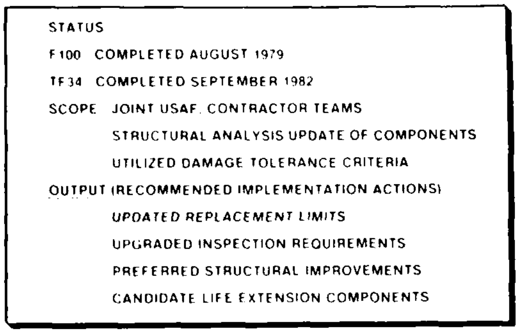

STATUS

F100 COMPLETED AUGUST 1979

TF34 COMPLETED SEPTEMBER 1982

SCOPE JOINT USAF, CONTRACTOR TEAMS

STRUCTURAL ANALYSIS UPDATE OF COMPONENTS

UTILIZED DAMAGE TOLERANCE CRITERIA

OUTPUT (RECOMMENDED IMPLEMENTATION ACTIONS)

UPDATED REPLACEMENT LIMITS

UPGRADED INSPECTION REQUIREMENTS

PREFERRED STRUCTURAL IMPROVEMENTS

CANDIDATE LIFE EXTENSION COMPONENTS

Figure 6 - Engine Durability and Damage Tolerance Assessments

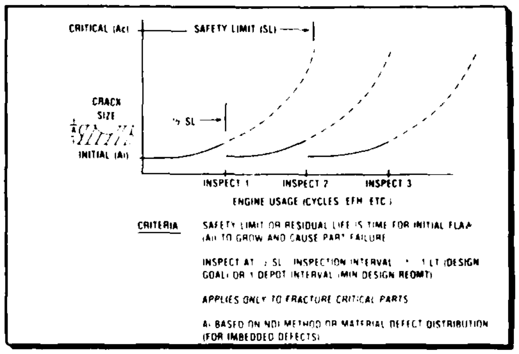

CRITERIA SAFETY LIMIT OR RESIDUAL LIFE IS TIME FOR INITIAL FLAW (Ai) TO GROW AND CAUSE PART FAILURE

INSPECT AT ½ SL INSPECTION INTERVAL [illegible] 1 LT (DESIGN GOAL) OR 1 DEPOT INTERVAL (MIN DESIGN REQMT)

APPLIES ONLY TO FRACTURE CRITICAL PARTS

Ai BASED ON NDI METHOD OR MATERIAL DEFECT DISTRIBUTION (FOR IMBEDDED DEFECTS)

Figure 7 - Damage Tolerance Approach to Life Management of Cyclic Limited Engine Components

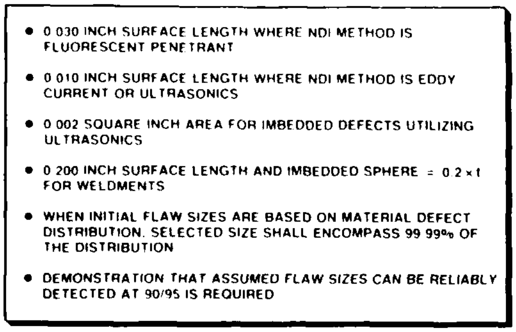

- 0 030 INCH SURFACE LENGTH WHERE NDI METHOD IS FLUORESCENT PENETRANT
- 0 010 INCH SURFACE LENGTH WHERE NDI METHOD IS EDDY CURRENT OR ULTRASONICS
- 0 002 SQUARE INCH AREA FOR IMBEDDED DEFECTS UTILIZING ULTRASONICS
- 0 200 INCH SURFACE LENGTH AND IMBEDDED SPHERE = 0 2 × t FOR WELDMENTS
- WHEN INITIAL FLAW SIZES ARE BASED ON MATERIAL DEFECT DISTRIBUTION, SELECTED SIZE SHALL ENCOMPASS 99 99% OF THE DISTRIBUTION
- DEMONSTRATION THAT ASSUMED FLAW SIZES CAN BE RELIABLY DETECTED AT 90/95 IS REQUIRED

Figure 8 - Assumed Initial Flaw Sizes Used In Design

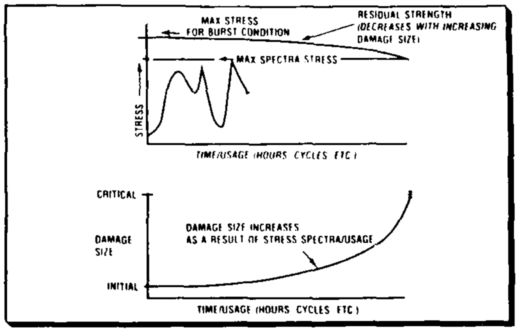

Figure 9 - The Residual Strength Requirement

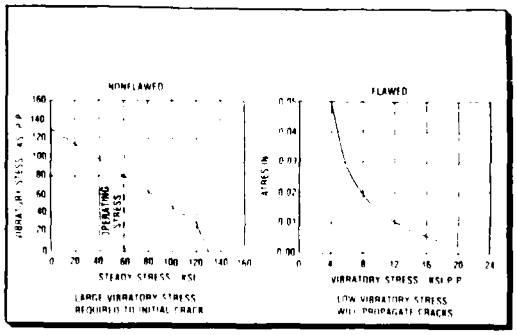

Figure 10 - Interaction of Vibratory Stress and Initial Flaws

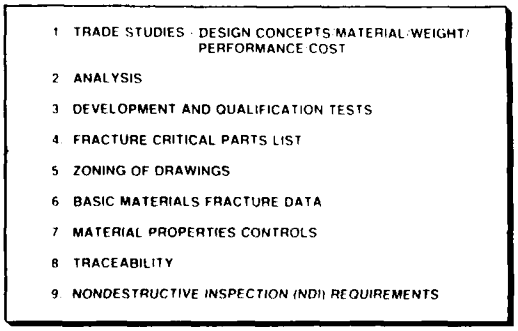

1 TRADE STUDIES - DESIGN CONCEPTS/MATERIAL/WEIGHT/ PERFORMANCE COST
2 ANALYSIS
3 DEVELOPMENT AND QUALIFICATION TESTS
4 FRACTURE CRITICAL PARTS LIST
5 ZONING OF DRAWINGS
6 BASIC MATERIALS FRACTURE DATA
7 MATERIAL PROPERTIES CONTROLS
8 TRACEABILITY
9 *NONDESTRUCTIVE INSPECTION (NDI) REQUIREMENTS*

Figure 11 - Tasks - Damage Tolerance Control Plan

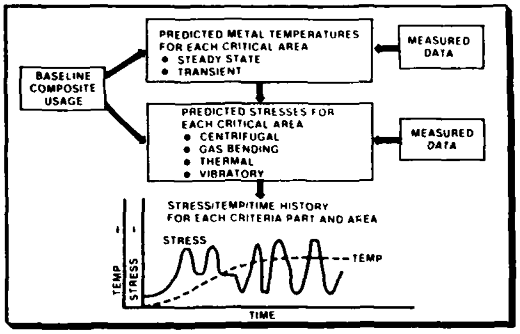
BASELINE COMPOSITE USAGE
PREDICTED METAL TEMPERATURES FOR EACH CRITICAL AREA
• STEADY STATE
• TRANSIENT
MEASURED DATA
PREDICTED STRESSES FOR EACH CRITICAL AREA
• CENTRIFUGAL
• GAS BENDING
• THERMAL
• VIBRATORY
MEASURED DATA
STRESS/TEMP/TIME HISTORY FOR EACH CRITERIA PART AND AREA
STRESS
TEMP
TEMP
STRESS
TIME

Figure 12 - Development of Stress Spectra

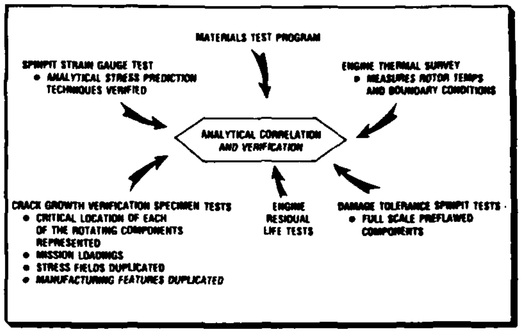
MATERIALS TEST PROGRAM
SPINPIT STRAIN GAUGE TEST
• ANALYTICAL STRESS PREDICTION TECHNIQUES VERIFIED
ENGINE THERMAL SURVEY
• MEASURES ROTOR TEMPS AND BOUNDARY CONDITIONS
ANALYTICAL CORRELATION AND VERIFICATION
CRACK GROWTH VERIFICATION SPECIMEN TESTS
• CRITICAL LOCATION OF EACH OF THE ROTATING COMPONENTS REPRESENTED
• MISSION LOADINGS
• STRESS FIELDS DUPLICATED
• MANUFACTURING FEATURES DUPLICATED
ENGINE RESIDUAL LIFE TESTS
DAMAGE TOLERANCE SPINPIT TESTS
• FULL SCALE PREFLAWED COMPONENTS

Figure 13 - Residual Life Analysis and Test Procedure

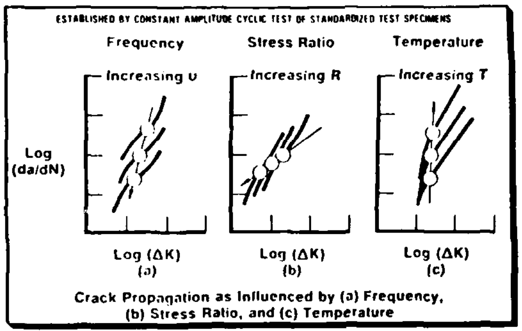

Figure 14 - Effects of Basic Variables

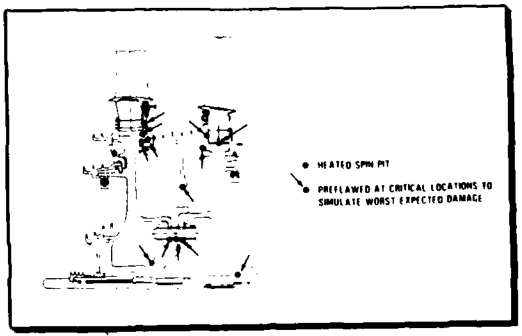
• HEATED SPIN PIT
• PREFLAWED AT CRITICAL LOCATIONS TO SIMULATE WORST EXPECTED DAMAGE

Figure 15 - Turbine Rotor Cyclic Spin Test

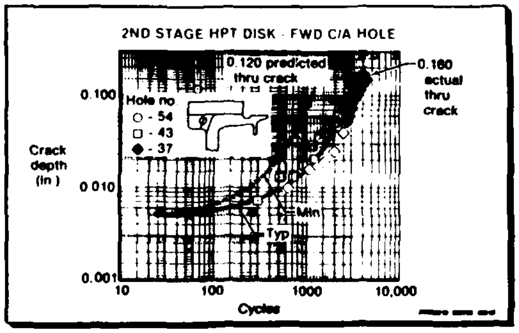

Figure 16 - Actual and Predicted Flaw Growth (Engine Test)

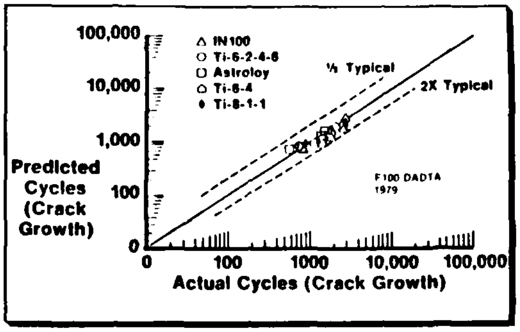

Figure 17 - Methodology Correlation (Specimens and Components)

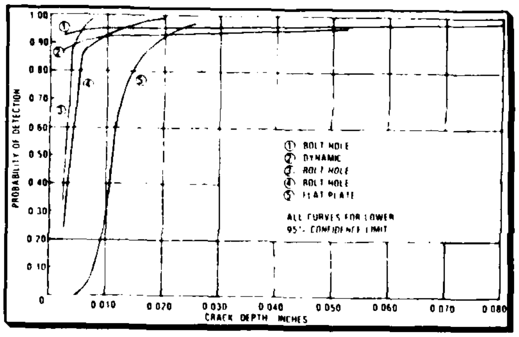

Figure 18 - Probability of Detection - Eddy Current

F100 ENGINE

EDDY CURRENT / DEPOT
EDDY CURRENT / PRODUCTION
FAN DISK CRYOGENIC PROOF TEST

TF34 ENGINE

EDDY CURRENT / DEPOT

F101 ENGINE

EDDY CURRENT / PRODUCTION
& DEPOT

FUTURE IMPLEMENTATIONS

F110
F109
ATFE

Figure 19 - STATUS - Implementation of Upgraded NDI Requirements (Includes FPI Improvements)

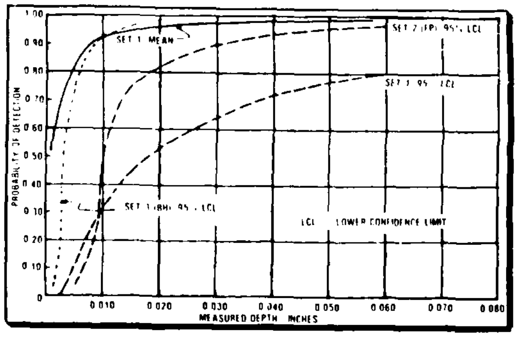

Figure 20 - Probability of Detection - Fluorescent Penetrant Inspection (FPI)

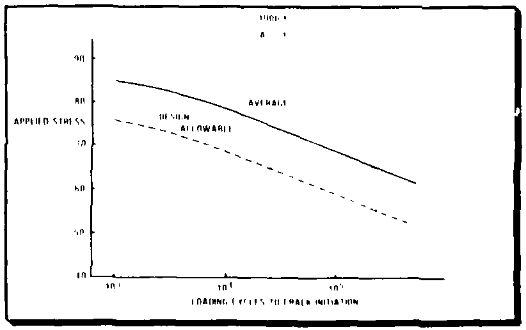

Figure 21 - INCONEL 718 S-N CURVE

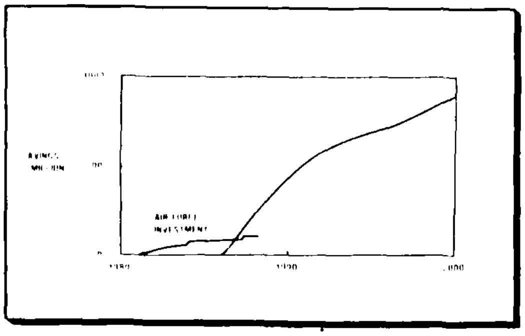

Figure 22 - Retirement For Cause Cost Savings

PARAMETERS THAT INPUT TO APPLICATION OF DAMAGE TOLERANCE CONCEPTS TO CRITICAL ENGINE COMPONENTS

by

D.W. Hoeppner, P.E., Ph.D
Cockburn Professor of Engineering Design and
Director, Structural Integrity, Fatigue, and
Fracture Research Laboratories
Department of Mechanical Engineering
University of Toronto
Toronto, Ontario M5S 1A4

after May 5, 1985 D. Hoeppner will become

Chairman and Professor
Department of Mechanical and Industrial
Engineering and
Director, Center for Design and
Materials Engineering
University of Utah
Salt Lake City, Utah 84112

ABSTRACT:

Numerous parameters affect the application of damage tolerance concepts to engine components. These parameters are reviewed in the paper in relation to overall integration of each parameter into the damage tolerance design methodology. Parameters such as initial crack size, "defect" level associated with the material and process, and model of the initial crack will be discussed as related to non-destructive inspection and modelling the discontinuity within a framework such as generalized fracture mechanics. Subsequent to characterization of the initial discontinuity or heterogeneity (d,h), or the likelihood of forming one in the service cycle, it is necessary to evaluate the potential for growth of a (d,h). Factors that affect the growth of a discontinuity in engines are: material, manufacturing route, stress magnitude, stress state, (uniaxial, biaxial, triaxial), residual stress, temperature, loading waveform, frequency of loading, loading spectrum, chemical environment. Furthermore, material properties of importance are thresholds of growth, fatigue crack growth behavior, and toughness. Numerous synergisms such as "creep-fatigue", "corrosion-fatigue", and fretting fatigue occur and must be considered. Evaluation of these parameters will be discussed, gaps identified and, an overall plan to integrate these into a safety critical component design methodology presented.

INTRODUCTION:

In 1920 Alan Griffith (1) published a paper that has become the basis for the modern theory of fracture mechanics. It is said by many who knew Dr. Griffith well that the theory was developed to help improve safety and durability of reciprocating engines that, allegedly, were failing at an alarming rate during and after, World War I. This theory also is the basis for this conference in a sense along with another of Dr. Griffith's contributions. Both Sir Frank Whittle (2) and Hayne Constant (3), among others review that Dr. Griffith wrote his theory of turbine design treatise in 1926, six years after his significant contribution to the physics of Materials Behavior (1). Griffith's contributions to gas turbine development until his death are well known. Here we are, forty five years after the former to review applications of damage tolerance concepts to gas turbine engines.

The "early pioneers" of gas turbine engines, such as Dr. Griffith, Mr. Whittle, Dr. Meyer (Brown-Baveri), Mr. Constant, Dr. Von Ohain, all were concerned with the early failures of discs, blades, shafts, bearings and other parts. As with most design innovations and evolution they (and their respective teams) were more concerned with getting the turbines to work - see Figure 1(4). This is always our first concern in design of a new system. In the case of gas turbines design modifications were introduced to deal with premature failures as they were encountered. As with almost all designs we find, subsequent to getting the system to work, that our assumptions, simplifications, oversights, naivete; all help to get us in serious difficulty. The right side of Figure 1 tells us that in design we then get into questions related to safety, reliability, durability, and integrity - the subject of this specialist meeting.

Before I begin the technical discourse I wish to express my thanks to the organizers of the conference and to the Structures and Materials Panel and Propulsion Panel of AGARD for asking me to give this lecture. As many of you know this subject is near to my spirit and heart and I am thus deeply honored and wish to formally say thanks. Inasmuch as I view my task as philosophical the paper presents concepts, discusses integration and synthesis of these concepts into a structural integrity (SI design system, and discusses needs for rather intensive research on the parameters involved to improve engine design for structural integrity. Other papers in this conference will present more specific details, in some cases with data, that complement this overview. Hopefully by the end of this brief two days everyone will have a clearer picture of how to deal with structural integrity, ENSIP and the right side of Figure 1.

THE FRAMEWORK OF STRUCTURAL INTEGRITY:

Figure 2(5) illustrates the important stages of structural integrity planning. Specifications written to precise technical requirements become the basis to implement SI technology and quality levels for control are established as early as feasible. At the beginning stages of SI planning, consideration is given to all of the following factors/parameters:

1) Stress, strain, loads, and temperature analysis,
2) Material selection,
3) Manufacturing processes,
4) Inspectability of component(s),
5) Maintainability,
6) Non-destructive inspection,
7) Material deformation and "failure" mechanisms,
8) Failure criteria,
9) Cracked component (fracture mechanics) analysis,
10) Fatigue design policy,
11) Wear design policy,
12) Creep design policy,
13) Corrosion design policy.

It is the job of teams of people, working through a well coordinated system, that all of these parameters/factors are considered in assuring damage tolerance through a structural integrity program such as ENSIP.

Inasmuch as this paper deals with parameters that input to damage tolerance it would be prudent to define these terms so all of us are using the same definition. A parameter is defined as:

1) An arbitrary constant whose value characterizes a number of a system; a quantity that describes a statistical population.

2) Any of a set of physical properties whose values determine the characteristics or behavior of something.

3) A characteristic element or factor.

In this paper definition 3 and/or 2 are considered. DAMAGE, means loss due to injury or harm, is rather nebulous and thus it will have to be defined more precisely. In relation to structural integrity it has become clear that damage should be trackable; i.e. at any time some physical measurements could be taken such that it could be determined whether "DAMAGE" has in fact occurred. Furthermore, in combination with the measurement(s) various analyses could be conducted to assess the likelihood of an undesirable event (such as fracture) occurring. This is depicted conceptually in Figure 3. It should be pointed out that damage (e.g. cracks) in many metals takes on the nature of highly discontinuous (tortuous) crack growth if they are preferentially oriented/anisotropic. Many gas turbine materials; particularly blades and single crystals, disc alloys, and welds present many problems related to "DAMAGE" analysis. In SI planning it is essential that we have both correlative and predictive tools. These should always be used in conjunction with each other and the industry accumulated experience. It is important to keep this in mind since we don't know everything to be as predictive as we would like.

Many of the elements that input to Damage Tolerant Design are shown in Figure 4(5). It is obvious that I cannot go into every one of the items shown in the figure. Rather, in this paper I will relate to the concepts involved in evaluating each of the elements shown. The need for a systematic approach cannot be overemphasized at this point. As with all component designs the process begins by considering all four of the following:

1) Material Behavior and Processing,

2) Force/Load/Deflection/Temperature determination that inputs to stress, strain, and/or stress intensity analysis,

3) Failure criteria, where the failure criteria are defined explicitly,

4) Inspection and monitoring to establish the state of the material/component/system.

In stress analysis, and the concomitant materials characterization to lead to configurational design, most components are analyzed initially as if they were crack-free, homogeneous, and continuous. This is mathematically convenient although often not correct. As is well known this very assumption of the mathematical theory of elasticity has provided extreme resistance to Griffith's concept (1), ENSIP and damage tolerant philosophies in general. The safe-life concept of design, and particularly fatigue design of gas turbine components, evolved to support this perspective. However, from a sampling of reality, as well as Griffith's theory and reasonable grounding in materials and their methods of manufacture/assembly it is clear that one of the major hypotheses of the Griffith theory (1), i.e. that all materials contain inherent discontinuities (d) and heterogeneities (h) and at times they can be crack-like (cld, clh), is true. Then, using modifications and extensions of Griffith's concepts (modern "Fracture Mechanics") it is possible to conduct cracked-body analysis. Since a crack is one form of damage manifestation another world of analysis becomes possible and this is one of the important aspects of damage tolerant based design.

The left column on Figure 4 shows methods by which a (cld) can be formed, given one (or more) are not present initially. On the other hand, if one is there initially then only the later three columns on Figure 4 are necessary. Nonetheless, the SIP must permit all of the elements shown to be dealt with in some manner as part of the damage tolerance evaluation. Inasmuch as all of the items shown in Figure

4 provide a rather broad design challenge I am going to tone it down a bit for this paper. Since fatigue is a large enough subject, I am going to use it as the process to unfold the concepts and discussion. In the last part of the paper I will return to synergisms between cyclic loading and some of the other processes. It will also become clearer why fatigue was picked for other reasons as well.

FATIGUE DESIGN POLICY:

Although economic/time, functional, and aesthetic constraints frequently provide the limit for fatigue design of gas turbines (as well as most other components) those of us who are idealists would like to think that some sort of Fatigue Design Policy would guide the fatigue design process. An example of this is shown in Figure 5. The first dilemma we are confronted with is the concept of safe-life fatigue design or damage tolerant fatigue design. (A recent U.S.F.A.A. workshop on fatigue design of engine discs reviewed this aspect (6)).

At one of the precursors to this meeting two papers were presented that discussed some aspects of this dilemma (7,8). Furthermore, reference 5,6 and 9 discuss other aspects of this dilemma. Basically the dilemma has traditionally revolved around whether to assume crack-free material or cracked material. This aspect also has bveen described by Alexander (10), and Jeal (11), as well as others, related to gas turbine components.

The philosophies, as applied to aircraft fatigue design particularly, are summarized as follows:

STRUCTURAL FATIGUE DESIGN PHILOSOPHIES

SAFE-LIFE DESIGN:	Require analysis or testing to show that the probability of any failure is "Extremely remote" for the assumed life of the structure; finite life or "Infinite" life; no cracks.
DAMAGE TOLERANT (including FAIL-SAFE) DESIGN:	Require a damaged structure to continue satisfactory performance until "Damage" is discovered and remedial action complete. . Critical Components (Areas on Components), . Multiple Load Paths (Redundancy), . Crack Stoppers, . Proof Testing, . Crack Growth Prediction Techniques, . Inspection (Types).

The details of the safe-life concept are summarized in (12). Damage tolerance considers all the elements of Figure 4 including the left column, which, as indicated earlier deals with the details of damage formation and damage propagation (for the remainder of the discussion the aspects of crack formation and crack propagation will be emphasized). Conceptually this is presented in "simple" form in Figure 6. This figure forms the basis of much of the following discussion and thus should be thoroughly scrutinized and comprehended before proceeding.

DAMAGE TOLERANT DESIGN:

At the AGARD propulsion panel meeting last year A. Mom provided an overview of AGARD SMP activities and, in a sense, compared safe-life and the damage tolerant approach (13). His presentation stimulated a a great deal of discussion related to the concept of damage tolerance compared to safe-life. Many of the old misconceptions came out - as they have in other areas of activity. Similar discussions took place when ASIP was developed, as pointed out recently by U. Goranson (14) and T. Swift (15,16).

When damage tolerance considerations are made it is by far easiest to consider, either by knowledge or assumption, that a crack-like discontinuity already exists. Then, we need to only deal with the three right columns of Figure 4. Even dealing with these is a large challenge however, because we need to know all of the following parameters to accurately conduct the damage tolerant design:

A) Failure Criteria - end of life, risk analysis.

B) Crack - size, location in stress field, type, location with respect to inspection, potential mode of extension (I,II,III or other), crack size with respect to microstructure. Do continuum assumptions apply?

C) Forces/Loads/Deflections/Temperatures - magnitude, direction, state (uniaxial, multiaxial), type - monotonic, sustained, cyclic, spectra, waveforms, phasing between force and temperature cycling (in-or out of phase).

D) Subcritical/Critical Crack Growth Response of Material and component - crack growth rates for conditions of interest, transfer functions (similitude), toughness (instability parameter), mechanisms of extension for materials of interest, predictability from "models". Considerations of environment, waveform, spectra, and frequency are essential here.

All of these above aspects are part of a general damage tolerant design and are noted within Figures 4,6. Discussion on each of the above is presented in the following subsections.

A) Failure Criteria:

The failure criterion is an implicit portion of the fatigue design philosophy and regrettably is not taken seriously by most engineers/scientists. For example, in fatigue design of gas turbines many "designers" have considered that they design for "initiation". The 'stages" of fatigue often have been characterized by two parts as follows:

$N_t = N_i + N_p$ where: (1)

N_t is to be total life for a given failure criteria,

N_i is the cycles to "initiation", actually this is cycles to crack detection but has frequently been mistated by the community,

N_p is the "cycles of propagation" of cld's.

Even though formulation one is simplistic it does not appear to present a clear picture in relation to the models needed for predictability. In the later 1960's and early 1970's it was decided other ways to divide the process were required and these divisions could relate to the process of fatigue, the micromechanics and macromechanics, the mechanics models to be used for prediction, and our understanding (or lack thereof). This has recently been reviewed elsewhere (8,12,16,17). The essence of these divisions is contained in Figures 7 and 8. Figure 7 relates to Figure 4. The four divisions of Figure 7 should be self-explanatory. Figure 8 simply indicates that the number of cycles to any time (ΔN_x) is a parametric relationship with all of the factors listed. This will make our challenge very great as we try to develop models for "prediction" of life.

If we can always state the failure criteria (fracture, crack detection, crack propagation of some amount, deflection, etc) it would seem our job will be simplified a great deal. Furthermore, when this is done, and if crack detection is a failure criterion then it becomes obvious that inspection must be coupled with any damage tolerance program (this is depicted in Figure 9) and discussed in (5,9,14-16). In addition, the paper following this one will undoubtedly cover this aspect in great detail. As indicated by A. Mom (13) the coupling of inspection to fatigue design is required for either damage tolerant design or safe-life ("initiation" based) designs. In damage tolerant design this requirement is obvious. Apparently in safe-life design it is not so obvious to people. Figure 10 attempts to illustrate why inspection is important in safe life design. If, as shown in the lower portion of the figure, the critical crack size (determined by toughness/final fracture criteria/loads) becomes approximately equal to or smaller than the "first crack" detectability size then fractures occur. Due to the evolution of gas turbine design philosophy this has been, and currently often is, the case (6-8,10).

B) The Crack:

Inasmuch as item B will be discussed extensively by other speakers it will not be covered here. The entire concept of inspection must be factored into fatigue design in all cases to assure that the boundary conditions used in any life prediction are met. If one wishes to use one of the four fracture mechanics formulations shown in Figure 11 then the crack(s) must be characterized as completely as feasible.

C) Forces/Loads/Deflections/Temperatures:

The gas turbine design community has expended significant effort on this area for obvious reasons. In my own view the effort has often been disproportionate to our knowledge of material bvehavior and items A,B, and D in this discussion. This is not to say this area is unimportant because it is very important. If we consider for a moment what are the minimal requirements for sustained load and cyclic loading (fatigue) as depicted in Figures 12 and 13 respectively it is obvious why we must know as much about these parameters as feasible. While we know a great deal about how to analytically model to calculate forces, and in recent years have become more and more proficient at engine force/load monitoring, it is another matter to know how to use the loads in life prediction related to item D and the synthesis into a damage tolerant life prediction methodology. T. Swift (9,15) has discussed the importance of this field and T. Cruse (6) has emphasized its importance for gas turbines. This aspect will be addressed further in this conference by G. Asquith in general and A. Mom/L.ten Haave related to TURBISTAN. The numerous aspects to be considered in relation to the load and its interaction with/on the material is a fascinating - as well as frustrating field (Figure 12 and 13). The aspects of thermomechanical fatigue, which in a sense results from combining the two figures, will be discussed more by G. Harrison and T. Edmonds in this conference. In addition, R. Bill (18,19) has presented the results of two workshops on thermomechanical fatigue held at NASA-Lewis recently. This aspect must receive a great deal more attention as we improve our gas turbine designs - with either philosophy.

In damage tolerant design we not only need the loads etc.to design the components but to use them to establish material/component subcritical crack growth characteristics.

D) Subcritical Crack Growth and Critical Crack Growth of Materials/Components:

With guidance from all of the first three areas this area becomes essential to successful implementation of damage tolerance. As with A-C above this area is full of misconceptions and great challenges - partly because the knowledge of B and C dictate a great deal of what can and must be done in this area. The procedure for subcritical crack growth using fracture mechanics based methods has been outlined on numerous occasions - see for example (5,8,9,12,14-17). As discussed in all of these references the following are necessary for satistactory provision of the required information:

1) Subcritical crack growth characteristics of material for conditions of interest, consider:

Proper fracture mechanics model, LEFM, EPFM, load spectra effects including waveform, environmental effects, stress state effects, temperature (tmf), data analysis, presentation, and test standards.

2) Understanding of material crack propagation so proper models can be formulated and used.
3) Boundary conditions.

4) Critical crack growth characteristics.

The above items are summarized in Figures 14,15 and were developed in conjunction with R. Jeal over the past 13 years. These two figures can be used as a guide and forthcoming papers in the International Journal of Fatigue will discuss them extensively. However, in the generation of subcritical crack growth data for use in damage tolerant design it is essential that less emphasis be given to the fitting of data unless it is for very specific conditions. Many people still believe there is a single fitting function such as the Paris relation that works everywhere - this is not the case (see 9,12,14-17,20,21). Swift(9) and this writer (16), as well as others, have recommended that actual fatigue crack growth data be integrated to obtain either inspection intervals or total life for subcritical crack growth.

In order to successfully implement these data in design many items are required that we currently have little information on. Some of these items are:

1) Boundary between region 2-3 in Figure 14.

2) Mechanics based method to describe crack growth in region 2 of Figure 14 (see 12, 22-29).

3) Details of formation of cld in region 1 (see 12, 22) for gas turbine materials.

4) Effects of Spectra. Dwell (see Larsen 21,25,29 and the TURBISTAN discussion of this conference) effects.

5) Multiaxial effects on crack growth.

6) TMF effects.

All of the above items must be known to the extent feasible for successful implementation of damage tolerance.

SUMMARY:

The conceptual damage tolerance considerations to be used are shown in Figure 16. The items shown assume we are in areas of Figure 14 where the appropriate models apply. Thus, it is clear that Figure 16 mainly is concerned with Figure 14 region 3 as long as plasticity effects are not too large to violate the appropriate assumptions. Regions 1 and 2 of Figures 14/15 obviously require a great deal more information before we can confidently exploit damage tolerant design to assure life and durability. Kolf(30) undoubtedly knew this when he wrote "However, durability or life is not readily determined during development and remains a promise to be designed into the engine to achieve the life requirements and reasonable cost of ownership". In order to fulfill the promise we are going to have to collectively work very hard on all the items discussed no matter what philosophy we use. However, the Damage Tolerant Philosophy provides the philosophical basis for a rational design philosophy because it emphasizes trackable damage. The safe-life concept does not offer this advantage on a philosophical basis. However, one can always say, in design of gas turbine components as well as others, design will be for no-cracks and the detection of a defined crack constitutes failure as explicitly defined. On economic, as well as safety, grounds this does not appear prudent. The following section presents some recommendations related to this presentation.

RECOMMENDATIONS:

Throughout the text many of the requirements for information were noted. Some of the major requirements are presented in this section. It must be emphasized that additional insights are required on each of the areas cited. To overemphasize certain areas at the expense of others will undoubtedly create difficulties. It is not clear to me how priorities can realistically be established. This does give us the advantage (as many generals are quoted as claiming) of attacking on all fronts.

Inspection:

I am sure Mr. Taylor will address this issue extensively. It is clear from many works, particularly encouraged by USAF to develop both ASIP and ENSIP, that improvement in inspection at all levels offers real improvement. While this improves our damage tracking and "quality" assessment capability it does not, however, solve the problem. It only provides a tool to keep track of things being there or not there. We must improve our capabilities here but not lose perspective on its importance.

Material Behavior and Process Control:

These are areas that need very much more attention under the context of ENSIP and to improve gas turbine design in general (31). Regions one and two are very much dominated by our collective knowledge in these areas and it is very inadequate at present. Better understanding of crack formation by fatigue, creep, corrosion, fretting, and "anomalous" behavior is essential to develop physics based models, improve materials, develop standard evaluation procedures (e.g.TURBISTAN), develop improved methods; and to know the boundary conditions that relate to application of the models. Improvements in understanding crack growth when cracks are small with respect to structure are essential (7,8,12,17,22,32) to improve models for life prediction, materials and processing improvements for improved crack propagation resistance. Better understanding of crack growth for EPFM or FPFM (elastic-plastic fracture mechanics) is essential.

The roll of dwell effects must be researched and understood much better in future. Also, stress state considerations in uncracked and cracked body design are not understood well at this stage. Finally, the role of thermomechanical aspects must be understood better to improve tmf life estimation.

Coupled to all of the above is the need for a data compilation and collection for gas turbine engine materials. Also, greater effort must be expended on standard test methods for materials characterization. Many of these aspects already are underway within AGARD, several companies, and under the auspices of military agencies. Undoubtedly this meeting will lead to expanded activity and discussion.

Loads and Temperature Monitoring:

This aspect was discussed at the Propulsion panel meeting in the Netherlands last year as well as ion previous AGARD activities. There is no doubt that this area has improved in recent years and further improvements are forthcoming.

Analysis:

The development of computer hardware and software has outstripped our knowledge related to inspection, materials behavior, rational models, processing effects, data generation techniques and methods developments. Undoubtedly further progress is needed here but greater emphasis is needed to improve the materials behavior - mechanics interfaces before improved analysis will get us far in improving damage tolerance capability. It probably need not be said, but emphasis on analysis and model development when cracks are short with respect to structure or when cracks are propagating in highly anisotropic elements is essential to progress.

Continued work on systematic integration of all of these parameters is essential but the damage tolerant design philosophy provides a framework for this to occur. Even so, many of us find this all so complex at times we try to revert to "no cracks".

ACKNOWLEDGEMENT:

I am indeed grateful to the planners of this specialist meeting for asking me to present this keynote lecture. It is always much easier to deliver a research result or new model than to provide a small overview into this challenging problem and I am grateful for the opportunity provided to attempt to do it. Many people have provided me both spiritual and emotional support during the many years that even make this possible. My special thanks to Sue, my wife, Laura, Lynne, and Amy (my daughters) for encouragement and insights. Nothing like this could be attempted without a very competent secretary I have a super one. Thanks to Janet Lambert. Also, my appreciation to all my friends and "students" who have encouraged me to go ahead.

REFFRENCES:

1. Griffith, A.A., "The Phenomena of Rupture and Flow in Solids", Philosophical Transactions of the Royal Society, vol. 221 A (1920), p. 163-198.
2. Whittle, F., "The Early History of the Whittle Jet Propulsion Gas Turbine", The First James Clayton Lecture, Institution of Mechanical Engineers, 1945, vol. 152, pp 419-435.
3. Constant, H., "The Early History of the Axial Type of Gas Turbine Engine", Institution of Mechanical Engineers, Proceedings, vol. 153, 1946, pp 411-440.
4. Hoeppner, D.W., Structural Integrity Principals to Engineering Design, Wiley-Interscience, to be published.
5. Hoeppner, D.W., Ekvall, J., McCammond, D., Poon, C., Venter, R., Aircraft Structural Fatigue - Vol. I, II, III, University of Toronto lecture notes prepared for courses delivered to U.S. Federal Aviation Agency. Presented 7 times between 1979-1984. To be presented at U. of Utah.
6. Salvano, D., Compilation of presentations from different portions of Aerospace Industry on Damage Tolerance, FAA Meeting, March 12/13, 1984, Burlington Mass.
7. J.A. Harris, Jr., C.G. Annis, M.C. Van Wanderham, D. Sims, "Engine Component Retirement for Course", paper No 5 in AGARD-CP-317, Proceeding of Conference on Maintenance of High Temperature Parts in Service, January 1982.
8. R. Jeal, "Defects and Their Effect on the Behaviour of Gas Turbine Discs", paper No 5, ibid-(ref.7).

9. T. Swift, "Verification of Methods for Damage Tolerance - Evaluation of Aircraft Structures to FAA Requirements", ICAF Symposium 12 proceedings, Doc No. 1336, Toulouse, France Mar 25-27,1983, paper 1.1.

10. J.D. Alexander, "Design Philosophy for Engine Forgings", Forging and Properties of Aerospace Materials, The Metals Society, London, pp 1-8.

11. R.H. Jeal, "Relationship Between Fatigue Modelling and Component Integrity", Presented at Conference on Fatigue Thresholds held at Birmingham, England, 1984 to be published.

12. D.W. Hoeppner, "Estimation of Component Life by Application of Fatigue Crack Growth Knowledge", Fatigue, Creep, and Pressure Vessels for Elevated Temperature Service, MPC-17, ASME, NY, NY, 1981. pp 1-84.

13. A. Mom, "Overview of the AGARD SMP Activities on Turbine Engine Materials Technology in the 1972-1982 Period", paper No 5, AGARD-CP-368, Conference Proceedings on Engine Cyclic Durability by Analysis and Testing held at Lisse-Netherlands, 1984.

14. U. Goranson, J. Rogers, "Elements of Damage Tolerance Verification", Paper 1-8, ICAF, Twelfth Symposium, Toulouse, France, May 1983.

15. T. Swift, "Annual Fatigue Lecture ASTM E-9 Committee - Airworthiness Certification for Fatigue - the Changing Scene", Charleston S.C., March 20, 1985.

16. Hoeppner, D.W., Krupp, W.E., "Prediction of Component Life by Application of Fatigue Crack Growth Knowledge", Engineering Fracture Mechanics, vol. 6, 1974, pp 47-70.

17. D.W. Hoeppner, "Application of Damage Tolerance Concepts to Short Cracks in Safety Critical Components", ICAF No. 12, paper No 2-1, Toulouse, France, May 25-27, 1983.

18. R. Bill, Personal communication summarizing TMF workshop 1 held at NASA-Lewis, Sept 21-22, 1983, NASA Lewis letter ref. 5221, Dec 12, 1983.

19. R. Bill communication on TMF workshop 2 held at NASA-Lewis, Nov. 15,16, 1984.

20. G. Bowie, D.W. Hoeppner, "Numerical Modelling of Fatigue and Crack Propagation Results", Computer Simulations for Materials Applications, Nuclear Metallurgy, vol. 20 part 2, p 1171-1178.

21. J.M. Larsen, T. Nicholas, "Cumulative Damage Modelling of Fatigue Crack Growth", Paper No. 9. AGARD-CP-368, Conference Proceedings on Engine Cyclic Durability by Analysis and Testing, Lisse, Netherlands, May/June, 1984, AGARD (1984).

22. D.W. Cameron, Perspectives and Insights on the Cyclic Load Response of Metals, Ph.D. Thesis, Dept. of Mechanical Engineering, U. of Toronto, 1984.

23. K.S. Chan, J.E. Hack, G. Leverant, "Fatigue Crack Propagation in Ni Base Superalloy Single Crystals Under Multiaxial Cyclic Loads", to be published.

24. D. Wu, D. Hoeppner, "Observations and Characterization Considerations of Fatigue Crack Growth in a Single Crystal Nickel-Base Superalloy", to be published in April 1985 issue of Scripta Metallurgica.

25. P. Sooley, An Investigation of the Fatigue Crack Growth Rate Characteristics of Titanium Alloy IMI 829, Ph.D. Thesis, Dept. of Mechanical Engineering, U. of Toronto, Available from D.W. Hoeppner or P. Sooley in August 1985.

26. M. Hicks, C. Brown, "Short Fatigue Crack Growth Behaviour of Titanium Alloy IMI 685", International Journal of Fatigue, July 1982, pp 167-169.

27. S. Missana, A New Apparatus for Making In-Situ Observations of the Fatigue Process in Metals, MASc Thesis, Dept. of Mechanical Engineering, U. of Toronto, 1983.

28. D. Wu, D. Hoeppner, "Fatigue Crack Growth in a Single Crystal Nickel-Base Superalloy", submitted to Nineteenth Symposium on Fracture Mechanics (1986).

29. J.T. Ryder, D.E. Pettit, W.E. Krupp, D.W. Hoeppner, Evaluation of Mechanical Property Characteristics of IMI 685, Lockheed Calif Co., Burbank Calif, Oct. 1973.

30. B. Kolf, "Designing for Durability in Fighter Engines", 84-GT-164, ASME, Gas Turbine Division publication, June 1984.

31. J.D. Alexander, "Structural High Temperature Materials - A View with a Future", 19th John Player Lecture, I Mech Eng. 1983, vol. 197C, No 40, pp 1-8.

32. M. Gell, G. Leverant, "Mechanisms of High Temperature Fatigue", Fatigue at Elevated Temperatures ASTM STP 520, American Society for Testing and Materials, 1973, pp 37-67.

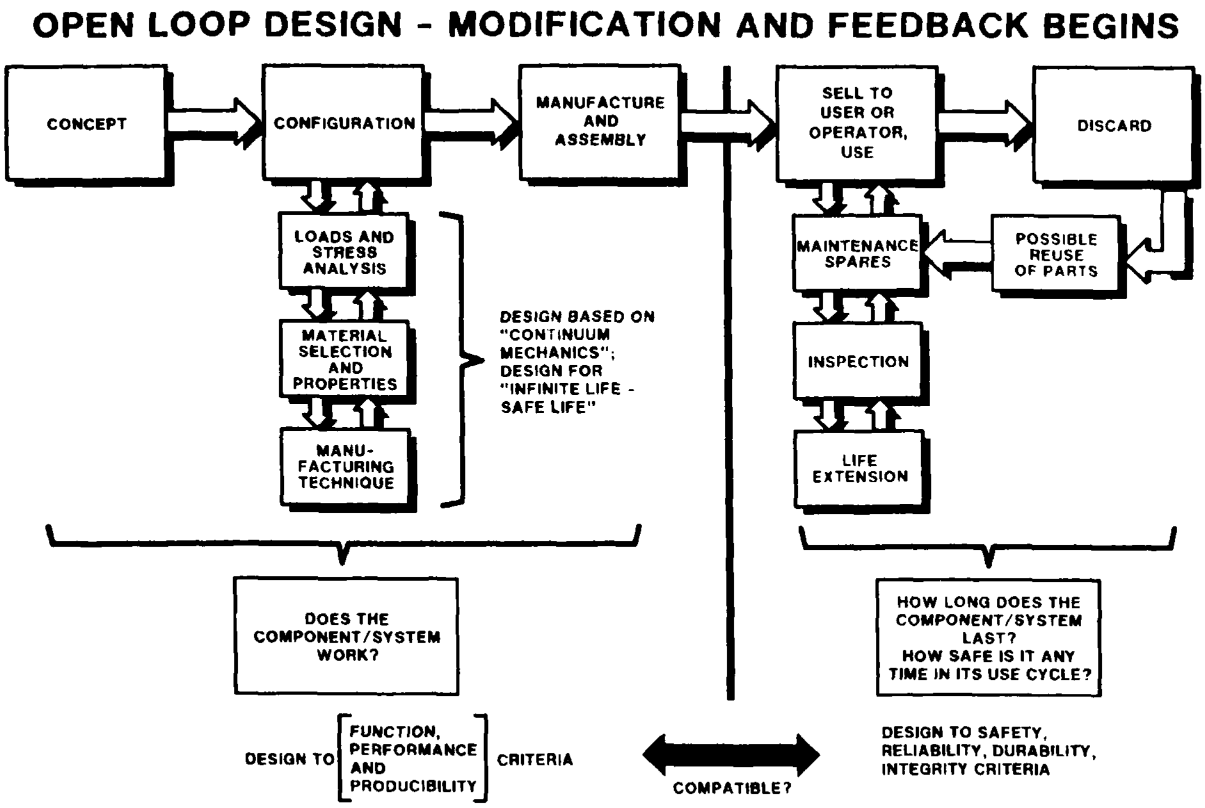
OPEN LOOP DESIGN - MODIFICATION AND FEEDBACK BEGINS
CONCEPT
CONFIGURATION
MANUFACTURE AND ASSEMBLY
SELL TO USER OR OPERATOR, USE
DISCARD
LOADS AND STRESS ANALYSIS
MATERIAL SELECTION AND PROPERTIES
MANU-FACTURING TECHNIQUE
DESIGN BASED ON "CONTINUUM MECHANICS"; DESIGN FOR "INFINITE LIFE - SAFE LIFE"
MAINTENANCE SPARES
POSSIBLE REUSE OF PARTS
INSPECTION
LIFE EXTENSION
DOES THE COMPONENT/SYSTEM WORK?
HOW LONG DOES THE COMPONENT/SYSTEM LAST? HOW SAFE IS IT ANY TIME IN ITS USE CYCLE?
DESIGN TO
FUNCTION, PERFORMANCE AND PRODUCIBILITY
CRITERIA
COMPATIBLE?
DESIGN TO SAFETY, RELIABILITY, DURABILITY, INTEGRITY CRITERIA

1. Open Loop Design - Modification and Feedback Begins. (4) Copyright D.W. Hoeppner and John Wiley Interscience.

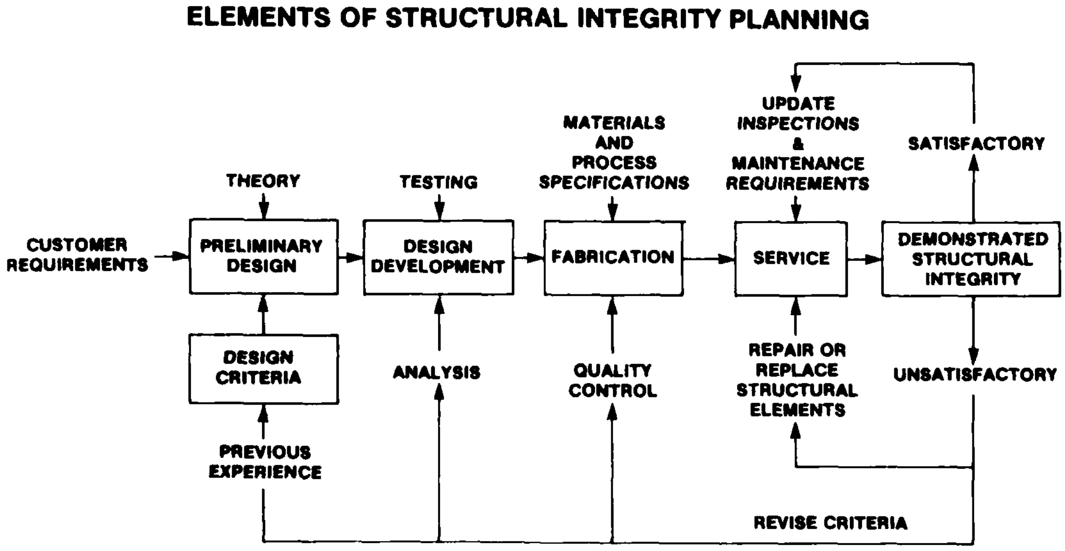
ELEMENTS OF STRUCTURAL INTEGRITY PLANNING
CUSTOMER REQUIREMENTS
THEORY
PRELIMINARY DESIGN
DESIGN CRITERIA
PREVIOUS EXPERIENCE
TESTING
DESIGN DEVELOPMENT
ANALYSIS
MATERIALS AND PROCESS SPECIFICATIONS
FABRICATION
QUALITY CONTROL
UPDATE INSPECTIONS & MAINTENANCE REQUIREMENTS
SERVICE
REPAIR OR REPLACE STRUCTURAL ELEMENTS
SATISFACTORY
DEMONSTRATED STRUCTURAL INTEGRITY
UNSATISFACTORY
REVISE CRITERIA

2. Basic elements of structural integrity planning (5).

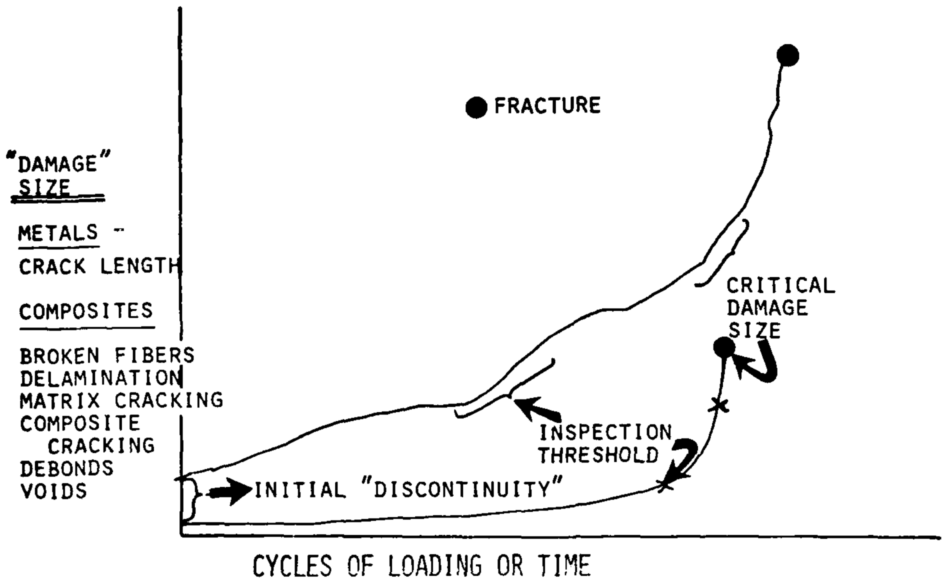

3. "Damage" accumulation with time or cycles. (Keynote lecture by D.W. Hoeppner on Fatigue of Fiber Reinforced Composites, ASTM Symposium 1979 (San Francisco, CA), cf. to M. Salkind, cf 1969/70 and cf D.W. Hoeppner 1965).

ELEMENTS OF DAMAGE TOLERANCE EVALUATION

NUCLEATION OF CRACK-LIKE DISCONTINUITY (d*)

- CREEP
- CORROSION
- FATIGUE
- WEAR
- FRETTING
- SYNERGYSMS
- HYDROGEN EMBRITTLEMENT
- FABRICATION
- MATERIAL QUALITY
- IN-SERVICE DAMAGE
- MAINTENANCE DAMAGE

SUBCRITICAL CRACK GROWTH

- INHERENT D*
- CORROSION FATIGUE
- SCC
- FATIGUE
- DATA-(COI)
- STANDARDS

UNSTABLE CRACK PROPAGATION

- STRESS INTENSITY
- ANALYSIS
- FRACTURE
- TOUGHNESS
- MEASUREMENTS

DAMAGE CONTAINMENT

- DYNAMIC CRACK ARREST
- RESIDUAL STRENGTH

RESIDUAL FATIGUE LIFE - METHODS DEVELOPMENT

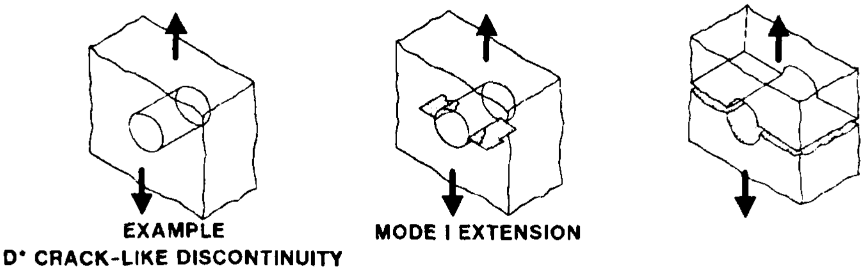

4. Some of the basic elements for a simple damage tolerance evaluation for a crack forming at a hole and propagating by Mode I crack propagation only.

FATIGUE DESIGN POLICY

- ● ESTABLISH FATIGUE LIFE GOALS
  - ● PHILOSOPHY - CRITERIA, METHOD (DESIGN RECIPE)
    - ▽ "SAFE-LIFE"
      - ○ NO CRACKS
        - ● "INFINITE LIFE"
        - ● SAFE-LIFE, FINITE-LIFE REPLACEMENT TIMES

          [FATIGUE SCATTER, QUALITY, TRANSFER]
    - ▽ DAMAGE-TOLERANT
      - ○ CRACK GROWTH
        - ● ESTABLISH DAMAGE TYPE
        - ● INITIAL STATE OF QUALITY
          - → QUANTITATIVE INSPECTION
        - ● INSPECTION INTERVALS
- ● PERFORM MISSION ANALYSIS; ACCUMULATE LOAD-LIFE HISTORY

  [Analytical and Experimental stress analysis]
- ● TEST MATERIAL - JOINT - STRUCTURAL DETAILS TO SPECIFIC LOAD SPECTRUM
- ● ESTABLISH FATIGUE QUALITY GOALS AND DESIGN STRESS LIMITS
- ● SELECT "BEST" MATERIAL FOR APPLICATION
  - ▽ CORROSION → "Thou shalt have no corrosion"
  - ▽ FRETTING → "Thou shalt have no fretting"
  - ▽ CREEP → "Thou shalt have no creep"
  - ▽ "FATIGUE" [No Cracks]
  - ▽ TOUGHNESS
    - → Rate of Damage Propagation, da/dN
    - → Residual Fatigue Life
    - → Residual Static Strength
  - ▽ STRESS CORROSION, K_{Iscc}, da/dt
  - ▽ INTERACTIONS or SYNERGISMS
  - ▽ STATIC STRENGTHS
- ● PROOF TEST DESIGNS (Components, Structural Systems)
- ● ESTABLISH INSPECTION, MAINTENANCE, REPAIR PROCEDURES.

5. Fatigue Design Policy (4).

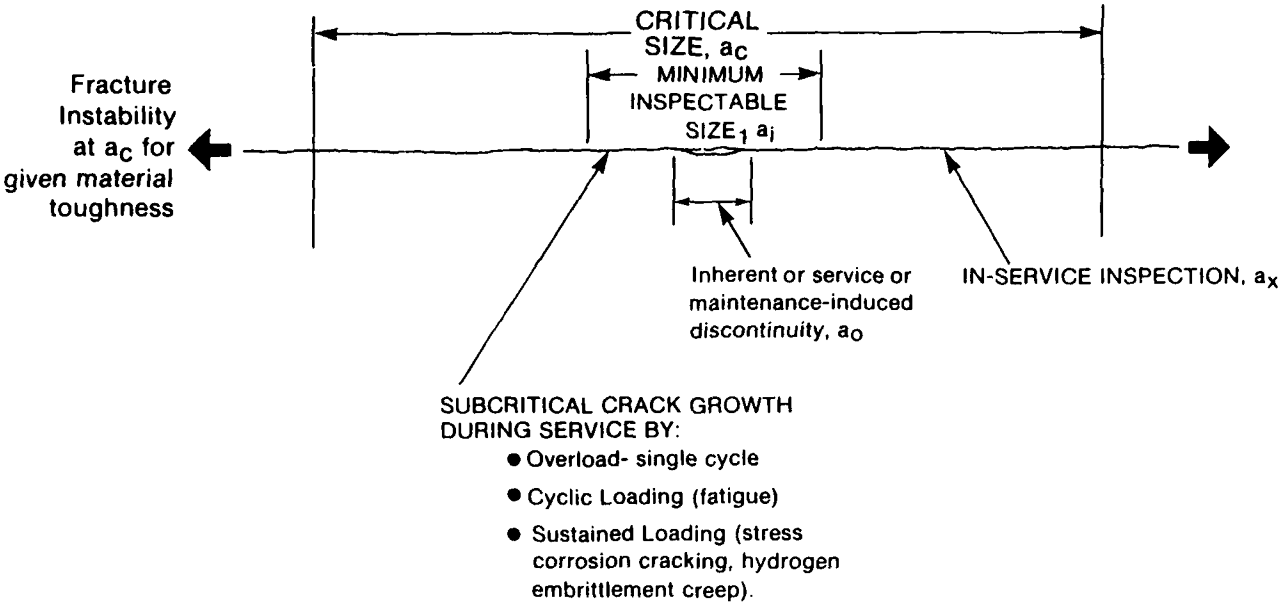
CRITICAL SIZE, a_c
MINIMUM INSPECTABLE SIZE, a_i
Fracture Instability at a_c for given material toughness
Inherent or service or maintenance-induced discontinuity, a_o
IN-SERVICE INSPECTION, a_x
SUBCRITICAL CRACK GROWTH DURING SERVICE BY:
● Overload- single cycle
● Cyclic Loading (fatigue)
● Sustained Loading (stress corrosion cracking, hydrogen embrittlement creep).

Given a discontinuity exists;

(1) Can it grow (propagate) in any way during use or storage?

(2) How fast can it propagate?

(3) If (1) occurs how big will the discontinuity become before yielding or fracture occur?

(4) Given (1), (2), (3), can it be detected prior to fracture?

6. The concept of crack extension (4,5).

$$\Delta N_T = \Delta N_n + \Delta N_S + \Delta N_{\sigma/p} + \Delta N_{\epsilon/p}$$

ΔN_T = total life - cycles

ΔN_n = cycles to nucleate a crack-like discontinuity (d*) given one is not there initially. Define d*!

ΔN_S = cycles of growth where growth is dependent on the Structure of the material or the Structural configuration

$\Delta N_{\sigma/p}$ = cycles of growth - characterizable by Linear Elastic Fracture Mechanics (LEFM); continuum regime

$\Delta N_{\epsilon/p}$ = cycles of growth - characterizable by plasticity which is too large to allow LEFM. Thus, use Elastic Plastic Crack Mechanics (EPCM) or Fully Plastic Crack Mechanics (FPCM)

7. Possible divisions of the fatigue crack growth process (4,5,6-DWH).

$\Delta N_{(x)}$

Varies with Material
Environment ⟨ T, Chemistry
Manufacturing
Radiation
Stress State
Geometry
Load Sequence (Spectrum, frequency)

Know the; Material
Inspectability
"Fatigue Quality"

8. The change of cycles from an initial number N_i to a final number (N_f) is given by $\Delta N_{(x)}$ which varies with the quantities shown.

fatigue
Quality

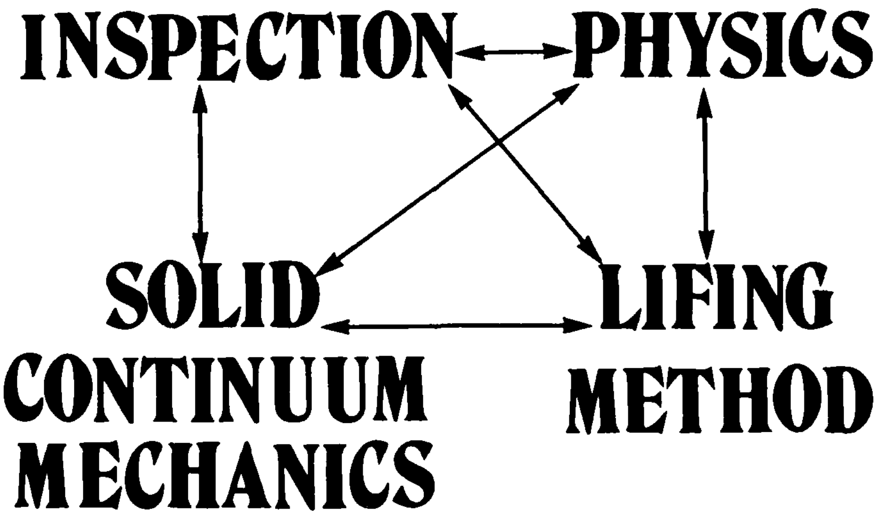

INSPECTION ⟷ PHYSICS

SOLID CONTINUUM MECHANICS ⟷ LIFING METHOD

LIFE GOAL

SAFETY & DURABILITY

9. Various factors that must be integrated into a damage tolerant design.

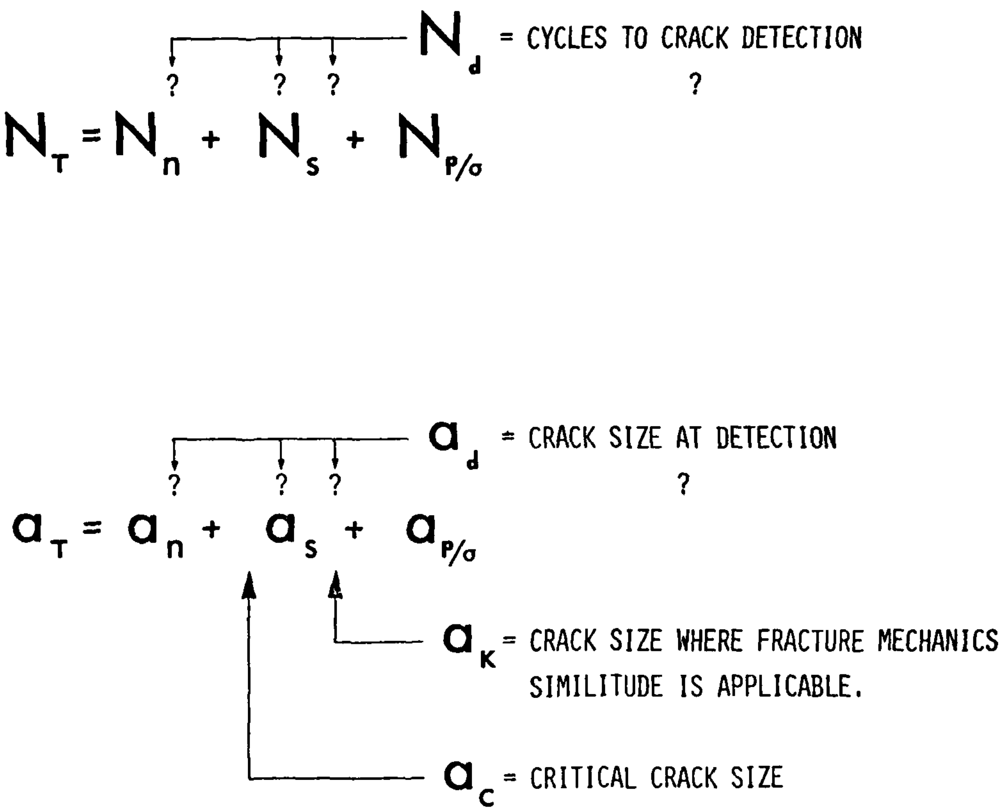

N_d = CYCLES TO CRACK DETECTION

?

$$N_T = N_n + N_s + N_{P/\sigma}$$

a_d = CRACK SIZE AT DETECTION

?

$$a_T = a_n + a_s + a_{P/\sigma}$$

a_K = CRACK SIZE WHERE FRACTURE MECHANICS SIMILITUDE IS APPLICABLE.

a_c = CRITICAL CRACK SIZE

10. The cycles to detect (N_d) a given crack (a_d) must be related to inspection capability, toughness, inspectability, and subcritical crack growth rate (da/dt) as well as the loads, temperatures and residual stresses. If these are not integrated, as a damage tolerance program emphasizes, then a_d could become equal to or less than the critical crack size (a_c) as shown in the lower part of the figure.

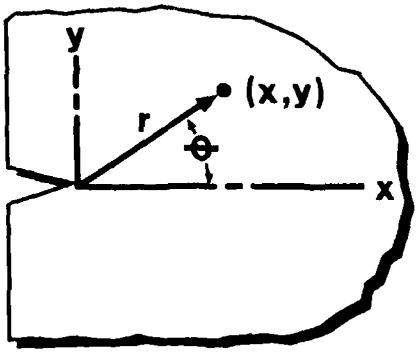

FRACTURE MECHANICS PROVIDES

A CRACK TIP ANALYSIS (A),
A CRACK TIP DISPLACEMENT ANALYSIS (B), OR
AN ENERGY RATE ANALYSIS (C)

	MATERIAL BEHAVIOR	
	LINEAR	NON-LINEAR
(A) CRACK TIP STRESS ANALYSIS	$\sigma_{ij} = \frac{K}{\sqrt{2\pi r}} f_{ij}(\theta)$	
(B) DISPLACEMENT ANALYSIS		$\delta = \alpha\left(\frac{J}{\sigma_y}\right)$ $\delta = f(\Delta, \sigma_y, l, B)$
(C) ENERGY RATE ANALYSIS	$\mathcal{G} = \frac{-\partial u}{\partial A}$ $\mathcal{G} = \frac{c^2\sigma^2\pi a}{E}$ $\mathcal{G}E' = K^2$	$J = -\frac{\partial u}{\partial A}$

FOUR PARAMETERS ARE AVAILABLE TO CHARACTERIZE THE CRACK TIP STRESS AND STRAIN FIELDS, viz. K, $\mathcal{G}$, δ, J

11. Some provisions of a fracture mechanics analysis.

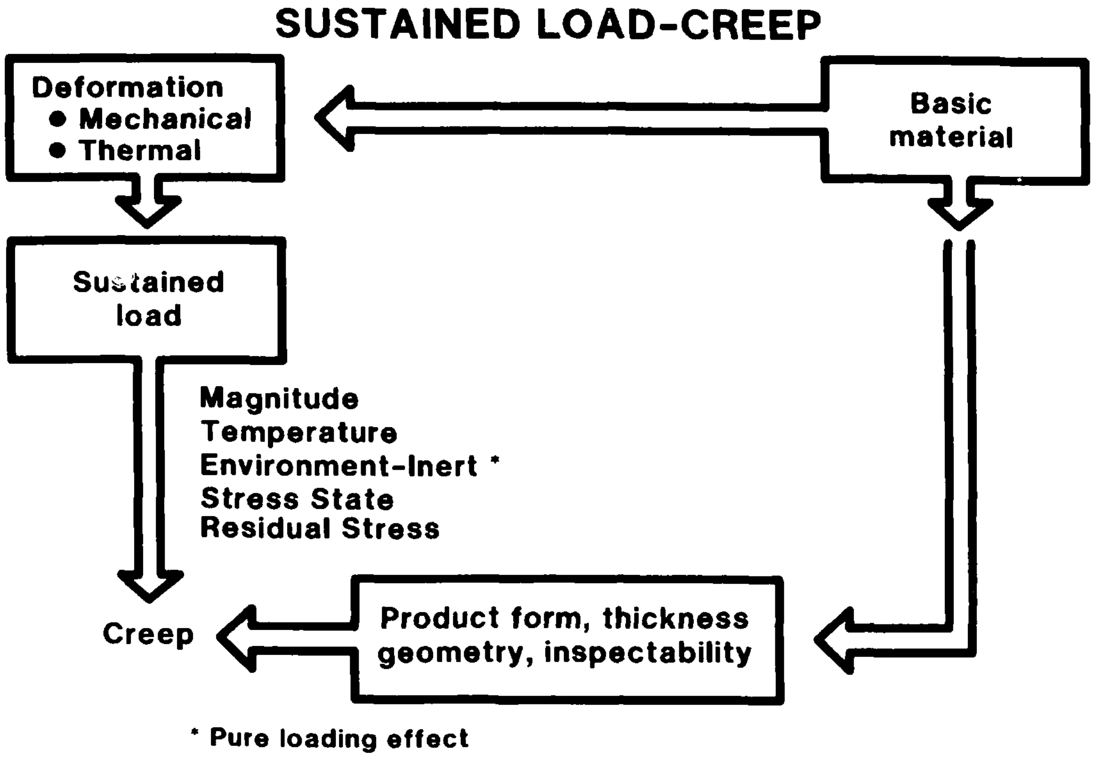
SUSTAINED LOAD-CREEP
Deformation
● Mechanical
● Thermal
Basic material
Sustained load
Magnitude
Temperature
Environment-Inert *
Stress State
Residual Stress
Creep
Product form, thickness geometry, inspectability
* Pure loading effect

12. Basic inputs for Sustained load considerations. (Creep for example - similar inputs are necessary for environmentally assisted sustained load crack; e.g. assisted by stress corrosion cracking or hydrogen embrittlement. In ceramics this could be "static fatigue").

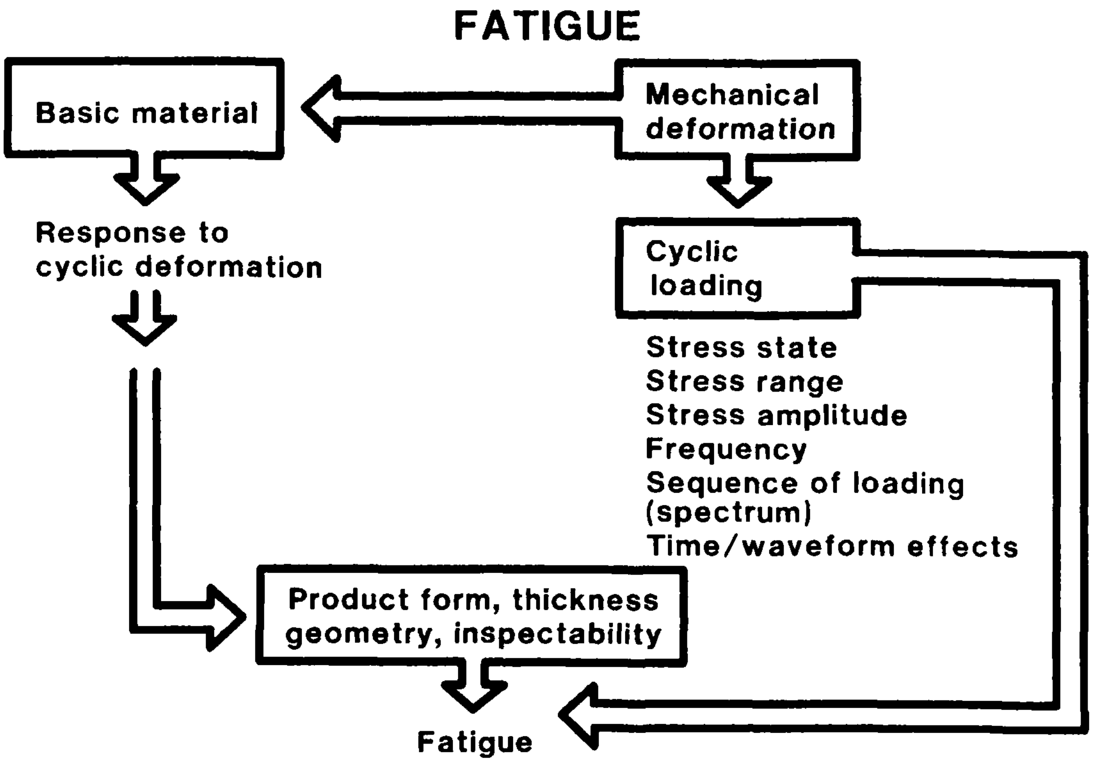
FATIGUE
Basic material
Mechanical deformation
Response to cyclic deformation
Cyclic loading
Stress state
Stress range
Stress amplitude
Frequency
Sequence of loading (spectrum)
Time/waveform effects
Product form, thickness geometry, inspectability
Fatigue

13. Basic inputs to Cyclic load considerations (Fatigue).

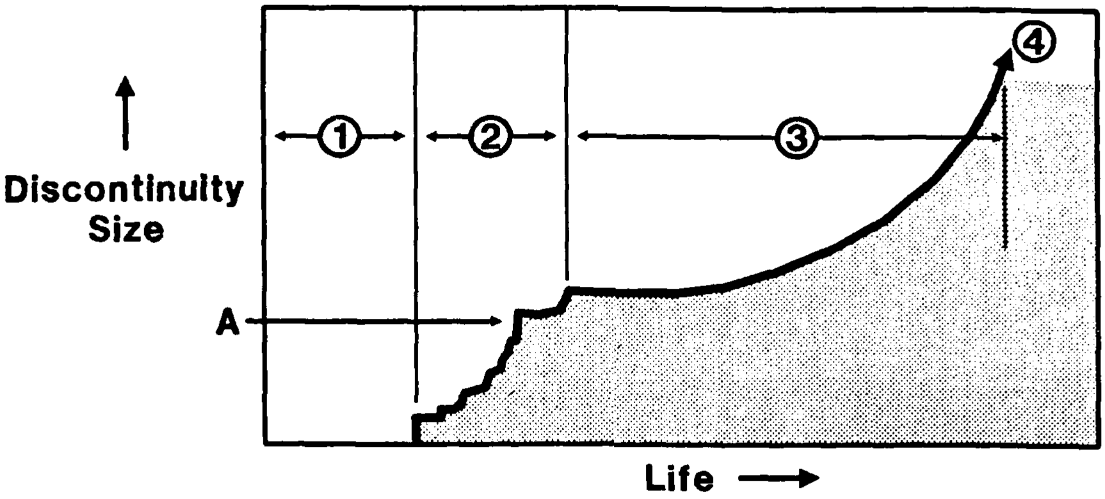

A: "FIRST" detectable crack
1: Nucleation phase, "NO CRACK"
2: "SMALL CRACK" phase - steps related to local structure (Anisotropy)
3: Stress dominated crack growth, LEFM ,EPFM
4: Crack at length to produce instability

14. Conceptual aspects of discontinuity extension (4,5,6-D.W.H, 8,11).

METHODS FOR EACH LIFE PHASE

Nucleation	"SMALL CRACK" Growth	Stress Dominated Crack Growth	Failure (Fracture)
Material failure mechanism with appropriate stress/strain life data	Crack Prop. threshold related to structure (micro)	Fracture mechanics •similitude •boundary cond. LEFM EPFM ?	K_{Ic} etc. C.O.D. Tensile/ compessive buckling
Nucleated discontinuity (not inherent) type,size,location	Structure dominated crack growth	Data base **	
Presence of malignant D*,H*	Mechanisms, rate	Appropriate stress intensity factor	
Possibility of extraneous effects • Corrosion • Fretting • Creep • Mechanical damage	Onset of stress dominated crack growth	Initial D*,H* Size,location,type	
	Effects of •R ratio •Stress state •Environment t chem T •Spectrum-waveform	Effects of •R ratio •Stress state •Environment t chem T •Spectrum -waveform	

15. Design methods for each life phase -(see Figure 4,6-8) (ibid Figure 14).

CONCEPTUAL DAMAGE TOLERANCE CONSIDERATIONS

	INITIAL DISCONTINUITY, DSC	SUBCRITICAL GROWTH	FRACTURE
ASSOCIATED CONCEPTUAL STEP	ASSUME ANY DSC BELOW A GIVEN DETECTION LIMIT IS PRESENT AT THE CRITICAL LOCATION	DSC PROPAGATES AS CRACK UNDER CYCLIC AND STATIC LOADING, RATE IS INFLUENCED BY ENVIRONMENT x	CRACK PROPAGATES UNTIL CRITICAL LOAD/CRACK SIZE IS REACHED: FRACTURE OCCURS
INFORMATION REQUIRED	NDI INSPECTION LIMITS AND/OR PROOF CYCLE SCREENED LIMITS	ANTICIPATED SERVICE STRESSES AND ENVIRONMENTS	INFLUENCE OF LOAD HISTORY & ENVIRONMENT ON FINAL FRACTURE
REQUIRED DATA	PROBABILITY OF DSC DETECTION VS. DSC SIZE AND SHAPE	$\frac{da}{dN}$ vs. ΔK, DETERMINE ΔK_{th}, da/dt vs. K_{max} IN SERVICE ENVIRONMENT	K_{Ic}, K_c, K_{Iscc}, K_{Ib}, K_{IIc}, J_{Ic}, S_{tu} OR STATIC FRACTURE CRITERIA
FRACTURE CONTROL STEPS	SET INITIAL INSPECTION REQUIREMENT SELECT MATERIALS & PROCESS CONTROLS	DETERMINE EXPECTED SERVICE LIFE	SET INSPECTION INTERVALS TO AVOID FRACTURE OR DETECT CRACK WELL BEFORE INSTABILITY

x STATE CRACK PROPAGATION MODE

16. Many of the conceptual damage tolerance considerations are represented in this chart (4,5).

LIMITATIONS OF MANUAL NDT SYSTEMS AND THE 'NO EYES' CONCEPT

R G Taylor
Chief of NDT Technology
Rolls-Royce Limited
Derby
UK

1. INTRODUCTION

For many years, the traditional role for non-destructive testing (NDT) has been confined to that of a goalkeeper, where it is assumed that NDT can prevent the entry into service of components with harmful defects or to remove from service those components that have become defective through usage.

Occasionally it is employed as a method of process control to highlight when significant changes take place in either the manufacturing or life cycle. However, the emphasis is usually placed on the 'goalkeeper' philosophy particularly in those industries, such as aerospace, where component failure is both costly and could result in loss of life.

Until recently, little or no attempt has been made to couple NDT with the life of a part and it is unusual to consider the NDT requirements (and limitations) during the design cycle. All too often the NDT requirements are only considered when the first components are made and when any limitations imposed on NDT by the shape, configuration or material is already a fact and beyond a stage when changes are acceptable. It is also unlikely that in-service inspection requirements will be considered until a problem arises in the field.

A further problem is the lack of understanding with respect to the reliability of NDT, although the majority of experienced NDT practitioners will admit to occasions when defects, which should have been detected and rejected, have slipped through the net. Recent studies carried out in the USA have demonstrated that unreliability in NDT is a very real problem and weaknesses have been recognised in the 'engineering' of NDT techniques on components and perhaps more disturbing are the human factors which lead to defects being missed when the NDT engineering and process parameters are correct.

It is not surprising, therefore, that premature component failure does occur due to the weaknesses of NDT and the result has been costly and embarrassing in a number of industries.

2. DEFECT TOLERANT DESIGN

The recent change from the traditional lifing concepts in the aircraft industry, which was established by component testing and an assumption that the material was free from harmful defects (due to the 'NDT goalkeeper philosophy'), to the defect tolerant design concept, has necessitated a serious review of both the strengths and weaknesses of non-destructive testing. The philosophy of designing and lifing a critical component with the possible presence of a defect, just below the 'assumed' detection threshold, places on current NDT methods (and attitudes) a responsibility they cannot achieve - to detect a defect with a very high degree of reliability and to size it with a high level of accuracy.

It is no longer acceptable to ask "what is the smallest defect that can be detected?" A much more important question to be answered is "what is the largest defect that can be missed?".

An analysis of the major problems associated with the current NDT technology can be summarised as follows:-

1. Lack of NDT Considerations at the Design stage.
2. Inadequate 'engineering' of the NDT techniques.
3. Defect Detection Requirements which are often too close to the detection threshold.
4. Human factors in the inspection cycle.

It may not be possible to totally eliminate all of the weaknesses of NDT in the foreseeable future but considerable improvements can be made by attention to the factors summarised above.

3. NDT CONSIDERATIONS AT THE DESIGN STAGE

In the past, lack of NDT involvement at the Design Stage has resulted in severe limitations in the ability to achieve adequate NDT on fracture crtitical components, particularly where sub-surface ultrasonic inspections are involved. The principal activity for the NDT Engineer, at this stage, is to highlight to the Designer, the limitations of NDT imposed by the shape and configuration of the part. This NDT, input together with the Material Engineers' knowledge of the type, distribution and orientation of defects, is intended to convey to the Designer, the likelihood of defects remaining in the part when all of the inspections have been carried out, to enable him to assess those implications on the intended lifing objectives. At this stage it may be possible to make minor modifications to the Design which would considerably improve the NDT capabilities, or alterations to the material configuration (forging shape) which would allow a more searching inspection to be carried out. Whether improvements can be made at this stage or not, it is essential that the Designer is made aware of the limitations of NDT on his part and that he finalises the design with that knowledge and agreement. Only when formal agreement is reached between the Designer, Materials Engineer and NDT Engineer on the limitations (in Rolls-Royce this is recognised by a formal statement and NDT limitations drawing) can be detailed inspection plan (Quality Control Procedure) be released. Final Agreement on the NDT limitations can not be completed until the first parts are produced and inspected. Ultrasonic Inspectability (for sub-surface defects) is dependant on the level of inherent material noise (grass) and the size of defect that is to be detected must have a greater amplitude than the noise level.

4. ENGINEERING OF THE NDT TECHNIQUE

The recent Reliability Study of NDT in the inspection of Aircraft Engine Components highlights the importance of NDT Engineering to reliable NDT application. Details of the specific critieria necessary for successful NDT engineering are contained in the report but in particular the objective of NDT Engineering concerns:

- Correct selection of the NDT method
- Obtain the maximum signal to noise ratio for the minimum defect size to be detected.
- Validation that the process can meet the intended specification consistently and reliably.
- Seal the NDT documentation
- Monitor, on a regular basis, that the process continues to meet the requirements.

In addition, it may be necessary to provide fixtures, tooling and defect panels or sensors to minimise the effect of human variations.

5. DEFECT DETECTION REQUIREMENTS (QUALITY STANDARDS)

One of the main problems for NDT is the increasing demand to detect smaller defects which are extremely close to current detection thresholds. This is true for all NDT methods and in particular to the ultrasonic inspection of critical parts for sub surface defects. During the past 10 years, the defect size required to be detected, has reduced from a No.3 hole (USA 3/64" dia) to a No.2 hole (2/64" dia) of a No.1 hole (1/64" dia) for some materials; in effect a reduction factor of 4 or greater of defect size, a reduction in the signal to noise ratio and a decrease in detection reliability. In order to increase detection reliability it is essential to increase the signal to noise ratio (ie. a greater difference between the defect signal and material noise). This increase is also required to introduce effective automation encessary to reduce the risks of human failure (see HUMAN FACTORS).

If we accept the argument that "the smaller the defect the lesser the confidence in detecting it" it is unlikely that current NDT methods alone can ever achieve the reliability necessary for defect tolerant design. Freedom from defects must be assured by both stricter process control together with improved NDT technology.

6. HUMAN FACTORS IN THE INSPECTION CYCLE

Although the 'HAVE CRACK' reliability study highlighted and quantified the human factors problem in NDT, experienced NDT practitioners are well aware of the failings of the human being in the inspection cycle. Radiography is the NDT method with the worst record of 'defect misses' simply because the 'evidence' is available after the event; however, it would be unwise (and untrue) to suggest that other NDT methods are less prone to human failure.

Whilst it may be possible, by careful personnel selection, to minimise the risk of human failure, defect miscalls by the inspector must be accepted as an established fact of life and a number of actions are required to eliminate the problem.

The most important requirement is to remove the human being from the inspection cycle or, reduce the incidence of failure by enhancing defect detection (improving signal to noise ratio) and to channel the attention of the inspector to the defects. Substantial research and development is required to achieve these ovjectives and within Rolls-Royce this was resulted in the "No Eyes" NDT R&D programme.

Although much has been accomplished by automating the 'Search' procedure and in certain cases warning the operator that a defect has been detected, in the majority of cases, the inspector is still required to determine whether the 'call' is true or false and to subsequently adjudicate on the acceptance or rejection of the real calls. Nevertheless, these advances represent a considerable improvement in the reliability of NDT since the tedium of distinguishing the good parts from 'bad' has been eliminated and the inspector can now concentrate on the parts on which definitive judgements have to be made. The areas where improvements have been made are:

- Real Time X-Ray of Turbine Blades
- Penetrant Inspection of Blades
- Ultrasonic Inspection of Discs
- Magnetic particle inspection of shafts
- Various eddy current applications.

In each of these, the system passes components with 'indications' below a defined level and rejects those parts with an indication above the level for adjudication by the inspector. In some cases this can result in more than 80% of the components being passed without any human intervention in either the processing or inspection cycle. Development is continuing, in all of these fields, in an attempt to completely eliminate the need for human involvement. However, a considerable problem is yet to be resolved. The majority of NDT methods produce 'indications' which may be real defects or 'the indications' may be spurious and non-malignant. Whilst modern technology is generally capable of detecting indications, reliably and consistently, modern technology does not yet possess the 'artificial intelligence' which will enable it to distinguish between the real and the spurious and until this is available the human being must remain in the inspection cycle.

Finally, where it is still a requirement to provide high NDT reliability and where it is not yet possible to utilise 'No Eyes' or 'semi-No Eyes' technology, the only recourse available is to carry out 'dual inspections' in order to prevent or, at best, minimise the number of defects that could slip through the net.

7. ACKNOLWEDGEMENT

Reliability of Non Destructive Inspections SA-ALC/MME 76.7.38.1 - December 1978 Prepared by Lockheed Georgia.

Reliability of Non Destructive Inspection of Aircraft Engine Components SA-ALC/MM-8151 - January 1984. Prepared by Martin Marietta Denver Aerospace.

NDT

Advent of fracture mechanics

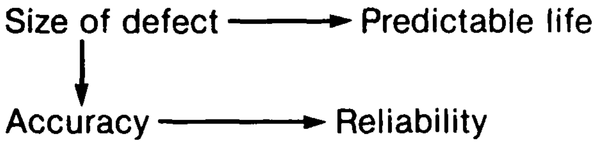
Size of defect
Predictable life
Accuracy
Reliability

VML 18079

ENSIP NDT requirements

- Equipment
  - Improve signal - noise ratio
  - Channel attention of inspector to flaws
  - Provide positive assurances equipment is performing intended function
  - Automate control and programme functions susceptible to human error

"No eyes"

VML 18070

Engineering

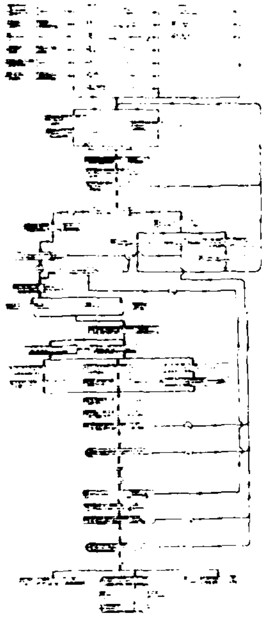

Define performance and life requirements

Optimise design & materials

Define methods of manufacture NDT methods and QAS

Rig & bench engine testing

Seal methods and release to production

VML 18073

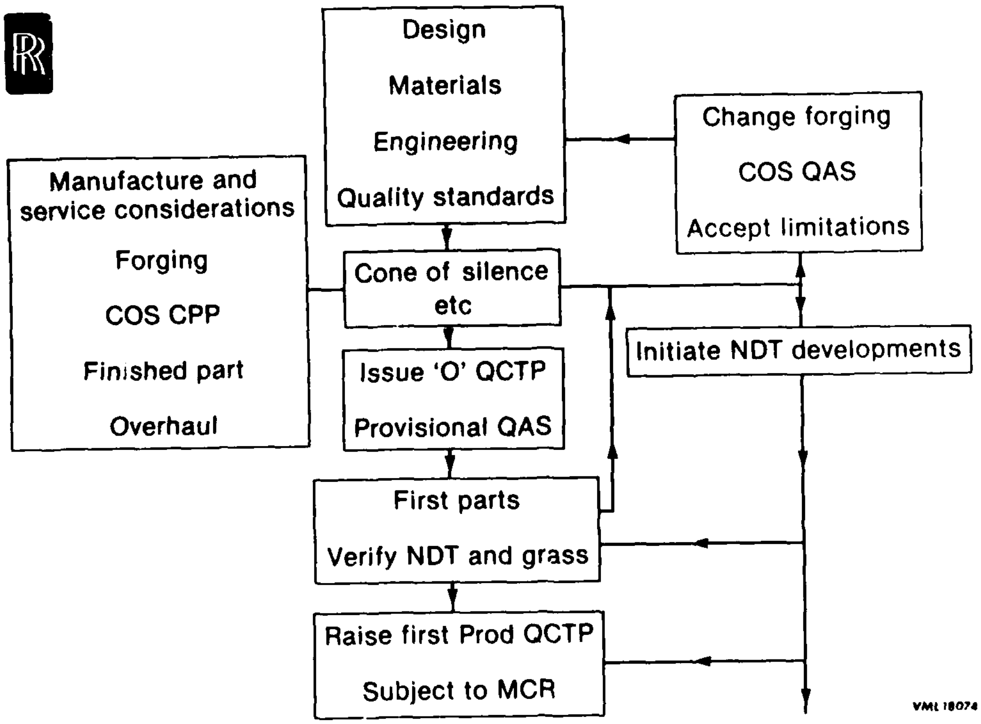

Design

Materials

Engineering

Quality standards

Change forging

COS QAS

Accept limitations

Manufacture and service considerations

Forging

COS CPP

Finished part

Overhaul

Cone of silence etc

Initiate NDT developments

Issue 'O' QCTP

Provisional QAS

First parts

Verify NDT and grass

Raise first Prod QCTP

Subject to MCR

VML 18074

Normal scans

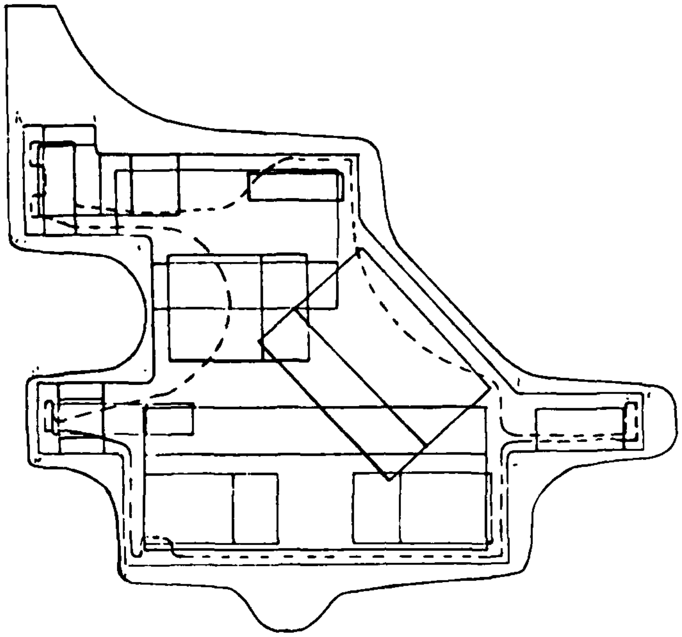

VML 18083

Ultrasonic limitations diagram

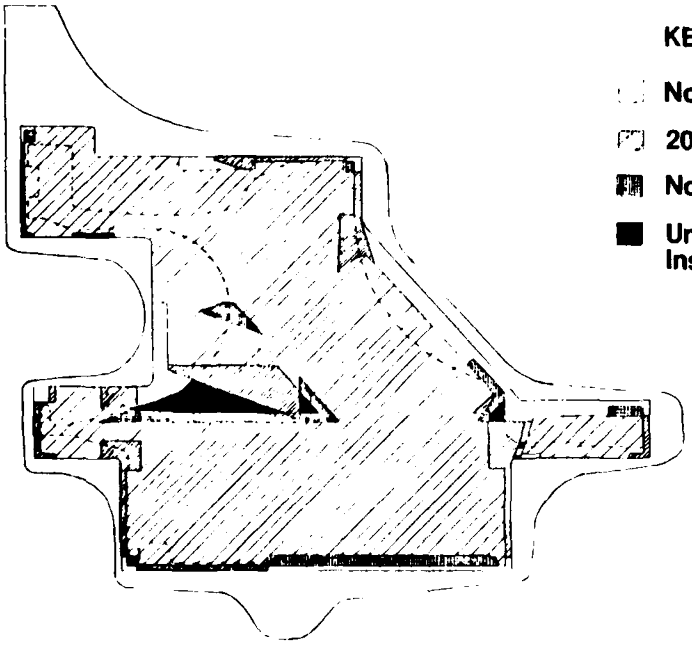

KEY

- ⬚ Normal 20° scans
- ▨ 20° scans only
- ▩ Normal only
- ■ Uncertain Inspection

ENSIP NDT

Preliminary conclusions — Aero engine parts

	Average	Best
Magnetic inspection POD	60% — .300" crack	65% — .250
Penetrant inspection	90% — .220"	90% — .175
Eddy current	90% — .090"	90% — .030"
Ultrasonic	80% — .375"	90% — .180

- Average results obtained from majority of technicians
- Best results obtained from top 10% technicians

DISCS WHEELS SHAFTS NDT R AND D SHEET 2

OBJECTIVE	POSSIBLE SOLUTION	ACTIVITY	BY	COST	80 81 82 83 84 85
	ACCOUSTIC EMISSION	Ongoing Programme	ARL RR	£30 K MoD	
	EDDY CURRENT g) Signal/Noise Enhancement and C Scan	Quotation Received	Pantatron	(£9 K)	Complete
	h) Signal Interpretation	Brochure Being Prepared		Not yet known	
Internal Drum Surface Inspection All surfaces	i) Scan UV Lasers (Pen)	Initial discussions		£7.5 K	
	j) Flying Spot (Vis)	Feasibility Study Done	SIRA	£10 K	£120 K for prototype
2. IMPROVED RELIABILITY SENSITIVITY FOR • PRODUCTION • SERVICE	AUTOMATION OF a) Penetrant Inspection b) Surface Preparation c) Magnetic Inspection	Prototype Ready RR Shop Trials Late 1980	Ardrox and RR	(£1 K) + RFC C$ 110 K	
	d) Eddy Current	Computer Programme of Existing System on Fan Disc/Blade Improved Probes	Reluxtrol	£ 20 K	Complete
	e) Ultrasonic	Programme ongoing	RR Sonic Open Univ	Already Funded	£50 K required
RERIREMENT FOR CAUSES (RFC)	All NDT Methods	USAF/SRL	RR and US Companies	C$ 175	

15 MAY '80 VML 18049

Rolls Royce Limited 198

Fluorescent penetrant inspection Lower 95% confidence limit

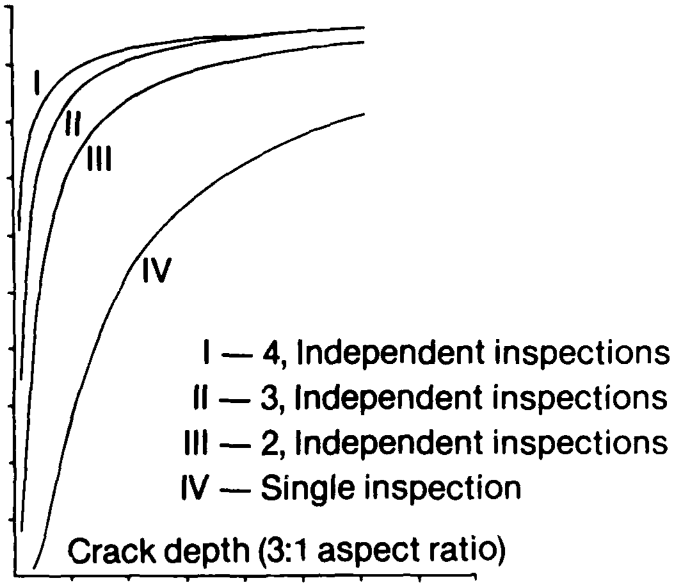

© Rolls-Royce Limited 198

Relative Amplitudes for 1/64", 2/64" & 3/64" F.B.H. Targets Set to the same Sensitivity.

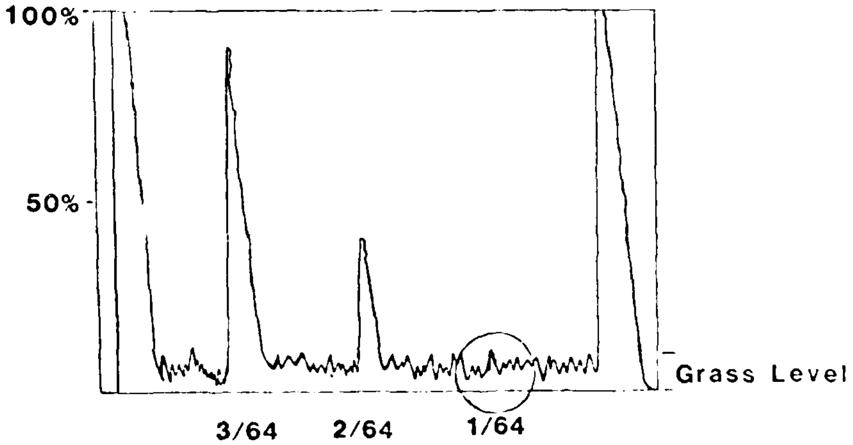

THE ROLE OF THERMAL AND STRESS ANALYSES IN THE APPLICATION OF DAMAGE TOLERANT DESIGN

by

G. F. Harrison
Propulsion Department,
RAE Pyestock, Farnborough,
Hants, ENGLAND
and
T. H. Edmunds
Rolls-Royce, Ltd
PO Box 3, Filton, Bristol,
ENGLAND

SUMMARY

The paper illustrates some of the important factors affecting the accuracy of proven analysis techniques in support of a damage tolerant design methodology. Temperature sensitivity analysis and the relevance of component geometry in controlling material response to external loading are discussed. The requirement to translate characterised material behaviour into models suitable in stress analysis is demonstrated. Examples identifying critical stresses and critical locations in typical engine discs are presented. The implementation of fracture mechanics analysis methods to these regions is discussed. Finally their relevance to damage tolerant design concepts is evaluated.

1 INTRODUCTION

One of the most significant consequences of the stringent lifing rules currently in force for aero engine components is that manufacturers have safety records of which they can be moderately satisfied. Between 1978 and 1981 all three major manufacturers of large fan engines - (Rolls-Royce, General Electric and Pratt & Whitney) - limited uncontained failures of rotating parts to 0.63 to 0.65 per million flying hours[1]. Such low failure rates are a consequence of the restricted lives placed on rotating components by the manufacturer.

The declared safe lives for these 'Group A' parts are derived from both full scale and laboratory test results, modified using statistical correction factors based on scatter in material properties and mission profiles. The safety criterion for UK engine discs is that on removal from service not more than 1 in 750 should exhibit a small but detectable crack. It is estimated that in achieving this rate, over 80% of the discs will have utilised less than half their safe lives.

In the current economic climate with airlines and airforces both trying to reduce 'cost of ownership' there is a strong motivation to extend overhaul periods and to alter or replace existing lifing procedures so that the maximum proportion of the disc life can be utilised without compromising safety. Of much greater importance than economic arguments is the fact that, to meet the increasing engine requirements of higher thrust-to-weight ratios, discs are being designed to run more highly stressed. These highly stressed components show an increased defect sensitivity and a 'life to first crack' philosophy may be neither conservative nor even meaningful. To fill this gap there has been a move to use fracture mechanics concepts for predicting service life and, more recently, to embody this within damage tolerant design concepts. Under this approach discs are removed from service before an assumed inherent flaw is calculated or observed to have grown to a critical size. Broadly the philosophy should allow a larger proportion of the safe life to be utilised.

For a typical disc material the failure distribution from -3σ to $+3\sigma$ (where σ is standard deviation) is likely to occur over a range in life of about a factor of 6. For a required life this is equivalent to the maximum stress that the weakest batch of a material can sustain being about 30% below the stress which the average material can sustain. In practice a further safety margin is allowed and the design line may be located at a position which is only 2/3 of that corresponding to the -3σ line. This gives an operating stress which is a further 15% below the stress that the average material can sustain for this life.

The additional margin anticipates inaccuracies in estimating stress and temperature distributions, material variability and variations in service usage. It implies that as the number of parameters controlling component life increases, the more accurately each must be calculated and weighted according to its contribution to life consumption. Furthermore if a greater proportion of the available disc life is to be used in service without a higher risk of failure, parameters affecting life must be calculated and monitored to a greater accuracy so that their effects on component life can be summated.

The major factors controlling the lives of discs in service are the magnitudes and variations in the stress and temperatures experienced. The role of thermal and stress analysis is to calculate these so that service lives may be optimised. However before discussing these factors it is useful to consider some practical aspects of numerical modelling techniques.

2 NUMERICAL MODELLING AND DISCRETISATION

This section relates mainly to the use of techniques in general rather than detailed characterisation of the material. The Finite Element Method is probably the most widely used method for calculating stresses and temperatures for service components. Assuming that the most appropriate element type has been selected and control parameters have been set to ensure converged solutions, the algorithm employed can have a marked influence on the required computing time. This was demonstrated in some recent work at RAE[2] in which several non-linear methods were applied to analyse the elasto-plastic stress distributions at the root of a notched cantilever bend specimen used for low cycle fatigue studies. To compare the speeds and the convergence rates, identical loading histories were used with each algorithm. The finite element idealisation of the specimen required 252 twenty-node isoparametric brick elements, 1719 nodes and a maximum front width of 498 degrees of freedom. Best and worst results are shown in Table 1.

Table 1

COMPARISON OF CPU TIME WITH DIFFERENT LOADING ALGORITHMS

Algorithm	Total number of iterations	CPU time
Initial stiffness	55	4h 36m
Tangent stiffness	23	24h 48m

When using the tangent stiffness algorithm, the stiffness matrix is recalculated at the start of each iteration. The results illustrate the expected rapid convergence of the iterative procedure and that the reduction of a new stiffness matrix for every iteration is computationally time consuming. In comparison the initial stiffness method needs many iterations but since the elastic stiffness matrix is used throughout, the method is extremely efficient.

These findings will apply to most computer problems involving large numbers of non-linear equations and show that suppressing reformulation of the stiffness matrix may reduce considerably the solution time without loss of accuracy.

In any analysis a compromise has to be reached between accuracy and computer CPU time (ie cost). For the example illustrated the less efficient tangent stiffness method took more than 5 times the CPU time of the initial stiffness method and so, with the same limitation on computer access, using the initial stiffness algorithm a much finer mesh can be employed. Table 2 illustrates the effects of mesh size on calculated stress levels for a typical feature in a turbine disc for a small engine.

The difference between the two sets of results is largely a consequence of the analysis procedure in which stress values are calculated for a discrete number of integration points within the element and then linearly extrapolated to the element boundaries to obtain nodal values. Thus the coarse mesh involves greater extrapolation but since surface stress levels can be critical, it is not good practice to extrapolate over relatively large distances.

Table 2

EFFECT OF MESH SIZE ON ELASTIC STRESS LEVELS

Mesh size	von Mises stress (MPa)	Principal stress (MPa)
Fine 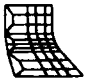	1170	1390
Coarse 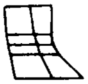	1089	1350

If the disc is loaded to a level that induces plasticity, then the difference in calculated peak stresses between coarse and fine discretisation will be reduced. Using a coarse mesh the peak principal stress may be calculated to be at the surface whereas with the finer mesh it can be shown to occur below the surface. The significance of this will be discussed later.

3 THERMAL STRESS MODELLING

Element size can also affect the accuracy obtained from thermal stress calculations. A typical converged thermal solution using second order elements may represent temperature as a piece-wise quadratic within each element. However, the same structural mesh cannot represent a quadratic variation of strain and hence local stress errors can be introduced. The position is worsened by the temperature dependence of the expansion coefficient.

An example illustrating the magnitude of this inaccuracy can be seen by considering a temperature variation across the cob of a disc. For illustration this has been simplified to a thin plate with the unidirectional temperature gradient shown in Table 3 and modelled using eight second order elements. Since the plate contains no geometric constraint it is free to expand and hence should be unstressed. The non-zero stresses calculated along the centreline of the plate are also presented in Table 3.

Table 3

THERMAL STRESS ANALYSIS OF AN UNCONSTRAINED THIN PLATE

Position	Temperature °C	Longitudinal stress MPa	Transverse stress MPa
Edge	525	-5.34	-10.4
	447	4.58	15.2
	380	-4.98	- 8.75
	327	4.21	15.9
	289	-1.06	- 5.53
	261	1.85	8.33
	241	-1.04	- 2.13
↓	231	0.78	4.29
Cob centre	225	-0.30	- 1.09

The errors illustrated are of the order of 2% of the peak service stresses but in the real situation they could be even greater. To minimise these it is necessary to use a fine mesh and/or higher order elements.

Additional to computational aspects, since material behaviour is highly sensitive to temperature, accurate determination of the latter is essential. Temperature gradients across rotating turbine discs are functions of conductive heat flow within the disc and convective and radiative heat flow at the surfaces. Boundary layer heat transfer coefficients are extremely difficult to quantify and in practice accurate temperatures are best determined by measurement using thermocouples, radiation pyrometers or thermal paint. Since these data are not available at the time of design it is necessary to use heat transfer coefficients based on past experience.

Qualitatively the effects of temperature can be summarised as follows. For a soaked high temperature condition, the rim of a disc is hotter than the bore. Differential expansions result in the diaphragm being subjected to radial tensile stresses, the cob to hoop tensile stresses and the rim to hoop compressive stresses. Conversely, during deceleration, the rim cools more quickly and a reverse temperature gradient can be established with the rim being subjected to high tensile hoop stress, the web to radial compressive and the cob to hoop compressive stresses.

The effects of temperature can be illustrated in more detail by reference to its influence during specific parts of the flight cycle.

Early in the take-off sequence a maximum temperature gradient is established between the cold interior of the cob and surrounding parts of the disc. A simple thermal sensitivity analysis can be performed to investigate the dependence of the induced stresses on temperature variations. The results of such an analysis are illustrated in Fig 1. The maximum hoop stress is linearly related to the temperature difference between the surface and the centre of the cob. The extrapolation to isothermal conditions indicates the hoop stress due solely to mechanical loading, and in the present case this is about 680 MPa. The additional diagram on Fig 1 exemplifies the 'onion ring' stress contours of a disc for a transient temperature difference of 300°C.

For this disc it is considered that during the take-off sequence the cob experiences a maximum temperature difference of 150 ± 25°C. This produces a variation of < 5% in the calculated peak transient hoop stress (1200 MPa ± 5%). A similar analysis shows that during the shutdown sequence the magnitude of the maximum thermally induced compressive stress is 40% of the peak tensile value.

A sensitivity analysis can also be carried out for an idealised cruise condition. For the case considered, temperatures at the rim and bore have been estimated to be 650°C and 300°C respectively. Calculations indicate that under these conditions the maximum steady state hoop stress at the bore is about 80% of the peak transient value. It is noteworthy that this calculated stress value is not particularly sensitive to inaccuracies in the estimated temperatures and variations of 50°C in the operating temperature difference alter the calculated peak hoop stresses by only 5%. Extrapolation to isothermal conditions confirms the previous value for the peak hoop stress due solely to mechanical loading (680 MPa). This is again about 70% of the peak steady state stress level. Although the latter situation is physically unrealistic this confirmation of the level of mechanical stresses provides confidence in the analyses.

4 MATERIAL MODELLING

In the discussions on temperature sensitivity, the stress calculations assumed that the disc remained elastic. In general it is good practice to carry out a full plastic analysis of the disc, which requires tensile stress-strain data over a range of temperatures likely to be experienced by the disc. The tensile stress-strain curves are affected not only by minor compositional and structural variations between samples of a material, but also by the strain rates during testing. The influence of the latter factor increases progressively as the testing temperature increases. Fig 2 shows a schematic tensile curve. Curves representing fully elastic and ideal plastic material have been added to illustrate extremes of mechanical behaviour.

The following examples have been selected to illustrate some of the effects of material properties on predicted stresses in components.

In general terms, for a stress concentration feature at low temperatures the strongest samples of a material might remain elastic whereas weaker samples of the same material might be expected to yield. Furthermore, for a stress concentration feature at a high temperature, stronger samples may behave in the typical elastic-plastic manner whereas weaker samples of the same material, could tend towards elastic-ideal plastic behaviour, especially at slow strain rates.

Figs 3(a), (b) and (c) show van Mises and maximum principal stress gradients at a typical stress concentration feature in a small turbine disc. The effects of extremes in material behaviour are illustrated in Figs 3(a) and (c), where respectively the material is assumed to behave in an elastic and in an ideal-plastic manner. Fig 3(b) illustrates the results likely to be obtained for a typical material.

These conventional stress analyses predict the response of the material to monotonic loading conditions. However prolonged engine service with complex mechanical and thermal cycling can alter the response of the material to the induced loads through processes such as creep relaxation or dynamic softening. Examples of these effects will be given by reference to the analyses of a titanium model disc which was cycled to failure in a spin-pit test. Fig 4(a) illustrates the hoop stress distribution along the centreline of the disc. The results were obtained using conventional tensile stress-strain data. On completion of the experimental test, standard fractographic examination revealed the location of the the initial cracked region in the disc and this has been identified in the figure. Typical of many situations in which stress redistribution takes place, the cracks occurred sub surface.

Neither von Mises stress nor the maximum principal (hoop) stress, which is illustrated in Fig 4(a), predict the failure region in the disc. However in practice at temperatures below 200°C, several titanium alloys are known to accumulate strain when under constant load[5] and a corollary to this is that in a disc rotating at constant speed, plastic strain will occur but in this case, at a stress concentration feature it will be accompanied by stress relaxation. Since the only relevant materials information used in a conventional stress analysis is stress-strain data no account is taken of this behaviour and so, before a more accurate estimation of the stress distribution can be obtained, an improved characterisation of material response to the induced mechanical cycle is required. In defining laboratory tests to achieve this, points to be considered include whether the tests should be stress or strain controlled and whether periods of time on or off load affect material behaviour. Additionally the stress analysis of Fig 4a is valid for the first loading cycle and shows that during this cycle the whole of the cob undergoes non-uniform plastic deformation. Hence the most satisfactory simulation of the material behaviour may be achieved by strain control tests.

Appropriate simulation of material behaviour requires recognition of two further points. Firstly, the model disc tests incorporate dwell periods at maximum speeds and this can be simulated in the strain control tests by sustaining the peak strain for a similar duration. Secondly, the minimum strains imposed during strain control testing must be selected to simulate the compressive stresses remaining in the disc after the load is removed. This is a much more difficult requirement to fulfil and needs detailed assessment. Results from the earlier analysis showed that on unloading the remaining compressive stresses are much less than the compressived yield point. However, practical experience warns that, for a typical zero to max strain test on a laboratory specimen, should yielding occur to the extent experienced in the disc, the accompanying stress cycle will alter from the initial zero to max stress such that at 'shakedown', stress levels will tend towards a fully reversed stress cycle. This implies that a zero minimum strain level is too severe to model accurately the small compressive stress levels remaining in the disc, and leads to the requirement that the lower strain control limit should have a tensile value.

A series of these tests can be used to characterise a material's response to cyclic loading. This has then to be represented as a materials behaviour model acceptable for analysis purposes. Peak shakedown stress against corresponding total accumulated strain provides a suitable form and allows a dynamic stress-strain curve to be constructed. The use of such a materials model in a stress analysis of the same problem as for Fig 4a gives the results shown in Fig 4b (static and dynamic stress strain curves are schematically compared in Fig 5).

The dynamic stress-strain curve reflects 'shakedown' conditions but provides no information on the progressive transition from initial to shakedown stress distributions. Equally it is impractical to model individually thousands of loading cycles. Nevertheless, since transient behaviour may influence final shakedown conditions, information on this may be important. It can be obtained by performing a time-dependent analysis. From such an analysis the estimated stress distribution after 100h load is presented in Fig 4c. The results were obtained using the MARC* analysis package with an RAE user-developed subroutine incorporating a creep equation for deformation behaviour. Comparing the predicted failure locations in Fig 4b and 4c the dynamic stress-strain curve gives a better result than the full creep analysis. Computing times on a Vax 11/750 minicomputer were 20 min for the dynamic curve analysis and 100 min for the creep, making the dynamic analysis particularly attractive.

The relatively poor predictions of the creep analysis arises because it is found that under cyclic loading with dwell-on-load, strain accumulates slightly faster than under simple static creep and so the creep equation used to predict Fig 4b still did not accurately model the material response to the imposed cyclic loading. If the additional effects of loading are taken into account, close agreement is obtained with the results from the dynamic analysis. The results in this section demonstrate that to obtain relevant stress distributions in discs care must be taken to characterise correctly material behaviour.

5 IDENTIFICATION OF CRITICAL STRESSES AND LOCATIONS

Having completed the stress analysis of a disc, a further problem is to determine whether, von Mises stress, equivalent plastic strain or maximum principal stress should be used to correlate behaviour. This section examines these options in respect to methods available for estimating disc life.

For the model disc associated with Fig 4, the von Mises stresses are highest at the bore although cracks initiate within the cob, the exact location coinciding with the peak hoop stress (ie maximum principal stress) as shown in Fig 4a.

The distribution of stresses around a stress concentration feature in a small cast disc are presented in Fig 6 and some details are given in Table 4.

Table 4

ASSESSMENT OF STRESSES AT VARYING DEPTHS IN THE FAILURE REGION
OF A SMALL GAS TURBINE DISC

Location		Stress MPa		Plastic strain $\varepsilon_p (\times 10^{-3})$	Cracking susceptibility	Relative crack growth rates
		von Mises	Maximum principal(σ_1)		$\sigma_1 \sqrt{\varepsilon_p}$	$\sigma_1 \sqrt{a}$* MNm$^{-3/2}$
Crack site	Surface	719	897	4.9	63	9.0
	5% depth	717	932	2.6	48	9.3
	10% depth	706	1013	0.7	27	10.1
	15% depth	700	1004	0.4	6	10.0
	20% depth	604	864	0.0	0	8.6
COB		716	608	2.7	32	6.1

* assumed flaw size a = 0.1 mm

The results show that for a range of locations there is little difference in the von Mises stress levels. In contrast, plastic strains and principal stresses show marked differences. Indeed the greatest plastic strain in the vicinity of the failure site is approximately twice that in the cob region and more significantly, peak maximum principal stress is almost twice that in the cob region. Similar results are obtained when increasing the peak rotational speed (Table 5) and as will be seen later, by altering the local geometry.

Table 5

EFFECT OF OVERSPEED ON STRESSES IN THE FAILURE REGION

Speed	Stress MPa		Plastic strain $\varepsilon_p (\times 10^{-3})$
	von Mises	Maximum principal	
Design speed	717	895	2.2
5% overspeed	718	933	3.6
10% overspeed	719	986	4.3

---

* Tradename of MARC Analysis Research Corporation

In Fig 7 lines have been drawn at selected nodes to indicate the operating directions of the maximum principal stresses in the failure region of the disc. The dots shown in this figure indicate that at these positions the principal stress perpendicular to this plane, (ie the hoop direction) has now become the maximum principal stress. Examination of cracked disc shows that the cracks grow perpendicular to these directions, supporting the importance of principal stress as a parameter controlling disc life. If flaws are present, relative crack growth rates at the various positions are also presented in Table 4. The results emphasise the importance of principal stress as a disc life limiting parameter and the significance of this will be discussed further in section 7.

The results also show that the plasticity is greatest in surface regions. In the absence of an inherent defect, the crack site will be related to a combination of the operating stress and the local plastic strain, and so an approximate crack susceptibility factor, $\sigma_1\sqrt{\varepsilon_p}$, can sometimes be used. This factor has been selected over the more physically attractive energy term ($\sigma\varepsilon_p$) because from the limited information available principal stress is more important in controlling crack initiation than plastic It should be noted that the factor is used to indicate the likely cracking position and is not associated with stress intensity.

6 DESIGN CONSIDERATIONS

Having identified the failure region in the disc as illustrated through the results in Tables 4 and 5 the next stage is to investigate possible design modifications which will increase the life at this location.

A useful concept in disc design is the 'free hoop radius'. This is the radius at which a thin free ring of the same material as the disc, would have the identical radial growth. If a design modification adds material inside this radius it should reduce local hoop stresses and should be self supporting. Material added outside the free hoop radius has to be partly supported by the existing disc and therefore increases stresses elsewhere.

Table 6 illustrates peak von Mises and principal stresses in the failure region of a disc as the local profile is altered. For comparison purposes peak bore region stresses are included. Again it can be seen that increasing the radius has an insignificant effect on the local von Mises stress level. In contrast there is a large reduction in local plastic strain, accompanied by a significant reduction in peak principal stress. As far as disc life limiting factors are concerned, a reduction in the critical radius by a factor of 6 still gives a peak principal stress level which is higher than that in the cob region. Thus if a flaw is present, the crack propagation rate will be higher than in the cob. However, the local plastic strain is only about 0.6 of the peak bore strain and so the susceptibility parameters, $\sigma_1\sqrt{\varepsilon_p}$, are similar, indicating that this is close to optimum design. Indeed, increasing the radius further adds material outside the free hoop radius and has therefore to be supported.

Table 6

EFFECT OF INCREASING CRITICAL RADIUS ON LOCAL STRESSES
AND SUSCEPTIBILITY TO CRACKING

Location	Stress MPa		Plastic strain	Cracking susceptibility	Relative crack growth rates
	von Mises	Peak maximum principal(σ_1)	$\varepsilon_p(\times 10^{-3})$	$\sigma_1\sqrt{\varepsilon_p}$	$\sigma_1\sqrt{a}$** $MNm^{-3/2}$
*R	721	1140	8.5	105	36
2R	719	1040	4.9	73	10.4
6R	713	880	1.6	35	9.8
Cob	716	608	2.7	32	6.1

*R is the original radius at the limiting feature
** assumed flaw size, a , = 0.1 mm

Designing components in which the stress systems redirect or turn the crack is a useful way of allowing larger crack growth prior to failure. This extra life should be used only as a safety factor if occurring in the cob region and in the rim it should be used to minimise the amount of material shed should a crack propagate.

It is well established that von Mises stress is most appropriate for characterising multiaxial creep processes and plastic flow. However, the results in Table 6 indicate for discs that equivalent plastic strain is a more sensitive measure of material behaviour and support its use as a control parameter in Low Cycle Fatigue studies. In plain specimen LCF testing, the imposed strain is applied over the whole gauge volume and the subsequent crack growth is rapid since it is in a constant or, following crack growth, an increasing stress field. In a disc, specific strain levels apply over very small volumes and growth is generally into a decreasing stress field. Hence failure in a simple laboratory test cannot be easily equated to failure in a disc. Nevertheless for a given strain level, crack initiation is likely to occur in a similar number of cycles and so the laboratory failure curve can be used to estimate crack initiation in the disc.

For cast materials incurring over 0.1% plastic strain, failure can occur in about 100 cycles so that for a range of loading conditions, crack initiation is a relatively easy event and therefore arguments with respect to inherent and induced cracks become largely irrelevent. Hence discs of these materials may be cracked for most or even all of their lives, although initially crack sizes may be below typical limits of detection. In practice, providing a suitable initial size is assumed in the crack propagation analysis, it should be possible to estimate safe lives for these discs. Indeed ENSIP lifing rules assume that flaws are present at critical locations and if applied to the results in Table 4 would lead to the prediction that cracks at the sub-surface position grow at a rate which would be 10% faster than at the surface and 66% faster than in the cob.

7 DISC LIFING PROCEDURES

Having established the important factors controlling material behaviour and identifying their distributions, the next stage is to use these in a life determination exercise. Two approaches have emerged, the traditional life to first crack and more recently the application of fracture mechanics and damage tolerant design concepts. Progressively the latter is assuming greater importance. Indeed the potential of modern high strength disc materials may only be fully exploited by instituting such procedures. Firstly however the 'life to first crack' approach will be examined briefly.

7.1 Life to first crack

Currently, design curves are based on disc spinning results and/or laboratory LCF data which have been modified using statistics to produce the design curve for the disc. Essentially this is a crack initiation approach in which the disc is considered to be life expired once a crack has been detected. Superficially it may be considered to have the advantage that no detailed understanding of the mechanisms of failure is required, however if life predictions are to be made with confidence it is essential to establish the limitations of the method employed.

In practice spin-pit tests are normally conducted isothermally and service thermal stress is allowed for by increasing the disc speed. Typical effects of test overspeed on stress distribution in the critical region of a disc are presented in Fig 8. It can be seen that the 40% overspeed test has achieved the peak stress level of the service disc, however the associated stress gradients do not correlate as well. This poor agreement is also reflected in both equivalent strain and principal stress values. For the reasons stated earlier, these differences should have little effect on the conventional "life to first crack". In contrast they will have a larger effect on the disc burst life which includes a significant contribution from the crack growth stage. Techniques for quantifying crack growth will be considered in the next section.

7.2 Crack propagation life

Within the overall fatigue endurance life of a disc, various phenomena operate in the crack initiation and propagation phases. Manufacturing induced defects and service imposed local strain events, separately, or in combination, control disc crack initiation. To assess fully the effects of the initial crack or defect, it is necessary to estimate its crack propagation life and the major numerical problem in this is the determination of the operating stress intensity factors. Detailed assessment of fracture mechanics computations is outside the scope of this paper. Nevertheless since stress intensities are calculated from the results of stress analyses a brief resume will be given of some of the techniques employed and the likely accuracies of the results.

The initial problem in such a stress analysis is the modelling of the mesh near the crack tip so that the singularity in stress can be represented with sufficient accuracy. Many methods are available, a typical one being to degenerate standard 8-noded isoparametric elements to triangles and to move the midside nodes adjacent to the crack tip to quarter point positions. Using such elements in a stress analysis satisfies the $1/\sqrt{r}$ singularity in the stress field. The resultant errors obtained in stress intensity values calculated from stresses and displacements or strain energy release rates are generally within ±3%.

Although only propagation life is controlled by the stress intensity parameter it is now known, thanks to greater sensitivity of laboratory methods, that crack propagation is occurring during the main part of a components life. However, there is a lower crack size limit to stress intensity controlled crack growth. Haddad[4] has proposed the use of an 'l_o' parameter which is function of threshold stress intensity and the fatigue endurance stress and in a simplified form relates to the crack size which must be exceeded before continuum mechanics can be applied.

The integrated form of the standard crack growth equation, $da/dN = c\Delta K^n$, can be used to estimate the number of cycles, N, between initial, a_o, and final safe crack size, a_1, as shown:

$$N = \int_{a_0}^{a_1} \frac{da}{c(\Delta K)^n}$$

and

$$\Delta K = G\sigma \sqrt{\frac{a}{\pi}}$$

where c and n are material parameters and can be determined by standard tests. G is a function of crack geometry.

Numerical procedures are frequently used to fit particular forms of f(ΔK) to the raw da/dN - ΔK data obtained from laboratory crack propagation tests. For illustration, Fig 9 shows two possible representations of the same data and Table 8 shows the results when these, and two additional expressions are applied to a typical propagation analysis. It can be seen that for this exercise the choice of law can influence the life by about 13%.

Table 7

CALCULATED LIVES WITH SELECTED CRACK PROPAGATION EQUATIONS

Form of law	RMS error in ΔK	Calculated life (cycles)
$C(\Delta K)^n$	15%	5169
$EXP(C_1 \sin h\,(C_2 \log \Delta K + C_3) + C_4)$	3.3%	5338
$C(\Delta K - \Delta K_{TH})^n / ((1-R)\,K_c - \Delta K)$	1.6%	4749
Linear interpolation on raw data	N/A	5412

To avoid cycle-by-cycle integration, a numerical quadrature scheme is often used and may include a second order, predictor-corrector algorithm with a fixed relative change in crack length per step. For a typical propagation analysis the associated accuracy is illustrated in Table 8.

Despite the importance of these results, non-through surface and corner cracks are more important to discs and will be discussed in the following section.

Table 8

TYPICAL ERRORS ASSOCIATED WITH CRACK STEP LENGTH

Relative change in crack length in one step	Number of evaluations of $\frac{da}{dN}$	% Error in life
0.01	742	-
0.02	372	-
0.05	152	0.03
0.1	78	0.25
0.2	40	0.80
0.5	18	4.64

Although a few 3D finite element analyses growing cracks in components have been reported, for example Ref 5, currently this is an expensive design procedure. For simple geometries, solutions have been tabulated in Refs 6 and 7, for example, and these are accurate to within 5%. However, for complex cases when the crack is of the same size as a local structural feature it is necessary to use an alternative method such as approximating the Green's function of the component by that of a rectangular block. It is then possible to use the stresses in the uncracked body and the tabulated solutions to estimate the stress intensity factors in the component. The accuracy of this type of procedure is hard to quantify but, without extreme care, the errors can be greater than 20%.[11]

Recently the approach in Ref 6 has been extended to the analysis of small non-through cracks occurring within the plastic strain fields of notch bend fatigue specimens[8]. It was shown that these behave similarly to long cracks, provided the appropriate stress values are used. In this case the plastic stresses adjacent to the crack fronts rather than the remote stresses were used to calculate the stress intensity. In practice, although disc materials may initially deform plastically, in most situations these components quickly shakedown to essentially elastic behaviour. Hence although the approach may not be strictly correct, when applied with caution, errors should be small.

With these assumptions and using average short crack stress intensity values, it is possible to superimpose both short corner and centre, crack propagation rate data on the long crack best fit line, Fig 10. As shown in this figure, the assumptions are also valid for short cracks in model discs.

The above technique has been applied to the small engine disc referred to previously. Modelling the cracks as semicircular flaws in a finite block gives a value for G = 2.32. Assuming a_0 = 0.5 mm and that after initial plastic flow has occurred the material behaves elastically, the estimated disc lives are within 15% of the values calculated from spin-pit test results.

8 SERVICE MONITORING

In any lifing procedure, it is essential that actual service usage be monitored and compared to the design assumptions. This requires the stresses and temperatures from flight recorded data. An approach to this formidable computational task is described in Ref 9. In this an algorithm is described which is capable of reproducing the results of the finite element models discussed earlier to an accuracy of ±5%.

9 DAMAGE TOLERANT CONCEPTS

The optimised design of severely loaded components such as gas turbine discs is a balance between low weight and high strength. Demands for increased engine performance have progressively resulted in higher stresses in discs and this has in turn resulted in the development and use of specialised high strength alloys. In general, these have a different failure criterion compared to conventional wrought discs, and hence require new lifing concepts (*eg* ENSIP) to realise their full potentials. Indeed the current paper is particularly relevant to two aspects of the proposed ENSIP lifing regulations.

Firstly, a main objective of these lifing rules is to apply damage tolerant concepts to those critical parts where failure could result in the loss of an aircraft. Engine discs with their high rotational energies fall into this category and to achieve adequate damage tolerance their stress distributions must be accurately predicted and controlled. The section on numerical analysis showed that if the disc is modelled with insufficient detail not only will there be errors in the calculated stress levels but also in the predicted failure positions. This can have serious ramifications when attempting to control the stress distribution to achieve damage tolerance.

Secondly, and of greater importance, it is suggested in ENSIP that structural properties used in design shall be the minimum of the specified values. This, surprisingly, may lead to the optimistic lifing of some components. The implication of Fig 3 is that, due to smaller amounts of plasticity, discs of higher strength batches of a given material may be stressed to a greater degree than discs manufactured from minimum strength samples of the material. Thus, in the presence of a flaw, they will have higher stress intensities and hence the paradox that the life expectancy of discs manufactured from high strength samples may be lower than those of poorer quality material and consequently may be lower than the predicted life using the method proposed in ENSIP.

The success, in the finite element analysis context, of using the dynamic stress-strain curve in modelling the material response to cyclic loading, indicates a requirement to develop and expand the material characterisation. Under cyclic loading conditions, material in the region of a stress concentration feature such as a bolt-hole may experience almost fully reversed stress cycles and, in contrast in the cob region, the situation may be closer to repeated tensile stress cycling. The significance is that different loading sequences can produce varying material responses and hence different dynamic stress-strain relationships. Thus in a stress analysis forming part of a service usage assessment, it may be necessary to employ a series of dynamic stress-strain curves which have been obtained under the cyclic conditions most appropriate to the specific regions.

Statistical analysis indicates that current lifing rules result in some 80% of turbine discs being retired from service having used less than half their available safe life. With reference to any alternative lifing technique having to achieve a greater utilisation of available safe life, the results in Table 6 are important. These show that even with the largest radius considered (the '6R' geometry), the maximum principal stress is much greater than at the cob and consequently, assuming the presence of flaws, crack propagation rates will be correspondingly faster. However in the absence of a flaw, plastic strain is greater in the cob region. Therefore, on the basis of results from simple strain controlled fatigue tests, cracking could occur in this region prior to the critical location. Complementary to this, the thermal analysis shows that the transient temperature differences during the take-off and landing sequences may induce the largest stresses experienced by the disc and again these are most severe in the cob. In practice, because of lower principal stresses in this region the crack should propagate at a slow rate. Unfortunately this crack is likely to initiate at a sub-surface location with the accompanying detection (and lifing) difficulties. These examples illustrate the requirement for careful inspection of the whole disc.

The effects of surface defects can possibly be simulated in spin-pit tests by introducing artificial cracks at critical locations. Unfortunately, as Fig 7 illustrates, for any region where plastic flow occurs, the critical location is sub-surface and it is not possible to simulate embedded defects in these locations, although pessimistic safe lives may be estimated by introducing an artificial surface flaw to the appropriate depth.

To calculate the full thermal contribution to life consumption, heat transfer models have to predict component temperatures as a function of flight conditions. In the past there has been inadequate identification of the service usage critical to the lifing of individual components. However in-flight recorders now allow accurate monitoring of service profiles. A recent approach to the analysis of such information is based on carrying out continuous but simplified thermal and stress analyses and then using correlating tables/constants for translating these results to corresponding full scale analyses. This has the potential for on-board installation, and accurate monitoring of damage accumulation. It may therefore provide a realistic way of meeting the requirement for in-flight transient thermal and stress analyses.

10 CONCLUDING REMARKS

In the design and subsequent life assessment of discs the requirement for accurate stress and temperature analyses has been demonstrated. The influences of mesh size and material response and the role of shakedown stress have been illustrated.

The importance of local strain and principal stress has been shown. A parameter to assess sensitivity to cracking has been suggested to aid the evaluation of design modifications.

Of the numerical inaccuracies considered, it has been recognised that the major problem relates to the determination of stress intensity factors at complex structural details.

Finally, the importance of accurately modelling materials behaviour has been considered in relation to a design code.

Acknowledgments

The authors would like to thank Mr P. Tranter who carried out several of the analyses discussed in this report and Dr W.J. Evans and Dr R. Dholiwar for helpful discussions.

11 REFERENCES

1. J.M. Ramsden, Uncontained engine failure: the 3 wide body turbofans compared. Flight International, 187-188, January 1982

2. T.J.W. Ward, C.G. Burton, Design and implementation of an efficient 3D finite element code for high temperature problems, presented at Mathematics of Finite Elements and Applications Conference, Brunel University, England. May 1984

3. W.J. Evans, C.R. Gostelow, The effect of hold time on the fatigue properties of a β-processed titanium alloy, Metallurgical Transactions, 10A, 1837, 1837-1346. 1979

4. M.M. El Haddad, K.N. Smith, T.H. Toffer, Fatigue crack propagation of short cracks, ASME, 101, 42-46. 1979

5. C.J. Lof Elangovan, G. Reibaldi, S.B. Welt, Numerical and experimental evaluation of stress intensity factors for curved crack fronts. Proceedings of 2nd International Conference on Numerical Methods, Pineridge, 671-686. 1980

6. A.C. Pickard, Stress intensity factors for cracks with circular and elliptical crack fronts. 2nd International Conference on Numerical Methods in Fracture Mechanics, Pineridge, 599-614. 1980

7. J.C. Newman Jr, I.S. Raju, Stress intensity factor equations for cracks in 3D bodies, NASA, TM83200. 1981

8. W.J. Evans, M.E.F. Smith, C.H.H. Williams, Disc life predictions for gas turbine engines, NATO-AGARD-CP 368, 11, 1-12. 1984

9. T.M. Edmunds, R.A. Lawrence, Monitoring engine thermal stresses, NATO-AGARD-CP-368 2, 1-19. 1984

Copyright © Controller HMSO, London, 1985

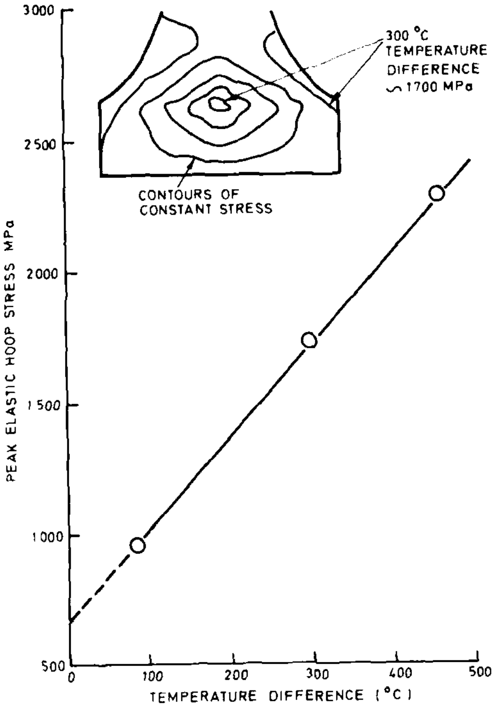

Fig.1 Effect of transient temperature differences on cob stresses

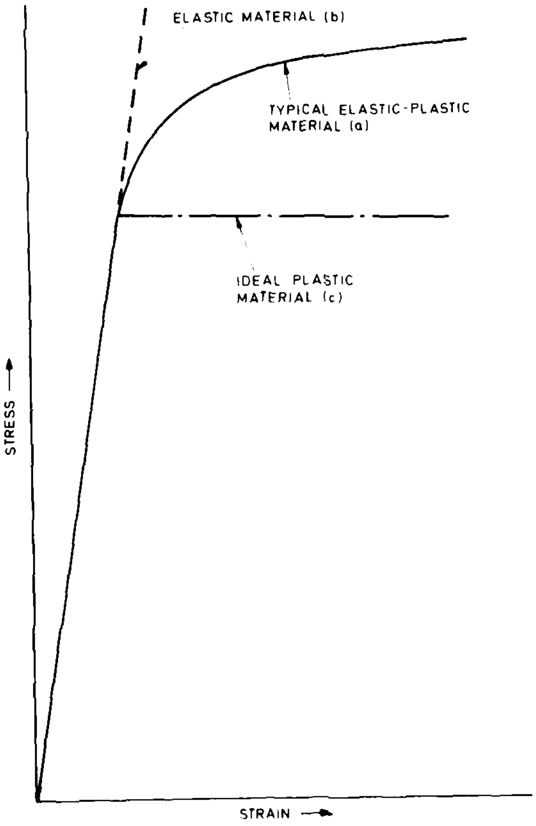

Fig.2 Typical stress-strain curve (a) with limits of elastic (b) and ideal plastic behaviour (c)

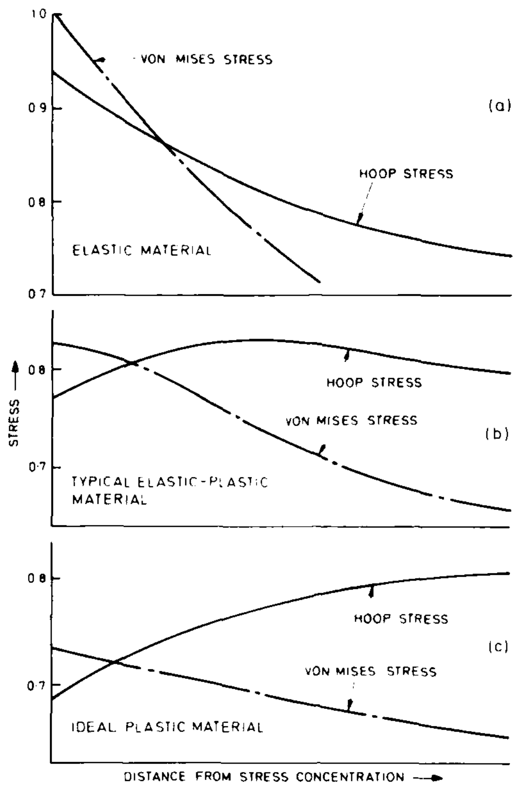

Fig.3 Effect of tensile properties on normalised stress distribution around a stress concentration feature

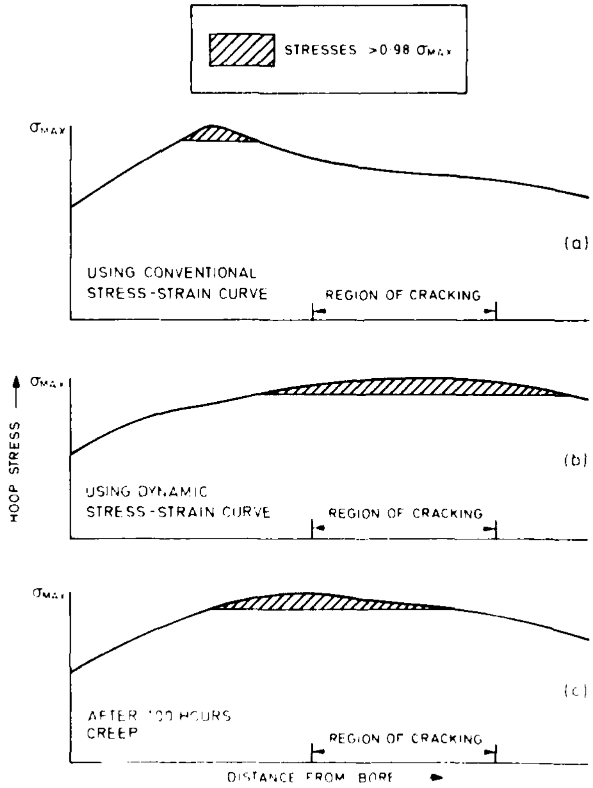

Fig.4 Computed stress distribution in a titanium disc

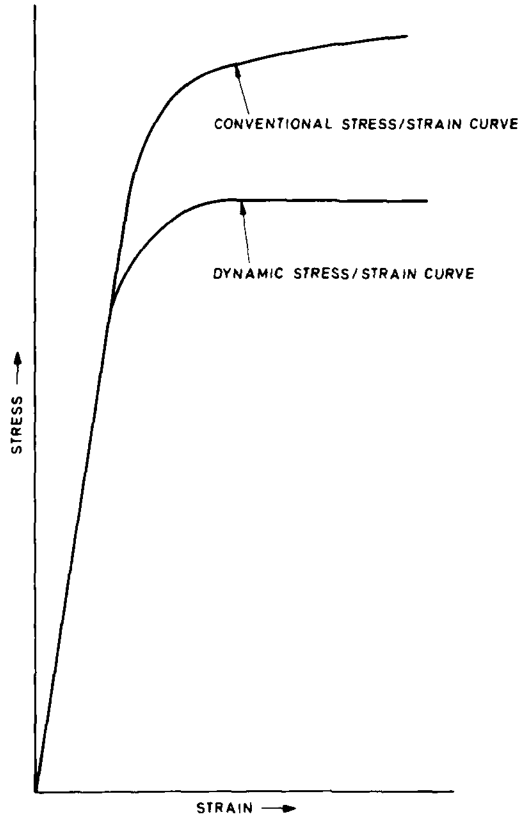

Fig.5 Schematic conventional and dynamic stress-strain curves

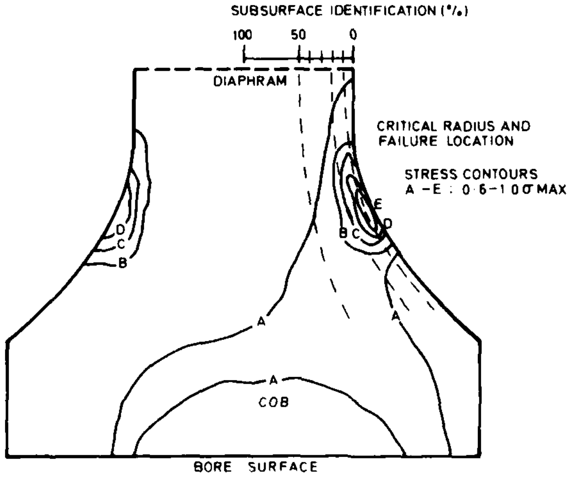
SUBSURFACE IDENTIFICATION (%)
100
50
0
DIAPHRAM
CRITICAL RADIUS AND FAILURE LOCATION
STRESS CONTOURS A – E : 0·6–1·0σ MAX
D
C
B
E
D
B
C
A
A
A
COB
BORE SURFACE

Fig.6 Distribution of maximum principal stresses in a small gas turbine disc

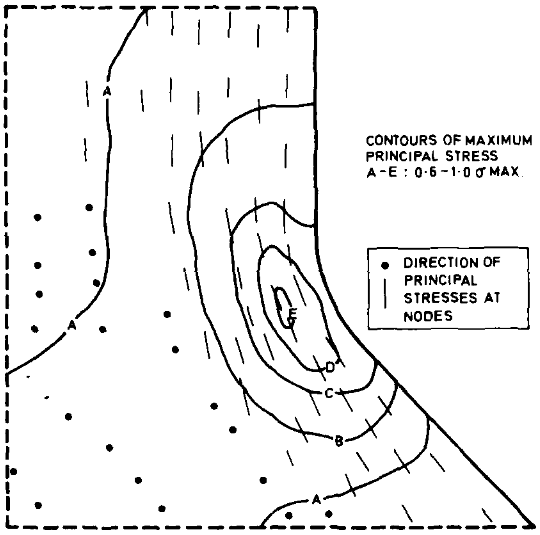
A
CONTOURS OF MAXIMUM
PRINCIPAL STRESS
A–E : 0·6–1·0 σMAX
● DIRECTION OF
| PRINCIPAL
STRESSES AT
NODES
E
D
C
B
A

Fig.7 Maximum principal stress and operating directions

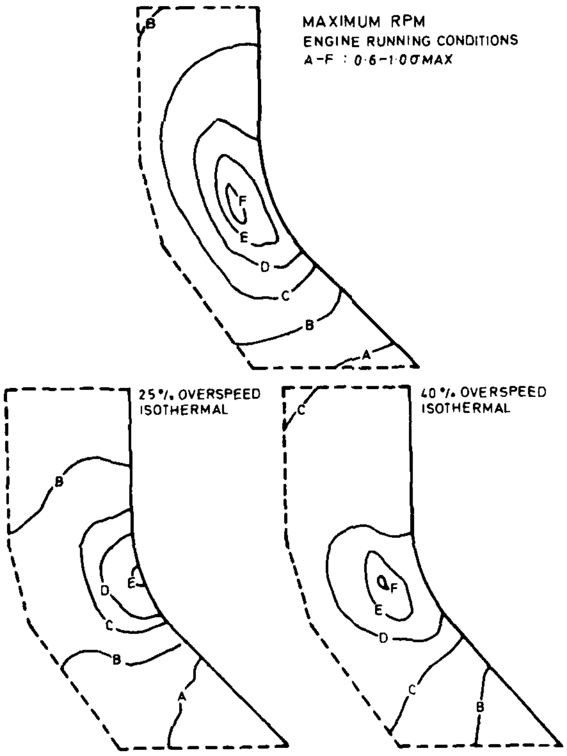
MAXIMUM RPM
ENGINE RUNNING CONDITIONS
A–F : 0·6–1·0σMAX
B
F
E
D
C
B
A
25% OVERSPEED
ISOTHERMAL
B
E
D
C
B
A
40% OVERSPEED
ISOTHERMAL
C
F
E
D
C
B

Fig.8 Effect of overspeed on maximum principal stress distributions

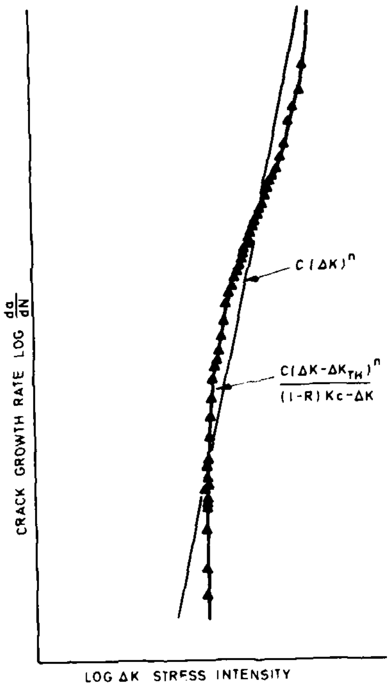

Fig.9 Typical empirical equations for crack propagation results

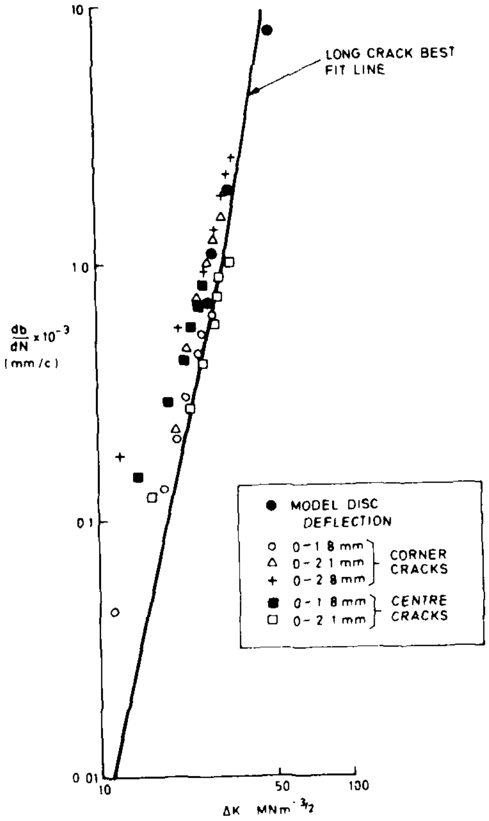

Fig.10 Short-crack crack propagation data and long-crack best fit line

DAMAGE TOLERANCE ACCEPTANCE METHODS IN STRUCTURAL COMPONENTS OF A MEDIUM CARBON STEEL AND A MEDIUM STRENGTH AL-Mg ALLOY

by
C.M.Branco
Professor
UNIVERSITY OF MINHO
4719 Braga Codex
PORTUGAL

SUMMARY

A review of the damage tolerance methodology is presented refering the main factors, parameters and computacional procedure for the assessment of flaws in the structure in order to avoid fatigue failures. Flaw acceptance and fatigue design methods are also reviewed and discussed.

Results of a defect tolerance study in cruciform welded joints of low and medium strength steels are presented. Theoretical defect tolerance curves relating initial flaw sizes, applied nominal stress, endurance and weld and plate geometry are obtained. The results are compared with some experimental data and also with the quality level curves proposed in the PD 6493 document for fusion welded joints.

The outline of the fatigue life prediction method and defect analysis in ductile materials such as the medium strength Al-Mg alloy 5083 is presented. COD and J integral data in this material is presented in the temperature range -120°C to 200°C.

1. THE DAMAGE TOLERANCE METHODOLOGY

Damage tolerance or defect tolerance acceptance methods are quite extensively used in the aircraft and aerospace industries. Many excelent reviews on the subject are available describing with some detail the damage tolerance methodology applied to components and structures in the aircraft field(1,2,3).While it is not the purpose of this paper to present the background of the damage tolerance it is important to start with refer the most important parameters of the damage tolerance analysis. Thus, parameters such as

- initial flaw size and flaw distribution
- stress spectra
- stress distribution and stress concentration factors
- environmental conditions (temperature,level of corrosion, etc.)
- stress intensity factor formulation
- threshold and fatigue crack propagation data
- stress corrosion data
- service life and endurance
- inspection intervals
- fracture toughness data

are the basis of any damage tolerance prediction method.

In many advanced industries such as the aircraft industry a damage tolerance assessment program is usually carried out either in the prototype stage of structural developement or in the early stages of the structure life. The main objective of the damage tolerance assessment is to define structural life,operational limits and establish improved structural inspection requirements. An operational life in terms of flight hours is previously defined and the structural life of the aircraft determined using Fracture Mechanics, should be greater then the operational life. A damage tolerance assessment program is normally carried out in five stages:

(1) Preliminary Damage Tolerance Assessment
(2) Initial Quality Assessment
(3) Stress Spectra Development
(4) Operational Limits and Inspection Requirements
(5) Individual Aircraft Tracking Program

Each one of these stages will now be explained with some detail.

In the Preliminary Damage Tolerance Assessment one selects and evaluates potentially critical structural areas which could affect safety. Candidate critical areas are systematically identified and screened using available stress and fatigue analysis data, service experience and nondestructive inspection data. Hence, the potentially critical structural items are identified, and to each location an assessment is made of its degree of criticality. The degree of criticality depends on several factors. For example there are areas where a single failure would result in the loss of the structure. These would be considered more critical than areas which could sustain a failure without loss of structure. Another important factor is the inspectability. Areas more difficult to inspect are considered more critical than others. In practice it means that, due to economic reasons, these areas will be inspected less frequently and this must be taken into account in the inspection intervals. Additional considerations affecting the degree of criticality are:

- material type and thickness
- strength and fatigue design margins
- crack growth rates
- stress concentrations
- load transfer
- service experience
- test data

Usually, after a detailed analysis has been carried out, only a few areas are judged sufficiently critical to warrant detailed analysis.

The purpose of the Initial Quality Assessment is to assess the initial manufacturing quality of the structure and to determine the maximum size of initial flaws that could be expected. A statistical distribution of initial manufacturing flaws could be obtained using either

(a) analysis of nondestructive records of flaw shape, distribution and location obtained in the actual or in a similar structure.
(b) analysis of crack propagation tests performed in selected parts of the structure

The nondestructive record analysis is comparatively straightforward to carry out, and only requires a well qualified and trained operator and a extensive collection of records for the selected critical areas. However NDT is not able to detect flaws with sizes below the values quoted in Table 1 (4)

However it is always possible to start the Fracture Mechanics with the assumption that an initial flaw (with a size equivalent to the flaw detection limits) exists in the critical location. However, this approach may not be adequate, due to all the factors affecting the detection limits. A better method(though more expensive) is to obtain the sizes of the initial manufacturing flaws as outlined in (b). The procedure is to fatigue test the selected component using a generally modified constant amplitude spectrum to allow adequate fatigue marking. The crack then initiates and propagates to failure. A fractographic analysis of the crack surfaces can reveal the initial size of the crack. After the initial sizes are obtained in each location, the data is statistically evaluated. Often a log normal probability distribution is obtained and in such a case the plot schematically shown in Figure 1 shows the percentage of cumulative number of flaws against its equivalent initial flaw size. Assuming a certain probability of occurence and a given confidence limit the maximum initial manufacturing flaw size can be obtained. This value defines the initial quality assessment in the structure.

TABLE 1-Estimated variations in flaw detection limits by type of inspection (in mm) (in Pettit & Krupp,1974).

NDT Technique	Surface cracks		Internal flaws	
	Processing	Fatigue	Voids	Cracks
Test specimens, laboratory inspection				
Visual†	1.25	0.75	+	+
Ultrasonic	0.12	0.12	0.35	2.0
Magnetic particle	0.75	0.75	7.5	7.5
Penetrant	0.25	0.5	+	+
Radiography	0.5	0.5	0.25	0.75
Eddy current	0.25	0.25	+	+
Production parts, production inspection				
Visual	2.5	6.0	+	+
Ultrasonic	3.0	3.0	5.0	3.0
Magnetic particle	2.5	4.0	+	+
Penetrant	1.5	1.5	+	+
Radiography	5.0	*	1.25	*
Eddy current	2.5	5.0	+	+
Cleaned structures, service inspection				
Visual	6.0	12.0	+	+
Ultrasonic	5.0	5.0	4.0	5.0
Magnetic particle	6.0	10.0	+	+
Penetrant	1.25	1.25	+	+
Radiography	12.0	*	4.0	*
Eddy current	5.0	6.0	+	+

+ Not applicable. † Use with magnifer. * Not possible for tight cracks. (Based on 25-mm ferritic steel, surface 63 RMS.)

The Stress Spectra Development task consists of the development of baseline representative stress spectra to be used to obtain the operational limits and inspection requirements for the critical items identified in the Preliminary Damage Tolerance Assessment. The principal stresses are then computed for the critical items and for each loading condition. The accuracy of the analytical stress equations can be checked against stresses measured in service.

The Operational Limits and Inspection Requirements are established conducting crack growth analysis and tests for the critical areas selected in the Preliminary Damage Tolerance using the results of the statistical distribution of initial manufacturing flaws and the stress spectra as the stress input. The operational limits are based upon conservative assumptions to prevent loss of the worst case situation. The operational limit is the service usage interval beyond which a potential failure of the unrepaired structure could result in a final or complete failure. The operational limits for each critical item or location can be calculated integrating an appropriate fatigue crack growth rate equation from an initial flaw size to a critical crack size. The initial flaw size could be either the initial manufacturing flaw size defined in Figure 1 or the largest flaw with a certain shape that would remain undetected during fabrication of the structure. The critical crack sizes are dependent on the residual strength of the structure which may be defined on the basis of two requirements, both schematically defined in Figure 2.

(a) the structure must be capable of sustaining design limit load

(b) the structure must be capable of sustaining the maximum load expected during the inspection period(e.g. one half of the operational limit)

The crack growth rate data selected for the analysis should be representative of the material, thickness, environment and stress ratio. The stress intensity factor formulation should be appropriate for the shape and type of defect and loading mode. The crack integration model should account for variable amplitude loading usually occuring in realistic service spectra and account also for crack growth retardation phenomena (5). Different retardation models can be used for that purpose (5,6) and the cycle-by-cycle integration process is the more commonly used. In this process crack growth is predicted based on accumulation of increments caused by each load application defined in the stress spectra and considering crack growth retardation. In some cases crack retardation is not considered if the currently applied load develops a plastic zone to or past one previously developed (greatest elastic-plastic interface). Retardation is generally taken into account if the current load develops a plastic zone smaller than the one which preceeded it.

The Paris (7) and Forman (8) crack growth rate equations are normally used in the crack growth computation.

The final element of the crack growth analysis is the determination of the critical stress intensity or fracture toughness. Fracture toughness data should be obtained for the materials, thickness and temperature of interest. Finally the crack length increments can be computed with the application of the stress cycles defined in the stress spectra and taking into account the details mentioned before. The calculation ends when the current crack length and minimum required residual strength load produced a stress intensity equal to the fracture toughness. The number of cycles obtained in the calculation constitutes the operational limit of the critical location being considered.

The corresponding crack sizes to the inspection interval chosen can be calculated using the same procedure. This calculated crack size can then be compared with the size measured during the inspections and therefore an assessment of component integrity can be done during the inspection period. If, for example, the measured crack size in the location is greater than the calculated or expected crack size the component must be removed or repaired.

In the aircraft industry the Individual Aircraft Tracking Program is applicable to monitor damage in individual aircraft. This turns out to be necessary because the operational limits and inspection intervals are usually established for baseline usage and this varies from aircraft to aircraft. More details of this method may be found in (9).

To summarise the individual points mentioned above the following diagram describes a typical damage tolerance computational sequence

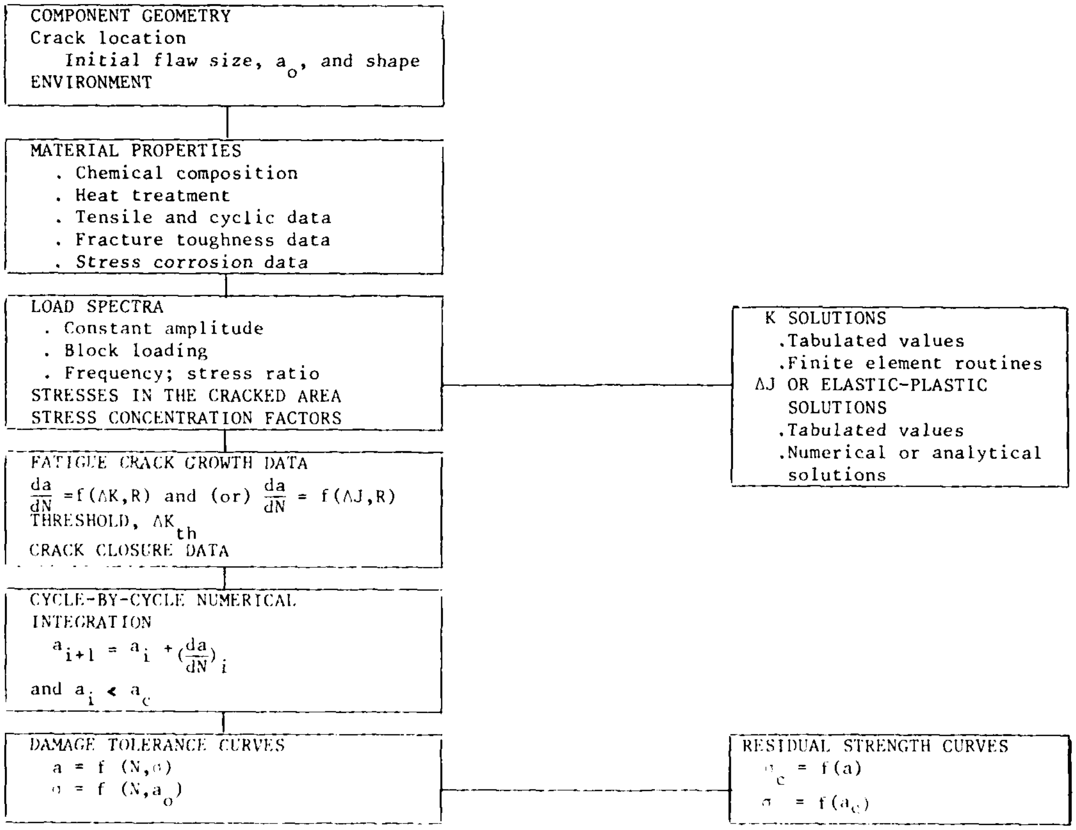
COMPONENT GEOMETRY
Crack location
Initial flaw size, a_o, and shape
ENVIRONMENT
MATERIAL PROPERTIES
. Chemical composition
. Heat treatment
. Tensile and cyclic data
. Fracture toughness data
. Stress corrosion data
LOAD SPECTRA
. Constant amplitude
. Block loading
. Frequency; stress ratio
STRESSES IN THE CRACKED AREA
STRESS CONCENTRATION FACTORS
K SOLUTIONS
.Tabulated values
.Finite element routines
ΔJ OR ELASTIC-PLASTIC SOLUTIONS
.Tabulated values
.Numerical or analytical solutions
FATIGUE CRACK GROWTH DATA
$\frac{da}{dN} = f(\Delta K, R)$ and (or) $\frac{da}{dN} = f(\Delta J, R)$
THRESHOLD, ΔK_{th}
CRACK CLOSURE DATA
CYCLE-BY-CYCLE NUMERICAL INTEGRATION
$a_{i+1} = a_i + (\frac{da}{dN})_i$
and $a_i < a_c$
DAMAGE TOLERANCE CURVES
$a = f(N, \sigma)$
$\sigma = f(N, a_o)$
RESIDUAL STRENGTH CURVES
$\sigma_c = f(a)$
$\sigma = f(a_c)$

In the present paper two applications of the damage tolerance methodology, not specific of aircraft structures, are described. The first one presents defect tolerance data for plate specimens and fillet(cruciform) welded joints of low and medium strength steels. The second study includes only the fracture toughness data and the outline of an elastic-plastic fracture mechanics analysis both for the medium strength Al-Mg alloy 5083.

2. FLAW ACCEPTANCE METHODOLOGY AND ANALYSIS IN WELDED JOINTS

Welded joints are quite extensively used in structural applications. For fatigue loading existing design codes(10,11) give a set of S-N curves each one applicable to a specific type detail and loading mode. The influence of weld defects and plate and weld geometry is not taken into account in these design curves, which are usually the lower bound of experimental results obtained for that type of weld detail.

In welded joints fatigue cracks usually initiate in stress concentration areas like the weld toe and weld root. Since the initiation period is generally small fatigue failure is mainly a crack propagation phenomenon occupying the total of the fatigue life.

In 1980 the BSI produced a document (PD 6493) (12) presenting for the first time a fatigue design methodology for welded joints where an assessment of pre-existing planar or non planar defects could be made using Fracture Mechanics methods. The technique is also applicable to estimate tolerable flaw sizes in a weldment as function of endurance and stress level.

PD 6493 (1980) describes two methods for the fatigue assessment of defects. The first method is the general fatigue crack propagation method refered above usingthe appropriate fatigue crack propagation equation. Provided the stress intensity formulation is available the analysis is comparatively straightforward for constant amplitude loading. For variable amplitude loading a linear damage law is assumed with no interaction effects. Since this method requires some research and development facilities, which may not be available for most of the users, the document describes a simplified method not requiring experimental data for the analysis.

The simplified method assumes the Paris' law with a value of $m=4$ for the exponent valid for all structural steels. This value m is the reciprocal of the assumed exponent of the S-N curves in UK codes for metallic construction (11). The value of C in Paris' law was adjusted to cover most of the experimental data obtained in welded steels and both values of m and C are claimed to be conservative.Figure 3 shows the design S-N curves for welded steel and aluminium alloys. Similar curves are available for stress-relieved steels.

Each curve in Fig.3 corresponds to a certain quality category ranging from Q1 to Q10 where Q1 is the higher grade and Q10 the lower grade. The quality categories are related with initial flaw sizes not specified in the document. Thus Q1 curve is for an initial flaw size smaller than Q2, etc. For variable amplitude loading an equivalent constant amplitude stress range may be computed and used in Figure 3. If the constant amplitude stress range or its equivalent is known together with the predicted or expected number of cycles the designer can get a point in the diagram of Figure 3 and therefore define the quality category.

The assessment of known defects may be carried out in a graphical form for both 97.5 and 99.5% survival probability. Several graphs are presented for the most important types of defects including defects at the fillet of weld toes. Surface and embedded defects are converted previously to equivalent "long" surface and embedded defects with a straight crack front. A stress parameter S is computed from assumed values of $\bar{a}_o$ and $\bar{a}_m$ where $\bar{a}_o$ is the equivalent initial or detected flaw size and $\bar{a}_m$ is the equivalent defect size for unstable fracture.

After computing the stress parameter S a quality category ranging also from Q1 to Q10 is defined for some minimum values of this parameter. Table 1 gives the quality categories and the minimum values of S for as received welds (without stress-relieved treatment).

Table 1 Values of S for 10^5 cycles for quality categories (as-welded)

Quality category	S Steel (MPa)	S Al-alloys (MPa)	Quality category	S Steel (MPa)	S Al-alloys (MPa)
Q0	>248	>83	Q6	115	38
Q1	248	83	Q7	100	33
Q2	218	73	Q8	85	28
Q3	185	61	Q9	73	24
Q4	163	54	Q10	62	21
Q5	135	45			

The defect is acceptable if the actual quality category obtained by this analysis(Table 1) is higher or the same as the quality category required by the design conditions and defined in Figure 3.

Both methods (the simplified and the general method) are also applicable to estimate tolerable flaw sizes. The calculation is carried out in reverse order starting with the final crack size and working backwards to obtain the initial flaw size for the accounted number of design fatigue cycles. The defect size at this stage is the tolerable initial flaw size.

The simplified method can lead to unrealistic results since some important parameters such as the crack growth equation weld geometryand plate thickness are not taken into account in the analysis. In an attempt to overcome these problems the simplified method of PD 6493 assumes conservative and uniform values of some variables, as refered before, and that leads to significative errors in most practical cases.

3. DEFECT TOLERANCE ANALYSIS IN CRUCIFORM JOINTS

Stress intensity factor computations using finite element methods have shown that fatigue crack porpagation in fillet weld joints depends on the geometrical variables like weld size and angle, plate thickness and the thickness of the attachment plate (13). Therefore an in-depth study of defect tolerance levels in cruciform welded joints was required in order to assess the size effect, predict fatigue design curves as a function of initial flaw size and compare these curves with the quality level curves of PD 6493 (Fig.3). First a stress intensity factor computation was done using the finite element method. The results were used in the integration of an experimentally obtained Paris' law equation for low carbon and medium strength steels. This led to theoretical S-N crack propagation curves funtion of weld geometry and initial flaw size which form the basis of the defect tolerance analysis. Finally these curves were compared against experimental fatigue data obtained in fillet welded specimens of medium strength steel St 52-3.

STRESS INTENSITY FACTOR COMPUTATION

The details of the computation and also the stress concentration and stress intensity factor results may be found in (14) and (15). Figure 4 shows the finite element mesh for the full penetration non load carrying cruciform weld and Figure 5 is the sketch of the specimen refering the nomenclature used in the analysis. In this figure B is the main plate thickness, B_1 the attachment plate thickness, LG the weld leg length and Θ the weld angle measured from the weld toe.

The mesh size shown in Fig.4 uses 2D eight node isoparametric elements with two degrees of freedom in each node and produced good results compared with several analytical and numerical solutions used as test cases having similar geometries as the joint in Fig.4.

Two loading modes were considered separately;an uniform tension, and cantilever bending both applied through the main plate of the weldment. The stresses were obtained at the Gauss integration points of the isoparametric elements and along lines 1 and 2 shown in Fig.5. The crack was assumed to propagate from the weld toe along line 1 in the thickness direction . Hence stress distribution plots were obtained along lines 1 and 2 and from those the values of the stress concentration coefficient at the weld toe, K_t, were derived from extrapolation of the stress distribution curve to the weld toe.

Table 2 - Geometrical parameters of the cruciform joint

B (mm)	B_1 (mm)	LG (mm)	Θ	B (mm)	B_1 (mm)	LG (mm)	Θ
4	10	5	26.57	24	10 and 20	5	63.43
12	10	5	26.57	48	10 and 20	5	63.43
4	10	5; 2.5 and 10	45	24	10 and 20	2.5 and 10	45
12	10	5; 2.5 and 10	45	48	10 and 20	2.5 and 10	45
4	10	5	63.43	24	10 and 20	5	45
12	10	5	63.43	48	10 and 20	5	45

The stress intensity factor was calculated using the Albrecht method (16). The basic equation is

$$K = M_K\, K' \tag{1}$$

where K' is the stress intensity factor equation for a similar geometry without the weldment and M_K is the stress intensifying factor which takes into account exclusively the stress gradient along the crack line induced by the weldment. The M_K computation is then based on the stress values obtained along the crack propagation line (line 1 in Fig. 5) but assuming that there is no physical crack along that line. To check the accuracy of the method K values were previously obtained for other stress concentration geometries (plate with a central hole in tension and V notch in a bar) and compared with K solutions obtained by the other basic methods. The errors in K values only ranged from 1 to 2% and that indicated that the method was accurate enough.

No correction for elliptical crack fronts was applied since fatigue tests have exhibited shallow crack fronts from the weld toe with values of the ratio (a/ 2c) between 1/8 and 1/10.

K values were obtained for all the cases refered in Table 2. It was possible to fit with a good correlation a power law equation for the M_K results in the form

$$M_K = p/\,(a/B)^q \tag{2}$$

where p and q are constant functions of the loading mode and of the weld and plate geometry (B,B_1,LG and Θ values indicated in Table 2). The complete list of M_K values may be found in (15), and typical plot of M_K against a/B is shown in Figure 6 for a joint where Θ=45°, B= 12 mm and B_1 = 10 mm. It is seen that M_K decreases as the crack ratio a/B increases and approaches the value of 1 (no influence of the weldment) for a/B values close to 0.1. Also it is seen that M_K increases with the weld leg length, but only with a minor increase for bending. The results in Fig. 6 also show that M_K is greater in tension than in bending and this difference increases as a/B increases.

For a few randomly chosen cases in Table 2, M_K values in tension and in bending were also obtained applying the Bueckner weight function method (17). Results of the Albrecht and the weight function method only differed from 1 to 3% and hence the Albrecht method was applied to all the cases in Table 2 since less time for computer running and preparation is required.

The main conclusions of the stress intensity factor computation are summarized below

(i) in cantilever bending K values are 20 to 30% less than in tension
(ii) K increases with the main plate thickness. However only a very small increase was observed for small values of the ratio LG/B and B_1/B
(iii) K increases with both weld leg length and weld angle, but only a slignt increase was obtained when the attachment plate thickness was increased
(iv) For a/B values greater than 0.12 in bending and 0.2 in tension M_K values are very close to 1 and hence K=K'

DEFECT TOLERANCE ANALYSIS

Using the K equations the integration of Paris' law of the material was carried out. To simplify the analysis only constant amplitude loading was considered. The values of m and C of Paris' law were taken as m=3.1 and $C=1.33\times10^{-13}|N\ mm^{-3/2}, mm/cycle|$ and these were obtained in previous fatigue crack propagation tests in plate specimens of several low and medium carbon welded steels (14). These values are in agreement with usual data for weldable steels.

The Paris' law for fatigue life in crack propagation is

$$N_r = \int_{a_i}^{B} \frac{da}{C\,(M_K Y \sigma_{max} \sqrt{\pi a})^m} \qquad (3)$$

Equation (3) was conveniently solved by numerical integration using Simpson's rule and an interval optimization technique. Four types of relations were obtained:

- plots initial crack size against thichness as a function of LG, Θ and B_1 keeping N_r = constant = 2×10^6 cycles and for stress values of 95 and 118 MPa
- plots initial crack size against N_r as a function of LG,Θ,B_1 and B and for the same stress values as above
- plots nominal stress range σ against main plate thickness B for the values of LG,Θ and B_1 indicated in Table 2 and for N_r = 2×10^6 cycles
- plots nominal stress range σ against N_r(S-N plot) as a function of initial flaw size a_i for the range of thicknesses refered to in Table 2.

A plot a_i against N_r is shown in Figure 7 to illustrate the combined influence of the weld angle Θ and thickness B. An increase of weld angle and plate thickness lowers the tolerable initial flaw size for fatigue failure. Fig. 8 is the plot nominal stress against thickness B where the data for all the cases given in Table 2 was plotted. Line 1 is the upper bound refering to minimum values of Θ and line 2 gives the lower bound of the results (higher values of Θ and B_1). Thus to obtain fatigue failure in 2×10^6 cycles the value of nominal stress and thickness should fall in the shaded area represented in the figure.

The results showed that the S-N crack propagation curves could be plotted in the form of paralell bands function of one parameter. Typical plots are shown in Figure 9a). for bending and Figure 9b for tension. In this plot the initial flaw size was assumed as 0.2 mm (typical fabrication flaw size in a weldment) and the S-N curves were plotted as a function of main plate thickness. Each band represented in Figure 9 includes the results obtained with all the values of LG,B, and Θ indicated in Table 2.

The curves in Fig. 9 indicate that in bending thickness is the main geometrical parameter for fatigue life. For low thickness values weld geometry has a minor influence in the position of the S-N curves in comparison with thickness (the bands of S-N curves are very narrow for thicknesses below 12 mm). However for higher thickness values (>24 mm) weld geometry has a considerable influence in fatigue life (Fig. 9 a). In tension (Fig. 9b) the effect of thickness and weld geometry is not so important as in bending. Howeber in tension higher fatigue strengths were obtained with the thickness of 100 mm exactly the opposite as observed in bending. Hence for low initial flaw sizes the thickness effect on the fatigue life of weldment is closely associated with the stress gradient.

The quality category curves of the PD6493,are superimposed in Figs.9a, b. In tension categories between Q1 and Q3 fit in the theoretical curves for a_i=0.2 mm. Quality categories below Q3 should give tolerable flaw sizes above 0.2 mm. For example the results for initial flaw sizes between 2 and 2.4 mm fall between Q5 and Q6 categories. Categories below Q7 refer to flaw sizes above 2.4 mm. In bending only the Q1 category lies within the band for the thickness of 100 mm.

The analysis presented above clearly shows that in cruciform welded joints the quality categories below Q4-Q5 will only be obtained with initial flaw sizes outside the values usually found and accepted in welded constructions. Bearing in mind that cruciform welded joints have the lowest fatigue strength it is recommended that quality categories above Q1 should be introduced in the document to cover fillet welded joints in bending (Fig. 9 a), K joints and butt welded joints. Quality categories below Q5 should not be recommended since the defect tolerance levels are too unsafe.

The theoretical results were compared with experimental S-N results obtained in St 52-3 medium strength steel cruciform non-load carrying joints (14). The results are plotted in Figure 10 together with the theoretical S-N curves for the same plate and weld geometry and for initial flaw sizes of 0.012mm, 0.3, 0.6 and 1.2 mm. The experimental S-N curves for the St 52-3 medium strength steel are considerable above the theoretical curves even for the lowest initial flaw size (0.012 mm). The difference is probably due to a crack initiation phase in the long life region, ($N_r > 10^6$ cycles).Note that the theoretical S-N crack propagation curves can safely be used in the fatigue design of these weldments (Fig.10).

Data contained in Figs.7 to 10 can be used to assess the fatigue life of cruciform joints as a function of stress, thickness, weld geometry, loading mode and initial flaw size. Any particular set of values of these parameters can be selected to meet specific design requirements.Moreover feasibility analysis of fatigue failures in these joints, resulting from preexisting flaws, can be carried out applying the data and methodology explained above. A decision can then be made either to tolerate a particular flaw observed in the weldment or to eliminate it by weld repair. In the latter case the defect should grow by fatigue to a size that can affect the integrity of the structure.

4. DAMAGE TOLERANCE WORK IN THE AL-MG ALLOY 5083

The Al-alloy 5083 is a medium strength, ductile Al-alloy quite suited for structural applications at low temperatures. Little work has been published on the fracture and fatigue behaviour of this alloy. Comparison of fracture toughness and fatigue crack propagation with those for high strength aluminium alloys used in aircraft structures is **important** and this was one of the main objectives of the investigation. Since ductile behaviour is observed in this material a computer analysis of damage tolerance will require the use of elastic-plastic methods in the fatigue analysis. Consequently the applicability of parameters such as ΔJ integral in the loading cycle, is being envisaged (18,19). Also a detailed investigation of short cracks in the light of elastic-plastic fracture mechanics parameters was another objective of the work.

The chemical composition and mechanical properties of the 5083 Al-alloy are refered in Table 3. The material was supplied in the normalized state(no HT) and in plates with 12 mm thickness. The tensile tests were carried out in cilindrical specimens with 8 mm diameter taken from the longitudinal(rolling) direction and transverse direction in the plate.

Table 3 - Chemical composition and mechanical properties or the Al-Mg alloy 5083

Chemical composition

Mg	Mn	Fe	Ni	Cu	Zn	Si	Sn	Pb	Ti	AL
4.5	0.55	0.37	<0.5	0.12	0.10	<0.10	<0.05	<0.05	<0.05	Balance

Mechanical properties

	Longitudinal direction	Transverse direction
Hardness HRF	78	72
σ_{ys} (MPa)	179.7	159
σ_{UTS} (MPa)	320.8	314.1
ε_f(%)	18.2	24.0
K_1 n_1	369.9 0.129	379.4 0.156
K_2 n_2	609.8 0.253	616.6 0.276
correlation coeficients	0.997 0.9996	0.996 0.9998

σ_{ys} - 0.2% yield stress

σ_{UTS}-ultimate tensile strength

The monotonic stress-strain curve was approximated by two straigt lines in the logatitmic plot true stress $\bar{\sigma}$ against true strain $\bar{\varepsilon}$. The equation of the curve is the power law $\bar{\sigma} = K \bar{\varepsilon}$ and the two values of K and n (strain hardening exponent) for the longitudinal and transverse directions are given in Table 3. From the results in Table 3 it is seen that this alloy exhibits considerable ductility namely in the transverse direction. However more strength was obtained in the longitudinal(rolling) direction.

Basic cyclic data was also obtained. The S-N curves in rotating bending of plain polished specimens in the rolling and transverse directions were determined. The equations were

$$\log\sigma=0.017(\log N)^2-0.27\log N+3.26 \qquad (4a)$$
$$\log\sigma=0.015(\log N)^2-0.24\log N+3.16 \qquad (4b)$$

Strain cycling and load cycling tests are in progress to obtain the cyclic stress-strain curves, Coffin--Manson relations and cyclic creep or stress relaxation data.

COD data was obtained in the temperature range -60°C to + 100°C. The specimens were three point bend and taken in the LS and LT directions of the plate material. Fatigue precracked was carried out at room temperature and the dimensions of the specimen cross section were 12x24 mm for the LT direction and 12x12 mm for the LS and LT directions. A typical plot applied vertical load, P against clip-gauge displacement Vg, at the mouth of the notch is shown in Fig.11. In all the tests failure occured past maximum load and hence considerable ductility was observed with extensive shear lip formation. Maximum COD values, δ_m were taken from the graphs and the plot COD against temperature in the range -60 to 100°C is plotted in Fig.12. In this alloy

COD tends to increase when the temperature is lowered and this effect is more noticeable in the LT direction. The COD values are comparatively high (range between 0.1 and 0.35 mm).

Fractographic examinations with the SEM indicated two different failure modes respectively for the low temperature and high temperature range. More details of the analysis may be found in (20).

Slow bend tests in Charpy type specimens 10x10 mm cross section were also carried out. To assess notch sensitivity of the material one set of specimens was tested with blunt notches and in the other group of tests the specimens had fatigue cracks with size $a/w \simeq 0.5$. The tests were conducted in the temperature range -60°C to 90°C according to the ASTM specification E 812-81 (21). The measured specific absorved energy per unit thickness U (area under the load deflection curve) is plotted against temperature in Fig.13. A decrease in energy is aparent when the temperature increases from -60°C to 0°C . Above 0°C the energy remains practically constant. The LT direction is tougher then the LS direction and the U values are on average 80% higher in the LT direction than in the LS direction. For both directions considerably higher energy values were obtained with the blunt noched specimens in comparison with the specimens provided with fatigue cracks. Hence notch toughness in this material should be evaluated with fatigue cracks.

Further COD and slow bend tests are in progress in the temperature range-60 to -120°C and from 90 to 200°C in order to clarify the observed trend of decreasing values of these parameters in the bottom ends of the temperature range.

The J resistance curve (J against slow crack growth Δa) was also obtained but at room temperature only. The same type of specimens and dimensions were used as in the COD tests and the tests were conducted following the ASTM specification E 813-81 (22). All the J data was analysed and linear regression lines were fitted to more than 50 experimental points of J against Δa for both LT and LS directions. These J, Δa lines are plotted in Fig.14. It is seen that at room temperature the J resistance curve for LT direction lies above the one for the LS direction. Critical values of J, J_c were taken as 6.5 kJ/m^2 for the LS direction. The equivalent values of critical K, K_c, could be taken as 21.7 $MPa\sqrt{m}$ for the LT direction and 18MPa $\sqrt{m}$ for the LS direction. The multiple specimen method and the single specimen method with unloading were used.

ELASTIC-PLASTIC FATIGUE ANALYSIS

For the damage tolerance analysis the computational sequence presented in 1 will be used. Since the 5083 Al-alloy has considerable ductile behaviour it is expected that an extensive range of fatigue crack growth rates will occur under elastic-plastic conditions. Both the growth of short and long cracks can be described using the ΔJ concept proposed by the author early in 1977 (23) and further developed in 1981(19). Fig.15 is illustrative of these operational definitions of ΔG and ΔJ in load cycling for a specified number of N loading cycles. If local or extensive yielding is developed in the specimen and the crack is growing under an elastic-plastic stress and strain field, ΔG and ΔJ are both given by the equation

$$\Delta G = -\frac{1}{B}\frac{d(\Delta U)}{da} = \Delta J \qquad (5)$$

where ΔU is the total accumulated potential energy in the specimen after N loading cycles and B is the thickness of the specimen. ΔG and ΔJ defined by equation (5) are operational definitions and for their determination analytical or numerical solutions could be used provided each loading cycle is treated separately.

In Fig.15 a) ΔG is valid for a linear elastic material where the unloading lines of the fatigue cycles converge to the origin. For an elastic-plastic material (Fig.15b) the parameter is ΔJ and in load cycling of a cracked specimen cyclic creep occurs and an accumulation of plastic strain is obtained in the specimen. Hence both strain hardening and cyclic creep behaviour of the material should be taken into account. The equation to calculate ΔJ after N loading cycles is

$$\Delta J = -\frac{1}{B}\left[\frac{d(\Delta\delta_1 + \Delta\delta_{cc})\Delta P}{da} + \frac{\Delta P}{2}\,\frac{d(\Delta\delta_{e\ell})}{da}\right] \qquad (6)$$

where $\Delta\delta_1$ is the extension at the point of maximum load in the first cycle, $\Delta\delta_{cc}$ is the cyclic creep extension accumulated after N loading cycles and $\Delta\delta_{e\ell}$ is the elastic specimen extension due to crack growth only (change in the elastic specimen compliance due to crack growth). It is assumed that due to plastic shake down, after few cycles the loading and unloading paths are straight lines and hence the specimen behaves essentially as an elastic body.

The displacement terms in equation (6) can be computed applying analytical numerical solutions. For a few simple cases analytical ΔJ solutions were obtained (19,23). These equations were compared with the ΔJ values directly obtained with equation (6) and where ΔU is taken from the experimental load deflection loops in the specimen. Good agreement was found between the ΔJ values calculated by the two processes. The advantage of calculating ΔJ with equation (6) is to eliminate the need of instrumented fatigue tests.

If ΔJ is the parameter controlling fatigue crack propagation then the fatigue crack growth rate should produce a good correlation with ΔJ. For ductile metals such as mild and low alloy steels a power law equation of the form

$$\frac{da}{dN} = C\,(\Delta J)^B \qquad (7)$$

was obtained in the range of da/dN values between 10^{-6} and 10^{-1}mm/cycle. As shown in Figure 16 both linear elastic data ($\Delta J = K^2/E$) and elastic-plastic data(ΔJ, equation 6) produced the same correlation with a significative overlap of data.

For the Al-alloy 5083 fatigue tests are now in progress to obtain linear elastic and elastic-plastic data similar to Fig.16. An extensive set of ΔJ solutions using equation (6) is being prepared and these will be applicable mainly to the more important mode I component geometries in bending and tension. ΔJ applicability to strain cycling, displacement cycling and also in the growth of very short cracks is being analysed. The results will form the basis of a damage tolerance computer routine applicable to fatigue crack growth in ductile materials where considerable life expectance could be obtained under extensive yielding or elastic-plastic conditions.

5. CONCLUSIONS

1. The results of an extensive study on the influence of plate and weld geometry in tolerable defect tolerance levels in the fatigue analysis of welded joints of low and medium strength steels have shown that there is a need for the revision of existing assessment methods such as the PD 6493 presently used for the fatigue assessment of defects in fusion welded joints.

2. In components made of ductile alloys such as the medium strength Al-Mg alloy 5083 the damage tolerance analysis should be based in elastic-plastic fracture mechanics parameters. Fatigue life prediction methods using these parameters were presented and discussed.

3. Fracture toughness data in the Al-Mg alloy 5083 was only validated in the temperature range-120°C to 200°C using elastic plastic fracture mechanics parameters. Maximum COD values tend to increase with the decrease in temperature. Similar trend was observed in the specific absorved energy results in slow bend but only from -60°C to 0°C. J_c data in 5083 was also obtained at room temperature both for the LT and LS directions in the plate material. At room temperature the J_c values were 6.5kJ/m^2 for the LT direction and 4.5kJ/m^2 in the LS direction.

REFERENCES

(1) - Fracture Mechanics Design Methodology, Session II: Damage Tolerance Analysis, AGARD LSP-97,AGARD, 1978

(2) - Fatigue Test Methodology, AGARD LS 118, 1981

(3) - Sih, G.C. and Faria, L.Ed., Fracture Mechanics Methodology, The Netherlands, Martinus Nijhoff Publishers, 1984

(4) - Pettit, D.E. and Krupp. W.E., "The Role of Nondestructive Inspection in Fracture Mechanics Application", In: ASM 3 Fracture Prevention and Control, American Society of Metals,1974

(5) - Wheeler, D.E., "Crack Growth under Spectrum Loading", Report No.EZM 5602, General Dynamics Corporation, Ft. Worth, Texas (1970)

(6) - Szamossi, M.,"Crack Propagation Analysis", Report No. NA 72-94, North American Rockwell, Los Angeles, USA (1972)

(7) - Paris, P.C. and Erdogan, F., "A Critical Analysis of Crack Propagation Laws", Journal of Bas. Eng., 85D, 9. pp. 528-534 (1963)

(8) - Forman, R.G., Kearney, V.E. and Engle, R.M., "Numerical Analysis of Crack Propagation in Cyclic Loaded Structures", J.Bas. Eng., Trans. ASME, 89, pp. 459-464 (1967)

(9) - Gray, T., "Individual Aircraft Tracking Methods for Fighter Aircraft Utilizing Counting Accelerometer Data", Technical Memorandum TM-78-1-FBE, Air Force Flight Dynamics Laboratory, Dayton, Ohio, USA (1978)

(10) - American Welding Society, Structural Welding Code-Steel, AWS, D.1.1-84, Part 10: Design of new tubular structures, Miami, USA, 1984

(11) - British Standards Institution, BS 5400, Part 10, Fatigue design rules for metallic bridges, London, 1980

(12) - British Standards Institution, BS: PD6493, Guidance on some Methods for the Derivation of Acceptance Levels for Defects in Fusion Welded Joints, London, 1980

(13) - Gurney, T.R., "Fatigue of Welded Structures", Ed. Cambridge University Press, England, 1979

(14) - Ferreira, J.M., Fracture Mechanics Application to Fatigue of Welded Joints, in portuguese, Doctorate thesis, University of Coimbra, Portugal, 1985

(15) - Ferreira, J.M. and Branco, C.M., "Fatigue of fillet Welded Joints", to be published in Fracture Mechanics Technology, 1985

(16) - Albrecht, P. and Yamada, K., "Rapid calculation of Stress Intensity Factors", J.Est. Div., Proc. ASCE, 103,p.337, 1977

(17) - Parker, A.P., "The Mechanics of Fracture and Fatigue. An Introcuction". Ed. F.N. Spon Ltd. London, 1981

(18) - Branco, C.M., Radon, J.C., "Analysis of Creep Cracking by the J Integral Concept", Proc. Conf.Eng. Aspects of Creep, ASTM/ASME/I. Mech.Eng./JSME, Sheffield, UK, 1980

(19) - Branco, C.M., Peres, J.S.,"Load Cycling of Cracked Plates in Tension", Proc. 3rd. European Conference on Fracture, ECF3, Ed. Pergamon Press, UK, 1981

(20) - Branco, C.M., Progress report of project P17, Development of Damage Tolerance Assessment Methods, AGARD/NATO, Ref.ASP13, January 1985

(21) - American Society for Testing and Materials, ASTM E 812-81, Standard Test Method for Crack Strength of Slow Bend Precracked Charpy Specimens of High Strength Metallic Materials, USA, 1984

(22) - American Society for Testing and Materials, ASTM E 813-81, Standard Test Method for J_{1c}, A Measure of Fracture Toughness, USA, 1984

(23) - Branco, C.M., Radon, J.C. and Culver, L.E., "Elastic-Plastic Fatigue Crack Growth Under Load Cycling", J.St.Anal. Eng.Des.,12,2,p.90 (1977)

ACKNOWLEDGEMENTS

The cooperation of Dr.John Radon from Imperial College, London is gratefully acknowledged.The present work is supported by AGARD (P17 project Ref. ASP 13)under the SMP Program Additional Support to Portugal and Turkey, and is a cooperative project between the University of Minho and Coimbra in Portugal, and Imperial College in the UK.

The fatigue and COD tests in the Al-Mg alloy 5093 were conducted by Mr.José Domingos da Costa of Coimbra University. The computational work was carried out by Dr.José António Ferreira as part of his doctorate thesis

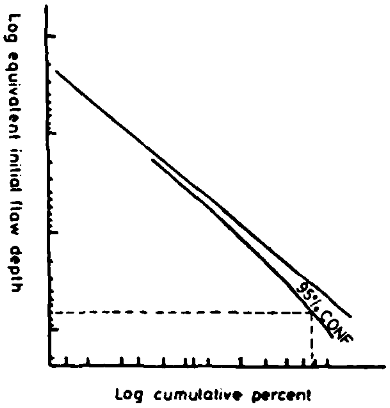

FIGURE 1 - Typical statistical distribution of initial manufacturing flaws

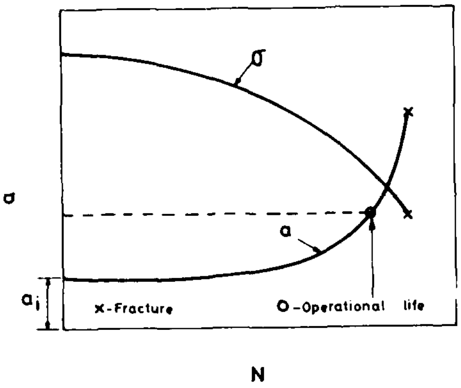

FIGURE 2 - Residual strength diagram

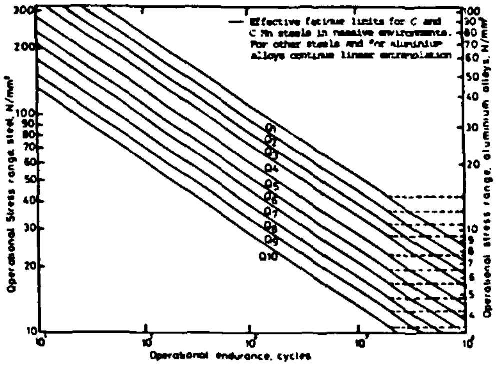

FIGURE 3 - Stress/endurance relationships function of quality categories for welded steels and aluminium alloys |12|

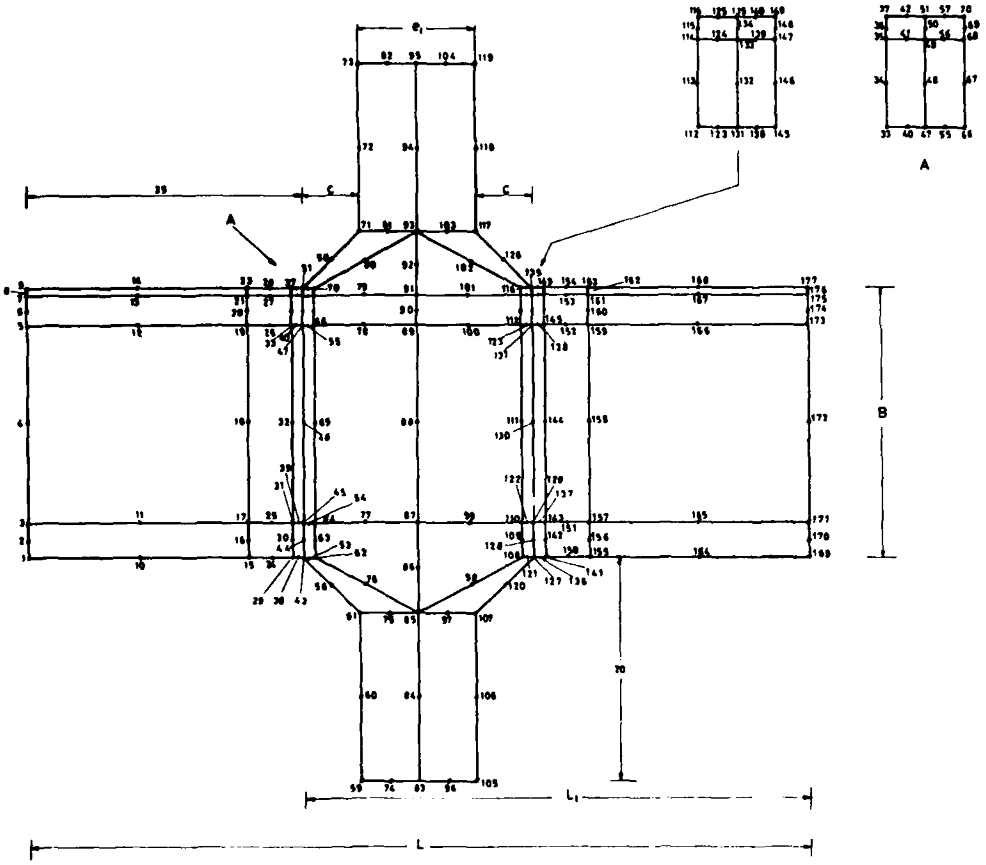
B1
C
C
A
A
B
L1
L

FIGURE 4-Finite element mesh for stress computation

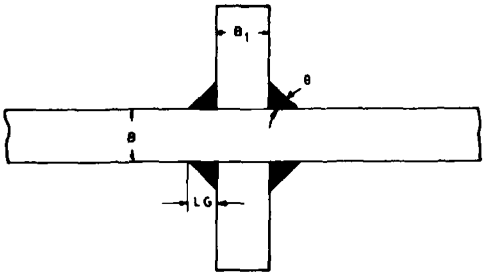

FIGURE 5-Nomenclature used in the analysis of the fillet weld

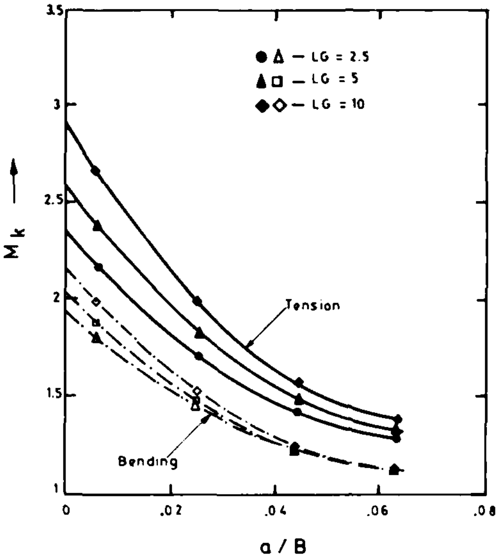

FIGURE 6-M_K against a/B as a function of LG in tension and cantilever bending. $\theta \cong 45^{o}$, B=12 mm; B_1= 10 mm.

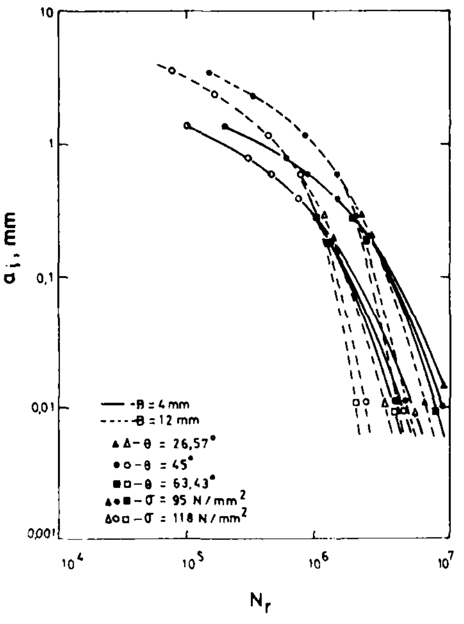

FIGURE 7-Initial crack size against N_r as a function of θ, LG= 5 mm. B_1=10 mm. σ= 95 and 118 MPa. Bending

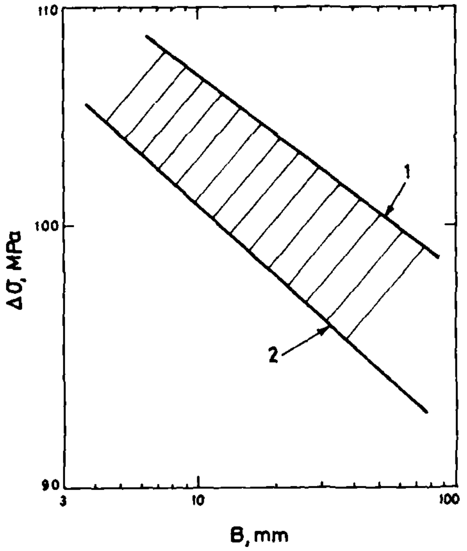

FIGURE 8-Nominal stress σ against B. a_i =0.2 mm. N_r =2x10^6 cycles. Bending

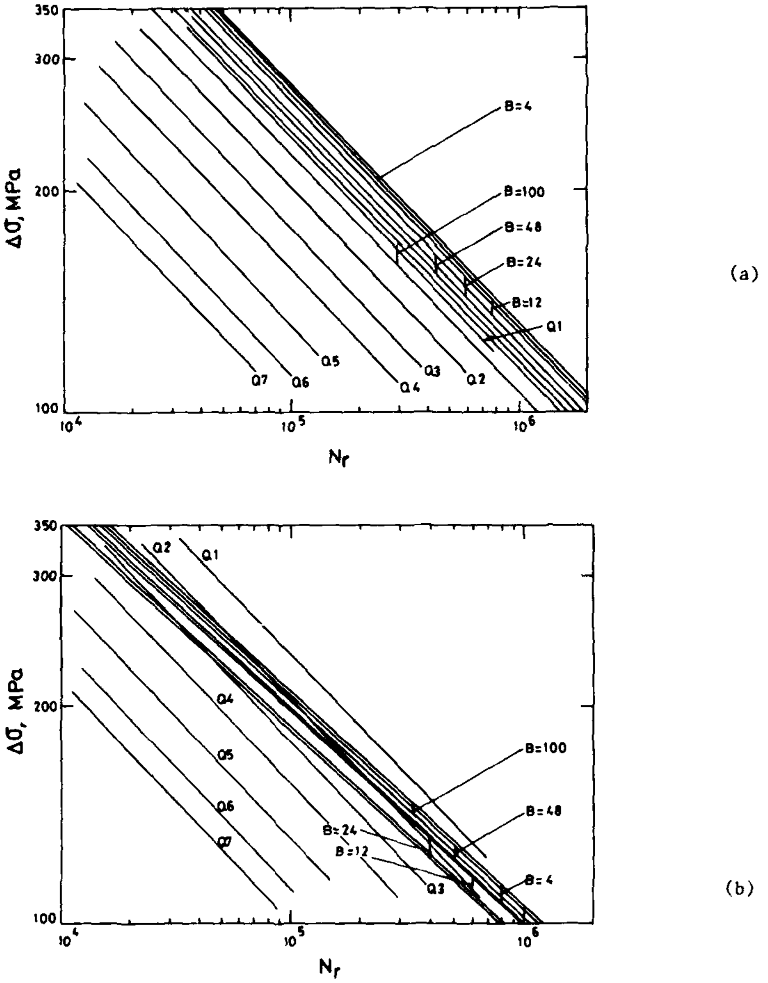

FIGURE 9 (a) S-N crack propagation curves in bending as a function of thickness. a_i=0.2 mm.
(b) S-N crack propagation curves in tension as a function of thickness. a_i=0.2 mm.

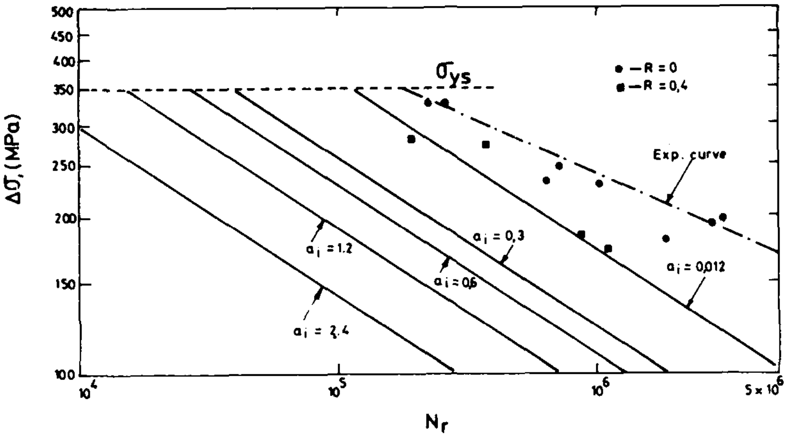

FIGURE 10-S-N curves. B=12 mm. $\Theta=45^{\circ}$. $B_1=10$ mm. LG=5 mm.

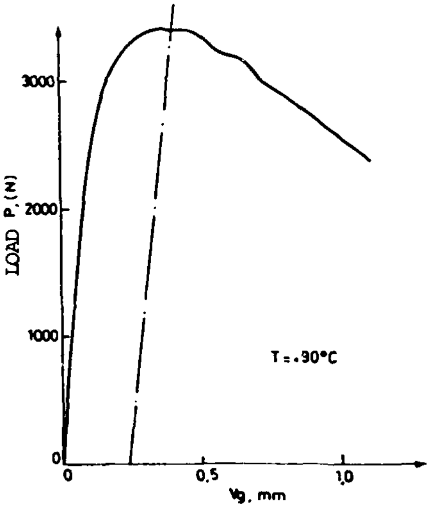

FIGURE 11-Load against clip-gauge displacement in a COD test. B=12 mm. Al-Mg alloy 5083

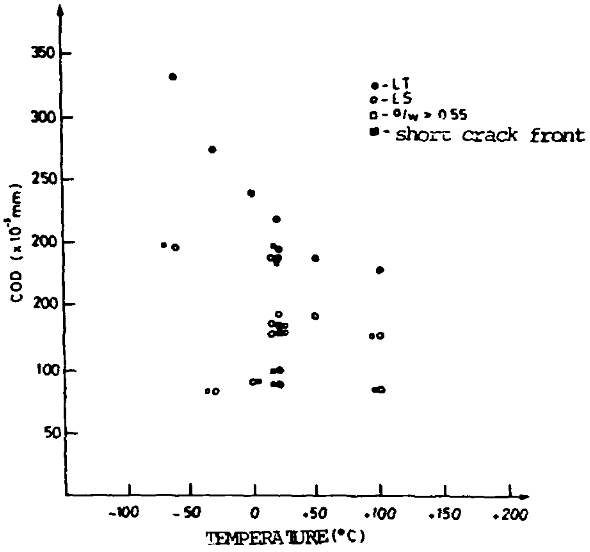

FIGURE 12-Maximum COD, δ_m, against temperature. B=12 mm. Al-Mg alloy 5083.

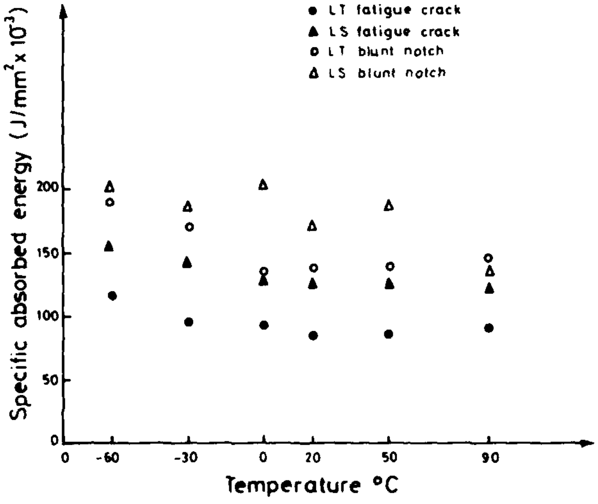

FIGURE 13-Specific absorbed energy against temperature in slow bend. B.=10 mm. Al-Mg alloy 5083

AD-A164 693 DAMAGE TOLERANCE CONCEPTS FOR CRITICAL ENGINE 2/4
COMPONENTS(U) ADVISORY GROUP FOR AEROSPACE RESEARCH AND
DEVELOPMENT NEUILLY-SUR-SEINE (FRANCE) OCT 85
UNCLASSIFIED AGARD-CP-393 F/G 21/5 NL

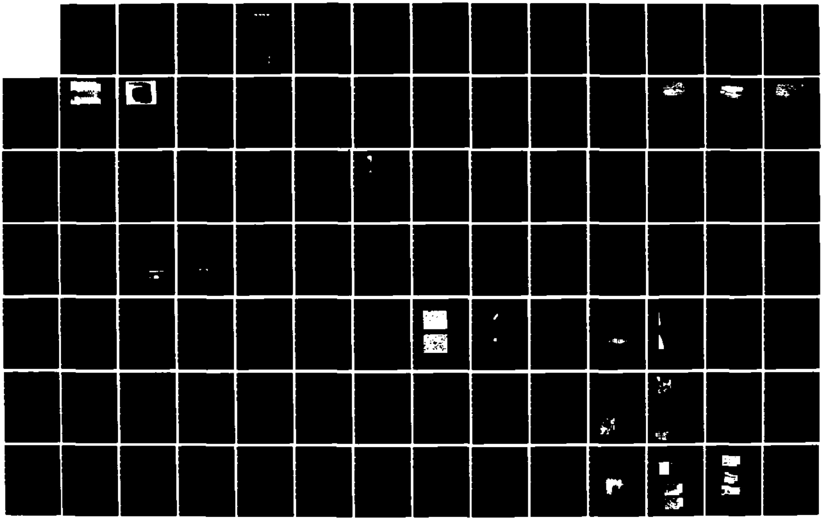

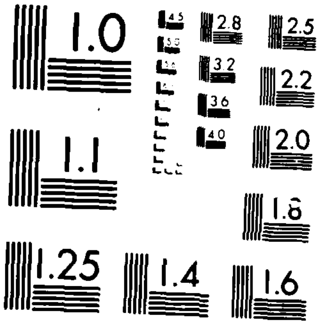
1.0
4.5
5.0
5.6
6.3
7.1
8.0
9.0
10
2.8
3.2
3.6
4.0
2.5
2.2
2.0
1.1
1.8
1.25
1.4
1.6

MICROCOPY RESOLUTION TEST CHART
NATIONAL BUREAU OF STANDARDS-1963-A

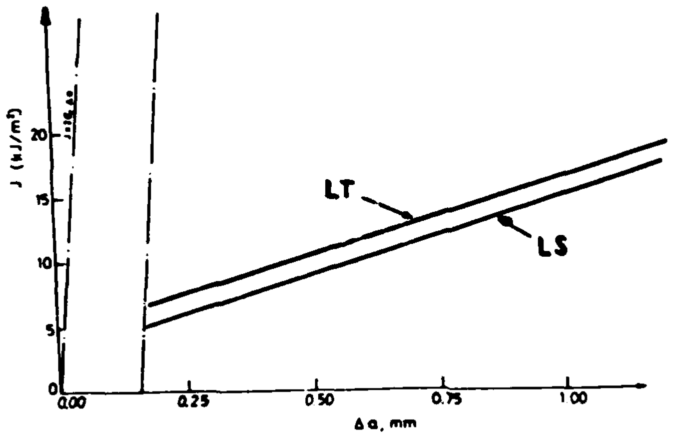

FIGURE 14 -J resistance curve at room temperature. B=12 mm. Al-Mg alloy 5083

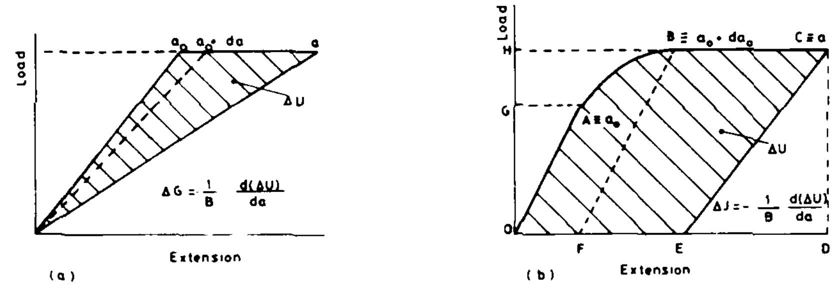
Load
a_o
$a_o + da$
a
ΔU
$\Delta G = \frac{1}{B} \frac{d(\Delta U)}{da}$
Extension
(a)
Load
$B \equiv a_o + da_o$
$C \equiv a$
H
G
$A \equiv a_o$
ΔU
$\Delta J = -\frac{1}{B} \frac{d(\Delta U)}{da}$
O
F
E
D
Extension
(b)

FIGURE 15 - Operational definitions of ΔJ in load cycling (a) Linear elastic material (b) Elastic-plastic material

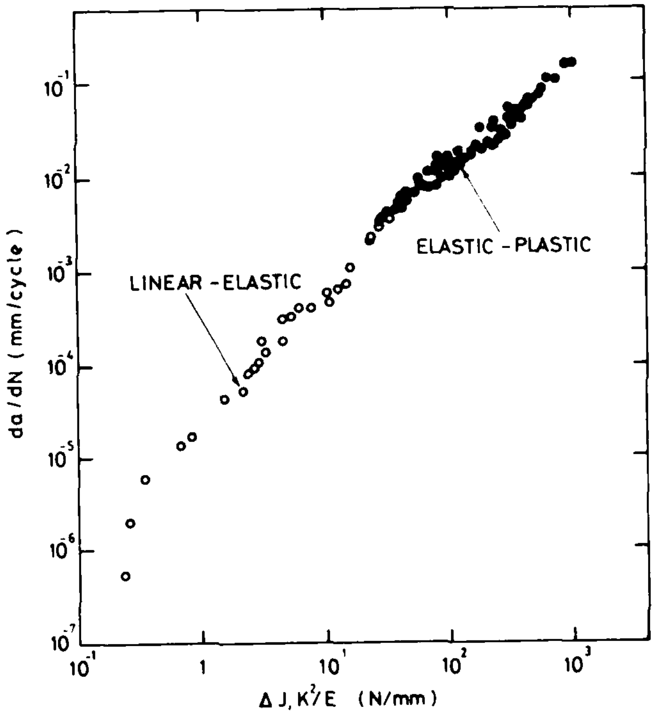

FIGURE 16 - da/dN against ΔJ. Mild and low alloy steels.

MANUFACTURING TECHNOLOGY FOR NONDESTRUCTIVE EVALUATION (NDE) SYSTEM TO IMPLEMENT RETIREMENT FOR CAUSE (RFC) PROCEDURES FOR GAS TURBINE ENGINE COMPONENTS

Donald L. Birx and Dena G. Doolin

SYSTEMS RESEARCH LABORATORIES, INC.
NDE Systems Division
2800 Indian Ripple Road
Dayton, Ohio 45440

SUMMARY

Systems Research Laboratories, Inc., with a team of subcontractors, has developed an automated NDE inspection system to detect surface flaws and inclusions in jet engine rotary parts. The system implements the Air Force Retirement for Cause philosophy in which good, used engine parts are returned to service, and flawed components are retired for cause. Emphasis has thus been placed on improving current flaw detection and characterization techniques by using computer algorithms (removing the human decision process) and achieving basic inspection and predictive capabilities via automated eddy current and ultrasonic inspection techniques.

The RFC/NDE Inspection System includes both state-of-the-art and proven NDE instrumentation and flaw detection/characterization techniques. The system is modular, uses standard communication interfaces, and has extensive computer capability to provide for future expansion, upgrade and modification. Backup capability, maintainability, and reliability have also been built into the system. Backup capability (50% throughput in the event of any major module or peripheral failure) is assured through redundant communication interfaces, inspection stations, and system computers. Maintainability is assured through self-diagnostics, simplicity, and a design influenced by a factory operating environment. Flaw detection reliability will be assessed using part specimens containing representative flaw geometries, and flaw analysis techniques including Least-Squares Log-Odds Mean Curve, Maximum Likelihood Estimator Log-Odds Mean Curve, and Least-Squares Log-Odds 90/95 Lower Bound.

The RFC/NDE contract was awarded to Systems Research Laboratories, Inc., in October 1981. During the first 2 years of the program, major effort was directed toward organizing and coordinating subcontractor program activities, establishing the core in-house project team, defining the inspection system's performance criteria and specifications, and designing and fabricating the prototype inspection system.

In March 1984, the prototype system, which consisted of 1 eddy current and 1 ultrasonic inspection station, the operator console, and 1 system computer, was successfully demonstrated to Air Force and subcontractor program participants. During 1984 and 1985, SRL has performed an in-depth performance evaluation and system upgrade to meet production inspection performance specifications. Initial system delivery to Kelly Air Force Base, San Antonio, Texas, is scheduled for fall 1985 with system integration/implementation activities scheduled to continue through the remainder of 1985. The RFC/NDE Inspection System is scheduled to begin actual production operation in March/April 1986.

SYSTEM DESCRIPTION

The RFC/NDE Inspection System was designed per structured analysis methodology and consists of an Operator Console, 2 System Computers, 3 Eddy Current and 2 Ultrasonic NDE Inspection Stations.

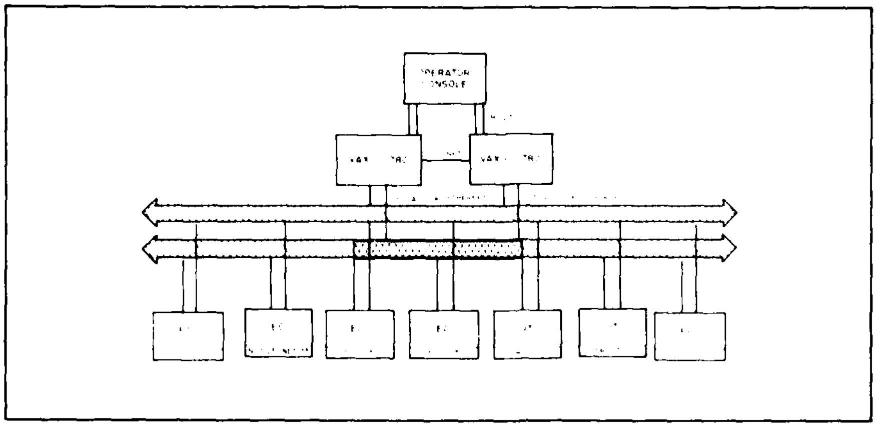

Figure 1. RFC/NDE INSPECTION SYSTEM

The Operator Console is a passive station used primarily to monitor the system's operational status, track the individual part inspections at the NDE inspection stations, and generate part inspection data reports.

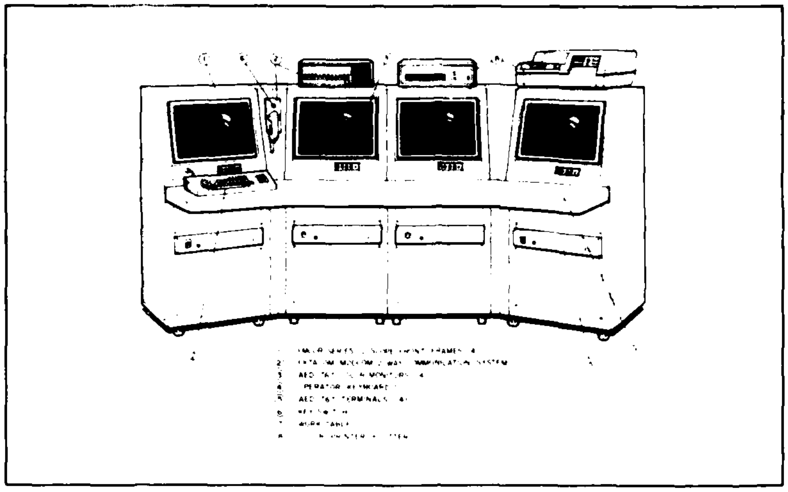
FRAMES 4
2 COMMUNICATION SYSTEM
3 AED 767 MONITORS 4
4 OPERATOR KEYBOARD
5 AED 767 TERMINALS 4
6
7 WORK TABLE
8

Figure 2. OPERATOR CONSOLE

The console has 4 color CRT displays functionally dedicated as follows. The Main Menu is a command-driven display used to generate part inspection data reports and graphic displays from previous part inspections. The Part/Defect Graphics Display provides color displays of part inspection results as they are generated at the NDE Inspection Stations. This display contains top- and side-view illustrations of the engine part with color-coded geometric flaw locations. The display also includes specific part inspection summary data such as relative flaw sizes and locations, inspection start/stop times, the cumulative number of part inspections, the date of inspection, and the part accept/reject decision. The System Diagnostic Display provides a continuously updated operational status display of the inspection system including the communication network, and the Inspection Status Display shows the current status of the part inspections at each NDE Inspection Station.

The Operator Console also has a 2-way intercom system for communication with the NDE Inspection Stations; a color printer/plotter for hardcopy color graphic print outs; and a line-printer for part inspection data reports. The Operator Console's software resides on the System Computers and all communication between the System Computers and the Operator Console is done over an RS232 data transfer link.

The dual VAX 11/780 System Computers provide the central intelligence for the entire RFC/NDE Inspection System. They perform advanced data processing, system-wide communication, and sophisticated, high-speed mathematical and scientific data analysis critical to the inspection process. The primary tasks of the System Computers are part tracking, Operator Console/NDE Inspection Station interface and communication, NDE data cross-correlation, archival data base storage, system diagnostics, advanced signal processing, RFC proprietary data analysis, and graphics processing.

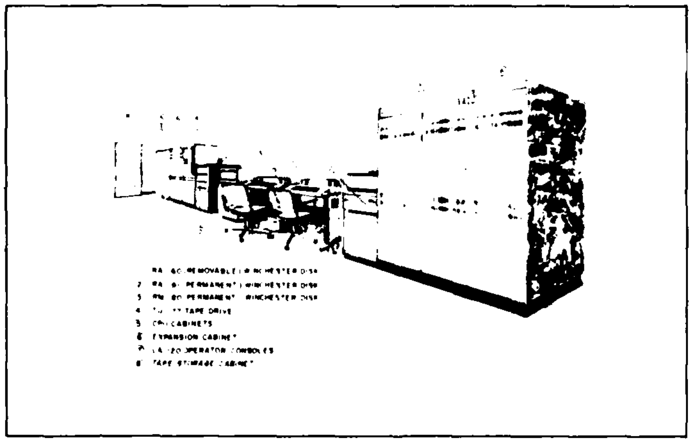
RA 60 REMOVABLE WINCHESTER DISK
2 RA 81 PERMANENT WINCHESTER DISK
3 RM 80 PERMANENT WINCHESTER DISK
4 TU 77 TAPE DRIVE
5 CPU CABINETS
6 EXPANSION CABINET
7 LA 120 OPERATOR CONSOLES
8 TAPE STORAGE CABINET

Figure 3. VAX 11/780 SYSTEM COMPUTERS

Each VAX 11/780 combines a 32-bit architecture, efficient memory management, and a virtual memory operating system to provide essentially unlimited program space. The VAX/VMS virtual memory operating system provides the multiuser, multiprogramming environment critical to the RFC System's application. In addition, the VAX floating-point instructions and accelerators, efficient scheduler, and FORTRAN-77 programming language are ideal for the System's realtime and scientific computational environments.

The combined disk space for the dual-VAX configuration totals 1,446 MB. The permanent on-line storage space has been dedicated to storing all archival data, RFC-application software, and engine manufacturer proprietary data thus ensuring ready-access and increased software security. The removable disks have been allocated for part-specific scan plan software storage thus providing easy software update and file expansion.

The dual-RS232 optical links provide the system-wide communication network between the System Computers and the NDE Inspection Stations. This dual structure provides enhanced system performance, increased data transfer rates, flexibility, and the capability to map functional elements around failed components. The communication link between the 2 VAX Computers is DECNET, and as stated earlier, a dual-RS232 serial link provides the communication between the System Computers and the Operator Console.

The RFC/NDE Inspection System employs both eddy current and ultrasonic inspection techniques to inspect the jet engine rotary parts. Ultrasonic "squirter" technology is used to detect volumetric flaws and voids, and eddy current is used for surface flaw detection. The RFC System consists of 5 NDE Inspection Stations (3 eddy current and 2 ultrasonic). Each eddy current and ultrasonic inspection station consists of a mechanical module and an instrumentation cabinet.

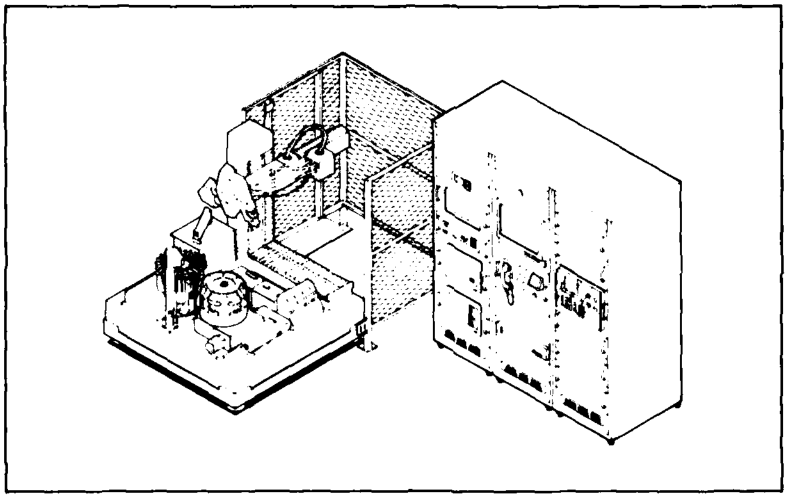

Figure 4. EDDY CURRENT INSPECTION STATION

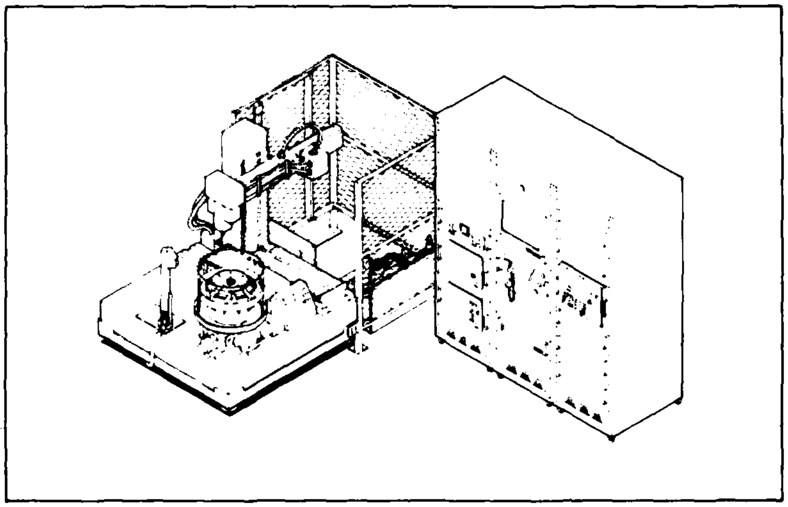

Figure 5. ULTRASONIC INSPECTION STATION

The eddy current and ultrasonic mechanical modules consist of an X-Y-Z axes mechanical manipulator (manufactured by M&M Precision Systems, Inc.) and the following subassemblies:

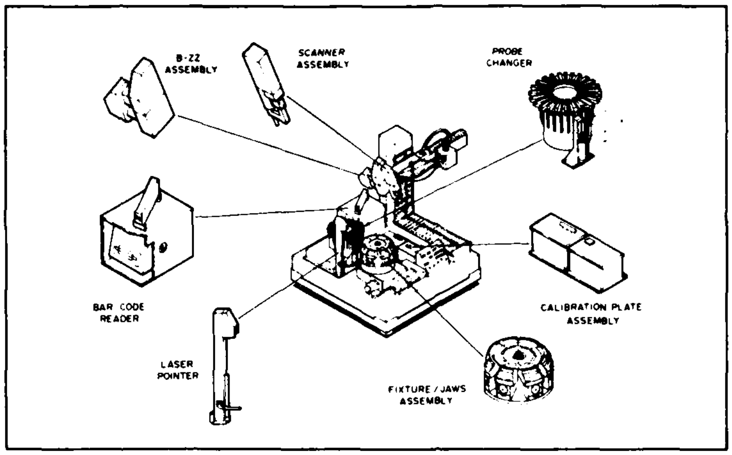

Figure 6. EDDY CURRENT MECHANICAL MODULE

The eddy current module has 7 primary subassemblies which are mounted directly to the base manipulator. The eddy current rotary scanner physically couples the probe to the mechanical manipulator and electronically couples the flaw signals to the eddy current instrument. The scanner has a C' drive mechanism for rotating RECHII probes up to 1,500 rpm, an air plenum to supply air to the air-bearing surface probes, and rotary transformers and specialized printed circuit cards for signal transfer and enhancement.

The calibration plate assembly consists of a metal riser upon which calibration plates with known flaws are mounted. The calibration plates are used to do a 2-point calibration of the eddy current instrument and an operational check of the probes prior to and following a part inspection.

The rotary table/part fixture assembly clamps and rotates the engine part during an inspection. The rotary table can operate in either a continuous rotation mode (at 0 to 20 rpm) or an index mode. The part fixture is a pneumatic system which automatically clamps the part (either on the outer diameter or inner diameter as required) to the rotary table.

The probe changer is a carousel assembly which holds up to 24 eddy current probes on its outside diameter. The probe changer automatically indexes the correct probe into position for retrieval by the mechanical manipulator. The bar code reader scans each probe in the probe changer prior to the part inspection to ensure correct probe placement by the operator.

The laser pointer is a low-power coherent laser which emits a thin beam across the engine part after the part has been placed on the part fixture. The beam assists the operator in properly aligning the part on the fixture prior to clamping.

The B-Z' assembly provides the robotic wrist action for the eddy current mechanical manipulator. The B axis rotates in a sweep pattern parallel to the X axis and the Z' provides a linear thrust motion on the B radial.

The ultrasonic mechanical module has 6 major subassemblies, 2 of which (the rotary table/part fixture assembly and the laser pointer) are identical to the eddy current module.

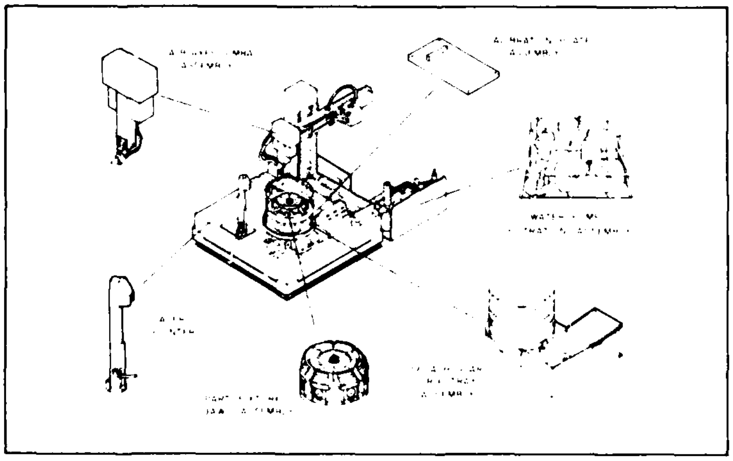

Figure 7. ULTRASONIC MECHANICAL MODULE

The 4 subassemblies which are unique to the ultrasonic station are the calibration plate assembly, the water pump/filtration assembly, the splash guard/drip tray assembly, and the A-B axes gimbal assembly. The ultrasonic calibration plate assembly is mounted inside the splash pan assembly and is used for squirter/NDT instrument calibration prior to and after each part inspection. The block contains 4 interior voids that are 20 mils in diameter and 1/2 inch deep.

The water pump/filtration assembly circulates and cleans the water during the squirter inspection process. The splash guard/drip tray assembly fits around and under the rotary table and catches the water used during the part inspection and returns it to the pump/filtration assembly.

The A-B axes gimbal assembly physically couples the squirter to the mechanical manipulator and provides the mechanical robotic wrist action for the X-Y-Z manipulator. The A axis has a 60° range of motion and the B axis has 130°.

The ultrasonic and eddy current instrumentation modules are the inspection station operator's control module. Each module contains an inspection module computer, an audio/visual alarm system, a color CRT display monitor, an operator pushbutton control panel and auxiliary keyboard, an intercom system to the Operator Console, the mechanical module's controller, and an NDE instrument.

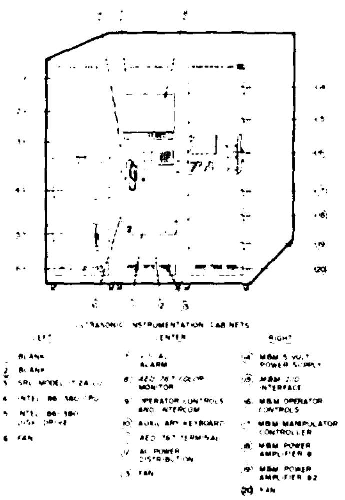
ULTRASONIC INSTRUMENTATION CABINETS
LEFT
BLANK
2 BLANK
3 SRL MODEL 1712A CUI
4 INTEL 86/380 CPU
5 INTEL 86/380 DISK DRIVE
6 FAN
CENTER
7 ALARM
8 AED 767 COLOR MONITOR
9 OPERATOR CONTROLS AND INTERCOM
10 AUXILIARY KEYBOARD
AED 767 TERMINAL
12 AC POWER DISTRIBUTION
13 FAN
RIGHT
14 MBM 5 VOLT POWER SUPPLY
15 MBM I/O INTERFACE
16 MBM OPERATOR CONTROLS
MBM MANIPULATOR CONTROLLER
18 MBM POWER AMPLIFIER
19 MBM POWER AMPLIFIER #2
20 FAN

Figure 8. INSTRUMENTATION MODULE

The RFC System's eddy current and ultrasonic NDE instruments represent the most advanced computer-controlled instrumentation available. The eddy current instrument is the NORTEC NDT-25 with dual channel digital sampler. The NDT-25 is a computer-controlled instrument with a frequency range of 10 KHz to 6 MHz. The ultrasonic instrument, the SRL Model 1712A Computerized Ultrasonic Instrument (CUI), is computer-interfaceable, and contains a microprocessor-controlled, square-wave pulser, high-speed digital sampler (55 MHz), and multibus-compatible receiver boards.

The inspection module computers provide local module intelligence and operator communication for the NDE Inspection Stations. The computer is an Intel 86/380 microprocessor which contains multiple Intel microcomputer boards for individual processing functions (e.g., I/O, mechanical system scan control, and instrument control) and specialized instrument boards. The Intel 86/380 System features a 32 MB Winchester disk drive, 1 MB floppy disk, iRMX operating system, and 12 multibus card slots for specialized user functions. The Intel 86/380 delineated functions, modularity, and component board plug-in capability enhance modification, diagnosis, and repair of the inspection module computer.

The RFC System's data acquisition module includes all probes and transducers used for flaw detection, adaptive positioning, dimensioning and scanning. Advanced technology that has been incorporated into this module include Southwest Research Institute's air-bearing probes and ultrasonic squirter, NORTEC's RECHII probes, and SRL's ultrasonic squirter.

AGARD COOPERATIVE TEST PROGRAMME ON TITANIUM ALLOY ENGINE DISC MATERIAL

by

A.J.A. Mom 1) and M.D. Raizenne 2)

1) National Aerospace Laboratory NLR
Anthony Fokkerweg 2
1059 AC Amsterdam
The Netherlands

2) National Aeronautical Establishment
National Research Council
Montreal Road, Ottawa, Ontario K1A OR6
Canada

SUMMARY

In recent years a strong interest in the application of damage tolerance techniques for lifing of gas turbine engine discs has developed. Before the damage tolerance approach can be safely implemented it requires sensitive and reliable crack detection techniques, operational loading information and improved knowledge of fatigue crack growth and fracture under service conditions. This latter aspect is the main subject of an international test programme, in which a number of laboratories from North America and Europe participate under AGARD coordination. The first phase of the programme is directed to test and specimen standardization and calibration of the different laboratories. The second phase will specifically address parameters relevant for real service operation like mission loading, sequence and dwell effects, temperature, fatigue threshold etc. The present paper will discuss the background and first phase of the programme.

1. INTRODUCTION

During the last 5-10 years a strong interest in the application of damage tolerance lifing methods with respect to gas turbine engine components has developed. While the damage tolerance design approach for aircraft structures was already introduced in 1970, and has been applied since then on a number of civil and military aircraft, the damage tolerance design of engine components is only a very recent development. Application of the damage tolerance approach with respect to disc lifing is now in consideration (and occasionally applied). Also, a preliminary specification on engine damage tolerance requirements has been developed [1]. However, no information on intial flaw assumptions and NDI requirements was available. This preliminary specification has undergone many modifications and is now part of an overall specification covering the entire engine. It is currently listed as MIL-STD-1783.
A damage tolerance design approach requires amongst other things a thorough understanding of material fatigue crack growth under actual operating conditions. To address this problem an international test programme has been set up in which a number of laboratories participate under AGARD coordination. The background and scope of the programme are reviewed below.

2. DISC LIFING METHODS

2.1 Safe life design

As indicated above the damage tolerance approach is only in an exploratory stage. Most discs are still designed based on the so-called "safe life" philosophy. In this respect "safe life" means that parts are designed for a finite service life during which no significant damage will occur. In safe life design no defects are assumed to be present in the new structure and no inspections are required during the design life. After reaching the life limit the part is retired from service.

With respect to aircraft engine discs the safe life is defined as the number of cycles at which, statistically, 1 of every 1000 components will develop a crack of 1/32 in (0.8 mm) surface length. This crack size has been chosen because (see [2]) (1) at this size high cycle fatigue (HCF) crack growth under vibratory conditions would not yet occur; (2) this crack size was, for existing materials, significantly smaller than the critical crack size for rupture, and (3) a 1/32 in crack was considered to be the smallest crack detectable in service (although the original safe life design approach does not implement inspections). The safe life design of discs implies that 999 out of 1000 components are rejected based on the statistical probability of a crack without the actual presence of a detectable crack. It has been shown [2-4] that owing to a large scatter in time to initiate and grow a crack to a detectable size, most of these retired components still have considerable service life left. If components could be withdrawn from service based on an actual crack then a much better usage of this inherent available life would become possible. This is in essence the basis of the damage tolerance approach, which is visualised schematically in figure 1.

2.2 Damage tolerance approach

In the damage tolerance philosophy the possibility of a crack or defect in a new structure is accounted for. The method is based on the assumption that crack growth at every critical location can be predicted under operational loading conditions. Inspections at regular intervals will screen out those components which have insufficient life to be returned into service, see figure 1. As can be seen from this figure the inspection interval is based on the maximum allowable crack size in service a_p, the minimum reliably detectable crack size by means of NDI or other techniques, and the availability of crack growth data.

From the foregoing it will be clear that some basic requirements should be met before the damage tolerance lifing approach can be successfully implemented, see also figure 2:

- the operational load history of discs should be well known
- material crack growth data should be available for the appropriate loading conditions
- NDI or other techniques should be available for a sensitive and reliable detection of very small cracks.

In recent years considerable progress has been made in inspection capability. It has been claimed [5] that under proper inspection conditions, working with well motivated people and very special equipment, cracks of 0.015 in surface length and 0.005 in depth (0.375 x 0.125 mm) can be detected at the 90 % probability/ 95 % confidence level. At present, however, it seems more realistic to assume a crack detection capability for cracks of at least 0.030 x 0.015 in (0.750 x 0.375 mm) [1]. In any event, NDI reliability, also with respect to the particular application, is an important factor in the damage tolerance lifing approach.

With respect to monitoring of operational load parameters several systems are presently in use, e.g. AIDS and EUMS. Analysis of the recorded signal in such a way that it can be used for an accurate life prediction is, however, still in an exploratory stage. A considerable amount of work in this area is performed in the Turbistan working group (which will report separately at this meeting) although with another incentive: the development of a standard or reference load sequence for discs. Anyhow, operational load monitoring and analysis is receiving increased attention.

The third basic requirement essential for the application of the damage tolerance philosophy is knowledge about material crack growth and fracture behaviour under operational conditions. This is the area to which the present AGARD cooperative programme is addressed. Only limited information exists to date and this information is restricted mainly to the engine manufacturer community. It would be extremely helpful if, by a common effort of the engine manufacturers and users, more information could be gathered on this subject so that application of new lifing procedures would become more nearly practicable.

3. THE AGARD PROGRAMME

3.1 Purpose and scope of the AGARD programme

An extensive amount of data and a basic understanding of material fatigue crack growth behaviour is needed before a damage tolerance lifing procedure can be adopted. Individual laboratories might not be capable in performing such a task. A common effort of a number of laboratories would definitely result in a broader data base, more confidence in each other's results because of standardisation of test procedures and specimens, and improved knowledge and understanding because of interacting activities. With this in mind a number of laboratories from Europe and North America decided to cooperate in this AGARD coordinated programme, which is directed to "an improved definition and understanding of the problems of fatigue and fracture in titanium alloy discs used in aircraft gas turbines" [6]. The ultimate goal of the programme is the establishment of a sound basis for a damage tolerance philosophy applied to these components. Table 1 shows a list of all participating laboratories and their representatives.

3.2 Framework of the programme

The programme consists of a CORE programme and a SUPPLEMENTARY programme. The CORE programme, performed on the basis of a commonly accepted test procedure including specimen types, is meant for calibration between the various laboratories. In this way it is possible to gain confidence in each other's results and to derive the necessary test standardisation. The CORE programme involves LCF life and crack growth testing on Ti-6Al-4V specimens under constant amplitude loading and room temperature conditions, see table 2.
The SUPPLEMENTARY programme, although not yet defined in detail, will address those parameters relevant to real engine operating conditions, spectrum load effects, major/minor cycling, sequence effects, dwell, HCF threshold etc. Furthermore, different materials and/or temperatures may be considered. The SUPPLEMENTARY programme in fact allows the various participating laboratories to direct their activities somewhat more to their own interest.

3.3 CORE programme

The CORE programme test matrix is given in table 2. Testing is performed on 4 different types of specimens (see figure 3), two of which are for LCF life and crack formation tests and two for crack growth testing. The corner crack (CC) specimen is especially meant for crack growth testing in the "short" crack regime. All specimens were machined from original Ti-6Al-4V disc forgings taking into account that the expected crack plane in relation to forging structure is similar for both the specimens and the real disc.
A working document [7] has been prepared in which all test procedures are specified in detail. An interesting aspect is that crack formation and growth is monitored by means of the potential drop (PD) technique. This technique requires that a constant current is passed through the specimen and that the electrical potential over the crack plane is measured by two probes located on both sides of the crack. If the relationship between crack length and voltage is known (a calibration curve should be available, see figure 4 [8]) accurate crack length detection can be achieved. The advantage of the PD-method is that crack length detection in a closed furnace is also possible and that automated data collection is easily attained. Additionally, the average crack length is determined instead of the surface crack length in the case of optical measurements. Changes in crack front curvature are thus accounted for.
A possible set-up for fatigue testing and crack length measurement is shown in figure 5. Note that apart from the notch voltage a reference voltage is measured to account for temperature effects and current variation. Thermoelectric effects and drift of the system are eliminated by taking the difference of two measurements, one with current on, one with current off. An instrumented corner crack specimen is shown in figure 6: note that for reasons of simplicity both the notch probe wires and the reference wires were welded on the same edge. In the actual test programme, to prevent the occurrence of a reference potential change due to crack growth, the reference probes are to be welded at a location at which the potential field is not affected by crack growth, e.g. at the opposite corner.

The results of a preliminary test on the specimen shown in figure 6 are presented in figure 7. An actual crack growth curve, i.e. average crack length a versus cycles N, might be constructed after calibration of notch voltage versus crack length. For this purpose the average crack size is measured at two distinct fracture surface markings, assuming the corresponding notch voltages to be known. The first marking has been obtained by heat tinting, the second marking is the clearly distinguishable transition line between fatigue and overload area (figure 8). The average crack length has been determined by taking the average of 5 readings; 2 at the side surfaces (the surface crack lengths), the other 3 at angles of 22.5°, 45° and 67.5°. This averaging method resulted in only a very minor difference from the real average crack length obtained by fracture area measurement. The calibration curve is now obtained by drawing a straight line through the two data points (see figure 9). The straight line assumption is justified based on figure 4 and the actual z/W value of about 0.014. Figure 9 also shows the relation between the notch voltage and crack size if measured optically at the specimen surface during the test. This curve indicates that the optical measurement underestimates the average crack length as used for the calibration curve. The reason for this effect is the crack front curvature at the specimen surface, see figure 8. This example clearly illustrates the advantage of the PD-method for crack length determination over the optical method. In addition, the PD-method sensitivity is very good. Our current system (figure 5) allows changes in crack length to be detected with better than 5 μm sensitivity.

4. CONCLUDING REMARKS

The application of the damage tolerance philosophy with respect to disc lifing requires sensitive and reliable NDI techniques for crack detection, knowledge of the operational loading conditions and a thorough understanding of fatigue crack growth characteristics. The present AGARD programme addresses the last subject. The first phase, the so-called CORE programme, is aimed at standardisation of test procedures and specimens and calibration of the participating laboratories. The potential drop technique is used to allow for very accurate crack detection and growth measurement. The second phase of the programme, the SUPPLEMENTARY programme, will address various parameters relevant for real service: major/minor cycle effects, spectrum loading, sequence effects, dwell, temperature, HCF threshold etc. This programme is yet to be defined in detail.

5. REFERENCES

[1] C.H. Cook, H.E. Johnson and C.E. Spaeth, Damage tolerant design for cold section turbine engine disks, AFWAL-TR-81-2045.

[2] S.A. Scatter and I.T. Hill, Design of jet engine rotors for long life, paper 750619 presented at SAE Air Transportation Meeting, Hartford 1975.

[3] C.G. Annis et al, Gas turbine engine disk retirement for cause: an application of fracture mechanics and NDE, ASME-80-GT-127.

[4] F.E. Reed, D.T. Hunter and R.J. Hill, LCC evaluation of advanced engine damage tolerance goals for a hot section disk, AIAA-83-1407.

[5] T.D. Cooper and D.M. Forney, Increased inspection requirements for critical air force engine components; paper presented at the Air Transport Association Non-destructive Testing Forum, Phoenix, September 1982.

[6] A.J.A. Mom, Proposal for an AGARD coordinated international test programme on damage tolerance in titanium alloy engine discs, NLR, Amsterdam 13-9-1983.

[7] A.J.A. Mom, Working document for the AGARD Cooperative test programme on titanium alloy engine disc material, NLR TR 84022 L.

[8] M.A. Hicks and A.C. Pickard, A comparison of theoretical and experimental methods of calibrating the electrical potential drop technique for crack length determination; Int. Journ. of Fracture, 20, 1982, pp. 91-101.

TABLE 1
List of participating laboratories and their representatives

North America	AFML, Dayton, USA	C. Harmsworth
	NADC, Warminster, USA	R. Mahorter
	NAE/NRC, Ottawa, Canada	D. Raizenne *
	NASA Lewis, Cleveland, USA	M. Hirschberg
	QETE, Ottawa, Canada	M. Bright
	University of Toronto, Canada	D. Hoeppner
Europe	CEAT, Toulouse, France	A. Liberge
	IABG, Ottobrunn, Germany	J. Foth
	NLR, Amsterdam, Netherlands	A. Mom *
	RAE, Farnborough, UK	C. Gostelow
	Rolls Royce, Derby, UK	R. Jeal
	University of Pisa, Italy	A. Frediani

* programme coordinators

TABLE 2
Overview of CORE programme; number of specimens indicated for each individual laboratory. All tests at room temperature

Type of test		LCF life / crack formation		Crack propagation	
Test specimen		Smooth cylindrical	flat notched $K_t \sim 2.2$	corner crack	ASTM CT
Number of specimens		6	6	3	3
CRACK DETECTION	potential drop	-	+	$+^{*)}$	+
	optical			+	
	GOAL		only initial crack formation	"short" crack range	total da/dN - ΔK curve

$^{*)}$ = optional

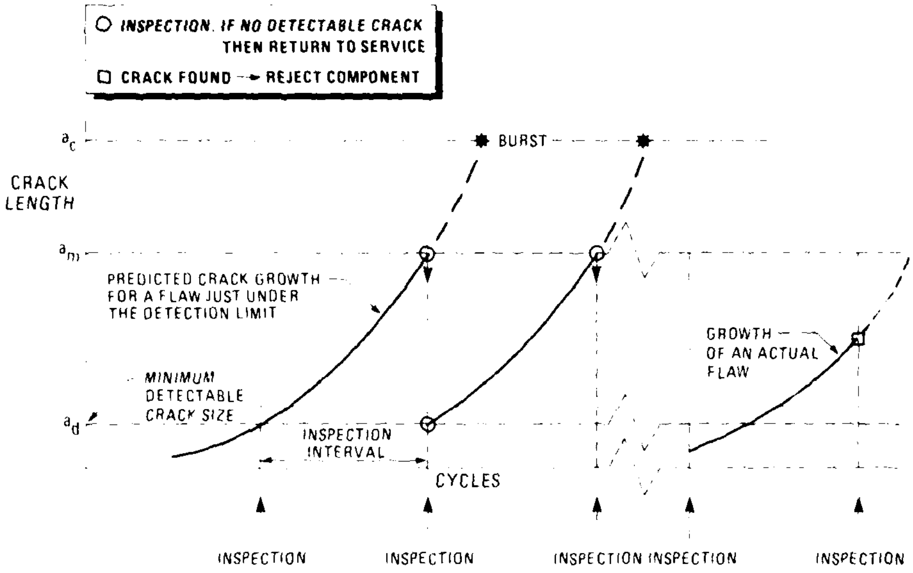

Fig. 1 Schematic of damage tolerance lifing approach
a_c = critical crack size
a_m = maximum allowable crack size in service
a_d = crack detection limit

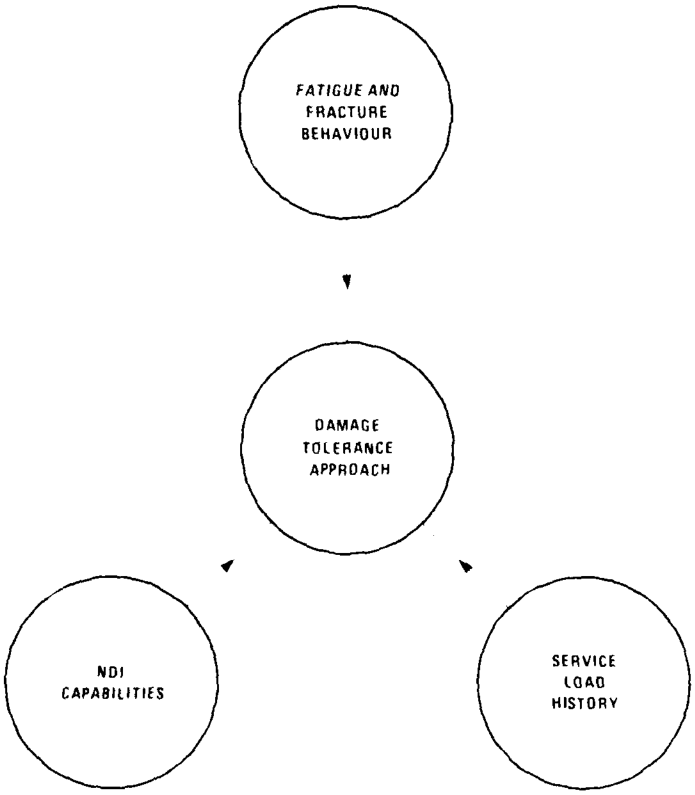
FATIGUE AND FRACTURE BEHAVIOUR
DAMAGE TOLERANCE APPROACH
NDI CAPABILITIES
SERVICE LOAD HISTORY

[illegible]

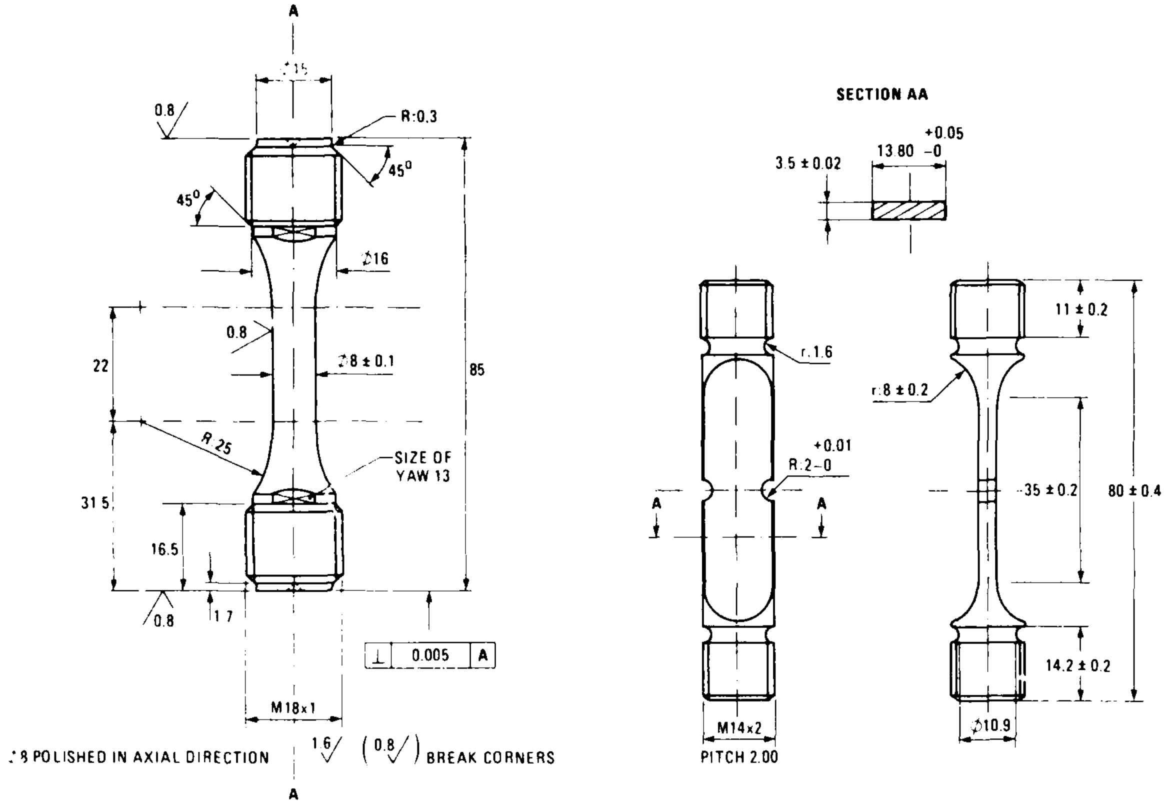
A
⌀15
0.8
R:0.3
45°
45°
⌀16
22
0.8
⌀8 ± 0.1
85
R 25
SIZE OF
YAW 13
31.5
16.5
0.8
1.7
⊥ 0.005 A
M18x1
⌀8 POLISHED IN AXIAL DIRECTION
1.6
0.8
BREAK CORNERS
A
SECTION AA
3.5 ± 0.02
13.80 +0.05 −0
r.1.6
r.8 ± 0.2
11 ± 0.2
+0.01
R.2−0
A
A
35 ± 0.2
80 ± 0.4
14.2 ± 0.2
M14x2
PITCH 2.00
⌀10.9

CYLINDRICAL UNNOTCHED LCF SPECIMEN

FLAT DOUBLE EDGE NOTCHED SPECIMEN ($K_t \approx 2.2$)

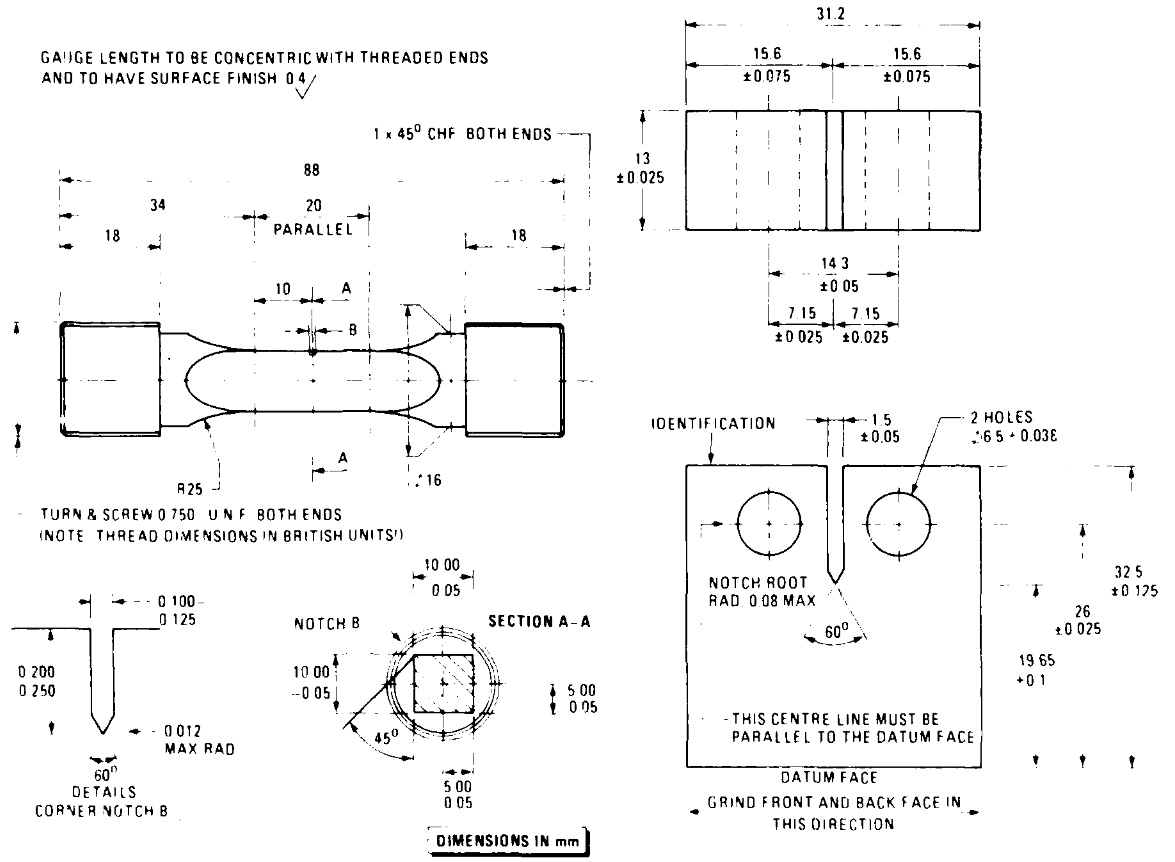
GAUGE LENGTH TO BE CONCENTRIC WITH THREADED ENDS
AND TO HAVE SURFACE FINISH 0.4
1 x 45° CHF BOTH ENDS
88
34
20
PARALLEL
18
18
10
A
B
A
R25
⌀16
TURN & SCREW 0.750 U.N.F. BOTH ENDS
(NOTE THREAD DIMENSIONS IN BRITISH UNITS!)
0.100−
0.125
0.200
0.250
0.012
MAX RAD
60°
DETAILS
CORNER NOTCH B
NOTCH B
10.00
0.05
SECTION A−A
10.00
−0.05
5.00
0.05
45°
5.00
0.05
DIMENSIONS IN mm
31.2
15.6
±0.075
15.6
±0.075
13
±0.025
14.3
±0.05
7.15
±0.025
7.15
±0.025
IDENTIFICATION
1.5
±0.05
2 HOLES
⌀6.5 + 0.038
NOTCH ROOT
RAD. 0.08 MAX
60°
32.5
±0.125
26
±0.025
19.65
+0.1
THIS CENTRE LINE MUST BE
PARALLEL TO THE DATUM FACE
DATUM FACE
GRIND FRONT AND BACK FACE IN
THIS DIRECTION

CORNER CRACK SPECIMEN

CT SPECIMEN

Fig. 3 Specimens used in the [illegible] programme

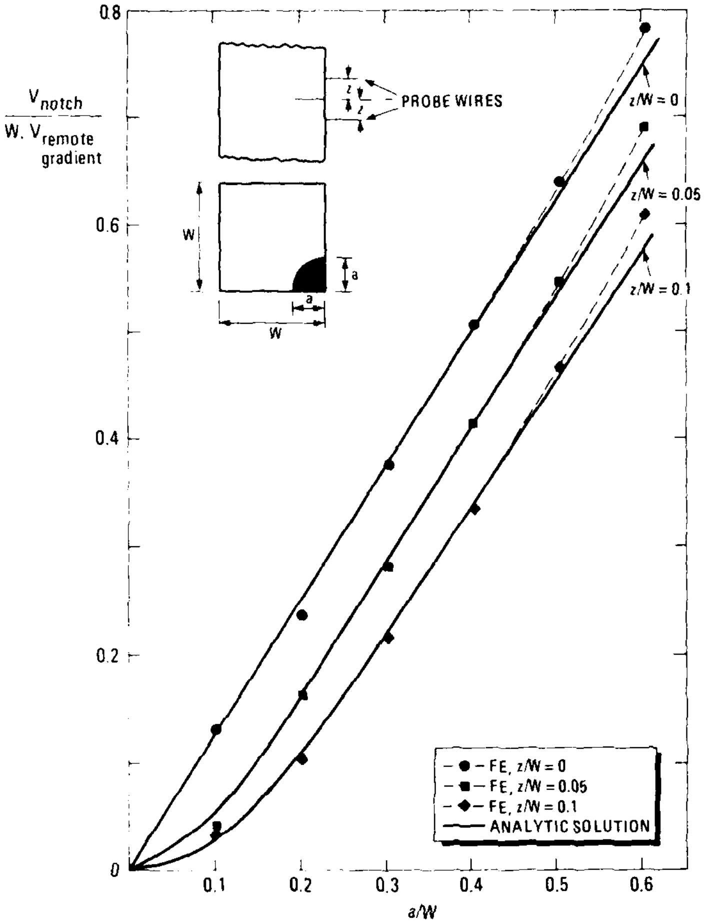

Fig. 4 Comparison of analytic and finite element solutions for various probe locations on the corner crack specimen (8)

Note: a quarter circular crack has been assumed with surface crack length = average crack length = a

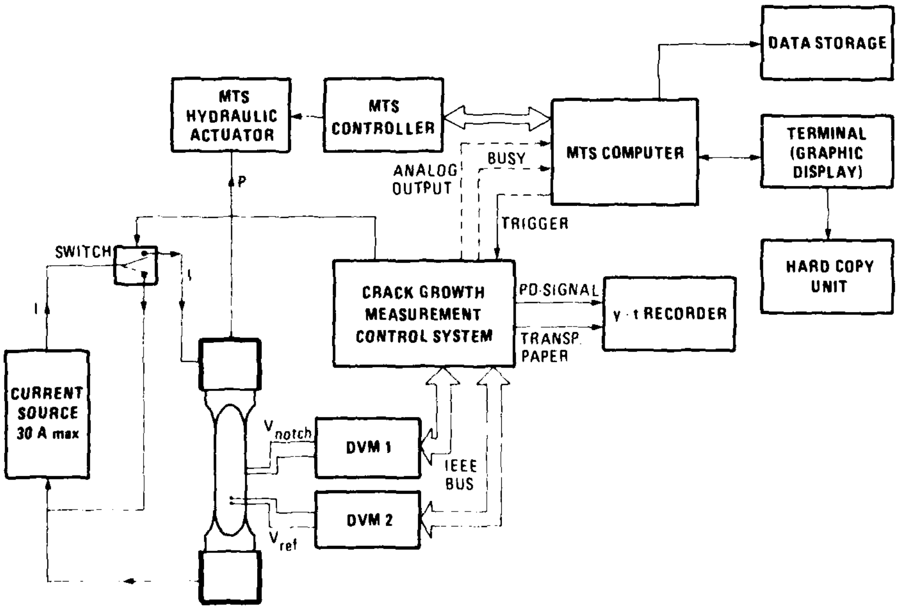

DATA STORAGE
MTS HYDRAULIC ACTUATOR
MTS CONTROLLER
MTS COMPUTER
TERMINAL (GRAPHIC DISPLAY)
BUSY
ANALOG OUTPUT
P
TRIGGER
HARD COPY UNIT
SWITCH
I
I
CRACK GROWTH MEASUREMENT CONTROL SYSTEM
PD-SIGNAL
TRANSP. PAPER
y - t RECORDER
CURRENT SOURCE 30 A max
V_{notch}
DVM 1
IEEE BUS
DVM 2
V_{ref}

Fig. 5 Instrumentation for fatigue testing and crack growth measurement

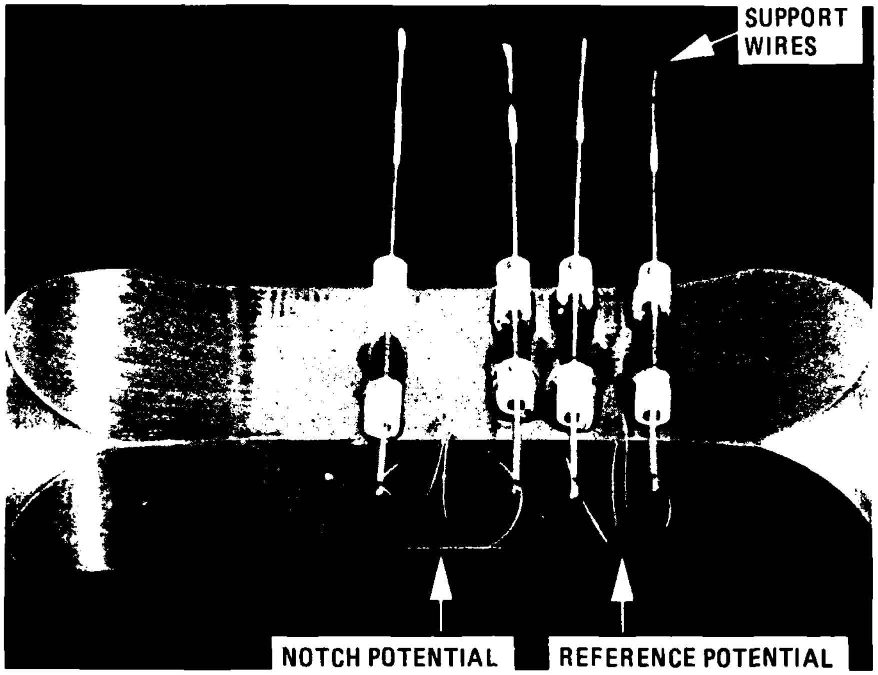
SUPPORT WIRES
NOTCH POTENTIAL
REFERENCE POTENTIAL

Fig. 6 Potential drop instrumentation of corner crack specimen. The 50 µm diameter notch probe wires are located on both sides of a 100 µm deep starter notch (not visible)

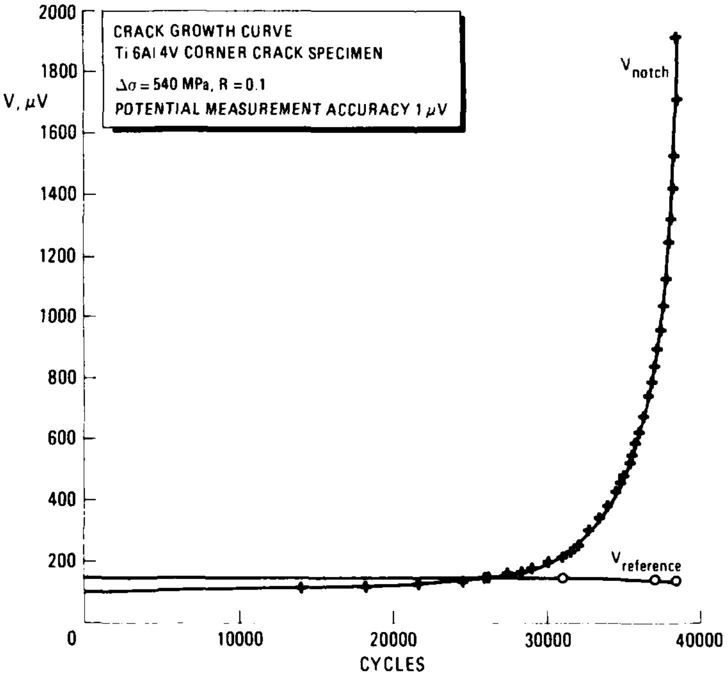

Fig. 7 Potential drop over crack versus number of cycles during fatigue test on corner crack specimen

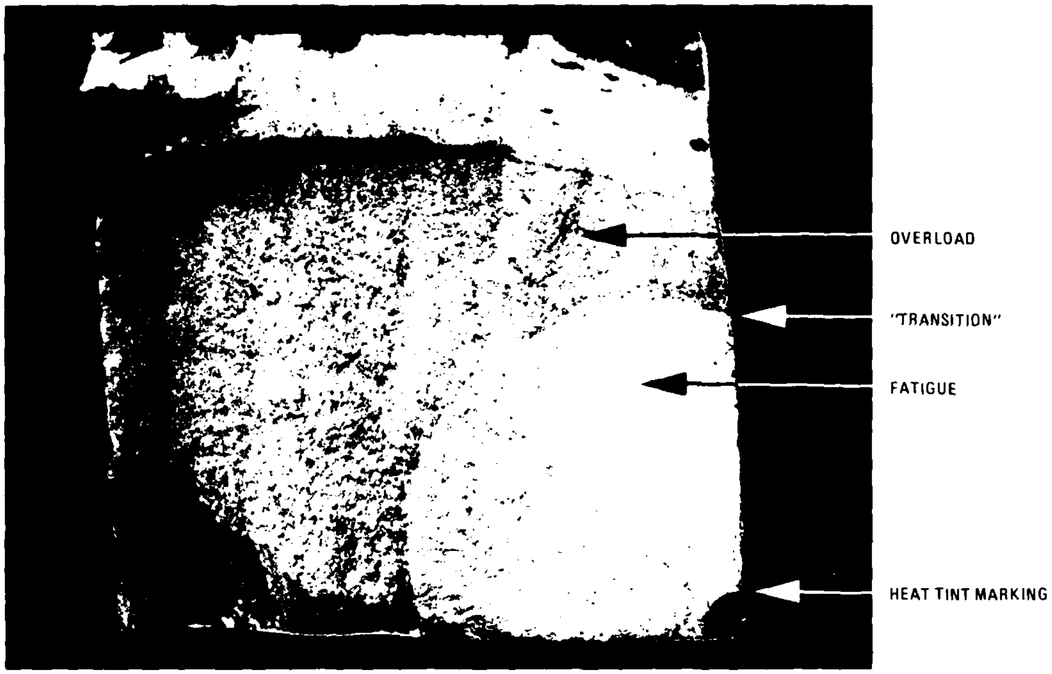
OVERLOAD
"TRANSITION"
FATIGUE
HEAT TINT MARKING

Fig. 8 Markings on fracture surface of corner crack specimen (x 9)

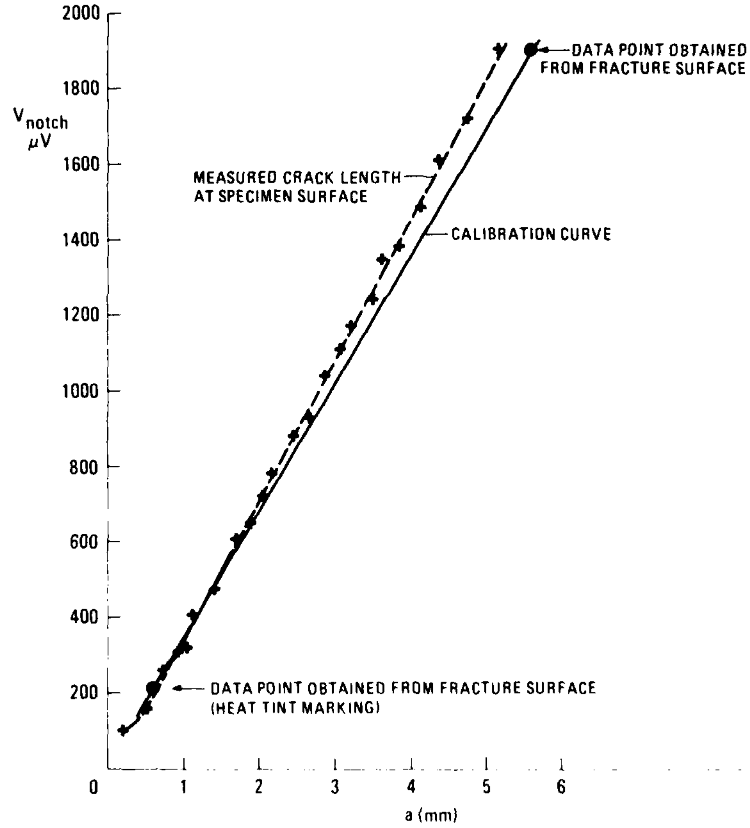

Fig. 9 Notch voltage versus crack length for corner crack specimen

ASPECTS OF SMALL CRACK GROWTH

M.N. James and J.F. Knott
Department of Metallurgy and Materials Science
University of Cambridge
Pembroke Street
Cambridge CB2 3QZ, England

SUMMARY

This paper addresses the nature of small defects which occur in engineering components and structures, and their subsequent growth to a size detectable by nondestructive inspection techniques. Consideration is given to fundamental aspects such as the modifying influence of residual stresses and "crack closure" on the growth of small cracks. Possible differences between laboratory test data and in-service crack growth are highlighted. Practical aspects are illustrated with specific reference to the example of the safety-critical high pressure turbine disc of an aeroengine.

1. INTRODUCTION

It is now well recognised that small pre-existing defects are an inherent feature of engineering components and structures. They may be formed as a direct result of material forming and fabrication techniques, or may be an adventitious result of careless transportation or handling. The sizes of such defects may range from the order of microns, for metallurgical inhomogeneities such as nonmetallic inclusions, to several millimetres for the case of welding defects such as slag inclusions or heat-affected-zone (HAZ) cracks. Over the majority of this range of crack sizes the major portion of the fatigue life is spent whilst the crack is smaller than the nondestructive inspection (NDI) limit, as illustrated in Fig.1. It is therefore convenient to define the upper bound of the small crack problem to correspond to the general NDI limit of around 0,5 - 1,0 mm.

The importance of the small crack regime in fatigue is apparent in Fig.1, and it is appealing to apply the principles of linear elastic fracture mechanics (LEFM) and, in particular, the defect tolerant design approach to this area. There are, however, certain practical and fundamental difficulties in extending fatigue design codes to include such small cracks. The practical difficulty relates to the NDI sizing limit. Many highly stressed components contain defect populations whose upper bounds are considerably lower than 0,5mm. This implies that, unless the upper bound on initial defect size can be determined by a feature of process control, e.g. by the mesh size employed in a powder metallurgy route, initial defect sizes cannot be quantified. Equally, estimates of the residual fatigue life of a component cannot be made until the crack has grown to a size that may be uncomfortably close to the critical failure size. Although in certain situations NDI may be able to detect surface-breaking flaws of perhaps 0,2mm, the above remarks still apply to very high strength materials with a correspondingly low defect tolerance.

The fundamental difficulties arise primarily from two factors. The first is that of applying LEFM to the high stress situations which usually characterise the growth of short cracks. A basic tenet in the use of LEFM is that applied stresses should be well below the yield stress and that the extent of crack tip plasticity should be small compared with crack size and component (specimen) dimensions. Associated with this is a possible "noncontinuum" aspect to crack tip plasticity when the crack size is small compared with some microstructural parameter. In this situation, several studies have indicated that the size of the crack tip plastic zone may then be determined primarily by the microstructure, rather than the applied stress intensity factor [1]. The second difficulty derives from the experimental observations of growth of short cracks at values of the applied stress intensity range (ΔK) well below the conventional "long crack" threshold value (ΔK_{th}). Such growth may occur at rates several orders of magnitude greater than might be expected from a supposedly conservative extrapolation of the Paris law regime to include low stress intensity values. It can then be inferred from such behaviour that in-service component failures could occur at a fraction of the expected lifetime. This emphasises the importance of understanding the growth of small cracks.

This paper addresses the nature of small defects which occur in practice and their subsequent growth to NDI detection size. Consideration is given to fundamental aspects such as the modifying influence of residual stresses and "crack closure" on the growth of small cracks. Possible differences between laboratory test data and in-service growth are highlighted. Practical aspects are illustrated with specific reference to the example of the safety-critical high pressure turbine disc of an aeroengine.

2. NATURE OF SMALL DEFECTS

The size and type of defect in a metallic product, and its initial stress state, reflect the processing route followed in its manufacture. In cast-to-shape products typical defects include porosity, shrinkage cavities, sand or slag entrapment due to abrasion of the mould surface by the metal flow, and solid nonmetallic deoxidation products. Although very high quality castings can be produced for small components such as gas turbine blades, castings generally contain a relatively large defect population. Probably the most important class of crack initiating casting defects are shrinkage cavities, which exist as essentially stress free geometric discontinuities with a wide range of sizes (up to 1mm or more in large castings).

For applications other than aeroengines, it is important to note that some casting alloys, designed to reduce macroscopic shrinkage, may contain phases of low density (graphite in cast iron; silicon in aluminium alloys) in the form of flakes and needles. These could be as deleterious as shrinkage cavities.

In cast-and-wrought products, the inclusion distribution represents the major class of defects. In addition to size and morphology, the chemical composition of inclusions is also of significance with respect to the growth of short cracks. Inclusions that are plastic at hot working temperatures, such as low-oxygen manganese sulphide inclusions in structural steels, can be rolled out to produce thin, crack-like platelets. Such inclusions can act as useful crack arresters in some orientations and significant crack initiators in others. Similar effects have been observed in stress-corrosion tests made on Al-Zn-Mg alloy forgings and extrusions where there is marked "pancaking" of grains [2].

The presence of inclusions also gives rise to local residual (or "tessellated") stresses on cooling, as a result of the strains produced by the differences in coefficients of thermal contraction between inclusion and matrix. Oxide or silicate particles contract less than a steel or nickel-base superalloy matrix, so that the inclusion is in compression. A weight function analysis shows that the net value of stress intensity due to the residual stress field is compressive, even for a crack of surface length twice the radius of a cylindrical inclusion [3]. The conclusion to be drawn is that it may be necessary to apply a tensile stress of at least the magnitude of the residual stress to provide a driving force for crack growth, even if the inclusion is already cracked. Such behaviour could induce a "fatigue limit" in the material, which would be expected to vary with temperature because this controls the value of mismatch strain between inclusion and matrix. The sign of such residual stresses, as well as their magnitude, can change with the chemical composition. In the case of manganese sulphide inclusions in steel, for example, a bonded inclusion would experience tensile strains.

A process route which appears to be particularly attractive for nickel-base superalloys, to attempt to overcome segregation problems associated with the conventional cast-and-wrought route, is the hot isostatic pressing (HIP-ping) and forging of atomised and sieved metal powder. This route is in use for the production of high pressure turbine discs in aeroengines. In general, the powder is uniform and surface oxidation is minimised, but it is possible for small refractory particles to be scoured off the mould and pass through the sieve to become mixed in with the metal powder [4]. The sizes of such particles will depend on the mesh size of the sieve (and the number of sieving operations), but are likely to be in the range 0,1 - 0,2mm [4]. The situation regarding residual tessellated stresses for these defects is similar to that for the oxide and silicate particles in cast-and-wrought alloys. Hipping and forging are carried out at high temperatures (in the range 1000 - 1150^{o}C), so that any mismatch strains are accommodated by plastic flow and diffusion: on cooling to lower temperatures, differences in thermal expansion coefficients again produce residual stresses.

With respect to defects introduced by fabrication techniques, it is probable that fusion welding is potentially able to produce the greatest variety of defects in metal-metal bonding. Included amongst these defects are solidification cracking, slag entrapment, lack of fusion and HAZ cracking produced by hydrogen up-take. The problem of treating small cracks at welds is compounded by the presence of residual stresses in the joint and, for fillet welds, by the stress gradient at the weld toe. Both sets of stresses can, however, be treated using suitable weight functions.

In conclusion, it is important to recognise that, although some defects may be initially essentially stress free, many defects are subject to residual elastic stresses which may be a substantial proportion of the materials yield stress. Such stresses are likely to influence the initial growth of cracks from defects and must be taken into account in realistic analyses of short crack growth.

3. SMALL CRACK GROWTH

When the growth of a fatigue crack from some small initial defect is analysed using LEFM parameters, different types of behaviour may be observed over the first millimetre or so of growth, as illustrated in Fig.2. In all cases, there is an initially high growth rate at ΔK values well below the conventional long crack threshold. The growth rate may then decrease to a minimum (or even arrest) as ΔK increases, before increasing again and joining the long crack growth curve. For tests employing constant values of maximum cyclic stress and stress ratio (R) ΔK may be replaced on the abscissa by crack length. The "short crack regime" can then be defined as existing for that range of crack sizes which exhibit enhanced growth rates relative to longer cracks. Such anomalous growth behaviour has been observed in many materials including steels [5-7], aluminium alloys [8], titanium alloys [9,10], nickel-base superalloys [11,12] and cast aluminium bronze [13].

Enhanced growth rates may be observed when:

1) Cracks are comparable in length to the scale of local plasticity. This is particularly the case when the crack is growing in a region of bulk plasticity, e.g. at a

notch root (see Fig.2), but can also occur when the crack is affected by the size of its own plastic zone. Such behaviour may in some cases be normalised by the use of a more appropriate fracture mechanics parameter, such as the J integral or crack tip opening displacement [14].

2) Cracks are similar in length to some microstructural dimension. This is essentially a breakdown in the homogeneous continuum requirement for the application of fracture mechanics [13]. This is likely to be more prevalent in coarse grained materials which exhibit very crystallographic growth.

3) Even when the crack is "long" in terms of microstructure and local plasticity, enhanced growth rates have been observed for physically short cracks, say less than 0,5 - 1,0 mm. This has been proposed to be due to a breakdown in the similitude concept of LEFM [15].

Similitude implies that two different sized cracks subjected to equal applied stress intensity values, in a given material/microstructure/environment system, will have plastic zones that are equal in size and have identical stress and strain distributions along the elastic/plastic boundary. The crack growth rates are then expected to be equal. Fracture mechanics parameters such as ΔK, however, define the nominal, applied, mechanical "driving force" for crack extension, since ΔK characterises the applied stress and strain fields ahead of the crack tip, whereas crack growth rates must reflect the local effective driving force at the crack tip. Conditions that affect this local driving force can therefore lead to a violation of similitude and subsequent anomalous growth behaviour. Local plasticity and noncontinuum behaviour can produce loss of similitude, but it may also arise from changes in crack growth mechanism and crack closure.

Several authors have proposed that changes in crack closure are the cause of observed short crack behaviour [6,7,9,11], and it has become increasingly apparent that closure is a major variable in fatigue crack growth, especially at near-threshold growth rates at low stress ratios ($R < 0,5 - 0,7$). One method of accounting for effects of closure on crack growth is based on the use of an effective stress intensity range (ΔK_{eff}), defined as $K_{max} - K_{op}$ where K_{op} is the stress intensity at which the crack tip opens. This definition assumes that K_{op} can be determined accurately. If the schematic data in Fig.2 were plotted versus ΔK_{eff}, the discrepancy between short and long crack growth rates, for most materials, would generally be reduced or, in others, such as quenched and tempered steels, eliminated.

Effects of crack closure, microstructure and plasticity on short crack growth may either act independently or in conjunction. It would therefore be expected that the extent of the short crack regime in a given alloy would vary with factors such as: heat treatment, which affects microstructure and yield strength; maximum stress intensity in the fatigue cycle, which could influence the retarding effect of grain boundaries [16]; and, independently, the minimum stress intensity (stress ratio) which determines the magnitude of the closure effect. In closure dominated situations short crack behaviour disappears at high stress ratios [7].

The effect of heat treatment is clearly demonstrated in two studies made on 0,4% carbon steels [17,18]. James and Smith [17] studied a quenched and tempered 0,4% carbon steel with a ferrite grain size of 10μm. They observed no microstructural dependence of growth for small cracks, with Stage II growth being established very early in life (see Fig.3). Enhanced growth rates were found for cracks whose surface length was less than 100μm. The short crack effect was explained by changes in closure. In a study of a normalised 0,4% carbon steel with a prior austenite grain size of 140μm, however, De Los Rios et al [18] observed microstructurally-dependent growth with cracks arresting at ferrite/pearlite interfaces. Short crack behaviour was observed for cracks with surface lengths in the range 200 - 300μm, which corresponded to the lengths of ferrite allotriomorphs in which the cracks had initiated.

Crack retardation at microstructural interfaces is one explanation for the initially decreasing growth rates shown schematically for short cracks in Fig.2. This decrease occurs despite the fact that ΔK, for constant amplitude loading, is increasing steadily as the crack length increases. This observation has been attributed to two factors [19]. The first is the difficulty in propagating slip across an interface, which may give rise to an incubation period, depending on the type of the interface, e.g. high angle grain boundary or interface with a second phase. The second factor is a possible increase in closure stress as a crack tip crosses an interface, caused by increased "noncontinuum" crack tip plasticity due to slip extending to the next interface. In a closure dominated situation the decrease in growth rates can be perceived as arising from an increase in closure stress (i.e. a reduced ΔK_{eff}) which more than offsets the increase in applied stress intensity. As the closure level approaches that of a long crack the increase in closure stress tapers off and the growth rate increases towards the long crack curve.

Several interesting facets of the behaviour of short cracks are shown in recent work by Hicks and Brown [12] on several aluminium, titanium and nickel-base alloys used in the aircraft industry. The nickel-base alloys tested were Astroloy with grain sizes of 5μm and 50μm, and single crystal specimens of SRR 99. Apparently, for initial coarsening of grain size short crack growth rates increased, relative to those for long cracks, but for the extreme of a single crystal specimen closer correspondence was obtained between short and long crack behaviour, as seen in Fig.4. It is likely that a single crystal specimen provides continuum conditions down to very small crack lengths. Short crack effects are then limited in extent as they will arise only from closure changes due to a limited crack wake and, at very short crack lengths, from plasticity effects. The data also indicate that crystal structure, which controls the mode of slip, may be used to rank the resistance of metals to short crack growth and that, within a particular crystal structure, increases in elastic modulus and yield strength further improve the crack propagation resistance.

It is clear from the above discussion that the prediction of short crack behaviour in a particular alloy is rendered difficult by the possibility of complex interactions between plasticity, microstructure and crack closure. Such data as those of Hicks and Brown [12] and Morris et al [19], however, indicate that there is considerable potential for developing more defect tolerant microstructures. This requires careful research programmes aimed at separating out the effects of the various factors which influence the growth of short cracks.

A further complication in studying short crack behaviour derives from the type of crack used in such work. Although many workers have considered semi-elliptical cracks [5,7,9,12], a significant number of studies have utilised through-thickness cracks [6,20]. These two types of crack are generated under very different loading conditions. Short through-cracks are generally obtained by machining away part of a crack produced under a load shedding or constant ΔK testing scheme, to leave a through-thickness crack of the desired length. Short semi-elliptical cracks, however, are usually generated under increasing ΔK conditions at stresses near, or above, yield. A stress relief operation may then be employed prior to subsequent testing. James and Knott [21] have recently critically examined the effects of these two crack generation techniques on the extent of short crack behaviour. Load shedding and constant ΔK techniques both lead to the development of considerable plasticity induced closure well behind the crack tip, as demonstrated in Fig.5, in both plane stress [22] and plane strain [21]. The length of crack wake which experiences "wedging" can be as much as 1-2mm. When part of the wake is removed, to produce short through-cracks of length less than the original "wedged" length, K_{op} is reduced and enhanced growth rates are observed during subsequent testing. The extent of the apparent short crack regime is then merely a reflection of the length of crack wake which contributed to closure during precracking. Effectively, the behaviour of such short through-cracks is the same as that of long through-cracks in which part of the wake has been removed by, say, electrodischarge machining [6,21] (see Fig.6). Crack growth under increasing ΔK conditions, however, appears to confine wake "wedging" to much smaller lengths directly behind the crack tip. Semi-elliptic surface crack tests conducted under increasing ΔK conditions should therefore furnish a more accurate estimate of the extent of any short crack behaviour in a particular alloy.

Surface cracks are, however, often generated by high stresses close to, or even exceeding, yield and are then stress relieved at relatively low temperatures (around 600°C). Initial fatigue crack growth could thus occur in the presence of significant plasticity, and there is then the possibility, at least for steels, of the incomplete removal of such plasticity during the stress relief treatment. Residual wake plasticity could then dominate short crack behaviour either directly, by invalidating the use of LEFM, or indirectly by contributing to the premature build-up of closure to a "long crack" value. An incorrect assessment of the extent of the short crack regime could result from this effect. The authors are currently examining this possibility, in QIN (HY80) steel, through a comparison between the behaviour of semi-elliptic surface cracks either initiated at inclusions by high stress, or initiated at low stresses by a novel application of hydrogen charging. This technique appears to have considerable potential in work on small cracks, as many natural cracks at welds are produced in a similar way. A typical hydrogen induced crack about 140μm deep and its final shape after subsequent threshold testing are shown in Fig.7.

4. DEFECT TOLERANCE IN TURBINE DISCS

Due to its rotational speed and mass, the high pressure disc of a gas turbine is generally considered to be the most safety-critical aeroengine component. The fatigue cycles of concern are the major "take-off/landing" cycles, in which the disc is stressed in parts virtually to its proof stress. Current powder metallurgy nickel-base disc alloys have 0,1% proof stresses of around 10^3 MPa, and a correspondingly low defect tolerance [4] as indicated in Fig.8. Considering the specific case of Astroloy, a useful depiction of short crack behaviour is that originally due to Kitagawa and Takahashi [23], shown in Fig.9. It represents the stress required to cause fatigue crack growth for a given crack length, and relates to threshold and endurance limit data. The crack lengths corresponding to the NDI limit, the onset of short crack behaviour [12] and the process control limit (sieve mesh size) are indicated in the figure.

It is clear that the initial defect sizes lie in the range where enhanced growth rates have been observed and that the entire short crack regime lies inside the NDI detection limit. The situation will be worsened by the high operating stresses experienced by the disc. Fig.4, based on data from laboratory test specimens, indicates that short crack growth rates will be at least an order of magnitude higher than an extrapolation of the linear growth rate regime would indicate. It is therefore instructive to examine the criticality of the initial defect size by applying a fracture mechanics crack growth analysis to the disc material.

The linear regime growth rate law for long fatigue cracks in Astroloy is [24]:

$$da/dN = 4 \times 10^{-12} \Delta K^{3,3} \qquad \ldots(1)$$

and this will apply to cracks as small as 0,25mm. Assuming that the applied stress range is equal to the proof stress (about 10^3 MPa), and that the final defect size is 0,8mm after a life of 10^4 flight cycles [25], equation (1) can be integrated to obtain an estimate of the allowable initial defect size. This process indicates than an initial surface defect would need to be only about 70μm deep to produce this growth, while the critical diameter of a penny-shaped buried defect would be about 100μm. This could cause concern on two counts; firstly the fact that the maximum size of initial defect which could pass through the process control sieves might be twice this size; secondly that the above analysis did not consider any enhanced growth rates in the initial portion of the life, when the crack was smaller than 0,25mm.

In actuality, experimental results from spin-rig testing of discs [4] suggest that the above fracture mechanics approach is somewhat pessimistic, as seen in Fig.10.

A possible explanation for this apparently contradictory short crack behaviour, compared with Fig.4, could be the local tessellated stresses around the refractory particles in the powder disc alloy. These particles would not be crack initiation sites in the laboratory specimens used to obtain the data in Fig.4. As discussed in an earlier section, such stresses will exert a clamping force on the fatigue crack during the initial stage of its growth from the inclusion. This could then lead to the "fatigue limit" type of behaviour seen in Fig.10.

The conclusion to be drawn from this is that a thorough analysis and understanding of the factors influencing the behaviour of small fatigue cracks is required, before experimental data acquired from small laboratory specimens can be reliably applied to service situations.

5. TESSELLATED STRESSES AROUND INCLUSIONS

As described in previous sections, the cooling of a powder-formed, nickel-base superalloy from the hipping or forging temperature is likely to generate local residual, or "tessellated", stresses around refractory inclusions as a result of differences in thermal expansion coefficient between inclusion and matrix. In this section, we attempt to show how the presence of such tessellated stresses could affect the early growth of short cracks and introduce an effective "fatigue limit". The approach followed is to load a hypothetical crack emanating from an inclusion with the residual stress distribution arising from the tessellated stresses, using an appropriate weight function. A similar method has been used with success to treat fatigue crack growth throughout the regions of residual compressive stress in autofrettaged gun barrels [26] and in regions of compressive stress in centre-cracked plates, where the residual stress was induced by indentation of the plate surfaces with rollers of length W/2, located centrally above and below the crack [27].

For an isolated inclusion in an infinite body, the circumferential stress at a total distance, r, from its centre is given by the following expressions [28]:

for a spherical inclusion:

$$\sigma_i = p \quad ; \quad \sigma_m = - p(r_i{}^3/2r^3)$$

where $p = \beta / [\{(1 + \nu_m)/2E_m\} + \{(1 - 2\nu_i)/E_i\}]$

for a cylindrical inclusion:

$$\sigma_i = p' \quad ; \quad \sigma_m = - p'(r_i{}^2/r^2)$$

where $p' = \beta(1 + \nu_i) / [\{(1 - 3\nu_i)/E_i\} + \{(1 + \nu_m)/E_m\}]$

and $\beta = (\alpha_m - \alpha_i)\ \Delta T$ for both types of inclusion. In these equations, the radius of the inclusion is r_i, suffix m refers to the matrix, suffix i refers to the inclusion, E is Young's modulus, ν is Poisson's ratio, α is the thermal expansion coefficient and ΔT is the difference in temperature between the hipping/forging temperature and the operating temperature.

A crack emanating from a spherical inclusion is ideally "penny-shaped": if it has radius a, it is loaded by a compression $\sigma_i = p$ between o and r_i, and a tension $\sigma_m = - p(r_i{}^3/r^3)$ between r_i and a. If $a > r_i$, the weight functions may be integrated to give stress intensities as follows:

$$K_1 \text{ (compression)} = 2(\pi a)^{-\frac{1}{2}} \int_o^{r_i} pr\ (a^2 - r^2)^{-\frac{1}{2}}\ dr$$

$$= 2p\ (\pi a)^{-\frac{1}{2}} \{a - (a^2 - r_i{}^2)^{\frac{1}{2}}\}$$

$$K_2 \text{ (tension)} = (\pi a)^{-\frac{1}{2}} \int_{r_i}^{a} - pr_i{}^3\ (a^2 - r^2)^{-\frac{1}{2}}\ r^{-2}\ dr$$

$$= - p\ (\pi a)^{-\frac{1}{2}} (r_i{}^2/a^2)\ (a^2 - r_i{}^2)^{\frac{1}{2}}$$

The net stress intensity (for $a > r_i$) is given by $K_3 = K_1 + K_2$.

For the specific geometry $a = 2r_i$, the result is that K_3 is given by:

$$K_3 = p(\pi a)^{-\frac{1}{2}} \{2(2 - \sqrt{3}) - \sqrt{3}/4\} r_i$$
$$= 0.051\ p\ \pi^{-\frac{1}{2}} a^{\frac{1}{2}} = 0.051\ p\ \pi^{-\frac{1}{2}} (2r_i)^{\frac{1}{2}}$$

i.e. the net stress intensity is still compressive. A similar result is obtained for the cylindrical inclusion [3]. For a crack of length $2a = 4r_i$ growing symmetrically from the centre of an inclusion, the compressive component is:

$$K_4 = 2p'(2r_i/\pi)^{\frac{1}{2}} \int_0^{r_i} (4r_i^2 - r^2)^{-\frac{1}{2}} dr$$
$$= (p'/3)\ (2\pi r_i)^{\frac{1}{2}}$$

Between r_i and $2r_i$, the tensile component is:

$$K_5 = -2p'(2r_i/\pi)^{\frac{1}{2}} \int_{r_i}^{2r_i} (r_i^2/r^2)\ (4r_i^2 - r^2)^{-\frac{1}{2}} dr$$
$$= -p'(3r_i/2\pi)^{\frac{1}{2}}$$

The net stress intensity $K_6 = K_4 + K_5$ is then given by:

$$K_6 = p'(\pi a)^{\frac{1}{2}} \{(1/3) - (\sqrt{3}/2\pi)\}$$
$$= 0.058p'(\pi a)^{\frac{1}{2}} = 0.058p'(2\pi r_i)^{\frac{1}{2}}$$

Again, the net stress intensity is compressive.

For forging temperatures slightly over 1100°C, the value of ΔT may be taken as 1100°C for the cold part of a disc and 500°C for the high temperature part. For a pure alumina inclusion, $E_i = 390$ GPa, $\nu_i = 0.25$, $\alpha_i = 8 \times 10^{-6}$, [28] and for a typical superalloy matrix, $E_m = 200$ GPa, $\nu_m = 0.29$, $\alpha_m = 13 \times 10^{-6}$ at room temperature [29,30]. For a spherical inclusion, the value of p is then calculated as 1220 MPa at room temperature and 555 MPa at an operating temperature of 600°C: for a cylindrical inclusion, the figures are 970 MPa and 440 MPa respectively. We see that the presence of the residual stresses can then induce a "fatigue limit", if sufficient tensile stress has to be applied either to overcome the pressure or to produce positive values of stress intensity. The order of magnitude of this "fatigue limit" is comparable with the material's yield stress (10^3 MPa) in agreement with the data shown in Fig.10. Differences in the value of p can be obtained for average values of α_m (20×10^{-6}) and for different inclusions, e.g. mullite ($3Al_2O_3.2SiO_2$) for which E_i is 145 GPa and α_i is 5×10^{-6} [31]. If a fatigue limit due to tessellated stresses does exist, it will be important to study inclusion/matrix combinations in detail to relate local stress levels to the precise values of fatigue limit observed.

6. CONCLUSIONS

This paper has drawn attention to a number of general aspects pertaining to short crack growth and to factors which produce differences in the growth rates of long and short cracks at the same nominal stress intensities. There is clearly a range of extremely small cracks in which behaviour is dominated by noncontinuum, microstructural effects. For larger defects, continuum fracture mechanics would be expected to be adequate, but the paper points out that most real defects, or short cracks studied in experimental tests, are not simply geometrical discontinuities, but are associated with residual stress fields, generated by plasticity (e.g. in the "wake" of a long crack) or by elastic fields due to surface hardening or differential thermal expansion. The last case has particular relevance to powder-formed discs and a possible method of analysis is proposed. The general point is that any assessment of the growth of small defects must simulate the local stress fields that exist around the defect in service and this demands a detailed knowledge of the microstructure, in addition to the use of weight function techniques to calculate the effects of the local stress fields on the stress intensity ahead of a small, growing crack.

7. REFERENCES

1. Morris W.L., The noncontinuum crack tip deformation behaviour of surface microcracks, Metall. Trans. 11A (1980), 1117-1123.
2. Day M.K.B., Cornish A.J. and Dent T.P., The relationship between structure and stress-corrosion life in an Al-Zn-Mg alloy, Metal. Sci. 3 (1969), 175-182.
3. Tsubota M., King J.E. and Knott J.F., Crack propagation and threshold behaviour in Ni-base superalloys and its implications for component life assessment, First Parsons International Turbine Conference, Dublin, Parsons Press, (1984), 189-196.
4. Wildgoose P., Turner N.G., Davies H.F., Helliwell B.J., Ubank R. and Harrison H., Powder metallurgical innovations for improved hot-section alloys in aeroengine applications, Powder Metallurgy 24 (1981), 75-86.
5. Kitagawa H., Takahashi S., Suh C.M. and Miyashita S., Quantitative analysis of fatigue process-microcracks and slip lines under cyclic strains, Fatigue Mechanisms, ASTM STP 675 (1979), 420-449.
6. Breat J.L., Mudry F. and Pineau A., Short crack propagation and closure effects in A508 steel, Fatigue Engng Mater. Struct. 6 (1983), 349-358.

7. James M.N. and Smith G.C., Short crack behaviour in A533B and En8 steels, Advances in Fracture Research, Proceedings of the Sixth International Conference on Fracture (edited by Valluri S.R. et al), New Delhi, India (1984) 3, 2117-2124.
8. Lankford J., The growth of small fatigue cracks in 7075-T6 aluminium, Fatigue Engng Mater. Struct. 5 (1982), 233-248.
9. James M.R. and Morris W.L., Effect of fracture surface roughness on growth of short fatigue cracks, Metall. Trans. 14A (1983), 153-155.
10. Brown C.W. and Hicks M.A., A study of short fatigue crack growth behaviour in titanium alloy IMI 685, Fatigue Engng Mater. Struct. 6 (1983), 67-76.
11. McCarver J.F. and Ritchie R.O., Fatigue crack propagation thresholds for long and short cracks in René 95 nickel-base superalloy, Mater. Sci. Engng 55 (1982), 63-67.
12. Hicks M.A. and Brown C.W., A comparison of short crack growth behaviour in engineering alloys, Fatigue 84, Proceedings of the Second International Conference on Fatigue and Fatigue Thresholds (edited by Beevers C.J. et al), Birmingham, England (1984) 3, 1337-1347.
13. Taylor D. and Knott J.F., Fatigue crack propagation behaviour of short cracks; the effect of microstructure, Fatigue Engng Mater. Struct. 4 (1981), 147-155.
14. Ahmad J., Hopper A.T., Kanninen M.F., Leis B.N. and Papaspyropoulos V., A nonlinear fracture mechanics predictive procedure for the short crack effect in fatigue, Battelle-Columbus Laboratories Report under Contract Number F-33615-81-C-5051 (1982).
15. Ritchie R.O. and Suresh S., The fracture mechanics similitude concept: questions concerning its application to the behaviour of short fatigue cracks, Mater. Sci. Engng 57 (1983), L27-L30.
16. James M.R., Morris W.L. and Zurek A.K., On the transition from near-threshold to intermediate growth rates in fatigue, Fatigue Engng Mater. Struct. 6 (1983), 293-305.
17. James M.N. and Smith G.C., Crack closure and surface microcrack thresholds - some experimental observations, Int. J. Fatigue 5 (1983), 75-78.
18. De Los Rios E.R., Tang Z. and Miller K.J., Short crack fatigue behaviour in a medium carbon steel, Fatigue Engng Mater. Struct. 7 (1984), 97-108.
19. Morris W.L., James M.R. and Buck O., Growth rate models for short surface cracks in Al 2219-T851, Metall. Trans. 12A (1981), 57-64.
20. Heubaum F. and Fine M.E., Short fatigue crack growth behaviour in a high strength low alloy steel, Scripta Metall. 18 (1984), 1235-1240.
21. James M.N. and Knott J.F., An assessment of crack closure and the extent of the short crack regime in QIN (HY80) steel, Fatigue Engng Mater. Struct. 8 (1985), in press.
22. Newman J.C. Jr, A nonlinear fracture mechanics approach to the growth of small cracks, Behaviour of Short Cracks in Airframe Components, Proceedings of the 55th Meeting of the AGARD Structures and Materials Panel, Toronto, Canada (1982).
23. Kitagawa H. and Takahashi S., Applicability of fracture mechanics to very small cracks or the cracks in the early stage, Proceedings of the Second International Conference on Mechanical Behaviour of Materials, Boston, USA (1976) 627-631.
24. Brown C.W. and Hicks M.A., Fatigue growth of surface cracks in nickel-based superalloys, Int. J. Fatigue 4 (1982), 73-81.
25. Coles A., Material considerations for gas turbine engines, Proceedings of the Third International Conference on Mechanical Behaviour of Materials, Cambridge, England, (1979) 1, 3-11.
26. Clark G., Fatigue crack growth in autofrettaged thick walled cylinders, Fracture Mechanics Technology Applied to Material Evaluation and Structure Design (edited by Sih G.C. et al), Martinus Nijhoff, The Hague (1983) 417-430.
27. Braid J.E.M., Fatigue crack propagation in residual stress fields, Ph.D Thesis, University of Cambridge (1983).
28. Brooksbank D. and Andrews K.M., Tessellated stresses associated with some inclusions in steels, J. Iron and Steel Inst. 207 (1969) 474-483.
29. Henry Wiggin and Co. Ltd., Introducing the Wiggin nickel alloys, Publication 3558 (1972).
30. Henry Wiggin and Co. Ltd., Nimonic alloys, Publication 25048E (1973).
31. Brooksbank D. and Andrews K.M., Stress fields around inclusions and their relation to mechanical properties, J. Iron and Steel Inst. 210 (1972) 246-255.

8. ACKNOWLEDGEMENTS

The authors thank Professor D. Hull for the provision of laboratory facilities, and the Ministry of Defence, Procurement Executive, for financial support for one of them (MNJ).

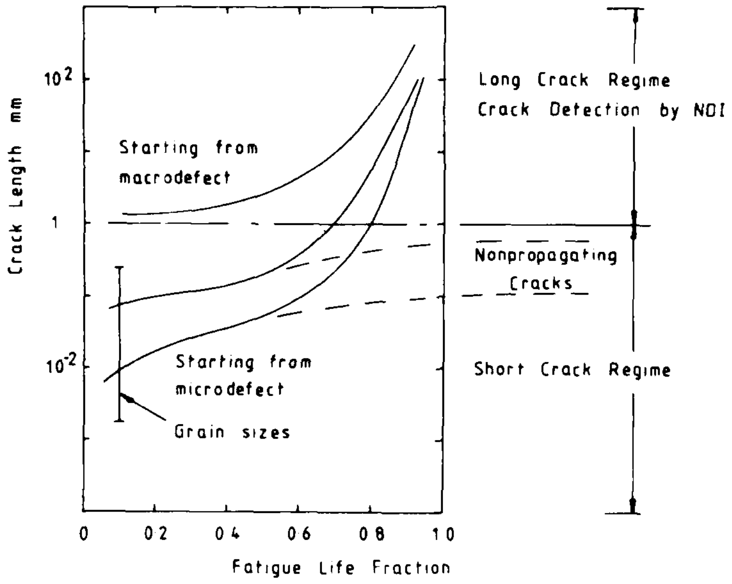

Fig. 1 Illustration of the importance of the small crack regime in fatigue. Where failure originates from microdefects, the majority of the fatigue life will be spent as cracks smaller than the NDI detection limit.

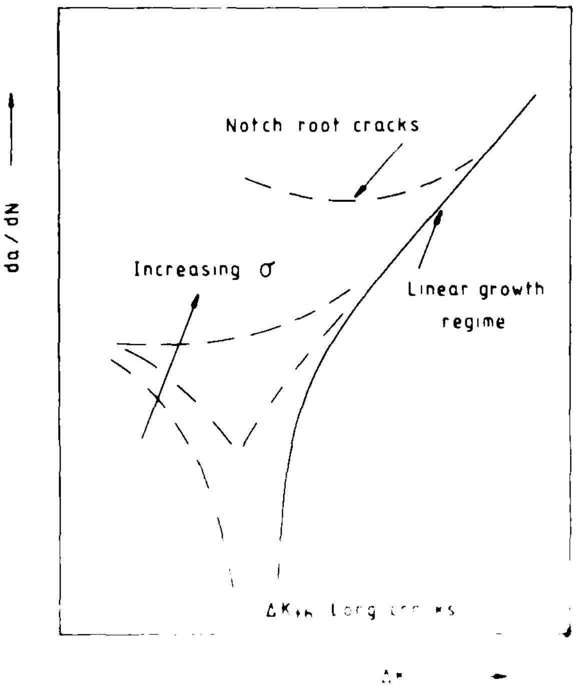

Fig. 2 Schematic illustration of types of short crack behaviour (dashed lines) which may be observed over the first millimetre or so of growth.

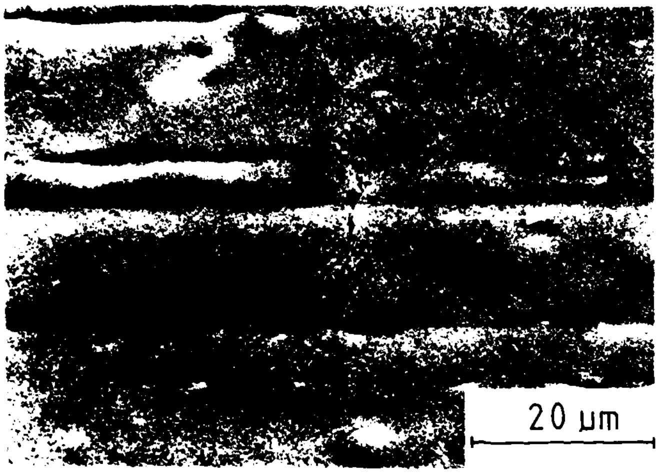

Fig. 3 Demonstration of the establishment of a Stage II crack at a very small size in a quenched and tempered 0,4% carbon steel [17]. The stress axis is indicated by the arrow. Initiation occurred at a subsurface alumina inclusion whose size was equal to the bottom of the "trough" in the central portion of the crack.

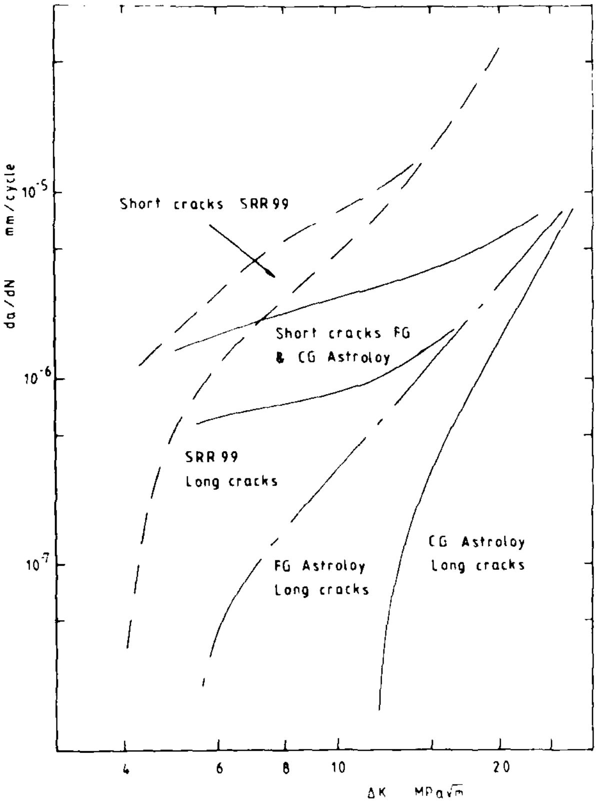

Fig. 4 Short crack behaviour in two nickel-base alloys, after Hicks and Brown [12]. The SRR99 data is for single crystal specimens, while the Astroloy had grain sizes of 5μm (FG) and 50μm (CG). Coarsening the grain size in the Astroloy gives rise to a larger difference between short and long crack behaviour, due to the higher threshold observed for the long cracks in the CG material. In the extreme of a single crystal specimen closer correspondence was obtained between short and long cracks.

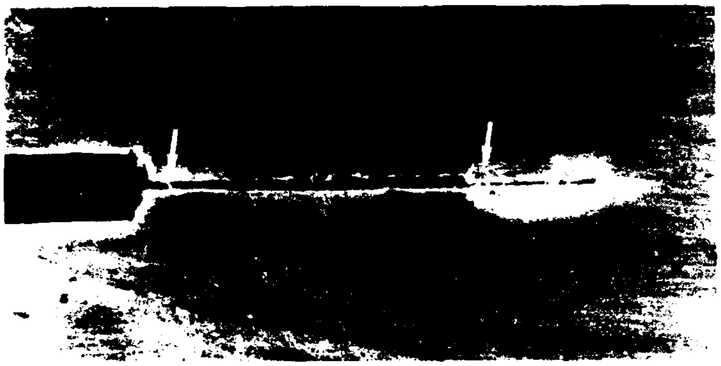

Fig. 5 Demonstration of the possibility of closure well behind the crack tip, in a simulated load shedding testing scheme involving a sequence of sawcuts from a notch in a sheet of polycarbonate [21]. The residual stresses in previous plastic zones reduce the width of the cut, as indicated by the arrows. Both cuts were made by the same saw.

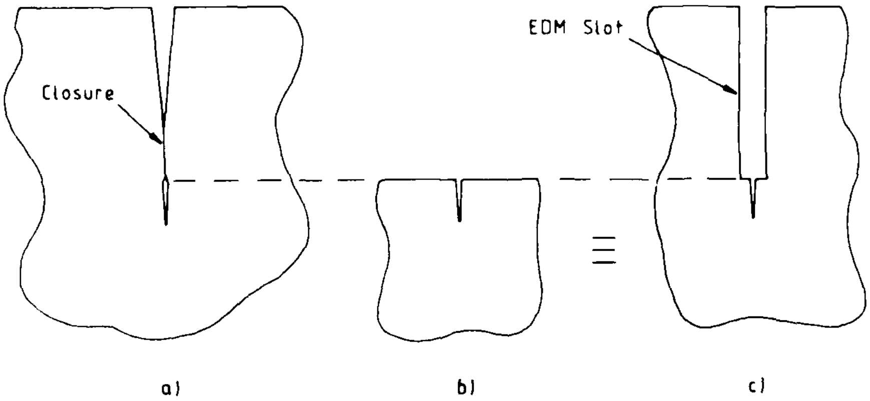

Fig. 6 Preparation of short through-thickness cracks.

a) the initial long through-crack, generated under a load shedding or constant ΔK scheme, will experience closure well behind the crack tip.

b) removal of the majority of the crack wake, to produce a short through-crack, decreases the crack tip opening load and thus reduces the influence of closure in subsequent fatigue cycling.

c) the equivalent situation can be obtained by removal of the majority of the wake of a long crack by, say, electrodischarge machining (EDM).

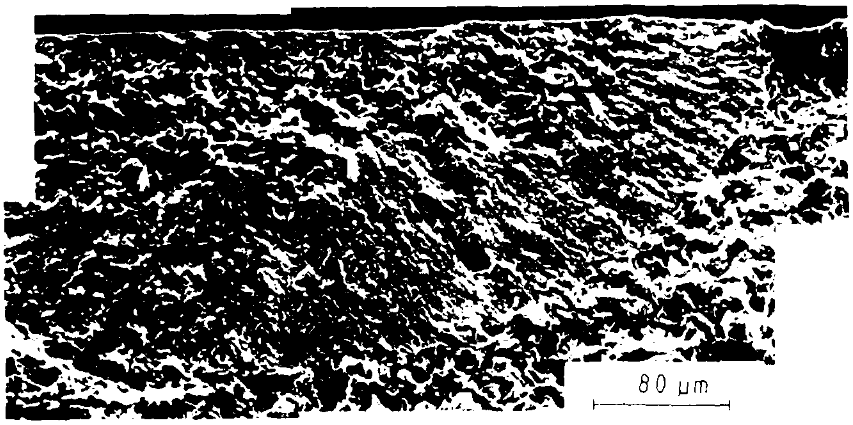

Fig. [illegible] Typical example of a surface crack initiated by hydrogen charging at low stresses, and its subsequent shape after threshold testing. The initial hydrogen-induced crack is indicated by the arrows, and has a depth of about 140 μm and an aspect ratio (2c/a) of about 4.

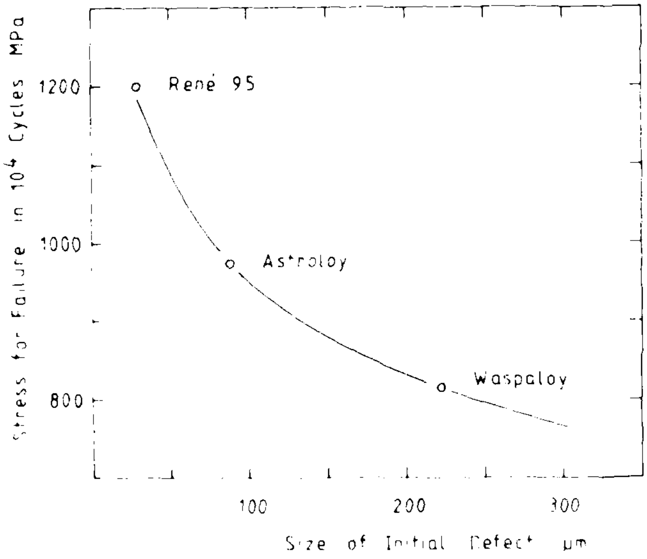

[illegible] permissible defect [illegible] in 10^4 flight cycles [illegible] turbine disc materials. [illegible] After [illegible]

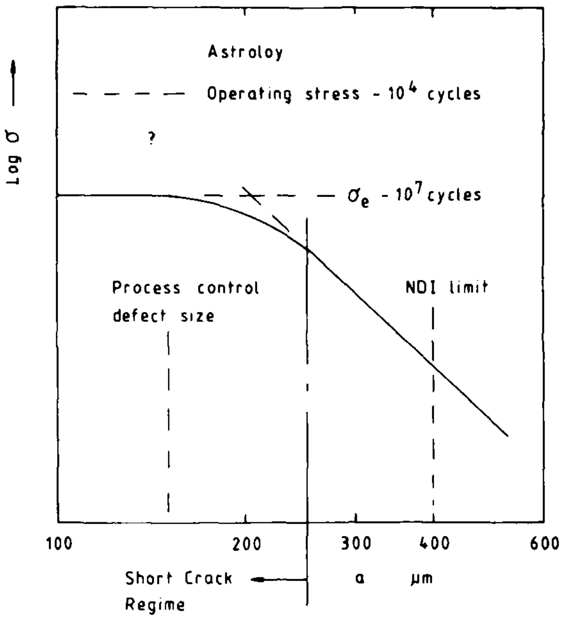

Fig. 9 Depiction of the relative positions of the short crack regime and NDI detection limit for Astroloy. The process control defect size is also shown, and the plot relates to threshold and endurance limit data. The data indicate that short crack effects should be of importance to crack growth in turbine discs, and that the situation is likely to be worsened by the high operating stresses experienced in service.

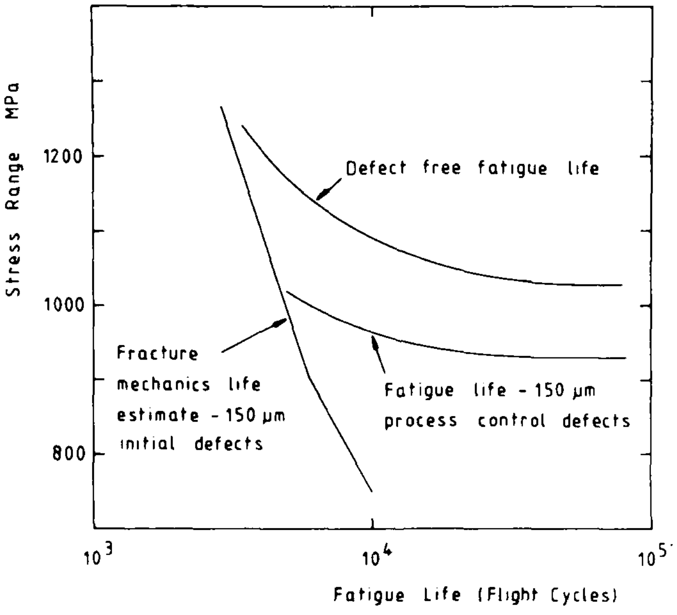

Fig. 10 Powder metallurgy Astroloy with 150μm defects: a comparison of the fracture mechanics life estimate (growth rate data from laboratory specimens) and the fatigue life observed from spin-rig tests. After Wildgoose et al [4]. A possible explanation for this observed difference could be that local residual ("tessellated") stresses around refractory inclusions, in the spin-rig discs, exert a clamping force on the fatigue crack.

CRACK GROWTH IN NEAR-ALPHA TITANIUM ALLOYS

C R Gostelow
Propulsion Dept, RAE Pyestock
Farnborough, Hants, UK.

1.0 INTRODUCTION

Ever since the first gas turbine aero engine entered into service there has been pressure to develop more powerful yet more efficient and lightweight units. To this end manufacturers have endeavoured to increase overall pressure ratios and maximum cycle temperatures whilst trying to limit engine size by using materials having higher strength-to-weight ratios and higher temperature capability.

Two main material approaches have been followed in order to help meet these requirements. These are the development of high-strength, high-temperature capability nickel base superalloys for extensive use in the turbine and the replacement of heavy steels and nickel alloys in the compressor by advanced lightweight titanium alloys. The latter approach was the driving force behind the development in the UK of a unique range of creep-resistant near-alpha titanium alloys suitable for use up to 600°C.

The objectives of this paper are:

1. to describe how a variety of parameters can influence the crack growth characteristics of near-alpha titanium alloys, with particular reference to the UK alloy IMI685;
2. to assess the relevance of these laboratory data to actual engine operation.

1.1 THE DEVELOPMENT OF CREEP RESISTANT TITANIUM ALLOYS

The UK philosophy has been to utilise as much titanium as possible for rotating components, and this has necessitated the continued development of a series of high temperature creep-resistant alloys. FIGURE 1.

In the mid 1950's the beneficial effects of small silicon additions on creep behaviour were patented and exploited in the alpha+beta alloy IMI 550.

By 1960 the enhanced performance of materials quenched rapidly from high in the alpha-beta phase field had been recognised. The best example of an alloy of this type is IMI 679. Here the amount of beta stabilisation has been reduced as too large an amount of the ductile retained beta phase was found to reduce creep strength.

The final development was the range of IMI alloys designed to be quenched from above the beta transus with a 100% transformed beta microstructure. These rely on the complexity of the transformed alpha phase to impart high temperature strength and have only small amounts of retained beta present, smeared out between the fine sub-grain structure. The role of silicon in these alloys is crucial, yet still not properly understood.

The first alloy in the series, IMI 684, was introduced at the beginning of the 1960's. This rapidly gave way to IMI685, a material that has proved itself in RB211, RB199 and Adour engines as a trouble-free compressor disc alloy.

With the proven success of IMI685 the 1970's saw research under way towards an alloy capable of usage at 600°C (1110 F). Based essentially on IMI685 this new alloy, Ti 5331S (IMI829), has met its temperature target and is now an important part of the Rolls-Royce strategy for the later RB211 developments.

The use of uncoated titanium alloys seems possible up to about [illegible] and this is seen as the highest temperature at which "conventional" alloys will see operation. A new alloy, IMI834, has now been developed by IMI Titanium and the Royal Aircraft Establishment at Pyestock to meet this target. It is currently the subject of large scale evaluation.

Unless otherwise stated, all results and discussion in this paper refer to the alloy IMI685. Alloy compositions are listed in Table 1.

1.2 METALLOGRAPHY OF TITANIUM ALLOYS

The creep resistant near-alpha alloys derive their good mechanical properties from the detail of the quenched-in microstructure. As might be anticipated microstructures are very sensitive to forging practice and heat treatment conditions. Two separate variables are significant; the prior beta grain size before quenching and the quenching rate itself.

To achieve their optimum properties near-alpha alloys depend on fast quench rates and a fine transformation product. In practice very fast rates cannot be achieved through thicker sections, and what is called "basketweave" microstructures normally result (FIGURE 2a). In very thick sections, or if the quench rate is too low, a more aligned structure can occur. In this non-preferred "aligned" microstructure the transformation product is a set of plates with crystallographic symmetry between adjoining plates. A prior beta grain can then act as a single crystal of hcp microstructure (FIGURE 2b).

The relatively large grain sizes associated with beta heat treated near-alpha alloys are compared to other alpha+beta alloys in FIGURE 2(c).

Much of the recent development work on near-alpha alloys has been aimed at controlling the prior beta grain size which, for thick section IMI865, can be up to 2mm. In the case of IMI829 grain sizes of 0.5mm are typical of the maximum found in components. The more complex alloys now available, such as IMI834, reduce this still further to levels more typical of the alpha+beta alloys.

2.0 CRACK GROWTH BEHAVIOUR OF IMI685

Much early work on fatigue crack growth concentrated on long cracks, it being assumed that the growth laws obeyed continuum mechanics such that long crack data could be extrapolated to short cracks.

Such an approach breaks down when the crack spans only a few grains, but for most non-aerospace materials this is of only academic importance.

For beta processed titanium alloys, on the other hand, a few grains could contain a crack 10 to 15mm long. Crack growth from an initiation site to this length might well form a significant part of the calculated fracture mechanics life. This has led to an increased interest in the behaviour of short cracks.

2.1 THE GROWTH OF LONG CRACKS

2.1.1 The effect of microstructure.

It has been shown that quenching at different rates gives rise to different microstructures in the material. The effect of microstructure on room temperature crack propagation at a frequency of 1Hz is illustrated in FIGURE 3. Although the actual differences seen between the basketweave and aligned microstructures are not large, they serve to illustrate the fact that microstructure is a relevant variable which cannot be ignored.

It should also be noted that, as the cooling rate through a thick section can vary, so can the crack growth rate.

For completeness a line for the alpha-beta heat-treated alloy Ti-6Al-4V is included on the Figure. This shows the significant improvement that can be obtained by beta heat treatment.

2.1.2. The influence of frequency and dwell on load.

When IMI685 is slow cooled to give an aligned microstructure, little difference is seen in the crack propagation rate at 1Hz and 10Hz. A similar result is obtained with an air cooled, basketweave, microstructure.

When dwell on load is applied there is a significant and detrimental effect on the crack propagation resistance of the slow cooled material. This is illustrated in FIGURE 4, where the effect of a 5-minute hold on load can, under some circumstances, lead to an order of magnitude increase in the measured crack growth rate.

Similar effects on this scale are not seen in other, preferred, microstructures.

Even in the slow-cooled aligned microstructure, dwell effects disappear at temperatures above about 120°C (260°F), well below the normal operating temperature of creep resistant titanium alloys.

The effect of dwell on load appears to be more noticeable at the higher stress intensity levels, the 1Hz and dwell data coming together at a stress intensity of about 20 $MN.m^{-3/2}$. For most situations crack growth at stress intensity levels above about 20 accounts for little of the expected life, and thus dwell on load may be of little practical relevance. It is, however, another reminder to ensure that the testing being conducted reproduces the failure mode seen in components.

2.1.3 The effect of R ratio

Most crack propagation tests, and the majority of components, are cycled at R ratios (minimum stress/maximum stress) at or just above zero. If the mean load is raised whilst maintaining the range constant, such that the R ratio increases to 0.5, an order of magnitude increase in crack propagation rate is observed in aligned IMI685 (FIGURE 5). Similar effects are also seen in basketweave microstructures.

The significance of these results is that they can be rationalised by invoking the concept of crack closure. Plastic deformation associated with crack advance can induce closure loads that hold the crack faces together. At high R ratios the minimum stress is such that the crack is open for the whole cycle. At low R ratios the crack remains closed for part of the cycle, thus reducing the effective cyclic stress range. The low R ratio results are thus an underestimate of the growth rate for a given effective stress.

In a component notch plasticity and other geometric effects can also affect the closure load, making the prediction of crack growth rate, and thus life, difficult.

2.1.4 Effect of environment (Aqueous Salt)

Titanium is known for its good corrosion resistance, and is widely used in both chemical and desalinisation plants. That its crack growth behaviour is significantly affected by aqueous salt may thus come as a surprise. In practice the effect of aqueous salt on all but a few titanium alloys is to cause enhanced crack growth above a certain threshold cyclic stress intensity level. This is illustrated in FIGURE 6 for aligned IMI685.

In no titanium alloy investigated has Kic been influenced by environment, but the onset of sustained load cracking, Kiscc, is. Additionally it is observed that enhanced cyclic crack growth occurs at lower stress intensities than predicted by Kiscc, a figure of 2/3 Kiscc being appropriate for most alloys.

Stress corrosion cracking is associated with static failure modes and as such is a function of the maximum stress intensity in the cycle, rather than the stress intensity range.

It is, however, useful to remember that environment rarely affects crack growth behaviour at lower stress intensities. As such the effect on overall crack propagation life of a component will normally be small.

2.1.5 Fatigue thresholds

When calculating the crack propagation life from a flaw or small crack the majority of that life is taken up by the crack growing at very low stress intensity levels. Extrapolating long crack data obtained at quite high crack growth rates down to these levels will predict a finite crack growth rate at all levels of cyclic stress intensity. In practice there is a lower level of cyclic stress intensity, the fatigue threshold, below which crack propagation does not appear to occur. This is analogous to the fatigue limit in a normal fatigue test.

Crack propagation curves at or near the fatigue threshold have been obtained by Hicks, Neal and Beevers for both basketweave and aligned structures in IMI685 (FIGURE 7). These curves indicate that, at a stress intensity range below about 5MN.m-3/2, no crack growth will be expected to occur. If these data on long cracks could be carried through to short cracks, then small defects in quite lowly stressed titanium alloys should not be a problem.

In practice it has been demonstrated that crack initiation and short crack growth, within the first few grains, cannot be predicted from long crack data.

[illegible] THE GROWTH OF SHORT CRACKS

Using again the non-preferred aligned microstructure and a deliberately increased grain size, Hicks and Brown have investigated the growth of cracks of the order of the grain size in IMI685. In a material with a conventional fatigue threshold of approx [illegible]MN.m-3/2, they have shown (FIGURE 8) that crack growth rates are between one and two orders of magnitude higher than predicted by long crack data. Additionally they have demonstrated that dwell in load is not significant for short cracks with stress intensities of less than approx [illegible] MN.m-3/2, a similar result to that observed with long cracks.

An important characteristic of the short crack data obtained is that it shows no tendency to [illegible] to a threshold value for crack growth. Perhaps if the cyclic stress levels were reduced to produce crack growth rates of 1E-8 or 1E-9 m/cycle thresholds would be found, but the practical significance of a threshold of about 1MN.m-3/2 is doubtful in terms of component life.

The data obtained on short crack growth of beta processed titanium alloys is consistent with that observed by [illegible] in the finer grain powder nickel alloys.

The understanding now available on the role and nature of short crack growth demonstrates the problems that can arise when crack propagation data are extrapolated beyond the limits of experimental variables; something that could preclude the derivation of a "universal" approach to damage tolerant design.

3.0 CONCLUSIONS

Many of the crack propagation features that were believed to be problems in near-alpha, beta heat-treated titanium alloys can be shown to be of little significance for component lifing. In particular the effect of dwell on load is only of importance in non-preferred microstructures and at cyclic stress intensities greater than around 20 MN.m-3/2, that is at stress intensity levels above which any reasonable lifing scheme would have rejected the component.

Environmental effects are also only of significance at faster crack growth rates, where little residual life is left in a component.

Operational experience has demonstrated that beta processed alloys can be used with confidence as disc materials, and has led to the development of the higher temperature alloy IMI829 (Ti-5331S) and to the latest in the line, IMI834. In both these alloys the material development process has had a two-fold objective; to achieve enhanced temperature capability and to restrict grain growth during thermo-mechanical processing.

Finally, the creep resistant titanium alloy story is one that has many implications for damage tolerant design. In particular it illustrates that when any major advances are made in a material's strength or temperature capability, by microstructural, compositional or processing route, it is dangerous to assume that design rules, data extrapolation techniques and predictive methods found viable for preceding materials will necessarily apply to the new development.

4.0 REFERENCES

Brown and Hicks, A Study of Short Fatigue Crack Growth Behaviour in Titanium Alloy IMI685.
Fatigue Eng Mat & Struc 6, 1983, 67-76.

Evans and Beale, Fatigue Crack Propagation in Wrought Titanium Alloys.
Proc Conf Forging and Properties of Aerospace Materials, The Metals Society, Leeds, Uk, Jan 1977.

Evans and Gostelow, The Effect of Hold Time on the Fatigue Properties of a Beta Processed Titanium Alloy.
Met Trans 10A, Dec 1979, 1837-1846.

Gostelow and Watt, Unpublished work at RAE, Pyestock.

Gostelow and Weaver, The Effects of Aqueous and Hot Salt Environments on the Fatigue and Crack Propagation Behaviour of Titanium Alloys.
Proc 4th US/UK NAVSEC Conf. Annapolis, 1979.

Hicks, Jeal and Beevers, Slow Fatigue Crack Growth and Threshold Behaviour in IMI685.
Fat Eng Mat Struc 6, 1983, 51-65.

Newman, PhD Thesis, University of Birmingham, 1984.

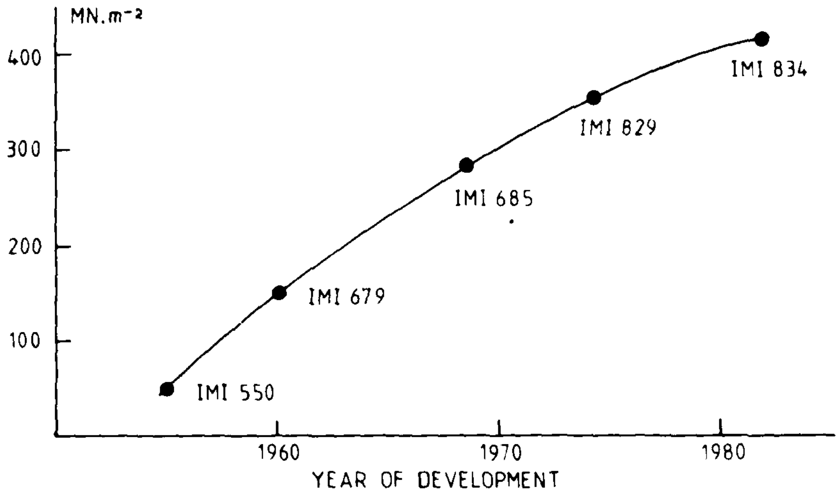

FIGURE 1.

Creep strengths of UK high temperature titanium alloys.

Alloy	Composition Wt-%							
	Ti	Al	V	Zr	Sn	Mo	Si	Nb
IMI 318	Bal	6	4	-	-	-	-	-
IMI 679	Bal	2.25	-	-	11	1	0.2	-
IMI 550	Bal	4	-	-	2	4	0.5	-
IMI 685	Bal	6	-	5	-	0.5	0.25	-
IMI 829	Bal	5.5	-	3	3.5	0.25	0.35	1

TABLE 1: Composition of UK Creep Resistant Titanium Alloys

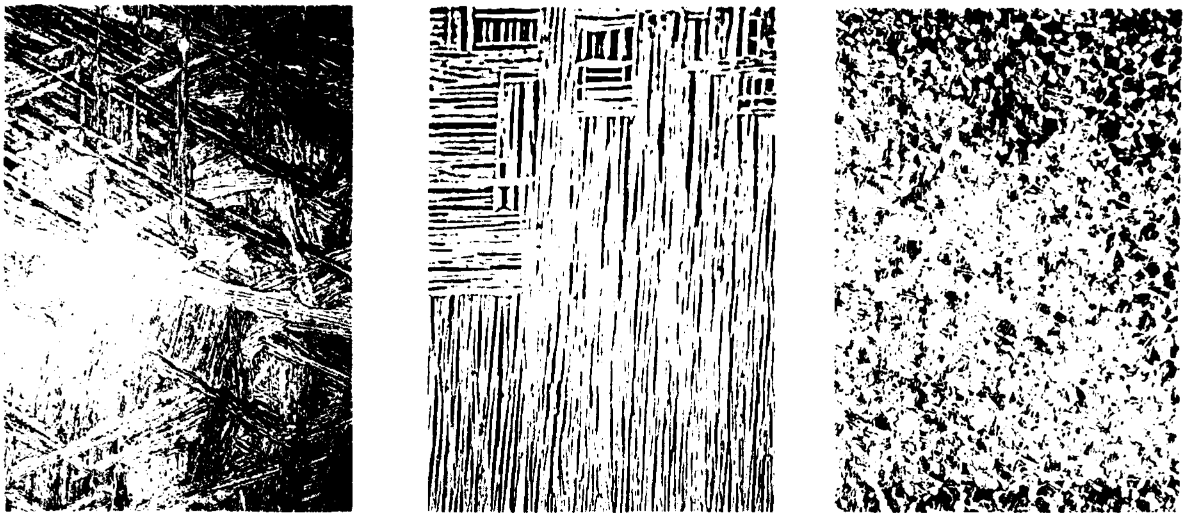

FIGURE 2.

Typical titanium alloy microstructure

(a) Fast-cooled "basketweave" IMI685.

(b) Slow-cooled "aligned" IMI685.

(c) Alpha+Beta Ti-6Al-4V showing finer grain size.

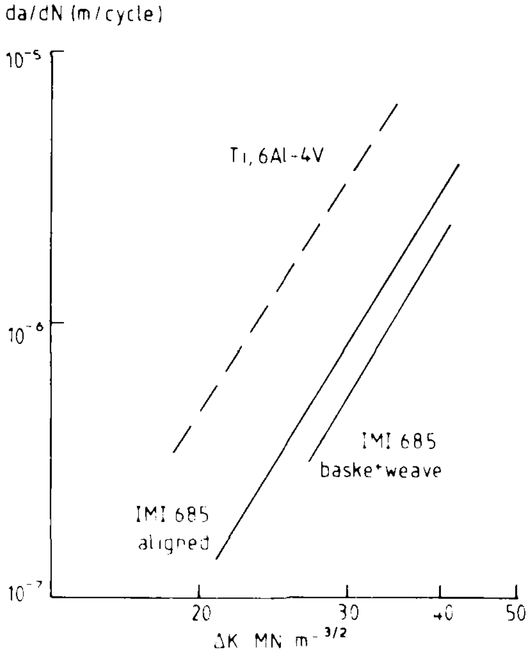

FIGURE 3.

Effect of microstructure on propagation rates in IMI685. (from Evans & Beale)

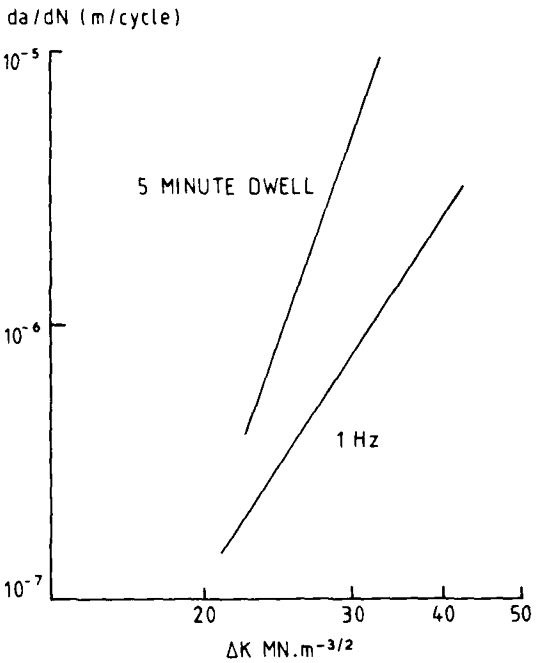

FIGURE 4.

Effect of dwell on load on crack growth of aligned IMI685.(from Evans & Gostelow)

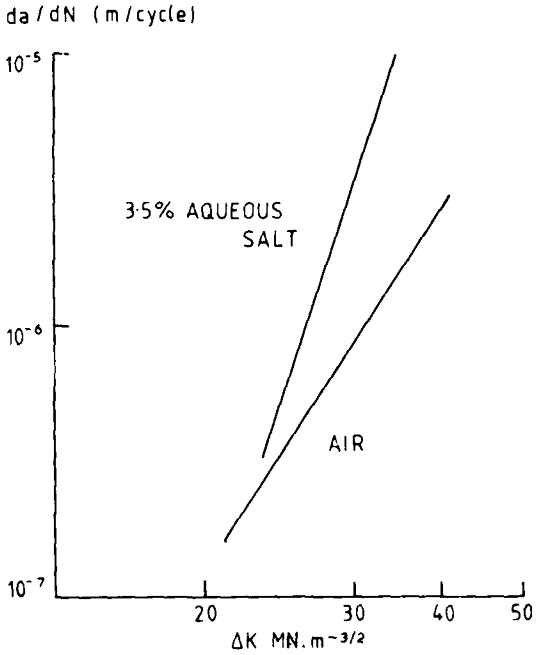

FIGURE 5.

Effect of aqueous salt on crack growth of aligned IMI685.(from Gostelow & Weaver)

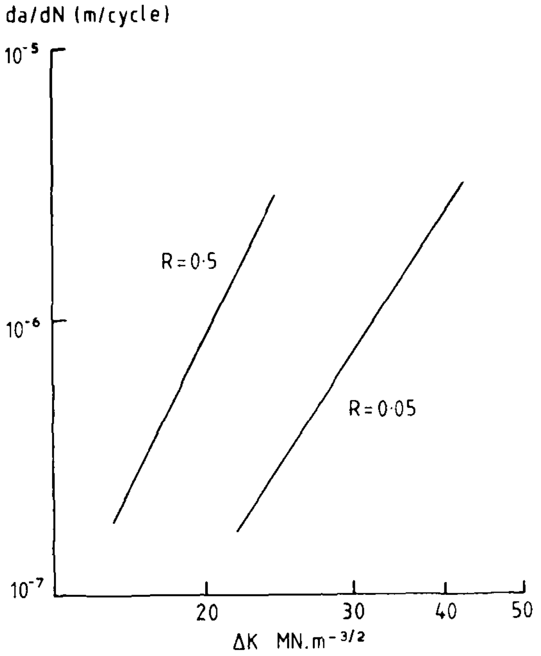

FIGURE 6.

Effect of mean stress on crack growth of aligned *IMI685*.(from Gostelow & Watt)

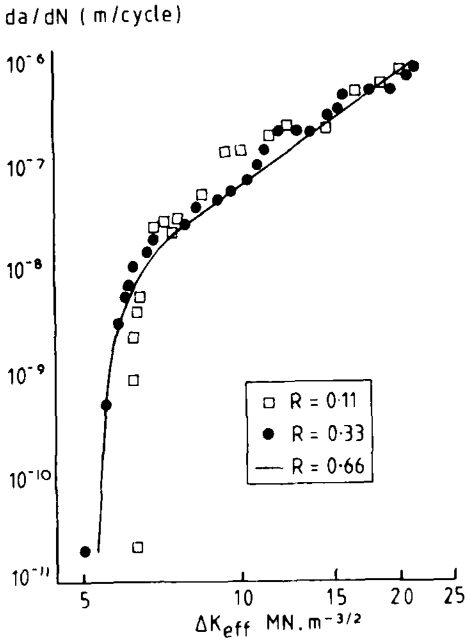

FIGURE 7.

Crack growth threshold behaviour in aligned and basketweave microstructures in IMI685.(from Hicks, Jeal & Beevers)

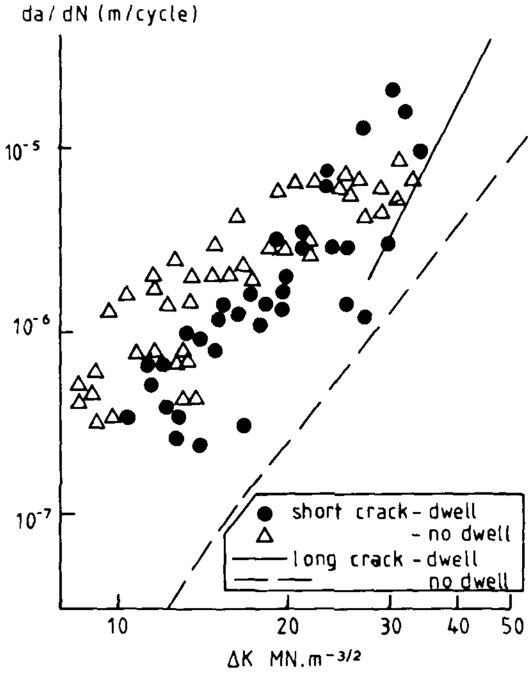

FIGURE 8.

Short crack growth behaviour in aligned IMI685. (from Brown & Hicks)

MESURE DE LONGUEUR DE FISSURE, DEFORMATION ET ENDOMMAGEMENT PAR UNE TECHNIQUE DE POTENTIEL ELECTRIQUE

par Humbert Policella, Georges Baudin et Georges Cailletaud

Office National d'Etudes et de Recherches Aérospatiales (ONERA)
92322 Châtillon Cedex (France)

RESUME

Cet article fait le point sur une nouvelle utilisation de la mesure du potentiel électrique et ses applications aux mesures de longueur de fissure, déformation et dommage. En premier lieu, nous présentons l'appareillage électronique développé à l'ONERA dont la caractéristique principale réside dans l'alimentation de l'éprouvette en courant pulsé. Deux types d'application sont ensuite présentés. Le premier type d'application a été effectué en fissuration sur de nombreux essais bidimensionnels pour des matériaux et températures différentes. Une extension de la méthode a également été appliquée à des fronts de fissures tridimensionnelles. Dans une seconde phase, nous avons supposé que la valeur du potentiel électrique sur un solide soumis à une sollicitation, était la somme de trois termes, respectivement dus à la déformation élastique, plastique et au dommage. Des applications ont été effectuées sur un acier AISI 316 à température ambiante, un INCO 718 à 650°C et un IN 100 à 900°C et 1000°C. Nous avons déterminé des valeurs de déformations plastiques et de dommage, comparées ensuite à d'autres types de mesure.

CRACK GROWTH, STRAIN AND DAMAGE MEASUREMENTS USING AN IMPROVED POTENTIAL DROP TECHNIQUE

SUMMARY

The paper deals with an improved version of the potential drop technique and its applications to crack length, strain and damage measurements. We present first the electronic device, developped at ONERA which supplies the specimen with a pulsed current. Two types of applications are then presented. In the first type several tests have been conducted on two-dimensionnal cracked specimens, made of different materials at different temperatures. An extension of the method has also been made to three dimensional crack fronts. In the second type we have supposed that the potential drop in an uncracked strained solid was the sum of three terms, respectively due, to elastic strain, plastic strain and damage. Applications have been performed on AISI 316 steel at room temperature, INCO 718 at 650°C and IN 100 at 900° and 1000°C. The plastic strain and damage determined with the P.D. technique are then compared with the ones measured using others methods.

I - INTRODUCTION

Dans la plupart des structures utilisées sous sollicitations mécaniques (cycliques ou non), il peut se produire au cours du temps une détérioration lente de certaines parties de celle-ci. Cette détérioration se manifeste le plus souvent par une apparition irréversible de défauts (microvides , microfissures) dont la croissance à terme entraîne une diminution de la résistance mécanique. Ce processus que l'on définit sous le terme de dommage est difficile à quantifier aussi bien du point de vue calcul que du point de vue expérimental [1], [2]. Le problème se pose ensuite de définir la dimension du défaut, de manière à connaître son évolution et permettre une utilisation de la structure dans les mêmes conditions de sécurité. De plus, la connaissance de la dimension du défaut peut être une donnée pour un calcul de prévision sur la durée de vie restante de la structure [3], [4]. On peut classiquement séparer le processus en deux phases distinctes. La première phase, liée à la mécanique de l'endommagement concerne les micro-défauts consécutifs à l'apparition de microvides de l'ordre de quelques microns, situés aux joints de grains et répartis d'une façon homogène dans le matériau.

La seconde phase se rapporte plus généralement à la mécanique de la rupture pour l'étude de fissures supérieures à 1 mm, avec un domaine de transition, celui des fissures dites "courtes" (0,1 à 1 mm) où la mécanique de la rupture s'applique mal.

Nous nous proposons d'étudier les deux aspects sous un angle expérimental, en définissant une manière de séparer les problèmes. Plusieurs méthodes peuvent être utilisées [5] pour la détection de défauts et leur progression, les plus employées actuellement sont :

- les ultra-sons
- les courants de Foucault
- la méthode électrique (Potential Drop Technique PDT)
- les rayons X
- la photographie Infrarouge.

Toutes ces méthodes présentent des avantages et des inconvénients selon les cas d'utilisation. Nous avons choisi d'utiliser et de perfectionner la méthode électrique [6], [7], parce que cette méthode, de mise en oeuvre aisée, est largement utilisée dans la plupart des laboratoires d'essais. En conséquence, nous présentons successivements les perfectionnements que nous avons apportés à la méthode électrique et l'appareillage qui en est résulté, l'application à la mesure des fissures [8] et, enfin, quelques extensions de la méthode, en particulier pour la mesure de l'endommagement.

II - DESCRIPTION DE L'APPAREIL

II.1 - Rappels sur la méthode électrique classique

Par principe, la méthode de mesure ne s'applique que sur des matériaux conducteurs électriques. Le principe de base bien connu, consiste à faire circuler un courant électrique d'amplitude constante dans une éprouvette isolée électriquement et à mesurer la tension qui en résulte entre deux points où l'on désire observer le phénomène [9] fig. 1a. L'apparition d'une fissure et sa progression entraînent une évolution de la tension mesurée et un étalonnage préalable permet dans le plupart des cas, de connaître la longueur et suivre de façon continue la progression de la fissure.

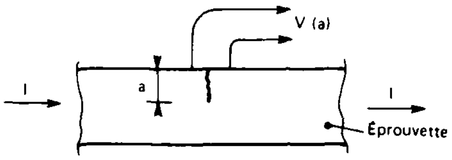

Fig. 1a) Principe de la méthode électrique.

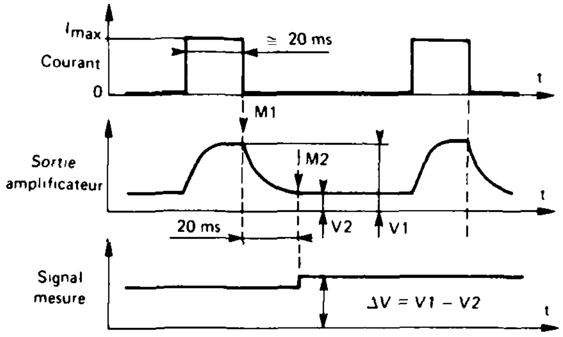

Fig. 1b) Principe de la mesure.

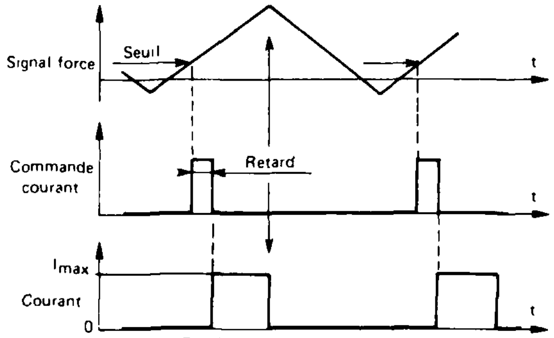

Fig. 1c) Synchronisation de la mesure.

Fig. 1 – Principe de mesure du système utilisé.

Cette méthode comporte toutefois quelques inconvenients lors de son utilisation. En effet, l'application d'un courant continu important peut dans certaines conditions provoquer des phénomènes électro-chimiques, ce qui peut en interdire son utilisation dans les études de fissuration sous corrosion. De plus, des précautions sont à prendre pour atténuer au maximum les effets de thermocouple. Enfin, le signal de mesure ayant une très faible valeur doit être amplifié, et cela pose alors le problème du bruit et de la stabilité de l'amplificateur.

II.2 - Perfectionnements apportés

Le principe de fonctionnement de l'appareil décrit sur la figure 1.b est le suivant :

- Le courant est injecté dans l'éprouvette sous forme d'une impulsion d'amplitude constante I_{max} et d'une durée d'environ 20 ms, temps au bout duquel le potentiel électrique est considéré comme établi. La tension de sortie V_1 de l'amplificateur est alors mémorisée analogiquement puis le courant s'annule.

- Exactement 20 ms plus tard, une deuxième mémorisation V_2 intervient. On dispose alors de la tension $\Delta V = V_1 - V_2$ exempte de tout parasite quasi-statique, qui est la valeur cherchée. Ces opérations se répètent ensuite à chaque impulsions de façon continue. Le niveau des bruits de fond parasite est atténué, d'abord en limitant la bande passante de l'amplificateur à 100 Hz, puis par les deux mémorisations décalées de 20 ms qui éliminent pratiquement les parasites dus au secteur (de période 20 ms). Enfin, un dernier filtrage de la tension de sortie ΔV permet d'obtenir une sensibilité de 0,1 μV pour un temps de réponse de 1 s. Une autre caractéristique importante de cet appareillage est de pouvoir synchroniser les impulsions, donc la mesure, avec le cycle de chargement en cours d'essai. La synchronisation s'effectue à l'aide d'un seuil, déclenché par le signal force de la machine d'essai, et d'un retard réglable fig. 1.c. La mesure du potentiel peut ainsi intervenir à force constante ou à force maximale, dans le cas de fissures très ouvertes.

III - APPLICATION A LA MESURE DE LONGUEUR DE FISSURE

III.1 - Etalonnage obtenu par une expression analytique. Cas bidimensionnel.

Un des exemples d'application les plus courants est celui où l'éprouvette prend l'une des formes simples indiquées sur la figure 2 et où les conditions d'alimentation assurent une densité de courant constante dans les sections "éloignées" de la fissure. Dans ce ces, l'étalonnage est donné par une expression analytique [6] :

(1) $$V(a,d) = \alpha U$$

avec

(2) $$U = \frac{2}{\pi} ch^{-1} . \frac{ch\,(\pi d/2W)}{Cos\,(\pi a/2W)}$$

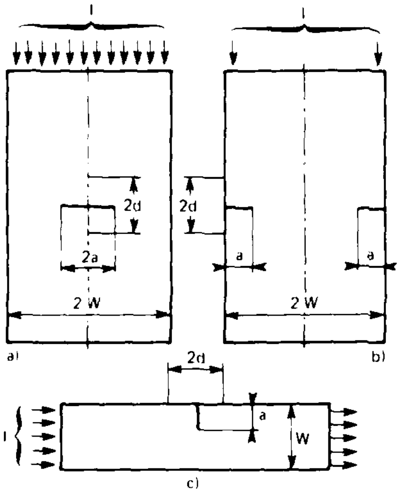

Fig. 2 – Méthode électrique : cas de calcul possible. Formes d'éprouvettes. a) Panneau en traction. b) Panneau en traction. c) Éprouvette flexion.

$V(a,d)$: tension mesurée

a : longueur ou demi-longueur de fissure

d : demi-distance des prises de potentiel

W : largeur ou demi-largeur de l'éprouvette

α : facteur de proportionnalité homogène à une tension et tenant compte de la densité de courant, de la résistivité et de l'amplification.

La fonction U paramétrée en d/W est représentée sur la figure 3 où l'on voit que la sensibilité est d'autant meilleure pour les fissures courtes que la distance d est petite.

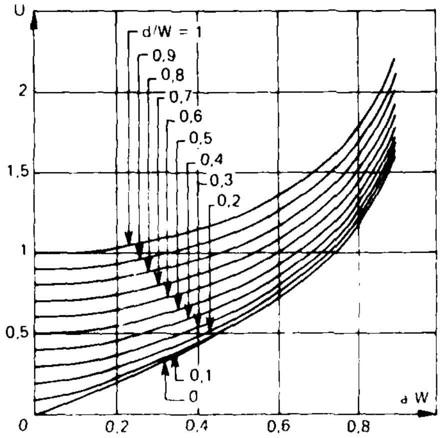

Fig. 3 – Représentation de la fonction U.

La procédure habituelle pour éliminer α est de tirer la valeur a de l'expression :

(3) $$\frac{V(a,d)}{V(a_0,d)} = \frac{U(a,d)}{U(a_0,d)}$$

a_0 étant la longueur initiale de la fissure au début de l'essai. Or, la précision sur d peut poser un problème surtout lors d'essais répétitifs. Pour éliminer cette incertitude éventuelle, nous proposons la procédure suivante, en remarquant que $\mathcal{U}(0, W) = 1$.

- Avant le départ de l'essai, une mesure préliminaire est exécutée avec des prises de potentiels distantes d'une valeur $2\,d^* = 2\,W$, à l'aide d'un calibre par exemple figure 4. Nous rappelons cette mesure V_{REF} (référence) qui est en fait la mesure de α :

(4)
$$V(0, W) = \alpha = V_{REF}$$

- La mesure $V(a_0, d)$, nous permet alors de déterminer indirectement d au travers de l'expression A (a_0 étant supposé connu d'une manière précise comme le résultat d'un usinage) :

(5)
$$A = \mathrm{ch}\left(\frac{\pi d}{2W}\right) = \cos\left(\frac{\pi a_0}{2W}\right) \cdot \mathrm{ch}\left[\mathcal{U}(a_0, d)\right]$$

et

(6)
$$\mathcal{U}(a_0, d) = \frac{V(a_0, d)}{V_{REF}}$$

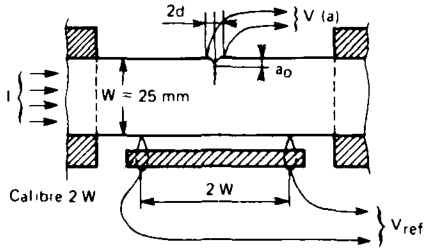

Fig. 4 – Éprouvette de flexion. Mesures initiales V_{ref} et $V(a_0)$.

Pendant l'essai, la longueur de fissure a est déterminée à partir de la mesure $V(a)$:

(7)
$$\frac{V(a)}{V_{REF}} = \frac{2}{\pi}\,\mathrm{ch}^{-1}\left[\frac{A}{\cos(\pi a/2W)}\right]$$

(8)
$$a = \frac{2W}{\pi}\cos^{-1}\left[\frac{A}{\mathrm{ch}\left(\frac{\pi}{2}\,\frac{V(a)}{V_{REF}}\right)}\right]$$

Cette procédure est couramment employée sur l'une de nos installations d'essais de fissuration et n'impose pas à l'opérateur de souder les prises de potentiel exactement à l'endroit prévu.

Pour une éprouvette en alliage léger de largeur 25 mm et d'épaisseur 2 mm la sensibilité est de $\pm\,10^{-2}$ mm et la précision supérieure à $\pm\,5\,10^{-2}$ mm avec un courant $I_{MAX} = 5$ A.

Le suivi en continu de la longueur de fissure et l'emploi d'un calculateur en temps réel offrent de grandes facilités d'automatisation. Comme exemple, la figure 5 montre la réalisation d'un essai de fissuration à vitesse constante.

Fig. 5 – Essai à vitesse de fissuration constante (éprouvette flexion).

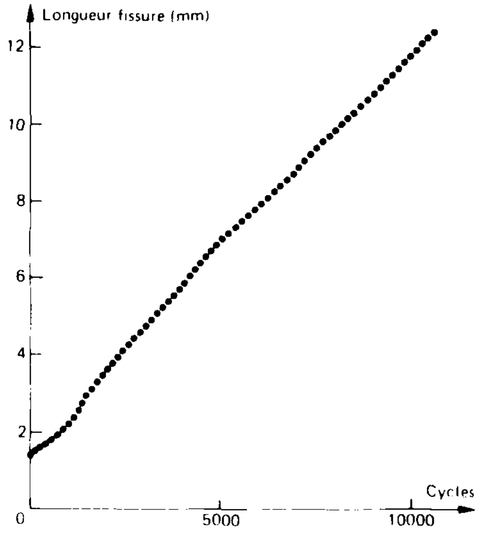

Lorsque l'essai se déroule dans des conditions isothermes, d'alimentation en courant et d'amplification de la mesure définis, il est toujours possible d'établir une courbe d'étalonnage V(a). Cette procédure s'utilise dans la majorité des cas en utilisant en parallèle une autre méthode telles que le marquage, la macrophotographie, le papier conducteur etc... Il faut toutefois prendre des précautions quand à la position des arrivées de courant et des prises de potentiel.

III.2 - Exemples d'application

III.2.1 Fissuration en flexion à haute température

L'éprouvette utilisée est en alliage réfractaire IN 100 alumisé de dimensions 170 x 25 x 9 mm, sollicitée en flexion, sur un montage représenté figure 6. L'éprouvette est isolée électriquement, les arrivées de courant sont placés aux extrémités de celle-ci et les prises de potentiels situées de part et d'autre de l'entaille initiale. La mise en température de l'éprouvette est faite au moyen d'une chauffage par induction *HF moyenne fréquence* (80 kHz) où la forme de l'inducteur permet d'obtenir une répartition uniforme de la température dans la partie utile de l'éprouvette. La courbe d'étalonnage de la valeur du potentiel en fonction de la longueur de fissure a été obtenue par comparaison avec macrophotographies infrarouge (fig. 7). Les résultats obtenus par cette méthode sont en bon accord avec la mesure électrique. Il apparaît également que pour des essais à très haute température (1000°C) cette méthode permet d'obtenir des mesures de variations de fissure de l'ordre de 0,01 mm.

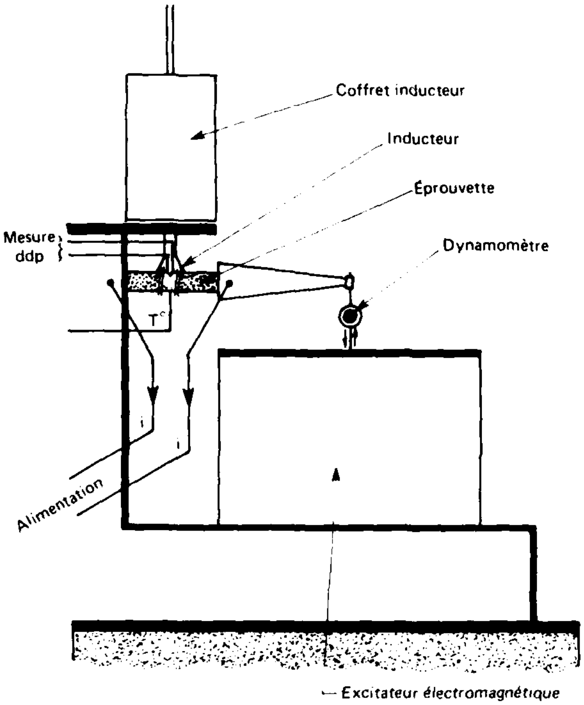

Fig. 6 – Montage pour essais de fissuration en flexion.

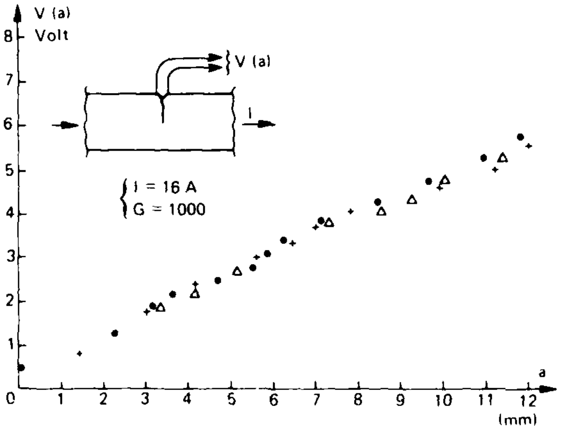

Fig. 7 – Essai en flexion. IN 100 à 1000° C. Courbe d'étalonnage.

III.2.2 Fissuration sous gradient thermique

L'éprouvette utilisée est en alliage réfractaire IN 100 aluminisé de dimensions 120 x 60 x 3 mm. Cette éprouvette est en appui sur une de ses extrémités et libre de tout mouvement. L'étude consiste à faire amorcer et croître une fissure sur un des bords libres, en créant des contraintes d'origines thermiques sur ces mêmes bords figure 8 [10]. Pour générer des gradients thermiques, nous utilisons un chauffage par induction HF dont l'inducteur a specialement été adapté pour obtenir ces gradients. Le cyclage thermique a une période de 300 s avec des temps de montée et descente de 60 s et un palier haut de 80 s. La température maximale sur les bords libres est de 1020°C et de 640°C au point bas, alors que la température au centre de l'éprouvette dans les mêmes conditions est de 610°C et 440°C et 440°C. Les arrivées de courant sont situées aux extrémités de la plaque et les prises de potentiel placées de part et d'autre des bords libres de celle-ci. L'étalonnage s'est effectué par comparaison avec des macrophotographies sur une éprouvette qui avait été préalablement équipée de repères tracés sur celle-ci. Ceci a permis au cours d'un essai de déterminer l'amorçage d'une fissure à 1 ou 2 cycles près, puis de mesurer sa progression en continu figure 9.

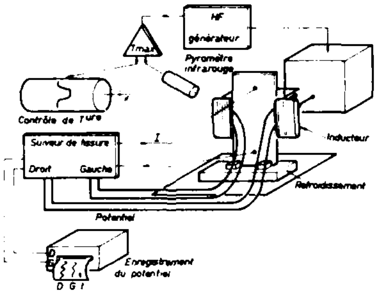

Fig. 8 – Fissuration sous gradient thermique.

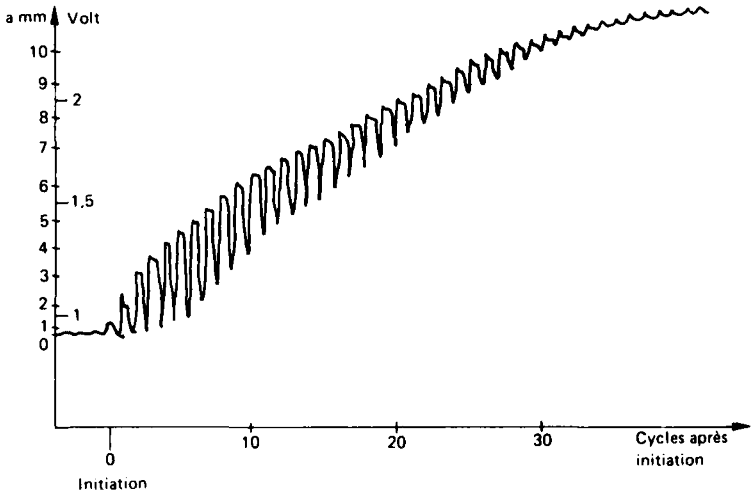

Fig. 9 – Variation du potentiel électrique lors de l'initiation de fissure.

III.2.3 Essai de bifurcation de fissure

Dans ces essais, l'éprouvette en alliage léger (2618 A) présente une partie centrale, plate, circulaire (Ø 300, ep 3) pouvant être sollicitée en traction, suivant deux axes perpendiculaires. A partir d'une fisssure artificielle inclinée d'un angle θ par rapport à un axe de traction, on provoque une fissure naturelle qui progresse dans la même direction θ sous l'effet de deux charges égales en amplitudes et synchrones.

Pour une longueur de fissure donnée, on modifie le rapport des charges, ce qui entraîne un changement de direction de la fissure après une période de réinitialisation. L'éprouvette est équipée de prises de potentiel et d'arrivées de courant de part et d'autre de la fissure artificielle (fig. 10). La grande sensibilité de la méthode a permis de mettre en évidence deux résultats importants :

Fig. 10 – Essai de bifurcation : courbe d'étalonnage de la mesure électrique. ● $\alpha = 80°$, $\theta = 64°$. + $\alpha = 50°$, $\theta = 55°$. Δ $\alpha = 0°$, $\theta = 0°$. ($I_{max} = 16$ A, $G = 25000$).

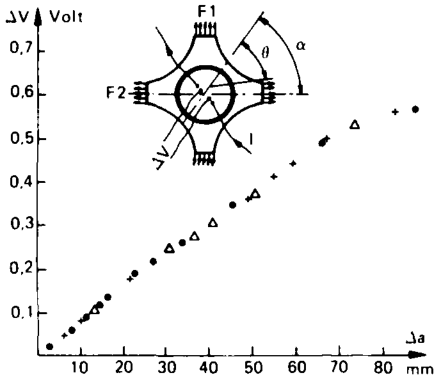

- Il est possible de définir avec précision l'instant de redémarrage de la fissure avec une sensibilité de quelques 1/10 mm.

- D'autre part, le signal de mesure est indépendant pour une large part de l'orientation du chemin de fissure et ne dépend que de sa longueur (fig. 10), avec une précision de l'ordre de 1 mm, ce qui est remarquable pour une éprouvette de cette dimension. Ce résultat résulte en partie du choix de la position des connexions d'alimentation et des prises de potentiel.

III.3 - Détermination de front de fissure dans les pièces Massives

Si pour les pièces de types bidimensionnels, la détection et la progression d'une fissure pose quelques problèmes, on peut toujours "visualiser" celle-ci par des moyens optiques. Sur les pièces massives, les moyens optiques ne peuvent visualiser que la partie externe de la fissure, la forme et la dimension du front restent alors des inconnues. Sur éprouvette, plusieurs méthodes ont été utilisées telles que le marquage ou le comptage des stries. Dans toutes ces méthodes, il faut toujours atteindre la rupture de l'éprouvette pour espérer accéder à la forme des fronts de fissure successifs.

Là encore, nous avons utilisé la méthode électrique pour déterminer les fronts de fissure sur des éprouvettes massives sous sollicitations cycliques [11]. Comme toute méthode expérimentale, elle comporte en plus de l'aspect mesure proprement dit, un aspect étalonnage qui dans ce cas s'avère délicat.

Le schéma de principe de cette mesure est représenté figure 11. Le relevé de points de mesure multiples de part et d'autre des lèvres de la fissure est réalisé par un palpeur à double contact, dont la translation peut être facilement automatisée si les formes de section d'éprouvette restent simples (rectangulaire ou circulaire par exemple). L'avantage d'un palpeur mobile est de permettre une mesure continue en fonction de son déplacement, toutefois une mesure par points à l'aide de contacts soudés et d'une commutation est également envisageable lors d'essais à haute température (jusqu'à 1000°C). Le signal issu du palpeur est ensuite amplifié et appliqué à l'appareillage électronique mentionné.

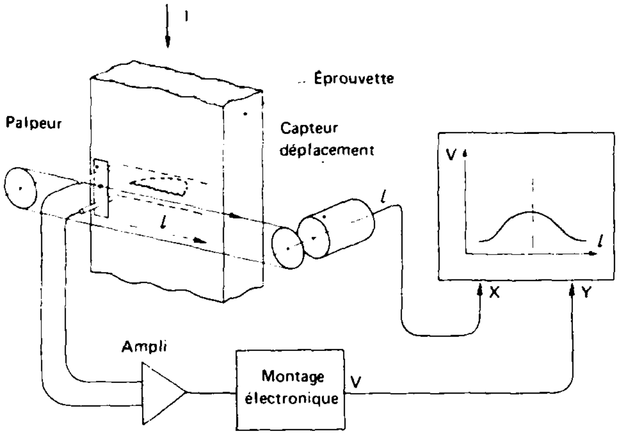

Fig. 11 – Principe de la mesure électrique sur éprouvette (3D).

Comme indiqué sur la figure 11 le signal mesuré est ensuite envoyé sur la voie Y d'un enregistreur graphique tandis que la voie X reçoit le signal proportionnel au déplacement du palpeur. Le résultat est par exemple l'une des courbes du réseau de la figure 12 réseau relevé au cours d'un premier essai de progression de fissure sur une éprouvette de section 80 x 20 mm en 2618 A sollicitée en traction, la fissure initiale étant semi-circulaire de rayon 7 mm. Ces courbes sont relatives à des fronts de fissure ayant une forme très proche d'arc de cercle comme le montre la vue figure 13 qui représente un front de fissure obtenu dans les mêmes conditions que l'essai précédent. La similitude entre courbe relevée et front de fissure est ici très nette, ce qui nous a encouragé à développer cette méthode de mesure en lui adjoignant une procédure d'étalonnage permettant de remonter au front de fissure à partir de la courbe relevée.

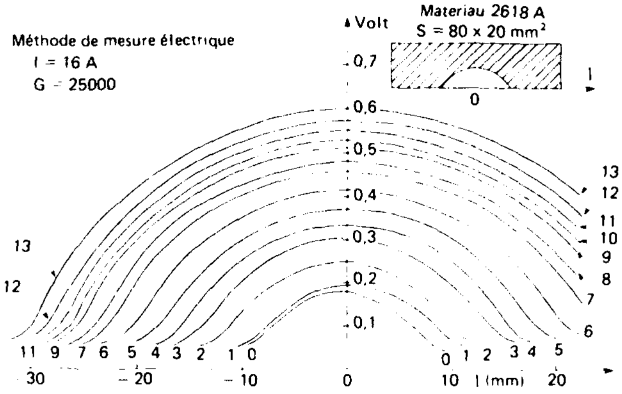

Fig. 12 – Essai de progression de fissure : relevés de tensions.

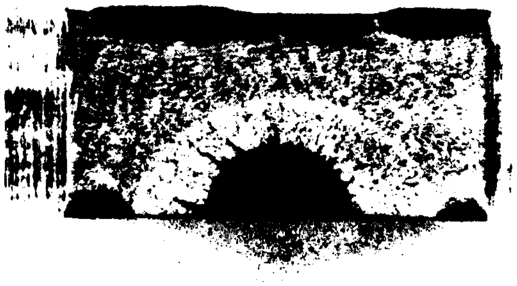

Fig. 13 – Faciès de rupture (S = 80 x 20 mm).

III.3.1 Etalonnage par moyen rhéologique

On reconstitue dans un milieu conducteur le potentiel électrique existant dans l'éprouvette ou la structure fissurée. Ce milieu conducteur est de l'eau et la cuve utilisée doit représenter la partie utile de l'éprouvette dans un rapport de similitude donné. Enfin la fissure est simulée par une plaque isolante et les prises de potentiel s'effectuent à l'aide d'un palpeur mobile d'une manière identique à celle de l'essai mécanique.

La figure 14 montre le principe de détermination du front de fissure dans une éprouvette à l'aide de cette cuve :

- on relève sur l'éprouvette la courbe $V(\ell)$ résultant de l'application de la mesure électrique (fig. 14a ;

- on cherche à reconstituer, sur la cuve rhéoélectrique, une courbe $V'(\ell')$ similaire à $V(\ell)$, par modifications successives de la plaque isolante représentant la surface fissurée (fig. 14b) ; ces approximations se réalisent par simple découpage de la plaque ;

- la concordance des courbes V et V' entraîne la conclusion que front de fissure réel et forme de fissure figurée sont dans le rapport de similitude éprouvette-cuve.

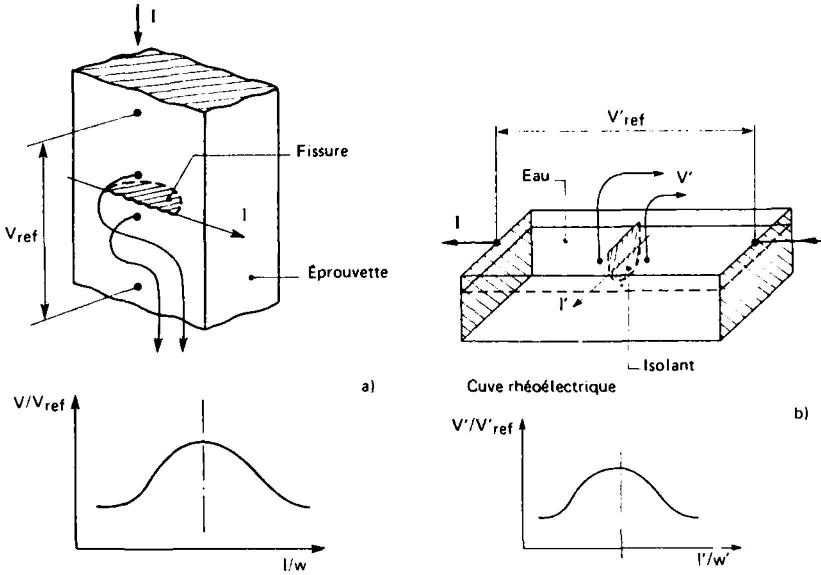

Fig. 14 – Détermination par analogie d'un front de fissure.

III.3.2 Applications

La figure 15 décrit un premier exemple sur une éprouvette en alliage léger (2618) A de section carrée, soumise à un chargement ondulé en flexion 4 points. Deux fissures de coin se propagent dans la section centrale à partir de 2 amorces de rayon 5 mm. Les conditions d'application de la méthode électrique sont indiquées sur la figure 15. Au cours de l'essai, plusieurs relevés de tension sont effectués le long des lèvres de la fissure en fonction de la progression de celle-ci. On procède également au marquage de certains fronts par injection de colorants, et aux enregistrements relatifs à ces marquages. Grâce à ces relevés, on peut avoir une bonne idée de la forme des fronts ainsi que de leur accroissement.

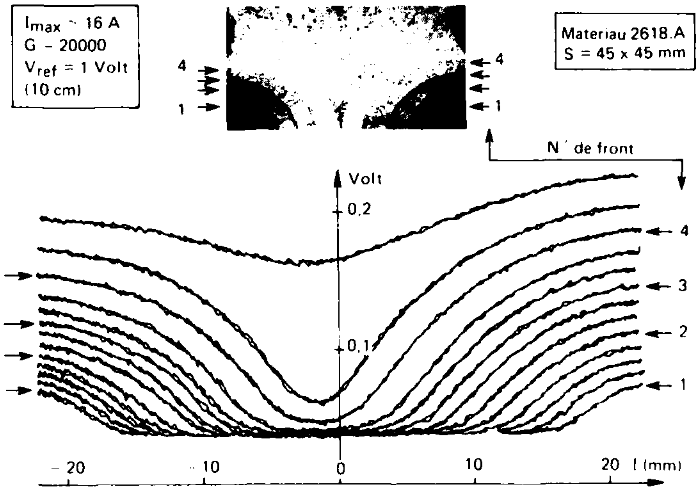

Fig. 15 – Progression de fissures dans un barreau. Mesure électrique.

On remarque en particulier que la fissure droite s'est propagée légèrement plus vite que la gauche. En supposant l'éprouvette non rompue, il faut alors établir leurs formes à partir des relevés correspondants. Nous avons alors appliqué trois méthodes, différentes dans leur principe (fig. 16). Dans le premier cas, nous avons cherché à faire correspondre en chaque point de relevé de tension, la profondeur de fissure donnée par l'étalonnage bidimensionnel de la figure 3. Cette première comparaison est évidemment très mauvaise. Dans le deuxième cas, nous utilisons un étalonnage 3D, tension maximale en fonction du rayon de fissure, pour fissure en quart de cercle qui nous donne un résultat plus réaliste. Enfin la méthode générale par approximation de la forme de la fissure artificielle donne un résultat très correct avec une incertitude inférieure à 0,2 mm sur le front réel.

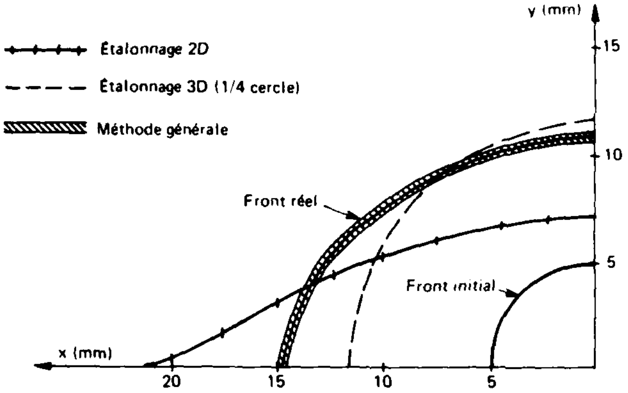

Fig. 16 – Détermination d'un front de fissure.

Un deuxième exemple concerne l'étude de l'amorçage sur une éprouvette cylindrique sollicitée en traction, de Ø 20 mm en AISI 316, comportant un coefficient de concentration de contrainte donné par une gorge de profondeur 2 mm et un rayon de fond d'entaille de 0,5 mm (fig. 17). Pour détecter l'amorçage en fonction du nombre de cycles de sollicitations, on enregistre simultanément l'évolution de la tension en trois points situés à 120° autour de la gorge. L'expérience montre que l'amorçage est quasi simultané en tout point du fond de gorge et que la fissure se propage presque à vitesse uniforme.

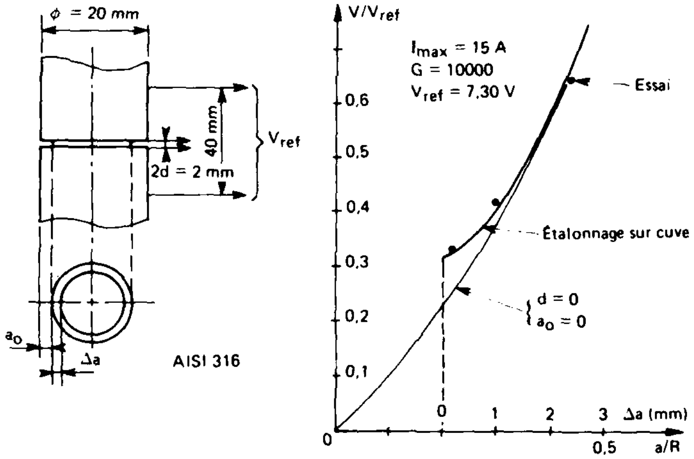

Fig. 17 – Amorçage et progression de fissure dans une éprouvette cylindrique entaillée.

On mesure donc une profondeur moyenne de fissure à partir de la moyenne des trois tensions et d'un étalonnage (figure 17). Le matériau étant très ductile, le début de l'évolution de la tension mesurée est due à la déformation plastique de l'éprouvette et non à l'amorçage. Nous avons donc enregistré également l'évolution de cette déformation et, compte tenu d'une relation linéaire entre tension et déplacement plastique explicitée plus loin [13], l'apparition d'un coude prononcé sur le graphe ΔV , ΔL_p (fig. 18) indique le début de l'amorçage. Ceci est confirmé par examen des faciès après rupture des éprouvettes et l'on peut voir sur la figure 17 que la mesure électrique donne des résultats très proches de la réalité, à environ 0,1 mm près.

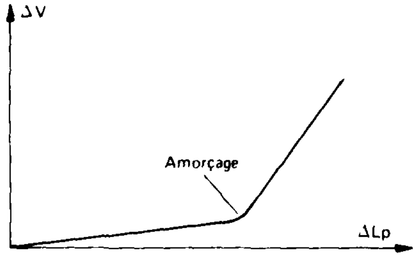

Fig. 18 – Détermination de l'amorçage.

VI - EXTENSION DES POSSIBILITES D'UTILISATION DE LA METHODE ELECTRIQUE

Ainsi que nous l'avons déjà mentionné en introduction, un élément de volume de matériau, soumis à des charges répétées dans le temps, est le siège d'un endommagement progressif, se traduisant par l'apparition de microvides ou microfissures. Mais, indépendamment de tout endommagement, ce même élément subit des déformations élastiques et, quelquefois, plastiques. Il est intéressant de noter que chacun de ces trois phénomènes : endommagement, déformation élastique, déformation plastique présente des aspects physiques spécifiques : variations de distance interatomiques pour le premier, activation de mécanismes de glissement pour le second, création de défauts microscopiques pour le troisième, qui tous doivent influencer la "fonction de transfert" électrique de l'élément ; d'où l'idée d'étendre les applications de la méthode électrique.

IV.1 - Etude électrique du problème

Considérons un élément de volume défini par un tube de courant élémentaire et deux surfaces équipotentielles voisines (fig. 19), de longueur dl et de section dS. A courant constant, et en supposant le matériau vierge de toute déformation, la différence de potentiel nous est donné par la relation classique :

(9)
$$dV = \rho \frac{dl}{dS} di$$

où ρ représente la résistivité du matériau. Si cet élément de volume élémentaire est soumis à une sollicitation de traction simple parallèle à la direction du courant, la nouvelle valeur de la ddp est alors :

(10)
$$dV' = \rho' \frac{dl'}{dS'} di$$

Les variations de ρ, dl, dS dépendent uniquement des variations de géométries dues aux déformations élastiques et plastiques. Si de plus, on suppose l'existence d'un endommagement, on peut le prendre en compte en utilisant le concept de la "contrainte effective" qui consiste à remplacer une section endommagée dS par une section équivalente dS (1-D), vis-à-vis du comportement mécanique (fig. 20), [3].

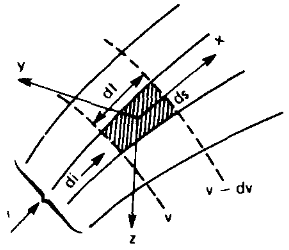

Fig. 19 – Volume élémentaire considérée.

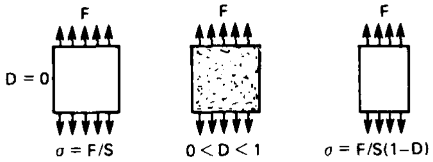

Fig. 20 – Représentation schématique du concept de la contrainte effective.

Il faut alors quantifier les valeurs de ρ, dl, dS, de manière à discerner au cours d'une variation de ddp, ce qui est réellement imputable à l'endommagement. Pour déterminer les valeurs relatives aux variations de déformation et d'endommagement nous faisons une première hypothèse, en supposant que le tenseur des déformations est constitué par la diagonale :

(11)
$$\varepsilon_e + \varepsilon_p \quad , \quad -\nu\varepsilon_e - \frac{1}{2}\varepsilon_p \quad , \quad -\nu\varepsilon_e - \frac{1}{2}\varepsilon_p$$

(ν coefficient de poisson et ε_p déformation plastique à volume constant). Ceci nous permet de définir les relations :

(12)
$$dl' = dl(1+\varepsilon_e+\varepsilon_p) \quad , \quad dS' = dS(1-\nu\varepsilon_e-\varepsilon_p)$$

La seconde hypothèse concerne la variation de résistivité due aux déformations [14]. Cet effet "piézoélectrique" étudié par Bridgman [15] traduit la variation relative de la résistivité, proportionnelle à la variation relative de volume ou aux déformations longitudinales et transversales [16], [17], à l'aide de deux coefficients C_1 et C_2. Si de plus on considère que l'endommagement n'influe pas sur la résistivité et qu'il est uniquement pris en compte par une réduction de section, on obtient alors :

(13)
$$\rho' = \rho\left[1 + C_1(\varepsilon_e+\varepsilon_p) - C_2(2\nu\varepsilon_e+\varepsilon_p)\right]$$

et

(14)
$$dl' = dl(1+\varepsilon_e+\varepsilon_p)$$

(15)
$$dS' = dS(1-D)(1-2\nu\varepsilon_e-\varepsilon_p)$$

d'où :

(16)
$$\frac{\Delta dV}{dV} = \frac{dV'-dV}{dV} \simeq \frac{k_e\varepsilon_e + k_p\varepsilon_p + D}{(1-D)}$$

avec

(17) $k_e = 1 + 2 \quad + C \quad - 2 \quad C$

(18) $k_p = 2 + C \quad - C$

Cette décomposition permet de retrouver la valeur expérimentale de Kp proche de 2, ce qui indique que l'influence de la déformation plastique sur la ddp se limite aux termes géométriques. Ce coefficient est le même que celui utilisé dans la théorie des Jauges.

IV.2 - Application de la méthode sur éprouvette

Comme nous venons de le voir, il est possible sur un élement géométrique simple de relier une mesure de ddp à une variation de déformation ou d'endommagement. Dans la pratique, il n'est pas toujours facile d'appliquer la méthode de mesure, à cause des géométries différentes de éprouvettes. Dans ce cas, il faut utiliser une méthode définie en [13] où la forme la plus générale de variation de ddp en fonction des divers impératifs de mesure s'écrit :

$$\Delta V = K_e \, \Delta \ell_e + K_p \, \Delta \ell_p + K_D \tag{19}$$

où K_e et K_p sont des coefficients qui relient la variation de ddp à la variation d'allongement élastique et plastique, et K_D coefficient qui rend compte du niveau de détérioration. Cette valeur que l'on peut qualifier de dommage est nulle lorsque le dommage est nul puis proportionnel a $\frac{D}{1-D}$.

Dans le cas précis d'essai d'écrouissage par exemple, une des applications immédiates de la méthode consiste à la détermination de courbe Force-Déplacement, connaissant la courbe Force-d.d.p. En effet, si l'on connaît les coefficients K_e et K_p du matériau en introduisant la raideur de l'éprouvette R, la relation (19) permet alors de définir

$$\Delta V = K_e \frac{F}{R} + K_p \, \Delta \ell_p \tag{20}$$

En supposant qu'il n'existe pas de dommage, on peut alors facilement déterminer la courbe F , $\Delta\ell$ (fig. 21).

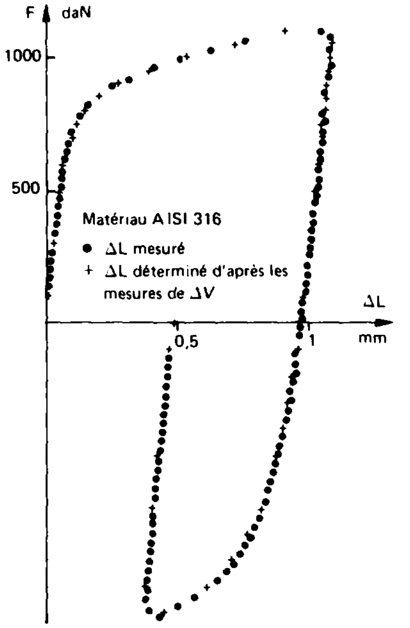

Fig. 21 – Détermination de la courbe F, Δl.

IV.3 - Evaluation du dommage

Sur de nombreux essais de fatigue oligocycliques que nous avons effectués à force imposée ou à déplacement imposé, l'ensemble des résultats obtenus nous a amené à faire les constatations suivantes :

- Essais à Force imposée : dans tous ces essais, la variation de l'amplitude du potentiel électrique ΔV apparaît plus rapidement et d'une façon plus importante que l'amplitude de déformation plastique à l'approche de la rupture de l'éprouvette.

- Essais à Déformation imposée : il est également apparu lors de ces essais qu'après stabilisation de l'amplitude de la force, l'évolution de ΔV se produisait bien avant une chute de l'amplitude de la force et d'une façon plus significative.

Dans ces deux types d'exemples, et comme il a été montre en [18], ceci est dû au fait que la mesure du potentiel électrique est sensible à la présence de micro-fissure.

D'après les hypothèses et relations écrites précédemment, le coefficient K_D traduit l'état d'endommagement de l'éprouvette ou de la structure. On peut voir sur la figure 22 un exemple de la manifestation de ce coefficient lors d'un essai de fatigue. Sur cette figure sont représentées les boucles Force-Déplacement et Force-d.d.p à différents nombres de cycles. A force nulle, on constate une dérive de la boucle Force-d.d.p. En fonction du nombre de cycles on peut évaluer la valeur de cette dérive grâce au terme $K_D = \Delta V_p - K_p \Delta \ell_p$ (21) proportionnel à $\frac{D}{1-D}$, puis comme il a été indiqué en [13] déterminer la valeur de D.

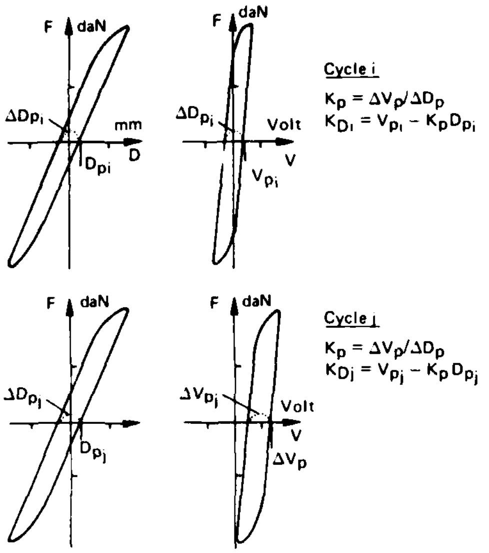

Fig. 22 – Évolution des coefficients K_p et K_D au cours des cycles.

Pour valider les résultats obtenus au cours de différents essais, nous les avons comparés à d'autres types de méthodes tels que :

- Mesure mécanique de l'évolution de la raideur de l'éprouvette en cours d'essai.

- Méthode de calcul de l'endommagement par un modèle développé à l'ONERA [19], ainsi qu'une représentation plus simple tenant compte de l'évolution de l'amplitude de déformation plastique.

D'autre part, pour "visualiser" le dommage, nous avons effectué quelques histogrammes de longueur de fissure (mesure de densités et longueurs de fissure sur coupe longitudinale) sur des essais interrompus à des valeurs de K_D définies à l'avance.

IV.4 - Résultats expérimentaux

Des essais à température ambiante ont été effectués sur des éprouvettes en AISI 316 de ∅ 6 mm et comportant une partie cylindrique de 12 mm (fig. 23). Pour la suite, tous les essais seront relatifs au même type d'éprouvette. La figure 24 montre les résultats obtenus sur un essai à force imposée à un niveau figure 24a et à deux niveaux figure 24b, dans le plan D, N/N_R. La comparaison se fait par rapport à un calcul du dommage utilisant des mesures de variation de raideur. De même sur la figure 24c, une comparaison identique a été faite sur un essai à déformation imposée.

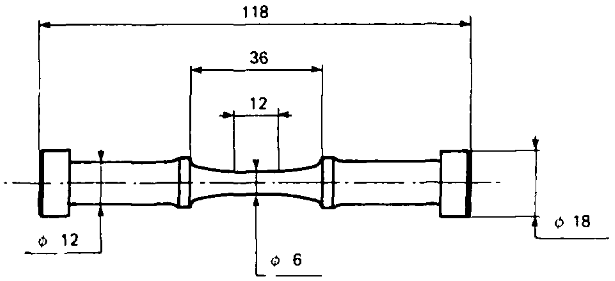

Fig. 23 – Type d'éprouvette utilisé.

Pour ces trois types d'essais, les valeurs du dommage calculées en utilisant la variation de raideur sont en bon accord avec les résultats obtenus par la méthode électrique.

Pour "visualiser" le dommage dans une éprouvette, nous avons interrompu un essai de déformation imposée (± 1 % , 0,3 Hz, 920 cycles) sur une éprouvette en AISI 316, pour une valeur de $K_D/V = 10^{-3}$ (V valeur de potentiel initial). Nous avons ensuite découpé cette éprouvette par électroérosion dans le sens de son plus grand axe puis poli les surfaces de manière à permettre une étude au microscope. L'ensemble des relevés est présenté sur l'histogramme des longueurs de fissures de la figure 25. Dans cet histogramme on visualise effectivement la notion de dommage, par l'existence d'un très grand nombre de fissures de l'ordre de 5 µ , réparties d'une façon aléatoire sur la partie centrale de l'éprouvette. Il existe seulement quelques fissures qui ont une dimension de l'ordre de 100 µ, ce qui peut signifier que celles-ci sont passées au stade du macro-amorçage. Le fait que l'éprouvette étudiée comporte un grand nombre de microfissure peut être lié à son comportement mécanique très viscoplastique et également à son mode d'usinage (tournage fin). A titre indicatif, le nombre de cycle à rupture sur une éprouvette sollicitée dans les mêmes conditions est de 1546 cycles, ce qui donne une idée de la détection $N/N_R = 0{,}6$.
Sur un autre exemple qui sera exposé par la suite (INCO 718, 650°C, rectifié-poli), un essai dans les mêmes conditions ne donne qu'une fissure.

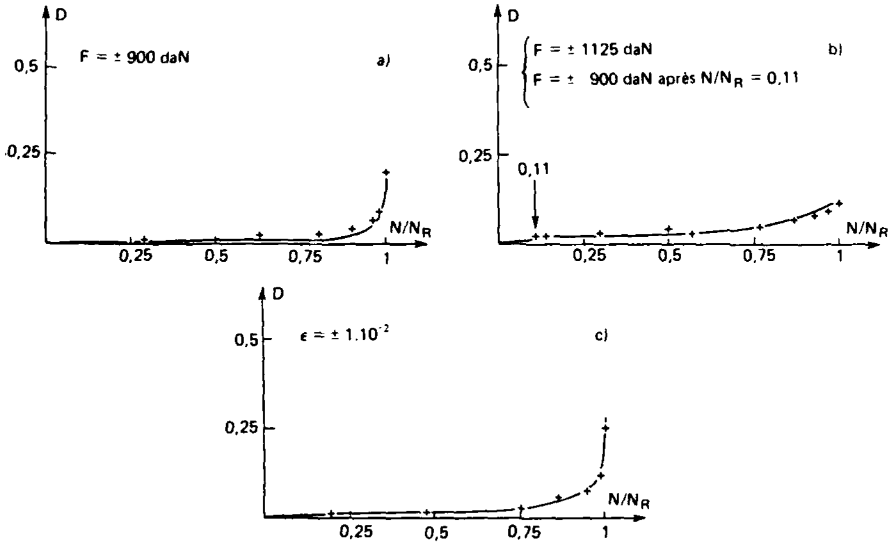

Fig. 24 – Comparaison entre les mesures d'endommagement par la méthode électrique (–) et la méthode de la raideur (+) (Aisi 316 ; T = 20°C ; fréquence 0,1 Hz).

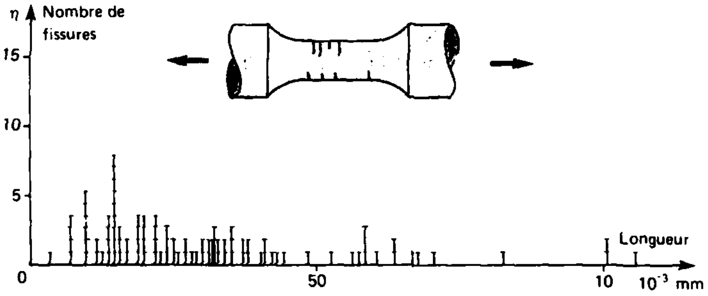

Fig. 25 – Histogramme des longueurs de fissure.

Nous avons également réalisé des essais de fatigue sur des éprouvettes en alliage IN 100 à 900°C et 1000°C. Sur l'essai de fatigue viscoplastique réalisé à 900°C, la comparaison du dommage a été faite par rapport à un calcul utilisant les lois de rupture de l'ONERA. Sur la figure 26 nous avons reporté l'évolution du coefficient K_D en présence de dommage, ainsi que la valeur de D obtenu grâce au terme K_D suivant [13], et l'on constate une bonne confrontation. Sur ce même matériau et à la température de 1000°C, nous avons réalisé un essai à contrainte imposée. Les résultats obtenus sont présentés sur la figure 27 ; l'évaluation du dommage s'est effectuée en considérant l'augmentation de la déformation plastique maximale. La comparaison entre ces deux types de mesure se révèle favorable compte tenu de l'incertitude non négligeable de ce genre de mesures obtenues par différence de deux états voisins.

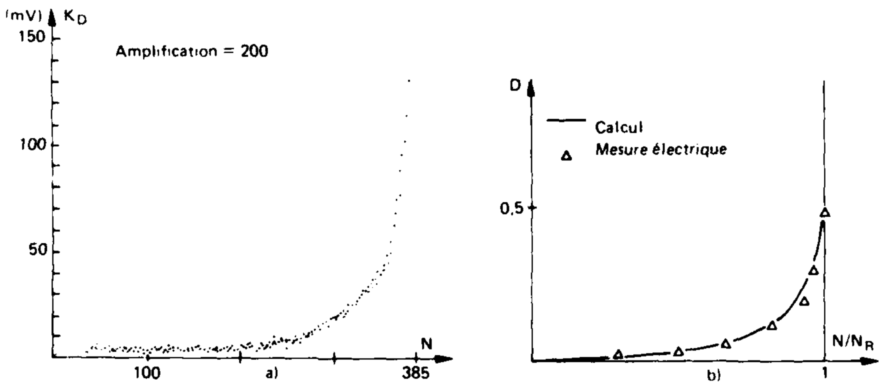

Fig. 26 – Essai de fatigue sur alliage IN 100 à 900°C. a) Détermination du coefficient K_D ; b) Comparaison du dommage mesuré avec un calcul.

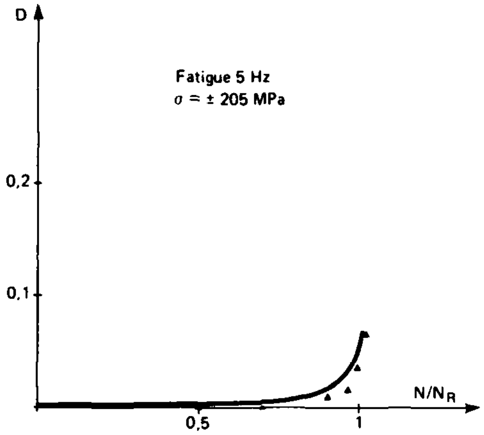

Fig. 27 – Détermination du dommage (—) méthode électrique, (▲ ▲) calcul.

L'application de cette méthode d'évaluation du dommage a également été utilisée sur des éprouvettes en INCO 718 à 650°C usinées par tournage fin puis polies. Certains essais ont été menés jusqu'à rupture, alors que d'autre ont été interrompus pour des valeurs de $K_D/V = 10^{-3}$, pour permettre des contrôles optiques éventuels (repliques, histogramme des fissures). On montre sur la figure 28, l'évolution du coefficient K_D en fonction du nombre de cycles pour un essai à déformation imposée. On constate que la valeur de K_D reste stable pendant la majeure partie de l'essai puis varie très rapidement jusqu'à la rupture de l'éprouvette. Ceci peut être lié à ce qui a été dit précédemment sur l'usinage et le comportement mécanique du matériau. Une grande partie de l'essai a été indispensable pour initier une microfissure au voisinage d'un défaut (début de l'endommagement) puis très rapidement il y a eu propagation et rupture de l'éprouvette sur une seule fissure.

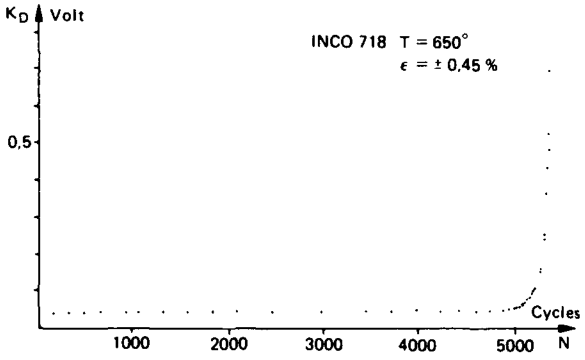

Fig. 28 – Évolution du coefficient K_D en cours d'essai.

Par la suite, et dans les mêmes conditions de sollicitations, nous avons interrompu l'essai pour une valeur de $K_D/V = 1,2.10^{-3}$. Sur la figure 29 on peut voir l'évolution du coefficient K_D en fonction du nombre de cycles jusqu'à l'arrêt de l'essai. Dans cet essai, on peut constater que l'obtention de K_D a été possible malgré une dispersion importante dans les nombres de cycles (19150 cycles, fissure extérieure $<$ 1 mm).

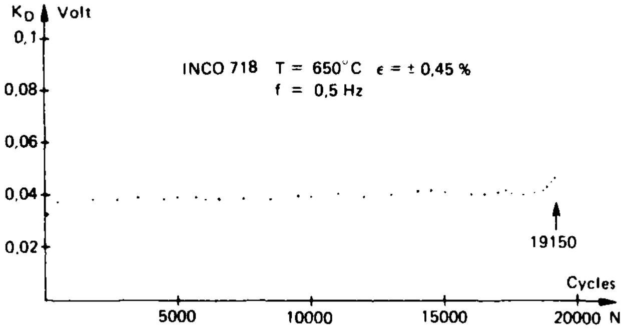

Fig. 29 – Évolution du coefficient K_D jusqu'à la valeur $K_D/V = 1,2.10^{-3}$

L'évaluation de la valeur de K_D représentative du dommage a également été appliquée sur des essais de fluage à haute température. Les éprouvettes en alliage IN 100 étaient chauffées par induction H.F. à 1000°C. Par ailleurs, nous avons également effectué des essais en fatigue-fluage, afin de vérifier l'additivité des dommages consécutifs à des sollicitations différentes.

Sur la figure 30, l'évolution du coefficient K_D est représentée en fonction de l'allongement des éprouvettes pour divers cas de chargement. Ces essais montrent l'influence d'un chargement préliminaire de fluage, suivi d'un essai de fatigue, où le dommage créé en fluage (microvides, microdéfauts) accélère le processus d'endommagement en fatigue. Au cours d'un essai de fluage, une comparaison de la mesure du dommage est faite par rapport à la loi de Norton (augmentation de la vitesse de déformation plastique) (fig. 31). Dans cette comparaison, il semble que la mesure électrique sous-estime les résultats obtenus avec la loi de Norton.

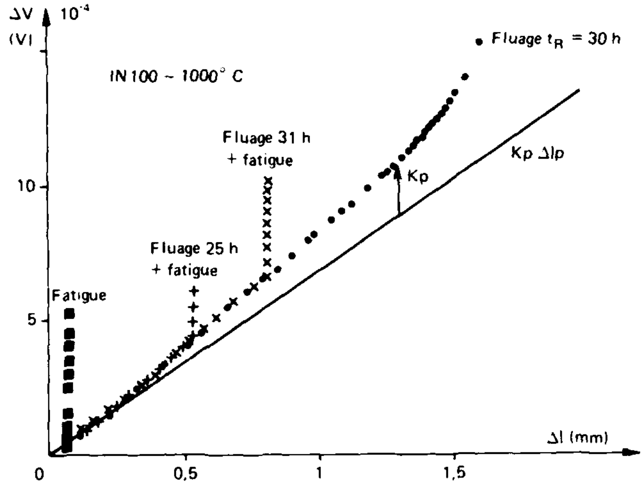

Fig. 30 – Évaluation du dommage par la mesure du coefficient K_D sur divers essais.

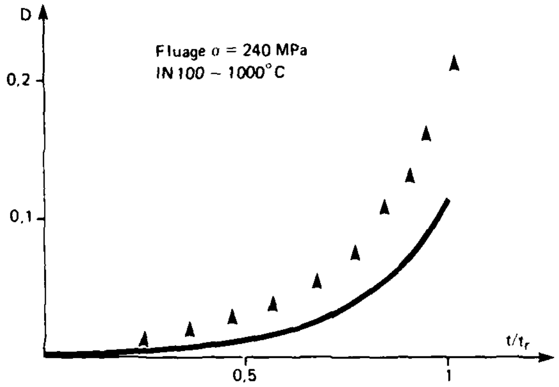

Fig. 31 – Comparaison entre les mesures de dommage par méthode électrique (——) et mécanique (▲).

Une application de la méthode est actuellement en cours sur une structure, mais n'a pas encore donnée de résultat. Cette application consiste à faire des mesures systématiques sur l'alésage et le fond d'alvéole d'un disque de turbine sollicitée par des cyclages en rotation, à la température de 600°C (fig. 32). Les mesures sont faites à température ambiante après arrêt de l'essai et démontage du disque, le but étant la détection d'une fissure de dimension inférieure à 1 mm.

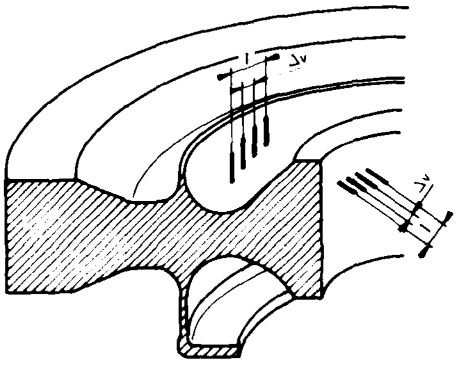

Fig. 32 – Essai de détection de fissure sur structure.

V - CONCLUSION

La méthode électrique (PDT) dans sa version améliorée s'avère particulièrement adaptée à la détection ou à la progression de fissure à *température ambiante et à haute température* dans son utilisation en laboratoire. Pour la détection de l'amorçage, un grand nombre d'essais ont mis en évidence la possibilité d'évaluer un dommage et de suivre son évolution au cours du temps. Cette mesure peut être acquise en continu et éventuellement en temps réel de manière à arrêter l'essai pour une valeur de dommage donnée.

La mesure du dommage obtenue par cette méthode est un complément expérimental précieux dans la recherche de lois d'endommagements tridimensionnelles. Son extension sur certaines structures de type industriel est en cours de réalisation et devrait permettre de suivre l'évolution de "défauts", "in situ", en temps réel.

Concernant la progression de fissure, la méthode constitue un maillon important dans la chaîne de comparaison essai-calcul, pour divers types de chargements (sinusoïdal, aléatoire, Falstaff, Twist) ainsi qu'à haute température.

Enfin, concernant les pièces massives, l'utilisation de la méthode du potentiel électrique a permis de connaître l'évolution de fronts de fissure avec une bonne sensibilité et une mise en oeuvre relativement aisée. Associée à une méthode d'étalonnage appropriée, cette méthode peut être d'une grande utilité pour les contrôles non destructifs sur des pièces réelles.

[1] - S. Savalle, G. Cailletaud
Microamorçage, Micropropagation et endommagement
Recherche Aérospatiale 1982 n° 6, p. 395-411.

[2] - J. Lemaître, J.L. Chaboche
Rupture par endommagement
Journal de Mécanique Appliquée, Vol. 2, n° 3 (1978).

[3] - Y.N. Rabotnov
Creep Rupture
Congress of applied Mechanics (1968), Standford - Springer

[4] - C. Levaillant, A. Pineau
Assesment of high temperature low cycle fatigue life of austenitic Stainless Steels, Using intergranular damage as a correlating parameter
Int. Symp. on low Cycle Fatigue and life Prediction, Firminy, France (1980).

[5] - M. Ragnet, G. Pluvinage
Mesures Physiques et Mécaniques de l'endommagement cyclique sous déformation plastique à haute température
Damage Mechanics, Euromech Colloquium 147, Cachan (22-25 septembre 1981).

[6] - H.H. Johnson
Calibrating the electrical potential method for studying slow crack growth
Material Research of Standards, Vol. 5 (1965) p. 442-445.

[7] - R.O. Ritche, G. Garrett, J.F. Knott
Crack growth monitoring ; optimisation of the electrical potential technic using an analogue method
Int. Journal of Fracture Mech., Vol. 7 (1971), p. 462-467.

[8] - G. Baudin, H. Policella
Nouvelle méthode de mesure électrique de longueur de fissure
Recherche Aérospatiale n° 1976-6, p. 340-358.

[9] - E. Bardal, T. Berge, M. Grower, P.J. Hargensen, B.M. Forre
A pulsed D.C. Method for the measurement of low-fatigue Rates of crack Growth
Advances in Crack Length Measurement, Editor Beevers C.J..

[10] - P.M. Lesne
Amorçage et propagation de fissure sous gradient thermique cyclique
Thèse Docteur Ingénieur (Lille Février 1985).

[11] - G. Baudin, H. Policella
Détermination de fronts de fissure dans les pièces métalliques tridimensionnelles par mesure électrique
Recherche Aérospatiale n° 1979-1, p. 73-85

[12] - R.O. Ritche, K.J. Bathe
On the calibration of electerical Potential Technic for monitoring Crack Growth using finite element Methods
Int. Journal of Fracture Mech., Vol. 15 (1979), p. 47-54.

[13] - G. Cailletaud, H. Policella, G. Baudin
Mesure de déformation et d'endommagement par méhtode électrique
Recherche Aérospatiale n° 1980-1, p. 69-75.

[14] - P.W. Bridgman
Proc. Am. Acad. 60, 423 (1925)

[15] - P.W. Bridgman
Collected experimental papers, Vol. 1-VIII
Harvard Univ. Press, Cambridge (1964).

[16] - E. Gruneinsen
Verh. Debteh. Gly. Gres. 15, 186 (1913)

[17] - H.K.P. Neubert
The elasto-resistive effect in metal wires and films
RAE Tech. Rep. 69272.

[18] - J. Lemaître
Sur la détermination des lois de comportement des matériaux viscoplastiques
Fac. Orsay (mai 1971).

[19] - J.L. Chaboche
Continuous damage mechanics : A tool describe phenomena before crack initiation
Nuclear Engineering and design 64, (1981), p. 233-247.

SMALL DEFECT CHARACTERIZATION IN POWDER METALLURGY MATERIALS

by
S. Re Fiorentin
FIAT Centro Ricerche
Strada Torino 50, 10043 Orbassano, Italy
and
H. Walther
FIAT Aviazione
Via Nizza, 312, 10127 Torino, Italy

SUMMARY

Powder metallurgy nickel-base superalloys are becoming important structural materials for the manufacturing of critical complex-shaped aircraft components (e.g. turbine disks). Since fatigue-life is largely affected by the presence of defects, in order to extend the limit of application of PM materials as far as possible, it is presently felt the need of a non-destructive technique capable of detecting defects of size down to approximately 50 micrometers.

An ultrasonic technique is presented which allows the detection and characterization of such small defects. It is based on the analysis of the signals backscattered by the material lying in the focal region of a short pulse transducer. During a first overall inspection of the component a real-time data processing allows both the detection of critical defects and the evaluation of average grain size. In successive local inspections, confined in the regions where inclusions have been detected, further information on their characteristics may be collected.

Some experimental results obtained on powder metallurgy samples containing seeded inclusions are presented.

PREFACE

Powder Metallurgy (PM) materials, more than conventionally produced ones, may be affected by foreign particles contamination causing life limiting defects, which are difficult to be avoided during the process. In order to extend the useful lifes as far as possible - and distinctly above those achievable in forged alloys - towards the limits prospected by the pure material, it is necessary on one side to better understand the life limiting influence of the particles size, type and orientation in order to establish the quality requirements, and on the other to define a testing procedure which guarantees the required quality level : that is the absence of defects above a certain size, etc.

In the case of PM materials, the most important particle-inclusions causing incipient crack formation are of ceramic, metallic or organic nature. Other types of defects (pores and undesired boundary structures) appear more easily avoidable. Fatigue tests, although subject to large data scatter, have shown that particle-inclusions cause remarkable reductions in the number of cycles to failure, depending upon their size and location in the specimen. At high stress levels such effects have been found down to defect sizes of 50 µm. Calculations on the crack propagation life (Paris law) also show considerable improvement, providing a crack starts at 50 µm rather than at 300 µm.
Besides of all the particular precautions to avoid inclusions or to remove them during the process, it seems necessary to require non-destructive testing down to such defect sizes, especially in critical P.M. components like turbine disks.

Non-Destructive Testing (NDT) methods however are presently not capable of detecting defects down to 50 µm : the detection limit of conventional ultrasonic techniques, which are the more widely used for defects in metals, was found to be placed somewhere between 500 and 300 µm, depending on the type of inclusion and on its depth in the material. X-Ray-radiography and Eddy-Current techniques are not at all able to detect these small defects in the range of depths generally required.

Our recent work showed us that ultrasonic techniques, after a suitable optimization of the experimental conditions, are well able to detect inclusions in the 50 µm size range.
This encouraged us to design a N.D.T. facility for the automatic inspection of P.M. turbine disks, which is presently under construction.
Scope of the following presentation is to review this optimization and to report the experimental results on detecting small inclusions in artificially doped P.M. samples.

1. CHOICE OF THE OPTIMAL TRANSDUCER CONFIGURATION

The ultrasonic (u.s.) parameters to be considered, all characterize the transducer :
- center frequency of the u.s. pulse
- bandwidth
- focal length
- diameter of the piezoelectric element.

Their optimal values evidently depend on the overall properties of the system under inspection:
- grain size
- porosity
- chemical composition of inclusions
- depth of inspection.

Since we are optimizing the operating conditions and not the ultrasonic equipment, we are not so much concerned with all other parameters which play a role in the final performance of the u.s. testing device, but do not depend on the material and inclusions properties.
While the final answer about the power of the technique is left to experiment, the search for the

optimal operating conditions can be carried out theoretically.

Theoretical models have been developed for the calculation of the probability of detection (POD) of flaws. Reference is made to the works of Fertig and Richardson [1], Thomson [2], Gray and Thomson [3,4], Elsley and Addison [5], Berens and Hovey [6]. Without aiming the calculation of the POD, one can use such models to optimize the above mentioned parameters.

The POD depends on the ratio between the amplitude of the signal coming from a certain inclusion and the noise produced by a series of other interactions. These might include, beside electronic noise, grain scattering noise, noise due to spurious scatterers, transducer ring-down, unwanted scattering from nearby surfaces, etc. The optimal values of the parameters are those that maximize the signal to noise ratio.

In a pulse-echo setup (Fig. 1) the transducer T launches an ultrasonic wave which passes from the coupling fluid through a generally curved surface, undergoes refraction at the surface, scatters off from any flaw in the volume element V, and is eventually received by the same transducer giving rise to a time dependent voltage Y(t) whose Fourier Transform Y(ω) can be represented by the sum [1] :

$$Y(\omega) = p_1(\omega)\ A_1(\omega, \vec{x}) + p_2(\omega)\ A_2(\omega) + \mu(\omega) \tag{1}$$

Here $p_1(\omega)$ is the system response function for a point scatterer on the axis of the ultrasonic beam and centered in the volume element V; $A(\omega, \vec{x})$ represents the scattering amplitude of the defect described by the vector $\vec{x}$. The function $p_2(\omega)$ is the system response function to distributed scatterers filling the sound beam, while $A_2(\omega)$ describes the scattering due to grain and randomly distributed spurious scatterers. The random process $\mu(\omega)$ represents the electronic noise. This last process is not convolved with either the point or distributed system response function because it does not represent a signal from any scattering process. The variance of $\mu(\omega)$ can be reduced through signal averaging while the variance of the noise process $A_2(\omega)$ cannot.

The point scatterer system response function has been derived in [2] and [3], and is given by :

$$\begin{aligned} p_1(\omega) = {} & R(\omega)\ C^2(z_1,z_2)\ T_{12}T_{21}\ [2\ c_2/(R_{1c}\ a_R^2\ \omega\ D(z_c))]\ \cdot \\ & \cdot \exp\ \{ -2\ [\alpha_1(\omega)\ (z_1-z_c) - \alpha_2(\omega)z_2]\} \cdot \exp\ \{ -2j\ [k_1(z_1-z_c)-k_2z_2]\} \end{aligned} \tag{2}$$

In this expression the voltage response of the transducer to the pressure wave has been determined through a calibration experiment with response R(ω). In this calibration, the transducer launches a wave normal to a planar interface at a distance z_c. The wave is reflected by the interface with a reflection coefficient R_{1c}. The functions $C(z_1,z_2)$, and $D(z_c)$ correct for diffraction effects in the measure and calibration experiment respectively; their detailed calculation is carried out in [3, 4]; z_1 and z_2 represent physical distances as indicated in Fig. 1. The factors T_{12}, T_{21} and $\alpha_1(\omega)$, $\alpha_2(\omega)$ represent the respective coefficients of transmission (water to solid, solid to water) and attenuation (water, solid).

The scattering amplitude $A_1(\omega, \vec{x})$ can be computed under the hypothesis of small linear dimension of the scatterer with respect to the wavelength λ (Rayleigh scattering). In this case, as it is well known, all scattering amplitudes (for scattering of longitudinal or transversal elastic waves from voids or elastic or fluid inclusions of any shape) are proportional to ω^2 :

$$A_1(\omega, \vec{x}) = \omega^2\ A_o(\vec{x}) \tag{3}$$

where $A_o(\vec{x})$ is the low frequency limit.

Regarding the system response function $p_2(\omega)$ it is shown in [1] that

$$p_2(\omega) = p_1(\omega) \cdot \mathrm{Vol}^{1/2}(\omega) \tag{4}$$

where Vol(ω) is proportional to the volume of material intercepted by the sound beam, and hence to its cross section area and to the pulse duration.

The scattering described by $A_2(\omega)$ can be considered as being composed of grain scattering and scattering from isolate and randomly distributed non-contributors to the predominant failure process (e.g. pores); both can be assumed to scatter in the Rayleigh regime. If the number of grains and voids intercepted by the sound beam is large, $A_2(\omega)$ may be taken to be a Gaussian process with zero moments (mean value and variance) :

$$E\{A_2\} = 0 \qquad , \qquad E\{A_2^2\} = \sigma_2^2\ \omega^4 \tag{5}$$

Also the noise process μ(ω) can be modeled as a white Gaussian stochastic process with moments :

$$E\{\mu\} = 0 \qquad , \qquad E\{\mu^2\} = \sigma_\mu{}^2 \tag{6}$$

With the foregoing evaluations, one can now calculate the signal to noise ratio as :

$$S/N = \frac{p_1(\omega)\ A_1(\omega, \vec{x})}{p_2(\omega)\sqrt{E\{A_2^2\}} + \sqrt{E\{\mu^2\}}} \tag{7}$$

which, with (3), (4), (5) and (6) can be put in the form :

$$S/N = \frac{A_o(\vec{x})}{\sigma_2\sqrt{\mathrm{Vol}(\omega)} + \sigma_\mu/[\omega^2 p_1(\omega)]} \tag{8}$$

If the standard deviation of electronic noise could be reduced to zero, the signal to noise ratio would practically be frequency independent, since the dependence of $\mathrm{Vol}(\omega)$ on ω is not very strong, being due to diffraction effects only.
Equation (8) suggests that it is convenient to reduce to a minimum the volume of material intercepted by the beam. That implies a focal spot of the u.s. wave as small as possible, and a short pulse duration (broadband pulse).

The optimal frequency must be computed maximizing the function $\omega^2 p_1(\omega)$. Making use of equation (2) and observing that the terms $R(\omega)$, $C(z_1,z_2)$, $D(z_c)$ describe diffraction effects which depend on the transducer parameters (diameter, focal length, etc.) and therefore cannot be ascribed to the characteristics of the system under inspection, we get :

$$\omega^2\ p_1(\omega) \sim \omega \exp\ [-\ \alpha_2(\omega)\ z_2] \equiv G(\omega) \tag{9}$$

where the attenuation of the ultrasonic beam in water has been neglected. Function (9) shows a maximum which depends on the attenuation properties in the solid.

In order to evaluate this optimum ω value we have measured experimentally the function $\alpha(\omega)$ for different grain sizes. The attenuation coefficient is composed of the coefficients of absorption α_a and of scattering α_s respectively :

$$\alpha(\omega) = \alpha_a(\omega) + \alpha_s(\omega) \tag{10}$$

The dependence of α_a and α_s on frequency ω and grain size d can be summarized as [7] :

$$\alpha_a \sim \omega \qquad \text{(for any } \lambda)$$

$$\alpha_s \sim \begin{cases} d^3\ \omega^4 & (\lambda >> d\ :\ \text{Rayleigh scattering}) \\ d\ \omega^2 & (\lambda \simeq d\ :\ \text{stochastic scattering}) \\ d^{-1} & (\lambda << d\ :\ \text{diffuse scattering}) \end{cases}$$

From these expressions derives the possibility of normalization with respect to the average grain size by introduction of the adimensional variables αd and ωd.
A series of measurements on 4 samples of Astroloy L.C. with different grain sizes led to the result shown in Figure 2. As it can be seen, all the experimental points fall on a single line, which is characteristic of the material. Performing an analytical regression of this curve and substituting into equation (9), we get a dependence of the G function on the variables ω, d and z_2. Figure 3 gives the plots of the function $G(\omega)$ in the case $d = 50\ \mu m$ for a few values of the depth of inspection z_2, while Fig. 4 presents the dependence of the optimal operating frequency on z_2 and d in the ranges of interest.

This result allowed us to conclude that for Astroloy type materials the frequency should be chosen accordingly in the range from 10 to 20 MHz. If ultrasonic inspection is to be carried out at depths up to 10 mm, a 20 MHz center frequency pulse can be considered optimal.

2. MEASUREMENT OF THE PROBABILITY OF DETECTION

2a. Samples preparation

The specimens used in the present investigation where flat cilinders (60 mm diameter and 10 mm height) of AP1 (Astroloy L.C.) and AF115 (René 95 type composition) containing Al_2O_3, Cr_2O_3, Zr_2O_3 or SiO_2 particles as inclusions. (*)
The grain size of the starting powder was kept smaller than 45 μm to avoid spurious particles in the size range of interest.
The hot isostatic pressing (hipping) of the powder was performed under the following conditions :

AP1 : $T_{max} = 1150°C$; $P_{max} = 1000$ bar; dwell time = 3 h ;
AF115 : $T_{max} = 1170°C$; $P_{max} = 1000$ bar; dwell time = 4 h .

The materials thus compacted were subjected to the following heat treatments:

AP1 : 1115°C/4 h - 650°C/24 h - 760°C/8 h ;
AF115 : 1175°C/4 h - 760°C/16 h .

The specimens were subsequently machined in order to obtain flat and parallel faces, with a roughness (Ra) smaller than 0.3 μm.
The characteristics of the samples and of their doping are reported in Table 1.
Figure 5 shows the typical aspect of loose Al_2O_3 and Zr_2O_3 particles, whilst Figure 6 shows them after embedment.

(*) Kindly prepared by MTU - München.

2b. The u.s. transducer

More than 10 transducers with frequencies in the range 15-25 MHz and focal distances from 1.5" to 5" in water have been tested. The best results have been obtained with a shock wave transducer of 22 MHz center frequency and 2" focal length. The lens has been optically worked and has a 5 μs delay line. Figure 7a shows the waveform of the pulse reflected in water by a flat surface placed at the focal distance, and Figure 7b its frequency spectrum. A C-scan type map of the maximum amplitude backscattered by a 250 μm radius sphere has shown that the cross section of the u.s. beam in the focal plane, measured at - 6 dB, has a diameter of approximately 300 μm (Fig. 8).

2c. - The experimental procedures

The ultrasonic testing must be carried out by inspecting the waveform backscattered by the material lying in the focal region : a cylinder of about 300 μm diameter and 1 mm height. A suitable scanning device has of course to be provided for the inspection of a component.

The heart of the detection process is however the "detection decision", which has to state if a defect is present or not in relation to the detection limit. Instead of basing this decision on the time dependence analysis of the received waveform, an advantage is seen to base it on an algorithm related to the spatial dependence of the peak height as measured in scanning steps of 100 μm an with a time window corresponding to a layer thickness of 1 mm. Such C-scan type data of each layer give rise to a spatial function $\tau(x,y)$, which is shown in Figs. 9a and 9b. The "peaks" there visible are due to inclusions, and the "grass level" to electronic and grain scattering noise. The signal to noise ratio is quite different in the two cases, because of differences in both grain and inclusion sizes (10 μm grain size and 200 μm inclusions in Fig. 9a; 50 μm grain size and 50 μm inclusions in Fig. 9b).

Plotting all the peak heights (from inclusions and noise) so far measured (and shown in Figs. 9a, 9b) in form of the histograms of Figs 10a, 10b (0.01 Volts have been choosen as interval), one observes *two very well distinguishable distribution functions. Extrapolation to zero frequency of the function* representing electrical noise and grain (and pore) scattering is easily possible and gives the limiting threshold value for inclusion detection on which the detection decision can be based.

This threshold value, together with the shape of the grain and pore scattering histogram, can give additional information about the microstructural properties of the material, and could allow a further quality assessment of the component. For a quantitative grain size estimation a calibration with reference standards is of course necessary and must be repeated for every depth of inspection.

Once obtained the optimal threshold value, a binary C-scan image of each inspected layer can be derived, plotting a dark spot in the points where the u.s. signal has a value greater than the threshold level. Such results have been compared with the radiographic indications (X-Rays) of the inclusions, after having separated the respective layer by machining. For the radiographic inspection of the sample layers containing the smaller inclusions, an X-Ray microfocus device had to be used. As a result of this comparison (an example is given in Figure 11) the POD is obtained. Fig. 12 summarizes the POD-results for the samples listed in Table 1 and for layers of 1 mm thickness at an inspection depth of 5 mm. As it is seen, the achieved POD is nearly 70% for 50 μm inclusions in a material (AF 115) with 10 μm grain size.

The particles not identified ultrasonically are probably the ones of not spherical shape and unfavourable orientation relative to the angle of beam incidence. The POD can therefore be increased by additional measurements either at other incidence angles or by using transversal waves.

Unfortunately however not all angles of incidence are accessible and not all inclusion shapes posses orientations much more favourable than others. In addition, the interference between grain and inclusion scattering can significantly modify the amplitude of the signal, so that it will never be satisfactory to describe the correlation between POD and particle size d by the step-wise function :

$$\mathrm{POD} = 1 \quad \text{if} \quad d > d^* \quad , \qquad \mathrm{POD} = 0 \quad \text{if} \quad d < d^* \ ,$$

the limiting value d^* being dependent on grain size, porosity and inspection depth.

3. A DEVICE FOR AUTOMATIC TESTING OF TURBINE DISKS

Ultrasonic methods for the N.D. identification of small defects in PM materials, such as explored above, may find practical application in turbine disks only if a series of additional requirements can be fulfilled. A suitably computerized and automized u.s. system must in fact have the following characteristics :

I. High mechanical precision
II. Fast scanning capabilities
III. Automated accept/reject criteria (based on damage-tolerant design concepts)
IV. Reasonably low memory consumption.

Whilst the first two characteristics can be achieved with mechanisms used in modern high precision gauging machines, one has to define the accept/reject criterion by correlating the identified defect (detection decision) with its influence on the component lifetime. This task must be handled separately inside any specific project. Concerning the fourth characteristic, a too large memory is needed in following the inspection procedure previously described, which requires the storage of the amplitude values of all inspected points, which in a turbine disk are several millions.

The detection algorithm has therefore been modified as follows : we have choosen to loose the information of the exact spatial localization of defects, keeping only the features necessary for the detection decision. If an inclusion is detected in a certain layer, the inspection must be repeated for its localization and sizing.

Even if the histogram of the frequencies of occurrence of the peak heights h (which in the following we shall indicate with N(h)) cannot be built up during the scanning, it can be reconstructed starting from the directly measurable function H(z), which gives the partial area of the inspected layer where the detected u.s. signal is greater than the threshold voltage z.

In fact, calling $H_o(z,h)$ the function measured for a sigle point reflector which gives rise to a peak of height h, the histogram $N(h)$ can be calculated solving the following integral equation :

$$H(z) = \int_0^\infty N(h)\, H_o(h,z)\, dh \tag{11}$$

Adopting the representation:

$$N(h) = \sum_{j=1}^{n} C_j\, \phi_j(v) \tag{12}$$

where

$$\phi_j(v) = \begin{cases} 1 & h_{j-1} < h < h_j \qquad (j=1,2,\ldots n) \\ 0 & \textit{elsewhere} \end{cases} \tag{13}$$

we get

$$H(z) = \sum_{j=1}^{n} C_j \int_{h_{j-1}}^{h_j} H_o(h,z)\, dh = \sum_{j=1}^{n} C_j\, H_{oj}(z) \tag{14}$$

The coefficients C_j can be computed by means of a least squares fit of the measured H(z) function with expression (14). Even if this procedure does not allow to get high resolution histograms, it gives anyhow correct average results.
The function H(z) can obviously be calculated from the $\tau(x,y)$ maps with the formula :

$$H(z) = \iint_{\tau(x,y) > z} dx\, dy \tag{15}$$

Fig. 13 shows the $H_o(z)$ function of the single point reflector obtained from the map of Fig. 8, while Figs. 14a and 14b show the H(z) function calculated from the maps plotted in Figs. 9a and 9b respectively. Fig. 15 is the H(z) function measured in a sample which does not contain any inclusion (sample No. 6 in Table 1), while Fig. 16 refers to a porous specimen (sample No. 10; porosity ~ 0.6%). As can be seen by inspection of Figs. 14-16, the presence of defects can be easily recognized in the shape of the H(z) function as well.

As far as the characterization of the defects is concerned, many algorithms are available which yield the size, shape and orientation of a flaw. The Inverse Born Approximation is one of the methods that recently have been more studied both experimentally and theoretically. The low signal to noise ratios that characterize the scattering from the smaller inclusions give sometime rise to larg uncertainties in the estimated size of the defects. Work is now in progress to overcome this problem and to allow an estimation of the acoustic impedence of the inclusions.

Fig. 17 shows a simplified block diagram of the test system whose main characteristics are reported in Table 2.

4. FINAL CONCLUSIONS

1. The probability of detection (POD) with ultrasonic methods of small ceramic inclusions in powder metal materials has been measured after a theoretical optimization of the experimental parameters.
2. A new detection decision algorithm, based on the "extrapolation of scattering functions" characteristic for the inclusions on one side and for the background scattering on the other has been used with advantage instead of the conventional "value comparison" method.
3. The detection limits for ceramic inclusions in AP1 and AF115 materials have this way been considerably improved (from ~ 300 μm to ~ 50 μm).
4. The POD of 50 μm ceramic inclusions in a 10 μm grain size PM material results to be ~ 70% and seems to be furthermore improvable. The POD depends on grain size.
5. A computerized ultrasonic scan system based on the results so far obtained, will allow testing of typical 300 mm diameter turbine disk in approximately 30 minutes.

5. REFERENCES

1. Fertig K.W. and Richardson J.M. , "Computer Simulation of Probability of Detection", Review of Progress in Quantitative NDE, Vol. 2A, Plenum Publishing Corp., New York (1982), pp. 147-169.
2. Thomson R.B., "Diffraction Corrections for Scattering Measurements", Internal Report, Center for Advanced Non-destructive Evaluation, Ames Laboratory, Iowa State University.

3. Thomson R.B., Gray T.A., Hsu D.K., Rose J.H. and Thomson D.O., "Foreward and Inverse Ultrasonic Scattering Measurements in Realistic Geometries", New Procedures in Non-destructive Testing, Springer-Verlag (1983), pp. 317-335.

4. Thomson R.B., Gray T.A., "Analytic Diffraction Corrections to Ultrasonic Scattering Measurements", Review of Progress in Quantitative NDE, Vol. 2A, Plenum Publising Corp., New York, (1982), pp. 567-586.

5. Elsley R.K., Addison R.C. and Graham L.J., "Detection of Flaws below Curved Surfaces", Review of Progress in Quantitative NDE, Vol. 2A, Plenum Publishing Corp., New York (1982), pp. 113-129.

6. Berens A.P. and Hovey P.W., "Evaluation POD/CL Characterizations of NDE Reliability", Review of Progress in Quantitative NDE, Vol. 2A, Plenum Publishing Corp., New York (1982), pp. 53-68.

7. Goebbels K., "Research Techniques in Non-Destructive Testing", Vol. IV, Academic Press, London (1980), Chapter 4, pp. 91-125.

N°	MATERIAL	GRAIN SIZE (μm)	DOPING MATERIAL	INCLUSIONS SIZE (μm)	DOPING (mg/Kg)
1	AP1	45 ± 5	Al_2O_3	149-177	95
2	AP1	55 ± 5	Al_2O_3	177-250	126
3	AP1	50 ± 5	Al_2O_3	250-297	203
4	AP1	55 ± 5	Cr_2O_3	177-250	223
5	AF 115	10 ± 2	Al_2O_3	177-250	126
6	AP1	45 ± 5	-	-	-
7	AP1	55 ± 5	Al_2O_3	44-53	2.1
8	AF 115	50 ± 5	-	-	-
9	AF 115	60 ± 5	Al_2O_3	44-53	2.1
10	AF 115	15 ± 5	-	-	-
11	AF 115	14 ± 3	Al_2O_3	44-53	1.6
12	AF 115	10 ± 3	Al_2O_3	44-53	0.64
13	AF 115	12 ± 3	Al_2O_3	88-105	7.125
14	AF 115	10 ± 3	Al_2O_3	88-105	14.25
15	AF 115	12 ± 3	SiO_2	37-44	0.83
16	AF 115	15 ± 3	SiO_2	44-53	1.06
17	AF 115	16 ± 3	SiO_2	88-105	12.92
18	AF 115	10 ± 3	SiO_2	177-250	16.36
19	AF 115	15 ± 3	Zr_2O_3	44-53	2.57
20	AF 115	18 ± 3	Zr_2O_3	44-53	1.22

TABLE 1 - Characteristics of doped samples

AXES	RANGE	POSITION ACCURACY	MAXIMUM SPEED	REPEATABILITY
X	800 mm	± 0.01 mm	12 m/mim	± 0.006 mm
Y	800 mm	± 0.01 mm	12 m/mim	± 0.005 mm
Z	450 mm	± 0.01 mm	12 m/mim	± 0.004 mm
θ	± 95°	± 0.02°	20 rpm	± 0.01°
φ	± 95°	± 0.02°	20 rpm	± 0.01°
T	CONTINUOUS	± 0.02°	27 rpm	± 0.005°

TABLE 2 - Mechanical characteristics of the scanning device for u.s. testing of gas turbine disks

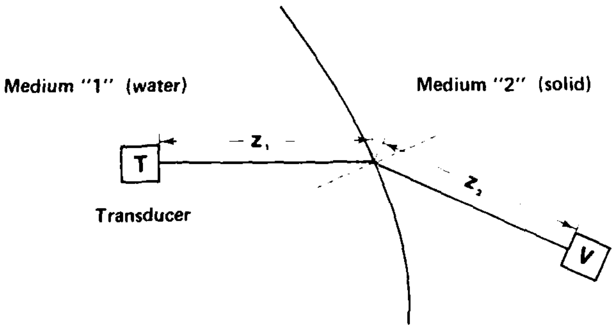
Medium "1" (water)
Medium "2" (solid)
z_1
z_2
T
Transducer
V

FIG. 1 - Pulse echo geometry

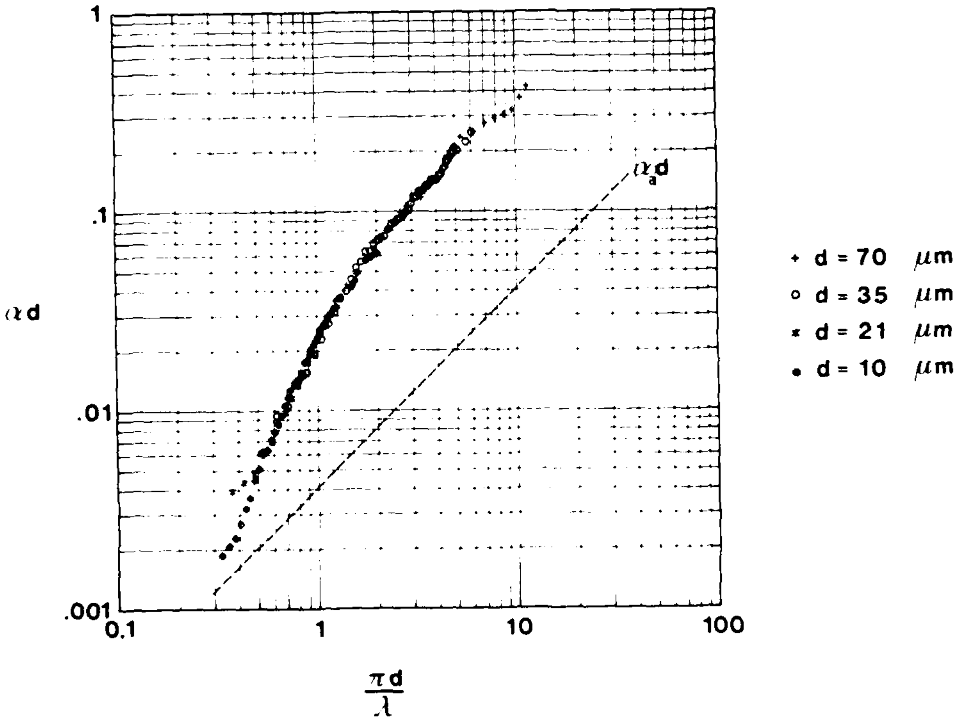

FIG. 2 - Normalized plot of the attenuation coefficient as a function of $\pi d/\lambda$

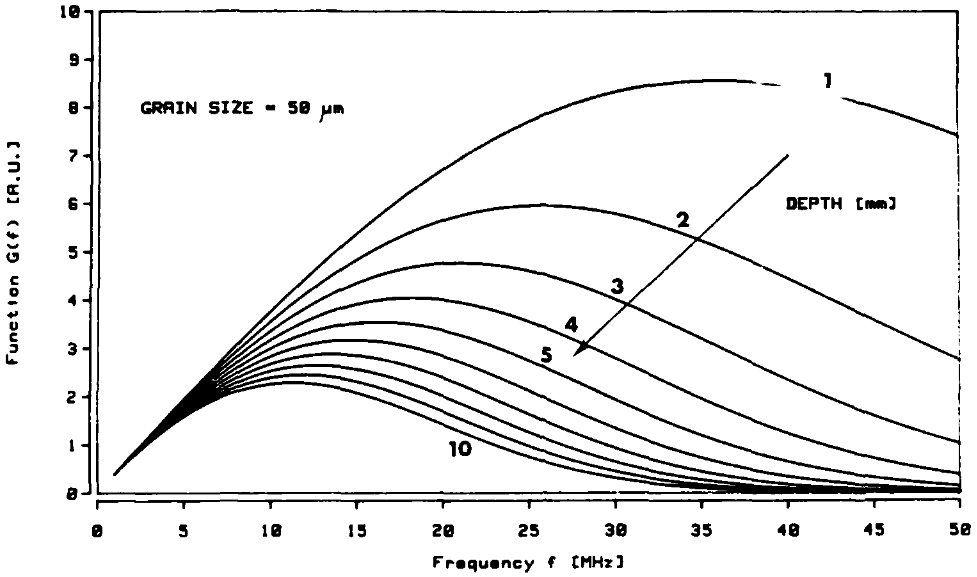

FIG. 3 - Behaviour of the G(f) function (to be maximized) for different depths of inspection

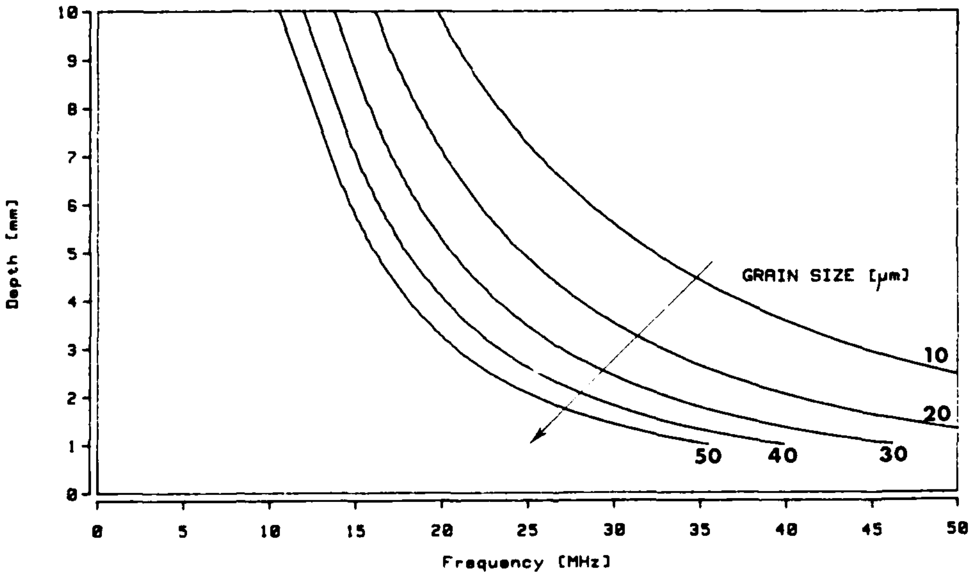

FIG. 4 - Dependence of the optimal operating frequency on inspection depth and grain size

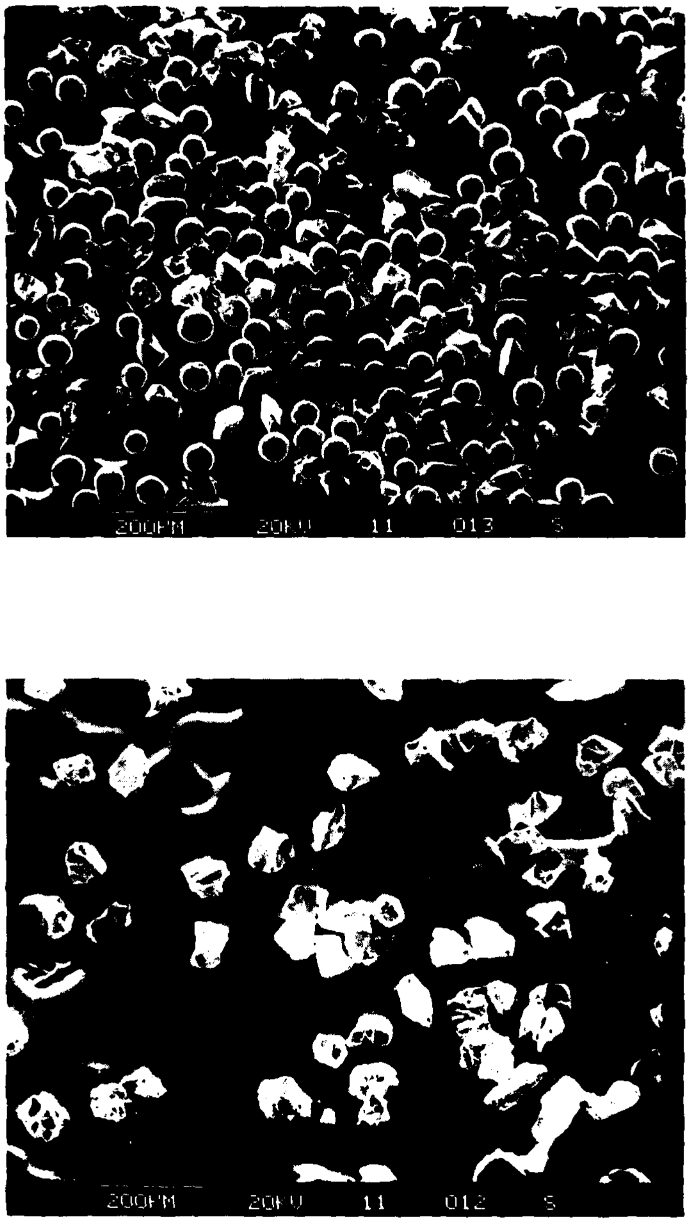
200PM 20KU 11 013 S
200PM 20KU 11 012 S

Al_2O_3

44 ÷ 55 μm

Zr_2O_3

44 ÷ 55 μm

FIG. 5 ~ Microphotographyes of some loose particles (100X)

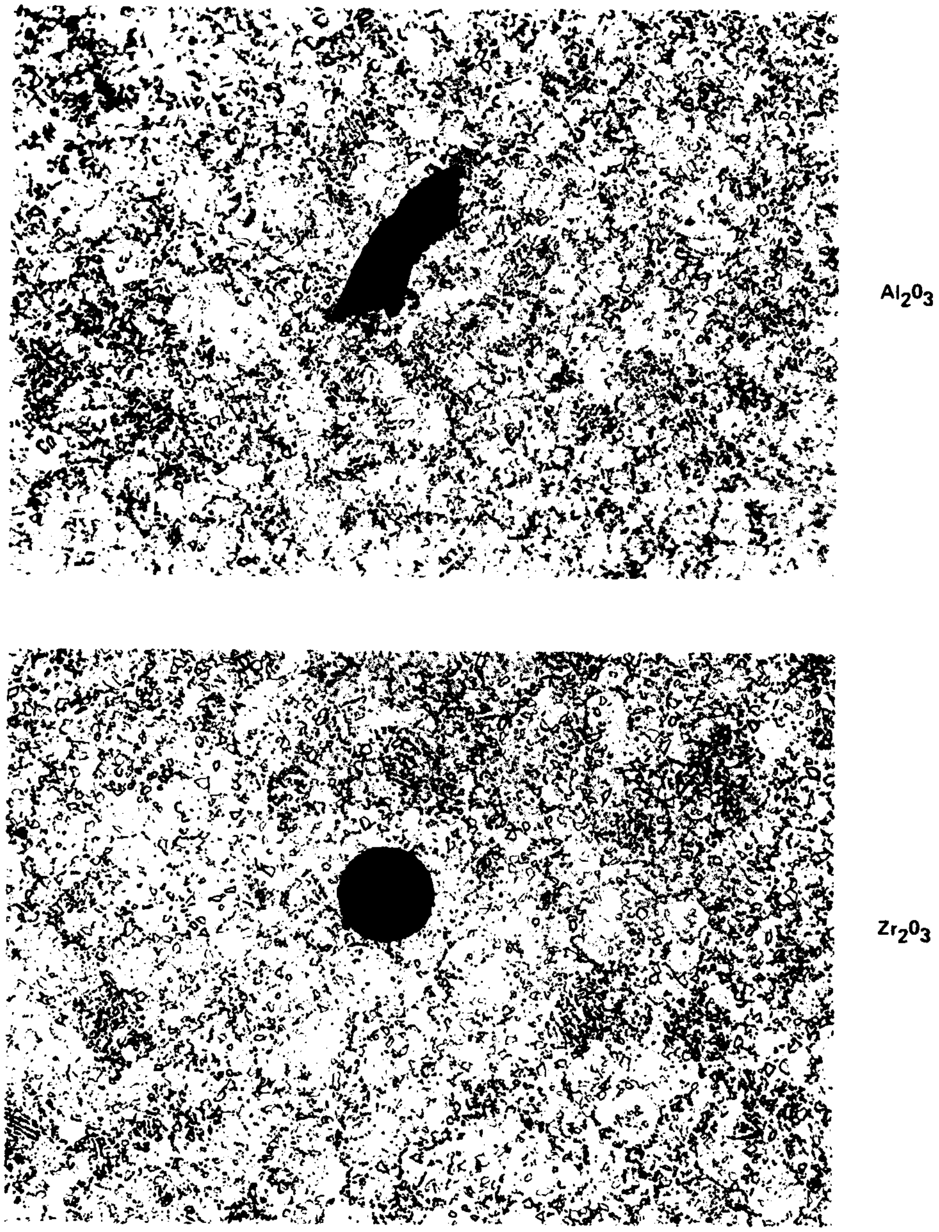
Al_2O_3
Zr_2O_3

FIG. 6 - Embedded particles in AF115 (500X)

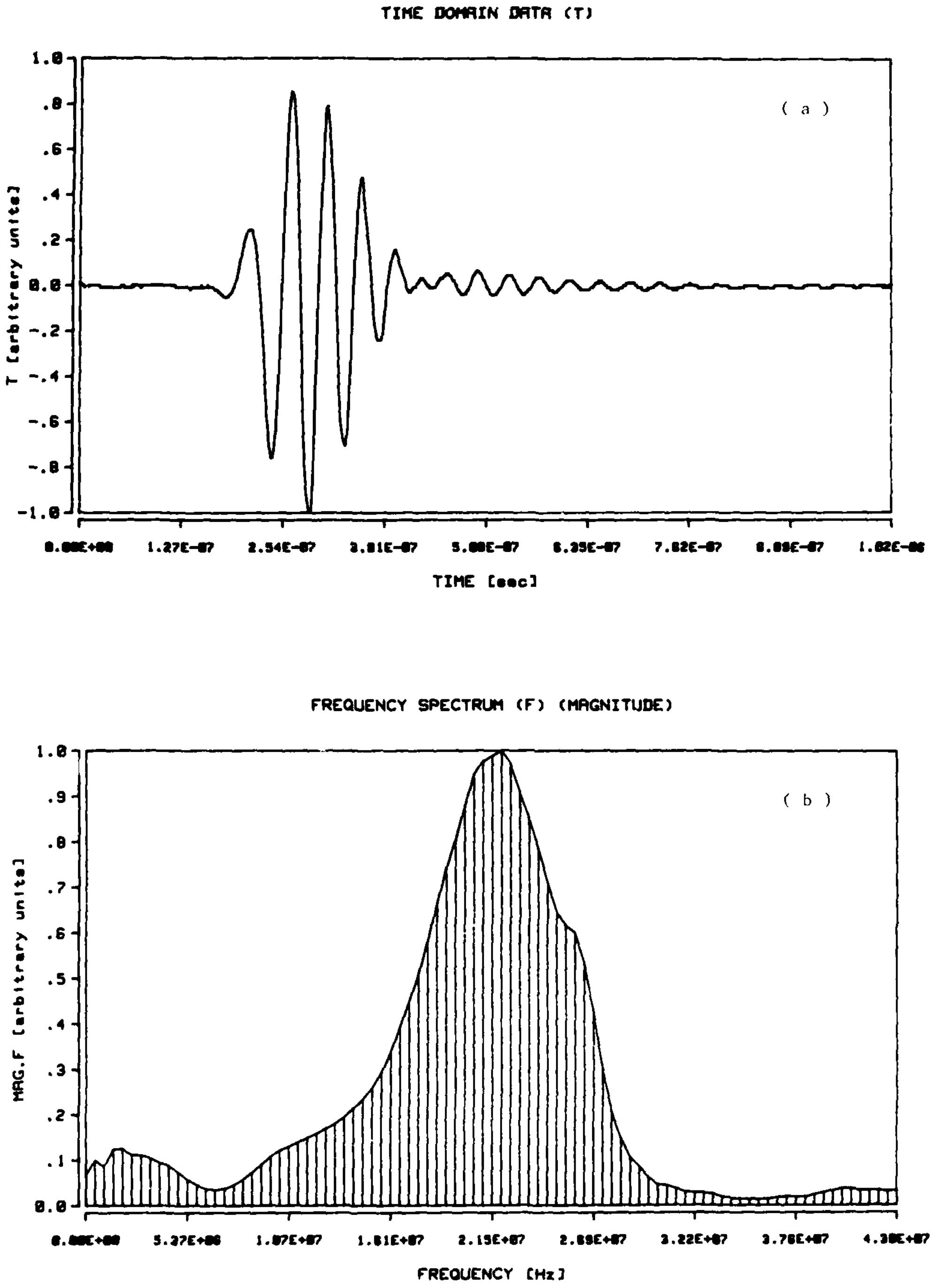

FIG. 7 - Characteristics of the u.s. pulse emitted by the transducer : pulse shape (a) and frequency spectrum (b)

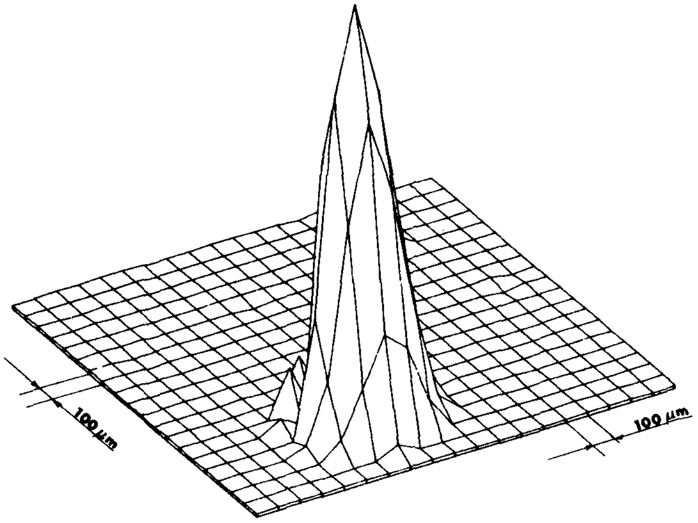

FIG. 8 - C-scan map of the amplitude of the u.s. wave backscattered by a 250 µm radius sphere

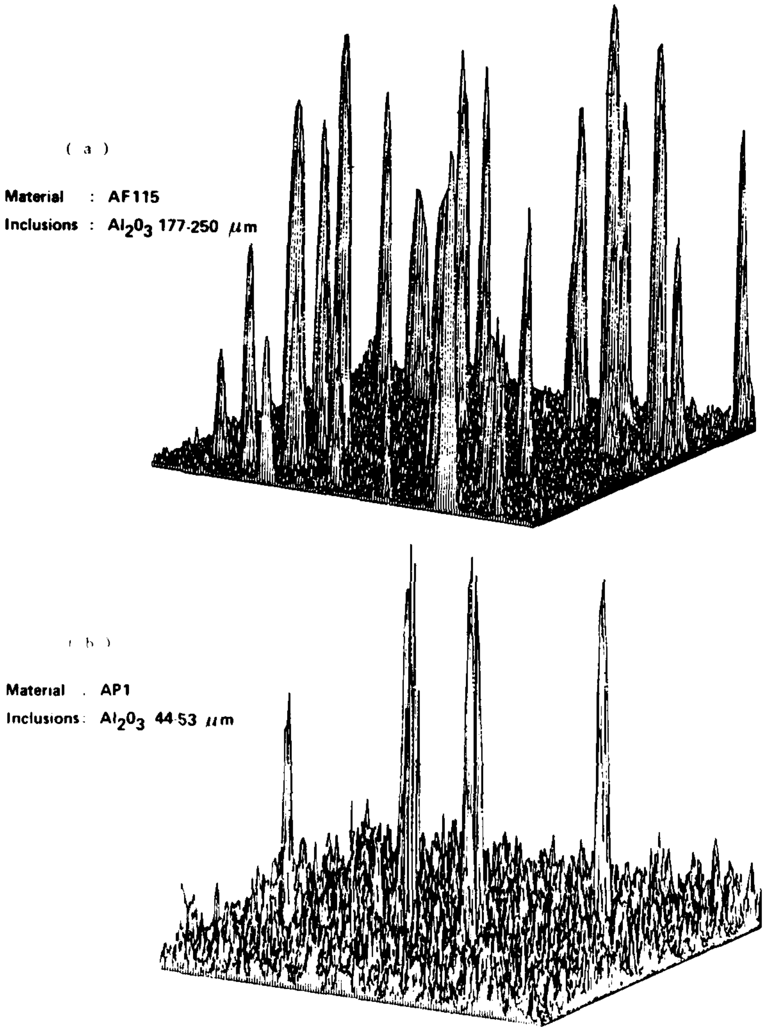

FIG. 9 - C-scan maps of the amplitude of the u.s. wave backscattered by a 30x30 mm^2 layer lying between 4.5 mm and 5.5 mm under the surface recorded in samples No. 5 (a) and No. 7 (b)

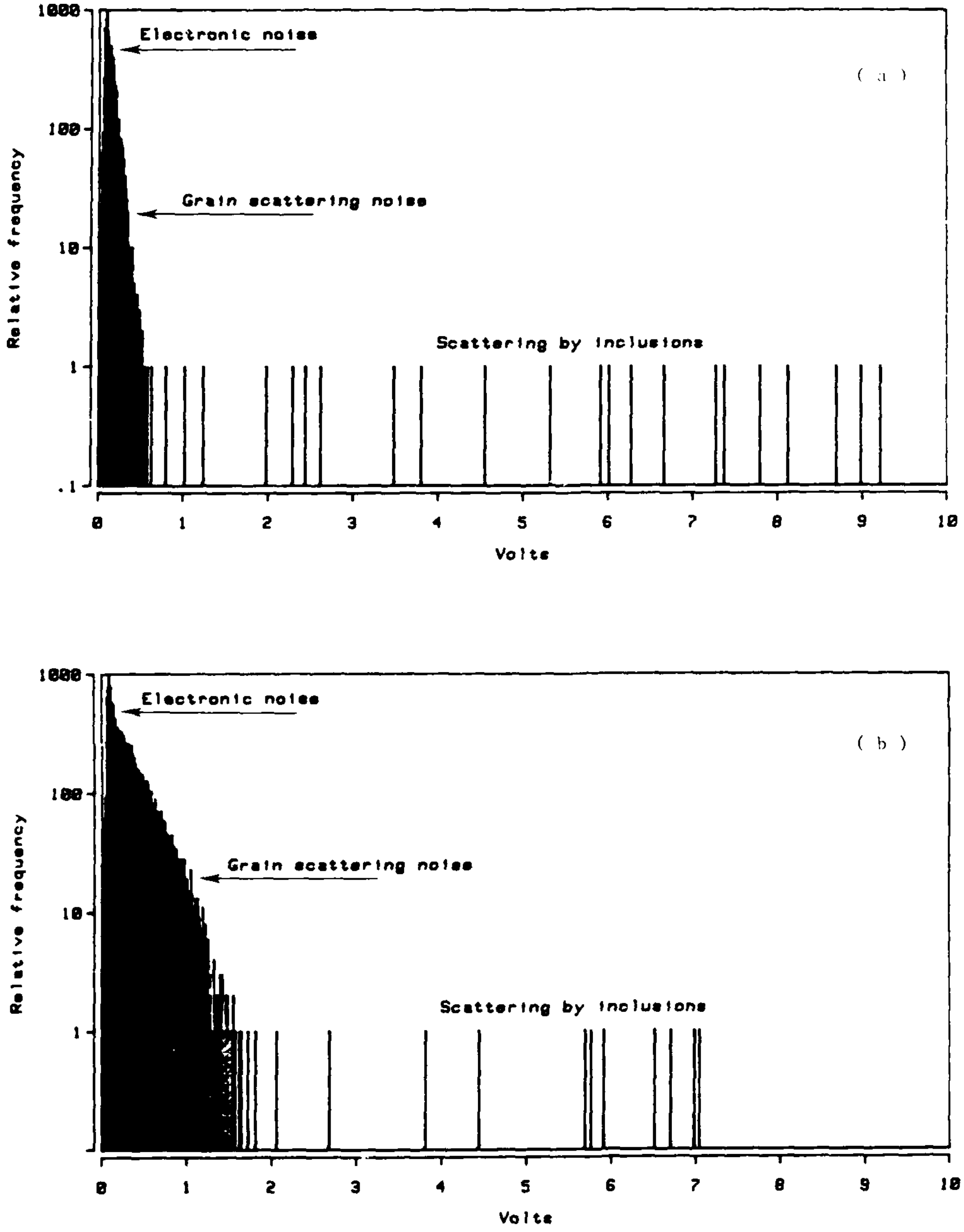

FIG. 10 - Histograms of the frequencies of occurrence of the peak heights obtained from the data of Fig. 9a (a) and Fig. 9b (b)

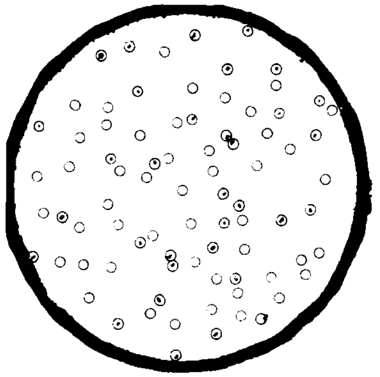

FIG. 11 - Evaluation of the probability of detection in Sample No. 7 (50 µm grain size). Circles show the regions where inclusions have been detected by X-Ray Radiography (Magnification 3X)

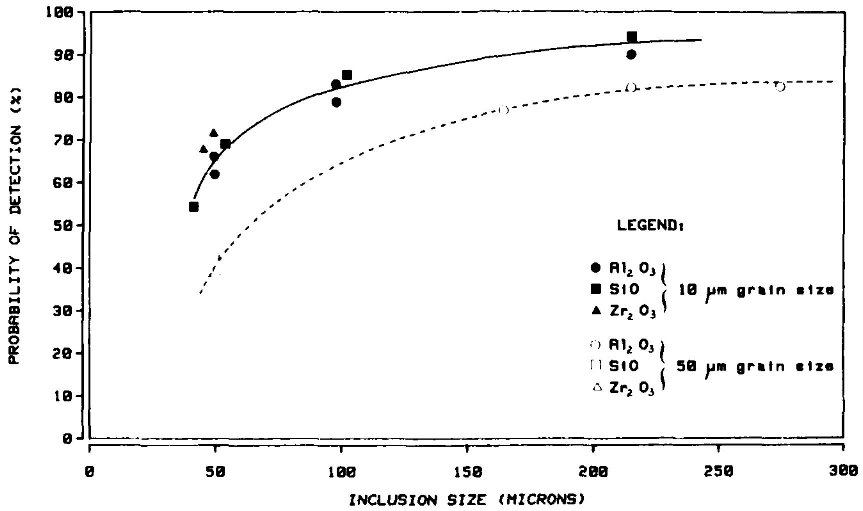

FIG. 12 - Probability of detection measured in the samples listed in Table 1

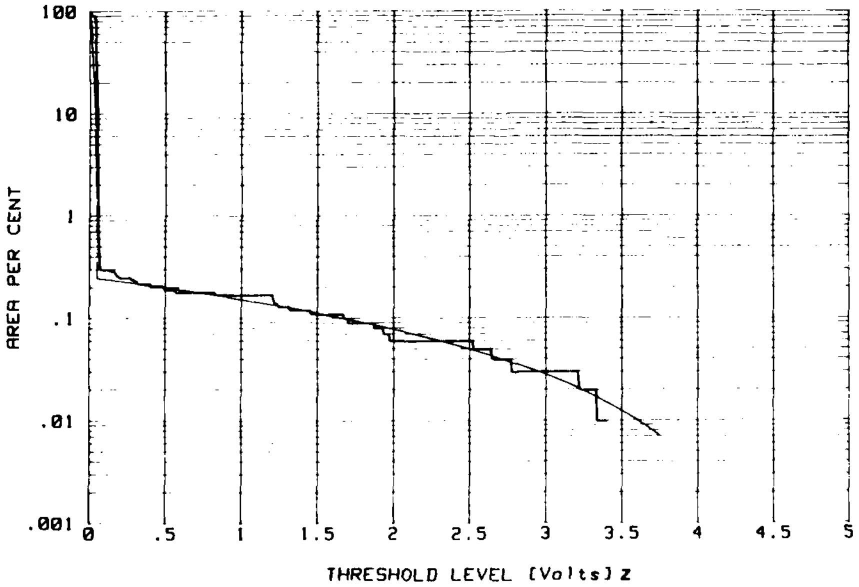

FIG. 13 - The point reflector response H_o : the step-wise curve is the measured function, while the smooth one is a theoretical fit

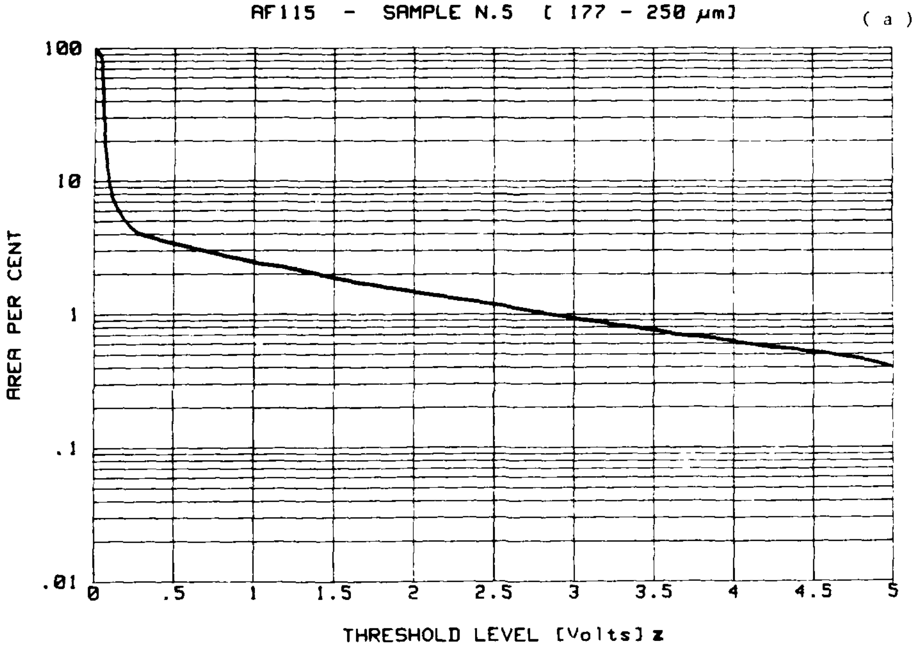

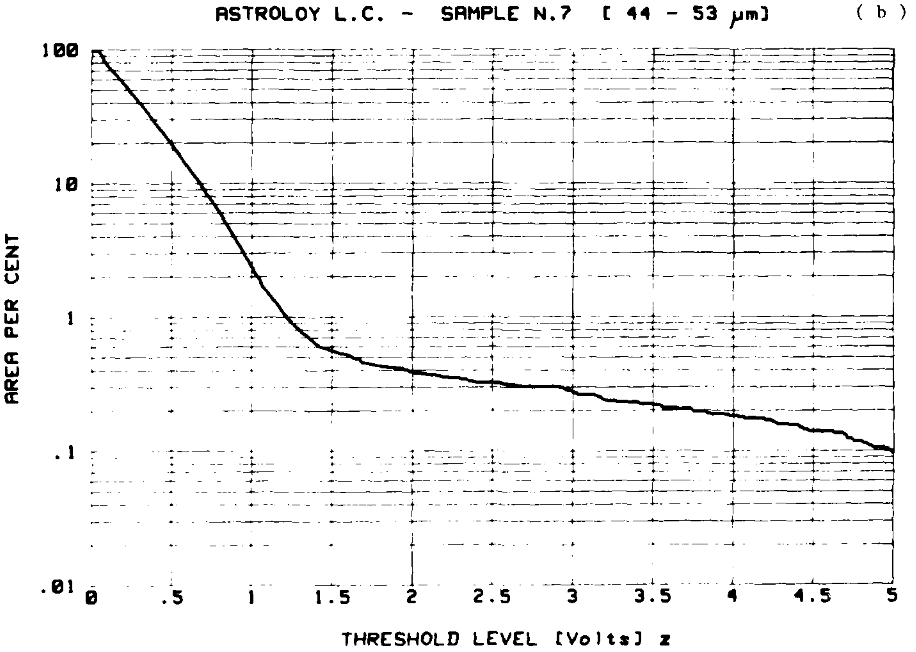

FIG. 14 - H(z) functions obtained from the maps reported in Fig. 9a (a) and Fig. 9b (b)

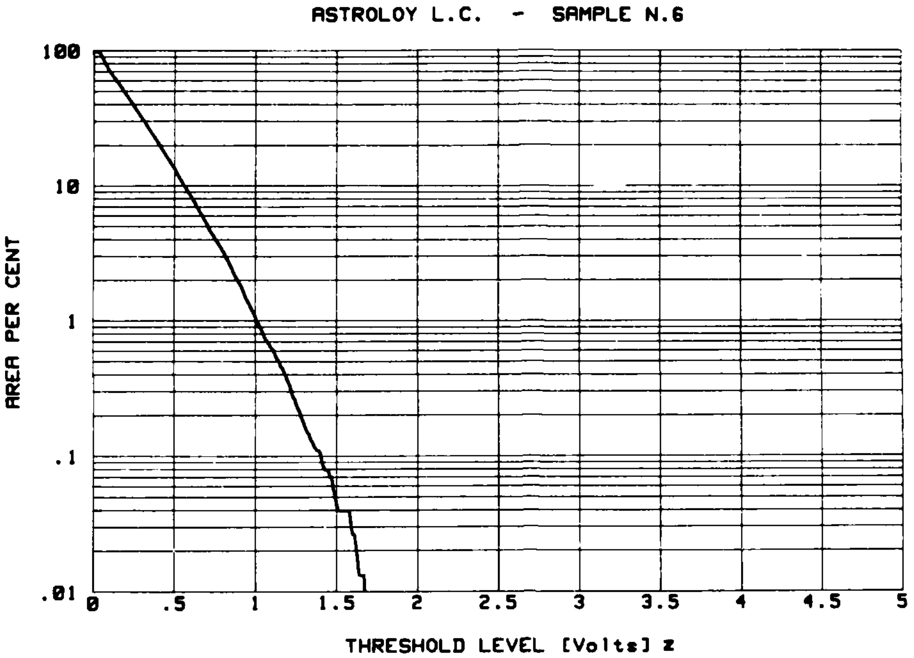

FIG. 15 - H(z) function measured in a sample without inclusions

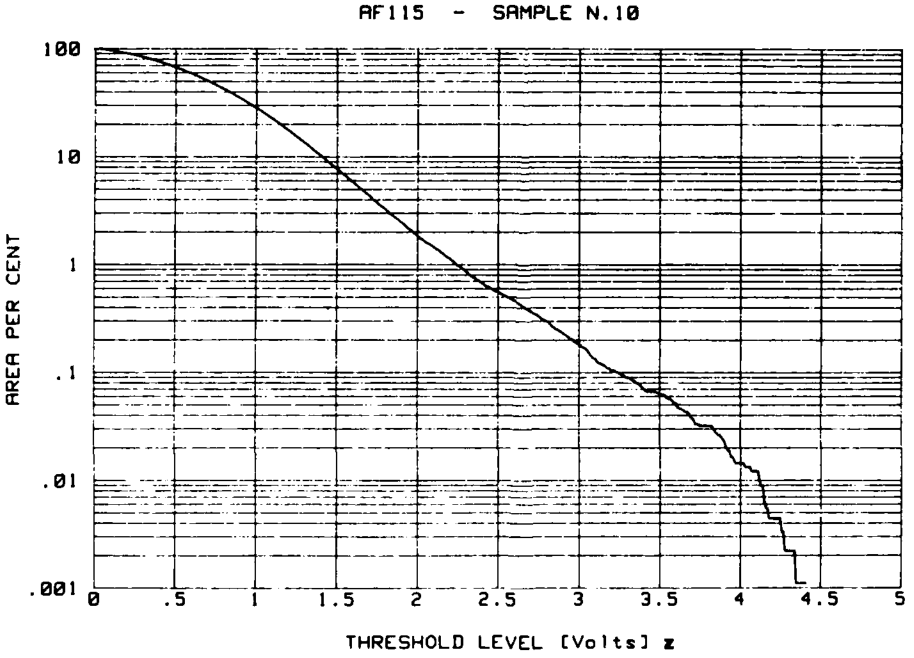

FIG. 16 - H(z) function of a porous specimen

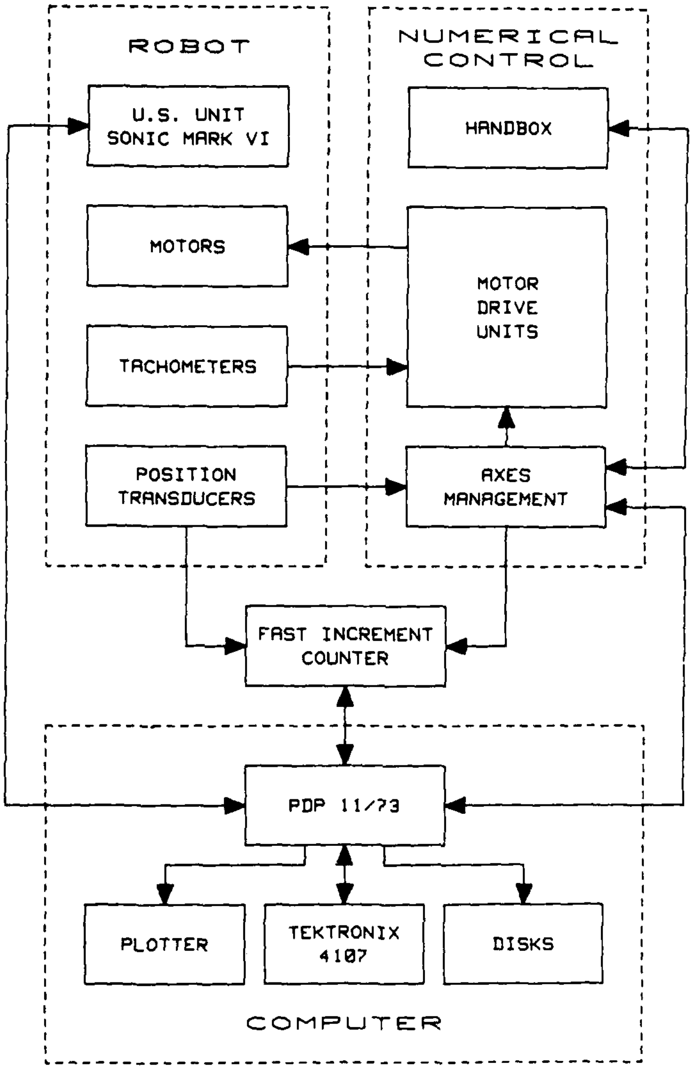
ROBOT
NUMERICAL CONTROL
U.S. UNIT SONIC MARK VI
HANDBOX
MOTORS
MOTOR DRIVE UNITS
TACHOMETERS
POSITION TRANSDUCERS
AXES MANAGEMENT
FAST INCREMENT COUNTER
PDP 11/73
PLOTTER
TEKTRONIX 4107
DISKS
COMPUTER

FIG. 17 - Simplified block diagram of the device for the ultrasonic inspection of gas turbine disks

ADVANCED EXPERIMENTAL METHODS
FOR MONITORING THE BEHAVIOR OF SMALL CRACKS

James M. Larsen
United States Air Force Wright Aeronautical Laboratories
AFWAL/MLLN, Wright-Patterson Air Force Base, Ohio, USA

SUMMARY

Two specialized techniques for monitoring the behavior of small fatigue cracks are discussed. The first of these is an automated photomicroscopic system that produces a permanent photographic record of the growth of small surface cracks. The system is automated by a microcomputer which controls fatigue testing and operates a 35 mm camera. Data are obtained for the growth of small cracks of approximate sizes ranging from 25 μm to fracture. The precision of the photographic measurements is approximately 1 μm for cracks of the order of 25 μm in length. In addition to the photographic technique, a unique interferometric displacement gage (IDG) which monitors the crack mouth opening behavior of small surface cracks is discussed. The IDG measurements produce a complete record of applied load vs. crack opening displacement. The load-displacement data are analyzed to determine effective crack length from compliance calibrations and to determine crack closure behavior. The capabilities of both the photomicroscopic and the interferometric techniques are discussed, and typical small crack data are presented.

INTRODUCTION

As part of an overall effort by the United States Air Force to implement a damage tolerant approach to life management of critical components in advanced turbine engines [1-3], considerable research has been performed to develop accurate predictive models of crack propagation under realistic engine operating conditions [4-9]. In general, experimental data have been generated by testing specimens containing relatively large cracks, and fracture mechanics methods have been used to predict the behavior of smaller, naturally occurring cracks in actual engine components. The accuracy of the damage tolerant approach has been demonstrated by extensive testing of specimens and actual engine components containing cracks of realistic sizes [6, 7, 10-12]. The minimum realistic crack size is defined by the detection limit of available methods of nondestructive inspection. Because the predicted life of a component is extremely dependent on this minimum size, an extensive research and development program has been dedicated to improving the reliable limit of nondestructive inspection of engine components [13]. There has been considerable success in this area, and additional improvements in inspection capability appear certain. As improvements continue, the accurate prediction of the growth of very small cracks will be of increased importance.

Recently, however, a number of investigators have observed that very small fatigue cracks may grow anomalously fast when compared to long cracks in conventional specimens subjected to a nominally equivalent crack driving force. In addition, small cracks have been observed to propagate under conditions that were well below the threshold stress intensity factor range (ΔK_{th}) that exists for long cracks. This "small crack effect" has been discussed at length [14] and extensively reviewed [15-17]. The inability of currently available fracture mechanics methods to predict the behavior of very small cracks has serious implications with regard to the damage tolerant approach, since such errors may lead to a significant overestimate of the actual component life. The anomalous behavior of small cracks has been attributed to a number of factors that include violation of the continuum assumption of solid mechanics, violation of the assumptions of linear elastic fracture mechanics (LEFM), or simply a failure to maintain similitude between the process zones that control the growth of long and short cracks. A number of models of the growth of small cracks have been proposed, and some of the small crack data presented in the literature have been effectively correlated. However, a general understanding of the factors responsible for the rapid growth of small cracks is lacking. As such, the practical crack size limit for the valid application of the available damage tolerant methods is uncertain.

Much of the research devoted to the study of small cracks to date has required relatively specialized methods to acquire experimental data. In general, testing methods that have been commonly used for conventional specimens containing large fatigue cracks have not been readily applicable to the study of small cracks. Although certain specialized optical methods have been used effectively to monitor the initiation and early growth of fatigue cracks [18-21], conventional optical techniques employed in testing of specimens containing large cracks have generally been inadequate to study small crack behavior in an efficient and cost effective manner. A number of alternative methods have been employed. Typically, length measurement of small cracks has been accomplished through the use of acetate replicas, by periodic examination with a scanning electron microscope (SEM), or by electric potential methods. Valuable data have been produced by each of these methods; however, there are disadvantages associated with each. Although replica and SEM methods offer excellent resolution, the use of these methods to track the propagation of very small cracks may be very time consuming, thereby limiting the number of data that can be realistically obtained. The use of electric potential monitoring generally requires an artificial crack starter to initiate the crack at a predetermined location between the electrical potential leads. The physical size of the crack starter defines the lower limit of crack size that can be investigated, and the crack starter may alter the normal mode of crack initiation.

Clearly, the selection of the crack length measurement technique to be used in the study of small cracks depends on the goals of the research. From the perspective of damage tolerance as applied to turbine engine components, experimental methods are needed to efficiently monitor the propagation of "engineering" size cracks initiated and grown under realistic service conditions. As such, the general objective that guided the present effort focused on a desire to study naturally initiated surface cracks of approximate sizes ranging from 25 μm to 2 mm grown under realistic engine service conditions. Data of crack size and crack mouth opening displacement were desired in order to develop a fundamental understanding of the physics and mechanics that pertain to the propagation of small fatigue cracks. This paper discusses the development and application of two techniques that offer promise in this area. Thus far, the research has focused on room temperature testing of titanium alloys; however, each technique has significant potential for elevated temperature application.

EXPERIMENTAL APPROACH

Materials

The size below which a small crack might be expected to exhibit unusually rapid rates of fatigue crack propagation may be approximated by the equation $a_o = (\Delta K_{th}/\Delta\sigma_e)^2/\pi$ [22] where ΔK_{th} is the material's threshold stress intensity factor, and $\Delta\sigma_e$ is the fatigue limit of the material. Using this equation for guidance, two alloys with radically different microstructures and mechanical properties were chosen for investigation. One of the alloys selected, Ti-6Al-2Sn-4Zr-6Mo, was a high strength material having a very fine microstructure, and this material was predicted to display a very limited "small crack effect." The alloy was cast and forged to the shape of circular disks and heat treated to produce a fine duplex microstructure of equiaxed primary α-phase (hexagonal close packed) in a matrix of Widmanstatten α + β (body centered cubic) phase as shown in Fig. 1. The forging and heat treatment procedure produced disks of high strength material (σ_y = yield strength = 1160 MPa; σ_u = ultimate strength = 1230 MPa) that was essentially isotropic as determined by sonic and mechanical testing. This material was ideal for developing and demonstrating the capability of the experimental techniques because its crack growth behavior was well described by linear elastic fracture mechanics for very small cracks.

The second material was a binary titanium alloy containing 7.7% aluminum by weight and having a low oxygen content of 0.065%. This alloy, hereafter referred to as Ti-8Al, was cast and hot rolled into the form of plate approximately 15 mm in thickness. The material was solution heat treated and quenched to produce a microstructure of equiaxed α-phase having an average grain size of 70 μm as shown in Fig. 2. The yield and ultimate strengths of this alloy were 673 and 759 MPa respectively. Based on the calculation of a_o, this material was anticipated to exhibit an exaggerated "small crack effect."

COMPUTERIZED OPTICAL PHOTOMICROSCOPY AS APPLIED TO SMALL CRACKS

All small crack testing was performed using the specimen shown in Fig. 3. This simple geometry, which resembled a design used earlier by Lankford [23], employed a mild notch to initiate surface cracks naturally in a localized field. The elastic stress concentration factor (K_t) due to the notches was originally estimated using handbook tabulations [24], and a subsequent 2-dimensional elastic finite element stress analysis confirmed that K_t = 1.027. Thus, the through-thickness stress was essentially uniform, while the reduced gage section effectively localized crack initiation within a small region that could be conveniently photographed. In order to eliminate surface residual stresses [25] and roughness produced during machining, the gage sections of all specimens were carefully electropolished to a depth of at least 0.20 mm. The electropolishing also produced a highly reflective surface that enhanced the detection and resolution of small surface cracks while highlighting the material's microstructure.

Crack growth data were acquired photographically using a metallurgical microscope mounted with a 35 mm camera having a 250 frame film magazine and powered by a standard motor drive. Fig. 4 shows this setup mounted on a custom built precision three-dimensional translation stage. The film plane magnification was limited to less than 5X in order to obtain a view of the full specimen width. However, it was found that crack initiation could be conveniently detected by periodic visual microscopic examination of a small region of the specimen notch. Thus, a small crack could be initiated, and the subsequent growth of the crack could be photographed at an increased magnification (usually 20 to 40X) which provided improved image resolution. Crack visibility was significantly enhanced through the use of reflected light illumination. Initially, microscope illumination was provided by a continuous lighting source, however, improved image resolution was achieved by lighting with an electronic flash. During testing, fatigue cycling was periodically interrupted, and photographs were taken while the specimen was held at maximum load for a period of approximately one second. Using Kodak Panatomic-X film, photographs were taken with virtually no loss of the microscope's available image resolution [26].

Testing using the photomicroscope was automated using the control system shown schematically in Fig. 5. This system employed an IBM Personal Computer to control all aspects of the testing. By programming a Wavetek 175 function generator, the microcomputer controlled the servo-hydraulic fatigue machine. Camera operation was facilitated by a Tecmar PC-Mate Lab Master digital-to-analog (D/A) converter, and the associated analog-to-digital (A/D) converter was used to provide feedback of fatigue machine performance throughout the test. During each test the microcomputer recorded pertinent data including the photograph frame numbers and the corresponding values of fatigue cycle count. At the conclusion of the test the film was developed, and a standard photographic enlarger was used to project the negative images of the small crack onto a computer digitizing tablet. The projected image magnification (up to approximately 600X) was calibrated using photographs taken of a microscope stage micrometer slide. The digitizing tablet was used to convert the photographs into data of surface crack length (calculated as the length projected onto a plane normal to the axis of loading), and these data were merged with their associated cycle counts to produce a computer file of surface crack length (2c) vs. cycles (N). The shapes of the surface cracks were determined by a heat tinting procedure to be discussed. Using these shapes, the crack growth data were reduced to the form of dc/dN vs. ΔK using the surface crack stress intensity solution of Newman and Raju [27].

Figure 6 presents a photograph of a typical small crack in the alloy Ti-6Al-2Sn-4Zr-6Mo. The resolution of the crack's image was enhanced by photographing the specimen under maximum load. For this alloy, a single small surface crack generally formed and quickly assumed an orientation that was normal to the loading axis. Thereafter, crack growth followed a relatively flat path having a low level of surface roughness. Generally, crack initiation occurred at a location that was well removed from the specimen corner, and the flaw propagated as a surface crack until fracture occurred. In order to determine the shape of the surface cracks, a number of tests were interrupted while the cracks were still short, and the specimens were heated to a temperature not exceeding 400°C to oxidize the crack surface. Upon failure of the specimens, the heat tinted surface cracks were measured to determine their shapes as projected onto a plane normal to the axis of loading. The resulting data of crack depth (a) vs. surface crack half-length (c) are presented in Fig. 7. The cracks were nearly semicircular over the full range of sizes examined and had an average aspect ratio of a/c = 1.03.

Typical crack growth data (c vs. N) obtained with the photomicroscopic system are presented in Fig. 8. These data are for a small crack in the alloy Ti-6Al-2Sn-4Zr-6Mo subjected to fatigue loading under a maximum stress equal to 75% of the material's yield strength. This specimen was tested in room temperature air at a frequency of 20 Hz with a stress ratio (minimum stress/maximum stress) of $R = 0.1$. The 25 μm initial crack length shown for this specimen was a typical detection size for the photomicroscopic system. For this crack size, the standard deviation of carefully repeated measurements of the crack length (c) was approximately 1 μm. This precision was considered excellent, since the value approached the theoretical optical resolution of the microscope. As the crack extended, the increasing level of crack tip plasticity made locating the crack tip more difficult, and the variability in measured crack length increased. As shown in Fig. 8, photographs of the small cracks were taken frequently. This provided a measure of the variation in growth rate as the crack extended, and the large number of data points could be treated statistically to determine the mean crack growth behavior. Thus, it was possible to minimize the influence of the random error associated with the individual crack length measurements. The large amount of data produced by this method was considered to be of particular value, since it was possible to monitor the instantaneous crack growth rate and record any unusual events in the growth of a small crack. Examples of such events are crack bifurcation and crack deflection produced by interactions with alloy microstructure.

The data of Fig. 8 were reduced to the form of dc/dN vs. ΔK, as shown in Fig. 9. The solid curve represents crack growth in conventional compact type (CT) specimens that were 10 mm in thickness. Except for the shortest crack lengths, the data from the small surface crack corresponded closely with the long crack behavior. The growth rates for short and long cracks became essentially equivalent for an approximate surface crack size of c > 75 μm. This transition crack size was in agreement with the independent findings of James and Morris [28] on the same material, who observed that, above this size, LEFM effectively correlated data of the growth of surface cracks. The 75 μm crack size was slightly larger than the value of the short crack correction factor defined by El Haddad et al [22], which was calculated as $a_o = (\Delta K_{th}/\Delta\sigma_e)^2/\pi = 23$ μm, where $\Delta K_{th} = 3.4$ MPa$\sqrt{m}$ and $\Delta\sigma_e = 400$ MPa are the long crack threshold stress intensity factor range and the fatigue limit respectively. The transition crack size was somewhat larger than the size of the two primary microstructural dimensions - the primary α-phase grain size (~5 μm) and the prior β-phase grain size (~15 μm). For all tests performed, the ratio of the size of the plane stress monotonic plastic zone (estimated as $(K/\sigma_y)^2/\pi$) [29, 30] was 0.25 or less, and the similar ratio involving the plane stress cyclic plastic zone (estimated as $(K/2\sigma_y)^2/\pi$) [29] was less than 0.065.

The fine scale of the microstructure of the Ti-6Al-2Sn-4Zr-6Mo, limited crack tip plasticity, and limited tendency for anomalous growth of small cracks under the test conditions investigated provided an ideal demonstration of the capabilities of the photomicroscopic system. The excellent agreement between the data for small surface cracks and long cracks in CT specimens illustrated the accuracy of the experimental and analytical procedures. Having demonstrated its capability, the photomicroscopic system was used to gather data from the second alloy which was anticipated to display a significant "small crack effect."

Data from tests of the Ti-8Al alloy produced results that were markedly different from those found for the Ti-6Al-2Sn-4Zr-6Mo. Typical data of the growth of a small crack in Ti-8Al fatigued under a maximum stress of $0.6\sigma_y$ are presented in Fig. 10. A number of discontinuities in the crack growth curve produced by crack interactions with alloy microstructure are evident. Small cracks in the Ti-8Al generally formed along slip bands that were inclined to the axis of loading and subsequently took on an orientation roughly perpendicular to the loading axis. When the crack growth data were reduced to the from of da/dN vs. ΔK, as shown in Fig. 11, the small cracks propagated rapidly under nominal applied stress intensity levels that were well below the ΔK_{th} obtained in testing of conventional specimens containing long cracks. While the discontinuous nature of crack growth in this alloy produced accentuated variations in crack growth rate, the mean trend of the data was clearly above that of long cracks when correlated with ΔK. As shown, this trend persisted until the half-length of the small surface crack reached $c \approx 1.5$ mm. This length was approximately 20 times the average grain size of the Ti-8Al. As was done previously, estimates were made of the ratio of the size plane stress plastic zone to the crack length. This ratio for the monotonic plastic zone was approximately 0.16, while the ratio involving the cyclic plastic zone was approximately 0.04.

Due to the preliminary nature of the Ti-Al small crack data, it is premature to speculate about the underlying causes of the anomalous small crack behavior in this alloy. However, the failure of the conventional fracture mechanics approach to correlate the behavior of small and large cracks in this material underscores the need for a more complete understanding of the analytical and physical bases for the rapid growth of small cracks. An extensive research program is in progress to study fundamental aspects pertaining to the growth of small cracks in titanium alloys.

COMPLIANCE AND CLOSURE MEASUREMENT FOR SMALL CRACKS

It has often been suggested that the anomalous behavior of small fatigue cracks may be due, at least in part, to differences in the crack closure response for short and long cracks. The general subject of crack closure has recently been reviewed in detail [31]. Essentially, the phenomenon of crack closure may be described as the premature contact of the crack's fracture surfaces during the unloading portion of a fatigue cycle. As a result of crack closure, the tip of a crack that is subjected to a nominal applied stress intensity factor range of $\Delta K = K_{max} - K_{min}$ actually experiences an effective stress intensity factor range, $\Delta K_{eff} = K_{max} - K_{cl}$, where K_{cl} = closure stress intensity factor. During the fatigue cycle the crack remains closed throughout the portion of the cycle for which $K < K_{cl}$, and the crack tip stress intensity factor remains constant at $K = K_{cl}$ until the crack reopens. Crack closure has been shown to be produced by three primary mechanisms associated with fracture surface plasticity [32,33], oxides [34], and fracture surface roughness [35]. The three mechanisms operate simultaneously, and their individual contributions to the total closure process depend on loading conditions, environment, and material.

Since crack closure, as a general phenomenon, operates behind the crack tip, a finite length of closure wake must exist in order to develop the full effect of the mechanism. A crack that grows from a length of zero has no closure wake initially, and the full development of closure is argued to require some finite crack extension. During the period of initial crack extension, the minimum crack tip stress intensity factor increases from K_{min} to K_{cl}, and the stress intensity factor range at the crack tip changes from ΔK to ΔK_{eff}. Newman [36] has used the finite element method to show that such a mechanism can account for the anomalous behavior of small cracks under conditions for which plasticity induced closure is dominant. However, experimental measurement of the closure level of small cracks is extremely difficult, and few data exist.

The experimental determination of crack closure load is generally accomplished by measuring crack opening displacement as a function of applied load. The difficulty in making such measurements on small cracks arises primarily from two sources. The first is the very fine scale of the crack mouth opening displacements (CMOD) that must be measured for small cracks. For a semicircular surface crack that is small relative to the specimen dimensions, the total crack mouth opening displacement is given approximately by the equation [37]

$$\mathrm{CMOD} = 2.892\sigma c/E \qquad (1)$$

where σ is the applied stress, c is the surface crack half-length, and E is Young's modulus. For a surface crack 50 μm long in the alloy Ti-6Al-2Sn-4Zr-6Mo loaded to 60% of the material's yield stress, CMOD ≈ 0.018c ≈ 0.45 μm. In order to determine crack closure from measurements of CMOD vs. applied load, displacement measurements must resolve much less than 0.45 μm.

The second difficulty encountered in making closure measurements for small cracks arises from the need to monitor crack opening displacement at a location very near the crack mouth. This requirement may be appreciated by consideration of St. Venant's Principle which generally states that the stress concentration produced by a mechanical notch becomes negligible as the distance from the notch becomes large with respect to the notch size. Thus, measurements of local displacement in the field of a small crack become insensitive to CMOD as the distance from the crack to the measurement location increases. The importance of this factor was estimated by considering the relationship between elastic compliance and measurement location. Since a general solution to this three-dimensional problem for a surface crack was not available, an estimate was made by performing a two-dimensional finite element analysis for a through-thickness center crack in a panel of finite width. The results are illustrated in Fig. 12 which plots the ratio of crack length (2a) to gage length (2h) vs. normalized compliance. The solid line represents the analytical relationship between crack length and compliance as determined from displacement measurements at the crack mouth ($h \to 0$). The individual data points represent the finite element calculations for $h > 0$. For the uncracked case ($a/h = 0$) the measured compliance corresponds to the modulus of the material alone. As a/h increases, the component of compliance due to the presence of the crack increases and dominates the measurement. Thus, experimental methods that use compliance to monitor the behavior of small cracks must use a very short gage length in order to attain sensitivity to the crack opening. This presents no problem for scanning electron microscopy methods, since these measure CMOD at the fracture surface. However SEM measurements are very time consuming to perform, and the visual/photographic nature of raw data obtained precludes the use of convenient automated data processing methods normally used with compliance measurements. The following discussion describes an alternative experimental approach which we used for determining crack length and closure behavior of very small cracks from compliance measurements. A particular advantage of this approach is the ability to computer automate the process and obtain real time data.

THE INTERFEROMETRIC DISPLACEMENT GAGE

The determination of mouth opening compliance and closure of small fatigue cracks was accomplished using a unique laser interferometric displacement gage (IDG) originally developed by Sharpe [38-41]. Generally, the method utilizes the coherent light of a He-Ne laser to make very precise measurements of mouth opening displacement for a small surface crack. Fig. 13 illustrates the basic principle schematically. A beam of laser light impinges on a pair of Vicker's hardness indentations placed approximately 50 μm apart that span the crack mouth. Each indentation has the shape of a regular four-sided pyramid, and the four pairs of parallel faces of the indentations reflect the laser light to four positions in space. Of the four reflections, the two shown in the figure are used for crack mouth opening displacement measurement. Each of the pairs of reflections interfere optically to produce observable fringe patterns as illustrated. The relationship between a fringe pattern and the gage length, d, separating the indentations is given by the equation

$$n\lambda = d \sin(\alpha_o) \tag{2}$$

where n is the order of the interference fringe, λ is the wavelength of the laser light (0.6328 μm), and α_o (~44°) is the reflection angle shown in the figure. Solving for d and differentiating gives

$$\delta d = \delta n\lambda/\sin(\alpha_o) \approx 0.9\ \mu m \tag{3}$$

for this geometry. Thus, by simply counting the fringes that pass a fixed point in space, displacements between the indentations can be resolved to approximately 0.9 μm.

Improved displacement resolution may be attained by monitoring fractional motion of the interference fringes. This was accomplished using the system illustrated schematically in Fig. 14. The system employed servo-controlled rotating mirrors to sweep the fringe patterns across the photodetectors located at α_o. This allowed the system to monitor the fringe pattern as a function of time (indentation displacement), and real time numerical determination of the fringe position was performed by a Digital Equipment Corporation 1124 minicomputer. The procedure could locate the interference fringe position to within approximately 0.01 of the fringe wavelength, and this corresponded to a measurement precision for displacement between the indentations of $\delta d \approx 9$ nm. This precision was approximately equivalent to the resolution of scanning electron microscopy, and the numerical nature of the data produced by the interferometric system made this method more efficient and potentially much more accurate than SEM methods.

CRACK OPENING DISPLACEMENT MEASUREMENTS

The capability of the interferometric system was demonstrated on a small surface crack in the alloy Ti-6Al-2Sn-4Zr-6Mo. The specimen geometry and its preparation were the same as that discussed earlier for the photomicroscopic system. A small precrack was initiated under fully reversed loading ($R = -1.0$; $\sigma_{max} = 0.6\ \sigma_y$; frequency = 20 Hz) and detected visually. The specimen was removed from the testing machine in order to place the Vicker's hardness indentations across the crack. Subsequently, the specimen was replaced in the testing machine, and crack opening displacement measurements were performed periodically as the crack was extended under constant load amplitude tension-tension fatigue ($R = 0.1$). The crack opening displacement measurements were obtained by interrupting the sinusoidal fatigue cycling to apply a low frequency (0.025 Hz) loading cycle having a triangular waveform. During this cycle, 280 load vs. displacement measurements were made. Typical data are presented in Fig. 15 for a small surface crack of half-length c = 37 μm. The total crack mouth opening displacement measured under maximum load was approximately 0.5 μm, and the much higher precision of the individual displacement measurements is evident. The data corresponded to a complete fatigue cycle. Little hysteresis in the measurements made during the cycle is observed. The effective size of the small crack was calculated from the elastic compliance determined from the slope of the upper linear region of the data. The crack closure load (P_{cl}) was determined from the break in the load vs. displacement curve as illustrated. For the data shown, crack closure occurred at approximately 57% of the maximum load.

The crack mouth opening compliance was measured at numerous crack lengths throughout the test. These data are plotted against optically measured surface crack half-length in Fig. 16. The experimental data corresponded closely to the solid line which represents the analytical relationship given in equation 1 for a semicircular surface crack. The excellent correlation between the experimental data and the analytical expression indicates that the interferometric compliance measurement may be used to determine the effective length of small surface cracks. In fact, much of the variation in the data presented is believed to be due to the error associated with the optical measurements which were made using a long focusing microscope mounted with a filar eyepiece. The optical resolution of this microscope was inferior to that of the more conventional optics used in the photomicroscopic system. However, the physical geometry of the interferometric system precluded direct access to the specimen, and optical measurements were made by mounting the long focusing microscope to the side of the specimen and using a mirror arrangement to view the crack. In the future, it should be possible to replace the long focusing microscope with the photomicroscopic system. However, unless a permanent record of the incremental crack extension is desired, the optical data would be required only to periodically confirm the accuracy of the compliance determined crack length.

As discussed, crack closure measurements were made from the load-displacements curves obtained as the crack extended. These data are presented as a function of crack length in Fig. 17. Data were obtained for surface crack lengths of 2c = 58 μm and greater. Over this range in crack size, the greatest crack closure was recorded for the shortest crack lengths, and the measured closure load approached the minimum applied load as the crack extended. The closure measurements varied significantly for 2c ≤ 200 μm and became more consistent as the crack extended. The behavior of the crack closure data may be more easily examined when replotted as a function of fatigue cycle count as shown in Fig. 18. The level of crack closure is observed to change abruptly three times, with the most obvious change occurring at the approximate midpoint of the test (27000 cycles). Although, to the author's knowledge, this behavior has not been previously reported, the data are believed to be accurate. The discontinuous change in crack closure level that occurred at this point in the test corresponded exactly to a bifurcation of one of the two visible tips of the surface crack. During the same period the crack length increased continuously (as independently determined by optical measurement of the longest branch and by compliance measurement). It is speculated that the change in closure load was the result of the creation of a major feature on the fracture surface which produced an abrupt change in the level of roughness induced closure. If this is true, then it is likely that the changes in closure level that were observed earlier in the test (at 4800 and 11000 cycles) also corresponded to the creation of dominant features on the fracture surface. Note that the closure level only increased abruptly; it never decreased in this fashion.

As shown in Fig. 19, the crack growth rate data generated during the test corresponded closely to data obtained from tests of long cracks in conventional specimens fatigued under equivalent conditions. The small crack data presented were obtained from optical measurements, although the data taken from compliance measurements were essentially the same. The data did not display the "small crack effect." The lack of this behavior may have been the result of the reduced stress level ($\sigma_{max} = 0.6\,\sigma_y$) for these data as compared to the data of Fig. 9 where $\sigma_{max} = 0.75\,\sigma_y$. However, additional research is required to resolve this issue.

In general the interferometric system demonstrated a unique capability for making crack opening displacement measurements of small fatigue cracks. The very short gage length and extreme measurement precision that are characteristic of the interferometric technique offer potential for novel research of the mechanisms that control the growth of small cracks. Crack length and crack closure data can be acquired as a small crack extends, and the natural development of the steady state crack growth process can be monitored. Crack closure data such as those presented have previously been difficult or impossible to obtain. The computerized interferometric system can acquire and analyze these data extremely efficiently and quickly. By combining the photomicroscopic and interferometric systems on a single test, fundamental study of fatigue mechanisms and mechanics of small cracks can be performed. Additional research is in progress to fully utilize the unique capabilities of both experimental methods to investigate the basic nature of small cracks.

SUMMARY AND CONCLUSIONS

The development and application of two experimental methods for monitoring the behavior of very small fatigue cracks were discussed. The first of these was an automated photomicroscopic system which recorded crack propagation directly. The second method employed laser interferometry to monitor crack mouth opening displacements which were analyzed to determine crack length and crack closure behavior. All small crack tests were performed using a specimen that allowed natural crack initiation to be localized within a small region. In the photomicroscopic method, a 35 mm camera mounted on a reflected light microscope was used to record the growth of small surface cracks of approximate sizes ranging from 25 μm to 2 mm. The system employed a microcomputer to control fatigue crack growth testing, operate the camera, and record pertinent data. Upon completion of a test, the photographs of the small cracks were projected onto a computer digitizing tablet which was used to obtain numerical crack length data. The capabilities of the photomicroscopic system were demonstrated in testing of the high strength titanium alloy Ti-6Al-2Sn-4Zr-6Mo. The measurement precision of the complete system was found to be approximately 1 μm for cracks of the order of 25 μm in length. For the Ti-6Al-2Sn-4Zr-6Mo, the data of small and large cracks were well correlated with the applied stress intensity factor range, ΔK, for all but the very smallest cracks. However, ΔK failed to consolidate similar crack growth data in a Ti-8Al alloy. Small crack growth in this material was much faster than equivalent long crack data, and the small crack growth occurred under loading conditions that were well below the long crack threshold stress intensity factor range, ΔK_{th}. The rapid growth of small cracks in this material persisted for total crack lengths as great as 3 mm. In general, the photomicroscopic system provided an efficient and cost effective method for monitoring the growth of small, naturally occurring fatigue cracks. A particular advantage of this method is the creation of a detailed permanent record of crack growth which includes information of crack path and microstructural interaction.

The second experimental method used a computerized interferometric displacement gage (IDG) to monitor the crack mouth opening behavior of small fatigue cracks. This method provided very precise measurements of crack mouth opening displacements as a function of applied load, and these data were analyzed to determine effective crack length and crack closure load. Complete load vs. displacement curves were obtained for naturally initiated surface cracks of total length less than 60 μm. For a crack of this size, the maximum crack mouth opening displacement was less than 0.5 μm. The precision of the displacement measurements was of the order of 10 nm, and this provided excellent definition of the load vs. mouth opening displacement behavior for small cracks. Both crack length and crack closure load were easily determined from the data. An excellent correlation between crack mouth opening compliance and surface crack length was demonstrated, and these data were shown to agree with an analytical expression for part-through surface cracks. As a result, it was suggested that the interferometric displacement gage might be used to obtain the effective length of small cracks in real time testing. Crack closure measurements obtained for a small crack suggested that closure develops discontinuously as the crack extends initially. This behavior was speculated to result from the formation of individual features on the fracture surface. At this time the data are preliminary, and further research is in progress to examine small crack phenomena. In general, the interferometric method proved to be remarkably effective for determining both crack length and crack closure behavior of very small fatigue cracks.

REFERENCES

1. J.A. Harris, Jr., D.L. Sims, and C.G. Annis, Jr., "Concept Definition: Retirement for Cause of F100 Rotor Components," Air Force Wright Aeronautical Laboratories Report AFWAL-TR-80-4118, Wright-Patterson Air Force Base OH, 1980.

2. United States Air Force, "Engine Structural Integrity Program," Military Standard 1783, Aeronautical Systems Division, Wright-Patterson Air Force Base OH, 1984.

3. W.H. Reimann and W.D. Cowie, "Damage Tolerant Design Concepts for Military Engines," in this publication, 1985.

4. C.G. Annis, Jr., R.M. Wallace, and D.L. Sims, Pratt and Whitney Aircraft, "An Interpolative Model for Elevated Temperature Fatigue Crack Propagation," Air Force Materials Laboratory Report AFML-TR-76-176, Part I, Wright-Patterson Air Force Base OH, 1976.

5. R.M. Wallace, C.G. Annis, Jr., and D.L. Sims, Pratt and Whitney Aircraft, "Application of Fracture Mechanics at Elevated Temperature," Air Force Materials Laboratory Report AFML-TR-76-176, Part II, Wright-Patterson Air Force Base OH, 1976.

6. D.L. Sims, C.G. Annis, Jr., and R.M. Wallace, Pratt and Whitney Aircraft, "Cumulative Damage Fracture Mechanics at Elevated Temperature," Air Force Materials Laboratory Report AFML-TR-76-176, Part III, Wright-Patterson Air Force Base OH, 1976.

7. J.M. Larsen, B.J. Schwartz, and C.G. Annis, Jr., Pratt and Whitney Aircraft, "Cumulative Damage Fracture Mechanics Under Engine Spectra," Air Force Materials Laboratory Report AFML-TR-79-4159, Wright-Patterson Air Force Base OH, 1979.

8. D.A. Utah, General Electric Co., "Crack Growth Modeling in an Advanced Powder Metallurgy Alloy," Air Force Wright Aeronautical Laboratories Report AFWAL-TR-80-4098, Wright-Patterson Air Force Base OH, 1980.

9. J.M. Larsen and T. Nicholas, "Cumulative Damage Modeling of Fatigue Crack Growth," Engine Cyclic Durability by Analysis and Testing, Proceedings of the 63rd Meeting of the AGARD Propulsion and Energetics Panel, AGARD Conference Proceedings No. 368, NATO Advisory Group for Aerospace Research and Development, 1984, pp. 9.1-9.15.

10. C.H. Cook, H.E. Johnson, and C.E. Spaeth, Pratt and Whitney Aircraft, "Damage Tolerant Design for Cold Section Turbine Engine Disks," Air Force Wright Aeronautical Laboratories Report AFWAL-TR-81-2045, Wright-Patterson Air Force Base OH, 1981.

11. J.H. Adams, M. Doner, and D.L. Vaccari, Detroit Diesel Allison Co., "Turbine Engine Structural Life Prediction/Correlation," Air Force Wright Aeronautical Laboratories Report AFWAL-TR-82-2116, Part 1, Wright-Patterson Air Force Base OH, 1982.

12. J. Walcher, D. Gray, and J. Pratl, Teledyne Corp., "Structural Life Prediction/Correlation Program," Air Force Aero Propulsion Laboratory Report AFAPL-TR-82-2027, Vol. 1, Wright-Patterson Air Force Base OH, 1982.

13. D.L. Birx and F.M. Taylor, "Manufacturing Technology for a Nondestructive Evaluation (NDE) System to Implement Retirement for Cause (RFC) Procedures for Gas Turbine Engine Components," in this publication, 1985.

14. Behavior of Short Cracks in Airframe Components, Proceedings of the 55th meeting of the AGARD Structures and Materials Panel, AGARD Conference Proceedings No. 328, NATO Advisory Group for Aerospace Research and Development, 1982.

15. S.J. Hudak, Jr., "Small Crack Behavior and the Prediction of Fatigue Life," Journal of Engineering Materials and Technology, Transactions of the ASME, Vol. 10, 1981, pp. 26-35.

16. S. Suresh and R.O. Ritchie, "Propagation of Short Fatigue Cracks," International Metals Review, Vol. 29, 1984, pp. 445-476.

17. B.N. Leis, M.F. Kanninen, A.T. Hopper, J. Ahmad, and D. Broek, "A Critical Review of the Short Crack Problem in Fatigue," Air Force Wright Aeronautical Laboratories Report AFWAL-TR-83-4019, Wright-Patterson Air Force Base OH, 1983.

18. R. Papirno and B.S. Parker, "An Automatic Flash Photomicroscopic System for Fatigue Crack Initiation Studies," Cyclic Stress-Strain Behavior-Analysis, Experimentation and Failure Prediction, ASTM STP 519, American Society for Testing and Materials, 1973, pp. 98-108.

19. J. Lankford, T.S. Cook, and G.P. Sheldon, "Growth of Small Fatigue Cracks at High Temperatures," Advances in Fracture Research, ICF-5, D. Francois, et al., Ed., Pergamon Press, 1980, pp. 2449-2456.

20. Y.H. Kim, T. Mura, and M.E. Fine, "Fatigue Crack Initiation and Microcrack Growth in 4140 Steel," Metallurgical Transactions, Vol. 9A, 1978, pp. 1679-1683.

21. C.Y. Kung, and M.E. Fine, "Fatigue Crack Initiation and Microcrack Growth in 2024-T4 and 2124-T4 Aluminum Alloys," Metallurgical Transactions, Vol. 10A, 1979, pp. 603-610.

22. M.L. El Haddad, K.N. Smith, and T.H. Topper, "Fatigue Crack Propagation of Short Cracks," Journal of Engineering Materials and Technology, Transactions of the ASME, Vol. 101, 1979, pp. 42-46.

23. J. Lankford, "The Growth of Small Fatigue Cracks in 7075-T6 Aluminum," Fatigue of Engineering Materials and Structures, Vol. 5, 1982, pp. 233-248.

24. R.E. Peterson, Stress Concentration Factors, Wiley Co., 1974, p. 37.

25. W.J. Pardee, W.F. Morris, and R.C. Addison, "Quantitative Nondestructive Evaluation (NDE) for Retirement-for-Cause," Annual Technical Report No. 1 on Defense Advanced Research Projects Agency Contract No. MDA903-80-C-0641, Rockwell International Science Center, Thousand Oaks, CA, 1981, p. 9.

26. Eastman Kodak Co., Kodak Professional Black-and-White Films, Second Addition, Eastman Kodak Co., 1976.

27. J.C. Newman, Jr., and I.S. Raju, "Stress-Intensity Factor Equations for Cracks in Three-Dimensional Finite Bodies," Fracture Mechanics: Fourteenth Symposium - Volume I: Theory and Analysis, ASTM STP 791, J.C. Lewis and G. Sines, Eds., American Society for Testing and Materials, 1983, pp. I-238-I-265.

28. M.R. James and W.L. Morris, "Effect of Fracture Surface Roughness on Growth of Short Fatigue Cracks," Metallurgical Transactions, Vol. 14A, 1983, pp. 153-155.

29. J.R. Rice, "Mechanics of Crack Tip Deformation and Extension by Fatigue," Fatigue Crack Propagation, ASTM STP 415, American Society for Testing and Materials, 1967, pp. 247-309.

30. D. Broek, Elementary Engineering Fracture Mechanics, Martinus Nijhoff Publishers, 1984, pp. 91-93.

31. S. Banerjee, "A Review of Crack Closure," Air Force Wright Aeronautical Laboratories Report AFWAL-TR-84-4031, Wright-Patterson Air Force Base OH, 1984.

32. W. Elber, "Fatigue Crack Closure Under Cyclic Tension," Engineering Fracture Mechanics, Vol. 2, 1970, pp. 37-45.

33. W. Elber, "The Significance of Fatigue Crack Closure," Damage Tolerance in Aircraft Structures, ASTM STP 486, American Society for Testing and Materials, 1971, pp. 230-242.

34. R.O. Ritchie, S. Suresh, and C.M. Moss, "Near-Threshold Fatigue Crack Growth in 2 1/4Cr-1Mo Pressure Vessel Steel in Air and Hydrogen," Journal of Engineering Materials and Technology, Transactions of the ASME, Vol. 102, 1980, pp. 293-299.

35. N. Walker and C.J. Beevers, "A Fatigue Crack Closure Mechanism in Titanium," Fatigue of Engineering Materials and Structures, Vol. 1, 1979, pp. 135-148.

36. J.C. Newman, Jr., "A Nonlinear Fracture Mechanics Approach to the Growth of Small Cracks," 55th Meeting of the AGARD Structures and Materials Panel on "Behavior of Short Cracks in Airframe Components," AGARD Conference Proceedings No. 328, NATO Advisory Group for Aerospace Research and Development, 1982, pp. 6.1-6.26.

37. C. Mattheck, P. Morawietz, and D. Munz, "Stress Intensity Factor at the Surface and Deepest Point of a Semi-Elliptical Surface Crack in Plates Under Stress Gradients," International Journal of Fracture, Vol. 23, 1983, pp. 201-212.

38. W.N. Sharpe, Jr., "Interferometric Surface Strain Measurement," International Journal of Nondestructive Testing, 1971, pp. 59-76.

39. D.E. Macha, W.N. Sharpe, Jr., and A.F. Grandt, Jr., "A Laser Interferometry Method for Experimental Stress Intensity Factor Calibration," Cracks and Fracture, ASTM STP 601, American Society for Testing and Materials, 1976, pp. 490-505.

40. W.N. Sharpe, Jr. and D.R. Martin, "An Optical Gage for Strain/Displacement Measurement at High Temperature Near Fatigue Crack Tips," Air Force Materials Laboratory Report AFML-TR-77-153, Wright-Patterson Air Force Base OH, 1977.

41. W.N. Sharpe, Jr., "A New Optical Technique for Rapid Determination of Creep and Fatigue Thresholds at High Temperature," Air Force Wright Aeronautical Laboratories Report AFWAL-TR-84-4028, Wright-Patterson Air Force Base OH, 1984.

ACKNOWLEDGMENTS

This research was performed under Materials Laboratory in-house research project number 2307P102, Air Force Wright Aeronautical Laboratories (AFWAL), Wright-Patterson Air Force Base, OH. The author wishes to acknowledge the helpful discussions of Dr. T. Nicholas of the Materials Laboratory and Dean J.C. Williams and Professor A.W. Thompson of Carnegie-Mellon University, Pittsburgh, PA. Grateful acknowledgement is also extended to Dr. A.M. Rajendran of the University of Dayton Research Institute (UDRI), Dayton, OH who performed the finite element stress analysis of the small crack specimen shown in Fig. 3 and to Capt. M. Bohun (AFWAL Materials Laboratory) who obtained the finite element results presented in Fig. 12. The efforts of J. Jira, Lt. R. Sincavage (both of the AFWAL Materials Laboratory), and Dr. T. Weerasooriya (UDRI) in developing and applying the interferometric displacement gage to monitor small cracks are deeply appreciated. The author's contribution to the research discussed in this paper was performed as partial fulfillment of the requirements for the degree Doctor of Philosophy in Metallurgical Engineering and Materials Science at Carnegie-Mellon University.

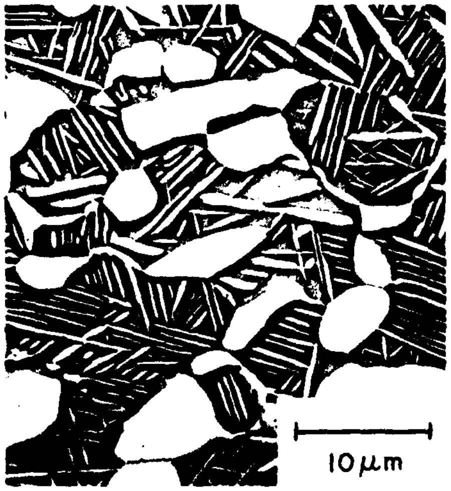

Fig. 1. Microstructure of the alloy Ti-6Al-2Sn-4Zr-6Mo.

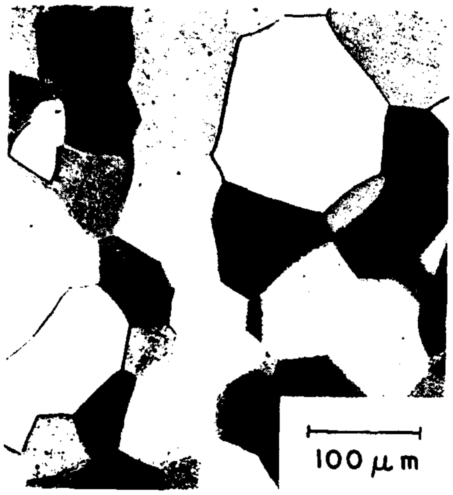

Fig. 2. Microstructure of the alloy Ti-8Al.

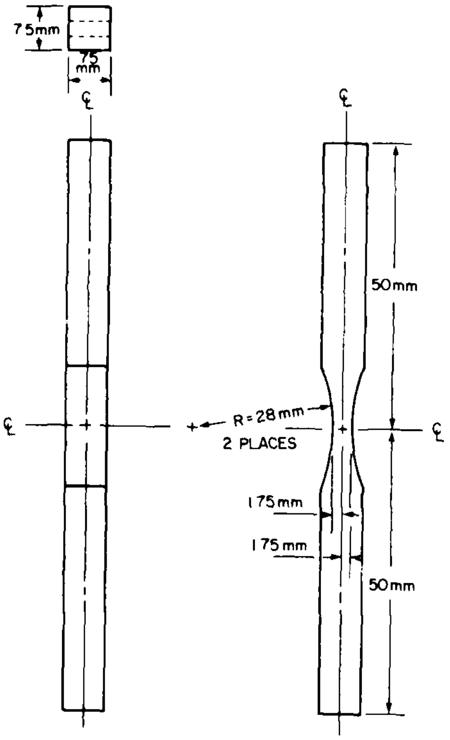
75mm
75 mm
℄
℄
℄
℄
50mm
R=28mm
2 PLACES
175mm
175mm
50mm

Fig. 3. Fatigue specimen used for small crack testing.

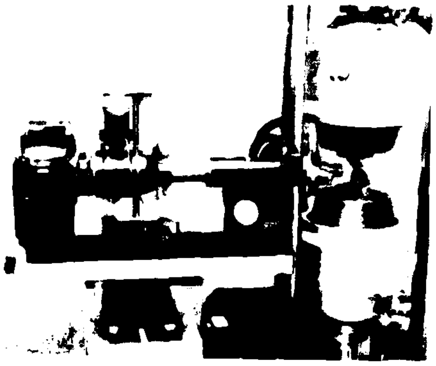

Fig. 4. Photomicroscope and small crack specimen.

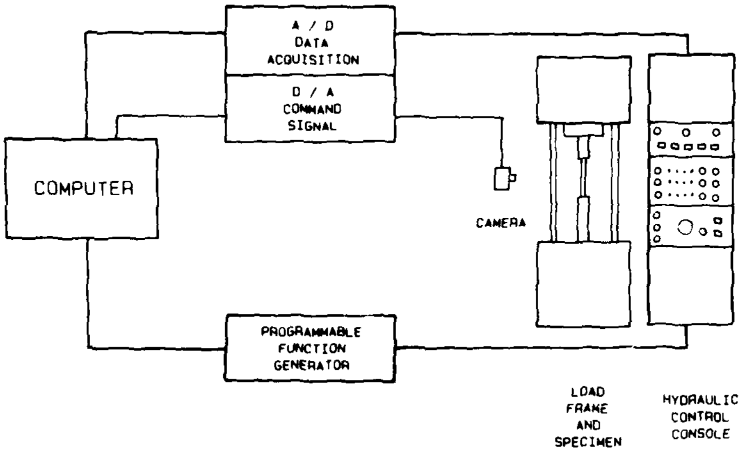
A / D
DATA
ACQUISITION
D / A
COMMAND
SIGNAL
COMPUTER
CAMERA
PROGRAMMABLE
FUNCTION
GENERATOR
LOAD
FRAME
AND
SPECIMEN
HYDRAULIC
CONTROL
CONSOLE

Fig. 5. Schematic illustration of the photomicroscopic testing system.

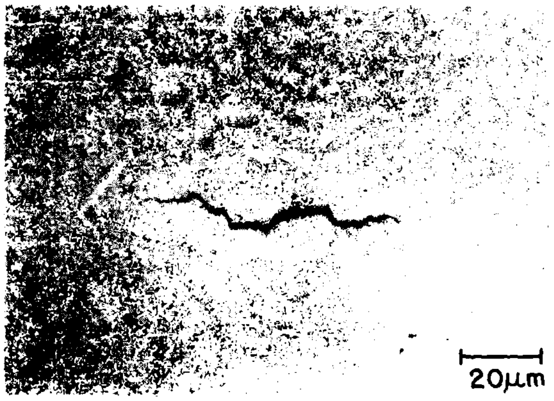

Fig. 6. Typical photograph of a small fatigue surface crack in the alloy Ti-6Al-2Sn-4Zr-6Mo.

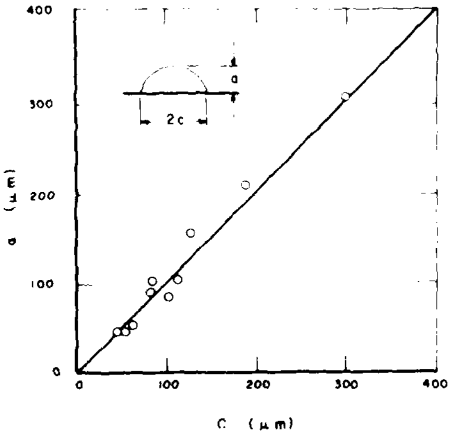

Fig. 7. Data of crack depth (a) vs. crack half-length (c) for small cracks of various sizes in Ti-6Al-2Sn-4Zr-6Mo.

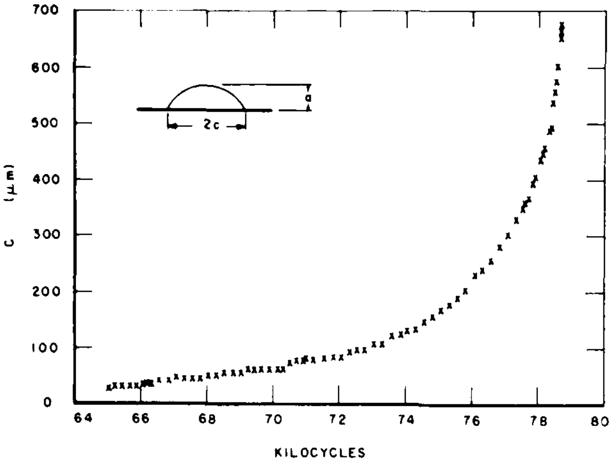

Fig. 8. Crack growth data for a small surface crack in the alloy Ti-6Al-2Sn-4Zr-6Mo.

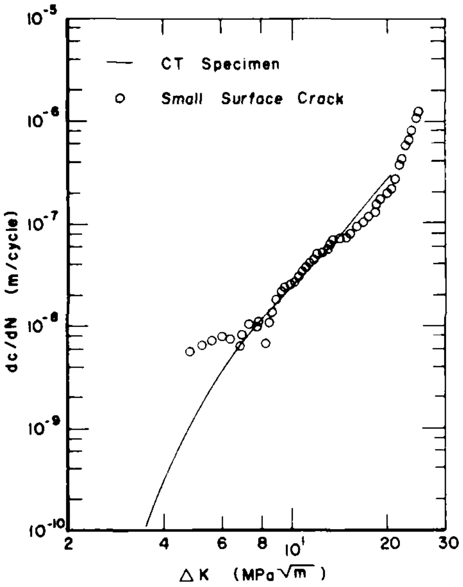

Fig. 9. Crack growth rate data for a small surface crack and more conventional long cracks grown in the alloy Ti-6Al-2Sn-4Zr-6Mo.

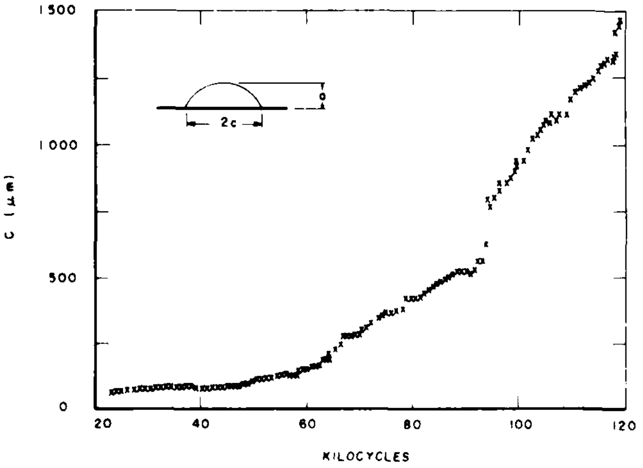

Fig. 10. Crack growth data for a small crack in the alloy Ti-8Al.

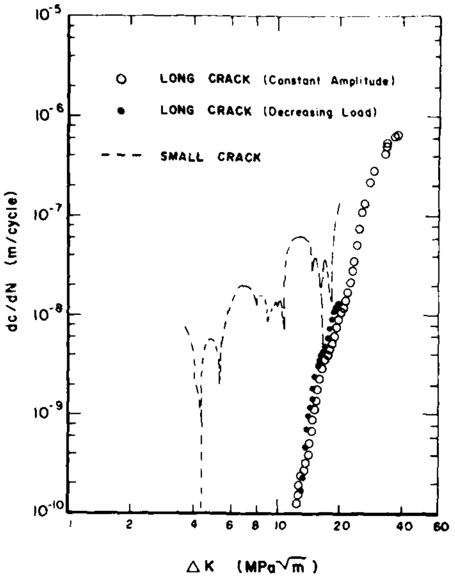

Fig. 11. Crack growth rate data for a small surface crack and more conventional long cracks grown in the alloy Ti-8Al.

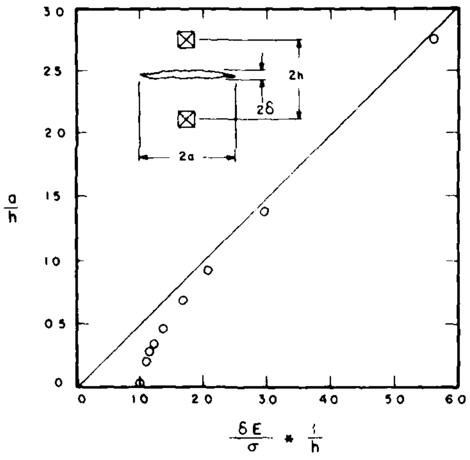

Fig. 12. Data illustrating the relationship between crack length (a) and normalized compliance ($\delta E/\sigma$). The data points illustrate the dependence of this relationship on the ratio of crack length to gage length (a/h). The solid line corresponds to the analytical relationship between crack length and compliance for $h \to 0$.

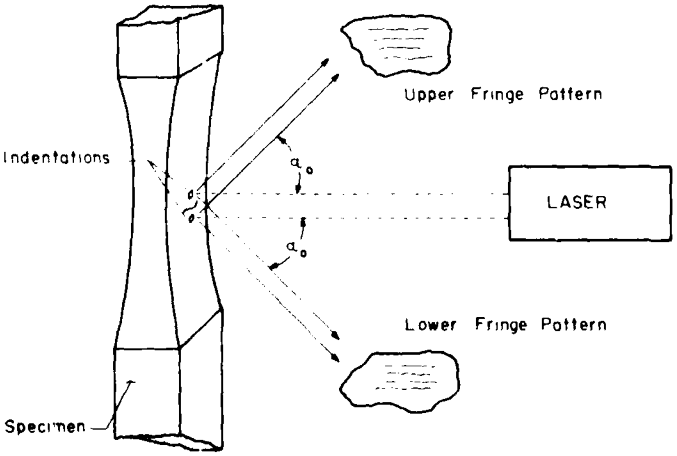
Upper Fringe Pattern
Indentations
α_0
LASER
α_0
Lower Fringe Pattern
Specimen

Fig. 13. Schematic illustration of the principle of operation of the interferometric displacement gage.

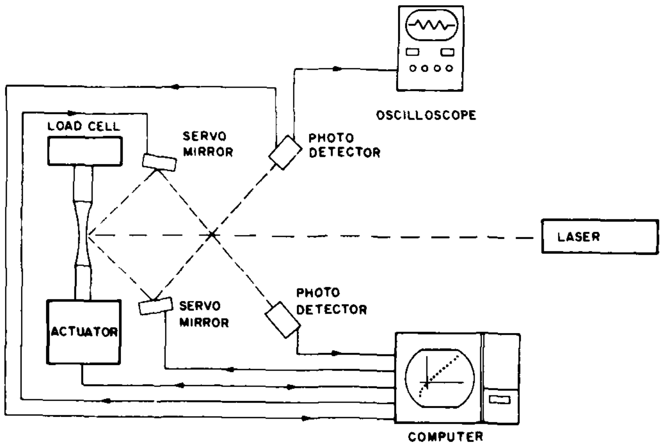
OSCILLOSCOPE
LOAD CELL
SERVO MIRROR
PHOTO DETECTOR
LASER
ACTUATOR
SERVO MIRROR
PHOTO DETECTOR
COMPUTER

Fig. 14. Schematic illustration of the computerized interferometric system.

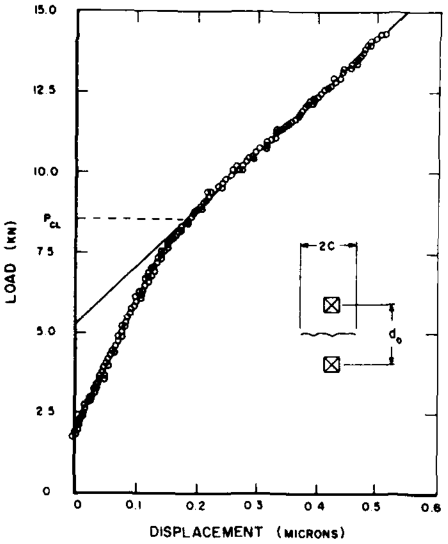

Fig. 15. Typical load vs. crack mouth opening displacement data for a small surface crack (c = 37 μm; d_o = 48 μm). The solid line corresponds to crack opening compliance, and the crack closure load (P_{CL}) is illustrated.

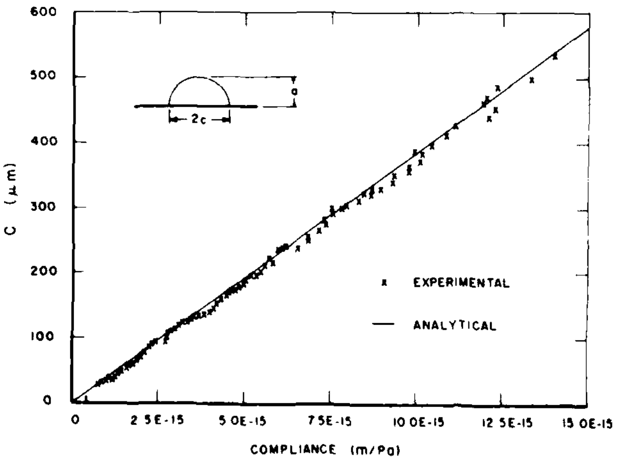

Fig. 16. Crack length vs. compliance data for a small surface crack in the alloy Ti-6Al-2Sn-4Zr-6Mo.

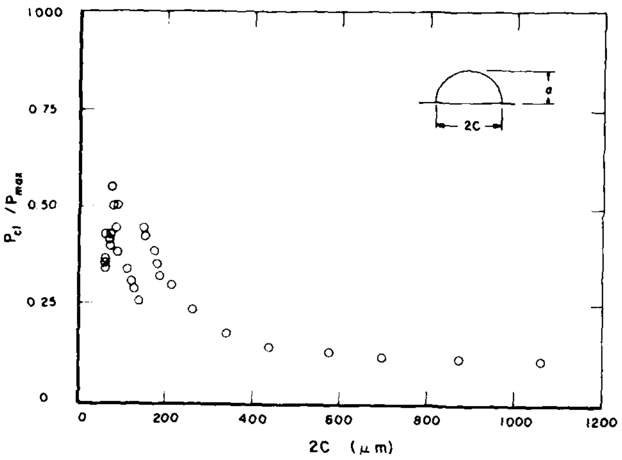

Fig. 17. Data of normalized crack closure load vs. crack length for a small crack.

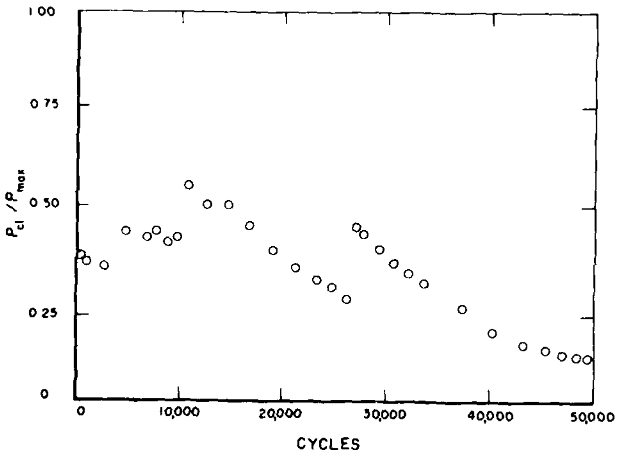

Fig. 18. Data of normalized crack closure load vs. the number of fatigue cycles applied to propagate a small crack.

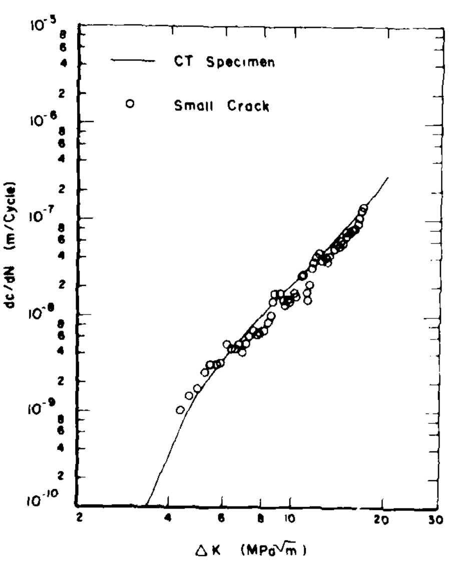

Fig. 19. Crack growth rate data corresponding to the data presented in Figs. 15-19.

MULTIAXIAL AND THERMOMECHANICAL FATIGUE CONSIDERATIONS IN DAMAGE TOLERANT DESIGN

by

Gail E. Leese
TRW, Aircraft Components Group
23555 Euclid Ave.
Cleveland, Ohio 44117
and
Robert C. Bill
U. S. Army R&T Labs. (AVSCOM)
NASA Lewis Research Center
21000 Brookpark Road
Cleveland, Ohio 44135

SUMMARY

In considering damage tolerant design concepts for gas turbine hot section components, several challenging concerns arise: Complex multiaxial loading situations are encountered; Thermomechanical fatigue loading involving very wide temperature ranges is imposed on components; Some hot section materials are extremely anisotropic; and coatings and environmental interactions play an important role in crack initiation and crack propagation. In this paper the effects of multiaxiality and thermomechanical fatigue are considered from the standpoint of their impact on damage tolerant design concepts. Recently obtained research results as well as results from the open literature are examined and their implications for damage tolerant design are discussed. Three important needs required to advance analytical capabilities in support of damage tolerant design become readily apparent: (1) a theoretical basis to account for the effect of non-proportional loading; (2) the development of practical crack growth parameters that are applicable to thermomechanical fatigue situations; (3) the development of crack growth models that address multiple crack failures.

INTRODUCTION

The demands for increased service reliability and reduced life cycle costs of aerospace structural components has stimulated the development and application of damage tolerant design concepts to component design. Damage tolerant design procedures are based on the assumed existence of a critically located flaw when the component enters service. The size of the assumed flaw is defined by the sensitivity and reliability of available NDT procedures that can be brought to bear at the critical location. A crack propagation analysis, based on loading representative of the mission profile, is then undertaken to determine the time required for the assumed flaw to grow from a size just below the threshold of detectability to criticality. A "safe fraction" of this time is used to define either an inspection interval or service life, depending on the component retirement philosophy.

Damage tolerant design concepts have been applied to airframe components, at least to the extent that fracture mechanics analyses have been employed [1]. However, engine components, in particular hot section parts, have generally been designed on the basis of crack initiation life using available LCF life prediction procedures. For purposes of providing enhanced engine durability, the military is presently interested in damage tolerant design concepts for engine critical components.

The Air Force has developed a programmed methodology to improve the structural integrity of its engines [2]. This methodology includes consideration of the entire engine life cycle from design inception through scheduled maintenance and finally retirement practices. A key element of this program is the incorporation of damage tolerant concepts in the engine design, combined with mission oriented testing directed toward the identified critical components. However, some special challenges arise when one considers applying damage tolerant design concepts to engine hot section components where complex multiaxial loading, material anisotropy, thermomechanical loading, and time dependent effects are commonly encountered.

The objective of this paper is to examine the effects of multiaxial loading and combined thermal and mechanical (henceforth thermomechanical fatigue - TMF) loading on crack initiation and cyclic crack propagation. These effects will be considered from the standpoint of their impact on damage tolerant design methods. Further, it is the objective of this paper to identify areas of research that will either extend the capabilities of crack growth analysis, or permit the reliable application of uniaxial, isothermal based analyses to more complex situations.

MULTIAXIAL FATIGUE

In the laboratory, multiaxial mechanical testing implies an excursion from traditional tensile or uniaxial fatigue tests, where 2 of the 3 principal stresses are zero. Biaxial fatigue testing is typically performed via combined tension and torsion cyclic loading on smooth round specimens. Such loading can be proportional (in-phase) such that the maximum and minimum loads of each cycle occur simultaneously or non-proportional (out-of-phase), such that a controlled phase difference exits between the two loads, resulting in hanging directions of principal stress throughout the cycle as illustrated in Figure 1. In addition to multiaxial stress states produced mechanically, thermal cycles may be applied producing in-phase or out-of-phase strains with respect to the mechanical profile.

The pertinence of such research in aircraft gas turbine engines is becoming more obvious as structural analysis techniques improve the description of the multiaxial stress states of hot path components. In recent NASA sponsored research [3] the biaxial stress state in a disk bore that would evolve from a realistic, simulated mission was presented as a complex spectrum of non-proportional, variable amplitude tangential and axial stresses. (See Figure 2.) In that same report it's suggested that vanes and combustor liners are likely to experience equally complex loading profiles. Frequently the non-proportional characteristics of such loading profiles results from the superposition of mechanical and thermal loads. Hence how to deal with multiaxial loading environments, as well as how to incorporate these solutions into design concepts such as damage tolerance, are relevant topics to existing engineering needs in the aeronautics and aerospace industries.

Applicability of Uniaxial Results

Many investigators have targeted their research towards the development and demonstration of ways of using existing uniaxial materials properties and response for the resolution of multiaxial problems. The most straightforward biaxial laboratory test germane to this effort is an isothermal constant amplitude torsion test. In this case the extrapolation of uniaxial fatigue strain-life properties to the biaxial stress state is frequently made by altering the power law strain-life relationships using conventional techniques. The axial representation of total strain-life law is [4,5,6]:

$$\Delta\epsilon_t = 2\epsilon'_f\ (2N_f)^{-c} + 2\sigma_f/E\ \ (2N_f)^{-b}$$

Where σ_f is the ultimate tensile strength, E the Young's Modulus, N_f the cyclic life, ϵ'_f is the fatigue ductility, and $\Delta\epsilon_t$ the total strain range.

The fatigue ductility and strength exponents, c and b, have been shown to be stress state independent at room temperature for several materials in these simple loading cases [7,8] and are therefore usually assumed to be constant. Some form of effective or equivalent criteria (such as von Mises or Tresca) is then used to modify the ductility and strength coefficients for the stress state of interest. (See Figure 3.) This approach is often adequate for the projection of fatigue properties in a simple stress state from another simple stress state.

However, in more complicated profiles that actually describe realistic component histories, including mean stresses, variable amplitude and non-proportional thermal and mechanical loading, there is no obvious way to extrapolate axial fatigue properties to the multiaxial environment. Indeed, the very accuracy of such an approach would be questionable for several reasons. Recent investigations have shown that non-proportionality as well as sequence effects of variable amplitude biaxial loading affect the cyclic strength ductility, as well as the cyclic strain hardening exponent [9,10]. Also, the actual modes of failure may vary with the bulk stress state applied, greatly reducing the physical basis on which one would justify such methodology.

Multiaxial Crack Propagation

Biaxial loading (primarily tension/torsion) of laboratory specimens in strain control has shown that the resulting damage states can be classified into 2 categories [7,11]:

1. Multiple crack systems, showing complex behavior of mixed mode growth and crack interactions, typically occurring in high strain, low cycle conditions.
2. Single dominant crack initiation and growth, characteristic of low strain, high cycle conditions.

These same trends have been observed in axial loading [11, 12], but due to recent advances in multiaxial testing capabilities, it has become apparent that they're greatly accentuated in multiaxial conditions, and cannot be overlooked as being merely of academic interest.

The multiple crack system response observed in high strain biaxial conditions is most interesting due to the complexity of the phenomenon, and due to the engineering implications in situations where finite life prediction is necessary. Testing laboratory specimens in torsion and combined tension/torsion promotes the initiation of cracks on planes of maximum shear stress at multiple sites on the surface. Early cracks form throughout the test section, grow to a size small in comparison to the specimen geometry, after which the growth is arrested while additional small cracks continue to start the same process. These cracks will grow along the specimen surface in planar shear, some linking with others until the resultant fissures are quite large relative to the specimen dimensions. Upon linking and growing in length on the surface, these cracks will eventually propagate through the thickness of the specimen in anti-plane shear, a mode of crack propagation quite different in terms of crack growth rate and critical crack lengths from that of surface crack propagation. It is this through thickness propagation that causes rapid degradation of the load carrying capability of a specimen.

Figure 4 shows this multiple cracking phenomenon in replicas of Waspaloy tested in torsion at room temperature. Similar modes of cracking have been reported with Hastelloy X.

These observations of multiple crack systems aren't peculiar to disk superalloys, and therefore have implications beyond the immediate application to disk materials. In Figure 5, similar multiple cracking patterns, observed early in the life of Inconel 718 are shown in replicas taken progressively throughout a strain controlled test at room temperature. To contrast further, medium carbon steels also exhibit these cracking modes in biaxial loading, as seen in the progression of cracking throughout the life of a 1045 steel in Figure 6.

Of course, high temperature response adds further to the complexity of multiaxial fatigue in superalloys. We have found that the temperature dependent material behavior and mechanisms are important in determining the critical planes housing the early LCF multiple cracks. Figure 7 shows the through thickness cracking that caused loss of load carrying ability in torsionally loaded Waspaloy at room temperature and at 650°C (1200°F). At room temperature the shear mode dominated initiation and failure on longitudinal shear planes, whereas at elevated temperature, the final failure occurred on the 45° planes across which the maximum principal stress occurs in torsion.

One might wonder whether the response of smooth, unnotched laboratory specimens is representative of the critical crack in the notched component that is addressed by damage tolerant design codes. There is very little information available generated from the controlled multiaxial testing of notched specimens, since this type of work is more on the order of component testing than research. However, experimental programs including combined bending and torsion on notched shafts have reported the same multiple initiation site behavior as seen in the smooth specimen tests. Until further experimentation shows otherwise, it is prudent to assume that notches in hot section components do not reduce the failure response to a single crack phenomena.

Single dominant crack failures (HCF), whether in axial or multiaxial stress states, obviously lend themselves to damage tolerant concepts directly. In the multiaxial case, the single crack may be growing in a mixed mode manner such that this must be considered in the methods of analysis. There is currently ongoing research under sponsorship of many different organizations investigating mixed mode crack growth.

TMF EFFECTS

Where are TMF Effects Significant

Two idealized but representative TMF cycles are shown in Figure 8, illustrating several significant features and parameters that together define the type and severity of the TMF cycle. An important feature is of course the temperature range represented by T_{max} and T_{min}. The phase relationship between the mechanical loading cycle and the temperature cycle can have a major effect on TMF life. Figure 8 represents an "in-phase" cycle wherein the material is under maximum tensile load at the maximum temperature. Conversely, Figure 8 shows an "out-of-phase" cycle in which the material is under maximum compression at the maximum temperature. The mechanical loading parameters that define the TMF cycle include the maximum, minimum, and mean stresses as well as the total strain range and the inelastic strain range.

In general, significant TMF effects on crack initiation and propagation lives are observed when the cyclic temperature range is large enough that significant variation in material mechanical behavior occurs. These conditions are certainly encountered during the operating cycle experienced by combustor liners, turbine airfoils, and to a lesser extent, turbine disk rims. Examples of TMF loading for critical locations of each of these components are shown in Figure 9 [13,14,15]. Both the turbine blade tip and the combustor liner are clear cases of out-of-phase cycling. In fact out-of-phase TMF cycles are more generally encountered in hot section components than are in-phase cycles. The disk rim example could also be considered an out-of-phase case with a high tensile mean stress since the maximum tensile stress occurs near the minimum temperature.

As is the case for isothermal fatigue, TMF life consists of a crack initiation stage followed by a crack propagation stage. Although the crack propagation stage is most pertinent to damage tolerant design, a brief consideration of initiation will help to establish some general trends and the overall significance of TMF cycle parameters on life.

Effects of TMF on Initiation Life

Analysis of component TMF life is presently based on isothermal life prediction models, some examples of which are listed in Table I. All of these models incorporate as input either the total or inelastic strain range, sometimes combined with various methods of accounting for interaction between time-dependent inelastic strain (creep) and cyclic time-independent plasticity. In some cases mean stress and maximum tensile stress effects are included in the life prediction models. Reference 16 summarizes the applicability of some of these models to TMF life prediction of a turbine blade alloy.

The experimental results in Figures 10 and 11 compare the TMF lives of 2 different turbine airfoil materials with results for isothermal testing. Unfortunately, comparable results are not available for a disk alloy. The tests were conducted in such a manner that the indicated lives are predominantly crack initiation lives.

Consider first the results for MAR-M 200 shown in Figure 10. The in-phase TMF lives are an order of magnitude lower than the isothermal lives, regardless of whether the isothermal data corresponding to the maximum TMF cyclic temperature or minimum temperature is used for comparison. The out-of-phase results however are comparable to the low temperature isothermal results.

The TMF crack initiation results for B-1900 show the same general trends as those for MAR-M 200, as may be seen in Figure 11. The in-phase lives are as much as an order of magnitude lower than corresponding isothermal lives. However, the out-of-phase results correspond more closely to the range of isothermal lives.

Although published TMF data is very limited, the results presented in Figures 10 and 11 are believed to be representative of the behavior one would see in a broad range of nickel based superalloys. A major phenomenon not generally predicted by the isothermal initiation life models is the relative ranking of the in-phase versus out-of-phase cycles. Note that in-phase cycling generally results in compressive mean stresses, and out-of-phase cycling generally results in tensile mean stresses. Most isothermal models are so structured with respect to the role of tensile stress or mean stress that out-of-phase lives would be predicted to be lower than in-phase. Apparently TMF cycling is introducing effects not captured in the isothermal models.

Effects of TMF on Crack Propagation

Some results from Pelloux's research on cyclic crack propagation under TMF conditions are summarized in Figure 12 [17]. The experiments were conducted on Inconel X-750, both in-phase and out-of-phase over a temperature range of 300°C to 650°C, representing disk rim conditions. A striking observation is that the highest crack propagation rates occurred under out-of-phase cycling conditions, with crack growth an order of magnitude faster for a given ΔK value than under isothermal conditions. Note that this phasing effect is the inverse of that seen in initiation dominated experiments. Crack growth for in-phase cycling was between the rates of isothermal and out-of-phase test. Pelloux attributes the high crack growth rates under out-of-phase conditions to non-closure at zero load, and shows that good correlation between TMF crack growth rates and isothermal results is realized if non-closure is accurately accounted for by substituting ΔK_{eff} for ΔK as illustrated in Figure 13. The practical difficulty here is accurately defining ΔK_{eff}, i.e. analytically quantifying crack non-closure, in the design of a turbine disk. Failure to do so would introduce potentially serious nonconservative errors in the predicted component crack growth life. It would appear that application of damage tolerant design to components subjected to significant TMF loading using linear elastic fracture mechanics (LEFM) principles will require considerable component and mission specific specimen testing as support.

Rau, Gemma and Leverant [18] conducted TMF crack propagation experiments similar to those of Pelloux, but on turbine airfoil materials and over a broader temperature range (320°C to 900°C typically). The results were correlated with cyclic strain intensity as the LEFM parameter. The same general trends were observed as for Inconel X-750 cited above, with crack propagation rates for out-of-phase cycling being significantly higher than for in-phase or isothermal cycling. These trends were attributed to oxidation assisted crack sharpening effects that may occur during the compressive portion of out-of-phase cycling. Again, accounting for these effects in the course of damage tolerant design analysis is difficult and errors incurred if isothermal crack propagation results alone are employed in conjunction with LEFM are likely to be nonconservative.

Jordan and Meyer [19] looked at the TMF crack propagation of Hastelloy-X from the standpoint of predicting TMF behavior on the basis of isothermal results. They developed a crack growth model based on ΔK_{Eff} with built-in corrections for temperature dependent crack growth rates determined in isothermal cycling. This model actually predicted TMF growth rates to within a factor of 2 to 3 of their experimental data, but was sometimes nonconservative and sometimes conservative, depending on loading conditions.

TMF crack propagation experiments conducted on a series of steel alloys important in the power generating industry were reported by Okazaki and Koizumi [20]. Though no direct comparisons with isothermal cycling fatigue data are shown, the authors did demonstrate very accurate predictions of crack propagation rate under TMF cycling using a J-Integral model. The accuracy of their prediction stems no doubt from their use of material hardening parameters determined from TMF cyclic stress-strain data. These cyclic constitutive parameters could, however, be determined in a test of limited duration not requiring the test time associated with crack growth measurement and life determination.

CONCLUSIONS

From the foregoing discussion of published results it is readily apparent that both multiaxial fatigue and thermomechanical fatigue have a significant impact on crack initiation and crack propagation. Several specific research needs are evident that will provide necessary improvements to crack propagation analysis, a vital part of damage tolerant design:

1. Theoretical basis to account for effects of non-proportional loading (mechanical and mechanical/thermal);
2. Crack growth models that address multiple crack failures;
3. Mixed mode failure models;
4. Development of practical crack growth parameters that are applicable to TMF load situations;
5. Crack initiation and growth models that accurately address TMF cycle phasing effects.

REFERENCES

1. Damage Tolerance in Aircraft Structures, ASTM STP-486, ASTM, Philadelphia, 1971.

2. Cowie, W. D.; Stein, T. A.: Development Trends in Engine Durability. ASME WAM, Dec. 10-15, 1978.

3. Laflen, J. H., and Cook, T. S., "Equivalent Damage - A Critical Assessment," (R82AEG533, General Electric Co.; NASA Contract NAS3-22534) NASA CR-167874, 1982.

4. Landgraf, R. W., Morrow, J., and Endo, T., "Determination of the Cyclic Stress-Strain Curve," *J. Mater.*, Vol. 4, 1969, pp. 176-188.

5. Morrow, J., "Modern View of Materials Testing," *Mechanical Behavior of Materials, Vol. 5*, The Society of Materials Science, Japan, 1972, pp. 362-379.

6. Socie, D. F., "Fatigue Life Prediction Using Local Stress-Strain Concepts," *Exp. Mech.*, Vol. 17, Feb. 1977, pp. 50-56.

7. Leese, G. E., and Morrow, J., "Low Cycle Fatigue Properties of a 1045 Steel in Torsion," *Biaxial Multiaxial Fatigue*. ASTM STP-853, ASTM, Philadelphia, 1985.

8. Halford, G. R. and Morrow, J., "Low Cycle Fatigue in Torsion," Department of Theoretical and Applied Mechanics Rep. No. 203, University of Illinois, Urbana, Oct. 1961.

9. McDowell, D. L., "Transient Nonproportional Cyclic Plasticity," Design and Materials Division Report No. 107, Dept. of Mechanical and Industrial Engineering, University of Il., Urbana-Champaign, June 1983.

10. McDowell, D. L., "On the Path Dependence of Transient Hardening and Softening to Stable States Under Complex Biaxial Cyclic Loading," Constitutive Laws for Engineering Materials, Univ. of Arizona, Tucson, 1983, pp. 125-132.

11. Hua, C.: Fatigue Damage and Small Crack Growth During Biaxial Loading. Materials Engineering - Mechanical Behavior, Report No. 109 July, 1984, University of Il. at Urbana-Champaign.

12. Dowling, N. E., "Crack Growth During Low-Cycle Fatigue of Smooth Axial Specimens," Cyclic Stress-Strain and Plastic Deformation Aspects of Fatigue Crack Growth, ASTM STP-637, ASTM, Philadelphia, 1977, pp. 97-121.

13. Moreno, V., "Combustor Liner Durability Analysis," (PWA-5684-19, Pratt and Whitney Aircraft Group; NASA Contract NAS3-21836) NASA CR-165250, 1981.

14. McKnight, R. L., Laflen, J. H., and Spamer, G. T., "Turbine Blade Tip Durability Analysis," (R81AEG372, General Electric Co.; NASA Contract NAS3-22020) NASA CR-165268, 1981.

15. Kaufman, A., "Advanced Turbine Disk Designs to Increase Reliability of Aircraft Engines," NASA TM-X-71804, 1976.

16. Bill, R. C., Verrilli, M. J., McGaw, M. A., and Halford, G. R., "Preliminary Study of Thermomechanical Fatigue of Polycrystalline MAR-M 200," NASA TP-2280, 1984.

17. Marchand, N., and Pelloux, R. M., "Thermal-Mechanical Fatigue Crack Growth in Inconel X-750," (Massachusetts Institute of Technology, NASA Grant NAG3-280) NASA CR-174740, 1984.

18. Rau, C. A., Gemma, A. E., and Leverant, G. R., "Thermal-Mechanical Fatigue Crack Propagation in Nickel- and Cobalt-Based Superalloys Under Various Strain Temperature Cycles," Fatigue at Elevated Temperatures, ASTM STP-520, ASTM, Philadelphia, 1973, pp. 166-178.

19. Jordan, E. H., and Meyers, G. J., "Fracture Mechanics Applied to Non-Isothermal Fatigue Crack Growth," (To be published in J. Appl. Mech.)

20. Okazaki, M., and Koizumi, T., "Crack Propagation of Steels During Low Cycle Thermal-Mechanical and Isothermal Fatigue at Elevated Temperatures," Metall. Trans. A, Vol. 14, Aug. 1983, pp. 1641-1648.

ACKNOWLEGEMENTS

The authors wish to thank Professor D. Socie of the University of Illinois for contributing Figures 5 and 6, and Professor S. Zamrik of Pennsylvania State University for contributing Figures 4 and 7.

TABLE I

HIGH TEMPERATURE LOW CYCLE FATIGUE MODELS AVAILABLE

o MANSON - COFFIN RULE

$$N_{PRED} = (C/\Delta\epsilon_{in})^{1/c}$$

o METHOD OF UNIVERSAL SLOPES

$$\Delta\epsilon_{TOT} = D^{0.6} N_f^{-0.6} + 3.5 \sigma_u / N_f^{-0.12}$$

o STRAIN RANGE PARTITIONING

$$1/N_f = F_{ij}/N_{ij}; \; ij \rightarrow (pp, pc, cp, cc)$$

$$F_{ij} = \Delta\epsilon_{ij}/\Delta\epsilon_{IN}$$

$$N_{ij} = (C_{ij}/\Delta\epsilon_{IN})^{1/c}$$

o OSTERGREN MODEL

$$\sigma_t \Delta\epsilon_p [N_f \nu^{(K-1)}]^{\beta} = C$$

o FREQUENCY SEPARATION MODEL

$$N_f = D\Delta\epsilon_p \, \nu_T^b \, (\nu_c/\nu_T)^c$$

o DAMAGE RATE MODEL

o TIME AND CYCLE FRACTION MODEL

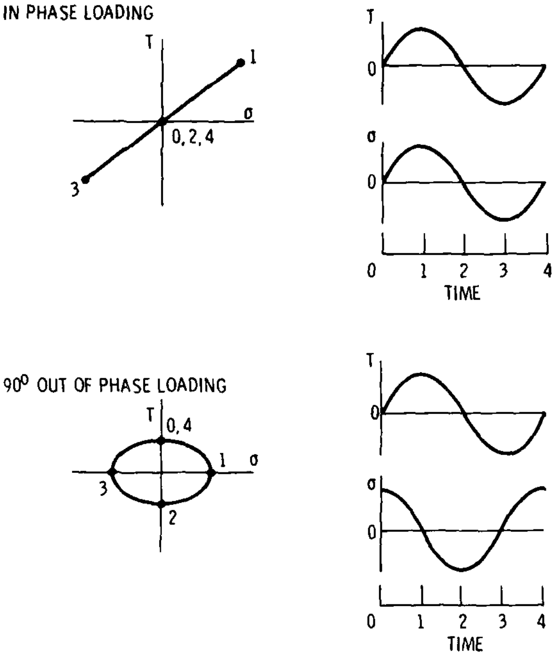

Figure 1. - In-phase and out-of-phase tension-torsion loading.

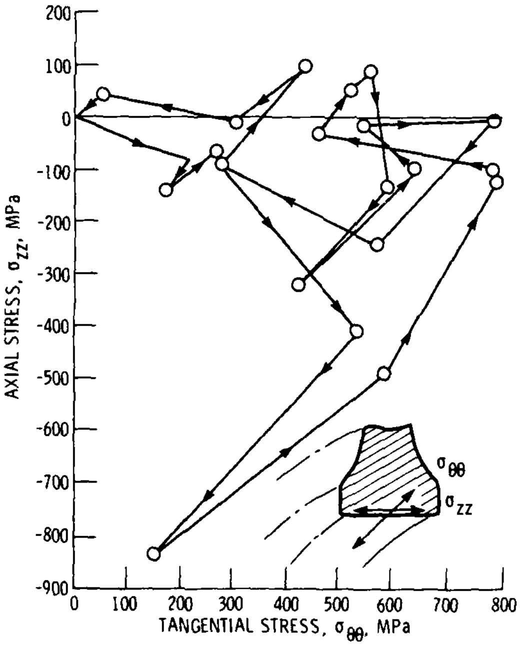

Figure 2. - Example of the complex states of stress that can evolve during a simulated mission in a disk bore.

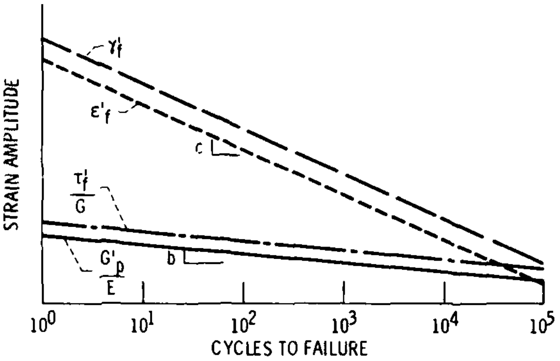

Figure 3. - First approximation of strain-life relationships in different stress states, assuming stress state independent slopes and modified strength and ductility coefficient.

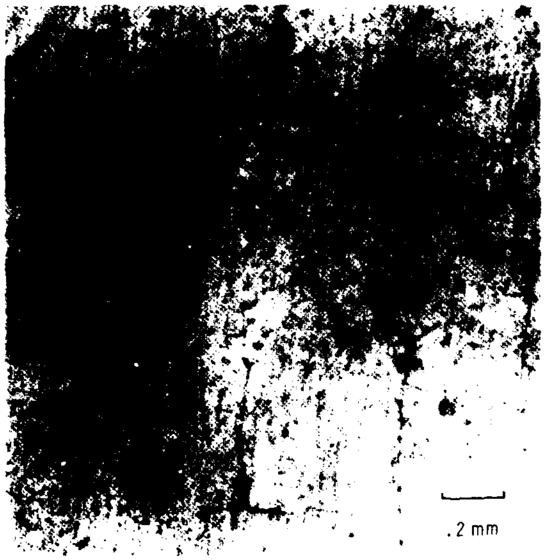

Figure 4. - Replicas showing multiple cracking in Waspaloy subjected to torsional loading ($\Delta\gamma_a$ = 0. 0196) at room temperature (N_f = 3965).

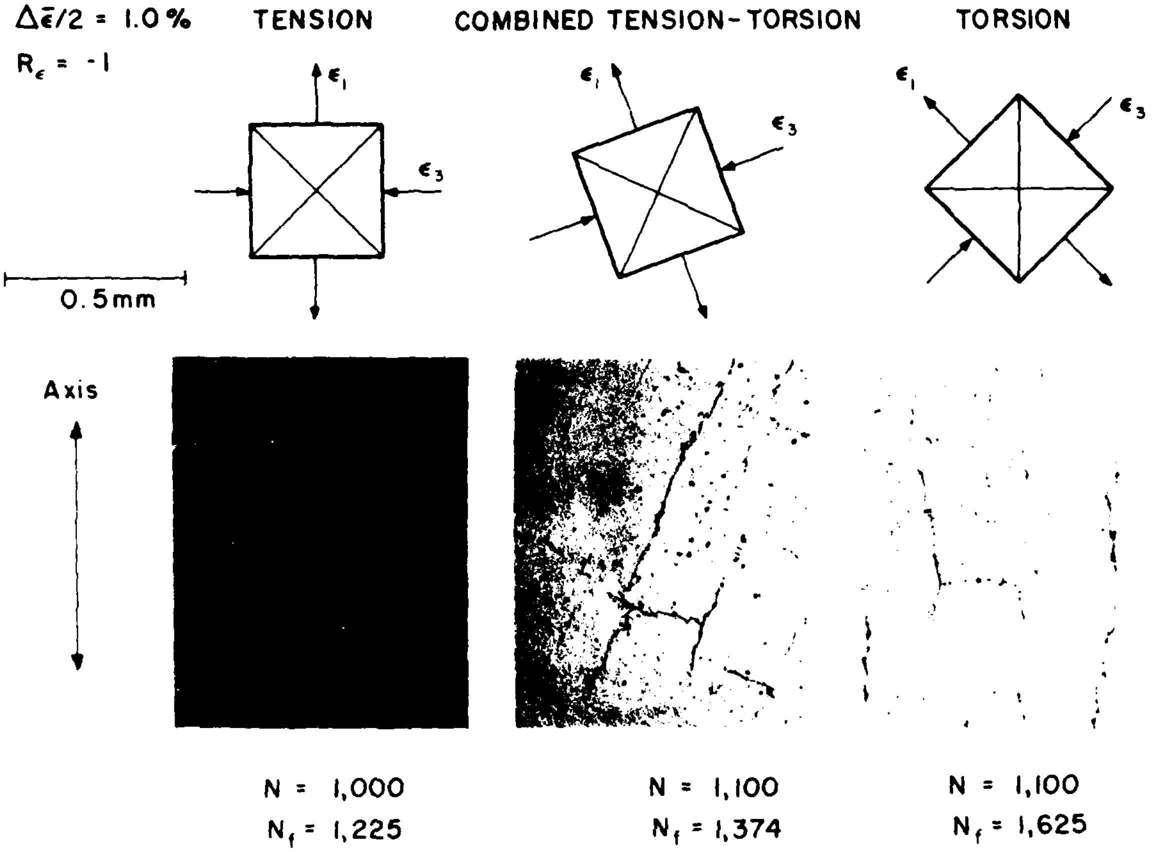
$\Delta\bar{\epsilon}/2 = 1.0\%$
$R_\epsilon = -1$
TENSION
COMBINED TENSION-TORSION
TORSION
ϵ_1
ϵ_3
ϵ_1
ϵ_3
ϵ_1
ϵ_3
0.5mm
Axis
N = 1,000
N_f = 1,225
N = 1,100
N_f = 1,374
N = 1,100
N_f = 1,625

Figure 5. - Progressive multiple cracking in Inconel-718 under tension-torsion loading.

(a) After 518 cycles.

(b) After 9266 cycles.

Figure 6. Progressive multiple cracking in medium carbon steel. $\gamma_a = +.8\%$; $2N_f = 11010$.

(c) After 10390 cylces.

Figure 6. - Concluded.

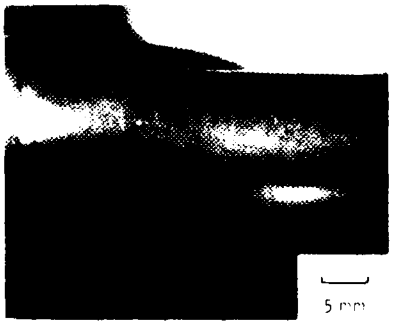

(a) Fine grain showing cracking on maximum shear planes, room temperature.

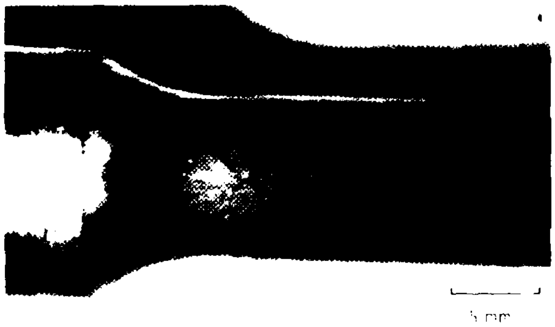

(b) Coarse grain showing cracking at 45^0 to specimen axis on planes of maximum tension, 650 °C.

Figure 7. - Macrophotos showing primary cracks in fine grain and coarse grain Waspaloy multiaxial specimens subjected to cyclic torsion.

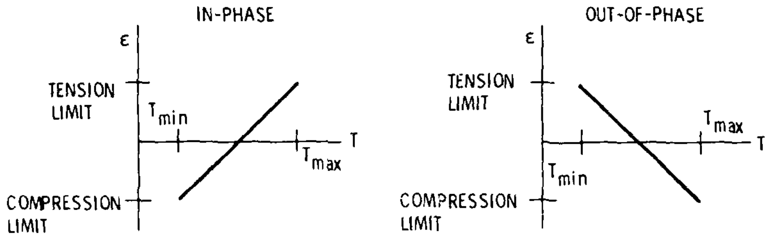
IN-PHASE
ε
TENSION LIMIT
T_{min}
T
T_{max}
COMPRESSION LIMIT
OUT-OF-PHASE
ε
TENSION LIMIT
T_{max}
T
T_{min}
COMPRESSION LIMIT

(a) Strain-temperature relationship.

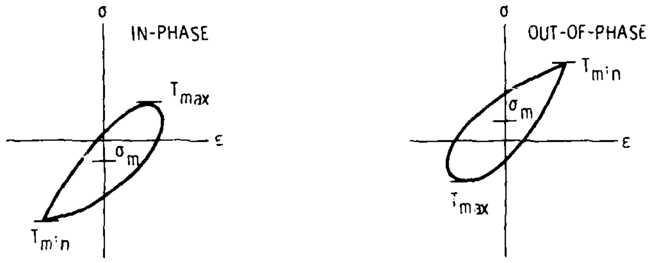
σ
IN-PHASE
T_{max}
ε
σ_m
T_{min}
σ
OUT-OF-PHASE
T_{min}
σ_m
ε
T_{max}

(b) Stress-strain relationship.

Figure 8. - Typical TMF test cycles showing mechanical strain versus temperature, and stress-strain relationships for in-phase and out-of-phase cycles.

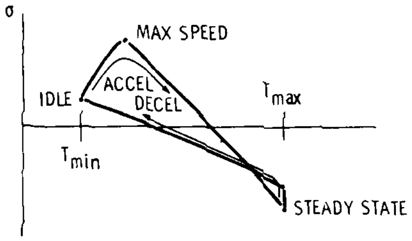
σ
MAX SPEED
ACCEL
IDLE
DECEL
T_{max}
T_{min}
STEADY STATE

(a) Turbine airfoil.

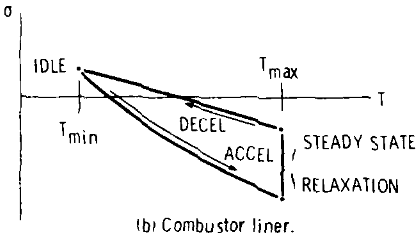
σ
IDLE
T_{max}
T
DECEL
T_{min}
ACCEL
STEADY STATE /
RELAXATION

(b) Combustor liner.

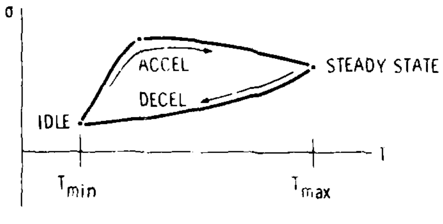
σ
ACCEL
STEADY STATE
DECEL
IDLE
T
T_{min}
T_{max}

(c) Disk rim.

Figure 9. - TMF loading cycle schematics representative of turbine airfoils, combustor liners and disk rims.

AD-A164 693 DAMAGE TOLERANCE CONCEPTS FOR CRITICAL ENGINE 3/4
COMPONENTS(U) ADVISORY GROUP FOR AEROSPACE RESEARCH AND
DEVELOPMENT NEUILLY-SUR-SEINE (FRANCE) OCT 85
UNCLASSIFIED AGARD-CP-393 F/G 21/5 NL

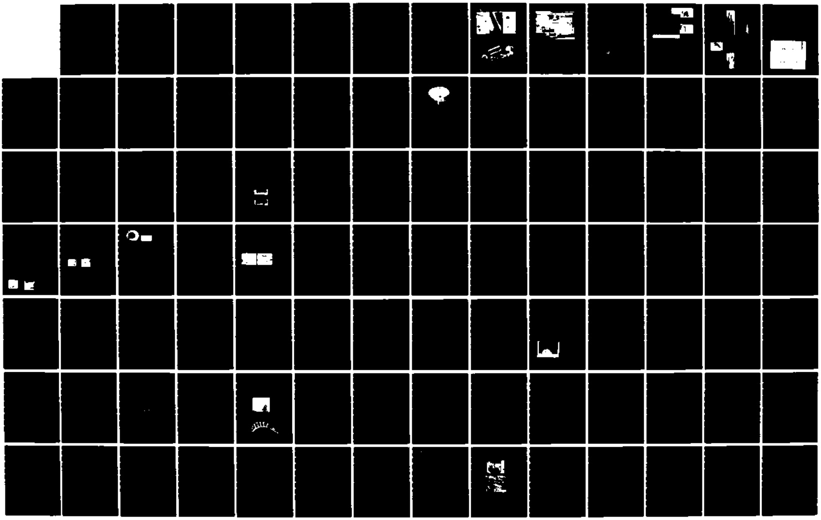

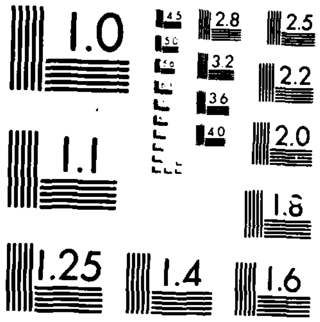
1.0
4.5
5.0
5.6
2.8
2.5
3.2
2.2
3.6
4.0
2.0
1.1
1.8
1.25
1.4
1.6

MICROCOPY RESOLUTION TEST CHART
NATIONAL BUREAU OF STANDARDS 1963 A

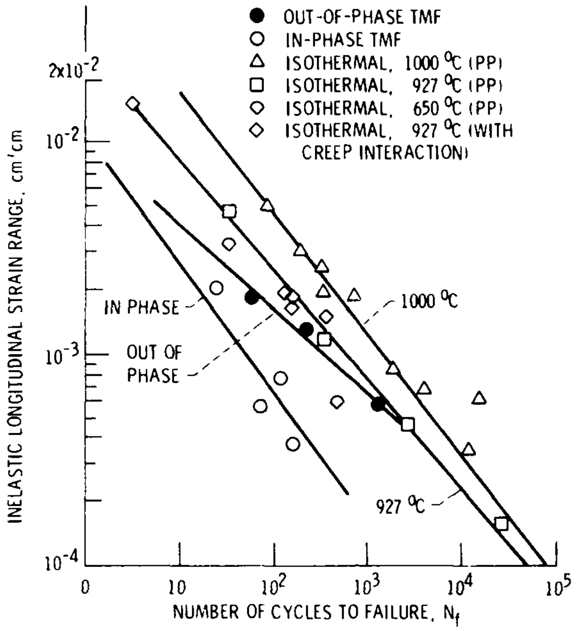

Figure 10. - Inelastic strain range as function of number of cycles to failure for polycrystalline MAR-M 200 under thermomechanical fatigue and isothermal cycling conditions.

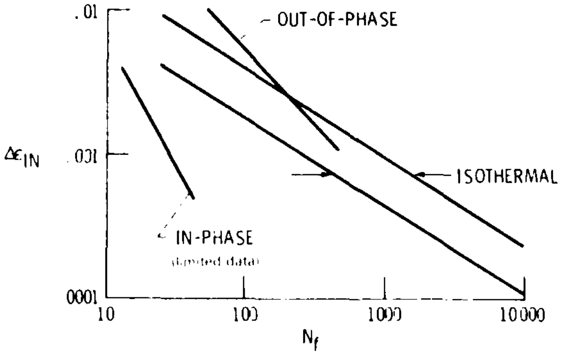

Figure 11 - In-phase and out-of-phase TMF lives compared to isothermal lives for B-1900 cycled between 520 °C and 870 °C.

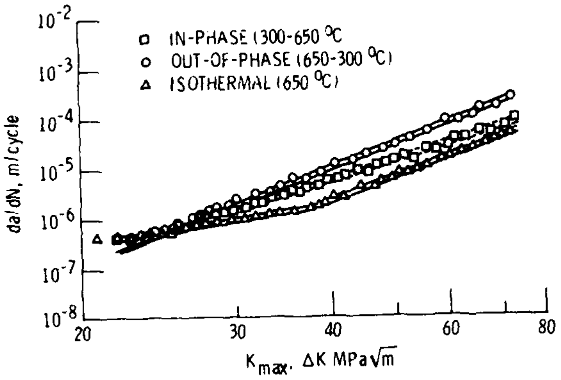

Figure 12. - Thermomechanical fatigue crack growth in Inconel X-750 as a function of ΔK, based on K_{max}, K_{min}.

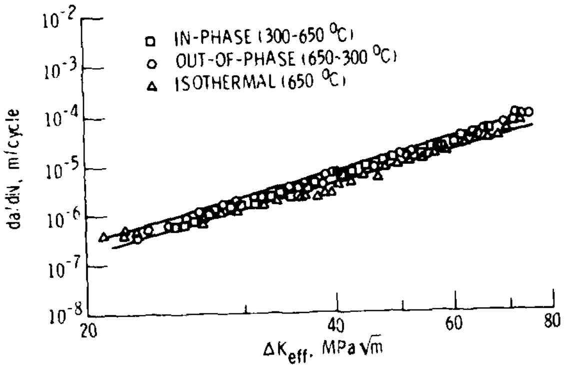

Figure 13. - Thermomechanical fatigue crack growth in Inconel X-750 as a function of ΔK_{eff}, accounting for crack closure effects.

ADVANCED QUANTITATIVE METHODS FOR NONDESTRUCTIVE EVALUATION

by
Dale E. Chimenti and Thomas J. Moran
Materials Laboratory
Air Force Wright Aeronautical Laboratories
Wright-Patterson Air Force Base, OH 45433

Abstract

Over the past decade and a half progress in nondestructive evaluation (NDE) methods which yield quantitative flaw information has been considerable and has sparked a revolution in the way industry and government view the capabilities and benefits of quality assurance or component integrity. Almost no NDE technique, new or established, is selected for research and development without examining its potential for providing accurate, quantitative defect information. Concurrent with this trend has been the increasing use of fracture mechanics in the design and life management of aircraft systems, placing in turn stringent requirements on quantitative nondestructive evaluation (QNDE). Nowhere are these demands heavier than in the case of advanced aircraft engine alloys where critical flaw sizes are measured in hundredths of an inch. Research in NDE, therefore, has concentrated on improving defect sensitivity and reliability and providing the quantitative information essential to the new system maintenance philosophies, such as "Retirement-for-Cause." In addition to the well known quantitative capabilities of standard techniques like radiography, dye penetrant, and in some cases, eddy current, developments in quantitative ultrasonics, eddy current, thermal wave techniques and exploitation of new medical x-ray imaging methods offer alternatives with enhanced capabilities and possibly reduced cost. In this paper the state of the art in QNDE will be discussed, as well as advanced methods currently in development.

Introduction

The implementations of the Aircraft Engine Structural Integrity Program (ENSIP) and the Retirement-For-Cause Program (RFC) require a quantitative nondestructive evaluation (NDE) capability of very high reliability. These requirements have provided the impetus for a considerable amount of research activity in the NDE area in the past decade. In this paper we will review the current capabilities of the various technologies being developed and project, to some extent, what capabilites will be available in the future.

Advanced Eddy-Current Probes

Figure 1 gives three examples of the potential for innovation in eddy-current technology. On the right is a close-up photograph of the YIG sphere ferromagnetic resonance device. This probe functions in a manner significantly different from familiar eddy-current coils. Its small size is an advantage for finding small surface cracks. In the middle frame is the detector coil of the electric current perturbation probe. Here again, small size combined with differential operation contribute to its unusual capabilities. Shortly, these two concepts will be discussed further. The last frame shows a research prototype of an eddy-current probe built by exploiting the well known technology of magnetic recording heads. In this case the magnetic fields sensing the presence of defects are confined to a closed ferrite loop, open for only 0.3 mm at one point along its length to allow magnetic flux to leak out near the metal surface. By severely limiting the spatial extent of the fields in the plane of the test surface, the vertical penetration of the magnetic flux can be confined as well to a depth much less than the classical skin depth. Therefore, sensitivity of this device to shallow cracks is better at 100 kHz than some conventional probes are at 1 MHz or more. Moreover, the magnetic-head probe can, because of its field-confinement properties, test very near corners and edges, where the response of conventional probes is perturbed by the geometry of the part.

YIG Sphere Device Assembly

As we saw earlier, eddy-current probes based on new technology offer possibilities now being explored. Here, we describe the YIG sphere ferromagnetic resonance concept and illustrate in Figure 2 a prototype device to reduce this technology to practice. At the extreme left side of the photograph, too small to resolve, is the YIG sphere, 0.5 mm in diameter. Instead of sensing the change in the impedance of a coil, this device relies on the resonance of atomic spins in the YIG (yttrium iron garnet) to detect a surface flaw. A static magnetic field of several hundred gauss is applied to the sphere and simultaneously it is excited by an oscillator whose frequency (typically 800 MHz) is determined by the resonance conditions. The presence of a surface crack interrupts eddy currents on the part and thus changes the radio-frequency electromagnetic environment. The YIG responds by varying its resonant frequency to accommodate the new conditions. The electronics we see in the disassembled probe in the figure sense the change in resonant frequency and the quality factor or sharpness of the resonance. These two quantities can be shown to be equivalent to the in- and out-of-phase components of a conventional eddy-current signal. The advantage of the YIG device is its small size, extreme sensitivity, and utility in thin-section components.

ECP Breadboard

One electromagnetic method currently under development primarily for increased crack detection reliability, but also partially to quantitative NDE, is the electric current perturbation method. The basis of the method is to induce a relatively uniform electric current sheet in the surface of the metal with a large coil and detect changes in normally small orthogonal components of the magnetic field with a small, properly oriented detection coil. Figure 3 shows an example of a breadboard probe and scanner produced by a recently completed Materials lab program which is capable of detected cracks as small as 250 micron in surface length in a complex-geometry area of a turbine disk.

ECP Signal Inversion

Comparisons have been made between simple features of ECP signals from an actual fatigue crack and those generated by an analytical model. Experimental results were obtained from a single, half-penny shaped fatigue crack grown to various lengths in a Ti 6-4 rod-type tensile specimen using a laboratory fatigue machine. Fracture of identical specimens containing cracks grown under similar conditions showed that true half-penny shaped fatigue cracks (2:1 aspect ratio) were obtained. Electric current flow was introduced into this specimen by direct contact at each end of the rod, and the perturbations were detected by a separate ECP probe scanned perpendicular to the crack. Theory and experiment were compared for the ECP signal amplitude as a function of interfacial area of the crack. These data are shown in Figure 4. It can be seen that the theory predicts an approximately linear relationship between signal amplitude and interfacial area of the crack. Experimental results show very close agreement with theory, thus indicating that crack interfacial area can be estimated by measurement of the ECP signal amplitude.

Eddy-Current Inversion

From a study of fracture mechanics we know that the depth of a fatigue crack is an important parameter in assessing the "severity" of the crack, or conversely, the continued fitness for service of the cracked component. It has long been a goal of those who employ alloys having small critical crack sizes to be able to extract crack-depth information from a standard eddy-current test. This prospect now seems close to reality. Using a conventional, air-core eddy-current coil researchers at the National Bureau of Standards in Boulder have achieved the promising results on electrodischarge-machined slots in a metal specimen, shown in Figure 5. Here, we plot the predicted slot depth versus the known depth for a series of four slots spanning a factor of four in depth. The eddy-current data were analyzed with an inversion theory developed under Air Force sponsorship at Stanford University. The agreement, even for these preliminary data, is quite good. Not shown here are similarly promising results for the slot lengths and opening displacements, all derived from the same set of eddy-current measurements. Currently, the technology is being further evaluated on a series of fatigue cracks in a variety of engine materials.

CT Schematic

In the area of radiography the Materials Laboratory has contributed, both in-house and on contract, to extend the medical computed tomography capabilities to the industrial and military environments. Figure 6 shows a simplified x-ray C/T machine designed specifically for industrial purposes. The instrument consists of a high energy source which emits a thin, fan-shaped beam which passes through a selected cross-section of the component being inspected. Then an x-ray detector array measures the flux of x-ray photons passing through given line elements in the component. Mechanical rotation and translation stages to move the component through the required angles for the acquisition of an adequate amount of data for a tomographic reconstruction. Typical inspection systems also possess a vertical motion capability which permits the acquisition of more conventional type of radiographic data in order to preview the part and select the location for the more time consuming tomographic reconstruction. These preview scans or digital radiographs can provide much quantitative information for the detection of dimensional errors and larger flaws.

IBIS XIM Module

The three AFWAL-sponsored systems currently in operation can inspect objects ranging in size from 5 cm. to 2.5 m. in diameter. Since the large systems are primarily concerned with the inspection of rocket components, we will not consider them here. The third system is a module in the General Electric Integrated Blade Inspection System (IBIS) and was designed specifically to inspect small engine blades. Figure 7 shows the type of data obtainable with this instrument. The digital radiograph shown in the lower portion of the figure shows the alignment of the cooling holes as seen from the side. The tomographic scan shown in the upper portion of the figure was made in the upper portion of the blade and clearly shows the cross-sections of the cooling holes. This method is currently the only way to determine if the cooling holes have adequate clearance from the sides. GE is using such data for the inspection of blades with integral tip caps, which are otherwise uninspectable. Future work in the engine area will involve the development of a high power microfocus source to enable the quantitative detection of such small flaws as casting defects using x-ray C/T instrumentation.

Thermal Wave Schematic

Figure 8 shows the geometry of the thermal wave imaging technique. The effect consists of a measurement, by one of several means, of the surface thermal properties of a component. A medium-power modulated laser at lower left causes periodic heating of a small region some 20 micron in diameter at the surface being tested. Because the mechanical condition of the surface and near-surface region will influence the diffusion of heat into the specimen interior, this method can reveal characteristics not detected by other methods. The periodic heating of the surface, in turn, results in a time-dependent temperature fluctuation of the small volume of air directly above the heated zone. A second low-power laser, at upper left, passes through the tiny volume of heated air and is optically deflected by an amount depending on the air's temperature. The amplitude of that temperature excursion and its phase relative to the heating pulse will be functions of the thermal properties of the surface: heat conductivity and heat capacity. A crack-like defect introduces a spatially dependent conductivity, while a void perturbs both the conductivity and the heat capacity near that point. These strong discontinuities change the thermal environment of the diffusing heat pulses, appearing as signals at the position-dependent probe-beam detector.

Bolt-Hole Crack

An example of this technology is seen here in Figure 9, where a real fatigue crack in the wall of a circular hole in a simulated bolt-hole specimen has been imaged thermally. The fatigue crack is clearly represented, including some subsurface features not visible in under an optical microscope. Because of the amount of time this technique currently requires to produce such a high resolution image of a crack, its major application, it is felt, will be as a tool for quantification of superficial defects once they have been detected by other means. Although the utility of the thermal methods for discrete defects is now well established, future applications might include measurement of case hardening depth, thickness or adhesion of thermal-barrier coatings, and concentration of distributed flaws, such as surface porosity.

IBIS IRIM Module

In addition to the advanced IR inspection methods currently under development, there exist lower technology systems which are already in use. An example of one of these systems is the Infrared Inspection Module (IRIM) in the GE IBIS system. It is designed to detect blocked cooling holes in turbine airfoil parts and verify the cooling efficiency. It operates by blowing heated air through the cooling holes and recording the time dependent local and global changes in the temperature of the component. Figure 10 shows two examples of its performance. In the upper left of the figure can be seen an end view of the tip of the blade. The air escaping from open cooling holes shows up as white in the figure. The circle indicates an area where an indication is missing and the hole is blocked. The center portion of the figure shows a side view of a similar blade which also has two blocked holes. In addition to the detection of the blockage, the thermal map of the side wall illustrates how this method could be used for determination of cooling efficiency in a quantitative manner.

Acoustic Microscope Schematic

In Figure 11 the principle of acoustic microscopy is illustrated. A radio-frequency tone burst is sent to a transducer, the resulting ultrasound emerging through a highly convergent acoustic lens into a couplant fluid. By arranging for the acoustic focal point to coincide with the surface to be examined, a microscopic image of near-subsurface detail can be obtained. In the operation mode illustrated in the figure, the focal point lies slightly below the surface. In this case, the microscope will generate leaky surface acoustic waves whose penetration allows imaging of subsurface defects. As the surface waves intercept a defect and reradiate into the fluid, returning to the transducer, the perturbed sound wave appears as a defect signal in the device's electronics. Scanning the lens over the surface of interest yields a two-dimensional image of high potential for NDE.

Acoustic Micrograph

In Figure 12 is an example of the capabilities of an acoustic microscope adapted to NDE problems. Operating frequency has been chosen to provide reliable defect detection for the size range of interest here, while retaining good penetration of the Rayleigh surface waves to permit coverage of the first 1 mm or so. This image is of a fabricated defect specimen, where the known defect sizes are indicated on the figure. Reliable detection of 0.4-mm horizontally oriented, planar flaws is clearly feasible with the first-generation laboratory prototype with which this image was made. The goal here is to provide an inspection tool for net-shape components where no "sonic" envelope will be machined away. In that sense this technique is complementary to conventional C-scan ultrasonics. However, on the horizon we can begin to see engine materials for use in very high-temperature, next-generation power plants whose NDE-critical flaw sizes may be measured in tenths of a millimeter. Whether these materials are ceramic, ceramic-composite, or some other advanced multiphase system, leaky surface waves generated and detected by the acoustic microscope will offer a high-sensitivity, tailorable probe of near-surface condition.

Born Inversion Procedure

One of the early objectives of the Air Force's entry into fundamental NDE was to render standard ultrasonics a quantitative tool. While the scattered elastic waves from a flaw contains a great deal of information concerning the size, shape, orientation and composition of the flaw, the mathematical nature of the inversion problem makes this technique one of the most difficult to quantify. This Figure 13 shows one realization of quantitative ultrasonics. Based on the widely used Born scattering approximation, this technique seeks to infer the size, and perhaps additional information, from an ultrasonic flaw reflection. Beginning at the left, a transducer sends a broadband pulse of sound through a couplant fluid to the part under test. There, it reflects from a defect, the echo arriving at the transducer some time later. That echo corresponds to the flaw signal indicated in (1). In the same test a measure of the transducer response (2) is acquired by observing the echo from a flat surface of the part. The frequency spectra of these two signals are now divided to obtain the pure flaw response (3) within a bandwidth limited by the transducer's frequency properties. A calculation is performed on the reflection data to deduce the exact position of the flaw's center (4). This step is important as an input to the mathematical operations which now follow to estimate the size of the flaw. The resulting graph (5) is a flaw function having a value of one inside the flaw and zero outside. As we see from the figure, there is not a sharp boundary, but a transition zone over which the function decreases continuously. This effect is due to the bandwidth limiting of the transducer. Another undesirable effect of bandlimited transducers is that the inversion algorithm to estimate the flaw radius can be confused if the transducer bandwidth is not favorable for sizing the particular flaw under study. This fact leads to a presizing step in which the correct transducer is selected, making the technique difficult to automate. Work is continuing to eliminate these limitations and increase the bandwidth and reproducibility of fabricated ultrasonic transducers.

Quantitative Ultrasonic Data

Figure 14 shows the results obtained when the Born procedure was applied to a number of spherical internal flaw types ranging from voids to inclusions with sizes from 350 to 1200 microns in diameter. As can be seen, the procedure can estimate the flaw size within roughly 50% which is probably the best obtainable given the limited transducer bandwidths and the single physical model required by an automated technique. For comparison, the results obtained using a highly operator dependent, multiple measurement inversion scheme known as the satellite pulse technique are shown in Figure 15 for the same set of flaws. Here the accuracy has improved to about 20% of the dimension for the larger flaws. These results are all for isolated single flaws, extensive research remains to be done for multiple flaws which should be even more difficult to deal with.

ADVANCED ELECTROMAGNETIC NDI/E PROBE CONCEPTS

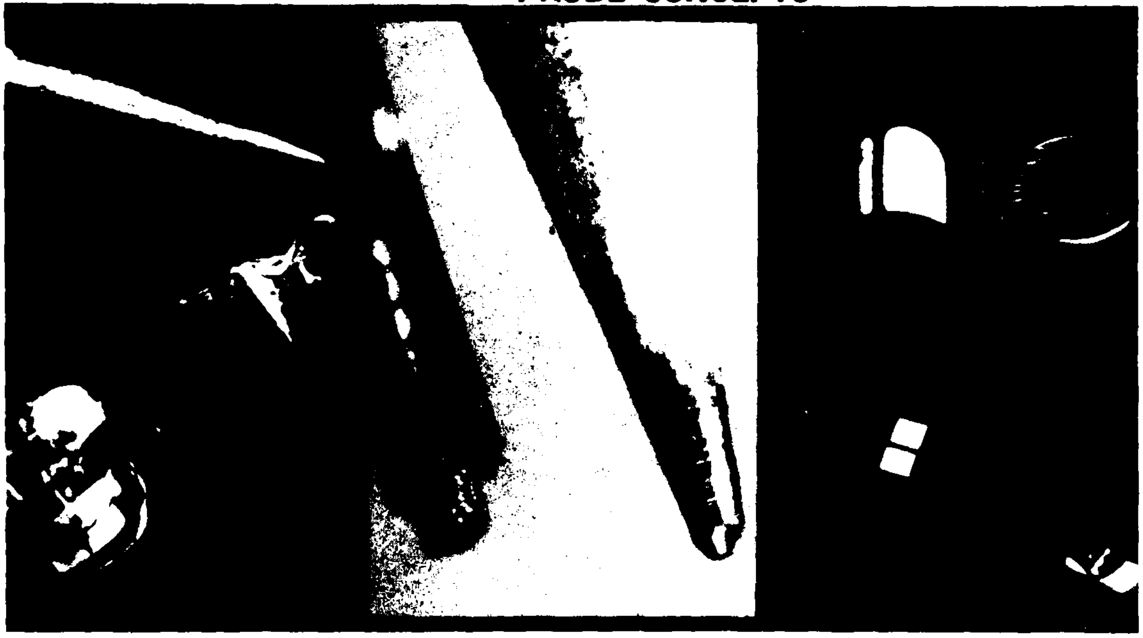

RESONANT YIG SPHERE PROBE

ELECTRIC CURRENT INJECTION PROBE

DIFFERENTIAL TAPE-HEAD PROBE

Figure 1

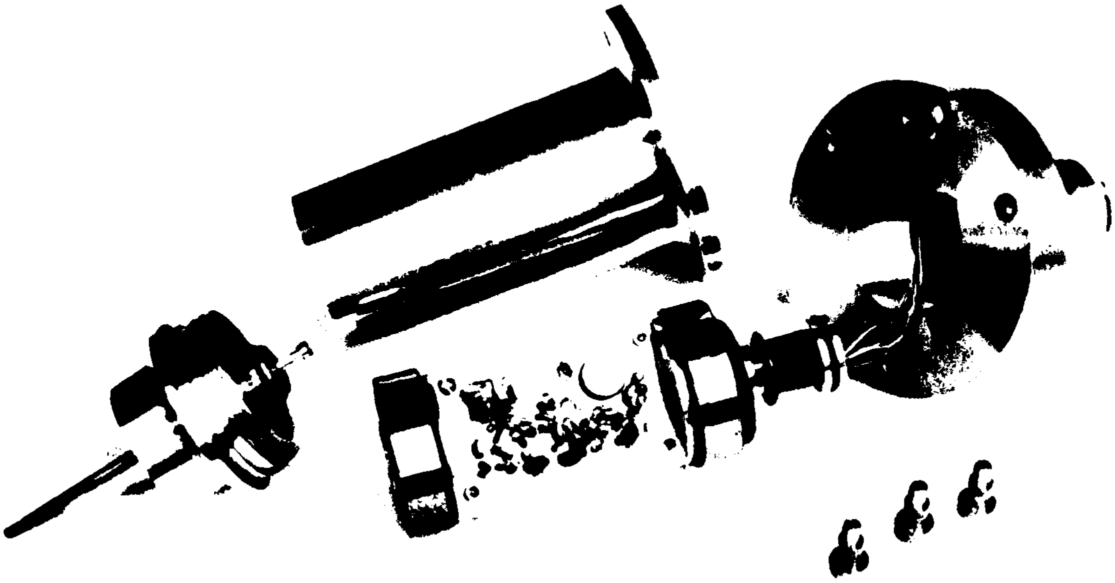

Figure 2

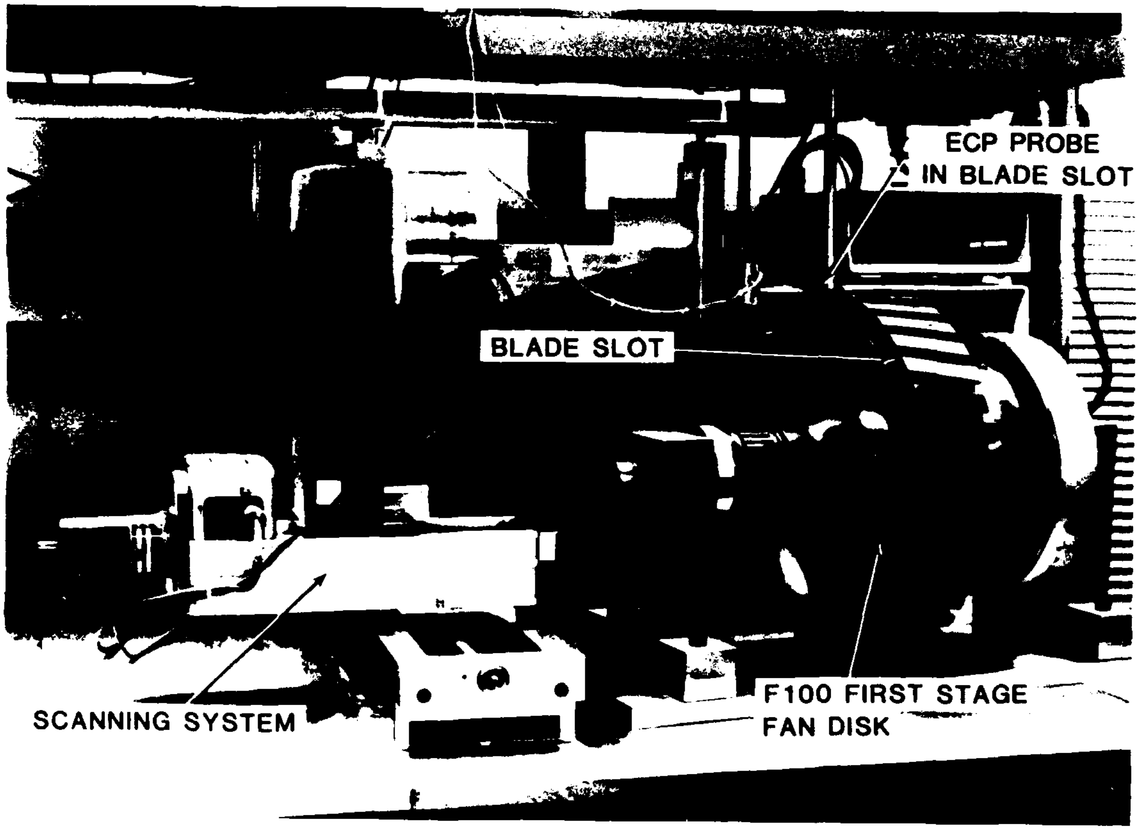
ECP PROBE IN BLADE SLOT
BLADE SLOT
SCANNING SYSTEM
F100 FIRST STAGE FAN DISK

Figure 3 ECP laboratory breadboard scanning system with F-100 first stage fan disk in place

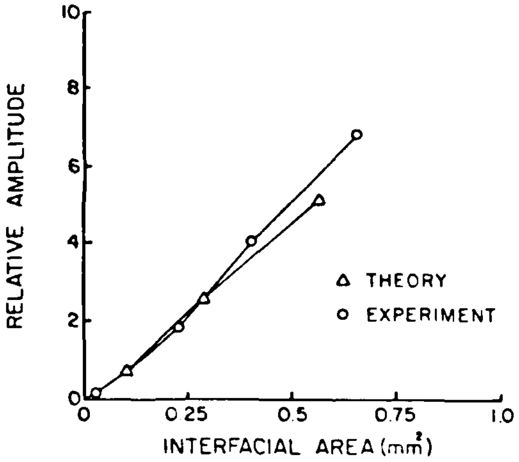

Figure 4

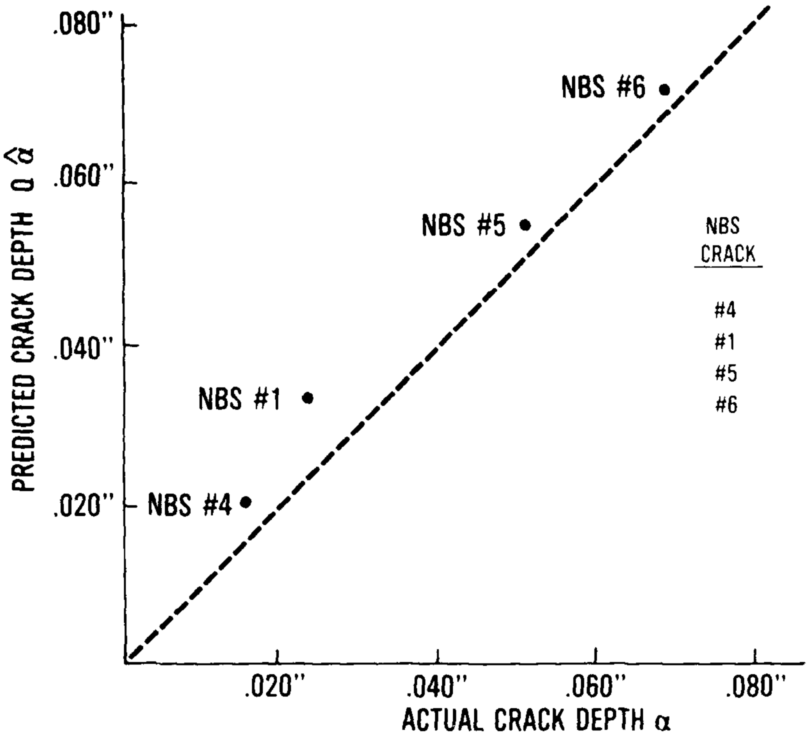

NBS CRACK	ACTUAL DEPTH	PREDICTED DEPTH
#4	.0158"	.020"
#1	.0236"	.033"
#5	.0512"	.055"
#6	.0690"	.072"

Figure 5 Crack depth

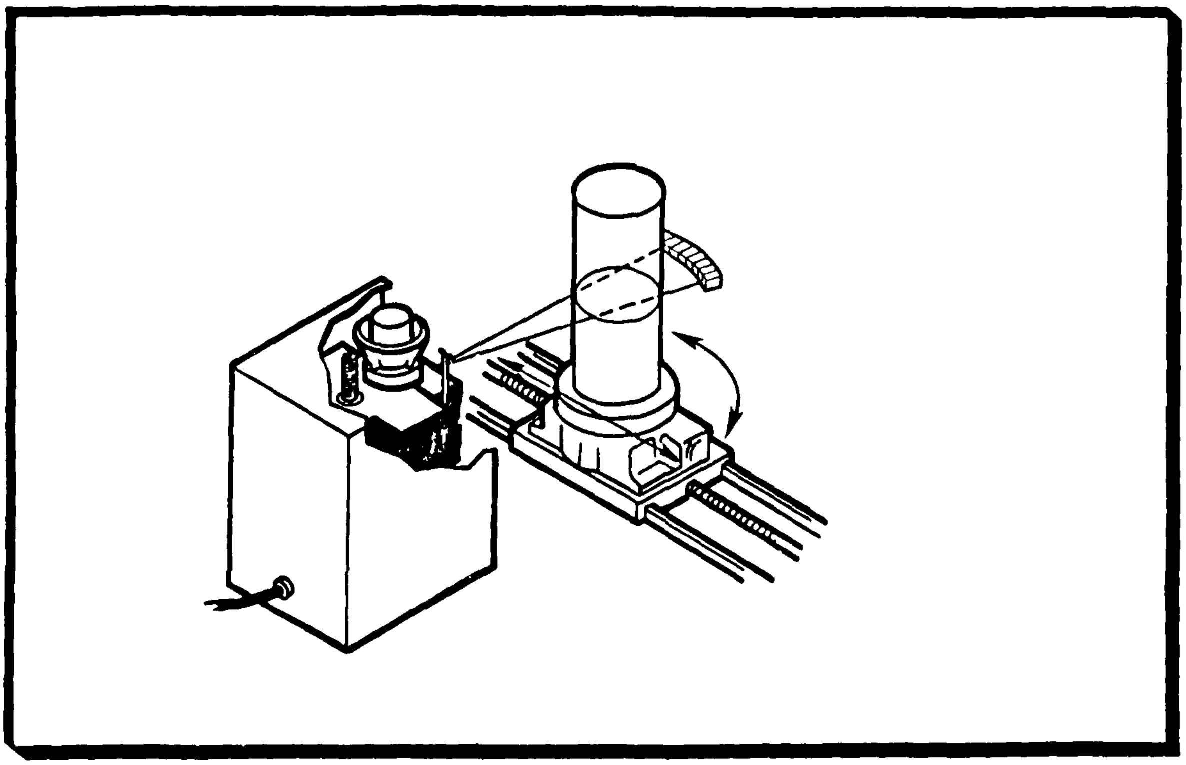

Figure 6 Computed tomography

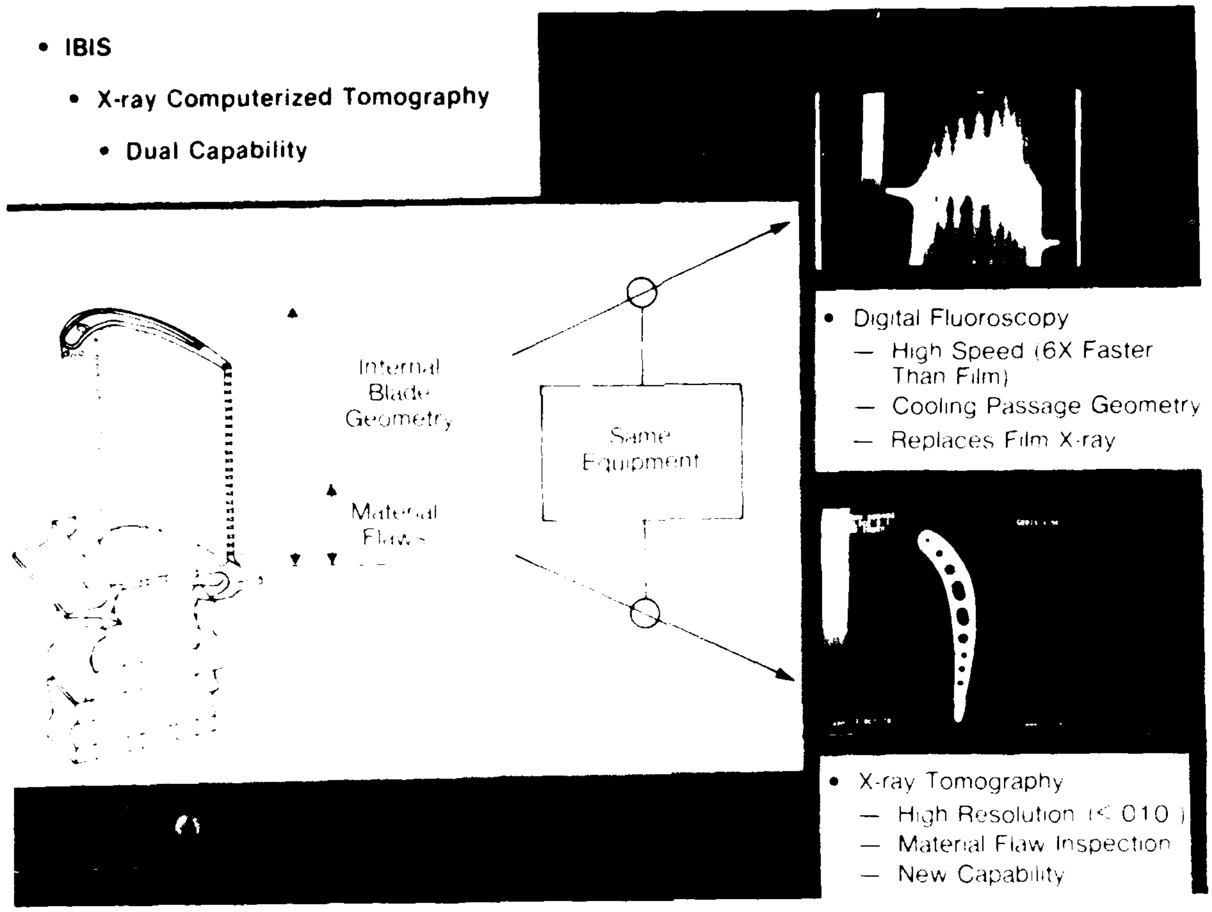

- **IBIS**
  - **X-ray Computerized Tomography**
    - **Dual Capability**

Internal
Blade
Geometry
Material
Flaws
Same
Equipment

- Digital Fluoroscopy
  - — High Speed (6X Faster Than Film)
  - — Cooling Passage Geometry
  - — Replaces Film X-ray
- X-ray Tomography
  - — High Resolution (< 010)
  - — Material Flaw Inspection
  - — New Capability

Figure 7

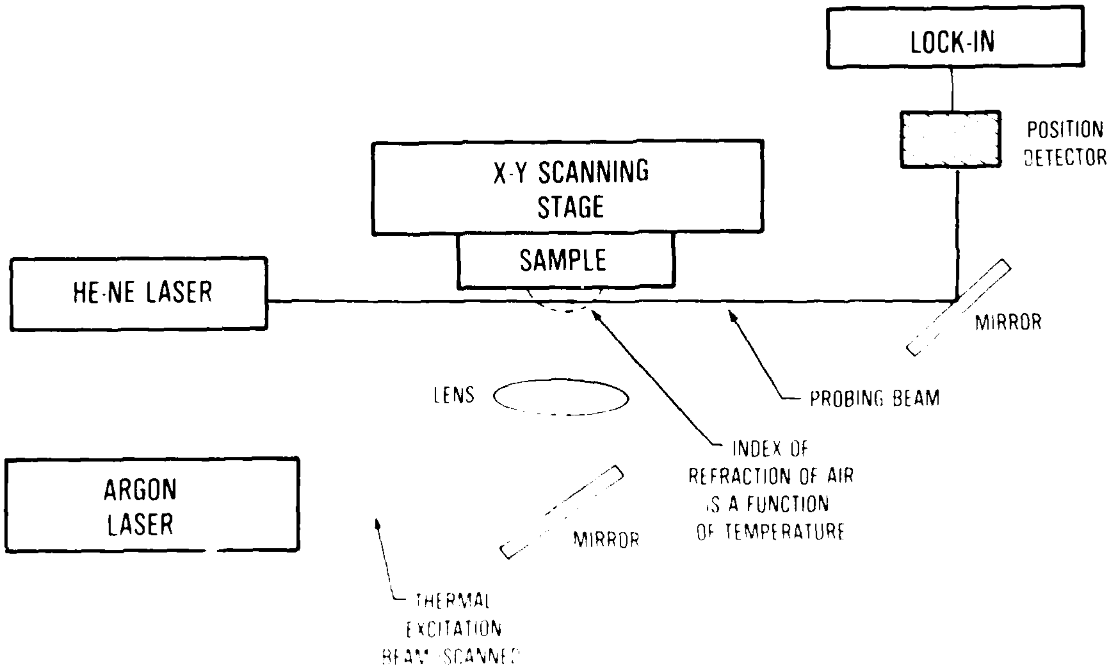
LOCK-IN
POSITION
DETECTOR
X-Y SCANNING
STAGE
SAMPLE
HE-NE LASER
MIRROR
LENS
PROBING BEAM
INDEX OF
REFRACTION OF AIR
IS A FUNCTION
OF TEMPERATURE
ARGON
LASER
MIRROR
THERMAL
EXCITATION
BEAM SCANNED

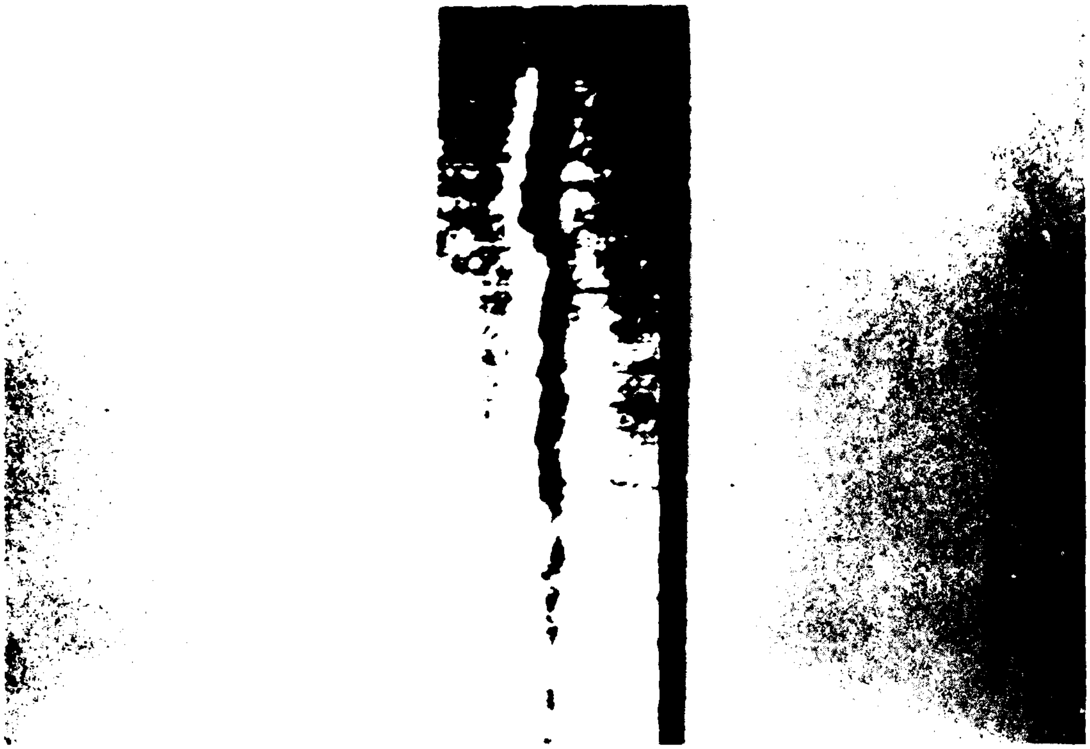

Figure 9

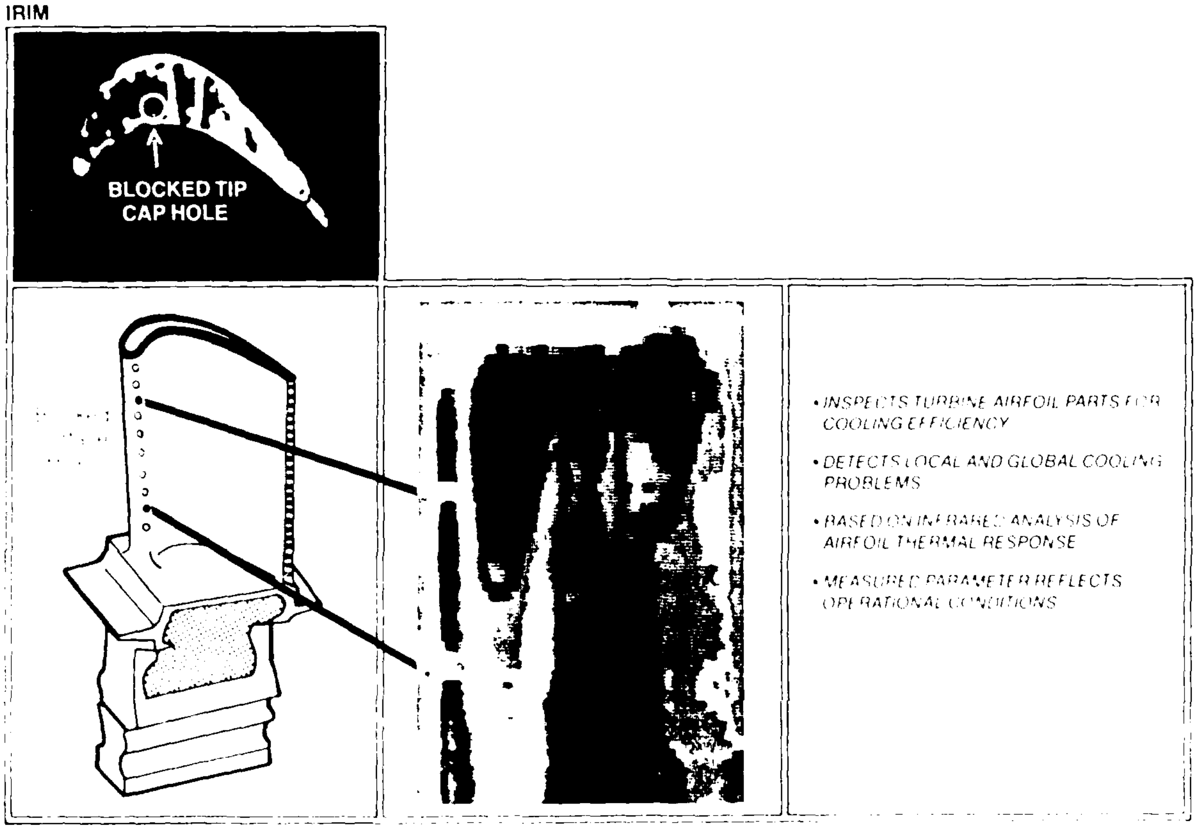

- INSPECTS TURBINE AIRFOIL PARTS FOR COOLING EFFICIENCY
- DETECTS LOCAL AND GLOBAL COOLING PROBLEMS
- BASED ON INFRARED ANALYSIS OF AIRFOIL THERMAL RESPONSE
- MEASURED PARAMETER REFLECTS OPERATIONAL CONDITIONS

Figure 10 IRIM infrared inspection module

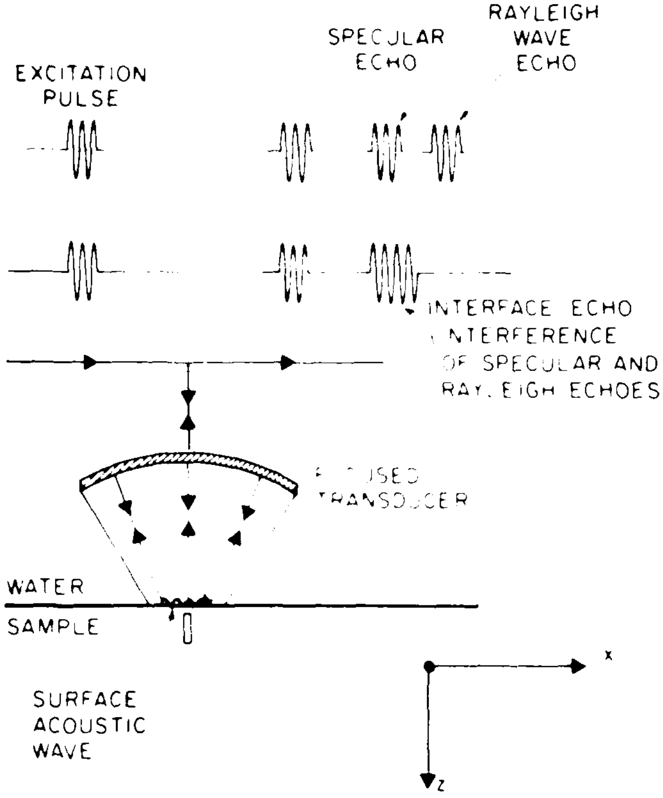
EXCITATION PULSE
SPECULAR ECHO
RAYLEIGH WAVE ECHO
INTERFACE ECHO
(INTERFERENCE OF SPECULAR AND RAYLEIGH ECHOES)
FOCUSED TRANSDUCER
WATER
SAMPLE
SURFACE ACOUSTIC WAVE
x
z

Figure 11

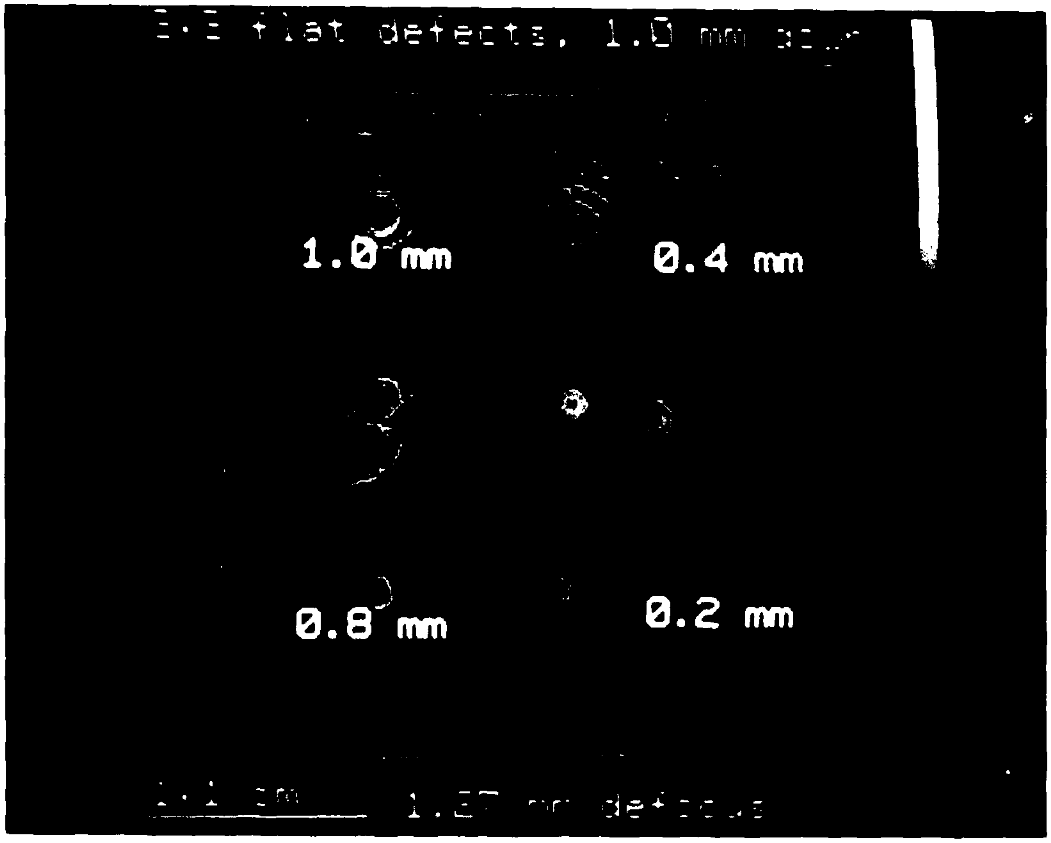
flat defects, 1.0 mm
1.0 mm
0.4 mm
0.8 mm
0.2 mm
1.27 mm defocus

Figure 12

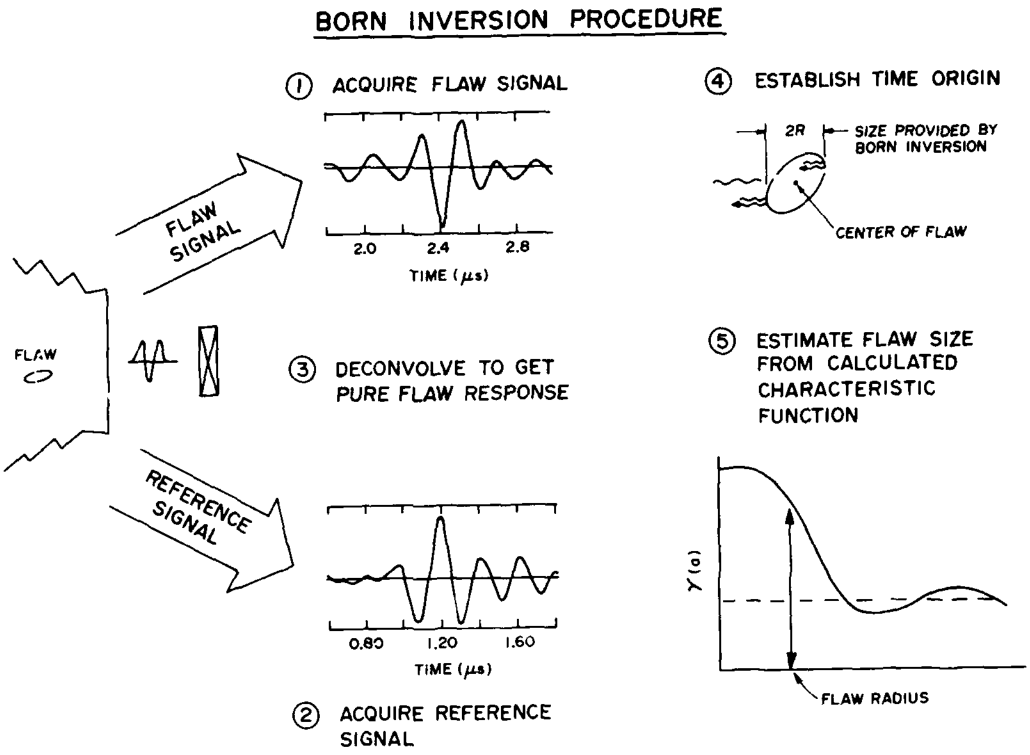
BORN INVERSION PROCEDURE
① ACQUIRE FLAW SIGNAL
2.0
2.4
2.8
TIME (μs)
FLAW SIGNAL
FLAW
REFERENCE SIGNAL
③ DECONVOLVE TO GET PURE FLAW RESPONSE
0.80
1.20
1.60
TIME (μs)
② ACQUIRE REFERENCE SIGNAL
④ ESTABLISH TIME ORIGIN
2R
SIZE PROVIDED BY BORN INVERSION
CENTER OF FLAW
⑤ ESTIMATE FLAW SIZE FROM CALCULATED CHARACTERISTIC FUNCTION
γ(a)
FLAW RADIUS

Figure 13

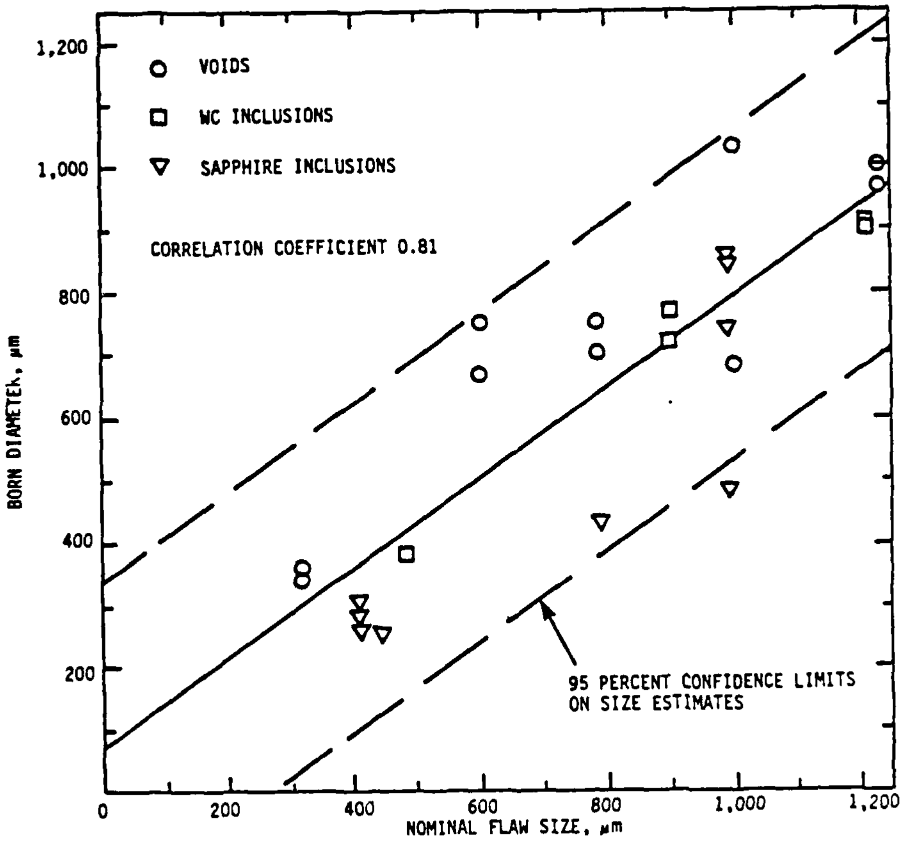

Figure 14 Correlation of nominal flaw sizes with estimates obtained by the Born Inversion Procedures (BIP)

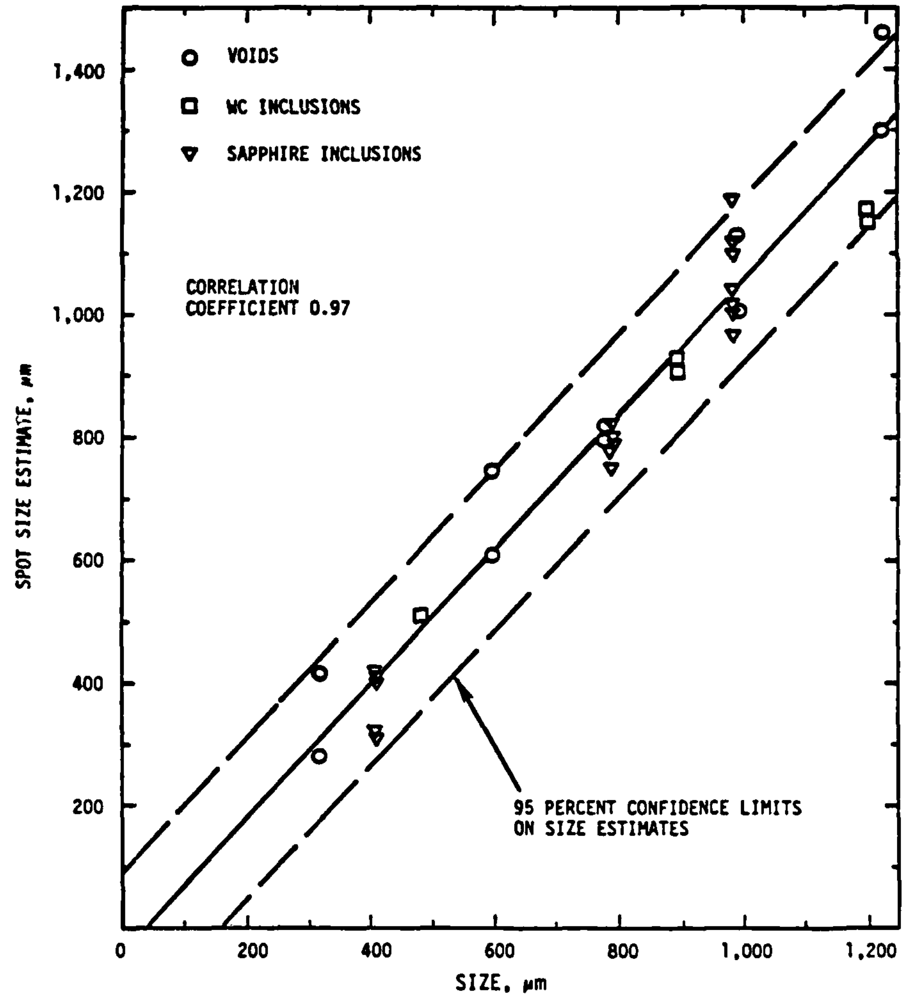

Figure 15 Correlation of nominal flaw sizes with estimates obtained by the Satellite-Pulse Observation Technique (SPOT)

STATISTICAL ANALYSIS OF SPIN PIT FAILURE DATA TO PREDICT INSERVICE B.1 LIVES OF GAS TURBINE DISKS

R. Mahorter and S. Fowler

Naval Air Development Center
Warminster, PA 18974

And

J. Salvino

Naval Air Propulsion Center
Trenton, NJ 08628

SUMMARY:

Currently used analytical predictive methods for establishing gas turbine disk lives have basic limitations associated with stress, thermal, and mission analyses among other factors. The difference between predicted life and actual in-service life is usually not known since most parts are removed from service prior to crack formation. The Navy is developing a predictive method based on statistical analysis of data from parts run to crack initiation in spin pit testing. As part of this work, the minimum number of disks needed to establish a viable predictive method will be determined. Although data from the small sample size (5) used has a great deal of statistical uncertainty, it appears that analytical predictions may be anti-conservative.

INTRODUCTION:

This program involves an approach to engine disc life prediction that incorporates extensive testing of used parts, statistical analysis predictive methods and feed back and reanalysis of currently used predictive methods to identify where these methods must be modified to achieve much more accurate predicted part lives. Part life is defined as the time at which one part in a thousand develops a 1/32" crack. This is also called the B.1 life.

The phase of the program being reported hereon is the testing to failure of a limited number of each of two disks. The times to failure were analyzed to predict a B.1 life by means of Weibull statistics. The Weibull method was chosen because it is the most common procedure in the aircraft engine field. A separate program is under way at George Washington University to determine the statistical distribution best suited to describing aircraft disk failures.

BACKGROUND:

The engine disc life prediction methodology currently used for naval aircraft consists first of analytically calculating operating stresses from rotational speeds, disc geometry and temperature distributions. The cyclic rates of these stresses are then inferred from mission analysis and experience from pilot interviews. The stresses and cyclic rates are combined to give a low cycle fatigue (LCF) spectrum. This spectrum is broken down into groups of discrete cycles. The life is predicted by comparing the number of cycles in each group with statistical materials data and summing the fractional lives by Minor's Rule (a linear summation model). Verification of the predicted life usually consists of running one or two engines to that life and inspecting for cracks. Cracks are not usually found since the design philosophy is quite conservative.

The predicted lives are used in engine management to plan overhauls and part replacement. Since new parts have lead times for procurement of up to two years, significant errors in life prediction can have drastic consequences on replacement part availability. Errors in life prediction have occurred with several engines. Replacement parts were not available and it became necessary to use engines to times significantly longer than the predicted lives. This overflying was accomplished by arduous non-destructive inspection techniques (NDI) and crack propagation calculations.

The program being reported upon is an attempt to establish a statistically meaningful failure distribution for a limited number of components. An experimental B.1 life can be determined and compared with the analytical life. The basic method for obtaining the data is by cyclic spin pit testing. This method duplicates the stresses in the part without the complicating factors of thermal gradients and cycle variations.

Weibull distributions have a wide variety of applications, particularly as a model for product life. The Weibull method allows fatigue test results to be plotted and used to project cumulative percentages of failures. The result is a graphical description of the fatigue-life distribution pattern of a product. Basic Weibull function equations are generally complex and will not be described in detail in this report. A brief description of how to apply Weibull techniques to fatigue test data is included. However, if the reader desires to investigate the mathematics of the Weibull techniques to a further degree, he can consult any of the references listed at the end of the paper.

The Weibull reliability function (R), the proportion of the product population surviving an age of at least time (t), is:

$$R(t) = \exp\left(-\left(t/\alpha\right)^{\beta}\right)$$

with β being the slope or shape parameter, and α being the scale parameter or characteristic life defined as the time at which 63.2% of the product population has failed. This can be reduced to:

$$\ln \ln (1/R) = \beta \ln (t) - \beta \ln (\alpha)$$

that gives a linear relation for R in terms of t when plotted on Weibull probability paper.

To construct a Weibull plot from the results of a fatigue test, the failure times are plotted against the median rank or percent failed which is a function of the sample size. These points can be approximated by a straight line which can be used to project cumulative percentages of failures as a function of part life with a 50% confidence level. The particular percentage of failure of interest in this study is 0.1% or when one part in a 1000 fails, also known as the B.1 life.

EXPERIMENTAL PROCEDURE:

SELECTION OF TEST SAMPLE:

The disks to be tested were selected by several criteria. First the analytically predicted life had to be fairly low so that any life extension would be immediately useful. Second, the operating temperature had to be below the creep threshold for the disk material since testing was to be done at room temperature. Finally, the disks should be from an engine where the average operating time is close to the predicted life. Based on these criteria two adjacent early stage compressor disks from the same engine model were selected. Both were titanium - 6 Al-4V alloy.

Since they were adjacent disks it was possible to spin them as a unit and significantly reduce test time and cost. Disk A had two low life locations, a tiebolt hole of 3100 hours and the blade slot of 3750 hours. Disk B had as its limiting location a tie-bolt hole with a predicted life of 2400 hours. Figures 1 and 2 show sketches of the low life locations.

SPIN PIT TESTING:

The disks were run in pairs in the Naval Air Propulsion Center spin pits of Trenton, NJ. The built up unit was essentially a subsection of the compresser complete with spacers and blades as shown in Figure 3. The spin pit is evacuated to reduce drive load and prevent frictional heating.

Low cycle fatigue testing is accomplished by alternating between a maximum and minimum rotational speed. Acceleration and deceleration is by means of an air driven turbine. The cycle (shown in Figure 4) was developed by the engine manufacturer to relate to engine operating time. One cycle is equal to 1.45 flight hours for disk A and 1.54 flight hours for disk B.

Testing was stopped at intervals to allow inspection of the disks for crack initiation. The interval was chosen so that propagation of the crack from initiation to failure was unlikely to occur within one interval. Since the length of the interval has a large impact on total test time and cost, it was lengthend in increments from 600 cycles to 2000 cycles as experience and confidence increased.

INSPECTION PROCEDURE:

At the end of each test interval the predicted failure locations were inspected for cracks. Inspection of the bolt holes was by means of a rotating eddy current probe (RECHII type). The probe was calibrated against a corner notched standard supplied by the manufacturer of the engine. Based on the size of the notch in the standard a rough estimate of signal size equivalent to a .030" long crack was made. In the case of the blade slots in disk A, a sliding eddy current probe and standard supplied by the manufacturer was used for inspection.

Once a rejectable eddy current signal was observed, the bolt hole surface was metallographically polished, etched, and replicated using acetate tape. The tape was then examined using the scanning electron microscope (SEM) for evidence of a crack. The eddy current rejection limit was found to correspond to a 0.30" to 0.060" crack.

ANALYSIS OF RESULTS:

Table I summarizes the test sample part history and spin pit data. The values of total part time were obtained by summing the part "time since new" (time accumulated during fleet operations) and the NAPC LCF equivalent hours. Seven part failures have been observed since the spin pit testing was initiated: four A stage disks and three B stage disks. All the failures occurring for both the A and B stage discs were bolt-hole cracks that exceeded the 1/32" limit. Past gas turbine engine LCF analysis has shown that bolt-hole failures are the primary cause of low cycle fatigue in engine discs.

The Weibull analysis of the data found in Table II for the A and the B stage disks are shown in Figures 5 and 6 respectively. The Weibull slope for A was found to be 2.0 with a corresponding B.1 life of 1,100 hours. the slope of disc B was calculated at 3.2 with a B.1 life of 4,500 hours. It is important to note that these calculations were made assuming that all five test samples of each stage had failed. As spin pit testing on the non-failed parts continues, the parts with the highest running times will continue to accumulate more total hours. The effect on the Weibull plots from the continued testing will force the slope to decrease for both discs. This decrease in slope will be accompanied by a decrease in the B.1 life. Only after all the test samples have failed can the results be considered final. At this time the results must be considered preliminary.

As with any statistical method, the degree of confidence in the calculations increases as the sample size increases. However, when analyzing gas turbine engine disks the luxury of a large number of test samples is not feasible. The high cost of engine disks and limited availability of spin pit facilities limit the sample size which can be tested. The loss of accuracy due to the small test sample used in this study is discussed in the following text along with ways that this loss of accuracy may be minimized.

Figure 7 represents the probable error of Weibull slope as a function of the number of failures observed. It can be seen that the slope error corresponding to five failures is approximately 20% or ± 10%. The observed slope for disk A of 2.0 could be as low as 1.8 or as high as 2.2. This variation in slope translates graphically to approximately ± 400 hours in B.1 life. Similiarly, disk B slope of 3.2 lies between 2.9 and 3.5 which corresponds to ± 1,000 hours in B.1 life. These variations in B.1 life are for a failure time that is predicted with only 50% confidence. The variation of B.1 life due to slope variation is greatly magnified when the 90% confidence band is considered. This band can be graphically represented by locating the lines corresponding to both the 5% and 95% confidence levels around the data points that represent the 50% confidence level prediction. Any failure times that fall within this region can be said to have a 90% confidence level of prediction. The B.1 life for disk A can be predicted with a 90% confidence to fall between 0.0 and 10,000 hours and for disk B between 0.0 and 18,000 hours which can be seen in figures 8 and 9. It can be seen that the loss of accuracy due to the small sample size is considerable.

The large size of the 90% confidence band occurring at the B.1 life arises because the calculations for a test sample with five parts is being used to predict the life distribution for a population of 1,000 parts. A question of interest is how large must the sampel size be in order to bring the B.1 90% confidence level down to an acceptable width? Figures 10 and 11 show the same B.1 and β obtained for the two stages, however, it is assumed that these results were obtained from a sample size of 50 failures. The larger sample size increases the degree of confidence, which can be seen graphically by a reduction of the 90% confidence level band. The band for disk A assuming 50 test samples extends from less than 100 to 4,000 hours and for disk B from 1,000 to 10,000 hours. Even for the case where 50 discs are spun to failure, the confidence level provided by the Weibull method is unacceptable.

DISCUSSION OF RESULTS:

This discussion will not consider the range of possible B.1 lives based on the 90% confidence band shown in Figure 8 and 9. The major reason for ignoring this variation lies in the fact that a similar confidence band has not been established or even estimated for the analytical prediction.

The statistically predicted lives for the boltholes of each disk do not agree with the analytically predicted values is shown in Table II. The blade slot area of disk A is considered undefined since no cracks developed in that location. It should be noted that the order of failure in the two boltholes was contrary to that predicted even though material of the parts was identical and the geometry was very similar.

The most disturbing of the results lies in the anticonservative nature of the analytical prediction for the disk A bolthole. The assumption of conservatism was one of the major driving forces in the implementation of the project and the expected result was a lengthening of component lives. The observed result suggests the probability that numerous in-service parts (besides the components under test) are operating beyond the actual B.1 life.

The one positive result was that the low cycle fatigue (LCF) initiation site was in both cases correctly predicted by the manufacturer. The implication of this result is that in-service inspections can focus on particular areas of the disks and therefore more sensitive methods can be applied.

CONCLUSIONS:

1. Analytically and statistically determined lives do not agree even in terms of relative lives for similar geometrics features in identical material.

2. Analytically determined lives are not consistantly conservative.

3. The low life feature of each disk was correctly identified.

REFERENCES ON WEIBULL ANALYSIS:

1. Mann, N. R., Schafer, R. E., Singpurwalla, N. D., "Methods for Statistical Analysis of Reliability and Life Data", John Wiley and Sons. (1974)

2. McCool, John I., "Life Test and Weibull Analysis", ASME Winter Meeting Transactions, (Nov. 1981)

3. Nelson, W. "Applied Life Data Analysis", Wiley Series in Probability and Mathematical Statistics, (1982)

4. Wilks, S. S., "Mathematical Statistics", John Wiley and Sons, Inc., (1962).

TABLE I
PART HISTORY, ENGINE OPERATION AND SPIN PIT

ASSEMBLY NUMBER	STAGE	ENGINE OPERATING HOURS	NAPC LCF CYCLES	NAPC EQUIV HOURS	TOTAL TIME HOURS
1	A	4,272.7	33,100	47,995	*52,267
	B	5,293.0	12,100	18,634	*23,927
2	A	4,029.4	17,100	24,795	*28,824
	B	4,029.4	13,100	20,174	*24,203
3	A	4,281.1	11,100	16,095	*20,376
	B	4,272.7	30,110	46,354	50,643
4	A	5,293.0	21,100	30,595	35,888
	B	4,281.1	21,100	32,494	36,775
5	A	4,850.0	7,100	10,295	*15,145
	B	4,850.0	16,100	24,794	*29,644

*CRACK OBSERVED

TABLE II
ANALYTICAL AND STATISTICAL LIVES FOR LOW CYCLE FATIGUE CRITICAL LOCATIONS

LOCATION	ANALYTICAL LIFE	STATISTICAL LIFE
BOLTHOLE, DISK A	3100 HOURS	1100 HOURS
BLADE SLOT, DISK A	3750 HOURS	NOT DEFINED
BOLTHOLE, DISK B	2400 HOURS	4500 HOURS

FIGURE 1

LOW CYCLE FATIGUE CRITICAL LOCATIONS OF DISK A

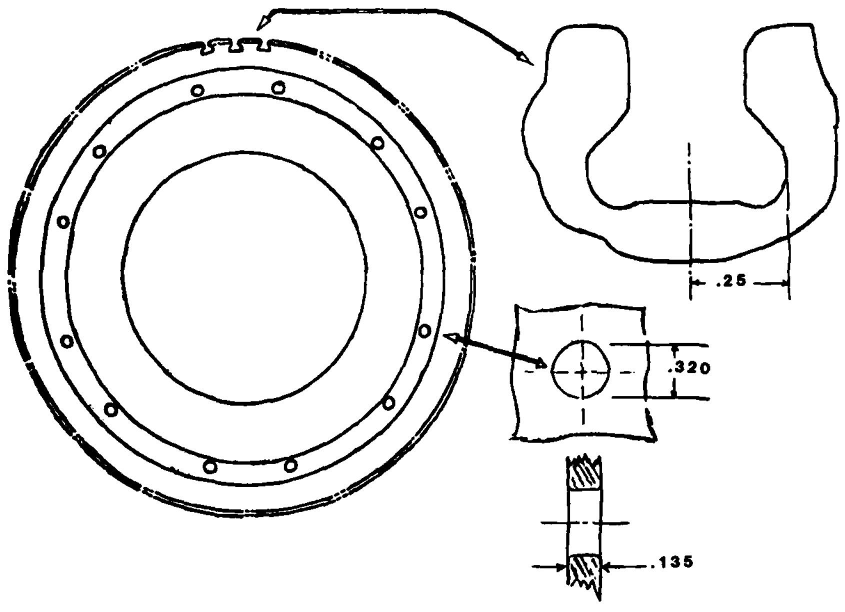

FIGURE 2

LOW CYCLE FATIGUE CRITICAL LOCATION ON DISK B

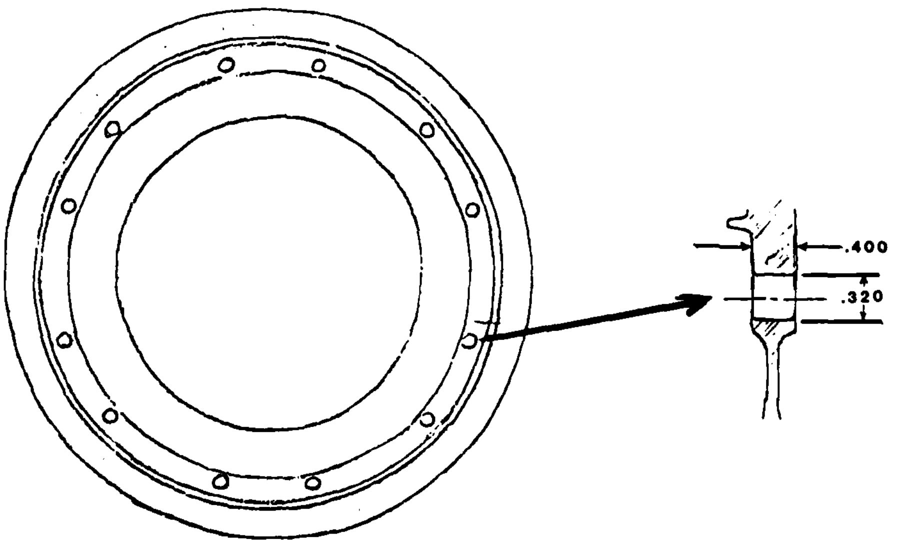

FIGURE 3
ASSEMBLY READY FOR SPIN PIT TESTING

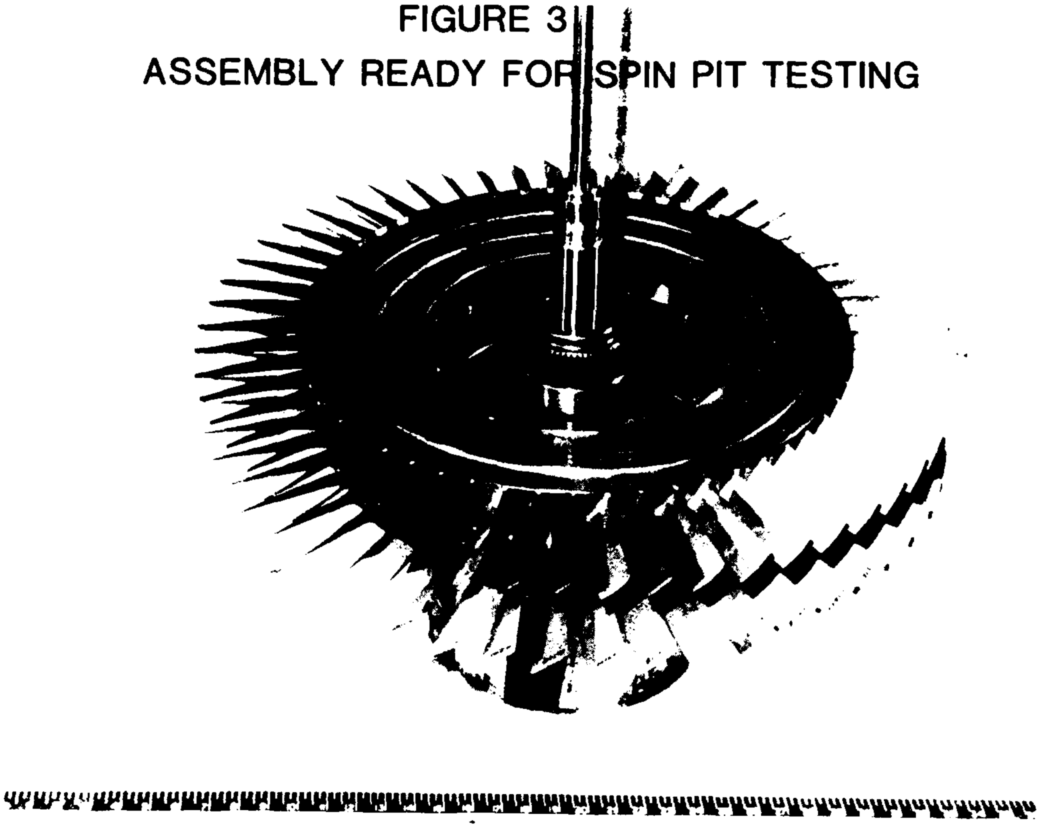

FIGURE 4
SPIN PIT TEST CYCLE

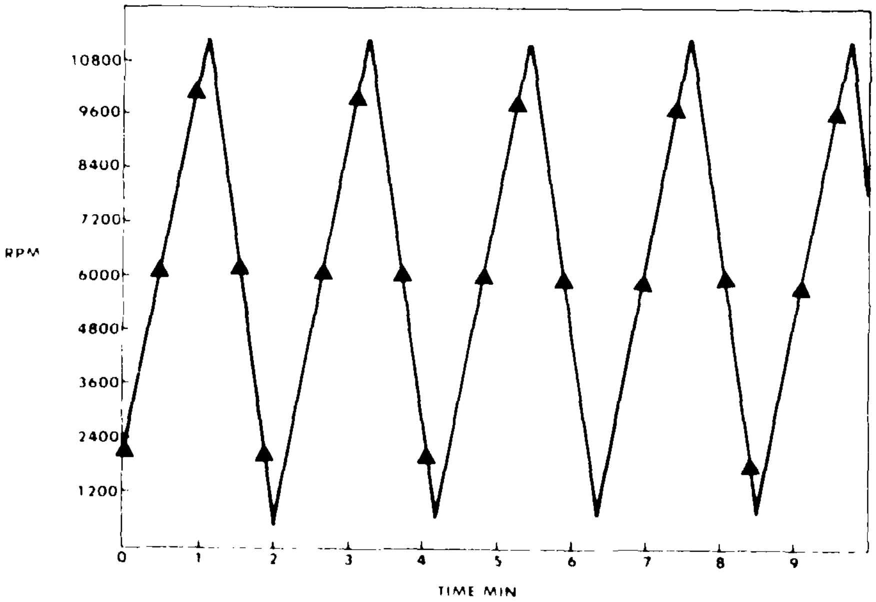

FIGURE 5

WEIBULL PLOT FOR STAGE A BOLTHOLE DATA B.1 = 1100 HRS, $\beta \approx 2.0$

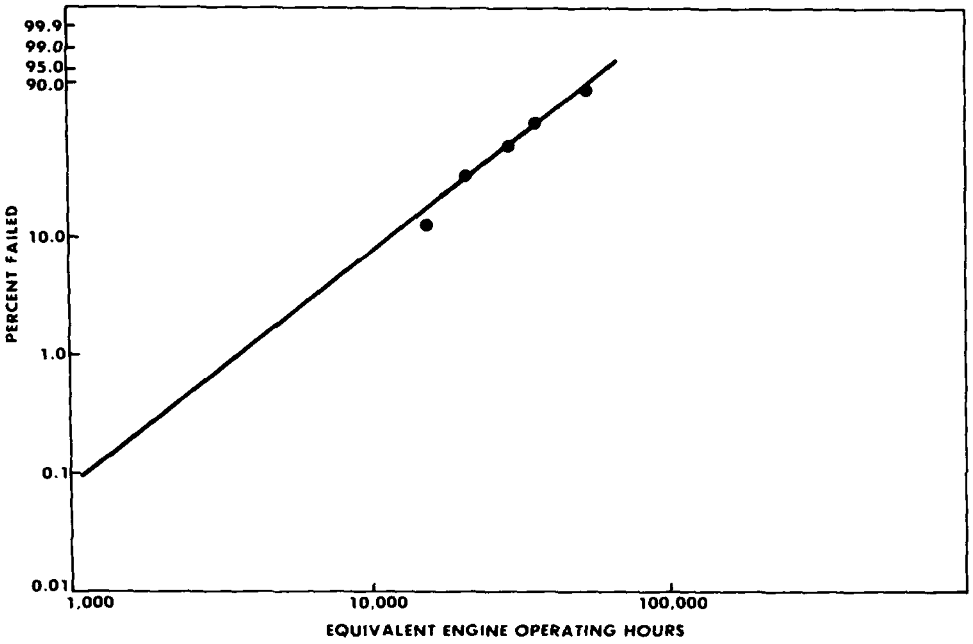

FIGURE 6

WEIBULL PLOT FOR STAGE B BOLTHOLE DATA B.1 = 4500 HRS, $\beta = 3.2$

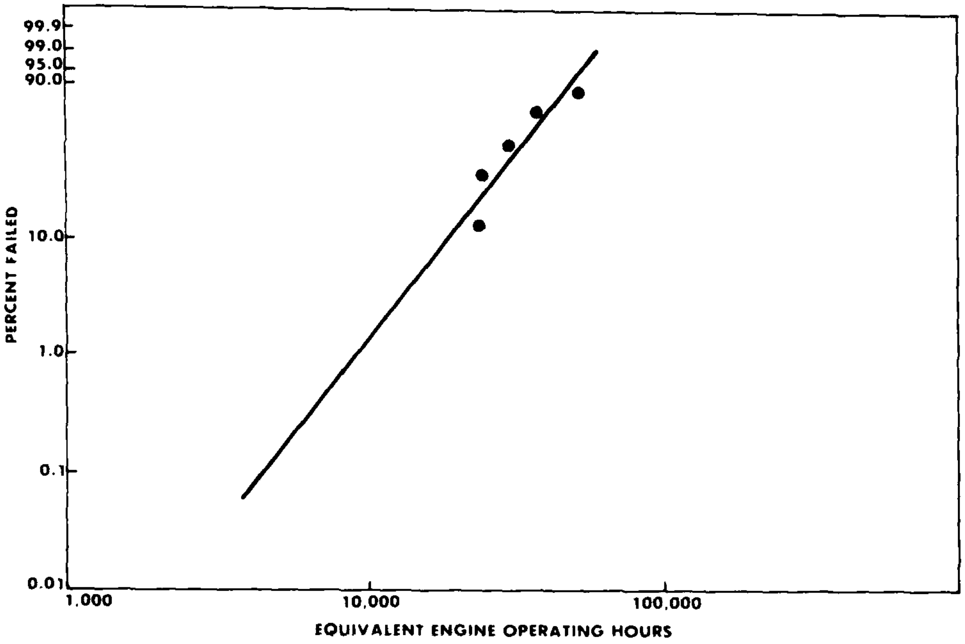

FIGURE 7

PROBABLE ERROR IN WEIBULL SLOPE WITH SAMPLE SIZE

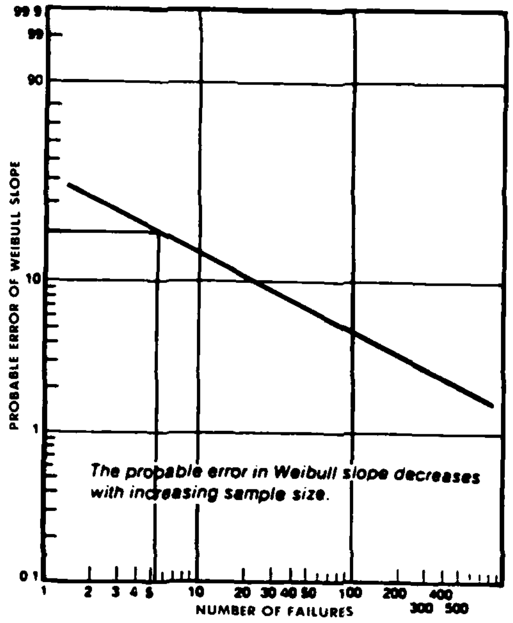

The probable error in Weibull slope decreases with increasing sample size.

FIGURE 8

WEIBULL PLOT FOR STAGE A BOLTHOLE DATA SHOWING 90% CONFIDENCE LEVEL AND EFFECT OF β VARIATIONS

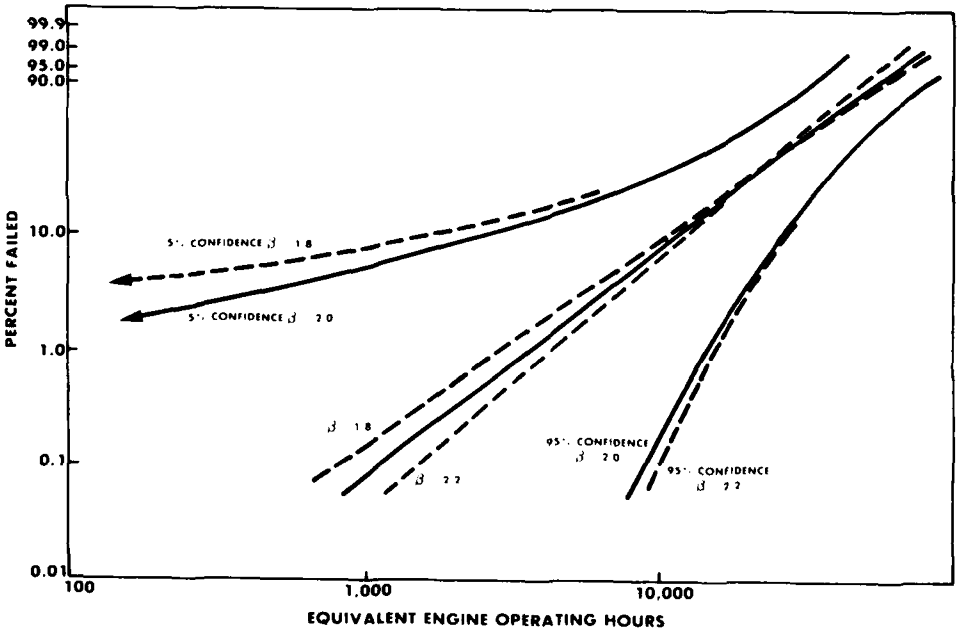

FIGURE 9

WEIBULL PLOT FOR STAGE B BOLTHOLE DATA SHOWING 90% CONFIDENCE LEVEL AND EFFECT OF β VARIATIONS

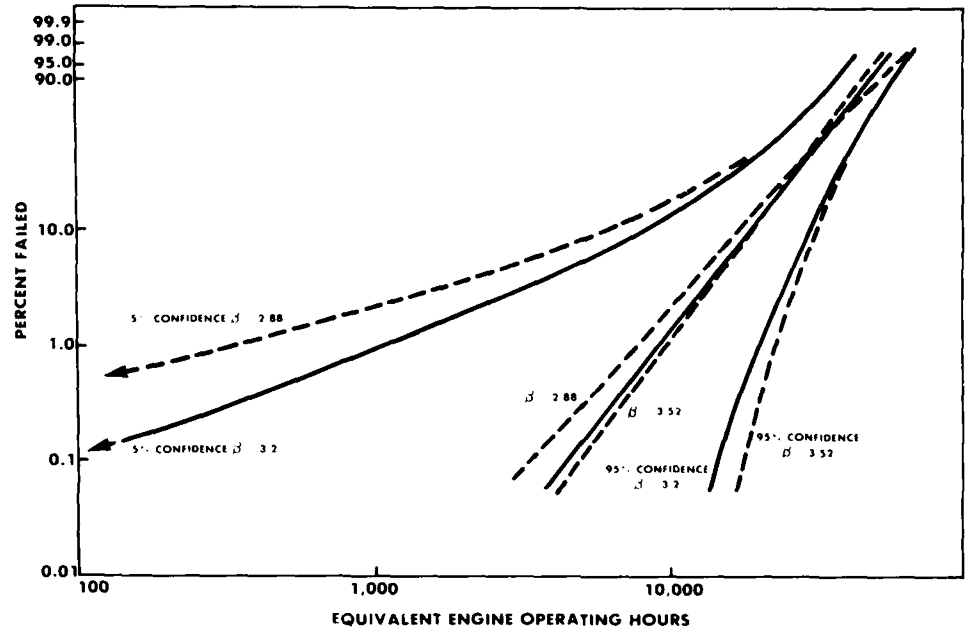

FIGURE 10

WEIBULL PLOT WITH 90% CONFIDENCE BAND ASSUMING 50 FAILURES, B.1 = 1100 HRS, β = 2.0

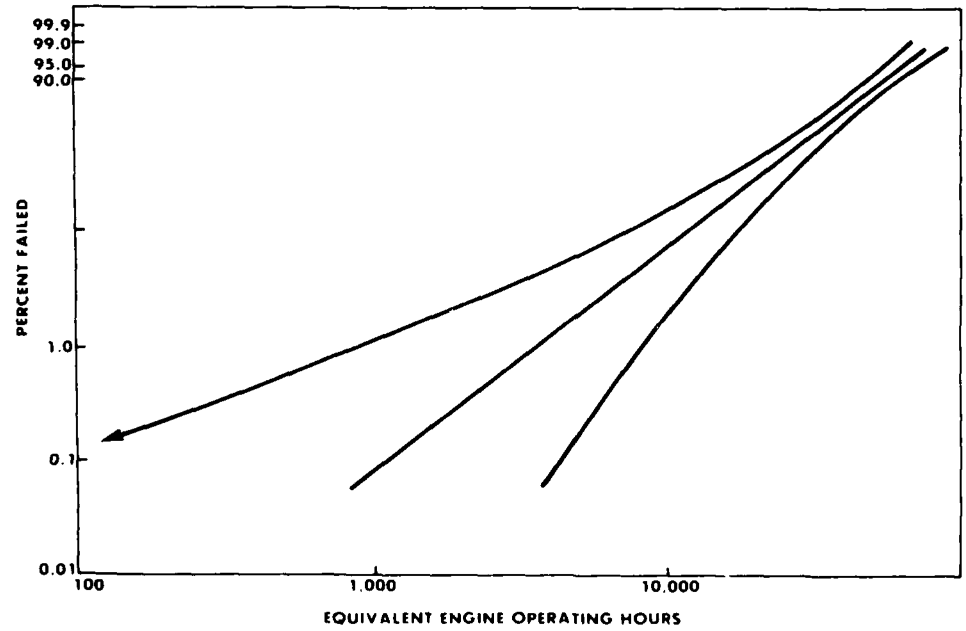

FIGURE 11
WEIBULL PLOT WITH 90% CONFIDENCE BAND ASSUMING 50 FAILURES, B.1 = 4500 HRS, β = 3.2

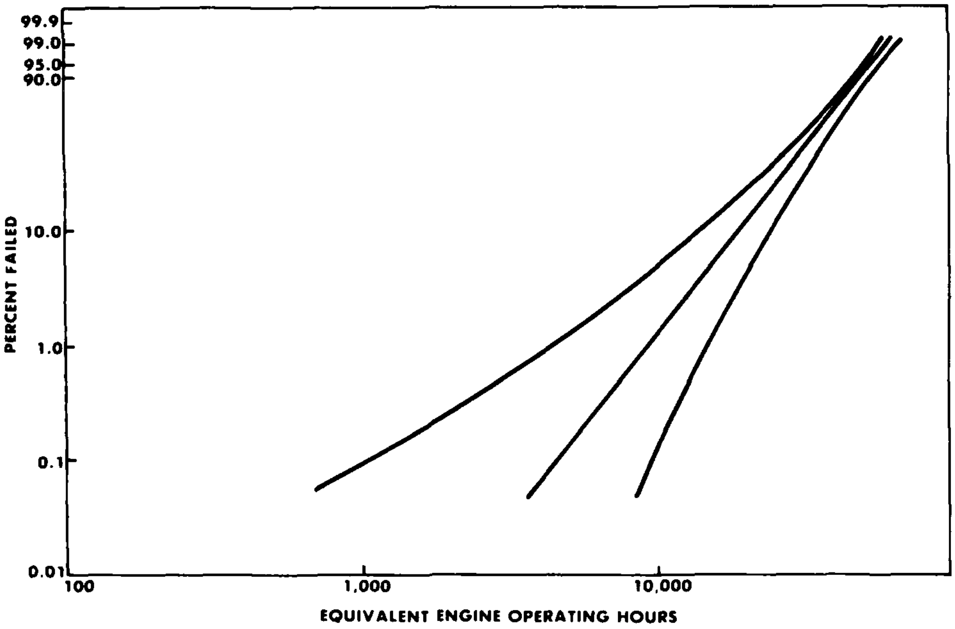

Fracture Mechanics and LCF-Properties of Engine Discs of Ti 6Al-4V,Inconel 718 and Udimet 700 P/M-HIP

by
Dr.Ing. Walter Schütz and
Dipl.Ing. R. Heidenreich

Industrieanlagen-Betriebsgesellschaft mbH
Einsteinstrasse 20, 8012 Ottobrunn, Germany

SUMMARY

Over the last decade IABG has carried out a large number of tests on gas turbine materials to determine the materials data necessary for the conventional lifing approach, that is LCF data, including dwell time effects and some HCF data. The data necessary for a damage tolerance approach, namely K_{IC} or K_Q respectively, as well as crack propagation properties i.e. da/dN vs. ΔK were also determined.

These tests were done at room and typical service temperatures. The materials were Ti 6Al 4V, Inconel 718 and Udimet 700 P/M-HIP.

The specimens were machined from a number of nominally identical compressor discs of Ti Al6 V4, from compressor discs of Inconel 718 and from disc-shaped "pancakes" of Udimet 700 P/M-HIP. Constant amplitude tests under strain control with unnotched specimens and under stress constrol with notched specimens were carried out, as well as a number of relatively simple variable amplitude tests.

1. INTRODUCTION

In view of the steadily increasing life and reliability requirements, fatigue life prediction of turbine and compressor discs - the so-called "lifing" - is becoming more and more important. In the design and dimensioning phases relevant specimen data are employed. In later phases, specimen data are still required, for example for checking the fatigue life prediction models used in the numerical fatigue life prediction of the disc or for obtaining statistically - derived scatter data which are necessary for determining the safety factor on life. Scatter of relevant materials data also is an extremely important property which can only be ascertained by specimen tests.

New materials will always be assessed - at least initially - by such relatively simple and inexpensive tests.

The above statements are valid both for the conventional "safe life" approach - **and** for the more recent "Retirement for Cause" (Damage Tolerance) approach in which cracks are tolerated.

2. TEST PROGRAMME

2.1 GENERAL

The test programme which is the basis of the present paper has been underway at the IABG /1-9/ for more than ten years.

The materials investigated were Ti Al6 V4, Inconel 718 and Udimet 700 P/M-HIP. LCF and some HCF data were obtained on unnotched and notched specimens under strain and load control at room- and typical service temperatures. Fracture thoughness K_{IC} and K_Q as well as fatigue crack propagation properties were also determined. If a sufficient number of specimens was available, a statistical evaluation was carried out.

Variable amplitude tests simulating the calculated local stress-time-history of a critical location in a turbine disc were also performed. The full programme also adressed the question of the correlation between microstructure and the above properties /10-12/. However, this will not be discussed in this paper; obviously only a fraction of the large number of results will be shown and discussed anyway.

2.2 MATERIALS AND SPECIMENS

The static properties of the materials investigated are shown in Table 1, the dimensions of the specimens employed in Figs. 1 and 2. The Ti 6Al 4V specimens were machined from compressor disc forgings; an example is shown in Fig. 3. For the tests on Inconel

718, two high pressure compressor discs of 380 mm diameter, see Fig. 4, were available for the specimens. Six "pancakes" were employed for the Udimet 700 P/M- HIP specimens.

3. RESULTS

3.1 LOW CYCLE FATIGUE

The monotonic and cyclic stress-strain curves of Inconel 718 for several temperatures are shown in Fig. 5, the crack initiation behaviour in the shape of strain-life curves in Fig. 6. The corresponding cyclic properties are contained in Table 2. Inconel 718 proves to be a strain-softening material, see Fig. 5. It is obvious from Fig. 6 that 600 °C represents an upper temperature limit for Inconel 718.

The results of stress controlled constant and variable amplitude tests with notched specimens are shown in Fig. 7. A 2 minute dwell time reduced the number of cycles to crack initiation **and** to failure by a factor of two to three. No such influence was found in strain controlled tests on unnotched specimens.

Three stress controlled tests with the simple flight-by-flight sequence shown in the upper right hand corner of Fig. 7 were also carried out. It is seen that the crack initiation phase takes up a lower percentage of the life to failure (i.e. the crack propagation phase is longer) than under constant stress amplitudes.

Similar results for Udimet 700 P/M-HIP are shown in Figs. 8 to 10 and included in Table 2. This material tends be strain softening at RT and low strain amplitudes, see Fig. 7, while it is strain hardening at 500 °C and 650 °C. Finally, at 700 °C, it is nearly neutral. The strain-life cur-ves in Fig. 9, together with the cyclic stress strain curves in Fig. 8, prove that Udimet 700 P/M-HIP can be utilised at higher temperatures than Inconel 718. In Fig. 10 more strain controlled tests are plotted, the specimens for which were machined from "pancakes" made by different firms. Details of their manufacture are listed in Table 3. As can be seen from Fig. 10, the results were similar, no manufacturer having a distinct advantage.

The stress controlled tests with notched specimens of Udimet 700 P/M-HIP are shown Fig. 11. A dwell time of two minutes was more detrimental than for Inconel 718, the life reduction factor being about five as against two to three. The simple flight-by-flight tests mentioned before were also performed with Udimet 700 P/M-HIP. The effect of the test temperature 650 °C on fatigue life is considerably larger than in the constant amplitude tests, probably because of the mean stress relaxation in the latter tests.

Based on the constant strain amplitude data, the fatigue life of the notched specimens at room temperature and at 650 °C was calculated by the local approach. The results are also shown in Fig. 11 (closed symbols, unbroken lines): The fatigue life under constant amplitudes was predicted accurately for 650 °C and 2 minutes dwell time, and conservatively for 650 °C and room temperature. The fatigue life under the flight-by-flight sequence was also predicted conservatively at 650 °C and room temperature.

Similar LCF data were also determined for Ti 6Al 4V, but are not presented in this paper.

3.2 DAMAGE TOLERANCE PROPERTIES

The fracture toughness of CT-specimens taken from the Ti 6Al 4V compressor disc forging shown in Fig. 3 was determined; the associated statistical evaluation of the C-R specimens is given in Fig. 12. It is seen that

- on the average, fracture toughness is higher in the hub area than in the rim area and
- there is no discernible difference between the R-C and C-R orientation of the specimens.

Scatter (at a coefficient of variation v = 0.060) is quite low, even if all the C-R-specimens (from the hub and the rim area) are evaluated together as in Fig. 12. By the way, the manufacturer of the jet engine in question requires a minimum fracture toughness for this compressor disc of 1650 N/mm in the C-R- orientation, the control specimen being taken from the rim area. One specimen at 1617 N/mm did not meet this requirement, see Fig. 3.

Relevant crack propagation properties are shown in Fig. 13: A one minute dwell time proved to be highly detrimental at room temperature and at 300 °C, while this temperature alone did not affect the results. The scatter bands of Fig. 13 are based on four to five tests per parameter.

The fracture toughness values K_{IC} and K_Q respectively for Inconel 718 (as well as for Ti 6Al 4V and Udimet 700 P/M-HIP) are summarized in Table 4.

The effects of a temperature of 620 °C and of a one minute dwell time is demonstrated in Fig. 14. At room temperature the dwell time resulted in such a large scatter that the results are not shown in Fig. 14: Two crack propagation specimens were not influenced by the dwell time, two others gave a reduction of the number of cycles to complete fracture (from 4 mm crack length) by a factor of 20!

In Fig. 15 the crack propagation properties of Inconel 718 and Udimet 700 P/M-HIP are compared at room temperature: Inconel 718 has a higher crack propagation rate over the whole range of stress intensity factors investigated. As Fig. 15 also shows, a one minute dwell time did not influence the crack rate of Udimet 700 P/M-HIP at 620°C (contrary to Inconel 718).

4. REFERENCES

/ 1/ Zenner, H. und W. Schütz:
Bauteilspezifische Werkstoffuntersuchungen - Untersuchungen an Triebwerksscheiben aus Ti 6Al 4V - Zusammenfassung und Diskussion der Ergebnisse.
IABG Report, No. TF-676.1, 1977

/ 2/ Zenner, H., H. Kratzer, R. Heidenreich, W. Oberparleiter und W. Schütz:
Bauteilspezifische Werkstoffuntersuchungen - Untersuchungen an Triebwerksscheiben aus Ti 6Al 4V - Niedrigwechselermüdung, Rißfortschritt und Bruchzähigkeit.
IABG Report, No. TF-676.3, 1977

/ 3/ Zenner, H., W. Scharfenberger und W. Schütz:
Bauteilspezifische Werkstoffuntersuchungen - Ergänzende Untersuchungen an Triebwerksscheiben aus Ti 6Al 4V.
IABG Report No. TF-873, 1979

/ 4/ Zenner, H., W. Scharfenberger und W. Schütz:
Bauteilspezifische Werkstoffuntersuchungen - Untersuchungen an Triebwerksscheiben aus Inconel 718 - Zusammenfassung und Diskussion der Ergebnisse.
IABG Report, No. TF-677.1, 1977

/ 5/ Zenner, H., H. Kratzer, R. Heidenreich, W. Oberparleiter und W. Schütz:
Bauteilspezifsche Werkstoffuntersuchungen - Untersuchungen an Triebwerksscheiben aus Inconel 718 - Niedrigwechselermüdung, Rißfortschritt und Bruchzähigkeit.
IABG Report, No. TF-677.3, 1977

/ 6/ Heidenreich, R., W. Scharfenberger und W. Schütz:
Bauteilspezifische Werkstoffuntersuchungen - Untersuchung von heiß-isostatisch gepreßten Triebwerksscheiben aus Udimet 700-Pulver, Phase I.
IABG Report, No. TF-1009, 1980

/ 7/ Heidenreich, R., H. Zeitler, W. Scharfenberger und W. Schütz:
Bauteilspezifische Werkstoffuntersuchungen - Untersuchung von heiß-isostatisch gepreßten Triebwerksscheiben aus Udimet 700-Pulver, Phase II.
IABG Report, No. TF-1158, 1981

/ 8/ Heidenreich, R., H. Stengel, H. Zeitler, W. Scharfenberger und W. Schütz:
Bauteilspezifische Werkstoffuntersuchungen - Untersuchung kennzeichnender Werkstoff-und Festigkeitseigenschaften an pulvermetallurgisch hergestellten Hohlzylindern und Triebwerksscheiben aus Udimet 700. IABG Report, No. TF-1159, 1981 IABG-Report, No. TF-1159, 1981

/ 9/ Heidenreich, R., J. Bergmann, H. Zeitler, W. Scharfenberger und W. Schütz:
Bauteilspezifische Werkstoffuntersuchungen - Zusammenfassende Diskussion und Beurteilung aller Untersuchungsergebnisse an heißisostatisch gepreßten Halbzeugen aus Udimet 700-Pulver.
IABG Report, No. TF-1160, 1981

/10/ Scharfenberger, W. und H. Zocher:
Bauteilspezifische Werkstoffuntersuchungen - Untersuchungen an Triebwerksscheiben aus Ti 6Al 4V - Gefügeaufbau und mechanisch-technologische Eigenschaften.
IABG Report, No. TF-676.2, 1977

/11/ Scharfenberger, W. und H. Zocher:
Bauteilspezifische Werkstoffuntersuchungen - Untersuchungen an Triebwerksscheiben aus Inconel 718 - Gefügeaufbau und mechanisch-technologische Eigenschaften.
IABG Report, No. TF 677.2, 1977

/12/ Fey, G., W. Scharfenberger und H. Zocher:
Bauteilspezifische Werkstoffuntersuchungen - Untersuchung von heiß-isostatisch gepreßten Triebwerksscheiben aus Udimet 700-Pulver, Phase I - Sonderband: Abbildungen der metallografischen und mikrofraktografischen Analysen.
IABG Report, No. TF-1009.2, 1980

Material	Test Temperature °C	0,2% Yield Strength N/mm²	Ultimate Tensile Strength N/mm²	Elongation %	Reduction of Area %
Ti 6Al 4V	20	938	1 027	13	38
	300	595	730	18	54
Inconel 718	500	1 000	1 203	-	38
	600	975	1 212	-	35
	620	920	1 135	-	37
	700	885	1 118	-	32
Udimet 700 P/M-HIP Wiggin/MBB/ Seilstorfer	20	948	1 298	23	24
	650	880	1 238	21	21
Röchling	20	953	1 295	20	21
	650	901	1 235	26	27
Seilstorfer	20	972	1 396	19	15
	650	909	1 245	26	28
Wiggin	20	981	1 386	17	13
	650	918	1 268	12	16

Tab. 1 Tensile Properties of Ti 6Al 4V, Inconel 718 and Udimet 700 P/M-HIP

Material	Test Temperature °C	σ_f' N/mm²	b -	ε_f' -	c -	K' N/mm²	n' -	E N/mm²
Inconel 718	500	1311	-0,0596	0,389	-0,631	1433	0,0945	158 000
	600	1237	-0,0609	0,431	-0,665	1336	0,0916	153 000
	620	1126	-0,0627	0,284	-0,657	1270	0,0954	151 000
	700	1056	-0,0644	0,288	-0,669	1191	0,0962	146 000
Udimet 700 P/M-HIP	20	1817	-0,0757	0,358	-0,552	2092	0,1373	212 000
	500	1965	-0,0846	7,274	-1,170	1513	0,0535	190 000
	650	1875	-0,100	0,052	-0,511	3342	0,1959	175 000
	700	1728	-0,100	0,018	-0,340	5644	0,2953	170 000
	650[1]	2767	-0,156	0,004	-0,215	15220	0,7258	177 000

1) with 2 minutes dwell time

σ_f' = Fatigue strength coefficient

b = Fatigue strength exponent

ε_f' = Fatigue ductility coefficient

c = Fatigue ductility exponent

K' = Strength coefficient

n' = Strain hardening exponent

E = Elastic modules

Strain-life-curve $$\frac{\Delta\varepsilon_t}{2} = \frac{\sigma_f'}{E}(2N_A)^b + \varepsilon_f'(2N_A)^c \quad \text{mm/mm}$$

Strain-stress-curve $$\frac{\Delta\varepsilon_t}{2} = \frac{\Delta\sigma}{2 \cdot E} \cdot \left(\frac{\Delta\sigma}{2 \cdot K'}\right)^{1/n'} \quad \text{mm/mm}$$

Tab. 2 Cyclic Properties of Inconel 718 and Udimet 700 P/M-HIP

Manufacturers	Powder	Powder Filling	HIPing ^{o}C/h/bar	Heat Treatment ^{o}C/h	Pancake Dimensions mm
Wiggin/ MBB/ Seilstorfer	Wiggin	MBB	Seilstorfer 980/ 3/1 000 1 150/ 2/1 000	MTU 1 110/ 4 650/24 760/ 8	300 x 62
Röchling	Wiggin	Röchling	ASEA 930/ 3/1 000 1 150/ 2/1 170	Röchling 1 115/ 4 650/24 760/ 8	193 x 185 tube
Seilstorfer	Homogeneous Metals	Seilstorfer	Seilstorfer 980/ 3/1 000 1 150/ 2/1 000	MTU 1 115/ 4 650/24 760/ 8	333 x 68
Wiggin	Wiggin	Wiggin	Wiggin 950/16/- 1 150/ 2/1 000	Wiggin 1 110/ 4 650/24 760/ 8	318 x 20

Tab. 3 Manufacturing Details

Material	Orientation	Specimen Thickness mm	Test Temperature	Arithmetic Mean N/mm$^{-3/2}$	K_{IC} or K_Q	Number of Specimens
Ti 6Al 4V	C-R rim area	15	RT	1 728	K_{IC}	8
	C-R hub area	15	RT	1 891	K_{IC}	5
	R-C rim area	15	RT	1 756	K_{IC}	3
	C-R rim area	15	300 ^{o}C	2 198	K_Q	3
	C-R hub area	9	RT	1 764	K_{IC}	3
	C-R rim area	6,5	RT	1 639	K_Q	3
Inconel 718	C - R	30	RT	4 657	K_Q	2
	R - C	30	RT	3 745	K_Q	2
	C - R	26	RT	4 671	K_Q	2
Udimet 700 P/M-HIP	C - R	26	RT	4 013	K_Q	2
	R - C	26	RT	3 858	K_Q	2
	C - R	15	RT	3 280	K_Q	2
	C - R	8	RT	2 184	K_Q	2

Tab. 4 Fracture Toughness of Ti 6Al 4V, Inconel 718 and Udimet 700 P/M-HIP

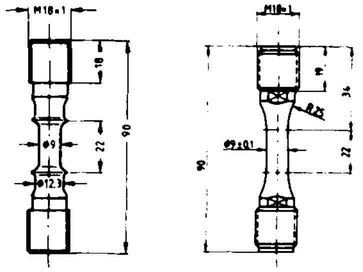
M18x1
18
90
Φ9
22
Φ12.3
M18x1
18
36
R25
Φ9±0.1
22
90

Ti6Al4V
Inconel 718

Udimet 700 P/M-HIP

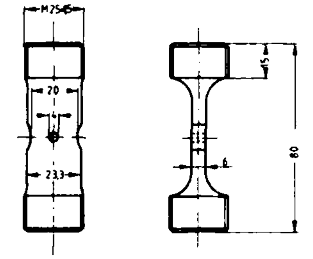
M25x1.5
20
23.3
15
6
80

Shape for all materials

Fig. 1 Specimens for Strain and Stress Controlled Tests

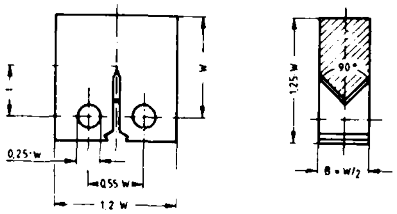
W
0.25·W
0.55 W
1.2 W
1.25 W
90°
B = W/2

Material	Thicknesses B mm
Ti6Al4V	6,5 , 9 , 15
Inconel 718	26 , 30
Udimet 700 P/M-HIP	8 , 15 , 26

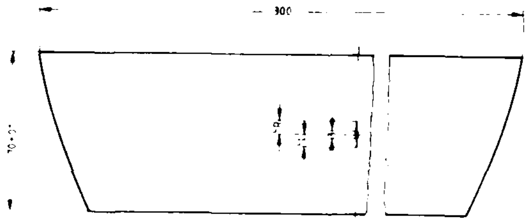

Shape for all materials

Fig.2 Compact Tension (CT) and Center Cracked Specimens

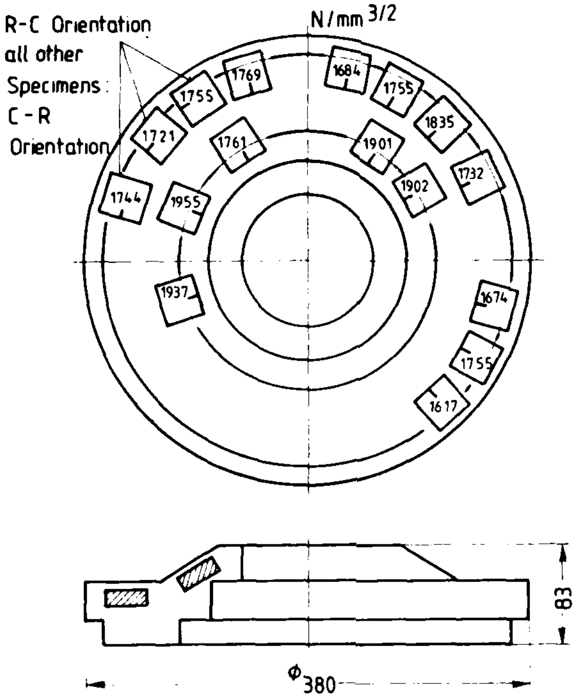
R-C Orientation
all other
Specimens:
C-R
Orientation
N/mm 3/2
1769
1755
1721
1744
1955
1761
1684
1755
1835
1901
1902
1732
1937
1674
1755
1617
83
Φ380

Forged Compressor Disc of Ti 6Al 4V

Fig. 3

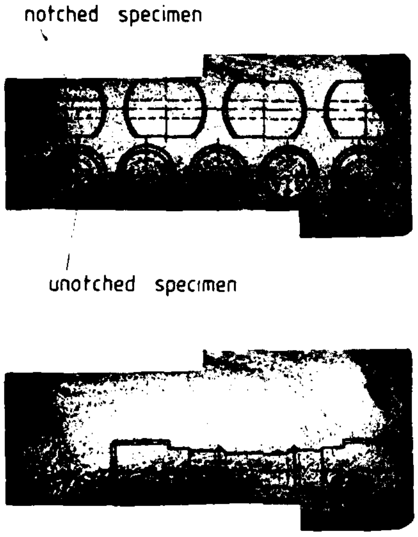
notched specimen
unotched specimen

Fig.4 Specimen Orientation in Inconel 718 Disc

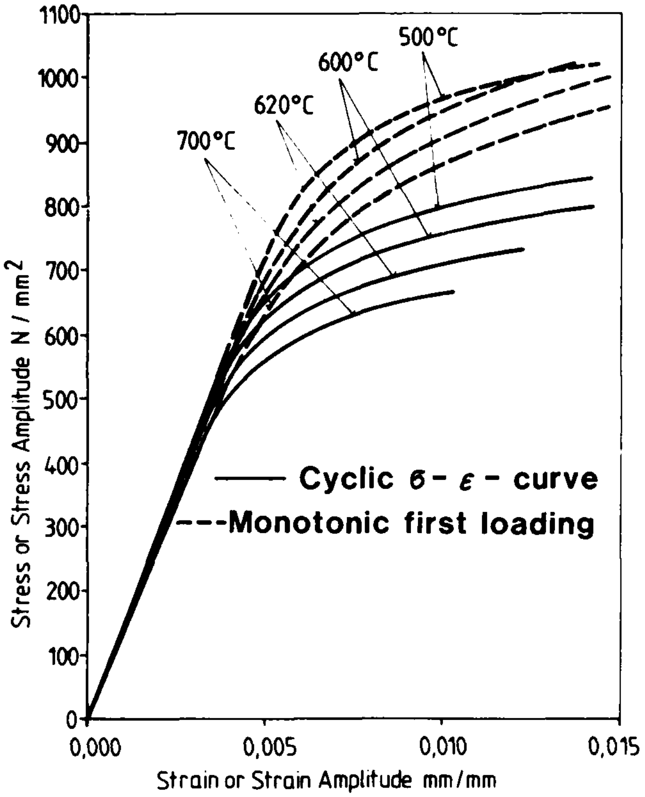

Fig. 5 **Stress - Strain Behaviour of Inconel 718 (Compressor Disc) Influence of Temperature**

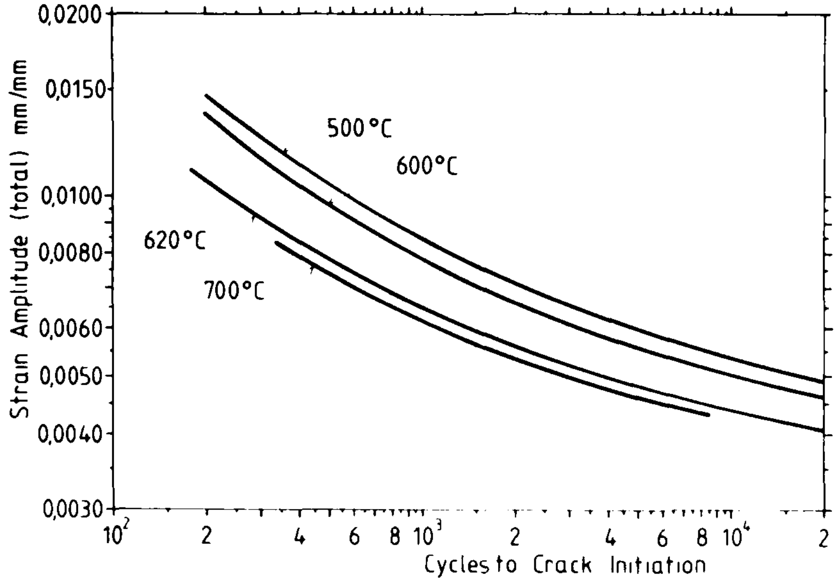

Fig. 6 **Crack Initiation Behaviour of Inconel 718 Influence of Temperature**

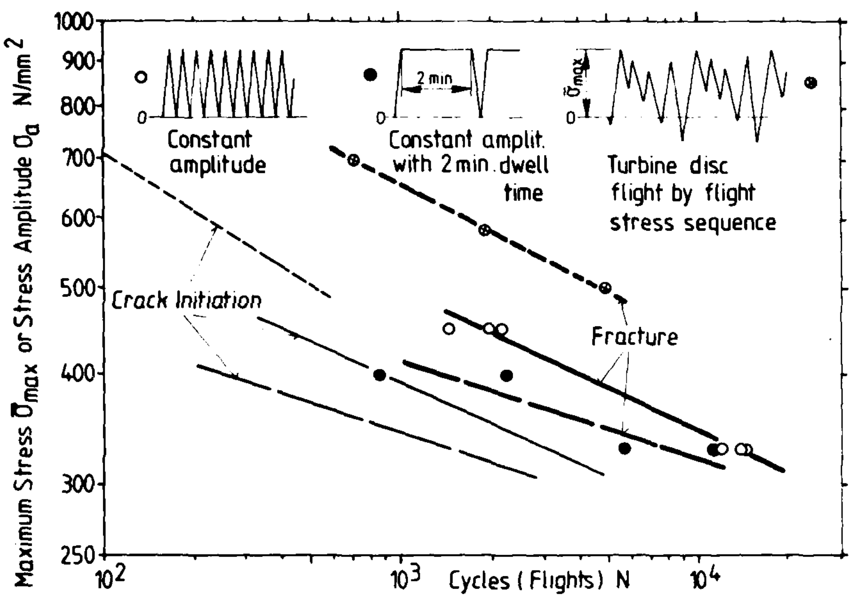

Fig. 7 Influence of Different Stress Sequences on Inconel 718 Specimens, K_t = 2,1; Temperature 620°C

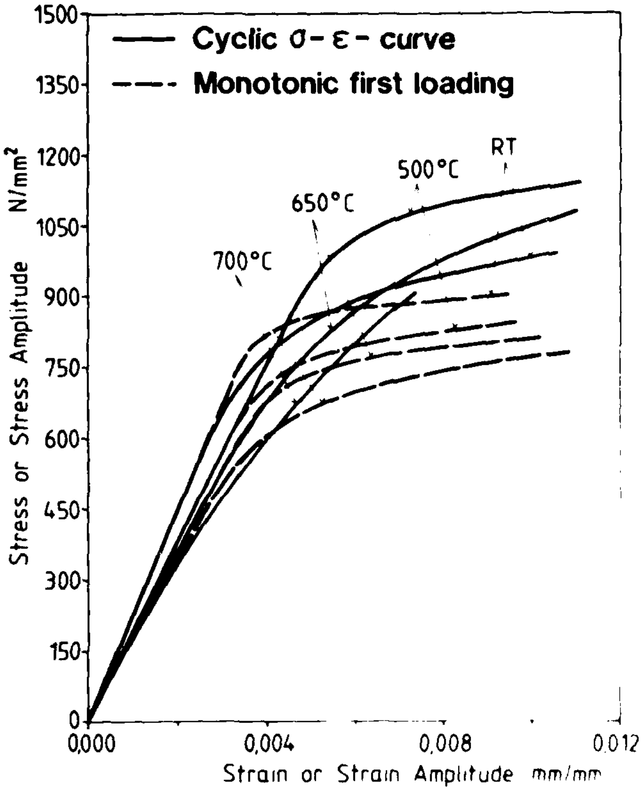

Fig. 8 Stress-Strain Behaviour of Udimet 700 P/M-HIP Influence of Temperature

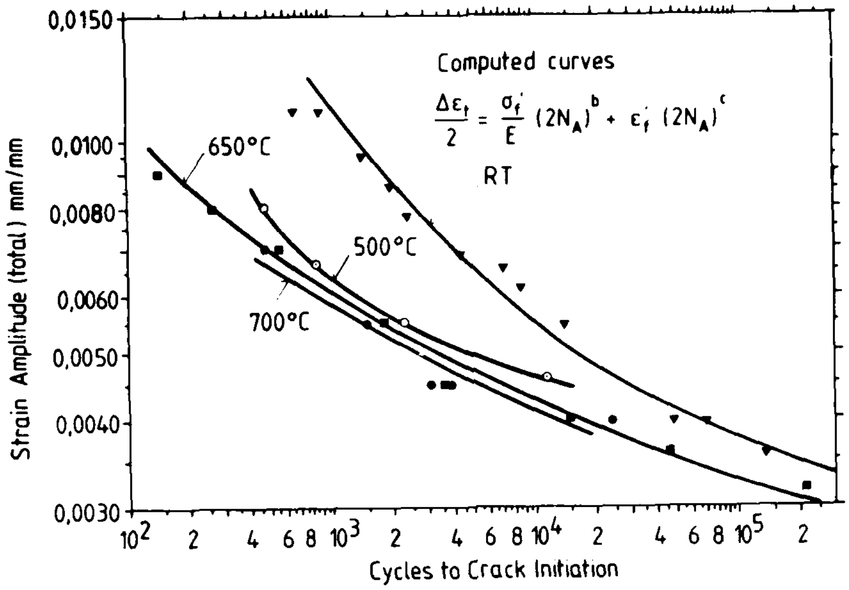

Fig. 9 Crack Initiation Behaviour of Udimet 700 P/M-HIP Influence of Temperature

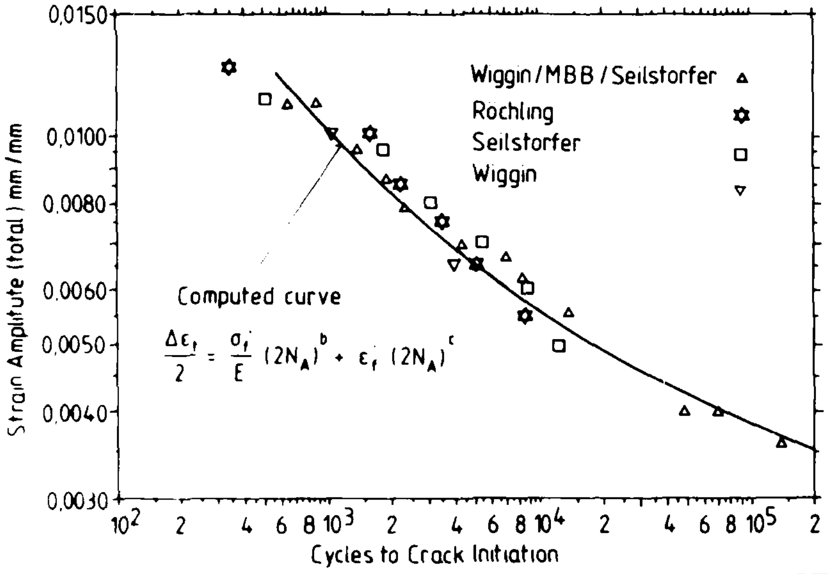

Fig. 10 Crack Initiation Behaviour of Udimet 700 P/M-HIP at RT Different Manufacturers

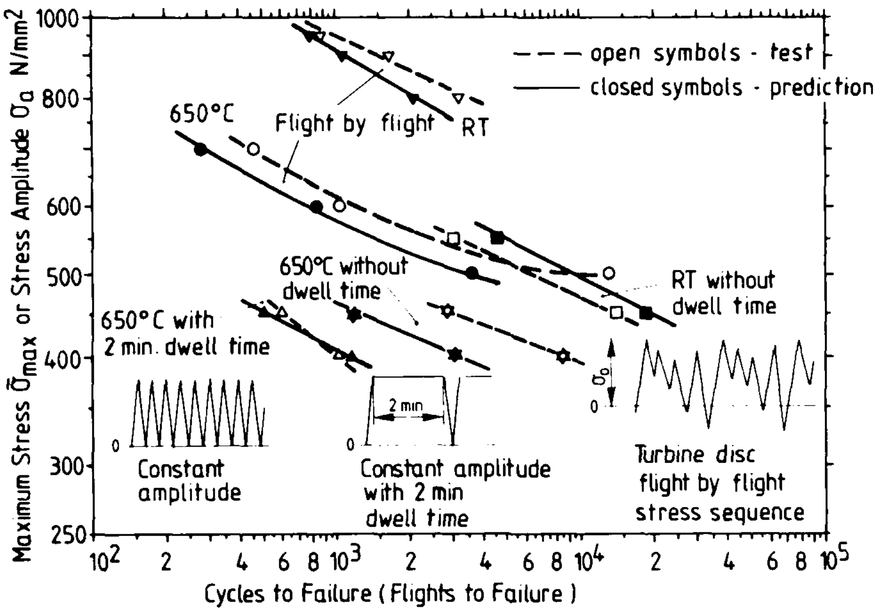

Fig. 11 Life Prediction by the Local Approach Udimet 700 P/M-HIP, Specimens $K_t = 2,1$

Ti6Al4V Forged Compressor Disc

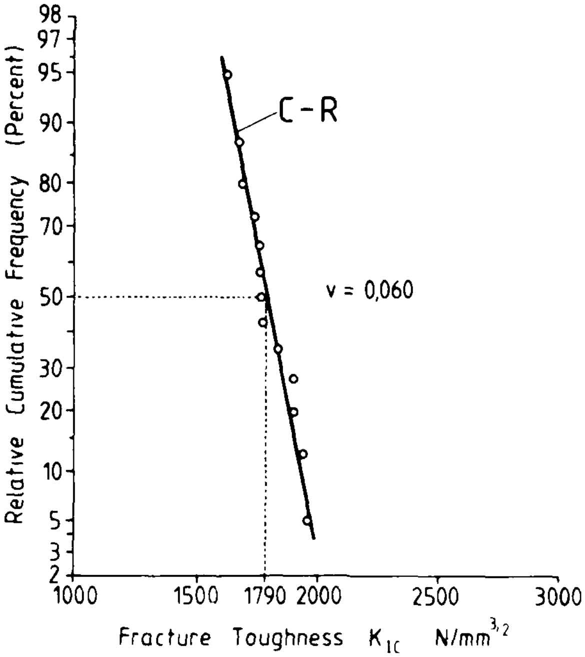

Statistical Evaluation of Fracture Toughness

Fig. 12

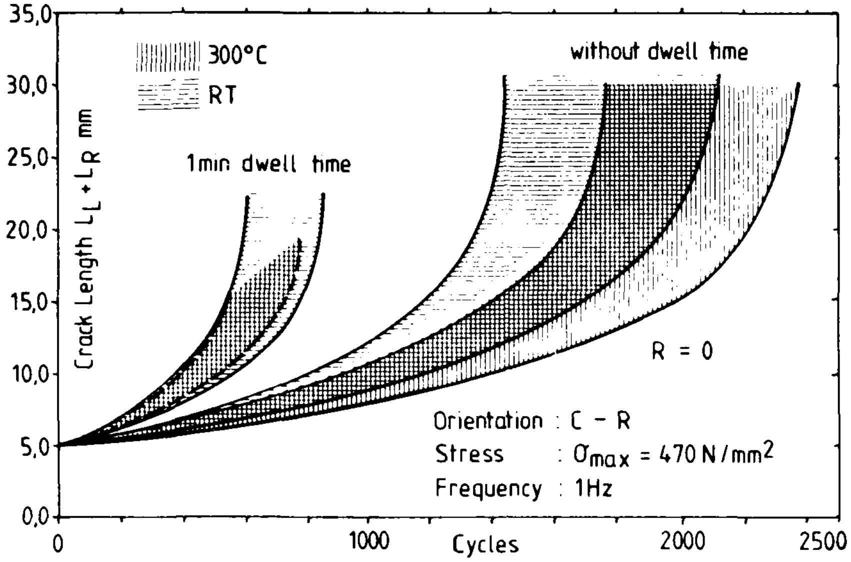

Fig. 13 Crack Propagation Curves of Ti 6Al 4V (Compressor Disc)
Influence of Temperature and Dwell Time

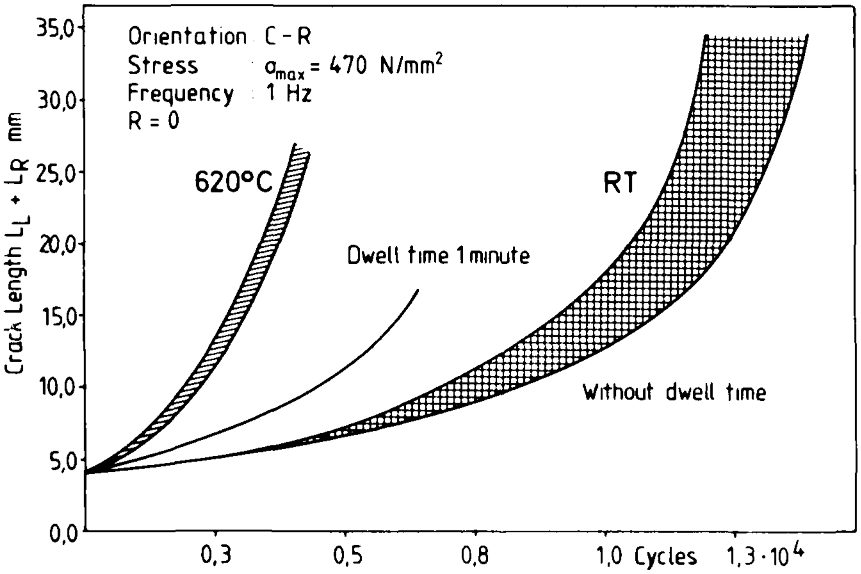

Fig. 14 Crack Propagation Curves of Inconel 718
Influence of Temperature and Dwell Time

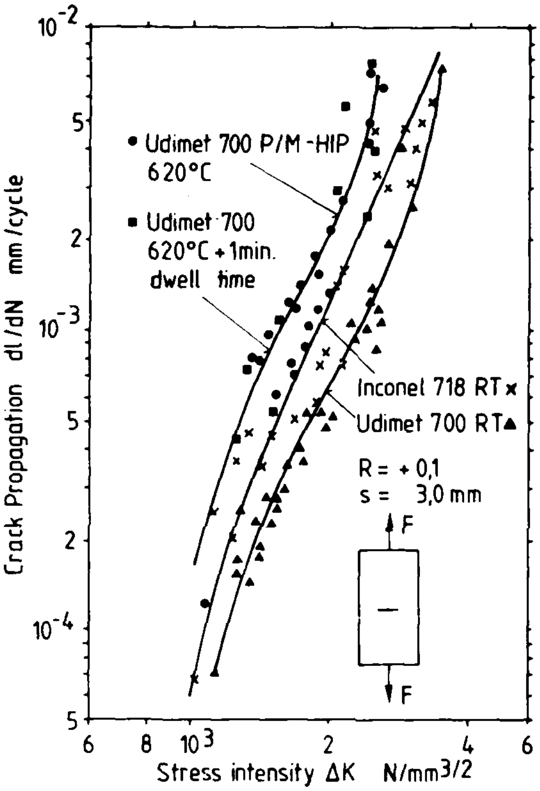

Fig. 15 Crack Propagation Rate Under Constant Amplitude Loading

EVALUATION OF CYCLIC SPIN PIT TESTS FOR THE DAMAGE TOLERANCE OF DISKS

by

H. Huff and G.W. König
Materials Laboratory
MTU
8000 Munich 50
West Germany

SUMMARY

In order to determine the damage tolerance at critical areas of nickelbase engine disks (bore, eccentric hole, blade slot) the crack propagation behaviour was investigated. The experiments include cyclic spin pit tests on disks and fracture mechanics tests on small-crack specimens. The results of the spin pit tests are compared with the crack propagation behaviour predicted by fracture mechanics. The tolerance of engine disks with respect to small crack-like defects is estimated and the potential of the crack propagation life for application in service is discussed.

It was found that at low and intermediate temperatures the crack propagation life is sufficient to cover a substantial portion of the life required for disks. With increasing temperature the influence of time-dependent processes results in a very strong reduction of the defect tolerance.

1. INTRODUCTION

The fatigue behaviour along with a sufficient burst strength is the most important criterion for the usable life of modern engine disks. Usually, in the total fatigue life two stages can be distinguished: the life to crack initiation and the life to crack propagation. Fig. 1 shows a typical representation of the crack initiation and propagation lives of a nickelbase alloy at room temperature. Most of the currently used design methods are based on the crack initiation life portion. This has led to the development of high-strength alloys with improved crack initiation resistance. However, since crack initiation and propagation are governed by different mechanisms, the consequence is often a decreased crack propagation life potential (1). In the meantime the crack propagation life of disks has attracted considerable attention (2, 3, 4). The main reasons are:

Small defects have a very strong influence on the crack initiation life. The number and size of these defects can be limited by quality control methods, but there is no way of avoiding defects completely. A conservative method to account for these defects is to assume that defects which are able to grow are present from the beginning. Therefore, the safe crack propagation life is an important safety margin for critical engine components.

The minimum defect size that can reliably be detected by modern non-destructive inspection methods is in the range of 0.1mm. This means that any lifing concept including inspections requires a sufficient crack propagation life from the detection limit to failure. Fig. 1 shows that the order of magnitude of the crack propagation life is about 10,000 cycles even at high loads. This is sufficient to cover the whole projected life or reasonable inspection intervals for many engine disks.

The objective of the present work was to assess the crack propagation life of nickelbase disks, which is most important to the damage tolerance of disks. The programme includes:

- The determination of crack propagation data under loading conditions relevant to engine disks
- The determination of the crack propagation behaviour at critical areas of disks during cyclic loading in a spin pit test. The areas under consideration are:
  - Bore
  - Eccentric hole
  - Blade slot

Each of these areas is characterized by different operational temperatures, stress gradients and crack shapes.

- The comparison between the predicted crack propagation behaviour based on specimen data and the disk behaviour.

While component testing is of fundamental importance to the lifing of disks, most parameters influencing the fatigue life (i.e. material, loading conditions, manufacturing parameters) are evaluated by specimen tests. It is therefore important to know how relevant specimen results are to predict component behaviour.

2. EXPERIMENTAL PROCEDURES

Fig. 2 shows the specimens which were used for the crack growth measurements. Since most of the crack growth life in disks is consumed in the range of small cracks, special specimens with small cracks were used. These specimens were preferred to long-crack specimens (i.e. CT-specimens) because of the better transferability of the data between specimen and disk. The crack size, stress intensity gradient and fracture mode of these specimens are very similar to those of disks. For loading conditions which are completely in the elastic range, the crack growth measurements were performed on rectangular specimens under stress control. At high stress ranges strain controlled tests were performed on round bar specimens. The starter notch for the fatigue crack is either an electric discharge machined notch, a drilled hole or a circumferential machining groove. The crack growth measurements were made by means of a potential drop device, replica, heat tinting and striation count.

3. RESULTS

The following results all refer to laboratory cylic spin pit tests of nickelbase superalloy disks. The tests were performed at constant temperature and one-step loading between zero and a fixed maximum spinning speed. The time for acceleration, deceleration and dwell at maximum spinning speed was each about 30 seconds.

3.1 CRACKS IN A DISK BORE

The following spin test results were obtained with a simplified turbine disk of the powder metallurgical nickelbase alloy U700. The temperature was 400°C and the total number of cycles of the test 11,255. During this test two fatigue cracks developed in the bore: a quarterelliptical corner crack and a semielliptical surface crack.

3.1.1 CORNER CRACK

The crack initiation site of the corner crack (Fig. 3) is at a small machining mark. During the spin test several dye penetrant inspections were made. The interruption of cycling during these inspections resulted in marks on the fracture surface (Fig. 3) which can be used to evaluate the crack growth behaviour during the spin pit test. Fig. 4 shows the crack depth as a function of the number of cycles for the corner crack. The figure also includes the predicted crack propagation behaviour. Since the stress range in the bore area was above the yield stress of the material the crack propagation data were measured under strain control. Contrary to the examples shown below, dwell effects were found to be unimportant at the testing temperature. The agreement between prediction and actual disk behaviour is very good: the predicted life is only about 6% less than the actual disk crack propagation life. This is less than the scatter of the crack propagation data used for the prediction. The figure also includes the crack depth indicated by dye penetrant inspection. It is evident that small cracks were not indicated by nondestructive testing and that the agreement with the actual crack size becomes reasonable only for large cracks.

3.1.2 SEMIELLIPTICAL CRACK

The location of the semielliptical surface crack in the bore is shown in Fig. 5. The crack starts at a nonmetallic inclusion. The comparison between the inspection marks in the fracture surface and the fracture mechanics prediction (Fig. 6) shows again good agreement (the difference in life is about 19%). Similarly to the corner crack situation, the crack size indicated by dye penetrant inspection is much smaller than the actual crack size.

3.2 CORNER CRACK AT AN ECCENTRIC HOLE

The cyclic spin test was performed with a model disk containing various eccentric holes to simulate the behaviour of bolt holes or cooling holes (Fig. 7). The disk material is powder metallurgical U700 and the testing temperature 600°C. After 9500 cycles the test was interrupted since several holes showed large fatigue cracks. Again the crack growth behaviour of these cracks could be established in the fracture surface by evaluating inspection marks. Fig. 8 shows the tangential stress in relation to the distance from the hole root. Because of plasticity the elastic tensile stress relaxes to a nearly constant level of about 1000 MPa while the compressive stress increases with the distance from the hole root. For the fracture mechanics calculation, crack growth data were used which were obtained under the strain conditions of the notch root. At 600C time-dependent effects strongly influence the crack growth rate. Therefore, the frequency and dwell time of the specimen tests were selected to be similar to the conditions of the spin pit test. Fig. 9 shows the comparison between the predicted and the actual (inspection marks) crack growth behaviour. The difference is about 18%, which is within the uncertainties of the underlying crack growth data. Good agreement between specimen and disk was also found with respect to the striation densities established in the fracture surface by scanning electron microscopy (Fig. 10).

3.3 CRACK AT A DISK BLADE SLOT

The following example illustrates the behaviour of blade slot cracks under testing conditions leading to extremely different crack growth behaviour. One test was performed with a disk of the conventional wrought nickel-base alloy Waspaloy (Fig. 11). The testing temperature was 450°C. After 17,000 cycles a large number of slots were cracked with the largest crack having a depth of 1.6 mm. A second test was performed with a disk of the powder metallurgical high-strength nickelbase alloy AF115 mod. (i.e. a modified version of the alloy AF115). The testing temperature was 600°C and the stress slightly higher than for the Waspaloy disk test. The fatigue life of the AF115 mod. disk was found to be much shorter than that of the Waspaloy disk: After only 2000 cycles bursting of the disk occurred at a final crack depth of 9 mm. The large difference in the fatigue lives of the two disks cannot be explained from the crack initiation data of the two alloys (Fig. 12). At 600°C the crack initiation life of AF115 mod. is about equal or superior to that of Waspaloy at 450°C. Since many slots were cracked in both disks the different behaviour must be considered as representative and cannot be attributed to singular material defects. The results can be explained by evaluating the crack propagation life of the two disks: The crack growth rate of AF115 mod. at 600°C is, by a factor of about ten, higher than that of Waspaloy at 450°C (Fig. 13). An important reason for the high crack growth rate of AF115 mod. is the influence of dwell leading to a change of the crack growth mode from transcrystalline (no dwell) to intercrystalline (dwell); Fig. 14. This behaviour is typical of high-strength and fine-grained nickel-base alloys such as AF115, Rene95, IN100 or IN718 (just to cite some of the currently used advanced disk alloys (1)). Fig. 15 shows the crack growth curves of the blade slot cracks in both materials assuming a small initial defect of 0.1mm in depth. The cracks found in the two disks are in good agreement with these crack growth curves. This indicates that the crack propagation life was the dominant part of the cyclic life of both disks.

4. SUMMARY AND CONCLUSIONS

1. The crack propagation life at critical areas of disks (bore, eccentric hole, blade slot) was found to be in good agreement with the fracture mechanics prediction based on short-crack specimen results.

2. These results show that fracture mechanics is able to predict the behaviour of disks containing propagating defects. At low and intermediate temperatures and stress levels typical of modern nickelbase disks the crack propagation life for small initial cracks is in the order of magnitude of 10,000 cycles. This means that many disks have a considerable defect tolerance which essentially contributes to their safety in service.

3. At high temperatures time-dependent processes lead to a substantial decrease in crack propagation life and hence defect tolerance. Under these conditions even small defects such as nonmetallic inclusions or machining marks greatly reduce the fatigue life of disks. The situation may improve if disk materials are developed the microstructure of which has been optimized with regard to fatigue crack growth at high temperatures. This, however, runs counter to the widespread tendency to optimize predominantly with regard to superior crack initiation life properties.

5. REFERENCES

1. König, G.W.: Comparison between the properties of conventional wrought and powder metallurgical alloys for turbine disk applications. in: Engine cyclic durability by analysis and testing; AGARD-CP-368; (1984)

2. Poret, L., Guedou, J.Y., Pineau, A.: Resistance à la propagation de fissures de l'alliage Inconel 718. in: Engine cyclic durability by analysis and testing; AGARD-CP-368; (1984)

3. Evans, W.J., Smith, M.F.F., Williams, C.H.H.: Disc fatigue life predictions for gas turbine engines. in: Engine cyclic durability by analysis and testing: AGARD-CP-368; (1984)

4. Huff, H., König, G.: Damage tolerance of aero-engine disks. in: Proceeding of the twelfth international committee on aeronautical fatigue; Toulouse, France, (1983)

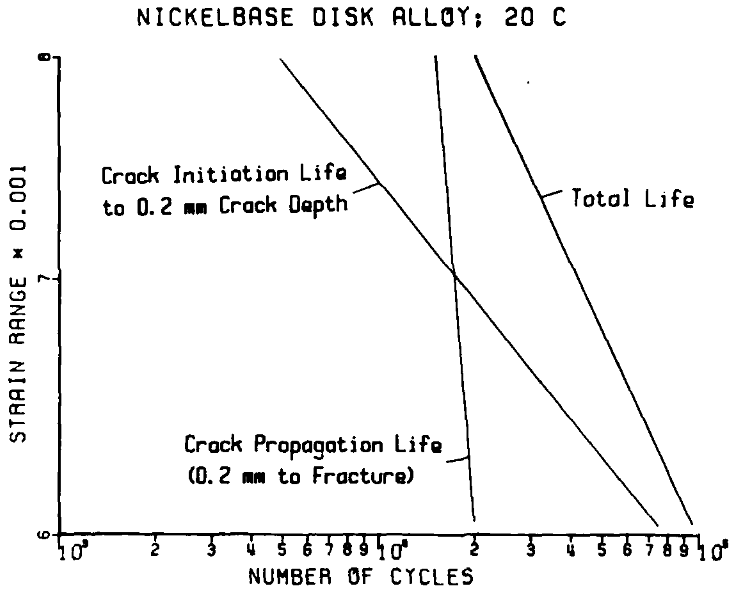

Fig. 1: Crack initiation life, crack propagation life and total life

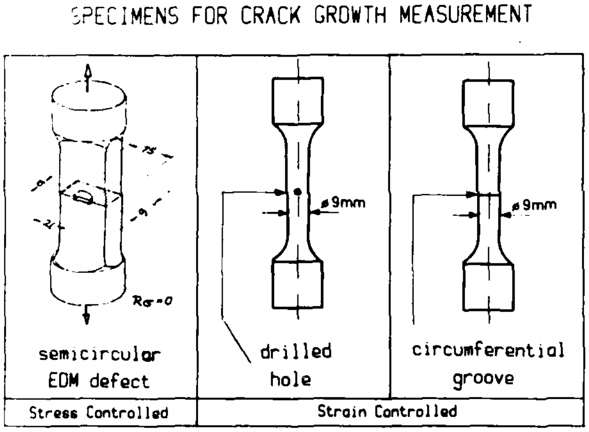
SPECIMENS FOR CRACK GROWTH MEASUREMENT
$R_\sigma = 0$
ø9mm
ø9mm
semicircular EDM defect
drilled hole
circumferential groove
Stress Controlled
Strain Controlled

Fig. 2: Specimen for crack growth measurement

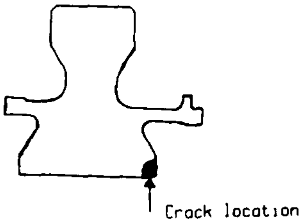
Crack location

CORNER CRACK IN A DISK BORE

- Cyclic spin pit test
- Material: U700 PM
- Temperature: 400 C
- Number of cycles: 11255

Fig. 3: Corner crack in a disk bore

Fatigue crack: General view
Final length: 6.[illegible] mm
Final depth: 5.8 mm

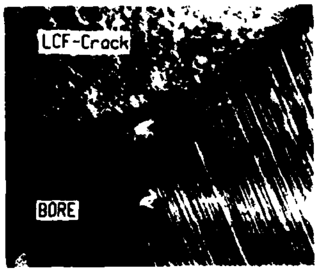
LCF-Crack
BORE

Crack initiation site: Machining mark

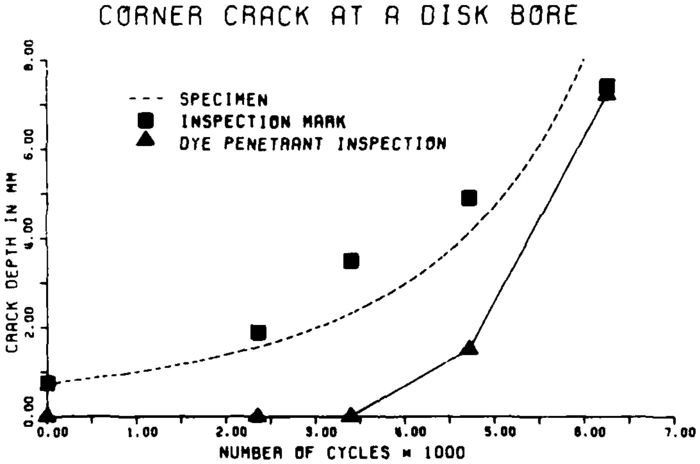

Fig. 4: Crack propagation life (corner crack). Comparison between specimen, disk (inspection mark) and dye penetrant inspection

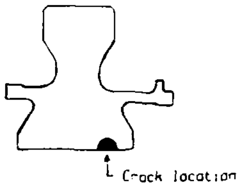

SEMIELLIPTICAL SURFACE-CRACK
IN A DISK BORE

- Cyclic spin pit test
- Material: U700 PM
- Temperature: 400 C
- Number of cycles: 11255

Fig. 5:
Semielliptical crack
in a disk bore

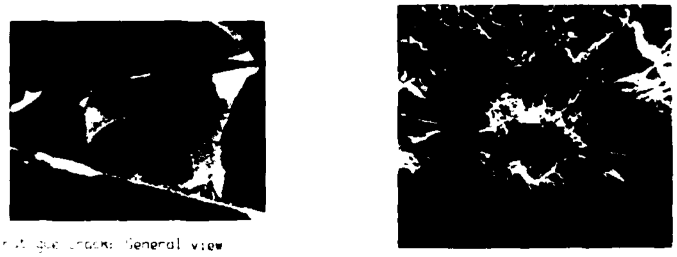

Fatigue crack: General view
Final depth: 3.8 mm
Final length: 6.2 mm

Crack initiation at an inclusion

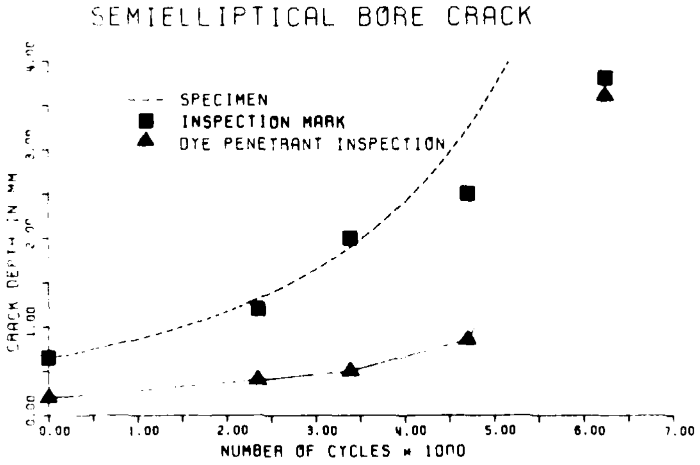

Fig. 6: Crack propagation life (semielliptical bore crack). Comparison between specimen, disk (inspection mark) and dye penetrant inspection

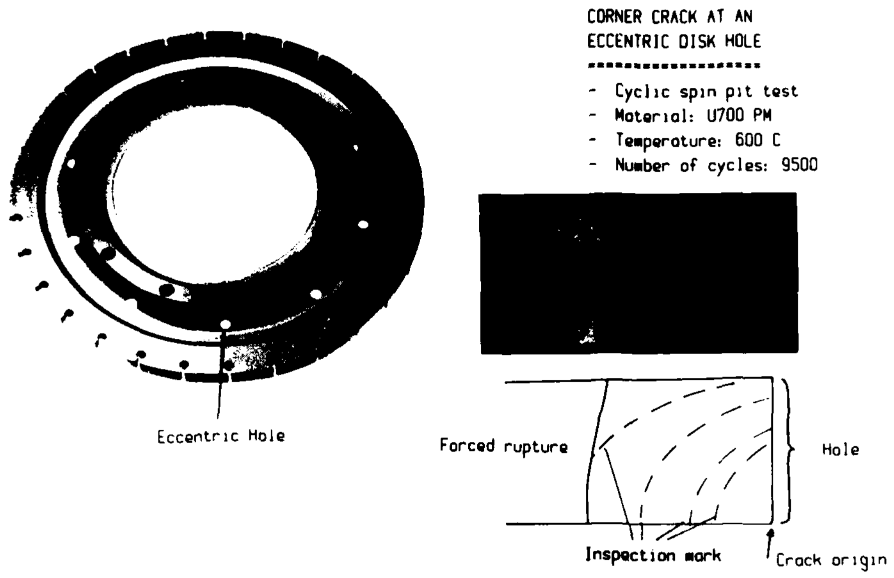

CORNER CRACK AT AN
ECCENTRIC DISK HOLE

- Cyclic spin pit test
- Material: U700 PM
- Temperature: 600 C
- Number of cycles: 9500

Eccentric Hole
Forced rupture
Hole
Inspection mark
Crack origin

Fig. 7:
Corner crack at an
eccentric disk hole

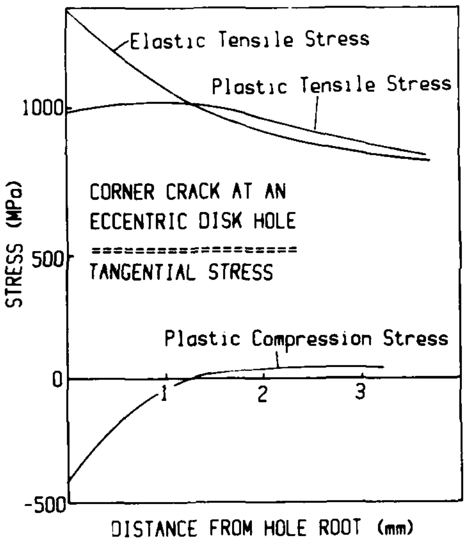

Fig. 8:
Tangential stress at the
hole root

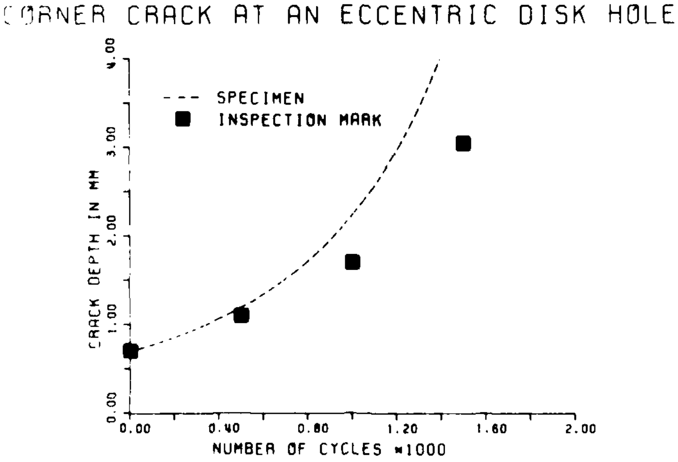

Fig. 9: Crack propagation life (eccentric disk hole). Comparison between specimen and disk (inspection mark)

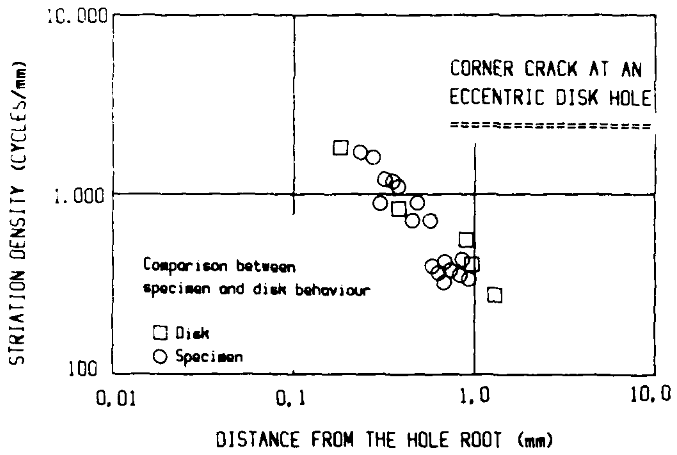

Fig. 10: Striation density
Comparison between specimen and disk

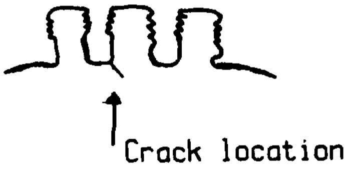

FATIGUE CRACK AT A
DISK BLADE SLOT

Cyclic spin pit test

1. WASPALOY DISK
   Temperature: 450 C
   Number of cycles: 17.000
   Final crack depth: 1,6 mm

2. AF115 Mod. Disk
   Temperature: 600 C
   Number of cycles: 2.000
   Final crack depth (burst): 9 mm

Fig. 11: Crack at a disk blade slot

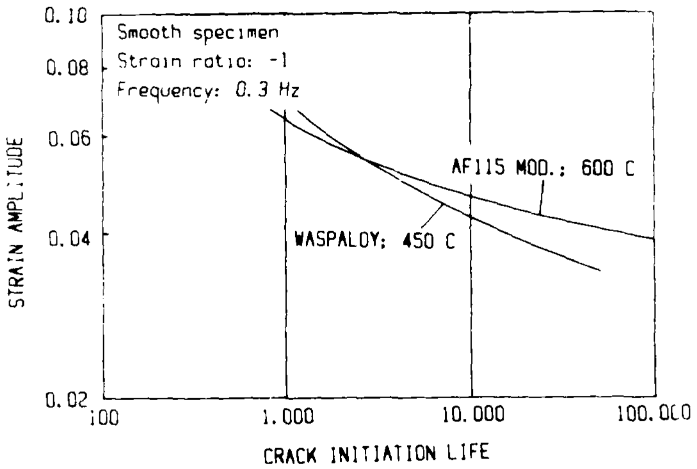

Fig. 12: Crack initation life of Waspaloy and
AF 115 mod.

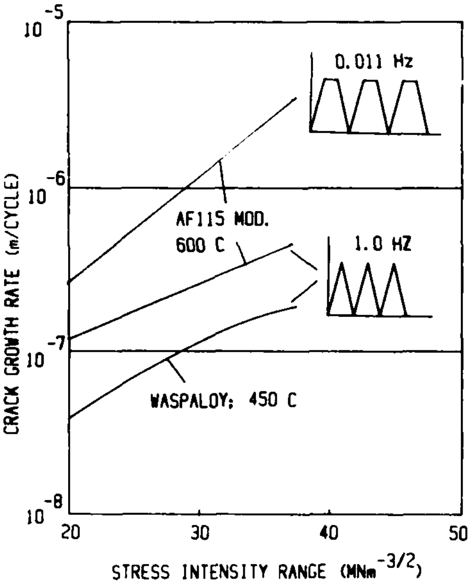

Fig. 13: Crack growth rate of Waspaloy and AF 115 mod.

CRACK GROWTH MODE OF AF115 MOD. AT 600 C

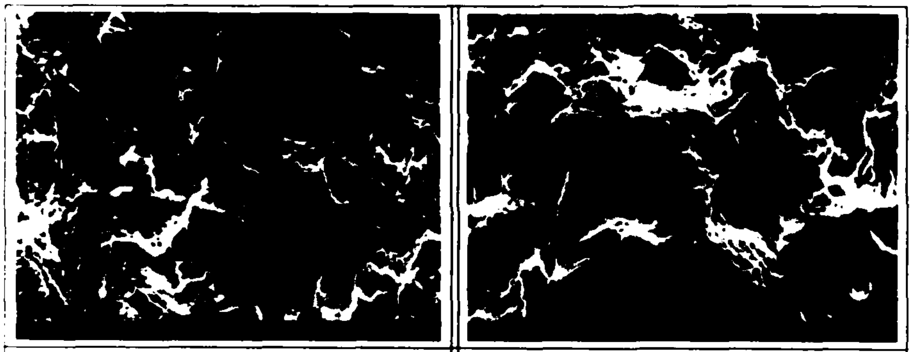

No Dwell	30 s Dwell
Predominantly Transgranular Crack Growth	Mixed Inter- and Transgranular Crack Growth

Fig. 14: The effect of dwell on the crack growth mode of AF 115 mod. at 600 °C

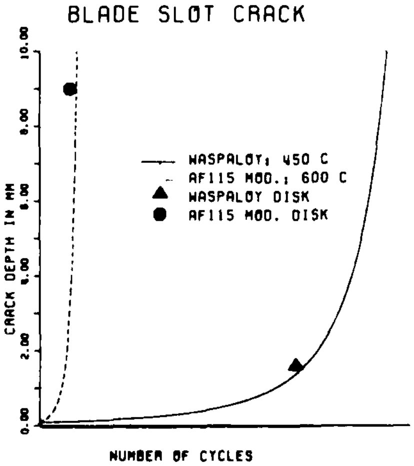

Fig. 15: Comparison between the crack propagation life of a blade slot crack in the Waspaloy and AF 115 mod. disk. Initial crack size: 0.1 mm

TURBISTAN,
A STANDARD LOAD SEQUENCE FOR AIRCRAFT ENGINE DISCS

by
A.J.A. Mom[1], W.J. Evans[2] and A.A. ten Have[1]

[1] National Aerospace Laboratory, NLR
Anthony Fokkerweg 2, 1059 CM AMSTERDAM
The Netherlands

[2] Materials Engineering Research Division
Propulsion Department
Royal Aircraft Establishment
Pyestock, Farnborough, Hants, GU14 OLS
England

SUMMARY

The development of TURBISTAN is a joint international effort to derive a loading standard representative for fighter aircraft engine disc usage. A representative loading standard offers considerable potential advantages over the present zero-max type of loading used for disc material evaluation. This is because the standard incorporates the effects of subcycles, their number, magnitude and sequence, which are known to seriously affect disc life and for which current life prediction techniques only partly account. Therefore usage of the standard in fatigue tests provides an improved evaluation of material properties, structural details, fabrication techniques, surface quality and life prediction.

The present paper describes the compilation of operational flight data, their analysis and the generation of a preliminary TURBISTAN sequence for "cold" compressor discs. The sequence contains about 8000 cycles which represent 100 flights. In addition the paper describes the background and philosophy of a material testing programme meant to assess the effectiveness of the standard and to explore the validity of the assumptions made in its derivation.

PROLOGUE

The development of TURBISTAN is a joint effort of the following engine manufacturers and laboratories and their representatives:

- CEAT, Toulouse, France (T. Pardessus)
- Fraunhofer Institut für Betriebsfestigkeit LBF, Darmstadt, Germany (D. Schütz, H. Köbler)
- Industrie-Anlagen Betriebsgesellschaft (IABG), Ottobrunn, Germany (W. Schütz, J. Bergmann)
- Motoren und Turbinen Union (MTU), Munich, Germany (G. Breitkopf, T. Speer, G. König)
- National Aerospace Laboratory NLR, Amsterdam, The Netherlands (A.J.A. Mom*, A.A. ten Have**)
- Royal Aircraft Establishment (RAE), Farnborough, United Kingdom (W.J. Evans***)
- Rolls Royce (RR), United Kingdom (R.H. Jeal, N.P. McLeod, R.F. Shellard)
- Snecma, Corbeil and Villaroche, France (C. Herman, J.Y. Guédou, L. Poret)
- Technical University Aachen (RWTH-Aachen), Germany (W. Koschel, A. Fischersworring)
- University of Toronto (UoT), Canada (D.W. Hoeppner)

* general secretary of TURBISTAN working group; ** chairman of mission analysis group; *** chairman of materials group

1 INTRODUCTION

The idea of the development of a loading standard for fighter aircraft engine discs arose first in 1980 and resulted in the establishment of the TURBISTAN working group in 1982. In the early discussions about the advantages and use of standards it turned out that to be accepted as a standard a load sequence should be really representative for its purpose. Furthermore it should be as simple as possible, its origin should be well documented and the sequence should be uniquely defined. If this is the case the standard has many advantages over the simple constant amplitude type of testing.

It then provides an improved evaluation of material properties, fabrication techniques, surface treatments, structural details, spectrum variation effects and analytical prediction techniques. This was and still is the basic philosophy behind the development of a standard or reference cycle. With this in mind the group decided to work along two different lines:

- The compilation and selection of operational flight data, analysis of these data and the generation of a basic sequence which might be subsequently simplified in different steps leading to a final TURBISTAN standard sequence.
- A review and selection of the main fatigue life affecting mission parameters (e.g. temperature, dwell, sequence, subcycle magnitude, rise time etc.) and the generation of fatigue life and crack growth test data on specimens subjected to the present simple 0-MAX loading cycle and to the various phases of the TURBISTAN loading sequence.

The combination of analysis and testing should finally result in a representative standard which contains all relevant parameters but which is also short and simple enough to be of practical interest. The present report describes the development of a preliminary sequence and the motivation of a material testing programme intended to enable derivation of the final TURBISTAN sequence.

2 BACKGROUND

Aircraft engine discs are often subject to complex loading patterns as a result of frequently occurring changes in throttle settings. For example, figure 1 illustrates a typical RPM profile obtained from a military aircraft mission. From this RPM profile a load pattern might easily be derived by taking $(RPM)^2$. Although the pattern looks quite complex, each mission might be simply regarded as consisting of a 0-max-0 main cycle, which is in fact the engine start - take off - shut down sequence, and a great number of sub-cycles as a result of engine check, taxiing or aircraft manoeuvring.

The life of a disc is in principle based on the number of main cycles, which correspond to the maximum stress range occurring in the mission. The effect of sub-cycles is sometimes taken into account but only in a very simplified way and in general only for military engines. Current design practice is that firstly a mission cycle is defined which the engine is assumed to perform in service. Such a predicted mission cycle is a very simplified version of the mission shown in figure 1 (e.g. there may be only one intermediate load level between 0 and max). Life evaluation is subsequently performed on the basis of constant amplitude testing, while the effect of the sub-cycles is accounted for by the application of Miner's rule (simply adding up the life fractions consumed by main and sub-cycles). This is done although the applicability of Miner's rule for these conditions has not been proven and might well result in highly erroneous life prediction.

The above illustrates that material evaluation for disc usage is principally based on constant amplitude testing. The effect of sub-cycles, e.g. the number and magnitude of sub-cycles and their sequence, and dwell effects are not incorporated in this evaluation. Because it is known that these parameters, and their mutual interaction, seriously affect life it is considered necessary to incorporate them in the fatigue testing programme. From this point of view, fatigue testing should be carried out under a realistic, operational loading pattern so that relevant material fatigue data are obtained. However, if each fatigue engineer were to define his own representative load sequence, representing his particular problem, this would result in a great number of load sequences. Material fatigue data comparison between laboratories and even within one laboratory would then become impossible. It seems much more desirable to have one common load sequence to be used as a standard or reference. It is the intention of the TURBISTAN working group to develop such a common, representative load sequence for discs of fighter aircraft engines.

Because of the complex task it was decided to concentrate efforts in the first instance on the development of a standard sequence for "cold" compressor parts, i.e. fan and early stage compressor discs. In this way temperature effects and therefore thermal stresses could be neglected: load sequences could then be derived easily from RPM sequences.

The next sections will discuss in detail the work performed for the two tasks mentioned before in the introduction to this paper.

3 DEVELOPMENT OF THE TURBISTAN LOAD SEQUENCE

3.1 Introduction

The entire development of TURBISTAN comprises the following phases:

- compilation and selection of operational mission profiles;
- analysis with respect to mission type, structure and content;
- determination of TURBISTAN sequence length and mission mix;
- TURBISTAN sequence generation;
- verification of TURBISTAN spectrum content;
- TURBISTAN sequence validity evaluation by material testing;
- definition of final TURBISTAN standard sequence.

The present paper deals with the first four phases and describes the scope of the material testing programme.

It may be questioned why the definition of the TURBISTAN loading standard was not performed in a more straightforward way by just putting together the available flights to form a sequence. This would eliminate extensive data processing while relevant results could still be obtained in fatigue tests. However, in this way only part of the potential value of a loading standard can be exploited.

A loading standard must adequately represent the loading on a particular engineering structure. All significant parameters affecting the material fatigue process must be included and recognised as such. This enables isolation of individual parameters within the standard to investigate their relative importance. At the same time many data based on the same well-documented standard will become available.

It should be realised that a loading standard is not intended to determine the fatigue life of a specific component under certain specified loading conditions, but that it is generally used during design and development phases to evaluate different materials, structural details, prediction techniques etc. This requires that the basic parameters in the standard are well described and easily accessible for modification. This is possible only if there is a systematic breakdown of the available flight data into basic elements from which the standard is subsequently generated.

The analysis and generation procedures of TURBISTAN are outlined in more detail below.

3.2 Mission analysis

Available flight data

The basis of TURBISTAN is a large number of operational mission profiles representing five tactical aircraft. The missions, in the form of RPM (or RPM^2)-time histories represent usage in France, Germany, The Netherlands and the United Kingdom. The analysis procedure is shown schematically in figure 2. Originally 46 flight profiles were made available from which 31 were selected for further processing. This was necessary since some missions were rather unrepresentative for common usage or contained unrepresentative mission parts.

Next, a mission type analysis was performed in order to define the number of different mission types for TURBISTAN. This was done in two ways:

- a grouping of associated missions could be achieved by comparing detailed flight schedules and RPM-time plots;
- by using a graphical tool the in-flight phases like cruise and manoeuvring were plotted such that differences in mission profiles and hence differences in flight character became clear, see e.g. figure 3.

The result of the mission type evaluation is given in table 1, which shows that the various input data are covered by four typical mission types: Air Combat (A), Transition/Training (B), Ground Attack (C) and Navigation (D).

Structure of a flight

The TURBISTAN loading sequence should adequately represent the general structure of operational flights. Therefore, it is logical to firstly analyse a flight with respect to its basic structure. Figure 4 [1] shows an example of how a flight can be broken down into flight events. In fact, the categorisation into nine flight events as shown in this figure was the procedure adopted for TURBISTAN to cover the structure of each mission.

Some flight events appear within a mission in a rather deterministic way, while other flight events are situated more or less randomly. As such a flight may also be described by the following three major blocks (see also Fig. 4):

- an Initial Block, containing Ground Handling, Engine Checks and Departure: each event occurs only once per flight and in this order;
- a Centre Block, containing the in-flight events Cruise, Low (Intensity) Manoeuvring, High (Intensity) Manoeuvring and Landing: these events, with the exception of Landing, appear in a more random order for an arbitrary number of times;
- a Final Block, containing Thrust Reversal and Taxi, again each occurring once per flight and in this order.

The terms stochastic and deterministic not only refer to the position of a particular event in a flight but may also be used for the type of loading within the event. For example, loading within Ground Handling (1), Cruise (3), Low Manoeuvring (4), High Manoeuvring (5), Landing (6) and Taxi (7) is considered stochastic with cyclic, non-predictable loading around some mean level.

Departure (2), a deterministic event, is described by a single load excursion to the overall maximum (100 %) load level and thus the maximum load level in TURBISTAN is reached in each flight. Engine Checks (8) and Thrust Reversal (9), also of deterministic nature, are of such significance that they are being handled as separate flight events. They are characterized by one or more load cycles from σ-idle to a certain σ-max.

Analysis

All 31 selected flights were broken down into the individual flight events as shown in figure 4. Subsequently, the analysis was performed along two different lines (see Fig. 2):

- information with regard to event sequence and duration was compiled. Note in this respect that centre block events were handled differently from initial and final block events;
- loading within each event was analysed in detail e.g. mean, alternating and maximum stress.

As stated above the analysis differed for certain types of events. This depended on the way in which, in a later phase, the TURBISTAN generation had to be performed for that specific event or for a specific flight block.

For centre block events, for example, a straightforward analysis method was used by taking the actual sequence, number of occurrences and duration as present in the basic flights. These actual data were later used during TURBISTAN generation. This approach, based on the consideration that the selected flights were representative and typical samples of various mission types, was the most simple one and probably more realistic than a detailed statistical analysis of the raw data followed by a generation procedure. The data blocks A and B in figure 2 indicate the registration of respectively sequencing and duration of centre block events for all selected missions.

For the initial and final block events Ground Handling and Taxi a different approach was chosen. These phases are generally independent from the tasks to be performed in a specific mission. Therefore information on duration is decoupled from the original flights and is handled in a statistical way. The durations for these events are randomised in time distribution functions (Block C).

The analysis of loading within individual flight events depends on the stochastic or deterministic nature of the event. For stochastic flight events, characterised by non-predictable stress cycles superimposed on a mean stress level, information is needed on cycle content and mean stress level. This information was obtained by performing a rainflow analysis, followed by a transformation procedure developed to arrive at summatrices for the overall cyclic content of flight event types (Block G). Information on mean stress level has been handled statistically by determining mean stress distribution functions (Block D). For deterministic flight events occurrence frequency distributions and maximum stress distribution functions were determined (Blocks E and F).

The topics concerning the above analysis procedures will be described in detail in the official TURBISTAN publication.

3.3 TURBISTAN generation

The TURBISTAN generation procedure, which is shown schematically in figure 5, is outlined in detail below.

Sequence length

The standard load sequence will be made up by a sequence of missions. For defining its total length opposing criteria have to be considered: the sequence of flights must be short enough to guarantee a sufficiently large number of repetitions in fatigue tests, but it must also be long enough to establish a representative mission mix. With respect to the maximum occurring load it must be realised that this is reached in every flight during Departure.

For TURBISTAN a sequence length of 100 flights has been chosen, which may be associated (approximately) with 100 flying hours. If a typical fatigue test is expected to last for about 1000 flights, then 10 repetitions of the total sequence will occur. This seems to be a reasonable compromise between testing time and possible sequence effects.

Mission mix

The TURBISTAN loading standard must distinguish between four typical mission types and thus the mission mix has to be established. The TURBISTAN mission mix which has been applied is composed in such a way that 75 % of the loading within the standard is due to combat conditions.

TURBISTAN mission sequence

With knowledge of the total sequence length (100 flights) and mission mix and by stating that all 31 flights of the pool will be taken into account with equal probability it is possible to define the actual mission sequence for TURBISTAN. This has been done by employing a once and for all random draw, resulting in a list of 100 flights representing the basic flights A1-A7, B1-B5, C1-C9 and D1-D10, see table 1. This list is used as an input table for the generation programme.

Individual mission generation

According to the flow chart in figure 5 each flight of TURBISTAN is constructed by lining up the various flight events and by generating the loading within each of them. The necessary quantitative information for the subsequent generation steps is indicated by the blocks A through G, (see also Fig. 2).
Since the analysis procedures are based on a 10 % class-width a resolution of 10 % is found in the final sequence. This was considered too rough and therefore a randomisation procedure has been applied afterwards to arrive at a loading sequence with a 1 % resolution. To do so "1 percent"-classes are drawn randomly within each 10 % class from a uniform distribution incorporating a 2 percent range filter.

Results

A sample of TURBISTAN is shown in figure 6. The standard contains 15452 loading reversals in total representing 100 flights, thus the average flight length is about 80 cycles. During the material testing programme this full preliminary TURBISTAN sequence is to be modified in various ways in order to find out if simplifications are possible and to control the validity of some basic assumptions, see section 4.

4 MATERIAL EVALUATION PROGRAMME ON VALIDITY OF TURBISTAN SEQUENCE

4.1 Introduction

In the initial part of this paper some material aspects dealing with disc lifing were shortly mentioned. In the following these will be discussed in more detail.

Current methods of lifing gas turbine discs are based on a "life to first visible crack" failure criterion. The visible crack is defined as an approximately 0.75 mm long surface feature that can be readily detected by routine inspection procedures. The number of cycles required to develop this size of defect is determined either through measurements made on laboratory test pieces or through full scale spin pit testing of disc components. In both cases, the test is carried out under a zero to maximum loading cycle and the measured lives are factored to arrive at a safe service life. These factors are statistically based so as to give, typically, a 1 in 1000 risk level for the formation of the visible crack [2].

For civil aircraft and military transport requirements this procedure is sufficient because the zero to maximum loading cycle can be equated with the take off-cruise-land missions flown. For combat aircraft, however, within the major fatigue cycle lie many minor cyclic excursions determined by the manoeuvre requirements of the mission. The fatigue damage caused by these minor cycles is often expressed in terms of an equivalent number of major cycles. Equivalent cycles are estimated by first identifying the minor cycles by techniques such as rainflow logic and then converting each minimum-maximum cyclic excursion to an equivalent zero-maximum major cycle through a Goodman diagram. This procedure is followed for the range of missions that the aircraft engine is likely to experience, i.e. low level attack, high level attack, training, and so on. The result is a frequency distribution of the cyclic usage (cycles/hour) for each component. From this distribution, a weighted mean value for the usage can be established. The weighting places this value towards the high side of the distribution. The mean usage or exchange rate is used with the factored laboratory and component test data to calculate a safe service life for each component in hours:

$$\text{Safe Service Life} = \frac{\text{Number of cycles to first crack}}{\text{Statistical safety factor x exchange rate}} \text{ (hours)}$$

The effectiveness of this approach is evident from the comparatively low number of disc failures that occur in service. This success is the result of the large safety factors used and the weighting applied in the exchange rate calculation. The requirements for lighter engines, however, demand that disc materials are used more efficiently. Calculations [3], in which a Monte Carlo routine has been used to "fly" a critical component through a range of missions on the computer, have indicated the extent to which a fixed exchange rate might misrepresent the fatigue damage incurred, see table 2.

One solution to this limitation is the continuous monitoring of the inflight usage experienced by critical components. Financial constraints, however, restrict the extent to which monitoring equipment can be deployed throughout a fleet of aircraft. At the same time, the computer algorithms which are used to convert the measured usage into component damage rely on conventional zero to maximum fatigue information. Once again, therefore, the calculated lives depend on the validity of:

- the methods used for identifying major/minor cycles;
- the technique for translating a minor cycle into an equivalent zero-maximum cycle, and
- the criterion adopted for summing up the damage incurred.

On the latter point, a Miner linear damage rule is often invoked even though it is known to break down under certain loading sequences [4].

The TURBISTAN programme seeks to remove some of these limitations by attacking the problem in a different way. The aim has been to develop a standard loading sequence that will be used to generate component design curves to complement the present approach based on repeated load cycles. The standard loading sequence incorporates and amalgamates the principal cyclic features from a range of missions flown by several aircraft types.

It is recognised that several standard sequences will be necessary because the stressing conditions, particularly with regard to the thermal contribution, are different between the front and rear of the compressor and within the high pressure turbine. However, in this first phase of the programme, attention is specifically focussed on fan disc characteristics where thermal stress effects are unimportant and where inflight RPM monitoring is sufficient for the derivation of a sequence. This was described in detail in the previous section.

The mission analysis exercise is supported by a comprehensive material testing programme. The programme is being used to assess the effectiveness of the standard and to explore the validity of assumptions made in its derivation. Details on philosophy, content and the experimental techniques employed are presented below.

4.2 Material testing programme

Material

The titanium alloy Ti-6Al-4V was selected because this alloy is typical of the materials used for fan and low pressure compressor discs. It is also an alloy for which the participating laboratories have gained much experience. The bulk of the testing is being carried out on material that has been given a STOA (solution treated and overaged) heat treatment. The laboratory specimens have been taken from full size fan disc forgings. Metallographic examination revealed a fairly uniform equiaxed microstrucure consisting of approximately 30 % primary alpha grains in a transformed beta matrix. A more limited test programme is being carried out on annealed Ti-6Al-4V in which there is an 80 % primary alpha content. Specimens in this case have been taken from a helicopter rotor forging.

Specimens

A range of specimens was selected that would allow TURBISTAN concepts to be explored for both crack initiation and propagation stages. It is reasonable to state that although existing fatigue design methods are based on a "life to first crack" or initiation philosophy there is much interest in moving to a crack propagation based criterion in which component life would be calculated on the basis of fracture mechanics principles [5]. The TURBISTAN experimental programme covers the requirements of both design philosophies.

- Plain Specimen

The cylindrical unnotched LCF test piece (see Fig. 7) is being used for both load and strain control testing. The unnotched geometry is believed to provide a good simulation of crack formation in regions of a component where the gradient in stress is low. For instance there is evidence to suggest that unnotched laboratory fatigue data correlate well with disc bore behaviour. Strain control testing is appropriate for regions where a plastic zone is constrained by elastically deformed material.

- Notched Specimen

The flat double edge notched specimen (see also Fig. 7) has been included to assess crack formation within a high stress gradient typical of that found at bolt holes and blade root fixtures in engine discs. Crack formation is being detected by means of a PD (potential drop) technique.

- Corner Crack Specimen (CC)

The dimensions of the corner crack specimen are shown in figure 7. This test-piece has been designed to simulate the growth of quarter circular cracks in engine components [6]. Crack growth is being monitored optically and by a PD method.

- Compact Tension Specimen (CT)

A standard CT specimen is being used as shown in figure 7. It is included to provide data on long crack growth behaviour. Crack monitoring is being carried out by PD techniques.

Fatigue testing programme

The test programme requires each specimen geometry to be subjected to five different loading cycles. The total programme for 30 % primary α material is summarised in table 3. It will be observed from this table that each laboratory is responsible for only one specimen type. This restriction was imposed to avoid complications due to differences in testing technique between the laboratories. At the same time, it enabled the programme to focus on a specialist capability in each of the test areas. The only general testing constraints placed on the participants were that the cyclic programme should be carried out in air at ambient temperature and a loading rate to give a rise time from zero to 100 % load of 0.5 seconds. The ideal cycle shape should be triangular although slight variations for measurement purposes are permissible. Control over test parameters, such as minimum loads in load control tests and calibration of test equipment, would be to the normal standards employed by the laboratory. The major criterion was that the same standard should apply throughout each individual laboratory programme. One final requirement was that at least 100 measurement points would be taken during crack growth monitoring.

Five loading cycles have been selected in order to satisfy the material testing programme objectives, which are:

- evaluation of the full preliminary TURBISTAN cycle;
- investigation of the degree to which the full cycle can be simplified;
- assessment of the validity of the assumptions made in constructing the TURBISTAN cycle.

It is appropriate to consider the purpose of each loading cycle separately:

- Zero-Maximum Cycle

The zero-maximum cycle tests are being used to establish baseline S-N curves or da/dn-ΔK plots for the material. Appropriate loading conditions will be selected from these curves for the remaining test programme. Typically, the 100 % stress condition will be the value which results in a life of about 16000 cycles.

- TURBISTAN Cycle

Design curves for the full TURBISTAN cycle are to be obtained at 3 different peak stress levels. As with the zero-maximum cycle, three specimens will be tested at each of the stresses. For the CT crack propagation work, only 2 specimens will be used for both the zero-maximum cycle and the TURBISTAN cycle.

- Zero-Maximum + Dwell

There is much evidence in the literature to support the view that titanium alloys are susceptible to dwell periods at peak stress and ambient temperatures [7]. The dwell sensitivity is readily apparent in low cycle fatigue tests under load control and evident also under certain crack propagation conditions. The magnitude of this sensitivity is greatest for large grained, β processed alloys but has been observed also in α/β materials such as Ti-6Al-4V. In developing the cold TURBISTAN cycle, it was decided to ignore the presence of dwell periods. It is necessary, however, to test the validity of this important assumption. An assessment will be made at one critical stress level only, although three specimens will be tested at that level. Within the test the total dwell period at peak stress will be the average TURBISTAN flight time.

- MINITURB Cycles

The cold full TURBISTAN sequence contains about 16000 load reversals representing 100 flights. The average flight length is thus 80 cycles. This figure arose through the application of a stress range filter to the raw engine data. The current filter is 2 % of the maximum stress range and any cycles less than this size are ignored. The MINITURB series of tests will explore the effect of reducing the number of minor cycles per flight on component life.

- SEQUITURB

There is evidence in the literature that the order in which minor cycles are placed can affect fatigue behaviour [3]. In the SEQUITURB programme the effect of minor cycle order will be evaluated. This will involve placing the minor cycles in the TURBISTAN mission into increasing and decreasing load sequences. Again one peak loading condition will be assessed using three specimens for the plain, notched and CC specimens and two for the CT specimen.

5 CONCLUDING REMARKS

Based on 31 selected operational mission profiles of several aircraft/engine types operating in Western Europe a load sequence for "cold" compressor discs has been derived which is considered representative for actual usage. This preliminary TURBISTAN sequence contains about 8000 cycles representing 100 flights. In this paper the compilation and selection of flight data, their analysis and the generation of this first TURBISTAN sequence was described.

A material fatigue testing programme was designed aimed at the verification of the assumptions made in the derivation of the standard sequence. In addition, the test programme should indicate to what extent the preliminary sequence can be simplified without compromising its validity. This test programme, including the current philosophy on material evaluation for disc lifing, has been reviewed.

It is the intention that the final TURBISTAN sequence will be ready within a year. It will then be available freely for all interested parties.

6 ACKNOWLEDGEMENT

The TURBISTAN working group would like to acknowledge the support of the Defence Ministries in their respective countries.

REFERENCES

1 Breitkopf, G.E., Speer, T.M., In-flight evaluation of LCF life consumption of critical rotor components subjected to high transient thermal stress, AGARD Conference on "Cyclic Durability by Analysis and Testing", Lisse, The Netherlands, 1984, AGARD CP-368, pp. 1/1-15

2 Evans, W.J., Smith, M.E.F., Williams, C.H.H., Disc fatigue life prediction for gas turbine engines, AGARD Conference on "Cyclic Durability by Analysis and Testing", Lisse, The Netherlands, 1984, AGARD CP-368, pp. 11/1-12

3 Leathart, A.B., Greig, A.W.M., A risk analysis of low cycle fatigue lives of engine components, Propulsion Department, RAE, Memorandum M79002, 1979

4 Cruse, T.A., Meyer, T.G., A cumulative fatigue damage model for gas turbine engine disks subjected to complex mission loading, ASME Winter Meeting, San Francisco, 1978

5 Hoeppner, D.W., Application of damage tolerance concepts to "short cracks" in safety critical components, Structures of High Fatigue Performance, ICAF, Toulouse, 1983

6 Brown, C.W., Hicks, M.A., Fatigue growth of surface cracks in nickel-based superalloys, Int. J. Fatigue, 1982, 4, pp. 73-81

7 Jeal, R.H., Defects and their effect on the behaviour of discs, AGARD Conference on "Maintenance in Service of High Temperature Parts", AGARD CP-317, 1982, 5/1-9

TABLE 1
Available missions in TURBISTAN

MISSION TYPE	MISSION DESCRIPTION	TOTAL NUMBER OF MISSIONS
A	Air Combat	7
B	Transition/Training	5
C	Ground attack	9
D	Navigation	10
	Total	31

TABLE 2
Calculated risk level for the development of a visible crack

Calculation method	Estimated risk of a crack in 400 hours	Estimated risk of a crack in 800 hours
Fixed exchange rate	1 in 1000	not estimated
Monte Carlo (i.e. variable exchange rate)	1 in 20000	1 in 1000

TABLE 3
Test programme

Test	Stress Levels	Cycle type	Fatigue life specimens			Crack growth specimens	
			plain		notched		
			σ control	ε control		CC	CT
1. 0 - MAX	3	No dwell	9	9	9	9	2
2. TURBISTAN	3	Full cycle (16000 revs)	9	9	9	9	2
3. 0 - MAX + DWELL (Total time = TURBISTAN time)	1	Dwell cycle (average time per flight)	3	3	3	3	2
4. MINITURB	1	Simple cycle (reduce number of reversals)	12	12	12	12	8
5. SEQUITURB	1	increasing	3	3	3	3	2
		decreasing	3	3	3	3	2
		Test Laboratory	LBF	IABG	CEAT	RR	UoT

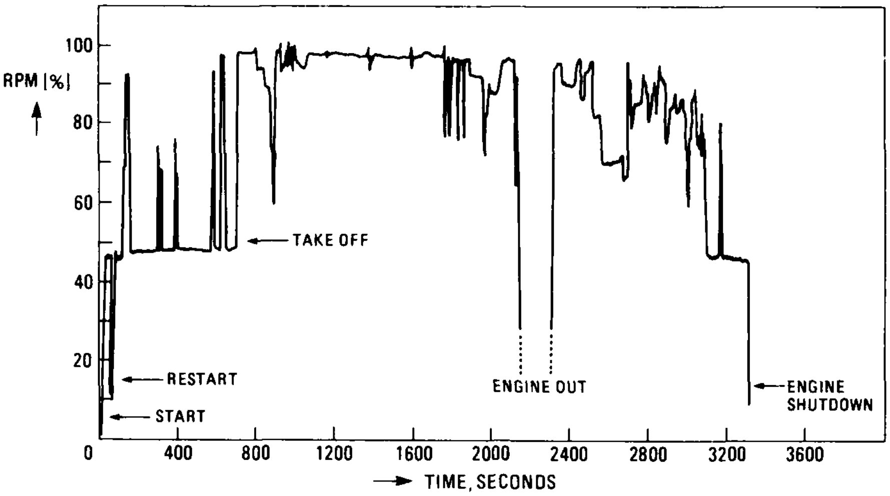

Fig. 1 Operational mission profile of fighter aircraft engine

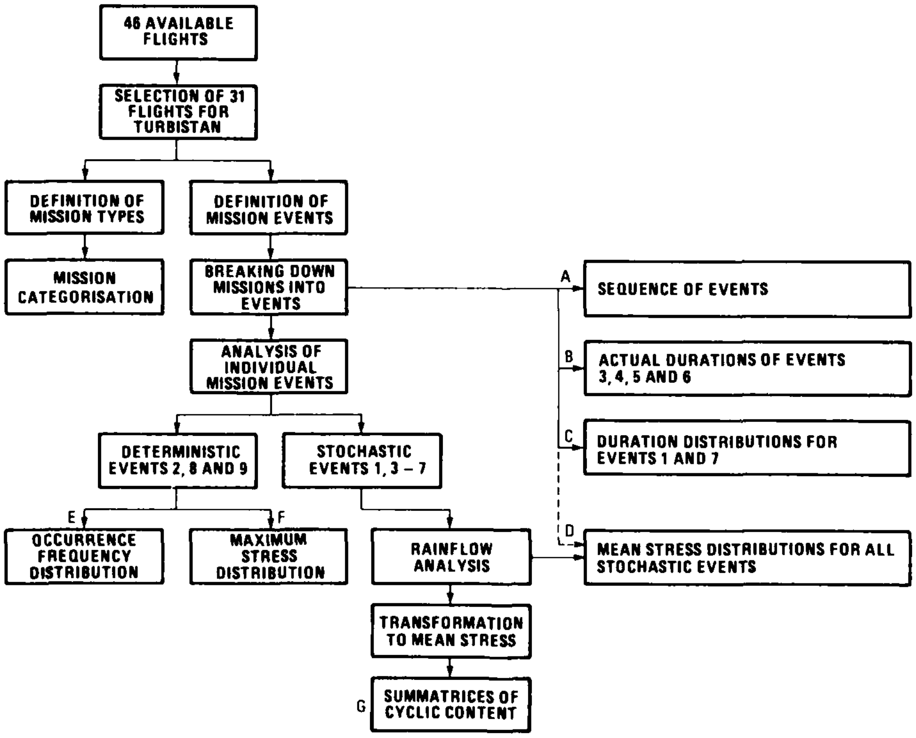
46 AVAILABLE FLIGHTS
SELECTION OF 31 FLIGHTS FOR TURBISTAN
DEFINITION OF MISSION TYPES
DEFINITION OF MISSION EVENTS
MISSION CATEGORISATION
BREAKING DOWN MISSIONS INTO EVENTS
ANALYSIS OF INDIVIDUAL MISSION EVENTS
DETERMINISTIC EVENTS 2, 8 AND 9
STOCHASTIC EVENTS 1, 3 – 7
E
F
OCCURRENCE FREQUENCY DISTRIBUTION
MAXIMUM STRESS DISTRIBUTION
RAINFLOW ANALYSIS
TRANSFORMATION TO MEAN STRESS
G
SUMMATRICES OF CYCLIC CONTENT
A
SEQUENCE OF EVENTS
B
ACTUAL DURATIONS OF EVENTS 3, 4, 5 AND 6
C
DURATION DISTRIBUTIONS FOR EVENTS 1 AND 7
D
MEAN STRESS DISTRIBUTIONS FOR ALL STOCHASTIC EVENTS

Fig. 2 Mission Analysis Procedure

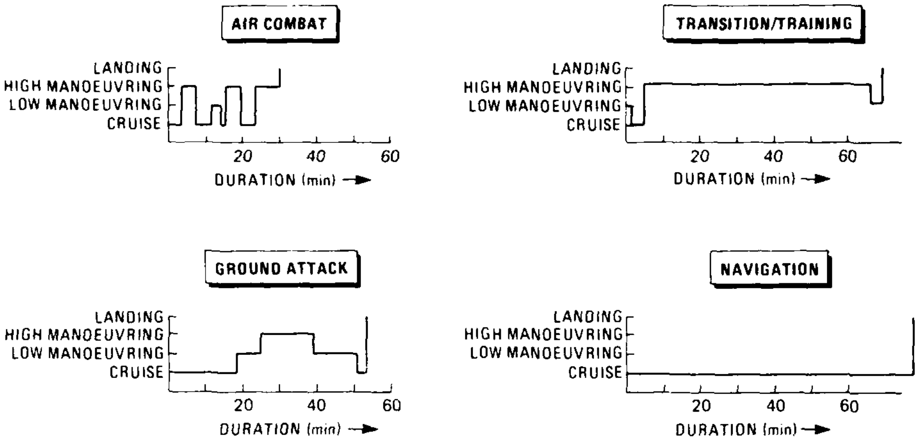

Fig. 3 Different character of in-flight phases schematised

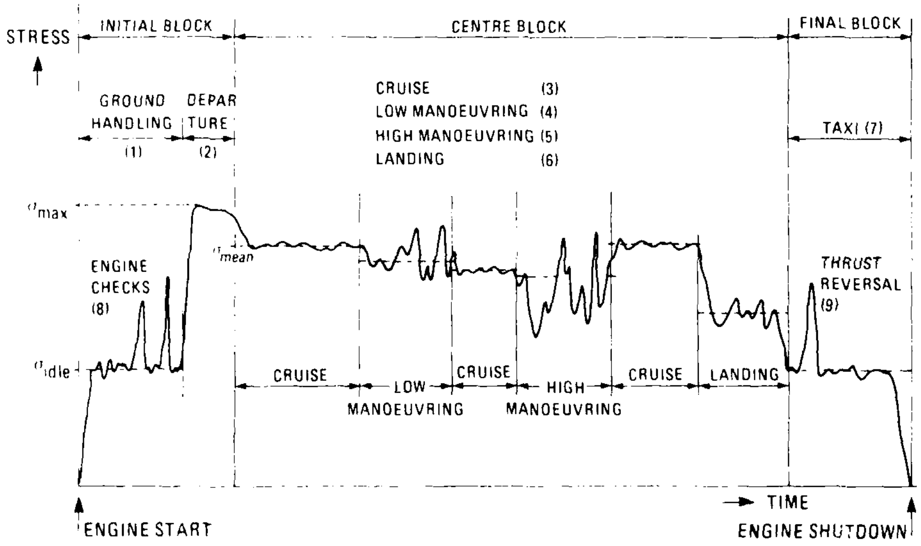

Fig. 4 The general structure of a flight

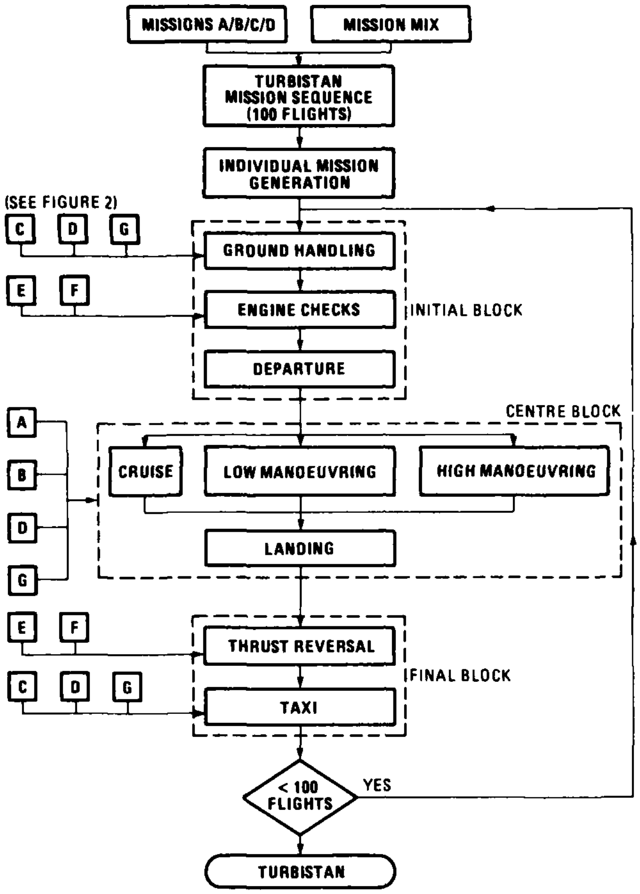
MISSIONS A/B/C/D
MISSION MIX
TURBISTAN MISSION SEQUENCE (100 FLIGHTS)
INDIVIDUAL MISSION GENERATION
(SEE FIGURE 2)
C
D
G
GROUND HANDLING
E
F
ENGINE CHECKS
INITIAL BLOCK
DEPARTURE
CENTRE BLOCK
A
B
D
G
CRUISE
LOW MANOEUVRING
HIGH MANOEUVRING
LANDING
E
F
THRUST REVERSAL
FINAL BLOCK
C
D
G
TAXI
< 100 FLIGHTS
YES
TURBISTAN

Fig. 5 Generation procedure

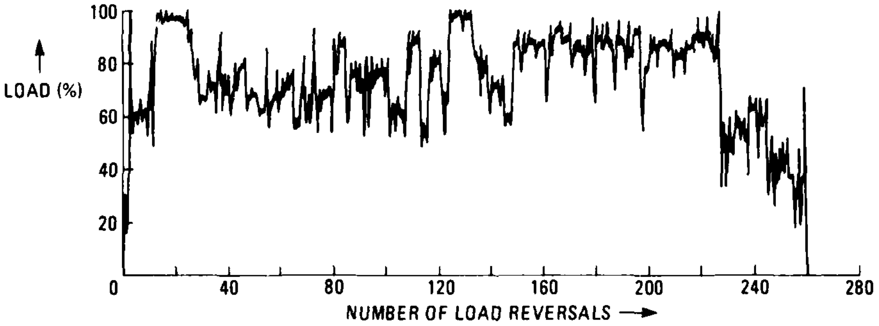

Fig. 6 Sample of TURBISTAN (Ground attack mission)

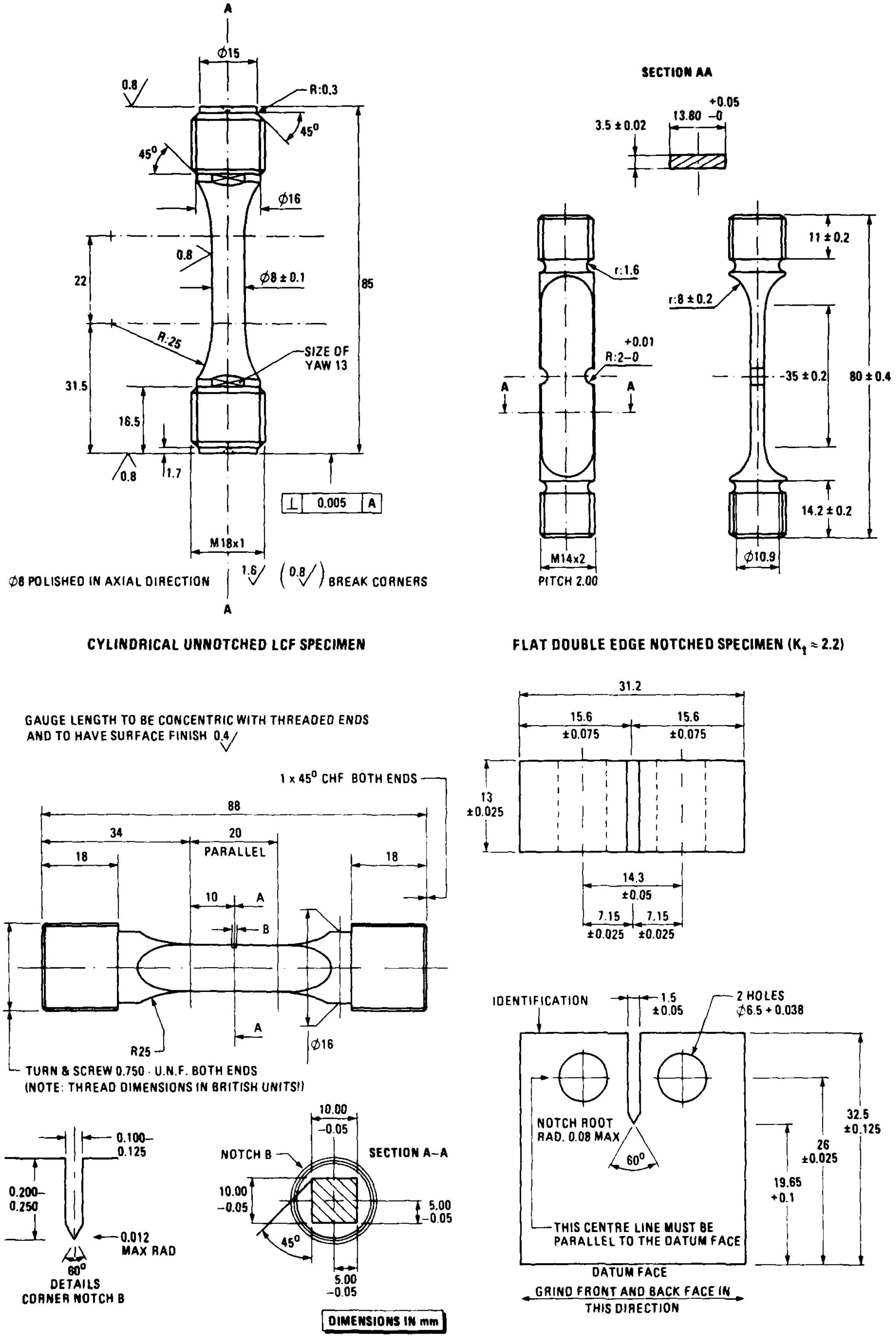
A
Ø15
0.8
R:0.3
45°
45°
Ø16
0.8
Ø8 ± 0.1
22
85
R:25
SIZE OF YAW 13
31.5
16.5
0.8
1.7
⊥ 0.005 A
M18x1
Ø8 POLISHED IN AXIAL DIRECTION
1.6
(0.8) BREAK CORNERS
A
SECTION AA
+0.05
13.80 -0
3.5 ± 0.02
r:1.6
r:8 ± 0.2
11 ± 0.2
+0.01
R:2-0
A
A
35 ± 0.2
80 ± 0.4
14.2 ± 0.2
M14x2
PITCH 2.00
Ø10.9
GAUGE LENGTH TO BE CONCENTRIC WITH THREADED ENDS AND TO HAVE SURFACE FINISH 0.4
1 x 45° CHF BOTH ENDS
88
34
20
PARALLEL
18
18
10
A
B
A
R25
Ø16
TURN & SCREW 0.750 - U.N.F. BOTH ENDS
(NOTE: THREAD DIMENSIONS IN BRITISH UNITS!)
0.100-0.125
0.200-0.250
0.012 MAX RAD
60°
DETAILS CORNER NOTCH B
10.00 -0.05
NOTCH B
SECTION A-A
10.00 -0.05
5.00 -0.05
45°
5.00 -0.05
DIMENSIONS IN mm
31.2
15.6 ±0.075
15.6 ±0.075
13 ±0.025
14.3 ±0.05
7.15 ±0.025
7.15 ±0.025
IDENTIFICATION
1.5 ±0.05
2 HOLES Ø6.5 + 0.038
NOTCH ROOT RAD. 0.08 MAX
60°
32.5 ±0.125
26 ±0.025
19.65 +0.1
THIS CENTRE LINE MUST BE PARALLEL TO THE DATUM FACE
DATUM FACE
GRIND FRONT AND BACK FACE IN THIS DIRECTION

CYLINDRICAL UNNOTCHED LCF SPECIMEN

FLAT DOUBLE EDGE NOTCHED SPECIMEN ($K_t \approx 2.2$)

CORNER CRACK SPECIMEN

CT-SPECIMEN

Fig. 7 Specimens used in TURBISTAN programme

AN ANALYSIS OF RIG TEST DISC FAILURES

by

G. Asquith
Mechanical Technology Department
Rolls-Royce Limited
Derby
DE2 8BJ

SUMMARY

A major objective in gas turbine engineering is the design and manufacture of discs that are reliable in service. Much depends on the accurate prediction of safe total lives and inspection intervals. Accurate predictions come from a complete understanding of material behaviour involving experimentation, interpretation and quantification, for which a balanced programme of laboratory specimen and full sized disc evaluation is required. Cyclic testing of full size discs is essential, this allows each disc to do its own "Monte Carlo" evaluation of the large number of variables that affect the final result. Where life can be predicted entirely by linear elastic fracture mechanics some simplification can be introduced; this encourages studies in the quantification of short crack propagation behaviour.

INTRODUCTION

A major objective in gas turbine engineering is the design and manufacture of discs that are reliable in service - that is, they can be relied upon not to grow too much or burst during the period of operation.

For many years three separate criteria have been used to prevent burst:

a) overspeed requirements (normally these cover growth).

b) low cycle fatigue life limitations; these cause the majority of discs to be withdrawn from service before any cracking can be observed by current inspection techniques.

c) the limitation of vibratory stresses to low levels considered by experience to be acceptable.

With the better understanding of the fracture process that has been obtained in recent years the burst criteria can be restated in a more rational form, as is done in ENSIP -

A crack in a disc must not be allowed to grow to a size that can lead to the onset of rapid fracture under any engine condition, i.e. commonly, a crack growing under low cycle fatigue must not be allowed to reach the length at which either vibration or an overspeed can promote rapid fracture. (Fig. 1).

> 'The service life must not reach the burst life or the onset of rapid fracture'
>
> This is the **fundamental criterion** for safety.

FIGURE 1 DISC LIFE CRITERIA (1)

Whichever set of criteria is used there is great emphasis on the reliability of LCF life prediction.

Ideally this reliability is obtained by:

i) UNDERSTANDING THE FRACTURE MECHANISM.

ii) QUANTIFICATION OF THE CONTROLLING PARAMETERS.

The case studies in this paper are mainly concerned with the quantification and the relationships between laboratory specimens and full size discs. Problems that can arise are illustrated, not all are solved.

CRACK GROWTH TO FRACTURE

In general there are four phases of crack growth. (Fig. 2).

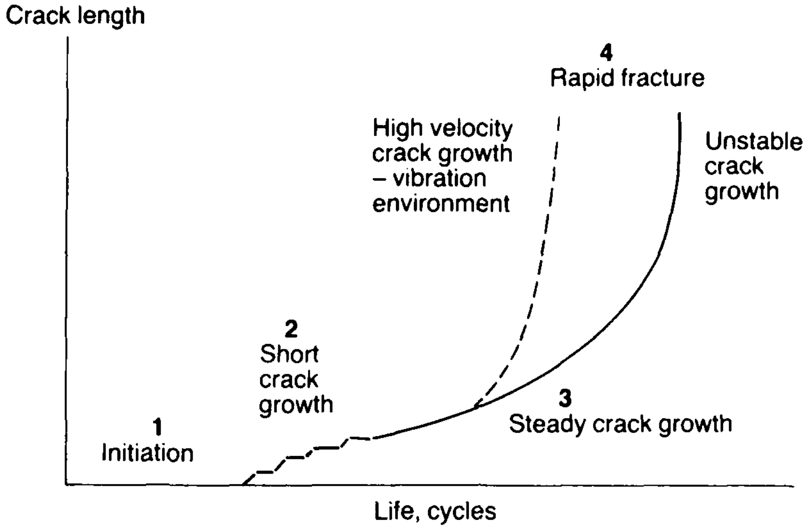

FIGURE 2 - STAGES OF CRACK INITIATION AND GROWTH

1. Initiation - the formation of small sub-grain-size cracks.
2. Short crack growth - mixture of growth within the grain and arrests at grain boundaries - structure dominated.
3. Steady crack growth - function of crack geometry and stress.
4. Rapid fracture - unstable crack growth under steady loading or high velocity crack growth due to high frequency stress oscillations superimposed on steady stress.

DESIGN REQUIREMENTS

Taking safety as the prime requirement there are two basic routes that may be chosen to arrive at a commercially acceptable design.

a) Safe predicted total life.

b) safe crack propagation life.

SAFE PREDICTED TOTAL LIFE

The objective here is to utilise as much of phases 1, 2 and 3 as safety permits. Whilst it is possible to distinguish between the three phases qualitatively the transition from one phase to the next is not necessarily clearly defined and there are difficulties in quantification of the life spent in each. Phase 1 is susceptible to scatter, crack propagation behaviour in phase 2 is still in the exploratory stage, phase 3 is the most amenable to quantification on a sound physical basis.

Standard practice has therefore been to quantify the total life to an arbitary end point without distinguishing between the individual phases other than to allow some of phase 3 as a safety margin between cracking and bursting.

The quantification of disc bore life in steel (FV 535) illustrates the traditional approach.

A disc bore is a large surface with no stress concentration features, the cheapest way to attain a stress-life relationship would therefore appear to be by testing load controlled plain specimens. On a probability basis one might expect to see the disc test results following the lower scatter boundary of the specimen S-N curve. The stressed volume/surface area of a disc is generally higher than a specimen, by one or two orders of magnitude, there is therefore a greater probability of exposing an unfavourably orientated grain to the stress field and as a consequence, earlier cracking may be expected (1).

Figure 3 shows the relationship of FV 535 disc bore test results to the plain specimen S-N curves, with all disc results above the typical specimen curve.

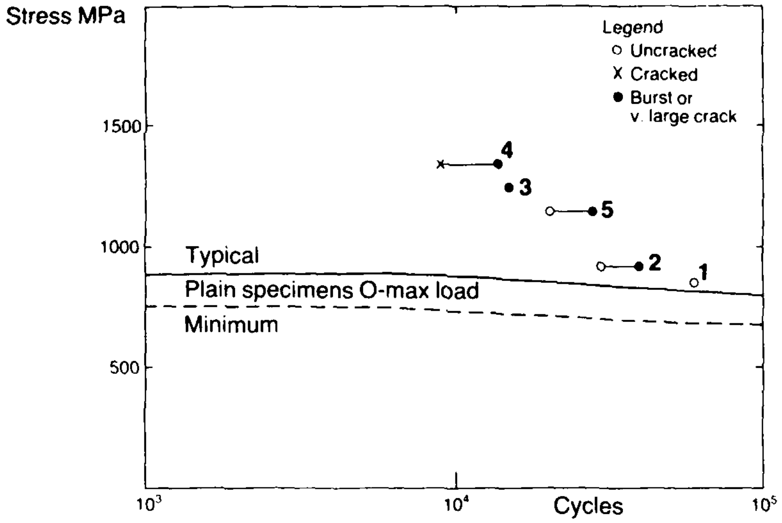

FIGURE 3 - FV535 BORES 300°C

The first point to note is that the stress values for the discs are quoted on the basis of elastic analysis, i.e. they are the first approximation to strain range $\Delta\varepsilon$ x Young's Modulus E, not the real stresses after yielding.

This opens up two alternative means of correlation with specimen results. Historically these were:

a) plastic analysis, followed by mean and alternating stress correlation on an R-M or Goodman diagram.

b) direct comparison with 0 - max. strain cycling specimen results.

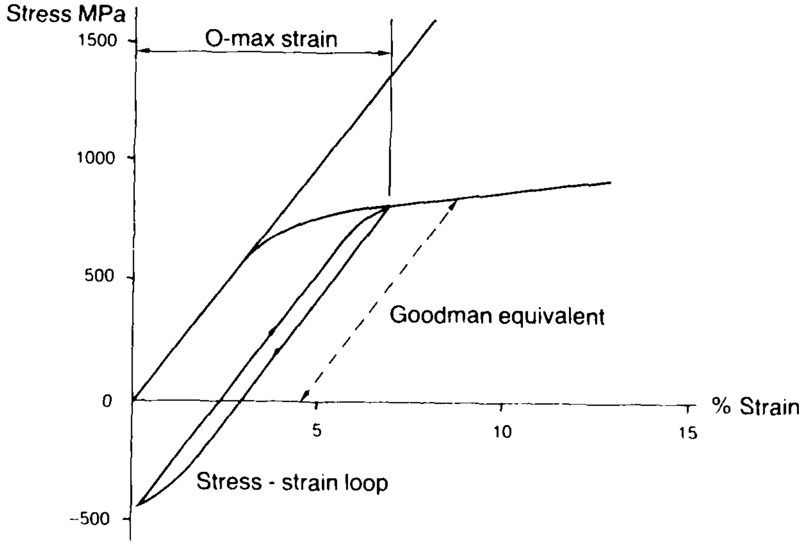

FIGURE 4 - FV535 BORES 300°C GOODMAN CONVERSION

Figure 4 shows diagrammatically the relationship of 0 - max. elastic strain to the maximum and minimum actual stresses subsequent to yielding. These stresses can be converted to the equivalent 0 - max. stress by the straight-line Goodman relationship.

$$\sigma = \frac{u\,\Delta\sigma}{u - \sigma_{min}} \qquad (1)$$

Where σ = 0 - max. stress equivalent.
u = Ultimate tensile strength.
$\Delta\sigma$ = stress range ($\sigma_{max} - \sigma_{min}$).
σ_{min} = minimum stress (+ve tensile).

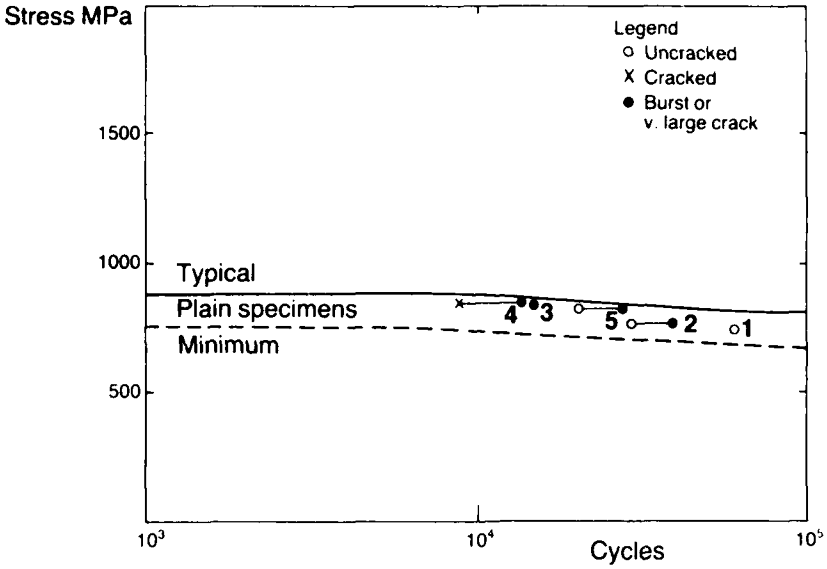

FIGURE 5 - O-MAX STRAIN CONVERSION TO O-MAX STRESS (GOODMAN)

Figure 5 shows the relationship of the disc test results to the plain specimen S-N curve after conversion by equation (1). The results fall into the anticipated scatter band and appear reasonable. Whilst this at first is gratifying, after further consideration it is seen that the lives all fall below the "typical" S-N ("typical" is used in the sense of approximate median) curve.

The discrepancy is emphasised by comparison with O - max strain cycling specimen results. (Figure 6).

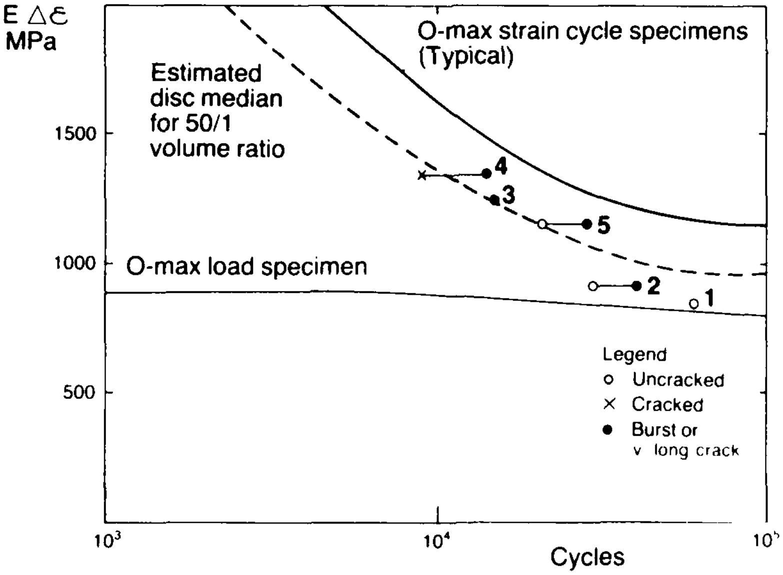

FIGURE 6 - FV535 BORES 300°C

First examining the volume effect, the ratio of highly stressed material in a disc compared with a strain cycle specimen gauge length was about 50/1. Accordingly a statistical analysis of the specimen strain-cycling results was made from which the predicted median S-N curve for the disc results was estimated. Using a log-normal distribution, discs would be expected to contain cracks as big as those in failed specimens at cyclic strain levels of about .84 times the specimen values (the specimens fail due to exceeding the UTS, not fracture toughness, equating to a semi-circular crack about 1mm radius). Discs were tested until cracks of 5-10mm developed, so that crack propagation lives of at least 6000 cycles in excess of specimen lives might be expected. Volume effects could therefore explain two results completely (4 and 5).

Corrosion was seen on all discs. This, together with the difference in specimen/disc surface finish might have depressed the other disc lives by reducing initiation life. (The specimens were turned and emery polished, the discs were simply turned).

For the largest crack in disc No.2 a striation count indicated over 18,000 cycles of propagation. This equated to a starting crack size of about 0.1 mm. (From the crack detection point of view it is worth noting that no cracking was observed 10,000 cycles before test completion, probably due to closure caused by residual compressive stresses). It had been postulated at one stage that as a result of the surface conditions the initiation phase had been completely eliminated. Crack propagation life estimates for various starting defect sizes are shown in Fig.7. From these the inference is that surface conditions have reduced the initiation life, not eliminated it.

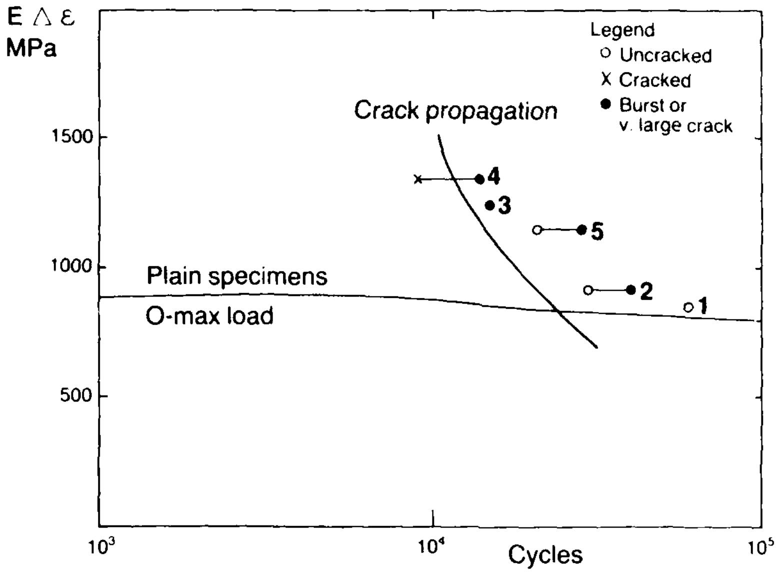

FIGURE 7 - FV535 BORES 300°C

Summarising, the above investigation indicates a number of factors having a potential significant influence on prediction of the total life of the disc -

Variation in initiation life, scatter.

Surface condition - machining.

- corrosion.

Yielding characteristics

Stress-strain loop.

Crack propagation - life fraction.

- initial crack size.

Disc/specimen - volume ratio.

- crack propagation life.

If each of the above factors were quantifiable in terms of its effect on life it would be possible to estimate the life of a disc analytically, either within bounds or by a Monte Carlo approach.

Where the factors and their interrelationships cannot be quantified with sufficient certainty, as in the example given, it is better to test a series of discs, allowing each to provide its own Monte Carlo solution, in order to establish a safe working life.

Material
- Microstructure
- Homogeneity
- Defect content

Surface
- Machining damage
- Scoring & burring
- Dents & bruises
- Fretting
- Processing

Residual stresses
- Quenching
- Welds
- Machining

Effects of yielding & creep
- Gross
- Local features

Relation of disc to specimen results
- Strain cycle
- Goodman
- Volume
- Crack propagation

Crack propagation prediction
- LCF cracks
- Structural discontinuities
- Manufacturing defects
- Artificial cracks

Inspection techniques
- Quality
- Definition
- Automation

Environment
- Vibration
- Temperature
- Corrosion

FIGURE 8 - ENGINEERING PROBLEMS IN ESTABLISHING SERVICE LIFE

SIGNIFICANT FACTORS

A more complete list of known factors of potential significance is shown in Figure 8. This emphasises the difficulty of quantifying each factor and hence the importance of testing engine discs in order to quantify the total combined effect.

By testing the discs to an advanced stage of cracking or failure and coupling this with laboratory and numerical analyses it is normally possible to deduce which are the most significant parameters. Further investigations can then concentrate on those features.

SAFE CRACK PROPAGATION LIFE

This may be treated as

a) a special case of total life, using damage tolerance concepts.

b) an incremental life between inspections.

Considering first a total life application, a number of Titanium 6-4 disc bore tests were carried out and compared to the 0 - max. load plain specimen curve, as was done for steel. (Figure 9). In this case however certain results tended to fall below the plain o-max. load specimen S/N data.

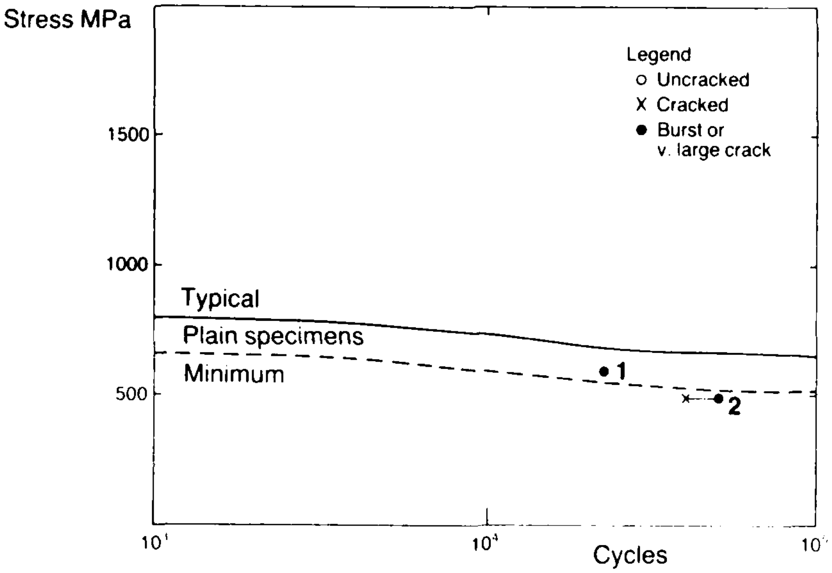

FIGURE 9 - TITANIUM 6 4 BORES 150°C

Laboratory investigation found handling damage marks from which the early cracking had originated and striation counting indicated that most if not all of the disc life was in the crack propagation phase.

Using crack propagation data obtained from laboratory specimens it was possible to correlate the damage and the total life by linear elastic fracture mechanics. (Fig. 10).

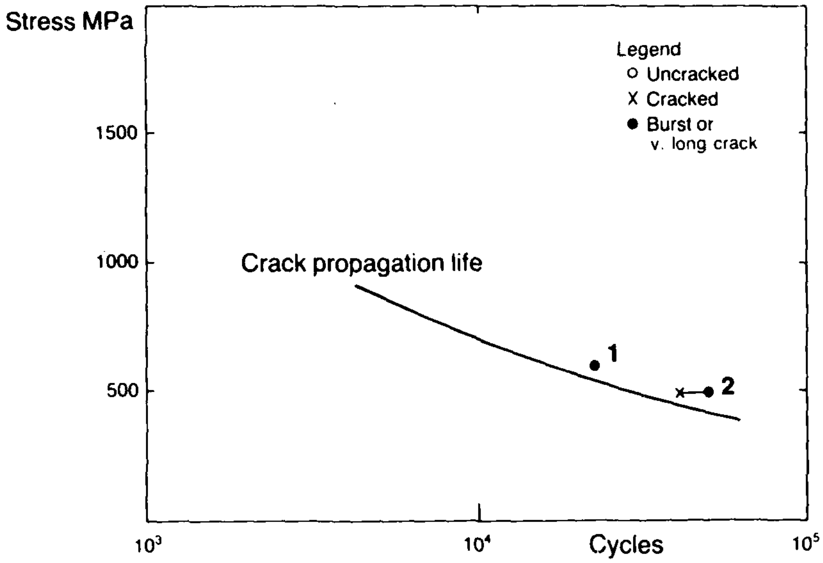

FIGURE 10 - TITANIUM 6-4 BORES 150°C

The result is that a minimum bound S/N curve can now be set up for service life estimation based on understood, quantifiable physical behaviour. This is scientifically more acceptable than phenomenological statistical approaches. The predicted life is commercially acceptable at reasonable stress levels that are within the elastic stress range and residual stresses are low enough to be neglected.

This case represents the ideal in simplicity.

To confirm the reliability of crack propagation on life estimation, and to assess inspection capability (and partly to develop a method that might later be applied to cracks growing in a field where residual stresses were significant) a series of cyclic spinning tests were carried out on similar Ti 6-4 discs into which bore cracks had been artificially induced by the slotted fin technique. (Fig.11). The discs were first

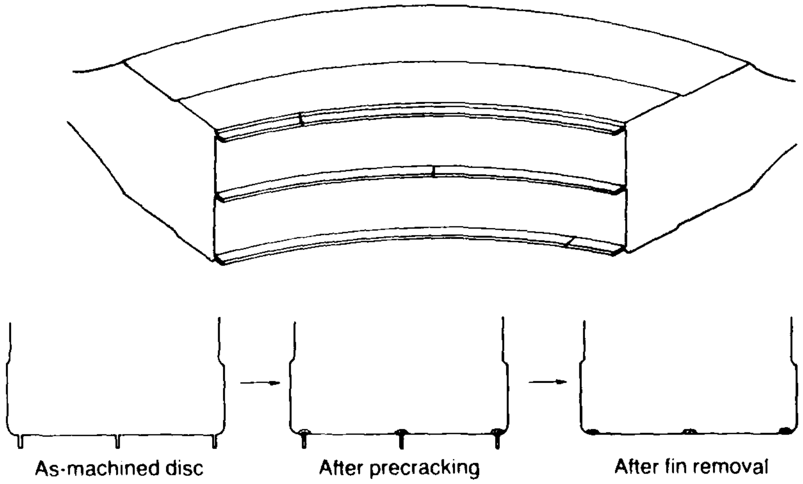

FIGURE 11 - ROLLS-ROYCE DISC BORE FIN CRACK TESTPIECE

cycled until cracks from the machined fin slots ran into the bore to a length of about .75 mm. The fins were then machined off, leaving the bore with a number of sharp starter cracks. Cyclic tests were then carried out and the cracks were monitored over a number of inspection increments. The relationship between predicted and observed growth

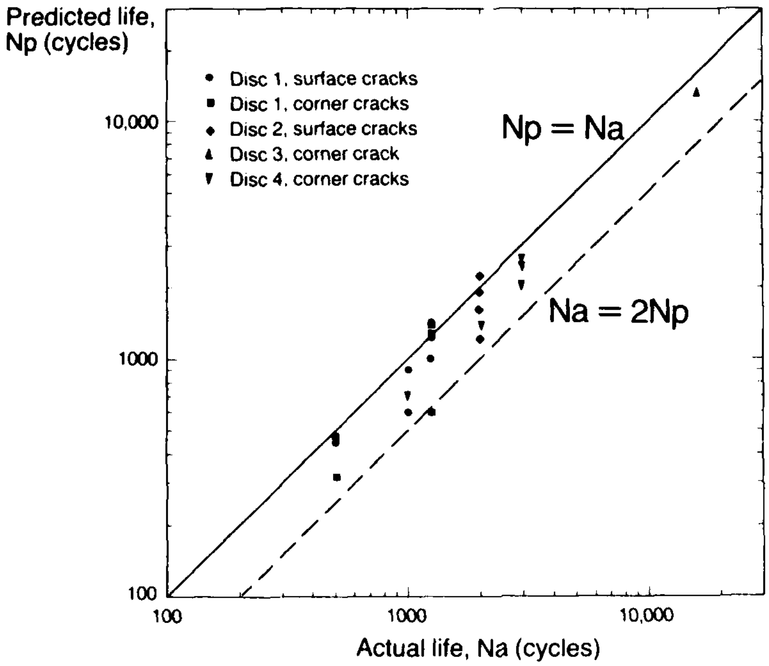

FIGURE 12 - BORE CRACK PROPAGATION RESULTS FOR ARTIFICIALLY CRACKED Ti-6-4 DISCS

is shown in Figure 12. This confirmed the viability of the predictions and indicated that crack monitoring by NDI methods would be possible. The viability of the technique as a means of disc testing was also demonstrated (2).

The cases examined above involved cracking from the surface. The complexity increases when

a) the material contains internal defects.

b) there are significant residual stresses.

c) stresses cannot be kept low enough to give adequate life in the steady crack growth LEFM phase only.

The typical problem, for which there is yet no complete solution, can be illustrated by tests on Waspaloy discs.

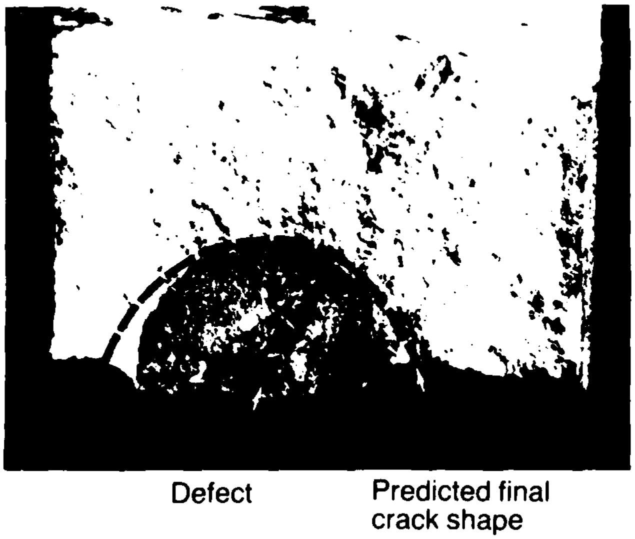

During manufacture, a defect was detected in the bore using ultrasonics, at −11dB to −12dB level.

The disc was rig tested until failure occurred in the rim region. The bore crack shown was then opened.

Ratio of predicted to actual life, using CT specimen data, is 0·86.

Ratio of predicted to actual life, using corner crack data, is 1·07

FIGURE 13 - CRACK PROPAGATION FROM A SUBSURFACE DEFECT NICKEL BASE SUPERALLOY DISC RIG TEST

Figure 13 gives an example of an internal defect growing under cyclic hoop tensile stress in a field of residual compressive forging stress. Correlation of crack propagation life with laboratory test data indicated that the Walker relationships could be relied on for life predictions when compressive residual stresses reduced the rate of steady crack growth.

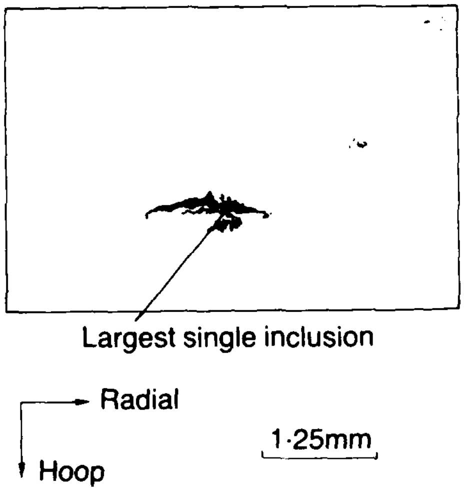

−1dB U/S indication initially

No cracking observed in 20,000 cycles

FIGURE 14 – BORE SUBSURFACE INCLUSION BEHAVIOUR NICKEL BASE SUPERALLOY DISC RIG TEST

Figure 14 illustrates internal defects that would have been expected to grow but simply did not. The fact that this was the case was potentially of great commercial benefit. It however emphasises the need for understanding and quantification of the conditions surrounding the change from initiation to short crack growth and then to steady crack growth in order to make the fullest economic use of any material.

GENERAL SUMMARY

The life of a disc can be influenced by a large number of parameters that are not necessarily independent of each other. The reliability of disc life prediction depends on understanding and quantification of material behaviour. This requires a balanced programme of laboratory investigation and component testing.

The role of engine size disc testing to cracking and failure is seen as:

- providing the most reliable means of life quantification by incorporating realistic representative samples of the variables (ie effectively doing the mathematical Monte Carlo analysis).

- demonstrating which variables are most likely to be significant so that follow-up investigations can be concentrated on these.

The Ti 6-4 testing illustrates how much more reliable life predictions become when they can be scientifically related to the true physical behaviour of the material.

The Waspaloy tests indicate the research needed in order to characterise the behaviour of internal defects and thus maximise the life potential from the initiation and small crack propagation phases.

References

1. CJ Waters and GM Norris. "A method for predicting the low cycle fatigue life of rotating discs from smooth specimen data for a titanium alloy" Private NGTE communication July 1974.

2. AC Pickard, CW Brown and MA Hicks. "The development of advanced specimen testing and analysis techniques applied to fracture mechanics lifing of gas turbine components" ASME International Conference on Advances in Life Prediction Methods, Albany, 1983.

Acknowledgements

The author wishes to thank Rolls-Royce Ltd. and RAE Pyestock for the provision of data on which these analyses were based and colleagues in RR Mechanical Technology and Laboratory departments, in particular Dr AC Pickard, for their co-operation and assistance.

CONTRIBUTION OF TURBINE BLADE SERVICE FAILURES TO A DAMAGE TOLERANCE APPROACH

by

R.J.H. Wanhill and A.J.A. Mom
National Aerospace Laboratory NLR
P.O.Box 90502
1006 BM Amsterdam
The Netherlands

SUMMARY

Modified repair of uprated first stage turbine blades from large turbofans was followed by several fatigue failures in service. The failure mode was low and high cycle fatigue starting at leading edge cooling holes. Fractographic and metallographic analysis by the NLR indicated that insufficient thickness of the leading edge walls was a primary cause of failure. A more comprehensive investigation by the engine manufacturer showed that other parameters besides leading edge wall thickness could be primary causes of failure, namely the leading edge and serpentine airflows and the backflow margin. Relative life reduction factors based on combinations of all four parameters were estimated for many failed, cracked and nominally undamaged blades. Then it became possible to reject blades with unacceptable life reduction factors both before and after repair. This is effectively a life-on-condition damage tolerance approach to blade use.

1. INTRODUCTION

Figure 1 shows the sequence of events leading to a life-on-condition damage tolerance approach for uprated first stage turbine blades from a type of large turbofan. In 1972 the original engine came into use on a number of wide-body aircraft. In 1975 the engines were uprated, which included a higher turbine entry temperature. To cope with this change the first stage turbine blades were redesigned, resulting in more cooling holes in the leading and trailing edges. Figure 2 illustrates the external configuration of these blades.

During service blade tips abrade by contact with the surrounding shroud. This necessitates repair, which for the blades illustrated in figure 2 originally included chemical stripping of the external protective coating, tip refurbishment by welding, external inspection for cracks, recoating, and airflow checks for individual blades. However, in 1977 and early 1978 a number of repaired blades failed or cracked in fatigue. These incidents were attributed to excessive increases in rotor set total airflow because chemical stripping widened the cooling holes during repair, see figure 3.

Owing to the previous incidents the engine manufacturer introduced the following changes in mid-1978:

- Blades already repaired
    - The set management system, whereby after airflow checks each blade must also meet certain criteria for satisfactory operation in a rotor set. The objective is to ensure all blades are adequately cooled in service. In principle this is a good system but it is tedious.
- Blades to be repaired
    - Dry grit blast stripping of the external coating. This avoids cooling hole size increase during repair, and the set management system is unnecessary in most cases.
    - Dump hole flow area reduction by brazing when repaired blades do not meet individual airflow check requirements.
    - Optional use of the set management system.

Despite these changes several incidents of blade failure and cracking occurred in late 1978 - early 1979. The NLR was requested to do a failure analysis. A more comprehensive investigation by the engine manufacturer led to development of a new lifing procedure that is effectively a life- on-condition damage tolerance approach to blade use.

2. BLADE DESIGN

The external configuration of the blades has already been illustrated in figure 2. The blades are René 80 precision investment castings. Ceramic cores provided for the internal cooling air cavities. After casting the cooling holes were drilled and Waspaloy perforated tubes were inserted into the leading edge cavities and fixed by brazing at platform level. Finally the tip caps were brazed on before coating.

The cooling airflow circuits are shown in figure 4. At the shank root the cooling air enters as two main flows W_A and W_B:

- Leading edge airflow airflow W_A
    - This leaves the tube insert and impingement cools the internal leading edge. The air then flows through the leading edge holes and gill holes and over the external surfaces to provide film cooling of the leading edge and mid-chord sections.

  - Cooling hole size and leading edge internal pressure determine the backflow margin (BFM) which is the percentage higher pressure inside the leading edge with respect to the external pressure. Hardware review showed that a minimum BFM of 1.1 % is required to maintain leading edge cooling characteristics. The BFM for individual blades can be calculated from bench measurements of P_D, the pressure drop through the leading edge concave wall gill holes, and the average $W_A + W_B$ for a rotor set.

- Mid-chord and trailing edge airflow W_B
  - Part of the air flows into the trailing edge cavity and leaves via the trailing edge holes. The remaining airflow, W_C, goes through the serpentine circuit. A small proportion of this airflow leaves via the film and tip cap holes. The rest, which is the serpentine airflow W_S, leaves via the dump hole.
  - W_S is a major parameter for the average temperature of the airfoil. An estimation of % W_S can be obtained from pressure differences at two tip cap holes across the serpentine circuit or from a correlation with W_C. The average pressure difference across the serpentine circuits of blades with unbrazed dump holes corresponds to 100 % W_S.

3. NLR FAILURE ANALYSIS

The NLR received one failed and three cracked blades that previously had been repaired and many unrepaired and repaired blades nominally undamaged by use. Two of the cracked blades had suffered foreign object damage (FOD) resulting in cooling loss and cracking at the leading edges.

Main results of the failure analysis follow:

- Fractography
  - Cracked blades were opened up for examination as well as the failed blade. Figure 5 summarises the most important results. Failure was by low and high cycle fatigue that gave fracture surface "beach markings" separated by fine striations. Cracks initiated at convex wall and nose centre cooling hole intersections with internal leading edges 23-25 mm above the platforms.
  - Secondary cracks were present at convex and concave wall gill holes.
- Metallography
  - Spanwise and chordwise cross-sections of unrepaired and repaired blades revealed many secondary cracks in the coatings and at feather edge intersections of cooling holes with the internal and external blade walls. The cracks often penetrated into the blade material.
  - Except for the failed blade, which had experienced overtemperature conditions, the microstructures were typical for solution treated and aged René 80 castings.
- Wall thickness
  - Leading edge wall thicknesses were measured for unrepaired and repaired blades, including the failed and cracked blades. Most cross-sections were 17.5 mm above the platforms. This enabled the failed blade to be compared with others while preserving the fracture surface. The non-FOD cracked blade was sectioned 27.5 mm above the platform, which is one of several cross-section heights with specified thickness minima for blade walls.
  - The failed blade cross-section is shown in figure 6 with actual and specified thickness minima. Note that the specified thickness minima refer to uncoated blade walls. Both the failed and non-FOD cracked blade had below minimum convex wall thicknesses, even though they were still coated and the failed blade had been sectioned at a lower height where blade walls, if anything, are thicker.
  - Cross-sections of unrepaired blades showed that wall thickness variations also occurred in these blades. Such variations are caused mainly by varying positions of the ceramic cores during casting.

The NLR concluded that insufficient thickness of leading edge convex walls was a primary cause of repaired blade failure and cracking. That this problem occurred only in repaired blades was attributed to metal removal during repair. Information from the engine manufacturer showed it had been possible for blades with below-minimum wall thickness to return to service because repair involved metal removal that could not be checked non-destructively at the leading edges until late 1979.

4. INVESTIGATION BY THE MANUFACTURER

Figure 7 gives a schematic overview of the investigation by the engine manufacturer. Design analysis identified four critical parameters that directly affect the blade airfoil temperatures, leading edge creep rates and hence fatigue life:

- Leading edge airflow W_A
- Backflow margin BFM

- Serpentine airflow W_S
- Leading edge convex wall thickness

The flow parameter influences on airfoil temperatures are illustrated in figure 8. Changes in W_A and BFM primarily affect the leading edge and W_S controls the average temperature.

As shown in figure 7, the analysis proceeded in several steps to derive life reduction factors (LRF) for all four parameters. Individual LRFs are arbitrary values for the relative influence of each parameter on leading edge creep rate, the formation of a low cycle fatigue crack and hence the susceptibility to high cycle fatigue crack growth and failure. The total LRF for each blade is the product of its individual LRFs.

Individual LRFs were determined first for the three flow parameters. Then the LRF for leading edge convex wall thickness was assigned different values during iterative best fit classification of total LRFs for many failed and unfailed blades. In other words, total LRFs were derived that clearly distinguished between failed and unfailed blades.

The best fit classification resulted in the individual LRF curves shown in figure 9. Note the relatively strong influence of serpentine flow reduction owing to dump hole brazing. Also shown are individual LRFs for nominal and minimum new blades. These have total LRFs of 1.0 and 7.3 respectively.

Based on these results the engine manufacturer proposed a new lifing procedure for both unrepaired and previously repaired blades (see also figure 7):

- Blades already repaired
    - Measure LRF parameters (including leading edge wall thickness by ultrasonic inspection).
    - Classify blades according to total LRFs.
    - Reject blades with high total LRFs.
    - Remove dump hole braze (if present) for satisfactory blades.
    - Internally coat blades for which dump hole brazing had been used. Internal coating provides a way of reducing serpentine airflow and balancing the leading edge and mid-chord and trailing edge airflows.
    - Return blades to service.
- Blades to be repaired
    - Measure LRF parameters.
    - Classify blades according to total LRFs.
    - Reject blades with high total LRFs.
    - Repair satisfactory blades. This includes initial dry grit blast stripping of the external coating, tip refurbishment by welding, external inspection for cracks, external recoating plus internal coating to re-establish airflows, airflow checks and measurement of LRF parameters.
    - Classify blades according to total LRFs.
    - Reject blades with high total LRFs.
    - Return satisfactory blades to service.

At the time of the proposal the maximum acceptable total LRF was not finalised. However, since minimum new blades (total LRF = 7.3) had not failed in service a provisional value of 5 was used for repaired blades. Finally the engine manufacturer reported ongoing development of two further improvements to the repair procedure:

- A recoating procedure to avoid complete stripping except at the location of tip repair. This is because complete stripping removes not only the coating but also some blade material.
- Ultrasonic non-destructive inspection to detect internal leading edge cracks.

In retrospect, not all the foregoing items were actually implemented. For example, internal coating was not incorporated in the lifing procedure, and ultrasonic inspection was not used to inspect for leading edge cracks.

5. DISCUSSION

LRF analysis and classification of blades is effectively a life-on-condition damage tolerance approach to blade use. Its development represents a significant advance in establishing blade acceptance criteria. However, an important part of the analysis is, in our opinion, questionable. This is the differing treatment of leading edge convex wall thickness with respect to the three flow parameters. The leading edge wall thickness has a direct effect on leading edge creep rate and hence the fatigue life. Thus it would be better to derive the LRF for leading edge convex wall thickness at an early stage of the analysis and not secondarily by iteration.

Figures 10 and 11 provide evidence for this viewpoint. Figure 10 shows that the leading edge convex wall thickness of failed and cracked blades investigated by the NLR were well below those of nominally undamaged blades. This strongly suggests that insufficient thickness of the leading edge convex wall was the primary cause of failure and cracking of these blades. However, the LRF curves in figure 11 show that serpentine flow reduction owing to dump hole brazing was apparently as important as wall thickness.

Looking to the future, it would be most worthwhile to try and develop LRF analyses directly relatable to blade service lives. This is a formidable problem. Its solution would, however, much extend current design philosophy concerning blade use.

6. CONCLUSIONS

- Uprated first stage turbine blades from a type of large turbofan failed after repair by a combination of low and high cycle fatigue.
- Failure was attributed mainly to the consequences of stripping the external protective coating and/or dump hole brazing during repair, for the following reasons:
  - Chemical stripping and dump hole brazing adversely affected blade cooling.
  - Dry grit blast stripping reduced blade wall thicknesses.
- Investigations by the NLR and engine manufacturer resulted in identification of four critical parameters that directly affect the blade airfoil temperatures, leading edge creep rates and hence fatigue life:
  - Leading edge airflow.
  - Backflow margin.
  - Serpentine airflow.
  - Leading edge convex wall thickness.
- These four critical parameters were each assigned a life reduction factor (LRF). For each blade the product of these LRFs gives the total LRF, which indicates the susceptibility to failure. A maximum total LRF for satisfactory service use was derived.
- The classification and acceptance of blades according to LRF values is effectively a life-on-condition damage tolerance approach to blade use. Its development represents a significant advance for blade design and lifing philosophy.

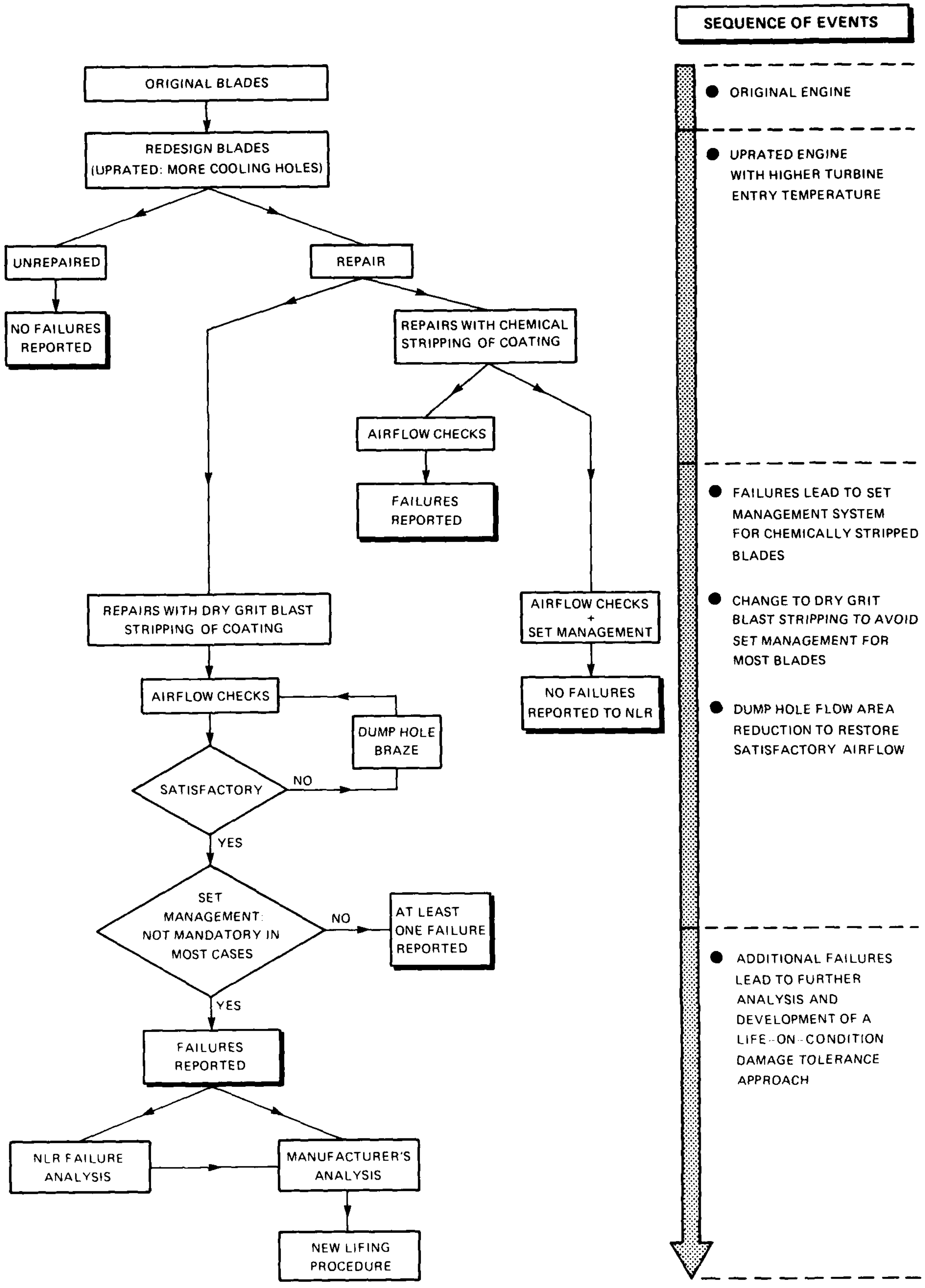
ORIGINAL BLADES
REDESIGN BLADES (UPRATED: MORE COOLING HOLES)
UNREPAIRED
REPAIR
NO FAILURES REPORTED
REPAIRS WITH CHEMICAL STRIPPING OF COATING
AIRFLOW CHECKS
FAILURES REPORTED
REPAIRS WITH DRY GRIT BLAST STRIPPING OF COATING
AIRFLOW CHECKS + SET MANAGEMENT
NO FAILURES REPORTED TO NLR
AIRFLOW CHECKS
DUMP HOLE BRAZE
SATISFACTORY
NO
YES
SET MANAGEMENT NOT MANDATORY IN MOST CASES
NO
AT LEAST ONE FAILURE REPORTED
YES
FAILURES REPORTED
NLR FAILURE ANALYSIS
MANUFACTURER'S ANALYSIS
NEW LIFING PROCEDURE
SEQUENCE OF EVENTS
ORIGINAL ENGINE
UPRATED ENGINE WITH HIGHER TURBINE ENTRY TEMPERATURE
FAILURES LEAD TO SET MANAGEMENT SYSTEM FOR CHEMICALLY STRIPPED BLADES
CHANGE TO DRY GRIT BLAST STRIPPING TO AVOID SET MANAGEMENT FOR MOST BLADES
DUMP HOLE FLOW AREA REDUCTION TO RESTORE SATISFACTORY AIRFLOW
ADDITIONAL FAILURES LEAD TO FURTHER ANALYSIS AND DEVELOPMENT OF A LIFE-ON-CONDITION DAMAGE TOLERANCE APPROACH

Fig. 1 Events leading to a damage tolerance approach for uprated first stage turbine blades from a type of large turbofan

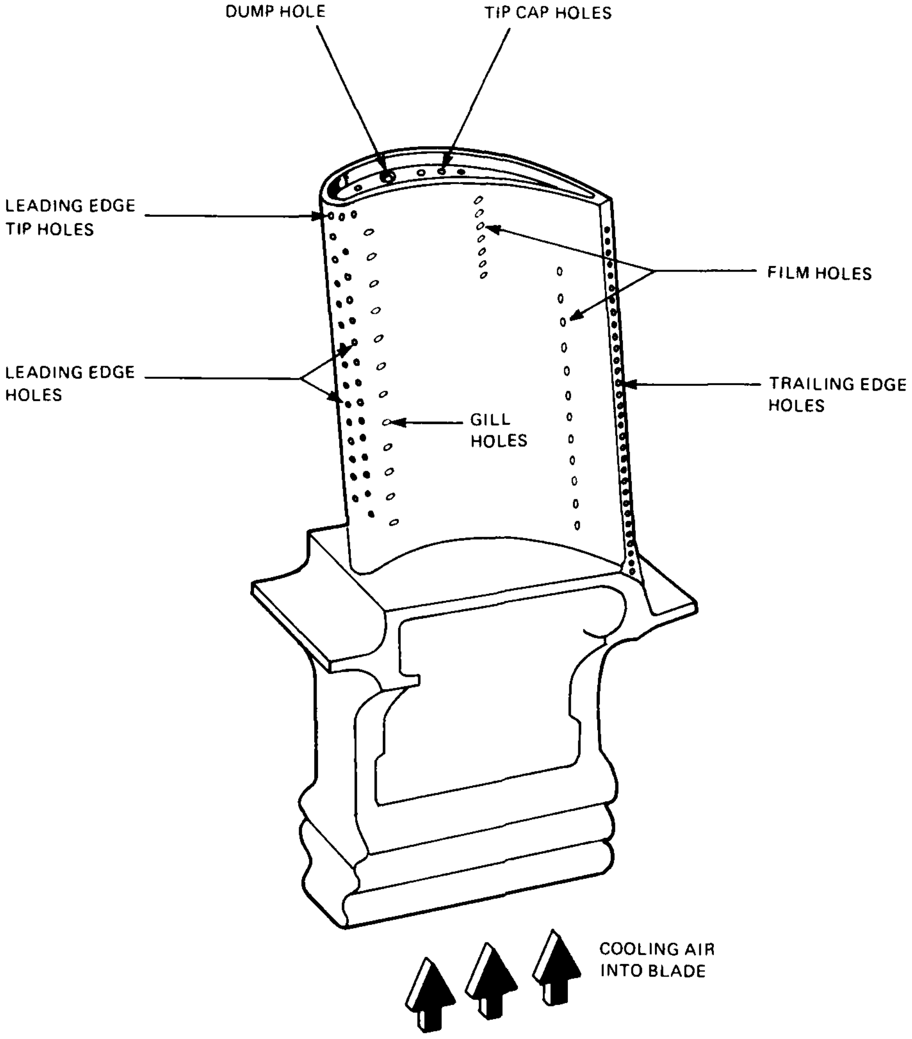
DUMP HOLE
TIP CAP HOLES
LEADING EDGE TIP HOLES
FILM HOLES
LEADING EDGE HOLES
GILL HOLES
TRAILING EDGE HOLES
COOLING AIR INTO BLADE

Fig. 2 Uprated first stage turbine blade external configuration

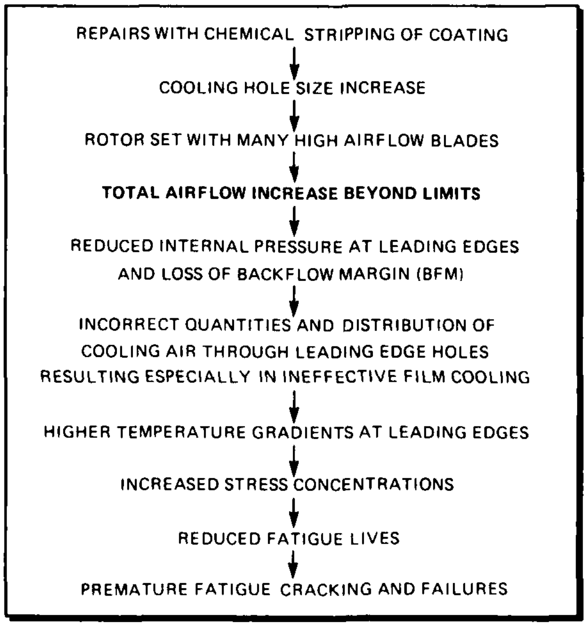
REPAIRS WITH CHEMICAL STRIPPING OF COATING
COOLING HOLE SIZE INCREASE
ROTOR SET WITH MANY HIGH AIRFLOW BLADES
TOTAL AIRFLOW INCREASE BEYOND LIMITS
REDUCED INTERNAL PRESSURE AT LEADING EDGES AND LOSS OF BACKFLOW MARGIN (BFM)
INCORRECT QUANTITIES AND DISTRIBUTION OF COOLING AIR THROUGH LEADING EDGE HOLES RESULTING ESPECIALLY IN INEFFECTIVE FILM COOLING
HIGHER TEMPERATURE GRADIENTS AT LEADING EDGES
INCREASED STRESS CONCENTRATIONS
REDUCED FATIGUE LIVES
PREMATURE FATIGUE CRACKING AND FAILURES

Fig. 3 Relation of chemical stripping during repair to subsequent cracking and failure of uprated first stage turbine blades

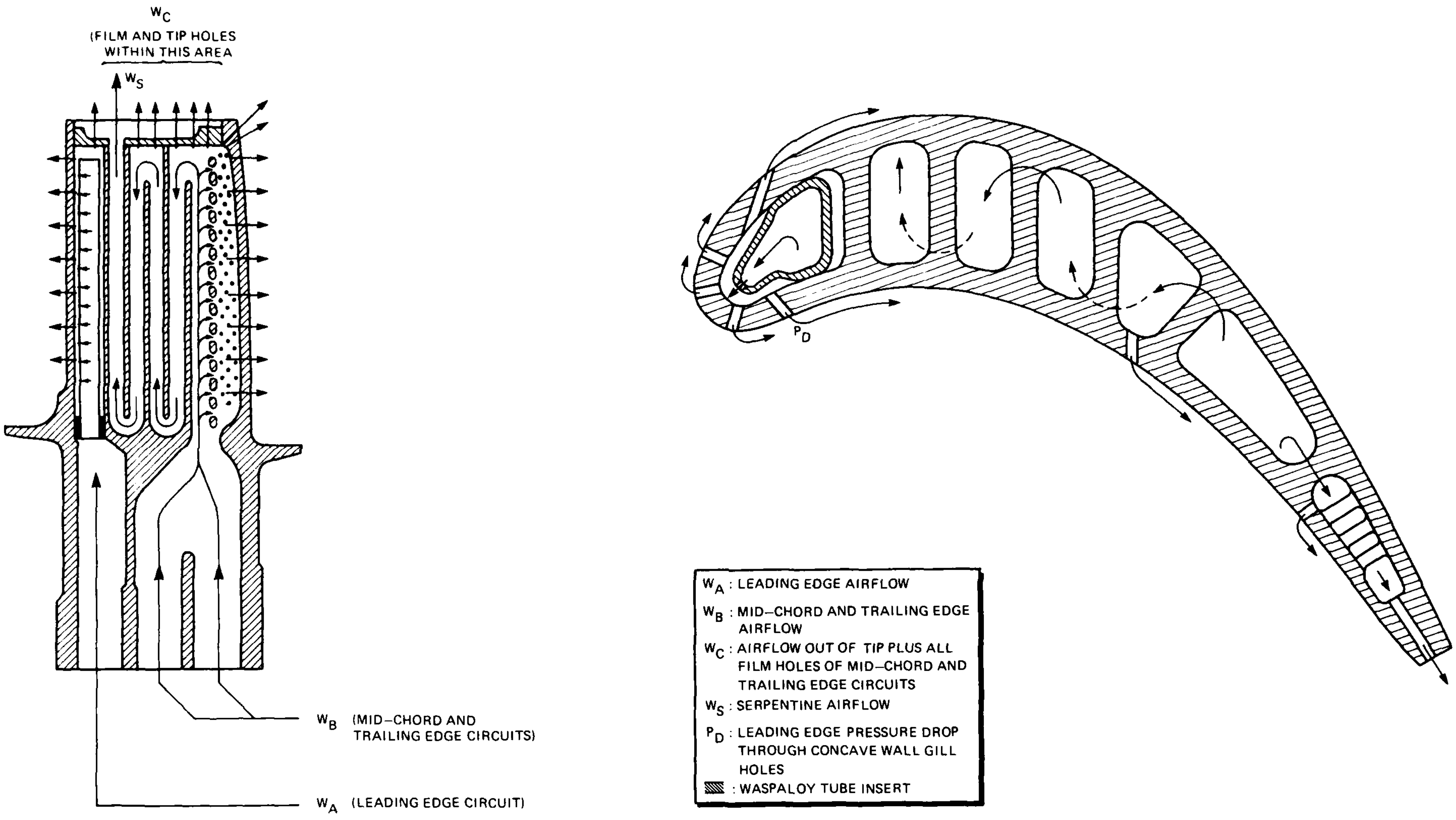
W_C
(FILM AND TIP HOLES
WITHIN THIS AREA
W_S
W_B (MID–CHORD AND TRAILING EDGE CIRCUITS)
W_A (LEADING EDGE CIRCUIT)
P_D
W_A : LEADING EDGE AIRFLOW
W_B : MID–CHORD AND TRAILING EDGE AIRFLOW
W_C : AIRFLOW OUT OF TIP PLUS ALL FILM HOLES OF MID–CHORD AND TRAILING EDGE CIRCUITS
W_S : SERPENTINE AIRFLOW
P_D : LEADING EDGE PRESSURE DROP THROUGH CONCAVE WALL GILL HOLES
▨ : WASPALOY TUBE INSERT

Fig. 4 Uprated first stage turbine blade cooling airflow circuits

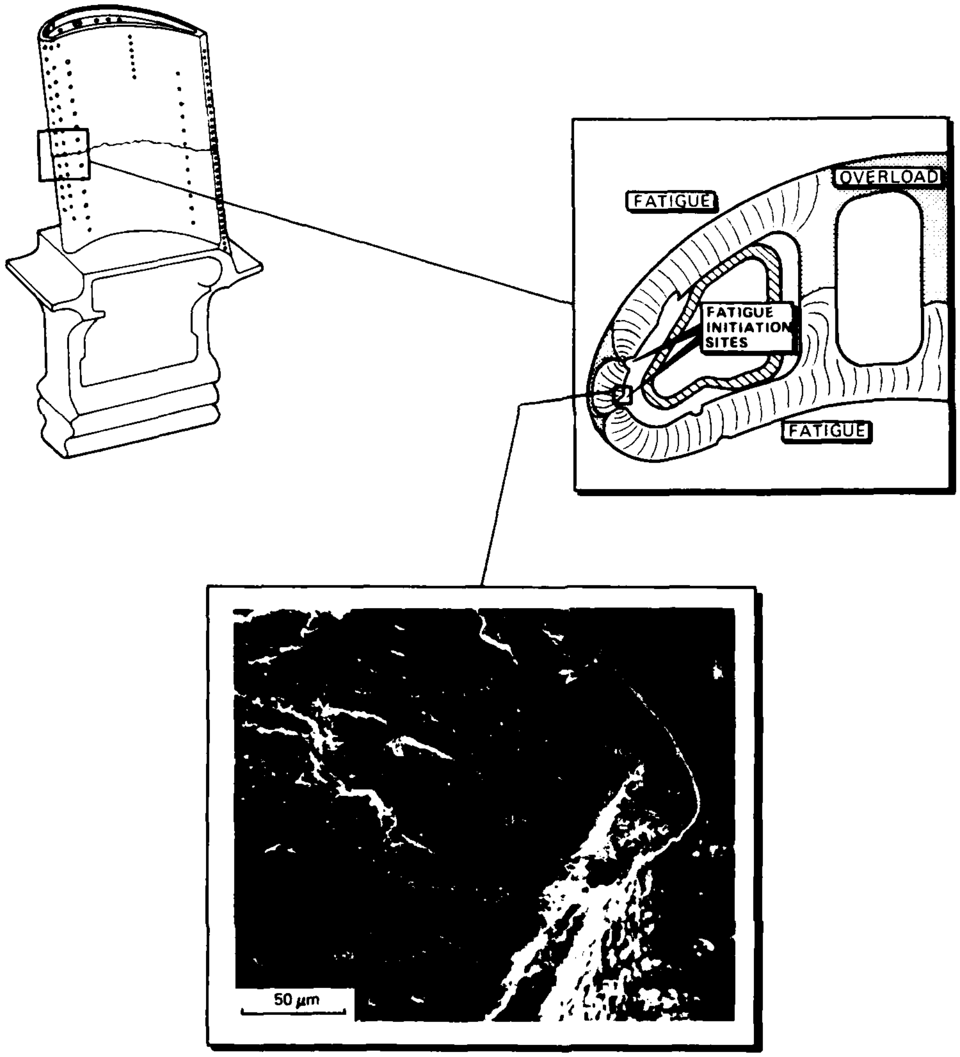
FATIGUE
OVERLOAD
FATIGUE INITIATION SITES
FATIGUE
50 μm

Fig. 5 Summary of fractographic results for failed and cracked blades supplied to the NLR

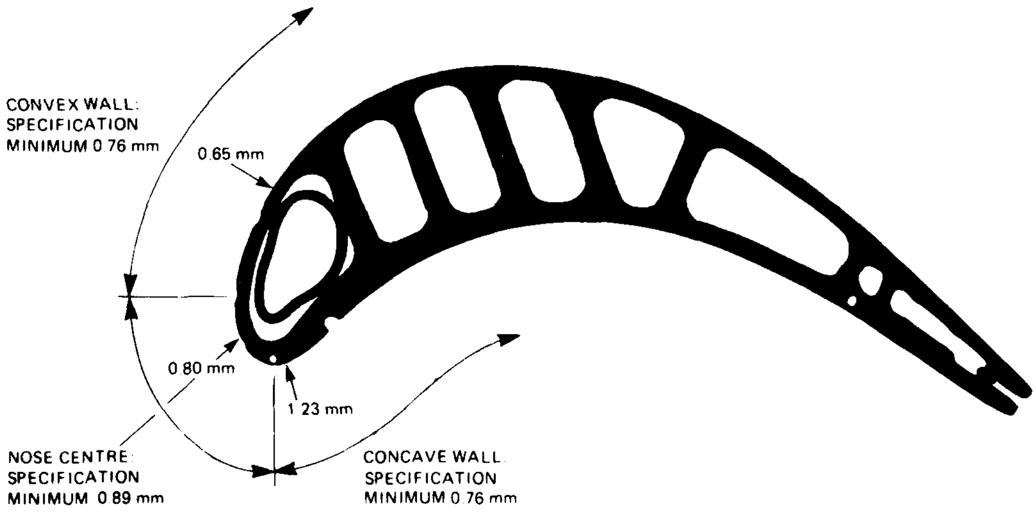
CONVEX WALL:
SPECIFICATION
MINIMUM 0.76 mm
0.65 mm
0.80 mm
1.23 mm
NOSE CENTRE:
SPECIFICATION
MINIMUM 0.89 mm
CONCAVE WALL:
SPECIFICATION
MINIMUM 0.76 mm

Fig. 6 Cross-section of the failed blade investigated by the NLR: height above platform 17.5 mm. Specification minima refer to 27.5 mm above platform for uncoated blades

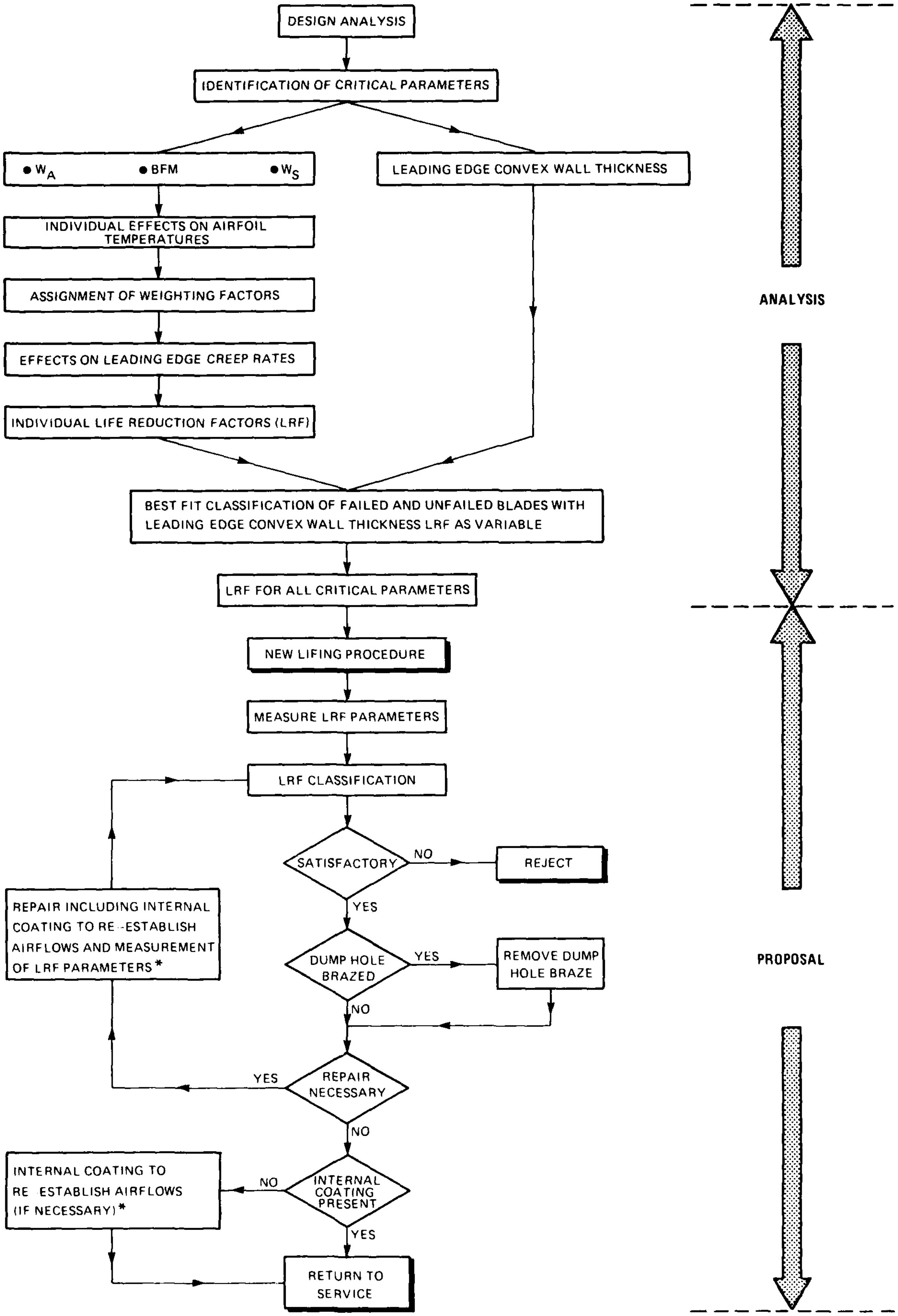
DESIGN ANALYSIS
IDENTIFICATION OF CRITICAL PARAMETERS
● W_A
● BFM
● W_S
LEADING EDGE CONVEX WALL THICKNESS
INDIVIDUAL EFFECTS ON AIRFOIL TEMPERATURES
ASSIGNMENT OF WEIGHTING FACTORS
EFFECTS ON LEADING EDGE CREEP RATES
INDIVIDUAL LIFE REDUCTION FACTORS (LRF)
BEST FIT CLASSIFICATION OF FAILED AND UNFAILED BLADES WITH LEADING EDGE CONVEX WALL THICKNESS LRF AS VARIABLE
LRF FOR ALL CRITICAL PARAMETERS
NEW LIFING PROCEDURE
MEASURE LRF PARAMETERS
LRF CLASSIFICATION
SATISFACTORY
NO
REJECT
YES
DUMP HOLE BRAZED
YES
REMOVE DUMP HOLE BRAZE
NO
REPAIR INCLUDING INTERNAL COATING TO RE-ESTABLISH AIRFLOWS AND MEASUREMENT OF LRF PARAMETERS*
YES
REPAIR NECESSARY
NO
INTERNAL COATING TO RE ESTABLISH AIRFLOWS (IF NECESSARY)*
NO
INTERNAL COATING PRESENT
YES
RETURN TO SERVICE
ANALYSIS
PROPOSAL

Fig. 7 Schematic of the investigation by the engine manufacturer.
* Note that internal coating was never incorporated

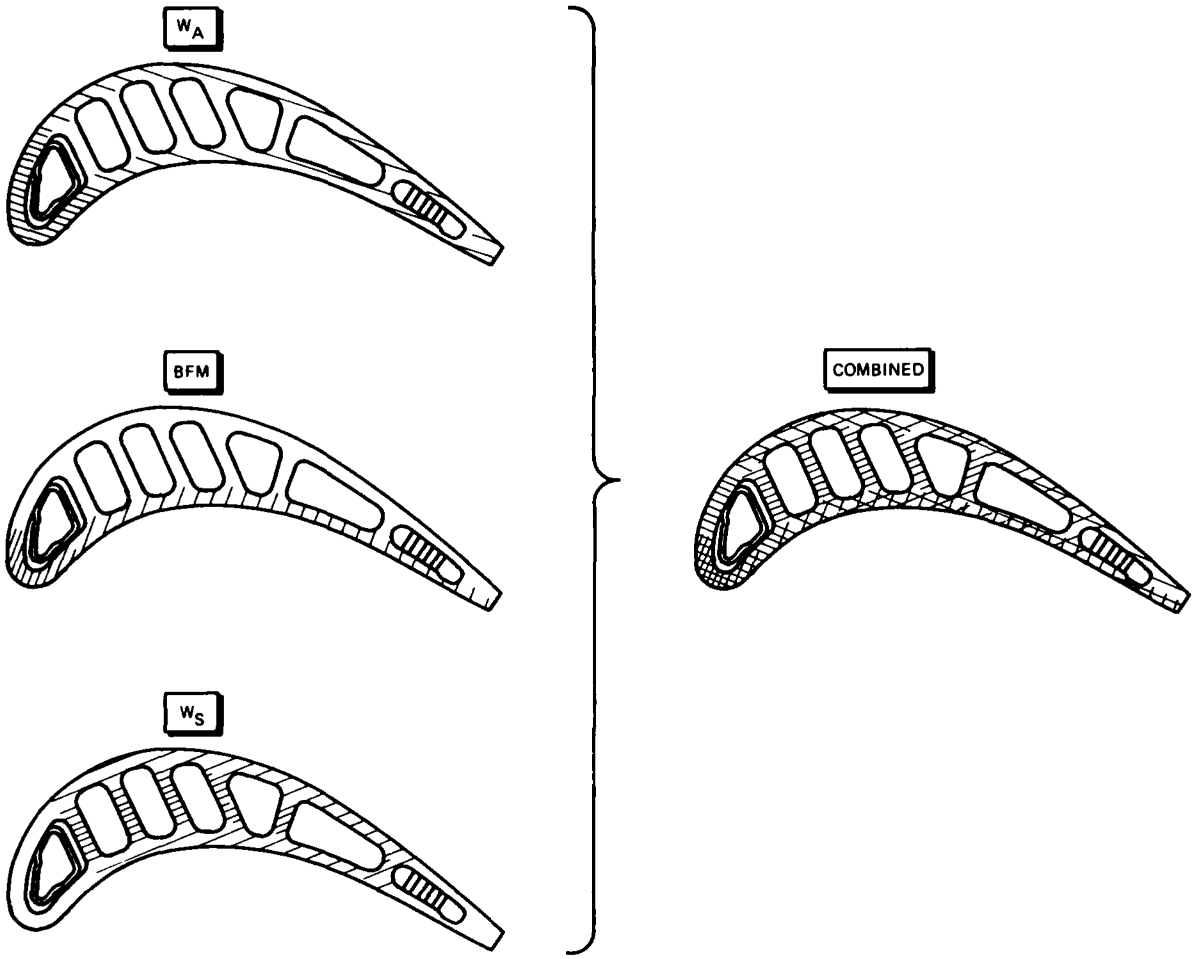

Fig. 8 Effects of leading edge airflow W_A, backflow margin BFM and serpentine airflow W_S on airfoil temperature

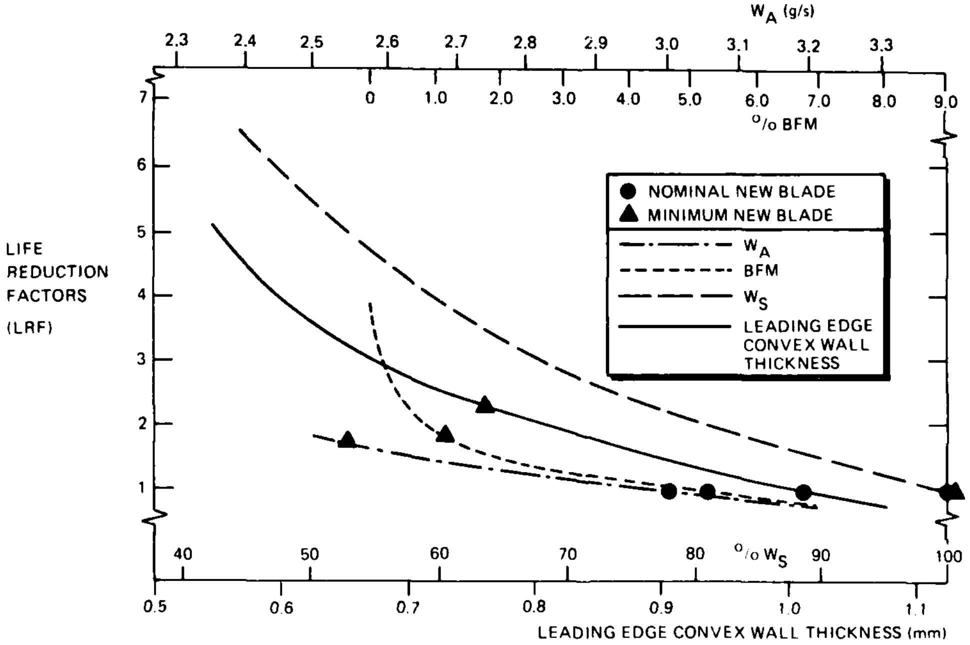

Fig. 9 Life reduction factors for leading edge airflow W_A, backflow margin BFM, serpentine airflow W_S and leading edge convex wall thickness

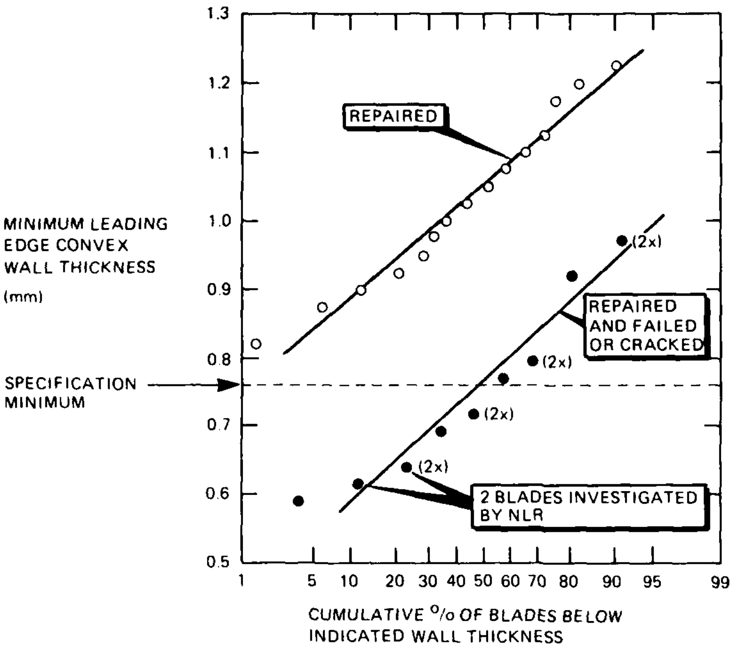

Fig. 10 Probability plots of leading edge convex wall thickness for repaired blades that were nominally undamaged or failed or cracked. Most data were supplied by the engine manufacturer

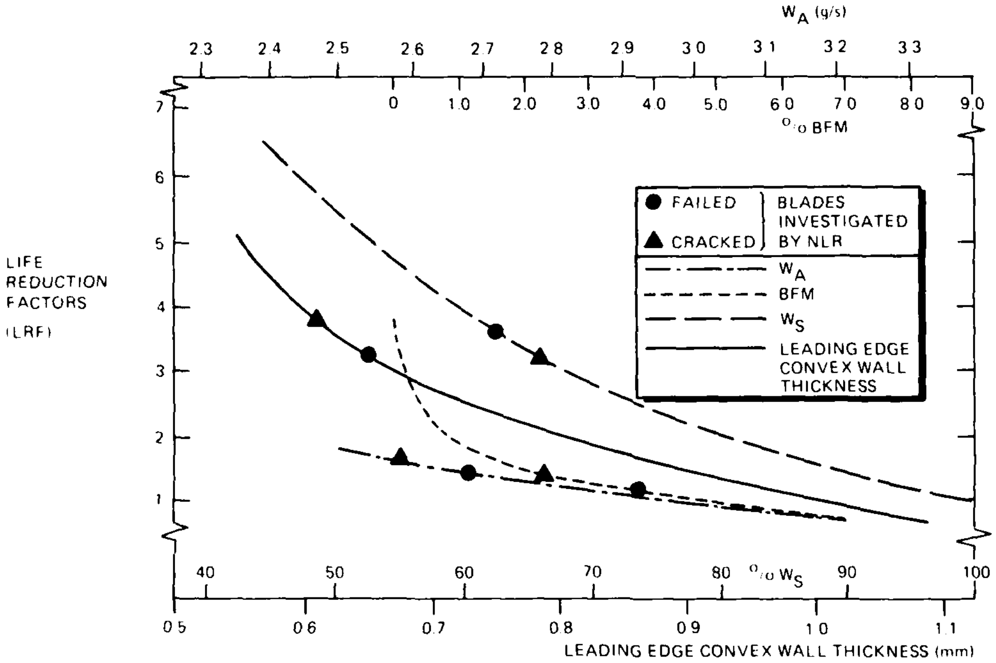

Fig. 11 Life reduction factors for leading edge airflow W_A, backflow margin BFM, serpentine airflow W_S and leading edge convex wall thickness of the failed and cracked blades investigated by the NLR

PRACTICAL EXPERIENCE WITH DAMAGE TOLERANCE BASED LIFE EXTENSION C TURBINE ENGINE COMPONENTS

by

A.K. Koul*, R. Thamburaj**, M.D. Raizenne*, W. Wallace*, M.C. DeMalherbe**

SUMMARY

This paper describes a detailed experimental and statistical analysis carried out to determine the risks and benefits of implementing a damage tolerance based lifing procedure for the General Electric J85-CAN40 engine. This is a "post-facto" investigation, using components of this engine retired by the Canadian Forces and the data available regarding these used parts. The emphasis in this paper is on the 5th stage compressor disc, which is one of the most crack prone components of this engine.

A number of procedures have been demonstrated by which the "safe life" and the "safe inspection interval" for this component can be calculated reliably. The possibility of improving the existing lifing procedure through a damage tolerance approach, and the limitations of the damage tolerance approach are discussed on the basis of experimental observations and information available from field experience.

1.0 INTRODUCTION

J85-CAN40 turbines were first purchased by Canadian Forces (CF) in the 1960's. At the time of purchase no low cycle fatigue (LCF) safe life limits were specified by the engine manufacturer for different rotating components, such as compressor discs and spacers and turbine discs. These safe life limits were eventually made available by the manufacturer in 1970, Table 1. These safe life limits are believed to have been determined on the basis of flying experience with the United States Air Force (USAF) J85-5 model engines(1). The USAF J85-5 and CF J85-CAN40 engines are used in T-38 and CF-114 trainer aircraft respectively. The assumption appears to have been made that the flight mission and therefore the safe lives of J85-5 and J85-CAN40 engines were comparable.

Between 1970 and 1981, the safe life limits of both J85-5 and J85-CAN40 compressor components were revised several times, based on the manufacturer's analysis of USAF and CF mission profiles(1). In 1981, premature LCF cracking was encountered in the 5th-7th stage compressor discs, and the spacers attached on either side of these discs, in the J85-CAN40 engines. It was realized that the CF usage was more severe than previously assumed, and the mission severity factor was increased to 1.8, relative to J85-5 usage. As a consequence, safe life limits for J85-CAN40 compressor parts were reduced even further as indicated in Table 1. The significantly reduced safe life limits created logistic problems since adequate quantities of replacement parts were not readily available, and in order to allow time for the purchase, delivery and installation of new parts a damage tolerance based maintenance methodology was developed to allow crack prone parts to be phased out systematically as required. The specific details can be found elsewhere(1,2).

It is the purpose of this paper to critically assess the merits and demerits of various analytical techniques proposed for implementing damage tolerance concepts in aero engines in general, and specifically those used in the case of J85-CAN40 engines. The usefulness of some of these procedures will be assessed by using "real life" data on the 5th stage compressor disc of the J85-CAN40 engine. In addition, factors influencing initiation and propagation of cracks, and the sensitivity and reliability of NDI procedures will also be critically examined. Finally, a damage tolerance approach that systematically utilizes the field experience to continuously update the safe inspection interval will also be outlined.

2.0 DAMAGE TOLERANCE CONCEPTS PROPOSED FOR LIFE EXTENSION

It is generally agreed that much of the useful life of most rotating components is not utilized through a safe design life approach, since only 1 in 1000 components will have developed a detectable crack at retirement(3-6). Marked reductions in the overall life cycle management costs would accrue by allowing the damage to develop in each component and retiring them on an individual basis. Damage tolerance concepts have thus emerged where it is proposed to utilize the remaining safe life of each component. It is assumed that flaws exist in parts as manufactured and these may be located in the most highly stressed regions or hot-spots of the component. It is further assumed that these flaws will grow in service, at a rate governed by the local stress distribution around the flaw, the operating temperature and the environment(3,4). The general objective of the damage tolerance approach is to establish expected crack growth rates under realistic operating conditions and to implement NDI procedures with an appropriate level of sensitivity, reliability, and frequency to ensure that cracks can be detected and if feasible monitored in service to a point where the *risk* of rapid or unstable crack propagation becomes severe(5,6).

A number of analytical procedures have been proposed for implementing damage tolerance concepts in rotating aero-engine components(7-16). These include, deterministic fracture mechanics (DFM), probabilistic fracture mechanics (PFM), combined analysis (CA) and traditional aircraft structural integrity programme (ASIP) approaches.

2.1 DFM Approach

The deterministic fracture mechanics (DFM) approach assumes that an initial flaw size a_i already exists in the critical location of a component, where a_i is defined as the maximum crack size that might be undetected by NDI equipment or that an NDI operator might miss. Stress analysis is used to calculate the maximum cyclic stress ($\Delta\sigma$) or steady stress (σ) in the critical component locations under realistic loading conditions. Fracture mechanics analysis is carried out to plot crack size (a) versus the number of LCF cycles (N) or the flight time (t) curves, Figure 1. In the case of LCF, the cyclic stress intensity factor (ΔK) is given by,

---

* Structures and Materials Laboratory, NAE NRC, Ottawa, Ontario, Canada K1A 0R6
** Carleton University, Ottawa, Ontario, Canada, K1S 5B6

$$\Delta K \propto \Delta\sigma\sqrt{\pi a} \tag{1}$$

Unstable crack growth is expected to occur when ΔK equals a critical value (ΔK_f). If $\Delta\sigma_f$ represents the residual fracture strengths, then a critical crack size (a_f) is given by(9),

$$\Delta\sigma_f = \Delta K_f / \sqrt{\pi a_f \lambda}$$

$$\text{or } a_f = \left(\frac{1}{\pi\lambda}\right)\left(\frac{\Delta K_f}{\Delta\sigma_f}\right)^2 \tag{2}$$

where λ is a factor that depends on the crack shape, structure and the gradient of stresses. In the regime of stable LCF crack growth, the residual number of cycles to failure (N) of a component containing a crack size a_i can be obtained by integrating the crack growth equation. The crack growth rate function is generally represented by an equation of the form,

$$\frac{da}{dN} = f(\Delta K) \tag{3}$$

$$\text{or } \frac{da}{dN} = C(\Delta K)^n \tag{4}$$

where constants C and n depend upon the loading mode, type of crack growth, material properties and environment. Upon rearranging Equation (4) and substituting for ΔK from Equation (1), the total number of cycles to failure (N_f) is given by,

$$N_f = \int_0^{N_f} dN = \int_{a_i}^{a_f} \frac{da}{C(\Delta K)^n}$$

$$= \frac{1}{C(\Delta\sigma\sqrt{\pi\lambda})^n} \int_{a_i}^{a_f} \frac{da}{a^{n/2}}$$

$$= \frac{(n/2-1)^{-1}}{C(\Delta\sigma\sqrt{\pi\lambda})^n}\left[\left(\frac{1}{a_i}\right)^{n/2-1} - \left(\frac{1}{a_f}\right)^{n/2-1}\right] \tag{5}$$

In practice, components such as compressor discs would be retired when a initial crack length (a_c) which can cause excessive vibration and/or unstable crack growth is likely to be present. This critical length (a_c) is usually called the "dysfunction limit" and should be distinguished from the crack length at failure, a_f, mentioned in the above equations. The life to dysfunction is referred to as N_d, later on in this paper.

Equations (1) to (5) can thus be used to determine the future worst performance of a rotating component if cracks can reliably be monitored during overhaul and inspection, Figure 1. To determine a safe inspection interval (SII) an appropriate safety factor based upon qualitative engineering judgement is superimposed on Figure 1. A safety factor of ~2 is generally used to establish damage tolerance allowables. The DFM approach is considered to be overly conservative since worst case assumptions impose unrealistic constraints on the overall maintenance methodology and many satisfactory components might be rejected unnecessarily(11-13).

2.2 ASIP Approach

A variety of methods for implementing damage tolerance concepts in airframe structures have also been proposed in the literature(14-16). However, the USAF damage tolerant design handbook specifies an ASIP approach which is very similar to that of the DFM approach, but in addition, specific guidelines regarding maximum undetectable flaw size are also laid down for various components(14). It is suggested that the maximum undetectable flaw size can only be specified in a meaningful manner if the probability of detecting (POD) that flaw and the confidence level associated with the probability are also specified. MIL-A-83444 requires that POD and confidence levels be 90% and 95% respectively for the slow crack growth category and 90% and 50% respectively for the fail safe category(17). A flaw size that satisfies these POD and confidence requirements is thus selected at the design stage of the component in order to specify an appropriate SII. However, Simpson(18) has argued that these POD and confidence requirements can also be satisfied by selecting a succession of SII provided the cumulative POD is 90/95. In this manner smaller a_i values can be chosen for DFM predictions and in addition, better reliability can be achieved with less sensitive (production type) NDI techniques.

ASIP specifies a 1.27 mm corner flaw at one side of the bolt hole as an assumption for a_i(14, 17). This flaw size is based on typical defects found in airframe structures and its applicability to aero engine components is questionable(19). In a USAF sponsored damage tolerance case study on a TF33 3rd stage turbine disc, the authors state that the assumption of initial flaw sizes 0.76 to 1.27 mm in surface length would provide adequate residual life for the safe application of damage tolerance concepts to many older disc designs(20). However, this methodology may not prove successful with advanced aero engine turbine discs that operate at very high temperatures and stresses and where maximum allowable crack length (a_c) might be of the order of 0.8 to 1 mm. In such an event it might be more appropriate to use a PFM approach rather than DFM and ASIP approaches.

2.3 PFM Approach

The probalistic fracture mechanics (PFM) damage tolerance approach is similar to the DFM approach in many respects, but instead of a specified a_i, the probability of occurrence of various flaw sizes ($P(a_i)$) is specified(7, 8,11). Similarly, instead of a maximum cyclic or steady stress, a probability distribution of various cyclic ($P(\Delta\sigma)$) and steady ($P(\sigma)$) stresses is used. Instead of assuming a specific crack propagation curve, Figure 1, the PFM calculation deduces a failure probability (P_f), ie. reliability, as a function of time. Also, rather than using a safety factor based on good engineering judgement, appropriate inspection intervals are selected to maintain a sufficiently low but cost effective failure probability(22,23).

The method uses a deterministic equation to compute residual LCF life of a cracked component from known values of input parameters such as $\Delta\sigma$, ΔK, a_i and a_c. These input parameters are treated as random variables with known or specified distributions. For simplicity, the observed scatter in crack growth rate in Equation (4) can be simulated by random variation in C rather than by some complex joint dependent variation of C and n, where C is assumed to show a log-normal distribution(7).

or

$$\log C = \mathrm{Gau}\,(\mu_c, S_c) \tag{6}$$

where μ_c *depicts the median and mean and* S_c is the standard deviation. Similarly, a normal stress variation can be represented by:

$$\Delta\sigma = \mathrm{Gau}\,(\mu_{\Delta\sigma}, S_{\Delta\sigma}) \tag{7}$$

Finally, the initial flaw size (a_i) and the critical flaw size (a_c) distributions are assumed to be log-normal,

or

$$\log a = \mathrm{Gau}\,(\mu_a, S_a) \tag{8}$$

where μ_a represents the mean and S_a is the standard deviation. The number of LCF cycles (N_{pr}) required to propagate a_i to a_c can be represented by,

$$N_{pr} = f\,(C, \Delta\sigma, a_i, a_c) \tag{9}$$

To obtain an analytical solution for the distribution of LCF propagation life, the theorem in (21) is generally utilized to combine equations (6-9) with a deterministic equation, e.g. Equation (5), to obtain a life distribution of the form,

$$\log N_{pr} = \mathrm{Gau}\,(\mu_N, S_N) \tag{10}$$

where,

$$\mu_N = \log B + p\,\mu_c + q\,\mu_{\Delta\sigma} + r\,\mu_{a_i} + s\,\mu_{a_c} \tag{11}$$

and

$$S_N = \left(p^2 S_c^2 + q^2 S_{\Delta\sigma}^2 + r^2 \mu_{a_i}^2 + s^2 \mu_{a_c}^2\right) \tag{12}$$

the number of cycles at a given failure probability α is given by

$$N_{pr} = 10^{(\mu_N + K_\alpha S_N)} \tag{13}$$

where K_α is the standard normal deviate (ie. the number of standard *deviations from* μ_N*) corresponding to a particular* value of α from the standard normal distribution function(7).

Jouris(22) has summarized various strengths and weaknesses of PFM versus DFM. One of the major criticisms against PFM is that the forms of various probability distributions, Equations 6 to 13, are not known exactly. However, an engineer generally has a reasonable idea about the approximate distribution from available engineering information and physical considerations. In addition, successful implementation of the PFM approach requires extensive measurements to obtain a statistically significant data base for developing appropriate distributions for Equations (6-8)(11, 22). Large deficiences in any one of those input parameters will require the use of conservative upper bounds, and thereby reduce the payoffs of PFM with respect to DFM.

2.4 CA Approach

The combined analysis (CA) approach is said to be the logical outgrowth of PFM and provides an optimum method for combining laboratory and field data with various analytical techniques to calculate life extension both safely and cost-effectively(9-13, 24). CA is less sensitive to design analysis errors since inspection information is used to continuously calibrate the original assumptions used in selecting an appropriate SII.

In one CA approach, fracture mechanics analysis and or laboratory test data are used to define a family of possible relationships between crack size 'a' and the number of LCF cycles 'N', Figure 2(24). The 'a' versus 'N' *curves in Figure 2 are bounded by* "A" and "B" which represent a broad range that can be defined analytically for all discs. The inspection results of each individual rotor tells the analyst (within some error band as shown in Fig. 2) which 'a' versus 'N' curve describes the absolute severity of the crack and the LCF performance of the disc. This 'a' versus 'N' curve in conjunction with a safety factor (SF), which compensates for any errors, is used to predict future disc performance. Thus, engineering analysis is used only to characterize the general nature of disc degradation in terms of the general shape of the 'a' versus 'N' curve. Field data is used to calibrate the analysis and to locate the single, correct 'a' versus 'N' curve for each disc with sufficient accuracy to permit life extension.

Life simulation is carried out by assuming that the total LCF life to dysfunction, N_d of a disc with a life limited by the rim serration or bolt hole or disc hub can be expressed by,

$$N_d = N_i + N_p \tag{14}$$

where 'N_d' is the life to dysfunction of the shortest-lived of all critical locations within a disc, 'N_i' is the life to initiation of a crack of some small defined depth 'a_i' and N_p is the life to propagate 'a_i' to a critical size 'a_c'. An analytical model is chosen to substitute for 'N_i' and 'N_p' to give an equation of the form,

$$N_d = \frac{C_i}{\Delta\sigma^{n_1}} + C_p \log(a_c/a_i)/\Delta\sigma^{n_2} \tag{15}$$

where C_i and C_p are treated as random variables which simulate the variation of crack initiation and crack growth at a given $\Delta\sigma$. Random variation in C_i and C_p is caused by localized microstructural and surface finish variations in the "hot spots" of a given set of discs. C_i and C_p are assumed to have log-normal distributions of the form,

$$\log C_i = \mathrm{Gau}\,(\mu_{c_i}, S_{c_i}) \tag{16}$$

and

$$\log C_p = \mathrm{Gau}\,(\mu_{c_p}, S_{c_p}) \tag{17}$$

The probability distribution assumed for '$\Delta\sigma$' is the same as in Equation (7) and the critical stress intensity factor 'ΔK_c' is also assumed to have a normal distribution, where

$$\Delta K_c = \mathrm{Gau}\,(\mu_{\Delta K_c}, S_{\Delta K_c}) \tag{18}$$

and a_c can be computed through an equation similar to that of Equation (2). Analytical solutions similar to those utilized in computing Equation (10) are then used to simulate 'N_i' and 'N_p' probability distributions. Equation (15) can also be used to relate an assumed crack depth 'a' to total number of LCF cycles where $a_i < a < a_c$. The overall results can be recast in the form of cumulative probability plots of the type shown in Figure 3. These plots can further be used to assign design lives, crack propagation intervals (CPI) and a SII for an assumed cumulative probability of failure. For example, the LCF design life is traditionally set at the 0.1% F* for a crack size 'a' in turbine discs, Figure 3. Upon using a given set of discs for a specified design life period, these discs are inspected and uncracked discs can be put back into service for a calculated SII from Figure 3, where

$$\mathrm{SII} = \frac{N_d - N_i}{\mathrm{SF}} \tag{19}$$

and N_d and N_i are selected for a cost-effective % F* and a SF is used by the analyst to compensate for the fact that N_d and N_i in Equation (19) are both estimates.

In the case of a cracked disc, the largest value of the apparent crack depth 'a′' measured in any critical location is recorded. Equation (15) is recast in the form,

$$N_t = C_i/\Delta\sigma^{n_1} + C_p \log(a'/a_i)/\Delta\sigma^{n_2} \tag{20}$$

where N_t is the life at inspection. Upon substituting for 'a′', Equation (20) is solved for $\Delta\sigma$. Substituting for $\Delta\sigma$ in Equation (15), an N_d value is predicted. Life extension can now be calculated through Equation (19). Errors caused by inspection uncertainity can also be treated in a probabilistic manner(9-13, 23, 24). These errors can further be quantified and incorporated in selecting an appropriate SII for a specific component. The entire analysis is usually performed with a computer program which employs Monte-Carlo simulation.

Whether a damage tolerance system is based upon DFM, ASIP, PFM or CA approaches, the selection of an appropriate life extension strategy for a specific application will be governed by relative cost and reliability associated with various options.

---

* Cumulative Probability of Failure

3.0 PRACTICAL EXPERIENCE WITH LIFE EXTENSION IN J85-CAN40 COMPONENTS

In 1981, the safe life limits of CF J85-CAN40 engines were determined by the manufacturer in a probabilistic manner, based on their experience with the USAF J85-5 model for which there was a broad data base available(1,2). The manufacturer appears to have assumed that the experimental or the field lifing data on time to crack initiation (N_i) and the time to form a critical crack size (N_d) in J85-5 components could be described by a simple Weibull model of the form,

$$F(t) = 1 - \exp\left[-(t/\eta)^{\beta}\right] \tag{21}$$

In practice β and η are the parameters to be determined from the experimental or the field data base. In the case of the J85-5 fifth stage compressor discs, β values of ~ 5 and ~ 9 were calculated from the N_i (0.8 mm crack length) and N_d (4.5 mm crack length) plots of Figure 4. The predicted J85-CAN40 N_i and N_d distributions were simply derived by dividing J85-5 N_i and N_d data bases by a mission severity factor (MSF) of 1.8, Figure 4. The J85-CAN40 Safe Inspection Interval was also determined by dividing the J85-5 interval (1000 hours for J85-5 fifth stage compressor disc) by a MSF of 1.8 (555 hours for J85-CAN40 fifth stage compressor disc). A limited amount of fracture mechanics and spin pit testing was carried out on a few selected service exposed components in order to verify predictions regarding SII for J85-CAN40 engines(1,2). The details of these data were not made available to the present investigators. It was also recommended to CF that *parts which are known to have been crack free at prior inspection may be operated for a maximum of one SII beyond that inspection with minimum additional risk.* At overhaul, CF subjected the service exposed discs to fluorescent penetrant inspection (FPI) and the crack-free components were returned to service. However, since prior to November 1981 CF were working to a safe life limit of 4680 h, fifth stage compressor discs already existed in service with lives more than 2.5 times the revised limit of 1777 h. As a result, discs had remained in service for times well in excess of the newly established safe inspection interval of 555 h and indeed the excess life was as much as five times the Safe Inspection Interval, as indicated in Table 2. This aspect of the problem will be discussed later.

By 1983, CF had accumulated a large amount of field data for cracked J85-CAN40 components. For example, 49 fifth stage compressor discs out of 201 had developed bolt hole cracks that were 4.5 mm or greater in length. CF analyzed these data in accordance with the model given by Equation (21) and the method outlined in Reference (1), and annotated the observed dysfunction data onto the predicted N_i and N_d lines, Figure 5. It was noted that the observed dysfunction life was longer than the predicted dysfunction life. These observations indicated that relative to the 1981 J85-5 mission, the J85-CAN40 mission was not as severe as originally predicted. At this point there was more confidence in the statistical significance of the 1983 N_d line and therefore the MSF was reduced from 1.8 to 1.4, Table 1 and Figure 5. Consequently, this revision of MSF led to an increase in N_i and N_d values for various rotating components. In essence, a CA life extension approach had been used since inspection analysis was used to recalibrate the original model given by Equation (21). At present, however, this damage tolerance based lifing procedure is not being applied by the engine user and components are being retired upon expiry of the safe life limit.

The following sub-section will focus on the available methodologies for determing N_i, N_d, and SII with special reference to J85-CAN40 engines. Attemps will also be made to incorporate the field experience to update the original predictions.

3.1 Crack Initiation Data Base (N_i)

A statistically significant date base on the number of high strain LCF cycles required to propagate a pre-existing flaw to a detectable size (0.8 mm) can be generated using smooth test specimens, assuming that the specimen simulates the local material behaviour at a geometric discontinuity in a disc. Providing the actual sequence of flight load cycles per hour of the flight is known, the number of service hours required to form a 0.8 mm crack can then be computed. The final step involves verification of the data base through spin-pit testing, since stress-strain distributions more typical of flight conditions can be generated in a spin-pit. The data can then be presented in the form of Weibull plots to select the 0.1% probability of failure N_i level, Figure 6. It should be noted that the N_i line presented in Figure 6 was computed by dividing the manufacturer's J85-5 predicted values by the 1983 revised MSF of 1.4.

In order to verify the J85-CAN40 predicted N_i line of 1983, ten 5th stage compressor discs that contained a maximum crack size of 6.4 mm were selected for quantitative fractographic studies. The bolt holes containing 6.4 mm long cracks were cut out and the crack faces were pried open for SEM examination, Figures 7(a) and 7(b). Fatigue striation spacings were measured along the entire crack length to determine crack growth rates at various points along the crack. Fatigue striations from 0.8-1 mm crack length onwards had a uniform spacing of ~ 1 μm. Below 0.8 mm crack length, smaller fatigue striation widths of the order of ~ 0.5 μm were observed. By using scanning electron microscopy, it was possible to derive a plot of crack length versus striation spacing for a bolt hole crack, Figure 8. It was also determined that the striations tended to be banded together (Fig. 7(b)), each band perhaps representing a set of major throttle excursions during a mission. The number of striations within a band were most often about 5, while in rare occasions 10-15 were seen. Counting backwards from 6.4 mm crack length up to 0.8 mm crack size and assuming that 5, 10 or 15 striations formed during one flight hour of actual engine operation it was possible to compute three N_i values for each bolt hole(25). The computed N_i values were analyzed in accordance with Equation (21) and the results were compared with the 1983 N_i line. The assumption of 5 striations flight hour gave the best fit with the 1983 N_i line as indicated in Figure 9. In a separate investigation on typical CF mission profiles of this type of engine it was shown(26) that the average number of major throttle excursions which occur during one flight hour of the engine would be between 3 and 6. Each LCF striation from 0.8 mm crack length onwards may thus correspond to a major throttle excursion during actual flight. It is concluded that providing the mission profile of an engine is known with a reasonable degree of accuracy, field experience in conjunction with quantitative fractographic techniques can be used to calibrate the predicted N_i data base.

Alternatively, a CA approach can also be employed to determine the in-service N_i distribution(1). The inspection information in conjunction with field data on Time Since New (TSN) and Time Since Overhaul (TSO) of discs containing cracks either equal to or greater than the dysfunction length (4.5 mm for J85-CAN40 fifth stage compressor discs) can be used to compute the N_i values. It could be assumed that the dysfunction cracks started on the first cycle following reassembly of the reportedly crack-free component after inspection. It is however unlikely that this condition occurred on all discs and equally unlikely that dysfunction crack sizes formed on the very last cycle. The best possible approach in determining N_i under these conditions would be to assume that a 0.8 mm crack was already present at previous overhaul and this crack went undetected due to the FPI detection threshold. In such an event, the difference between TSN and TSO of discs cracked to dysfunction or greater can give the N_i data points. Using this approach, the crack initiation life distribution for J85-CAN40 fifth stage compressor discs was deduced, Figure 10. The Weibull plots for these data are presented in Figure 11 where the 1983 N_i line is included for comparison purposes. The TSN-TSO line falls slightly on the right hand side of the 1983 N_i line. However, it should be remembered that the TSN-TSO line in Figure 11 estimates cycles to crack detection rather than cycles to 0.8 mm crack formation.

In fact, an investigation to evaluate the reliability (Probability of Detection, POD) and resolution (sensitivity of the technique) of the industrial FPI technique used, was also carried out. Complete description of the techniques used to collect the raw data from actual disc bolt holes and the analytical procedures employed can be found elsewhere(19). The lower bound of the 95% confidence limit for the industrial FPI technique used in the case of J85-CAN40 components is presented in Figure 12. It is evident that the industrial FPI technique is only successful in detecting those cracks that are greater than 1.5 mm in length. In the range of 0.8 to 1.0 mm bolt hole cracks, the POD is extremely low. Furthermore, it was also established that the maximum crack length which escaped detection during industrial FPI was ~ 1.75 mm(19). This detection limit is significantly higher than the 0.8 mm criterion used to plot the 1983 N_i line in Figure 11. Based on this argument one would expect the "cycles to detection" line or the TSN-TSO line of discs cracked to dysfunction to lie on the right of the 1983 N_i line. Nevertheless, the TSN-TSO criterion can still be useful in providing a rough estimate of the crack initiation distribution, Figure 10.

3.2 Dysfunction Data Base (N_d)

A dysfunction data base can be directly generated by allowing cracks to grow to a critical size during a spin-pit test, providing the critical crack length is already known. The field data can then be incorporated to recalibrate the original predictions in a manner similar to that described for J85-CAN40 components, Figure 5. However, in the case of J85-CAN40 5th stage compressor discs 49 dysfunction data points were taken from those discs that contained cracks 4.5 mm or greater in length(1). In strict mathematical terms, TSN of only those discs that contained a maximum crack size of 4.5 mm should have been used to compute the recalibrated N_d line in Figure 5. In theory, crack lengths longer than the precise dysfunction crack size cannot be treated as an integral part of the dysfunction life distribution, Figure 13.

More often than not, large data bases cannot be generated cost-effectively for applying damage tolerance concepts to older engines. However, statistical methods such as the Monte-Carlo simulation technique in conjunction with the Kolmogrov-Smirnof test can be used to generate large amounts of data from a limited amount of experimental or field data(27-29). In addition, initiation and propagation of cracks in different bolt hole locations of a given disc can be assumed to occur independently of one another. Using this approach, a 5th stage compressor disc with 40 bolt hole locations can yield 40 data points for Weibull analysis purposes. In the case of multiple cracking occurring in a given bolt hole, only the longest crack should be taken into account during analysis. These options are currently being evaluated at NRC and the findings of these investigations will be published at a later date.

3.3 Prediction of a Crack Propagation Interval (CPI)

A -3σ CPI is related to the predicted N_i and N_d distributions at 0.1% F providing the POD of cracks greater than 0.8 mm in length is high. Assuming that the lower values of TSN's in the N_d line arise due to undetectable cracks propagating to the dysfunction size, Figures 4 and 5, and a statistically significant number of precise dysfunction points exists within the overall N_d distribution, then

$$-3\sigma\ \mathrm{CPI} = \mathrm{TSN}\ (N_d)\ \text{at } 0.1\%\ \mathrm{F} - \mathrm{TSN}\ (N_i)\ \text{at } 0.1\%\ \mathrm{F} \tag{22}$$

where 1 disc in 1,000 discs will be expected to contain a dysfunction crack size after one CPI beyond crack initiation life. However, the industrial FPI technique used in the case of J85-CAN40 components could not reliably detect crack lengths of the order of 0.8 to 1 mm. In the case of J85-CAN40 components, a CPI calculated on the basis of Equation (22) would therefore prove overly optimistic since cracks lengths ~ 1.75 mm could be missed during inspection which would lead to dysfunction much earlier than that predicted by Equation (22). However, appropriate safety factors could be incorporated in Equation (22) in order to prevent any service failures. A safety factor of 2 is generally used to calculate the safe inspection interval in the damage tolerance approach(28) and applying Equation (22) to the case of the 5th stage compressor disc (Fig. 6)

$$\mathrm{SII} = 0.1\%\ \mathrm{F\ CPI}/2 = \frac{2285 - 1067}{2} \sim 600\ \mathrm{h}$$

which is a good approximation to the estimate of 555 h specified by the manufacturer.

A number of alternative methods are also possible and the CPI can be determined by experimental measurements, statistical techniques or a combination of both with field experience. These approaches are individually described as follows:

(1) A fracture mechanics calculation can be performed to determine the remaining propagation life assuming an initial flaw size just enough to have been missed during inspection (~ 1.75 mm in the case of J85-CAN40)(28), and substituting it in Equation (5) along with known '$\Delta\sigma$', 'λ', 'n', 'C' and 'a_c' values. However, the value of $\Delta\sigma$ would have to be determined by finite element stress analysis of the actual disc using known conditions of disc geometry, disc rpm, disc weight and the crack geometry. In addition, the value of the stress exponent 'n' and the constant 'C' in Equation (4) should be determined by laboratory testing of fracture mechanics specimens, Figures 14 and 15.

With increasing crack length, the stress distribution ahead of the crack tip would be expected to change since disc dimensions and the distance between the crack tip and the disc rotational axis are continuously changing. Finite element stress analysis was therefore carried out on the 5th stage compressor disc and the disc was assumed to rotate between a minimum of zero and a maximum of 16,500 rpm. The stress distribution ahead of the crack tip of a bolt hole thru crack (1.75 mm to 4.5 mm in length) was then computed under plane stress conditions. It is of interest to note that a constant ΔK value of the order of ~ 45 $\mathrm{MPa}\sqrt{\mathrm{m}}$ was observed over the entire crack length ranging between 1.75 and 4.5 mm(2,30,31). Microhardness measurements of the plastic zone sizes ahead of the crack tips in service exposed discs were also carried out to calculate the operative stress intensity factors at varying crack sizes(30). The predicted constant ΔK value of ~ 45 $\mathrm{MPa}\sqrt{\mathrm{m}}$ for crack lengths ranging between 1.75 to 4.5 mm was further verified in these investigations(2,30). Under constant ΔK conditions between 1.75 mm (a_i) and 4.5 mm (a_c) crack lengths, an integrated form of Equation (4) can be directly used to compute a CPI, where

$$\mathrm{CPI} = \frac{a_c - a_i}{C(\Delta K)^n} \tag{23}$$

An 'n' value of ~ 2.3 and an upperbound 'C' value of ~ 1.53×10^{-10} m/cycle was computed from the crack growth rate data of J85-CAN40 5th stage disc, Figure 15

$$\therefore \text{ CPI} = \frac{(4.5 \times 10^{-3} - 1.75 \times 10^{-3})}{1.53 \times 10^{-10} \times (45)^{2.3}} = 2833 \text{ cycles}$$

Since 5 major throttle excursions occur per flight hour in these engines, a CPI of ~ 567 hours is predicted for J85-CAN40 discs and this is very close to the manufacturer's estimated value of ~ 555 hours.

(2) An alternative approach investigated in this study involves a combination of Weibull analysis and quantitative fractography of service induced cracks. The details of the experimental technique and various other observations have already been presented in Section 3.1 of this paper. It is nevertheless important to point out that the observed striation spacings between 0.8 mm to 10 mm of crack length in the 5th stage compressor disc bolt holes were about 1 μm on an average, Figure 8. The striation spacings do not vary significantly over this range since ΔK values remain more or less constant over a significant crack length interval in this component(2,30,31). Based on these data, the CPI was estimated as,

$$\text{CPI} = \frac{\text{Dysfunction crack size} - \text{Max. crack size that escapes detection}}{\text{Av. striation spacing} \times \text{No. of striations per mission (per hour)}} \tag{24}$$

For the case of J85-CAN40 5th stage compressor discs, the CPI according to Equation 24 is given by:

$$\text{CPI} = \frac{4.5 - 1.75}{1 \times 10^{-3} \times 5} = 550 \text{ hours}$$

which is a strikingly close estimate to the value predicted by the manufacturer.

(3) Field experience may also be used to recalibrate or update the predicted CPI by plotting the TSO of discs cracked to dysfunction versus % F on a Weibull plot, Figure 16. Since crack propagation to the dysfunction limit occurs in these discs during the time between last overhaul and the time of retirement, it is felt that the TSO plot could be used to derive the CPI as well.

In the Weibull plot of TSO shown in Figure 16 which was supplied by the manufacturer, it appears that the CPI for the J85-CAN40 5th stage compressor discs would be ~ 250 h. However, it would be erroneous to interpret the plot in this manner, since the data indicates a strong tendency for the plot to have some curvature. A curved Weibull plot can be corrected for by a method suggested by Abernethy et al.(32). In this method a correction factor is calculated and subtracted from the TSO data. The corrected data is replotted as shown in Figure 17 and the TSO value read at the 0.135% F level (~ 50 h in this case). The correction factor (Figure 18) of 505 h is then added to the value of TSO measured from the replotted line to give the CPI. Thus, in this case, the CPI = 505 + 50 = 555 h, which is exactly the figure predicted by the engine manufacturer for the 5th stage compressor disc.

3.4 Limitations and Suggested Modifications of the Damage Tolerance Approach

At the beginning of Section 3 it was pointed out that the manufacturer advised CF not to use components for more than one CPI beyond the original safe life limit. These concerns can be rationalized in terms of continued microstructural degradation of turbine engine components with increasing service. At the end of the safe life limit plus one CPI, the microstructure of a component may be very different from that of the original material. Particularly, stress-temperature induced microstructural degradation would be expected to be more severe in hot section components. Thus, the population of discs that have been in service for say, three crack propagation intervals beyond the safe life may behave quite differently from those that have been in service for one crack propagation interval beyond the safe life. In fact, in the turbine wheels of the J85-CAN40 engine pronounced microstructural changes were found to take place with prolonged service exposure beyond the safe life limit, though no sign of cracking could be seen. The material of these wheels was A-286, an iron-base superalloy and it was found that with service exposure up to two or three times the safe life limit of 1111 h, a stress-induced transformation of the γ' strengthening phase to the possibly deleterious η-phase occurred. The quantity of the needle-like η-phase was virtually nil at the very rim of these discs, but the quantity and size of these particles increased on progressing to more highly stressed areas towards the bore, (Fig. 19). Thin foil transmission electron microscopy clearly indicated that the presence of η-phase occurred only in severely deformed regions. Areas in which intense dislocation activity could be seen were populated with η-phase particles, (Fig. 20) while in areas which had no dislocation substructure no evidence of η-phase precipitation could be found (Fig. 21). It therefore becomes apparent that the crack propagation interval for discs that have been in service well beyond the safe life limit could be entirely different from that for new discs. There may be considerable risk involved in assuming that crack-free components can be used repeatedly beyond the safe life limit for several crack propagation intervals unless the value of this crack propagation interval is continuously updated in relation to the deteriorating microstructural balance in the material. Thus, the manufacturer's specification that the engine components were to be used for a maximum of one crack propagation interval only, may be due to the behaviour of these components becoming unpredictable after this stage, according to their analysis.

However, it is clear that the potential life of the compressor discs extends beyond one crack propagation interval, since most of the retired components were used by CF for several propagation intervals prior to dysfunction. Therefore, it is felt that the lifing procedure suggested by the manufacturer can be improved by using more than one crack propagation interval, but with each interval calculated in relation to the added microstructural degradation occurring with each extra interval of service exposure.

It is also clear that the success of this damage tolerance approach depends upon positive identification of all cracks above the detection limit of 1.75 mm. This detection limit has been determined by using what may be considered a limited amount of data (160 sets) and it is essential to confirm this using modelling and simulation techniques to generate a large data base(28).

4.0 CONCLUSIONS

1. The compressor discs and spacers of this engine were used well beyond the same life limits specified.
2. The majority of retired compressor discs and spacers were severely cracked in bolt hole areas. Cracking was most severe in the 5th and 7th stage discs and in spacers on either side of them. The 5th stage discs were selected for the study described in this paper.
3. Cracks were determined to initiate and propagate as a result of low cycle fatigue damage. Crack propagation takes place under nearly constant ΔK conditions and hence, a nearly constant propagation rate over a significant crack length interval.
4. Cracks as long as 19 mm were found in the 5th stage discs. It is thought that cracks could have grown to this length due to cracked components being inadvertently reinstalled after an inspection, since the NDI procedure used was not capable of detecting all cracks below a certain "detection limit". This detection limit was found to be 1.75 mm even under ideal laboratory testing conditions.
5. The construction of Weibull cumulative failure probability plots was of considerable use in determining the basis upon which the lifing procedure was specified for these components.
6. The life to initiation (N_i) could be approximated by a Weibull plot using data on TSN-TSO of discs cracked to dysfunction and above. However, this appeared to yield a plot of "cycles to detection" rather than "cycles to initiation". The initiation line could be approximated better by a combination of experimental analysis and Weibull analysis. The experimental analysis consisted of determining the number of cycles to crack initiation in a number of discs by striation spacing measurements.
7. The safe life limit specified for these components is based on dysfunction. The dysfunction limit (N_d) could be easily determined by a Weibull plot of TSN's discs that had cracked to dysfunction and above.
8. The crack propagation interval (CPI) for the 5th stage disc could be determined by the various methods described below:

   (a) By taking the separation between the N_i (predicted) and N_d (observed) Weibull plots at the 0.1% F level and dividing this by a safety factor of 2.

   (b) By taking the separation between the N_d (observed) plot and the TSN-TSO (cycles to detection) plot at the 0.1% F level.

   (c) By using the following equation:

   $$\mathrm{CPI} = \frac{\text{Dysfunction crack size - Crack detection limit}}{\text{Striation spacing in cracked components} \times \text{No. of striations per mission}}$$

   (d) By using da/dN vs. ΔK data from laboratory simulation of crack propagation using fracture mechanics tests and calculating CPI as,

   $$\mathrm{CPI} = \frac{\text{Dysfunction crack size - Crack detection limit}}{C(\Delta K)^n \times \text{No. of LCF cycles/mission}}$$

   (e) By using a Weibull plot of TSO of discs cracked to dysfunction and above and measuring the TSO value at 0.1% F.

   The CPI was determined to be 550 to 576 h by methods (c), (d) and (e) while the manufacturer's prediction was 555 h.
9. It is clear that uncracked components can be used for at least one crack propagation interval beyond the specified safe life limit. Further life extension of uncracked components through additional crack propagation interval may be possible but these intervals would have to be calculated in relation to the increased microstructural degradation which occurs during these extra hours of service exposure.

5.0 REFERENCES

(1) Koul, A.K., Thamburaj, R., Schofield, J., Wallace, W.
Weibull Analysis in Turbine Engine Component Lifing.
NAE-NRC Report, LTR-ST-1528, June 1985.

(2) Koul, A.K., Wallace, W., Thamburaj, R.
Problems and Possibilities for Life Extension in Gas Turbine Components.
Proc. Conf. 63rd PEP-AGARD Meeting on, 'Engine Cyclic Durability by Analysis and Testing', AGARD-CP-368, 10-1, Lisse, Netherlands, May 28th - June 1st, 1984.

(3) Tiffany, C.F., Cowie, W.D.
Progress on ENSIP Approach to Improved Structural Integrity in Gas Turbine Engines An Overview.
ASME-78-WA/GT-13, Annual Winter Meeting, ASME Gas Turbine Division, San Francisco, Dec. 1978.

(4)	Harris, J.A. Jr. Sims, D.L. Annis, C.G. Jr.	*Concept Definition: Retirement for Cause of F100 Rotor Components.* Technical Report AFWAL-TR-80-4118.
(5)	Hill, R.J. Reiman, W.H. Ogg, J.S.	*A Retirement for Cause Study of an Engine Disc.* AIAA/SAE/ASME 15th Joint Propulsion Conference, Las Vegas, 18th-20th June 1979.
(6)	Annis, C.G. Cargill, J.S. Harris, J.A. Jr. Van Wanderham, M.C.	*Engine Component Retirement for Cause: A Non-Destructive Evaluation (NDE) and Fracture Mechanics Based Maintenance Concept.* Journal of Metals, July 1981, p. 24.
(7)	Besuner, P.M. Tetelman, A.S.	*Probabilistic Fracture Mechanics.* J. Nuclear Engineering and Design, Vol. 43, 1977, p. 99.
(8)	Hurchalla, J. Johnson, H.E. Wallace, R.M.	*Fracture Mechanics LCF Life Prediction System with Application to an Advanced Gas Turbine Alloy.* Proc. 11th AIAA/SAE Propulsion Conference, Anaheim, California, September 29-October 1, 1975.
(9)	Besuner, P.M. Sorenson, K.G. Johnson, D.P.	*A Workable Approach for Extending the Life of Turbine Rotors.* ASME Publication on Fatigue Life Technology, Eds. T. Cruse and J. Gallagher, 1977.
(10)	Besuner, P.M. Sorenson, K.G.	*RFC: A Workable Approach for Structural Life Extension and Response to In-service Problems.* EPRI-NP-855, Part 2, Aug. 1978.
(11)	Rau, C.A. Jr.	*The Impact of Inspection and Analysis Uncertainty on Reliability Prediction and Life Extension Strategy.* ARPA/AFML Review of Progress in Quantitative NDE, San Diego, July 1978, p. 150.
(12)	Rau, C.A. Jr. Besuner, P.M.	*Quantitative Decisions Relative to Structural Integrity.* Trans. ASME, Vol. 102, Jan. 1980, p. 56.
(13)	Rau, C.A. Jr. Besuner, P.M. Sorenson, K.G.	*Role of Micromechanical Models in Risk Analysis.* Metal Sci., August-September 1980, p. 463.
(14)	Wood, H.A. Engle, R.M. Jr.	*USAF Damage Tolerant Design Handbook: Guidelines for the Analysis and Design of Damage Tolerant Aircraft.* Technical Report AFFDL-TR-79-3021, March 1979.
(15)	Whittaker, I.C. Saunders, S.C.	*Application of Reliability Analysis to Aircraft Structures Subject to Fatigue Crack Growth and Periodic Structural Inspection.* Technical Report AFML-TR-73-92, March 1973.
(16)	Whittaker, I.C. Saunders, S.C.	*Further Development of Reliability Analysis Application to Structural Fatigue Evaluation.* Technical Report AFML-TR-75-191, Jan. 1976.
(17)		*Aircraft Damage Tolerance Requirements.* MIL-A-83444, 2nd July, 1974.
(18)	Simpson, D.L.	*Development of NDI-POD Curves Using Field Data.* NAE-NRC Report, LTR-ST-1285, August 1981.
(19)	Raizenne, M.D. Thamburaj, R. Koul, A.K. Doswell, W.	*POD Analysis of J85-CAN40 Compressor Discs.* NAE-NRC Report, LTR-ST-1529, Feb. 1984.
(20)	Hill, R.J. Reimann, W.H. Ogg, J.S.	*A RFC Study of an Engine Turbine Disc.* AFWAL-TR-81-20094 Report, Nov. 1981.
(21)	Burington, R.S. May, D.C.	Handbook of Probability and Statistics with Tables, 1st edn., McGraw-Hill, Sandusky, Ohio, 1958, p. 145.
(22)	Jouris, G.M.	*Some Comments on the Probabilistic Approach to Safety Analysis.* J. Nuc. Eng. and Design, 50, 1978, p. 169.
(23)	Rau, C.A. Jr. Besuner, P.M.	*Risk Analysis by PFM.* Product Engineering, October 1979, p. 41.
(24)	Besuner, P.M. Sorenson, K.G.	*A Workable Approach for Extending the Life of Life-Limited, Inspectable, Expensive Components.* Failure Analysis Associates Report, FAA-78-1-1, Palo Alto, California, 1978.

(25) Dainty, R.V. *Application of Optical and Electron Microscopic Techniques in the Fractographic Determination of of Fatigue Crack Growth Rates.* Proc. AGARD-SMP Conference on, 'Fatigue Crack Topography', Siena, Italy, 1st-6th April, 1984.

(26) Jones, J., Raizenne, M.D., Thamburaj, R. *Mission Profile Analysis of CF J85 Engines.* Unpublished Work, NAE-NRC, March 1985.

(27) Ostle, B., Mensing, R.W. *Statistics in Research.* The Iowa State University Press, 3rd Edition, 1975.

(28) Annis, C.G. Jr., Van Wanderham, M.C., Harris, J.A. Jr., Watkins, T. Jr. *Probabilistic Consequences of Imperfect NDE.* Proc. of the 10th Annual Review of Progress in Quantitative NDE, held in 1983 August 7th-12th, Univ. of Calif., Santa Cruz, California, USA, Eds. D.O. Thompson and D.E. Chimenti, Vol. 2B, p. 37, 1983.

(29) Yang, J.N., Donath, R.C. *Improving NDE Through Multiple Inspections.* ibid, p. 69.

(30) Thamburaj, R., Koul, A.K., Kirk, J., Kacprzynski, J.J. *Calculation of Stress Intensity Factors by Micro-hardness Measurements.* To be submitted for publication to J. Mat. Sci. and Eng.

(31) Kacprzynski, J.J. *Determination of Stress Intensity Factors in a J85-CAN40 5th Stage Compressor Disc by Finite Element Analysis.* NAE-NRC Unpublished Work, March 1984.

(32) Abernethy, R.B., Breneman, J.E., Medlin, C.H., Reinman, G.L. *Weibull Analysis Handbook.* AFWAL-TR-83-2079, November 1983.

6.0 ACKNOWLEDGEMENTS

Prepared on behalf of the Department of National Defence of Canada under cover of financial arrangement No. 325-F070. Thanks are also due to Mr. C.A. Bridges of Orenda division of Hawker Siddeley Canada Ltd. for many useful discussions. The authors also wish to express their sincere appreciation to Mrs. Shirley Dodds and her group for their assistance in preparing the final copy of the manuscript.

TABLE 1

SAFE LIVES AND MISSION SEVERITY FACTORS SUPPLIED BY G.E. AT VARIOUS DATES FOR THE 5th STAGE COMPRESSOR DISC.

DATE	SAFE LIFE J85-5 HOURS	MISSION SEVERITY FACTOR	SAFE LIFE CF HOURS
May 1970	3,000	1.00	3,000
June 1978	4,500	0.94	4,787
Sept. 1, 1979	4,000	0.94	4,255
Sept. 17, 1979	4,400	0.94	4,680
Nov. 24, 1981	3,200	1.80	1,777
Oct. 12, 1983	3,200	1.40	2,285

TABLE 2

SERVICE LIFE DATA OF J85-CAN40 COMPRESSOR AND TURBINE DISCS

COMPONENT	SAFE LIFE LIMIT HOURS	SAFE INSPECTION INTERVAL HRS.	LONGEST LIFE COMPONENT HRS.	MEAN LIFE (HRS.)	AVERAGE LIFE EXTENSION (HRS.)
4th Stage Compressor Disc	2333	555	4428.2	3863	1530
5th Stage Compressor Disc	1777	555	4473	3875	2098
6th Stage Compressor Disc	2222	722	5066.4	3971	1749
7th Stage Compressor Disc	2222	722	5066.4	3812.9	1590.95
8th Stage Compressor Disc	2944	722	5066.4	4080	1136
1st Stage Turbine Disc	1111	555	3737.6	2364	1253
2nd Stage Turbine Disc	1111	555	3791.6	2971	1860

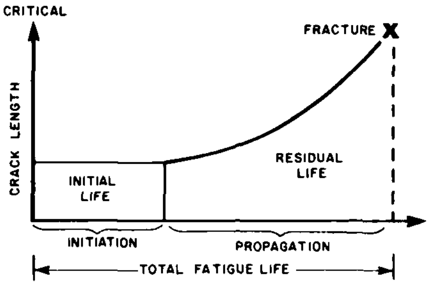
CRITICAL
CRACK LENGTH
FRACTURE X
INITIAL LIFE
RESIDUAL LIFE
INITIATION
PROPAGATION
TOTAL FATIGUE LIFE

Fig. 1 Total LCF Life Segmented into Stages of Crack Development, Sub-critical Growth and Final Fracture

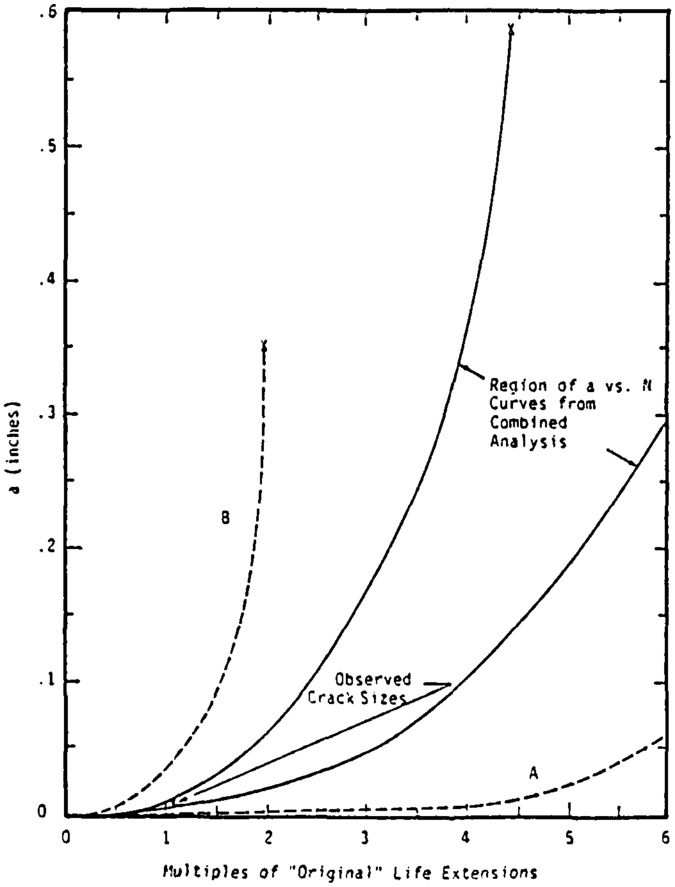

Fig. 2 Use of Combined Analysis to Narrow the Range of 'a' vs. N Curves for Cost-Effective RFC

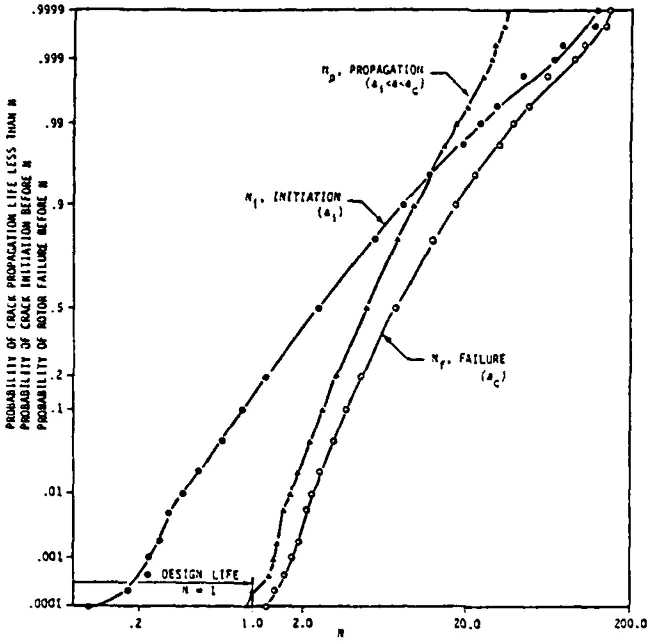

Fig. 3 Cumulative Probability Distributions of Lives Required for Crack Initiation, Crack Propagation and Failure

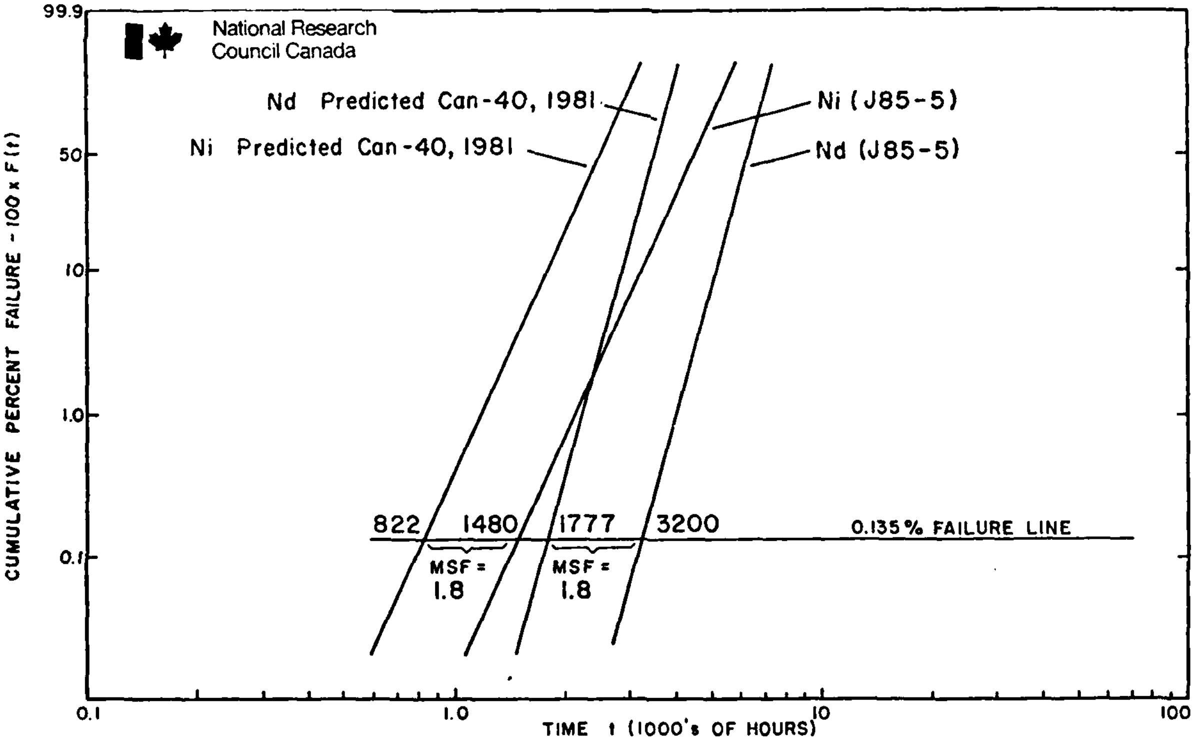

Fig.4 N_I AND N_D LINES (1981) FOR J85 AND J85-CAN40 5TH STAGE COMPRESSOR DISCS

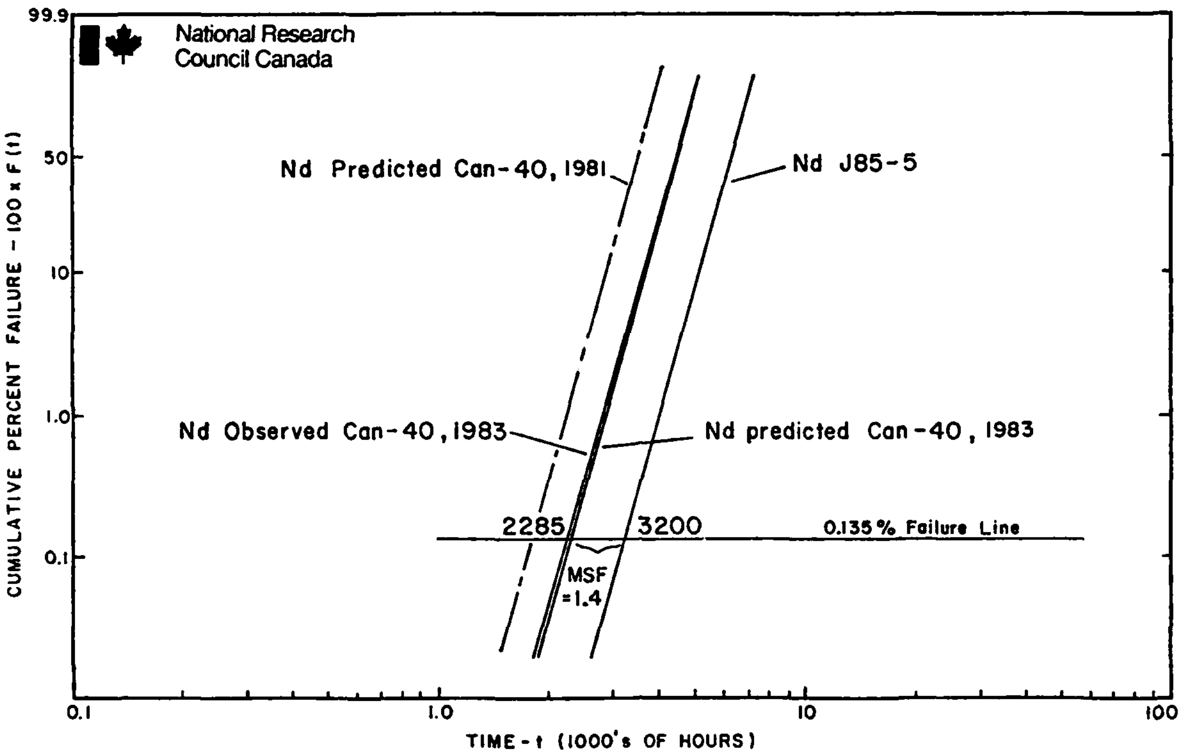

Fig.5 REVISION OF MISSION SEVERITY FACTORS

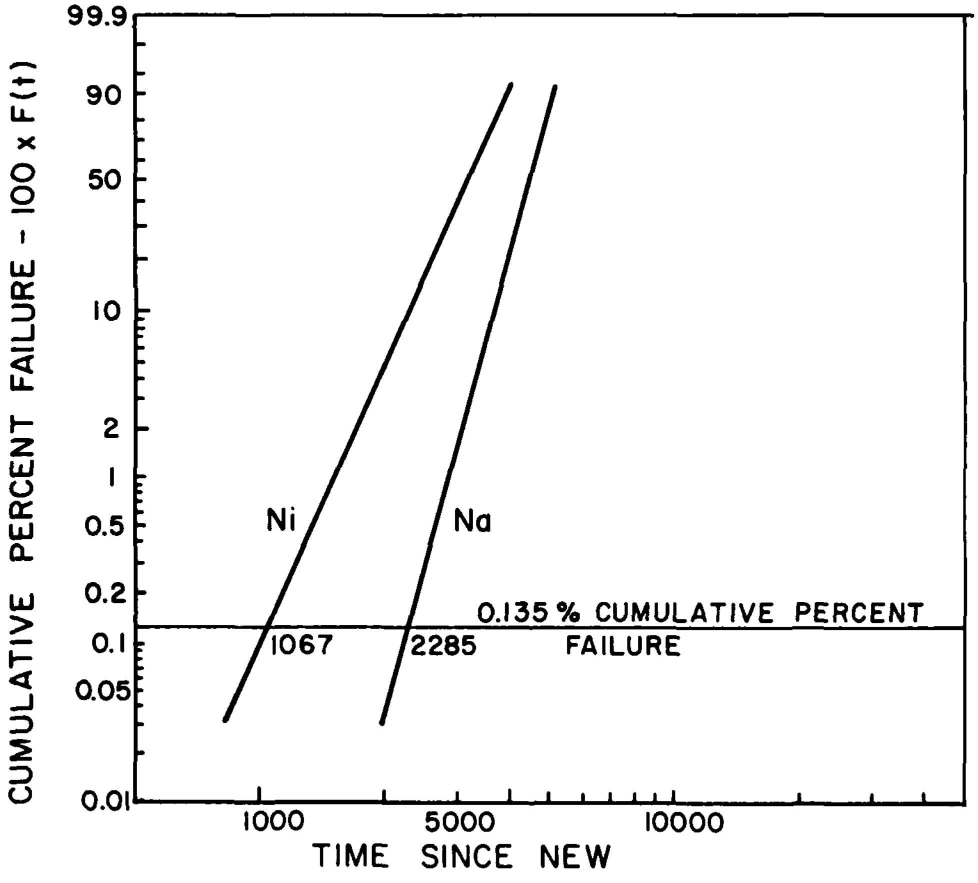

Fig. 6 Revised (1983) N_i and N_d Lines for 5th Stage Compressor Disc

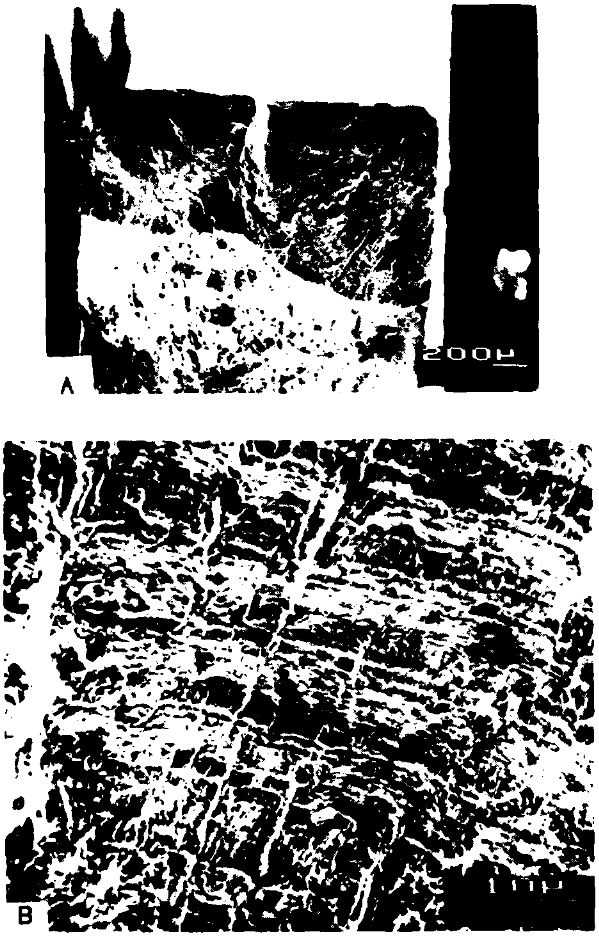

Fig. 7 FRACTURE MORPHOLOGY OF BOLT HOLE CRACKS IN 5TH STAGE COMPRESSOR DISC

(A) INITIATION SITE

(B) BANDED STRIATIONS

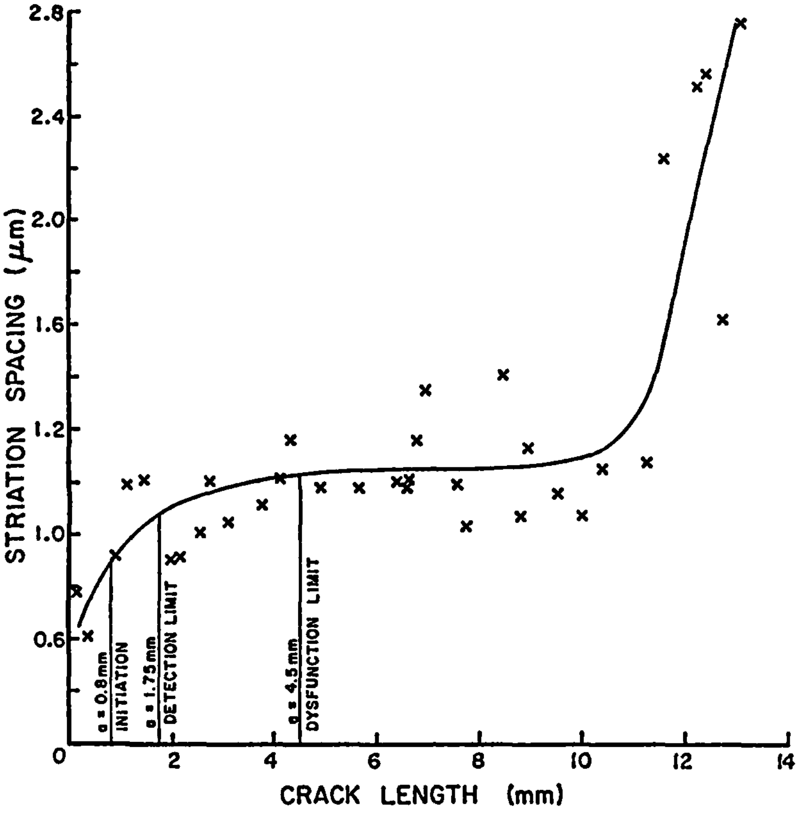

Fig. 8 RESULTS OF STRIATION SPACING MEASUREMENTS
- LONG CRACK IN A 5TH STAGE COMPRESSOR DISC

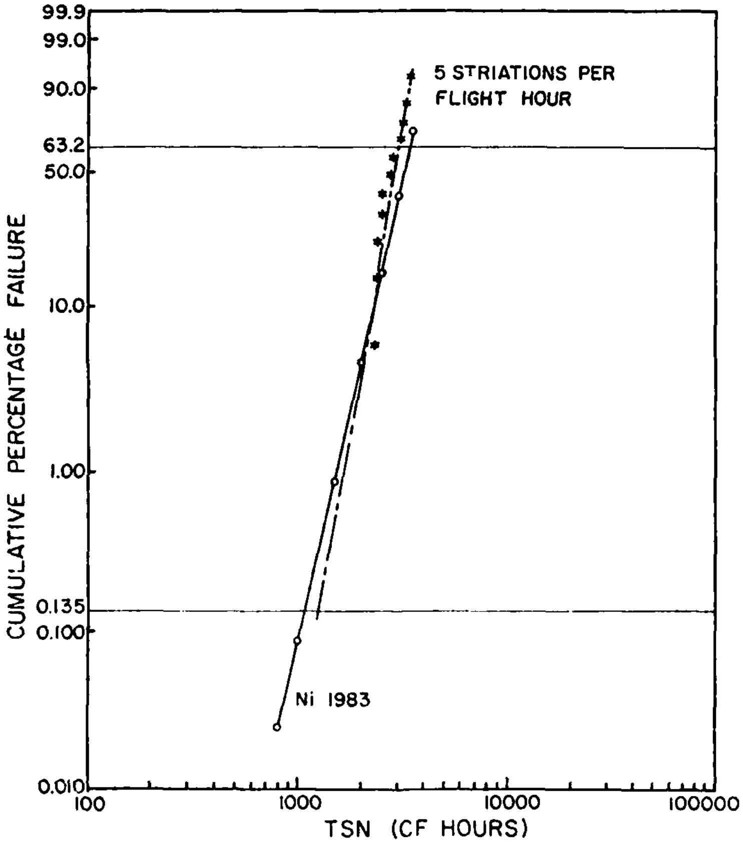

Fig. 9 N_i LINE BASED ON AN ASSUMPTION OF 5 STRIATIONS PER MISSION

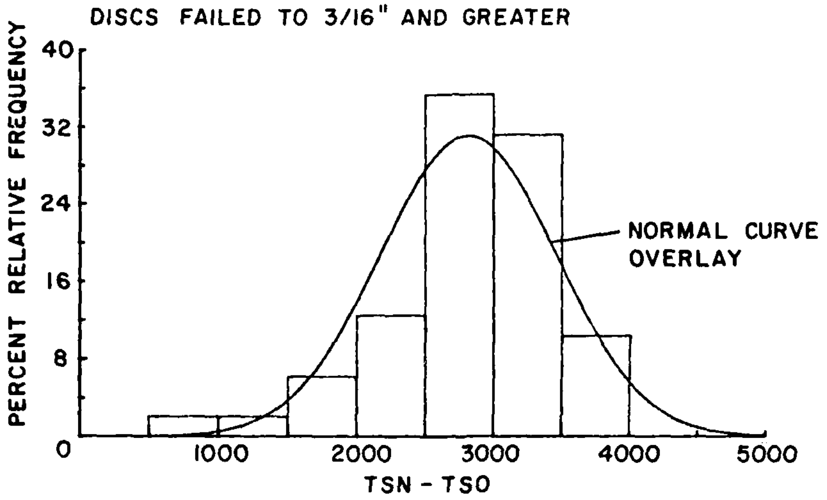

Fig. 10 LIFE DISTRIBUTION PLOT OF TSN - TSO FOR DISCS CRACKED TO DYSFUNCTION AND ABOVE

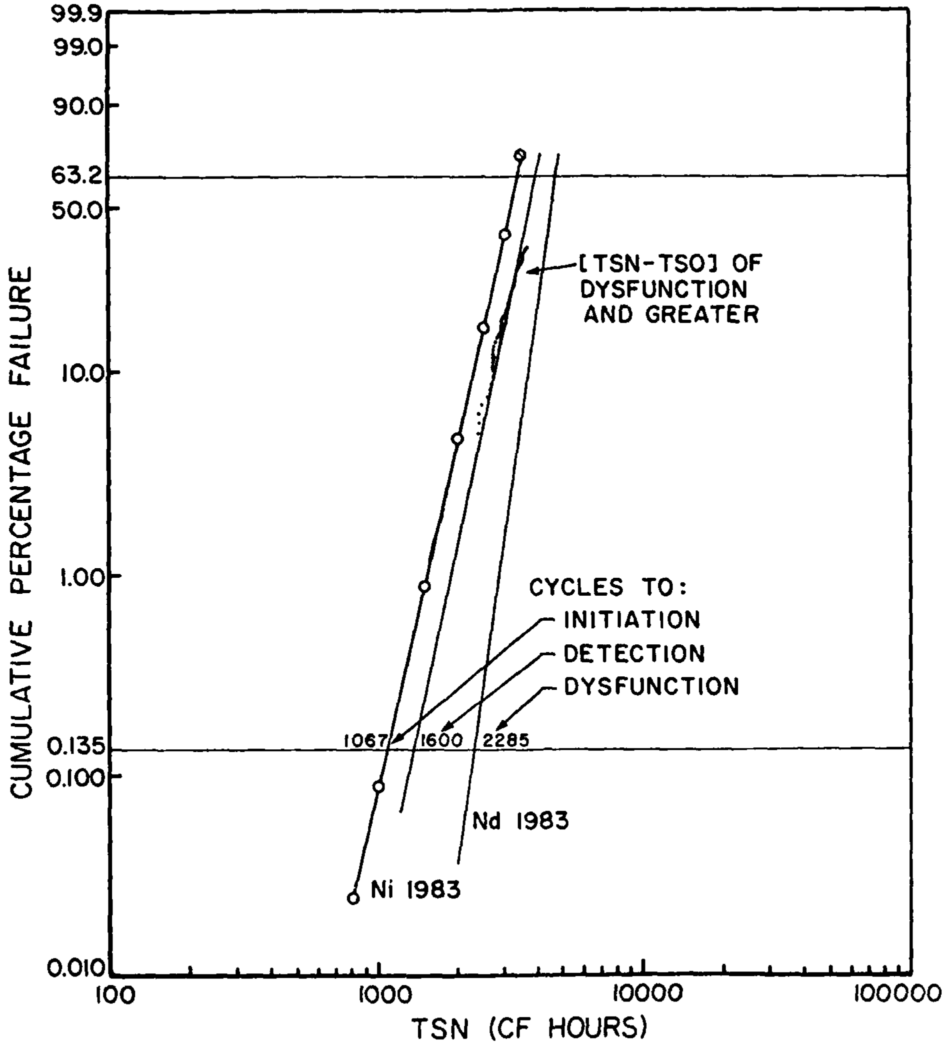

Fig. 11 WEIBULL PLOT OF TSN - TSO FOR DISCS CRACKED TO DYSFUNCTION AND ABOVE

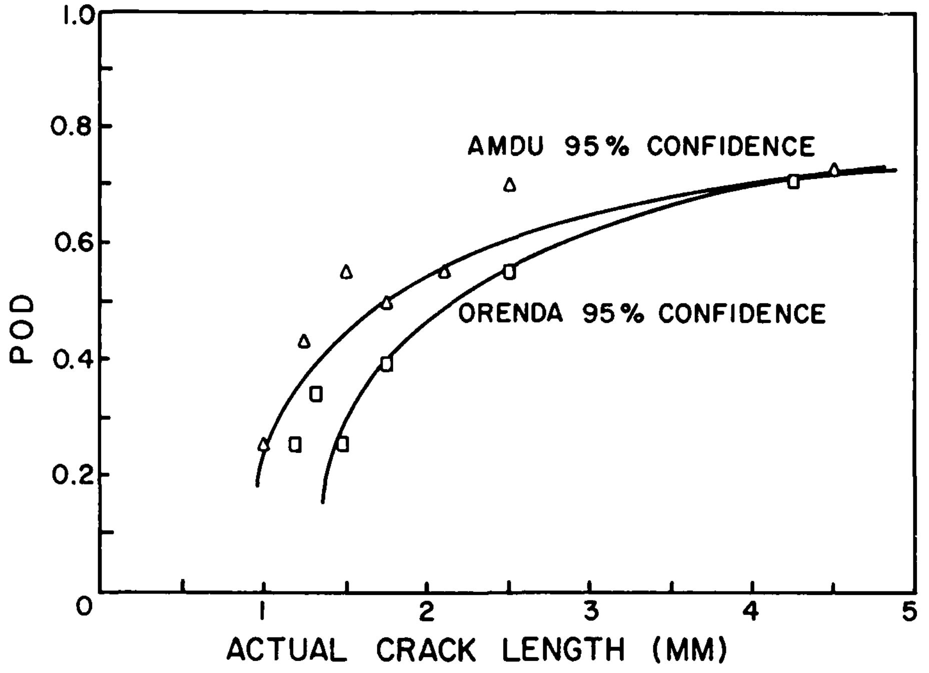

Fig. 12 PROBABILITY OF DETECTION - LOWER 95% CONFIDENCE BANDS

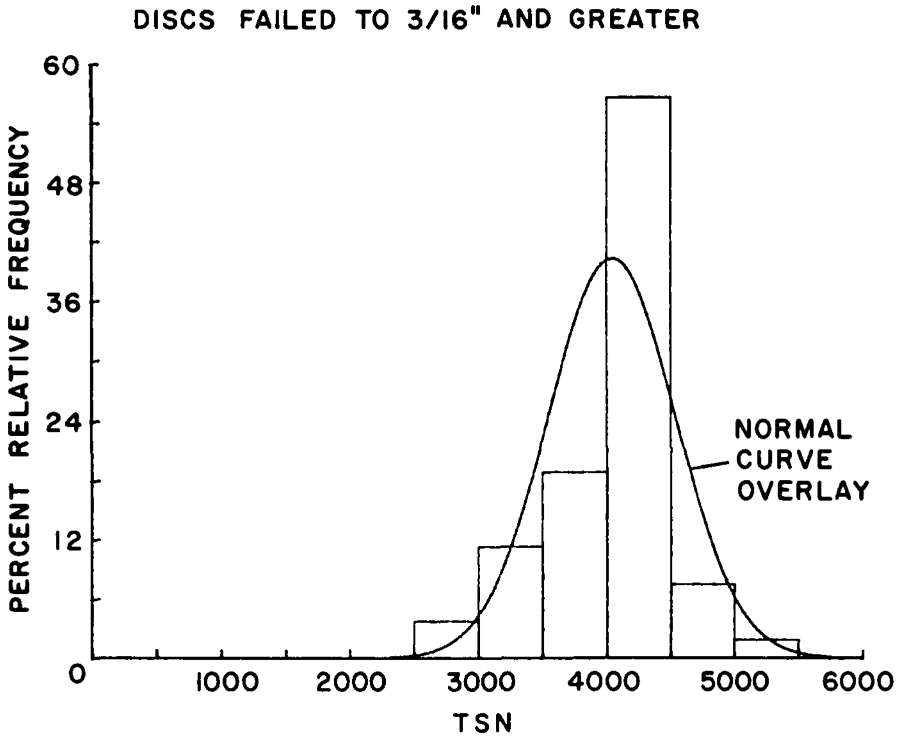

Fig. 13 WEIBULL PLOT OF TSN FOR DISCS CRACKED TO DYSFUNCTION AND ABOVE

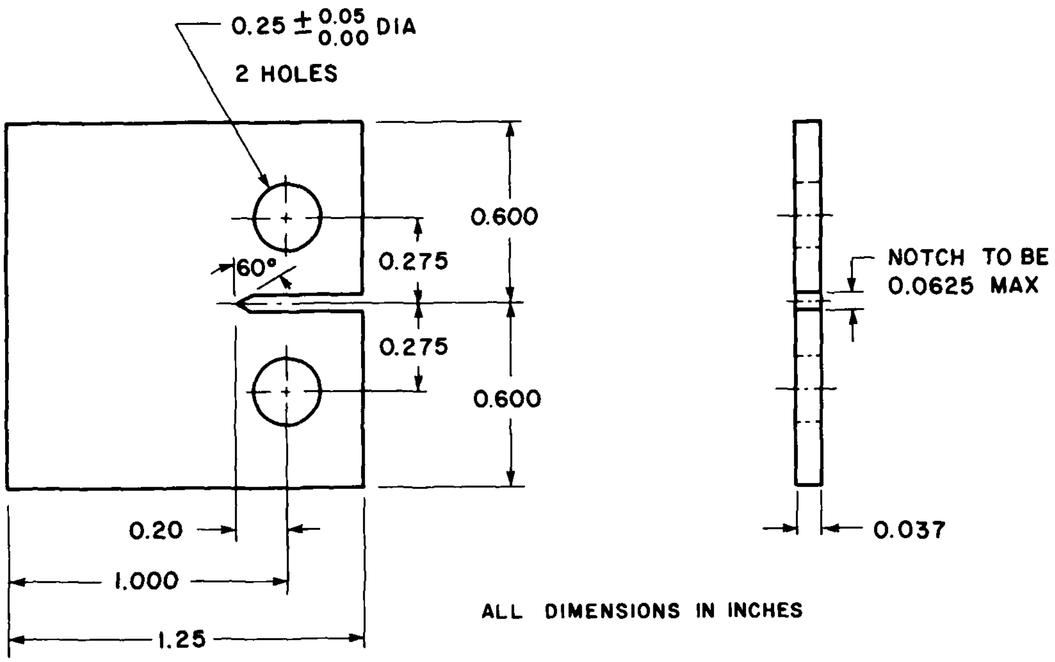
0.25 ± 0.05/0.00 DIA
2 HOLES
60°
0.275
0.275
0.600
0.600
0.20
1.000
1.25
NOTCH TO BE 0.0625 MAX
0.037
ALL DIMENSIONS IN INCHES

Fig. 14 Geometry of Compact Tension Specimen Used for Laboratory Measurement of Crack Propagation Rates

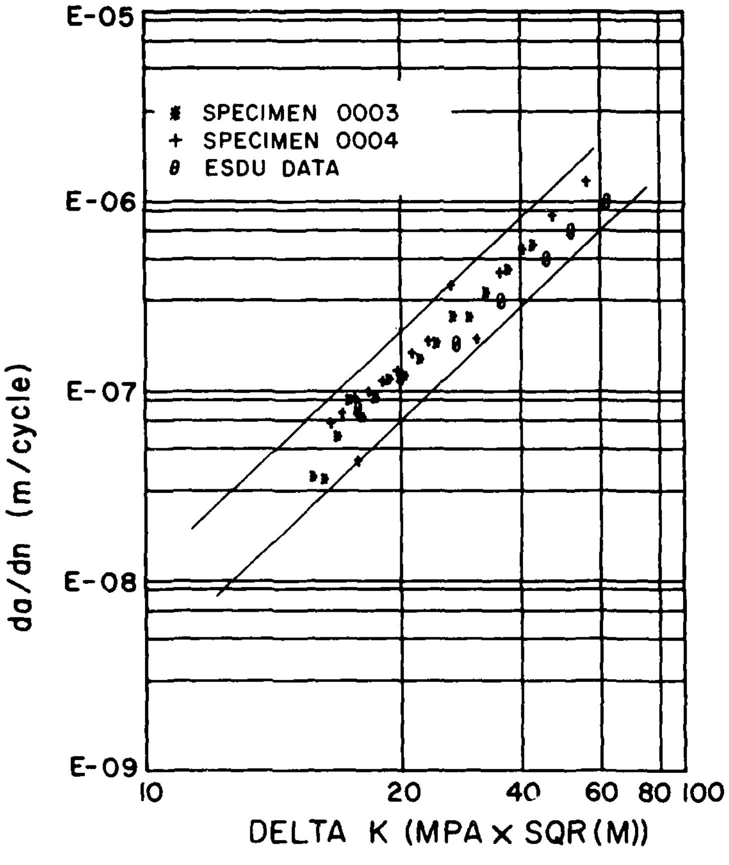

Fig. 15 Results of Crack Propagation Tests on Compact Tension Fracture Mechanics Specimen

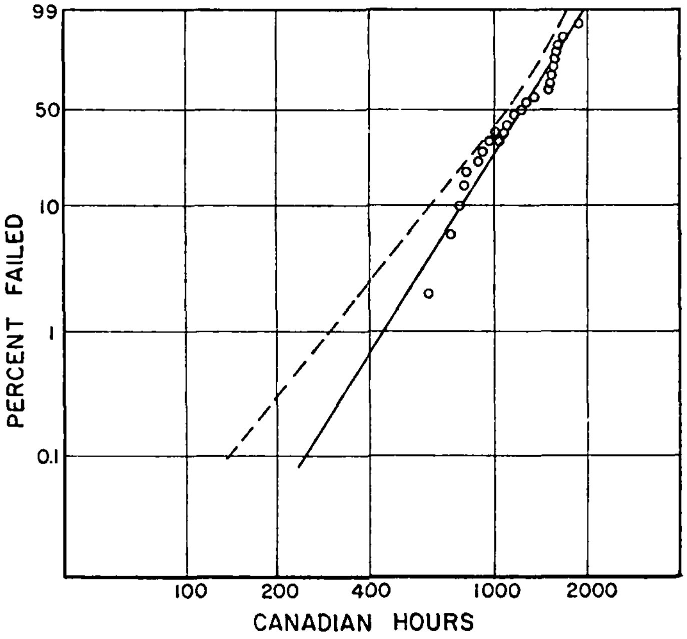

Fig. 16 WEIBULL PLOT OF TSO FOR DISCS CRACKED TO DYSFUNCTION AND ABOVE

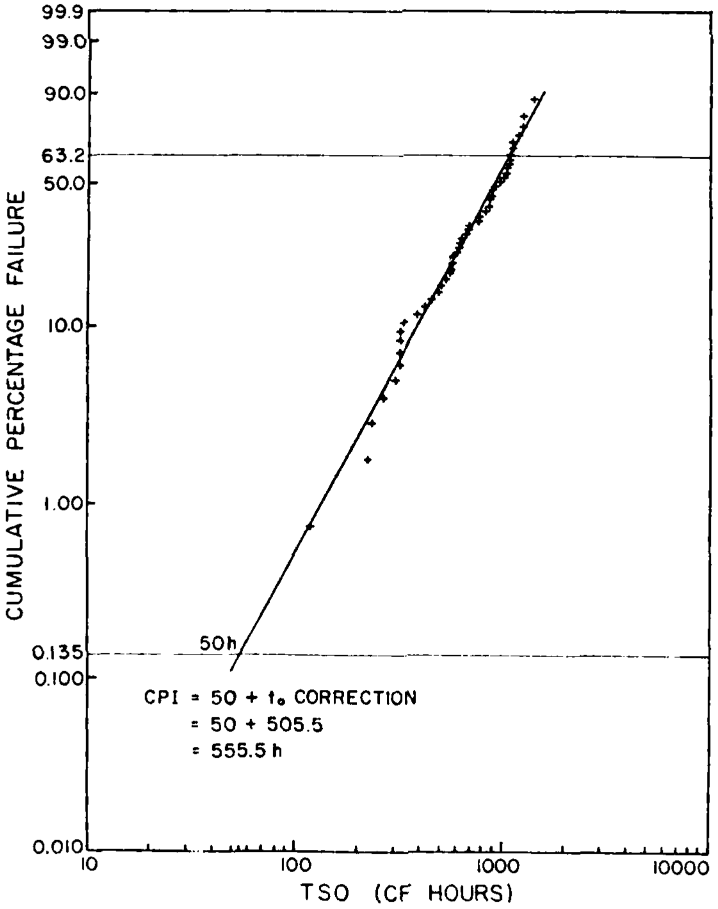

Fig. 17 WEIBULL PLOT OF TSO FOR DISCS CRACKED TO DYSFUNCTION AND ABOVE SHOWING CORRECTION APPLIED FOR CURVATURE

AD-A164 693 DAMAGE TOLERANCE CONCEPTS FOR CRITICAL ENGINE COMPONENTS(U) ADVISORY GROUP FOR AEROSPACE RESEARCH AND DEVELOPMENT NEUILLY-SUR-SEINE (FRANCE) OCT 85 4/4

UNCLASSIFIED AGARD-CP-393 F/G 21/5 NL

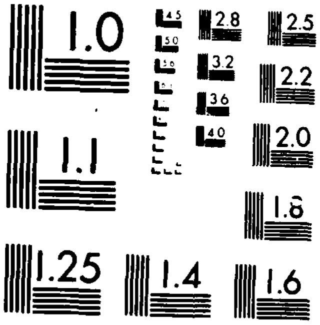
1.0
4.5
5.0
5.6
6.3
7.1
8.0
9.0
10.0
2.8
3.2
3.6
4.0
2.5
2.2
2.0
1.1
1.8
1.25
1.4
1.6

MICROCOPY RESOLUTION TEST CHART
NATIONAL BUREAU OF STANDARDS-1963-A

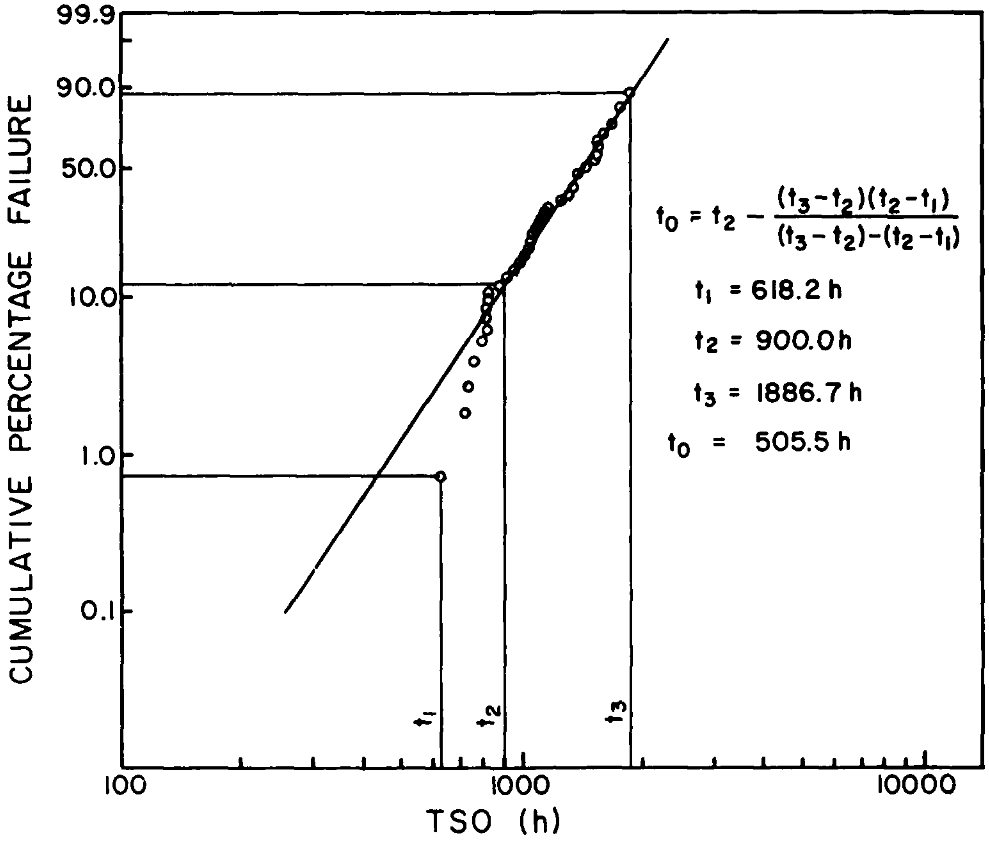

Fig. 18 WEIBULL PLOT OF TSO FOR FIFTH STAGE COMPRESSOR DISC SHOWING METHOD OF DETERMINING T_0

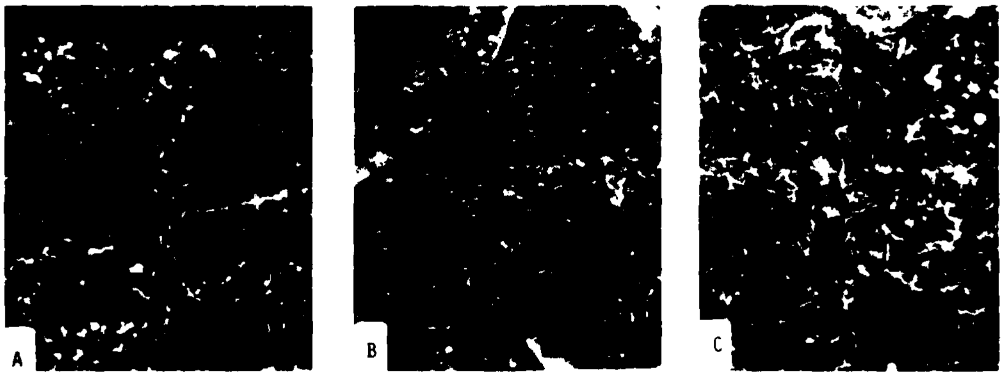

Fig. 19 PROGRESSIVE COARSENING OF NEEDLE-LIKE PHASE (η) ON PROCEEDING TOWARDS THE BORE

(A) AT RIM
(B) 5 MM FROM RIM
(C) 7.25 MM FROM RIM

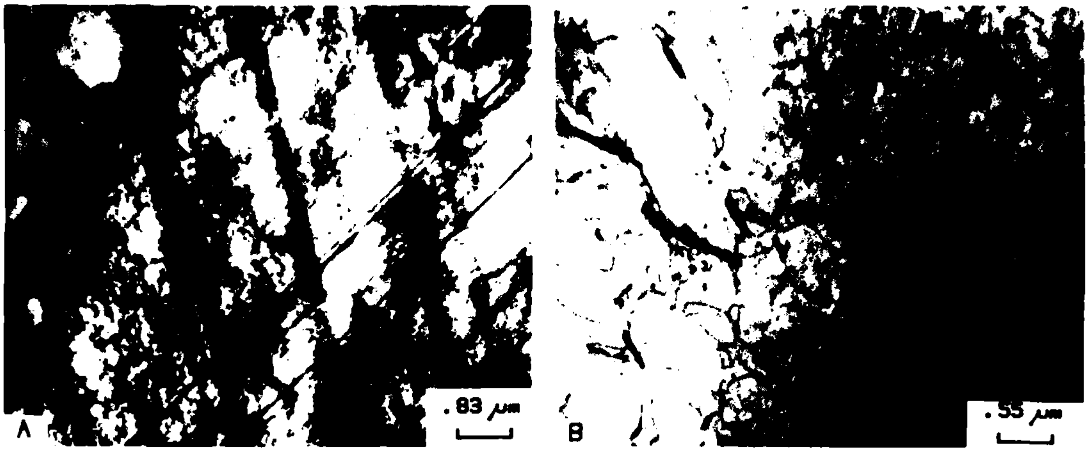
.83 µm
A
B
.55 µm

Fig. 20 η-PHASE PRECIPITATION ALONG SLIP BANDS AND REGIONS OF INTENSE DISLOCATION ACTIVITY

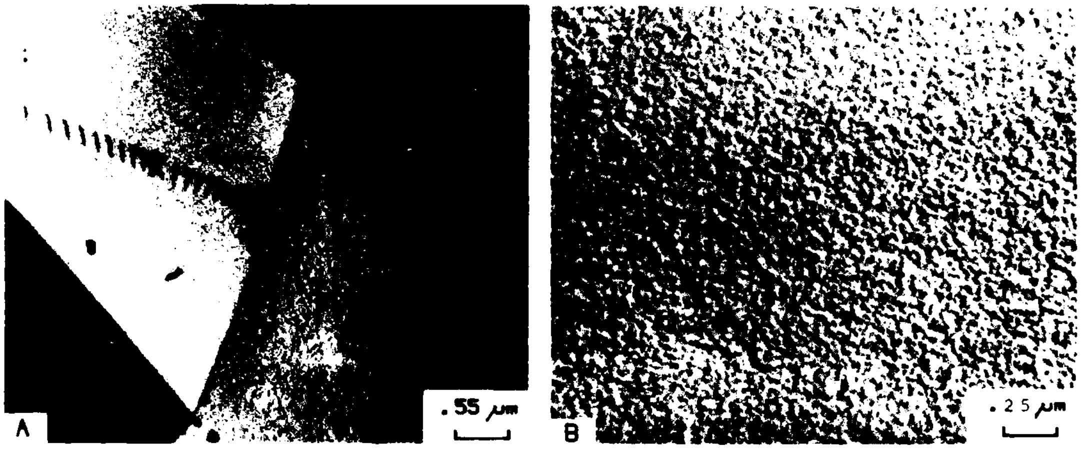
.55 µm
A
B
.25 µm

Fig. 21 ABSENCE OF DISLOCATION ACTIVITY AT THE VERY RIM OF STAGE 2 TURBINE WHEELS

RECORDER'S REPORT OF FINAL DISCUSSION

by

Dr G.F.Harrison
Royal Aircraft Establishment (Pyestock)
Pyestock,Farnborough,Hants GU140LS
UK

In the opening session of the Conference participants were asked to consider three important questions concerning engine related damage tolerance, namely *what is it, who needs it and is it safe?* Many of the views which had been expressed in the papers presented earlier were reiterated during the final discussion session. The ensuing debate went some way towards providing answers to these three questions.

i) What is damage tolerance?

There is general agreement that 'damage tolerance' is an alternative to the 'safe-life' philosophy currently used in the lifing of critical components in engines. It overcomes two limitations associated with a 'safe-life' approach, these being an inefficient use of available component life and an inability to take account of *the possible presence of rogue defects* which could initiate rapid crack growth and disc failure.

Inherent to the damage tolerance concept is the assumption that components are not necessarily defect-free. From this it follows that, having information available on defect size, on component stress distribution and on service cycle usage, fracture mechanics can be employed to estimate either the full service life or the safe time-between-overhauls which can be declared for a critical component.It is considered that the incorporation of damage tolerance within the full ENSIP lifing scheme should produce a more disciplined approach to the design of both civil and military engines. However *the discussion illustrated differences in emphasis between UK and American viewpoints.* In the American approach all components are considered to have defects, their maximum size generally being assumed to be the limit of NDI detectability. The UK approach accepts the use of fracture mechanics to predict component life but does not define the starting crack specifically by the NDI limit but by a limit related to strict control of processing and manufacturing routes and process inspection.

ii) Who needs damage tolerance?

In a war situation the essential requirement of engines is mission survivability and not the attainment of any specified design life. However, for a peacetime air force, with cost of ownership very much to the fore, it is necessary to compromise performance for increased durability. To minimise this drop in performance the maximum available life of engine components must be utilised. Damage tolerance offers a way of achieving this life. Indeed, it was stated that in designing the first engine to meet fully ENSIP requirements, only 14lbs was added to its weight, but a shortest component life in excess of 7,000 hours was achieved.

Although there is agreement with much of the design procedure package as expressed in ENSIP, it is considered in the UK that these procedures and concepts must be separated from a combined retirement-for-cause/fracture mechanics approach to life assessment. It was stated that, since the latter approach assumes the presence in components of cracks or flaws up to a limiting size, the manufacturer might relax manufacturing tolerances to take advantage of this. The UK emphasis is that damage tolerance is an added tool to ensure safety in the event of material deficiencies being present and it 'provides a way of living with an inadequate design'. Doubts were expressed as to whether it is the best way to handle new designs.

Additionally, there is a greater emphasis in the UK on the hard-lifing of components. In a fracture mechanics life assessment of such a component, where rigorous control of material processing and manufacture should be maintained, advantage can be taken of the cycles required to grow a crack from the limiting process flaw size, to a size detectable by NDI techniques. For many materials this is the major proportion of component cyclic life. There is, therefore, little or no further advantage to be gained in implementing fully RF procedures for the reward of relatively small increases in the declared lives of engine components.

iii) Is damage tolerance safe?

There is considerable difference between detecting under laboratory conditions known flaws in known locations and the capacity to detect rogue flaws in real components. A key issue therefore is the ability of NDI to detect, reliably, flaws of specified sizes. An omission from the final discussions, and indeed from the Conference in general, was any detailed information on probabilities of flaw detection. However, such figures must be established and must take account of geometric effects and differences in physical properties of engine materials. Information must also be obtained concerning the probability of rejecting unflawed components. Additionally, and of at least equal importance, since damage tolerance allows some form of defect to be present, it is necessary to identify the size levels below which detection becomes uneconomical. The unavailability of such information has been realised and, in association with ENSIP evaluation, reliability studies have been initiated. Results to date show that 5mil surface defects can be detected consistently, although information is not yet available on embedded flaws.

Damage tolerance is a useful concept which can be used to life certain engine components. However, many parameters and techniques are associated with this approach. Flaw size measurements, material physical properties, component stresses and mission cycle variability etc, all have uncertainties associated with them and so, before the method can be used to realise the full potential of the new high strength alloys, it is essential that these uncertainties are incorporated into total probabilistic analyses.

REPORT DOCUMENTATION PAGE

1. Recipient's Reference	**2. Originator's Reference** AGARD-CP-393	**3. Further Reference** ISBN 92-835-0380-5	**4. Security Classification of Document** UNCLASSIFIED

5. Originator Advisory Group for Aerospace Research and Development
North Atlantic Treaty Organization
7 rue Ancelle, 92200 Neuilly sur Seine, France

6. Title
DAMAGE TOLERANCE CONCEPTS FOR CRITICAL ENGINE COMPONENTS

7. Presented at
the 60th Meeting of the Structures and Materials Panel in San Antonio, Texas, USA on 22–26 April 1985.

8. Author(s)/Editor(s) Various	**9. Date** October 1985
10. Author's/Editor's Address Various	**11. Pages** 308

12. Distribution Statement This document is distributed in accordance with AGARD policies and regulations, which are outlined on the Outside Back Covers of all AGARD publications.

13. Keywords/Descriptors

Aircraft engines
Components
Damage
Tolerances (mechanics)
Acceptability

14. Abstract

This publication reports the proceedings of a Specialists' Meeting called by the AGARD Structures and Materials Panel on Damage Tolerance Concepts for Critical Engine Components. The meeting discussed the overall philosophy of Damage Tolerance as applied to aircraft engine parts considered and refined the parameters important in DTC, reviewed specialist techniques needed for the support of DTC, and lastly, surveyed the prospects for and experience of the implementation of DTC.

AGARD Conference Proceedings No.393
Advisory Group for Aerospace Research and Development, NATO
DAMAGE TOLERANCE CONCEPTS FOR CRITICAL ENGINE COMPONENTS
Published October 1985
308 pages

This publication reports the proceedings of a Specialists' Meeting called by the AGARD Structures and Materials Panel on Damage Tolerance Concepts for Critical Engine Components. The meeting discussed the overall philosophy of Damage Tolerance as applied to aircraft engine parts considered and refined the parameters important in DTC, reviewed specialist techniques needed for the support of DTC, and lastly, surveyed the prospects

P.T.O

AGARD-CP-393

Aircraft engines
Components
Damage
Tolerance (mechanics)
Acceptability

AGARD Conference Proceedings No.393
Advisory Group for Aerospace Research and Development, NATO
DAMAGE TOLERANCE CONCEPTS FOR CRITICAL ENGINE COMPONENTS
Published October 1985
308 pages

This publication reports the proceedings of a Specialists' Meeting called by the AGARD Structures and Materials Panel on Damage Tolerance Concepts for Critical Engine Components. The meeting discussed the overall philosophy of Damage Tolerance as applied to aircraft engine parts considered and refined the parameters important in DTC, reviewed specialist techniques needed for the support of DTC, and lastly, surveyed the prospects

P.T.O

AGARD-CP-393

Aircraft engines
Components
Damage
Tolerance (mechanics)
Acceptability

AGARD Conference Proceedings No.393
Advisory Group for Aerospace Research and Development, NATO
DAMAGE TOLERANCE CONCEPTS FOR CRITICAL ENGINE COMPONENTS
Published October 1985
308 pages

This publication reports the proceedings of a Specialists' Meeting called by the AGARD Structures and Materials Panel on Damage Tolerance Concepts for Critical Engine Components. The meeting discussed the overall philosophy of Damage Tolerance as applied to aircraft engine parts considered and refined the parameters important in DTC, reviewed specialist techniques needed for the support of DTC, and lastly, surveyed the prospects

P.T.O

AGARD-CP-393

Aircraft engines
Components
Damage
Tolerance (mechanics)
Acceptability

AGARD Conference Proceedings No.393
Advisory Group for Aerospace Research and Development, NATO
DAMAGE TOLERANCE CONCEPTS FOR CRITICAL ENGINE COMPONENTS
Published October 1985
308 pages

This publication reports the proceedings of a Specialists' Meeting called by the AGARD Structures and Materials Panel on Damage Tolerance Concepts for Critical Engine Components. The meeting discussed the overall philosophy of Damage Tolerance as applied to aircraft engine parts considered and refined the parameters important in DTC, reviewed specialist techniques needed for the support of DTC, and lastly, surveyed the prospects

P.T.O

AGARD-CP-393

Aircraft engines
Components
Damage
Tolerance (mechanics)
Acceptability

END
FILMED
4-86
DTIC